THE GEOLOGY AND GENESIS OF MASSIVE SULPHIDE, BARITE-GOLD DEPOSITS ON WETAR ISLAND, INDONESIA.

Philip M. Scotney

Southampton
Ocean & Earth Science

UNIVERSITY OF SOUTHAMPTON

A thesis presented for
the degree of
Doctor of Philosophy

Billiton

THE NATURAL HISTORY MUSEUM

School of Ocean and Earth Science
University of Southampton
August 2002

UNIVERSITY OF SOUTHAMPTON

ABSTRACT

FACULTY OF SCIENCE
DEPARTMENT OF GEOLOGY

Doctor of Philosophy

THE GEOLOGY AND GENESIS OF MASSIVE SULPHIDE, BARITE-GOLD DEPOSITS ON WETAR ISLAND, INDONESIA.

By Philip M. Scotney

Volcanic hosted massive sulphide mounds are preserved at Wetar Island, Indonesia with flanking Au-Ag-Hg bearing baritic ore bodies. Wetar Island measures 110 km × 40 km and is part of the Inner Banda Arc, formed during the arc-continent collision of the NNE moving Indian-Australian plate beneath the Eurasian plate. The island is composed entirely of Oligocene to Recent volcanics and minor oceanic sediments with centres of mineralisation at Kali Kuning (KK3) and Lerokis that are located approximately 3 km inland at an elevation of 400-500 m. The orebodies occur marginal to rhyodacite domes within hydrothermally altered calc-alkaline volcanics which overly ocean floor basaltic -andesites. $^{40}Ar/^{39}Ar$ dating of biotite grains from a syeno-granite intrusion from the Meron area yielded a Zanclian age of 4.72 ± 0.22 Ma, biotites from a post-mineralisation overlying dacitic flow yielded a Piacenzian age of 2.4 ± 0.28 Ma.

The massive sulphides are dominantly pyrite with minor chalcopyrite in upper parts, the pyrite is arsenian (up to 6.7 wt% As) and cut by late fractures infilled with covellite, chalcocite, tennantite-tetrahedrite, enargite, bornite and Fe-poor sphalerite. Mining removed the associated Au-Ag-bearing barite sands (2.17 Mt at 3.98g/t Au at Lerokis; 1.9 Mt at 4.63 g/t Au at Kali Kuning), with the sulphide mounds at each deposit remaining unexploited. The barite ores are generally friable and are cemented by a series of complex arsenates, sulphates with gold present as <10 μm free grains. Anhedral <20 μm inclusions of sulphides and sulphosalts are present within the barite. The morphology of the barite within the deposits ranges from euhedral rectangular, rhombohedral and polyhedral crystals up to 6 mm in diameter to finer subhedral to anhedral crystals towards the footwall and hangingwall of deposits. Linear and pipe-like barite- Fe-oxide structures are evident and are fluid feeders for the barite ore bodies. The ore bodies are covered by post mineralisation globigerina bearing limestone, lahars, sub-aqueous debris flows and pyroclastics.

Alteration is zoned around the orebodies and dominanted by illite-kaolinite-smectite assemblages. Inner advanced argillic mineral cores and the presence of native sulphur are indicative of acidic, oxidising fluids occurring proximal to mineralisation. A central zone of residual silica along with minor alunite and traces of pyrophyllite have been identified, laterally and vertically this zone passes into argillic and propylitic zones. K-Ar dated illite samples of altered footwall volcanics gives an age of mineralisation at 4.7 ± 0.16 Ma, $^{40}Ar/^{39}Ar$ dating of this same sample yields an age of 4.52 ± 0.22 Ma.

Fluid inclusions within barite are dominantly two phase liquid/vapour with homogenisation temperatures of 144°-314°C, salinities vary from 1.6-5.1 wt% NaCl with an average value of 3.2 wt% NaCl. The sulphur isotope composition ($\delta^{34}S$) of Wetar sulphides range between +3.3 and +11.7‰ (mean, 8.0‰ and standard deviation of 1.9‰, n=30) whereas $\delta^{34}S$ sulphate data vary between +22.4 and +31.0‰ (mean, 24.8‰ and standard deviation of 2.1‰, n=23). Native sulphur and post mineralisation gypsum from Kali Kuning yielded $\delta^{34}S$ values of 15.8‰ and 12.8‰ respectively. Late stage barite veins distal to mineralisation are isotopically heavy compared to all other barite from the mineralisation. Oxygen isotopes ($\delta^{18}O$) of sulphates vary between +5.8 and +11.3‰ (mean, 8.5‰ and standard deviation of 1.6‰, n=18). Post mineralisation gypsum from Kali Kuning yielded $\delta^{18}O$ value of 13.3‰. The range of $\delta^{34}S$ and $\delta^{18}O$ values for sulphides / sulphates are similar to published data from Kuroko deposits and TAG, a mean of 24.8‰ for all sulphate sulphur data strongly suggests derivation from Miocene seawater sulphate (22‰). The $\delta^{34}S$ ratios of the inner Banda Arc volcanics range between +2 and +7‰ compared to +0.1‰ for MORB. Wetar island sulphide $\delta^{34}S$ data (mean +8‰, n=30) suggest derivation of sulphur from associated host volcanics through extensive water / rock interaction. Values of $\delta^{34}S$ and $^{87}Sr/^{86}Sr$ within the hosting rocks reflect contributions from the subducting slab. Hydrothermal barite range from 0.7076 to 0.7088 (n=16) and suggests a dominant Miocene seawater component within the hydrothermal system. Despite evidence of low pH fluids, radiogenic and stable isotopes record a dominant seawater component within the hydrothermal system, the fracture related hypogene sulphosalt assemblages may record the late input of magmatic volatiles into the system confirmed by $^{3}He/^{4}He$ ratios > 1 R/Ra.

ACKNOWLEDGEMENTS

This project was initiated by Dr. R. Herrington and D. First and carried out as a collaborative link between the University of Southampton, Natural History Museum, London and Billiton plc. Financial support was provided by the aforementioned, fieldwork was supported by Billiton.

Many thanks, Richard, Steve and David for allowing me to undertake this project and for the encouragement throughout.

At Southampton I would like to thank Andy Barker, Rex Taylor, Damon Teagle, Bob Foster and Lawrence Hopkinson for discussions and suggestions, to Ian Croudace for assistance with XRF and to Posy for laboratory assistance. To Bob and John for the sample preparation, their intellectual conversations and to all the past and present postgraduate students.

At the Natural History Museum I would like to thank Terry Williams and John Spratt for their time on the Microprobe and Robin Armstrong for comments, suggestions and for being a good friend throughout.

During the fieldwork season on Wetar Island, thanks to Jon Booler and Irwan Santosa for their hospitality, all the mine staff and to Mr John and Mr Vincent who guided me through the spectacular environment carrying my samples.

Special thanks to James Macdonald, David Hopgood and Peter Gower for matching their support with financial assistance from Billiton.

At SUERC I would like to thank Adrian Boyce for introducing me to East Kilbride and to the "student flat" and all his assistance, to Anthony Fallick, Fin Stuart and all the lab people who assisted in the isotope research.

At the University of Manchester, many thanks to Ernie Rutter for allowing the Argon and Helium work to go ahead and to Ray Burgess, Daryl Harrison and Paul Harrop for assistance with these techniques. Thanks Tony Lewis for your friendship, I hope our beer and curry evenings continue for many years.

To Charles Catell for starting me off on the geological track and to all family and friends who have all endured the "thesis" with me.

Finally to Steve and Richard, I can never repay the help, advice, support and patience you have given during the course of this project, I hope you both feel it has been worth it, see you both on the golf course!

CONTENTS

	Page
Abstract	
Acknowledgements	
Contents	
List of Figures	
List of Tables	
Chapter 1 – INTRODUCTION	**1**
1.1 VMS Systems	1
1.2 High-Sulphidation VMS Systems	2
1.3 Wetar Island	8
1.4 Previous Work	10
1.5 Present Study	11
1.6 Thesis Layout	12
Chapter 2 – TECTONIC EVOLUTION OF THE SUNDA AND BANDA ARCS	**14**
2.1 General evolution and subdivision of the arcs	14
2.2 Detailed evolution of the arc	18
2.2.1 Australian continental shelf / margin	18
2.2.2 Timor trough / zone of subduction	18
2.2.3 Forearc	20
2.2.4 Collision complex / accretionary prism	20
2.2.5 Volcanic arc	22
2.2.6 Backarc region	23
2.3 Summary	24
Chapter 3 – VOLCANIC AND STRUCTURAL SETTING OF THE DEPOSITS	**26**
3.1 Introduction	26
3.2 Previous work	27
3.2.1 Structure	27
3.2.2 Stratigraphy	28
3.3 Present study	28
3.3.1 Structure and Stratigraphy	28
3.3.2 Kali Kuning deposit geology	38
3.3.3 Lerokis Zone 5 deposit geology	40
3.3.4 Lerokis Zone 4 deposit geology	42
3.3.5 Meron deposit geology	43
3.4 Discussion of stratigraphy and host geology	44
3.5 Summary	46
Chapter 4 – HYDROTHERMAL ALTERATION	**49**
4.1 Introduction	49
4.2 Previous work	49
4.3 Sample selection and analysis	52
4.4 Results	52
4.4.1 Kali Kuning	54
4.4.2 Lerokis Zone 5	54
4.4.3 Lerokis Zone 4	55
4.5 Alteration geochemistry / petrochemistry	62
4.6 Discussion of alteration	69
4.7 Summary	70
Chapter 5 – ORE MINERALOGY, TEXTURES AND CHEMISTRY	**72**
5.1 Introduction	72
5.2 Previous work	73
5.3 Sample selection	74
5.4 Field relationships	74
5.4.1 Sulphide mounds	74
5.4.2 Stockwork zones	81

5.4.3 Barite deposits 81
5.4.4 Barite / Fe-oxide feeder structures 85
5.5 Petrography and mineral chemistry 87
5.5.1 Massive sulphide mounds 87
5.5.1.1 Pyrite 91
5.5.1.2 Marcasite 91
5.5.1.3 Chalcopyrite 91
5.5.1.4 Sphalerite 92
5.5.1.5 Tennantite 92
5.5.1.6 Barite 92
5.5.1.7 Minor phases 93
5.5.2 Stockwork zones 93
5.5.2.1 Gold 93
5.5.2.2 Pyrite 100
5.5.2.3 Galena 100
5.5.2.4 Sphalerite 100
5.5.2.5 Chalcopyrite 101
5.5.2.6 Fahlore minerals 101
5.5.2.7 Covellite 101
5.5.2.8 Barite 102
5.5.2.9 Silica phases 102
5.5.3 Barite deposits 102
5.5.4 Barite cementing phases 103
5.6 Paragenesis 118
5.7 Discussion of mineralogy 122
5.8 Summary 125

Chapter 6 – FLUID INCLUSION STUDY **126**
6.1 Introduction 126
6.2 Analytical methods 126
6.3 Sample selection 127
6.4 Nature and occurrence 128
6.5 Microthermetric results 131
6.6.1 Discussion 135
6.6.2 Depth of formation and pressure estimates 143
6.7 Summary 146

Chapter 7 – STABLE ISOTOPES **147**
7.1 Introduction 147
7.2 Sulphur isotopes 148
7.3 Previous work 149
7.4 Present study 149
7.4.1 Sample selection 149
7.4.2 Results 150
7.5 Oxygen isotopes 156
7.6 Present study 156
7.6.1 Sample selection 156
7.6.2 Results 156
7.7 Discussion of isotopic data 158
7.7.2 Isotopic variation with depth 162
7.7.3 Isotopic geothermometers 162
7.7.4 Sources of sulphur and oxygen 166
7.8 Summary 167

Chapter 8 – HELIUM and STRONTIUM **168**
8.1 Introduction 168
8.2 Helium 168
8.2.1 Previous work 168

8.3 Helium ratios
8.3.1 Circum Pacific arcs 169
8.3.2 Sunda and Banda arcs 170
8.4 Sample Selection 172
8.5 Analytical techniques 172
8.6 Results 172
8.7 Discussion 174
8.7.1 Evolution of the arc 174
8.7.2 Hydrothermal system 174
8.8 Strontium isotopes 177
8.8.1 Previous work 177
8.9 Sample selection 179
8.10 Results 179
8.11 Discussion 182
8.11.1 Arc and petrogenetic evolution of strontium 182
8.11.2 Hydrothermal evolution 186
8.12 Argon 188
8.12.1 Previous work 188
8.13 Present Study 188
8.13.1 Sample selection 188
8.13.2 Analytical technique 188
8.13.1 Results 189
8.13.4 Discussion 189
8.13 Summary 193

Chapter 9 – DISCUSSION / GENETIC MODEL **194**
9.1 Host volcanic stratigraphy 194
9.2 Hydrothermal alteration 195
9.3 Mineralisation and style of deposits 197
9.4 Fluid composition 201
9.5 Depth and timing of mineralisation 204
9.6 Isotopes 205
9.7 Summary 208
9.8 Genetic Model 209
9.8.1 Tectonic, magmatic and geological evolution 209
9.8.2 Ore deposit evolution 214

Chapter 10 – CONCLUSIONS **218**
- Future Work / Recommendations 220

References **221**

Appendices
A. Abbreviations and samples during study
B. Thin sections
C. XRD, FTIR and XRF
D. SEM, MICROPROBE, mineralogical studies
E. Microthermetric data
F. Isotopic data (S, O, Sr, Ar/Ar, H)

List of Figures

Figure		Page
1.1	Volcanic Hydrothermal system typical of an emergent intrusion centred volcanoplutonic arc.	4
1.2	Location map of polymetallic massive sulphide deposits and modern hydrothermal seafloor systems.	5
1.3	Principal epithermal, VMS and porphyry deposits in the western Pacific.	6
1.4	Location of the Wetar field area.	8
1.5	Mine site, north coast Wetar.	9
1.6	Lerokis and Kali Kuning project area, pre-mining.	13
2.1	Principal geographic features of eastern Indonesia.	16
2.2	Principal tectonic and volcanic features of the Banda arc.	17
2.3	Simplified cross section of the Banda orogen.	19
3.1	View approximately east of the Lerokis mine area.	27
3.2	Schematic cross section through Wetar Island and age dates.	29
3.3	Simplified geological map of Wetar Island.	30
3.4	Deposit location and sites of mineralisation.	31
3.5	Aerial views of Kali Kuning and Lerokis Zone 5.	34
3.6	Schematic stratigraphy of the Kali Kuning, Lerokis and Meron area.	35
3.7	Volcanics and post mineralisation debris flows.	36
3.8	Photomicrographs of unaltered lithologies.	37
3.9	Post mineralisation debris flow, volcanoclastic sediment and limestone / gypsum / chert contact.	41
3.10	Lerokis Zone 4 field photo.	42
4.1	Extensive gossanous zones around mineralisation.	53
4.2	Alteration zonation around the Kali Kuning orebody.	56

4.3	Cross section through the Kali Kuning orebody.	57
4.4	Microphotographs of altered host volcanics.	58
4.5	Alteration around the Lerokis Zone 5 orebody.	59
4.6	Cross section through the Lerokis Zone 5 orebody.	59
4.7	Volcanic morphologies of host volcanics.	60
4.8	Alteration around the Lerokis Zone 4 orebody.	61
4.9	Alteration spectra in relation to zones of alteration.	63
4.10	IUGS chemical classification of volcanic rocks and intrusives.	65
4.11	Discrimination diagrams of Nb/Y and Zr/TiO2.	66
4.12	Discrimination diagram of Ti/Zr.	67
4.13	Schematic section through and idealized orebody and associated Alteration.	71
5.1	Exposed sulphide mounds at Kali Kuning and Lerokis Zone 5.	76
5.2	Sulphide mound textures.	77
5.3	Sulphide hand specimens.	78
5.4	Sulphide mound and footwall contacts.	79
5.5	Sulphide mound features.	80
5.6	Stockwork zone hand specimens.	82
5.7	Nature of in-situ barite ore, Lerokis Zone 4.	83
5.8	Nature of in-situ barite ore, Kali Kuning.	84
5.9	Distal vein barite.	85
5.10	Cemented barite – Fe oxide structures, Lerokis Zone 4.	86
5.11	Barite – Fe oxide structure at Kali Kuning.	89
5.12	Barite – Fe oxide structure at Lerokis Zone 5.	90
5.13	Reflected light microphotographs of sulphide mound assemblages.	94
5.14	Reflected light microphotographs of sulphide mound assemblages.	95

5.15	Back-scattered electron microphotographs of As zonation.	96
5.16	Copiapite and romerite crystals on barite.	99
5.17	Reflected light microphotographs of sulphide mound / stockwork Zone assemblages.	104
5.18	Reflected light microphotographs of sulphide mound / stockwork zone assemblages.	105
5.19	Reflected light microphotographs of sulphide mound / stockwork zone assemblages.	106
5.20	Reflected light microphotographs of sulphide mound / stockwork zone assemblages.	107
5.21	In-situ contact zone between sulphide mound / barite ore and altered footwall, location 84.	110
5.22	Morphology of barite ore crystals.	111
5.23	Barite blocks for microprobe and SEM study.	112
5.24	Back-scattered electron microphotographs of barite ore.	114
5.25	Back-scattered electron microphotographs of barite ore.	115
5.26	Wavelength dispersive analysis map of barite sample 111983.	116
5.27	Anhedral nature of gold grains associated with barite ore.	117
5.28	Back-scattered electron microphotographs of barite ore.	118
5.29	Paragenetic sequence of mineralisation.	119
6.1	Photomicrographs of barite hosted fluid inclusions.	129
6.2	Microthermetric results of fluid inclusions.	133
6.3	Microthermetric results of fluid inclusions.	134
6.4	Microthermetric results of fluid inclusions.	141
6.5	Homogenisation temperatures and salinities of inclusions.	142
6.6	Pressure-temperature diagram and comparative fluid data.	145
7.1	Sulphur isotopic compositions of Wetar data, de Ronde, 1995.	153
7.2	Sulphur isotopic compositions of Wetar data, present study.	153

7.3	Comparison of Wetar sulphur data.	154
7.4	Oxygen isotope compositions of Wetar sulphates.	157
7.5	Comparison of Wetar oxygen data.	157
7.6	Sulphur lateral variation at location 84, Kali Kuning.	159
7.7	Native sulphur at Kali Kuning.	161
7.8	Plots of sulphur and oxygen versus depth.	163
7.9	Calculated fluid $\delta^{18}O$ versus temperature for barite.	163
8.1	Helium isotopic ratios of volcanic lavas, gases and massive sulphides.	171
8.2	Helium summary data and comparisons.	175
8.3	Along arc variation in helium and strontium ratios.	178
8.4	Wetar island whole rock and sulphate strontium data.	181
8.5	Strontium concentrations in Banda arc volcanics.	183
8.6	Sr-isotope mixing diagram for Banda arc volcanics.	184
8.7	Banda arc strontium data.	185
8.8	Relationship between strontium and alteration.	187
8.9	$^{40}Ar/^{36}Ar$ correlation diagrams and Age versus %K release.	190
8.10	Schematic cross section through Wetar Island and age dates.	192
9.1	3D evolution model of the Wetar Island ore deposits.	211
9.2	Cartoon model for the development of mineralisation.	215

List of Tables

Table		Page
1.1	Size and grade for the Kali Kuning, Lerokis and Meron deposits.	9
3.1	Key mineralogical, geological and alteration characteristics of the principal mineralised areas.	32
4.1	Alteration mineralogy of the Wetar deposits.	50
4.2	Classification of alteration zones.	52
4.3	XRF data for Wetar host volcanics.	64
5.1	Abundance of sulphides in hand specimen.	87
5.2	Percentages of individual sulphide phases.	88
5.3	Representative electron microprobe analysis of sulphides.	97
5.4	Representative electron microprobe analysis of barite ore cements and inclusion phases.	98
5.5	Microscope analysis of barite ore and pyritic sands.	108
5.6	Results of SEM and Microprobe analysis of barite ores.	109
6.1	Microthermetric results and descriptions of fluid inclusions.	132
6.2	Fluid inclusion data from selected VMS systems.	139
7.1	Sulphur and oxygen data of sulphides and sulphates.	152
7.2	Summary of sulphur and oxygen data.	152
7.3	Calculated temperatures using sulphur geothermometers.	165
8.1	Noble gas composition of Wetar sulphides and sulphates.	173
8.2	Strontium results of whole rock and sulphates.	180
8.3	Stepped heating Ar/Ar data for the Wetar samples.	191

Chapter 1

INTRODUCTION

1.1 VMS SYSTEMS

The sulphide mineralogy of volcanogenic massive sulphide deposits (VMS) are typically dominated by a pyrite-pyrrhotite-chalcopyrite assemblage, with associated chlorite-sericite alteration of the underlying host volcanics. These mineralogical characteristics in concert with other geochemical data are considered to reflect systems where circulating seawater, with a chemistry buffered by water-rock interaction at high temperatures is the dominant hydrothermal component (Shanks et al., 1995). Typical VMS deposits contain 60% or more sulphide minerals, (Sangster and Scott, 1976) with 80% occurring in arc related strata, (Franklin et al., 1998) generally as concordant lenses that are stratigraphically underlain by discordant stockwork zones of sulphide veins contained within a pipe of hydrothermally altered host rock (Lydon, 1988). Morphologies of individual sulphide lenses are varied and can range from steep sided cones to tabular sheets and tend to occur in clusters within a single stratigraphical interval (Sangster, 1980). The textures and structures present are varied from laminated sulphides to massive, rubbly and brecciated forms but the most diagnostic feature is perhaps the zonation of the ores (Lydon, 1988). This zoning is perhaps most prominent with Noranda and Kuroko deposits with the latter consisting of seven zones, in ascending stratigraphic order they are as follows: siliceous ore (pyrite-chalcopyrite and extensive cryptocrystalline quartz), gypsum ore (gypsum-anhydrite-pyrite), pyrite ore (± chalcopyrite and quartz), yellow ore (pyrite-chalcopyrite-sphalerite-barite-quartz), black ore (sphalerite-galena-chalcopyrite-pyrite-barite-tetrahedrite-tennantite), barite ore and ferruginous chert. Two distinct groups of VMS deposits based on metal content are the Cu-Zn and Zn-Pb-Cu groups, (Franklin et al., 1981): the Cu-Zn type are generally contained within bimodal volcanic sequences whereas Zn-Pb-Cu types are dominated by felsic volcanics, barite is more abundant in the latter (reviews in Franklin et al., 1981). Alteration patterns associated with hydrothermal activity also differ in relation to these two groups however both suggest a reduced near neutral fluid, alteration pipes below Zn-Pb-Cu generally comprise sericite and quartz rich cores with chloritic outer zones, chlorite

rich cores with outer sericite zones in contrast are typical of Cu-Zn deposits. Models of VMS formation suggest that metalliferous hydrothermal solutions are primarily generated by seawater rock interaction at depth, leaching metals from the volcanic and sedimentary sub-strata which are subsequently discharged on the seafloor through faults into rifts, calderas and basins as a result of extensional tectonics. High temperature hydrothermal vents "black smokers" are the modern analogues of fossil VMS systems (Koski, 1995).

1.2 HIGH-SULPHIDATION VMS SYSTEMS

The division of terrestrial sub aerial epithermal deposits into *high* and *low-sulphidation* deposits are based on ore, gangue and alteration mineralogy, textures and fluid compositions (Hedenquist and Lowenstern, 1994; White and Hedenquist, 1995). This two-fold division is comparable with, and may also be termed acid sulphate and adularia-sericite types (Hayba et al., 1985; Heald et al., 1987). Isotopic evidence indicates a dominant magmatic component within *high-sulphidation* fluids in contrast to *low-sulphidation* type fluids which are typically dominated by meteoric water with a minor or transient magmatic input (Hedenquist and Lowenstern, 1994). Recent investigations of some active ocean floor and ancient VMS systems report the presence of a *high-sulphidation* (HS) mineralogy (Hedenquist, 1987; Herzig et al., 1993; Hannington and Herzig, 2000). Numerous polymetallic submarine VMS deposits are now recognised as *high-sulphidation* VMS deposits, defined like their subaerial epithermal counterparts by the presence of advanced argillic alteration and *high-sulphidation* mineral assemblages (Sillitoe et al. 1996; Hannington, 1997: Sillitoe, 1999). Pyrite, bornite, enargite, luzonite, tennantite-tetrahedrite, covellite and low-Fe sphalerite are reported, associated with advanced argillic alteration mineral assemblages, including residual silica, kaolinite, pyrophyllite, dickite, diaspore, alunite, barite and native sulphur (Herzig et al., 1994, 1997; Arribas Jr, 1995; Ishibashi and Urabe, 1995; Herzig et al., 1998). These mineralogical observations argue strongly for *high-sulphidation* conditions occurring proximal to the sea floor. The VMS deposits precipitated from oxidised hydrothermal fluids are considered to have contained a significant contribution from ascending magmatic volatiles which condensed into circulating seawater resulting in a highly acidic and corrosive fluid capable of extensive leaching and the formation of advanced argillic alteration

(Sillitoe et al., 1996; Hannington, 1997). However, these systems are significantly less abundant than *low-sulphidation* VMS deposits present in both modern and ancient settings (Sillitoe, 1999). The abundance of base metals and exhalative mineralisation including massive pyrite lenses, abundant barite and manganiferous horizons distinguishes them from sub aerial epithermal deposits.

Many deposits may be hybrids and a result of both epithermal style and VMS mineralisation (Hannington and Herzig, 2000). *High-sulphidation* systems are postulated by Sillitoe et al., (1996) to have been generated proximal to the source of magmatic fluids in contrast to more typical Zn-Pb-Cu VMS systems or equivalent *low-sulphidation* systems which are located distal to the heat source (see Figure 1.1). These *high-sulphidation* VMS deposits are not constrained by water depth, some modern systems are forming in near shore environments adjacent to sub aerial geothermal systems, ie. Lihir Harbour, PNG at <10 m, (Pichler et al., 1999). Shallow water deposits also include the Panarea Platform at 80 m, Aeolian Arc, Italy (Gamberi et al., 1999; Marani et al., 1997), and at the Bay of Plenty, Taupo volcanic zone, New Zealand at 200 m (Stoffers et al., 1999). Generation of *high-sulphidation* polymetallic sulphides occur at the Palinuro Seamount at depths of 600 m (Tufar, 1992; Minniti and Bonavia, 1984), at Conical Seamount (1000 m), south of Lihir (Herzig et al., 1999) and >2000 m in the Lau Basin (Herzig et al., 1998).

Modern *high-sulphidation* VMS systems have been described from the eastern Manus Basin (Gamo et al., 1997) including the DESMOS caldera (Gamo et al., 1997; Gemmell et al., 1999), the Hine Hina deposit in the southern Lau Basin (Fouquet et al., 1993; Herzig et al., 1993; Herzig et al., 1998) and the Brothers hydrothermal system, Southern Kermadec Arc (de Ronde et al., 2000). Ancient, on land deposits include the 180-170 Ma high grade Au sulphosalt Eskay Creek deposit, Iskut River area, British Columbia (Macdonald et al., 1996; Roth et al., 1999). The formation of these systems is poorly understood. If *high-sulphidation* fluids are to avoid neutralisation and conversion to the *low-sulphidation* fluid responsible for most VMS deposits, they must avoid dilution by copious quantities of deeply circulated seawater and excessive wall-rock interaction. Therefore the acidic magmatic fluids responsible for the *high-sulphidation* VMS deposits cannot have ascended from deep magmatic sources, but must have been generated nearby at shallow depths (Sillitoe, 1999). This thesis will report a detailed investigation of the well preserved Au-bearing barite and associated VMS deposits of Kali Kuning, Lerokis (Zones 4 and 5) and Meron

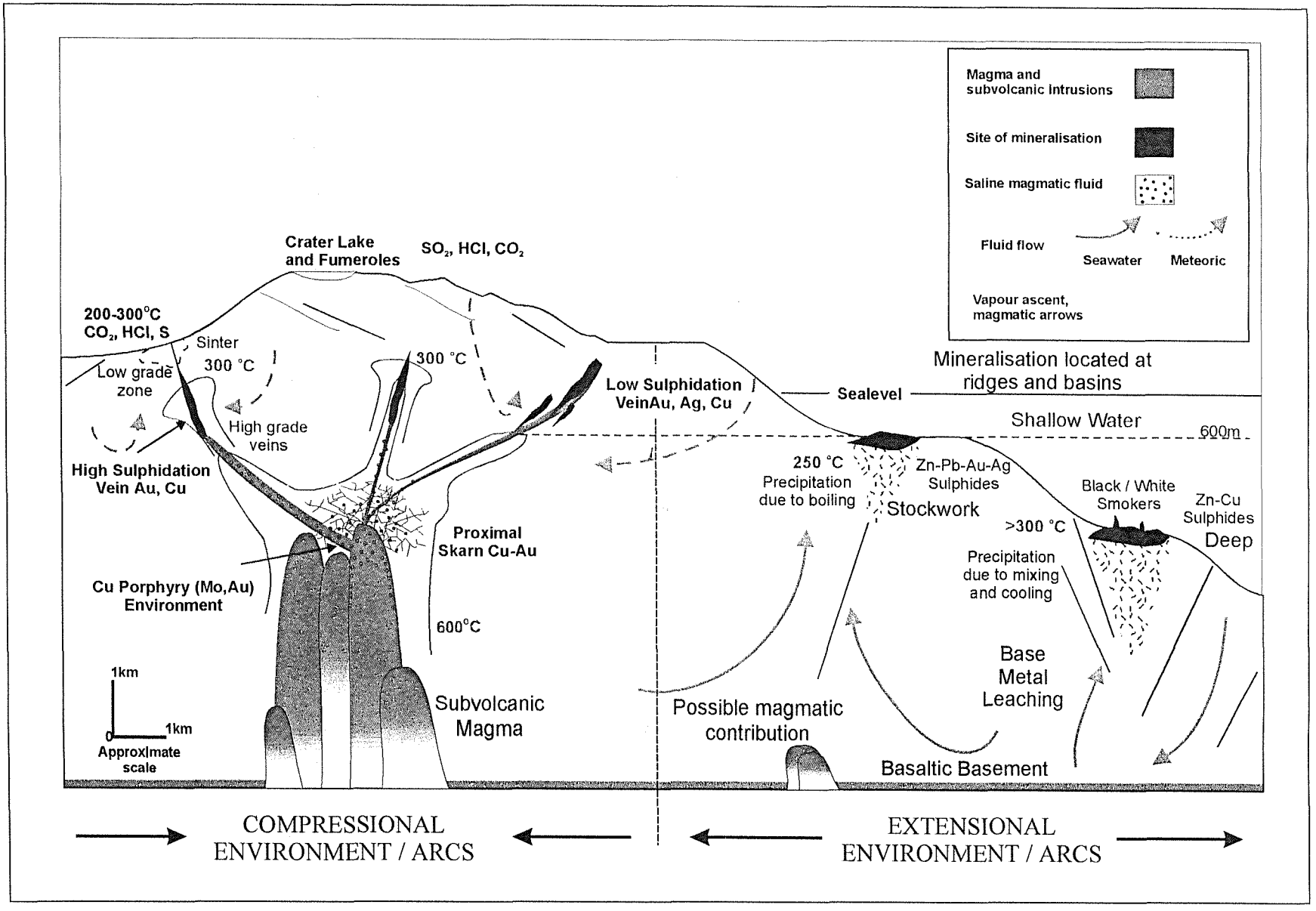


Figure 1.1. Volcanic - Hydrothermal system typical of an emergent intrusion centred volcanoplutonic arc, modified from Henley and Ellis 1983; Henley, 1985; Hedenquist and Lowenstern,1994; Sillitoe, 1995, 1999; Hannington and Herzig, 2000. The schematic section illustrates that in sub-aerial epithermal systems, fluids are dominated by meteoric waters, these may extend below sea level and may discharge as shallow water hot springs. Below sea level, fluids are dominantly sea water in origin, extensive fluid rock interactions and heating at depth results in base metal leaching and conventional formation of sulphide mounds on the sea floor at ridges, basins and calderas. In shallow water environments, boiling of the hydrothermal fluids may occur. The diagram illustrates that a broad spectrum of deposits may occur in a single arc edifice.

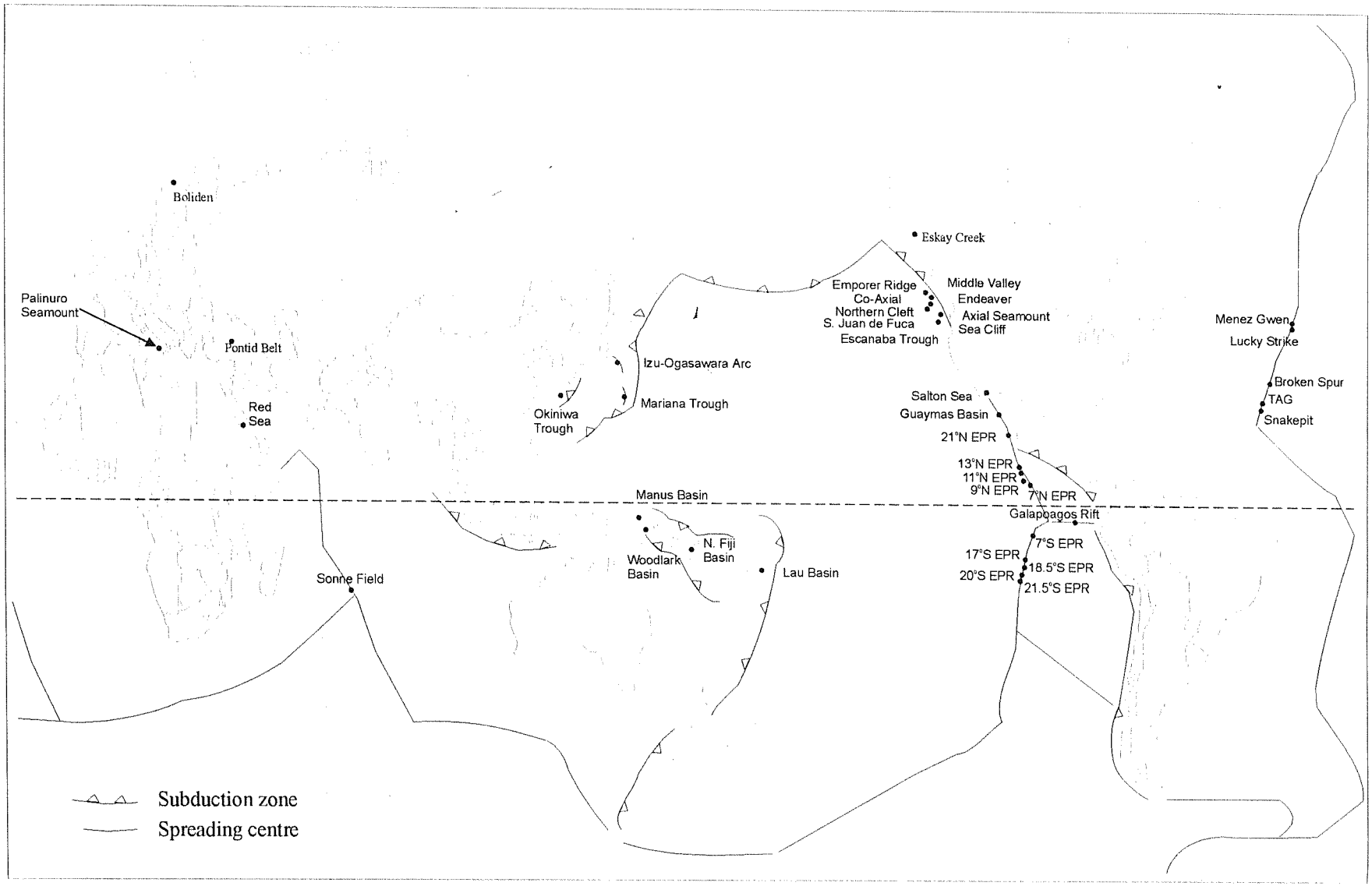


Figure 1.2. Location map of some selected polymetallic massive sulphide deposits and hydrothermal systems on the modern seafloor, modified from Hannington et al., 1994, Sillitoe et al., 1996 and Herzig and Hannington, 2000.

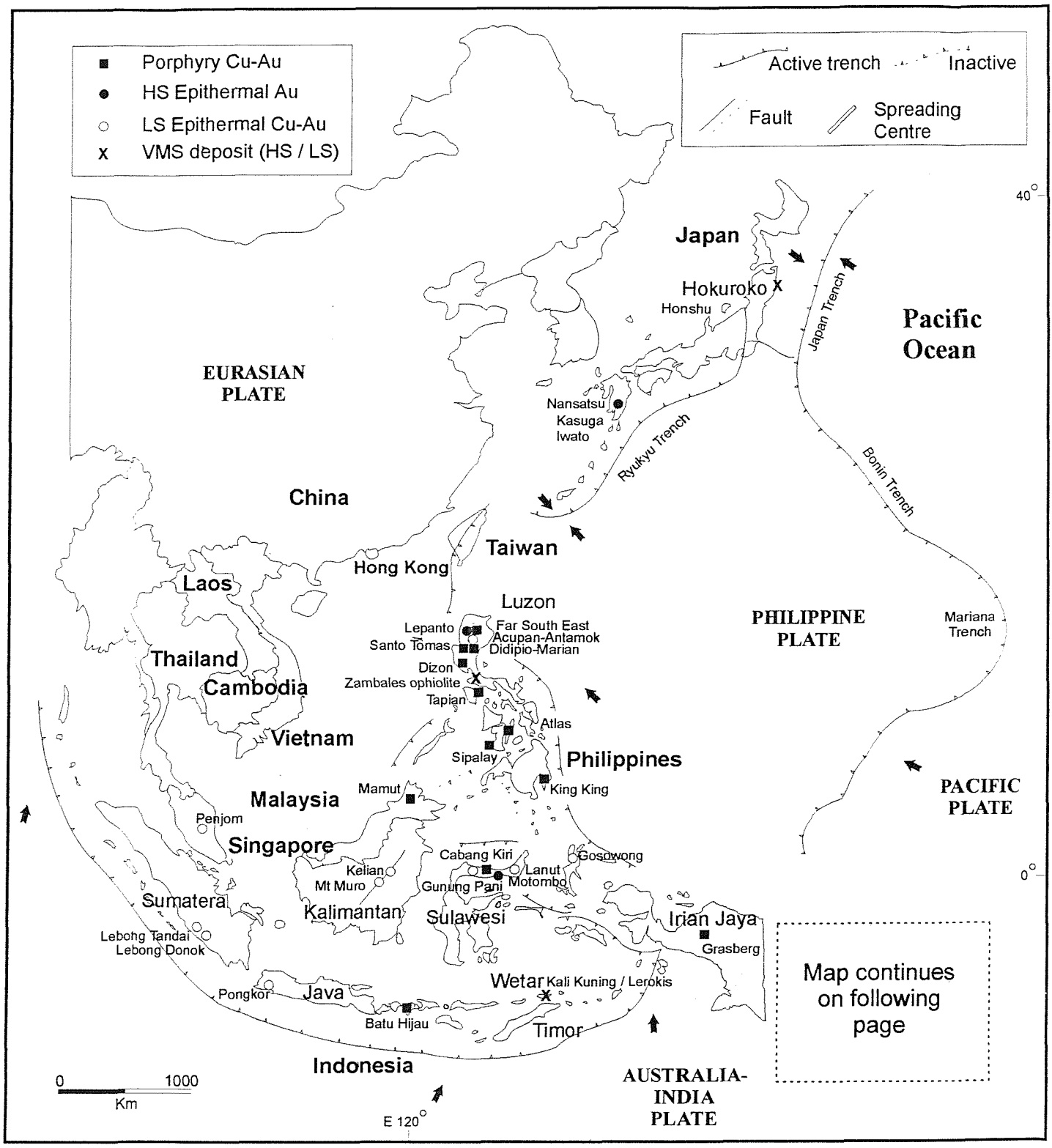


Fig 1.3. Principal epithermal, VMS and porphyry deposits (modern and ancient) in the western Pacific: Indonesia to Japan. Data from Sillitoe, 1989, Wheller et al., 1992, Herzig, 1995, Gemmell, 1995, Corbett and Leach, 1998. Arrows indicate plate movement direction.

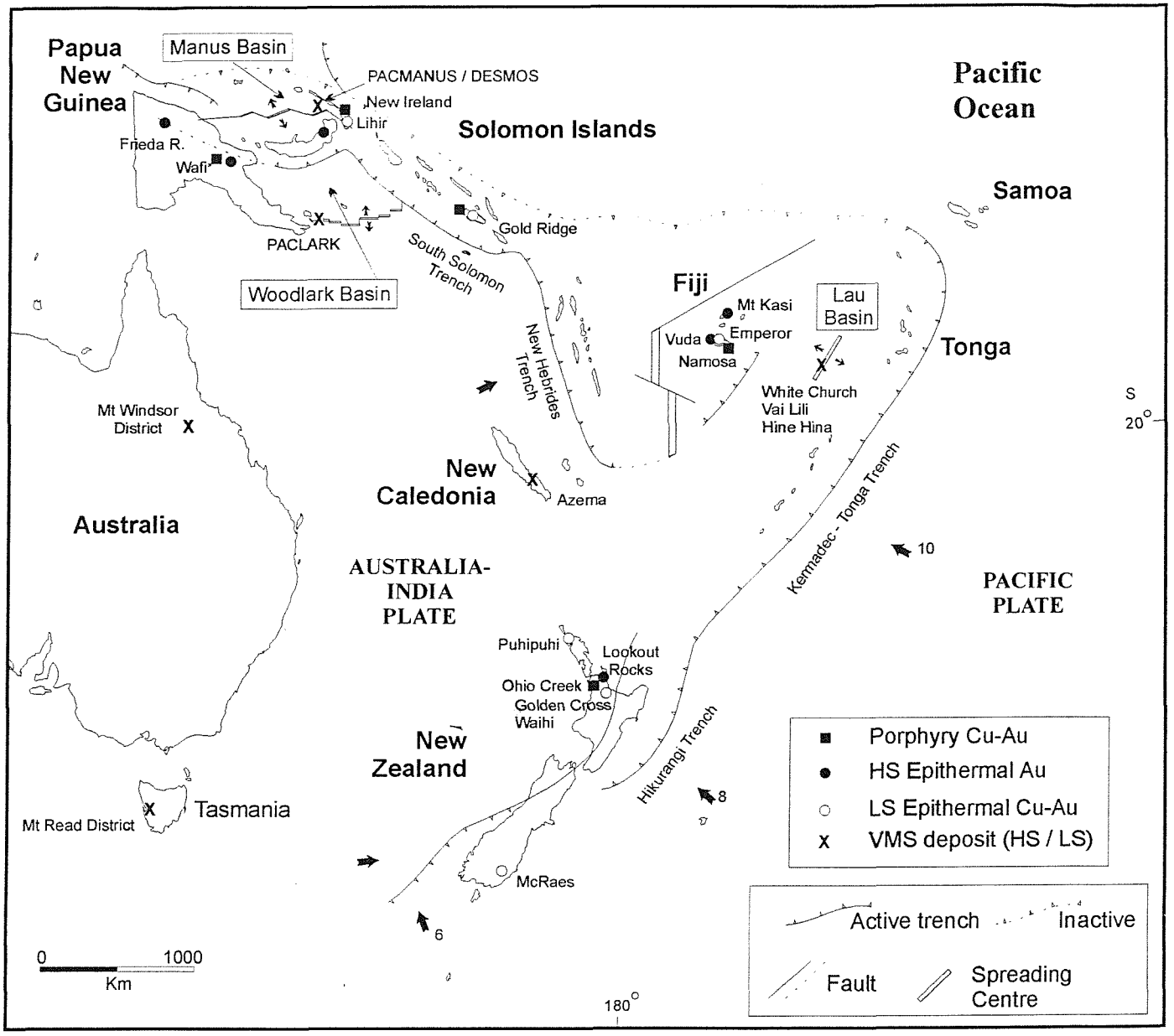


Fig 1.3. cont. Principal epithermal, VMS and porphyry deposits (modern and ancient) in the Western Pacific. Data from Sillitoe, 1989, Wheller et al., 1992, Herzig, 1995, Gemmell, 1995, Corbett and Leach, 1998. Arrows indicate plate movement direction and speed, cm/year.

orebodies of Wetar Island, Indonesia. Principal ore deposits discussed in the text (both modern and ancient) are shown on Figures 1.2 and 1.3, these are referred to throughout the thesis.

1.3 WETAR ISLAND

Wetar Island is located within the Maluku province of eastern Indonesia and is ~ 70 km north of Dilli, east Timor. The island measures ~110 km x 40 km, the study area is situated towards the north coast of the island ~ 4 km from the village of Lurang (Figure 1.4). Topography within the study area is rugged with heights reaching 650 m above sea level. An aerial photo is shown of the mine site on the north coast of the island (Figure 1.5). Recent geological research in the area started with the initiation of mineral exploration in 1984 (Sewell and Wheatley, 1994a). Two economic orebodies were defined at Kali Kuning and Lerokis (Figure 1.4), plus a smaller deposit at Meron, comprising asymmetric massive sulphide mounds flanked by generally poorly consolidated barite deposits.

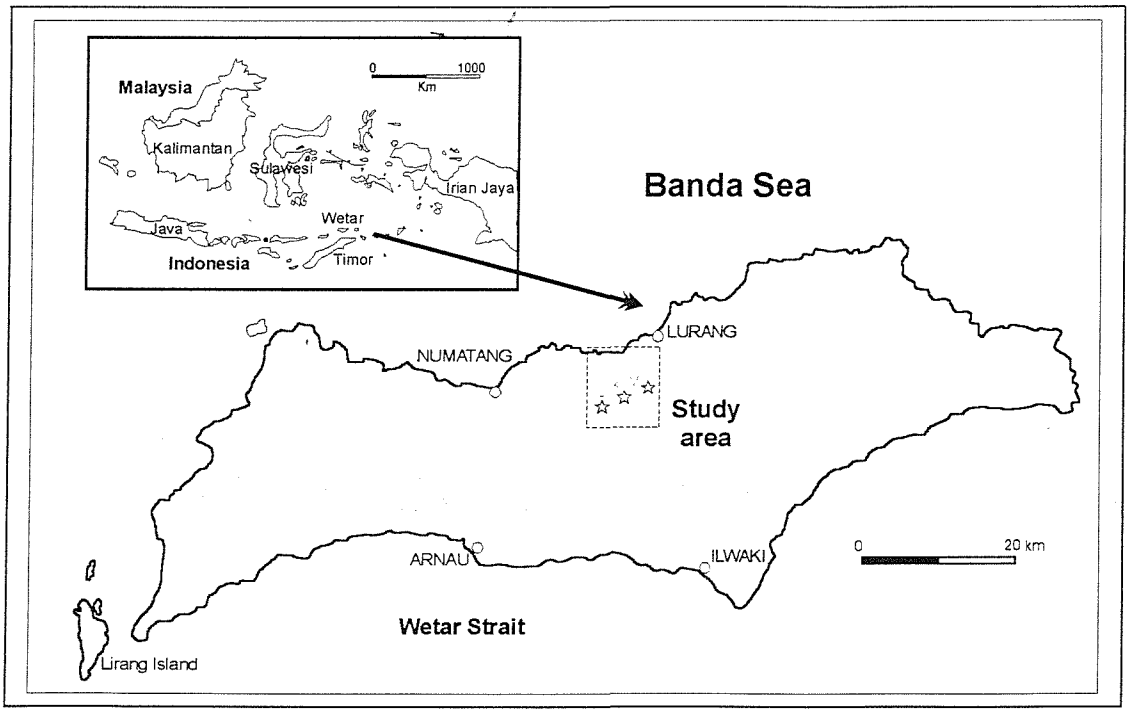


Figure 1.4. Location of the field area and Wetar Island, Eastern Indonesia. Principal villages are shown, L= Lerokis, K= Kali Kuning and M= Meron.

Mining focussed on the associated Au-Ag-bearing barite deposits with the sulphide mounds at each deposit remaining unexploited, grade and size of each deposit are reported in Table 1.1. Wetar is composed entirely of Oligocene to Recent volcanics and minor oceanic sediments. Mineralisation is hosted by volcanic flows and intrusions with post mineralisation lahars, sub-aqueous debris flows and pyroclastic rocks covering much of the deposits.

The deposits on Wetar are unusual in that they contain Au-Ag-Hg bearing barite deposits both onlapping and overlying typical VMS mounds. Originally described as VMS systems (Sewell and Wheatley, 1994a,b) there has been debate as to the deposits origin (Herrington and First, 1996). Recent evidence for *high-sulphidation* VMS systems (Sillitoe et al, 1996; Hannington et al., 1997) has fuelled this debate.

Table 1.1. Total size of deposits and grades for the Kali Kuning, Lerokis and Meron deposits, values given were calculated by Abadi (1996), Meron grades from Platt (1996) and Suryantoko (1997).

Deposit	Barite Deposit			Sulphide Mounds					
	Size (Mt)	Au g/t	Ag g/t	Size (Mt)	Cu %	Pb %	Zn %	Au g/t	Ag g/t
Kali Kuning	1.9	4.63	151	4.1	3.55	0.3	0.19	0.74	35
Lerokis	2.17	3.98	114	2.7	4.21	0.37	1.39	0.91	50
Meron	0.32	3.18	143	0.61	2.25	0.15	0.22	0.51	21
TOTAL	4.5	3.93	136	7.4	3.34	0.27	0.6	0.72	35.3

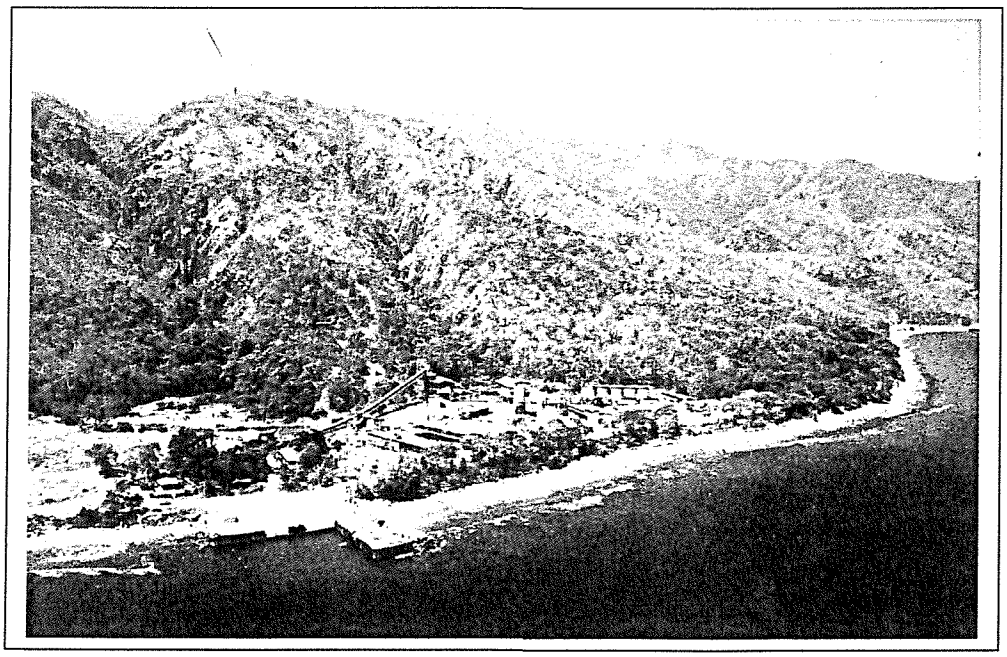


Figure 1.5. Mine site, north coast, Wetar Island, Indonesia.

1.4 PREVIOUS WORK

Limited published literature exists for the geology of Wetar Island (Sewell and Wheatley, 1994a,b). The first accounts of the geology of the island were given after an expedition to the Lesser Sunda islands by the University of Amsterdam in 1937 (Heering, 1941; Dejong, 1941; Van Bemmelen, 1949). Published conference abstracts (Herrington and First, 1996) and numerous internal company reports exist as a result of an extensive drilling programme based around exploration between 1984 and 1998. Structure, stratigraphy, mineralisation and alteration are discussed in Sewell and Wheatley (1994a & b). Age dates on volcanic events are given by Abbott and Chamalaun, (1981) sulphur isotopes are discussed by de Ronde (1995) giving $\delta^{34}S$ values for sulphates and sulphides for the deposits of Kali Kuning, Lerokis and Meron. Numerous unpublished reports document the mining / exploration history of Wetar, Hatfield and Budiono, (1995), Kavalieris, (1994), Heesterman, (1992) and Suriantoko, (1994). Alteration mineralogy is discussed by Herrington (1993b, 1995a, 1996), other work by Herrington includes petrological investigations (1993a, 1993b, 1996), microprobe analysis of the barite deposits (1995b), and whole rock geochemistry (1995a, 1996). Exploration on Wetar Island was initiated by CSR Minerals in 1984 and continued by Billiton Companies in Indonesia since 1988. Gold mineralisation was first reported in 1986 when stream float sampling, systematic soil and rockchip analysis showed Au assays of 13 g/t with associated high Ag, Pb, As and Ba values. Ground geophysical surveys (electromagnetics, induced polarization and resistivity) indicated several broad anomalies indicative of shallow conductors. Aerial reconnaissance was undertaken between 1987-88 to locate areas of visible alteration; integration with landsat TM defined seven colour anomalies. Follow up exploration and sampling of these anomalies discovered significant Au values at KK3 (Kali Kuning) and Lerokis, prior to mining no sulphide mounds were exposed at surface (Figure 1.6). From 1988-92 almost 20,000 m of diamond and reverse circulation drilling defined the geological resources outlined in Table 1.1. A previous study by Herrington (1993) on the barite ore revealed that Au occurs as free grains adhering to barite crystals and an association with jarositic material that occurs as a cementing phase. Exploration yielded over 20 tonnes of near surface Au within the baritic ore zones, mining terminated during the summer of 1997 with subsequent

backfilling of pits and replanting of vegetation. The massive pyrite mounds were not mined and were subsequently covered at the end of 1997.

1.5 PRESENT STUDY

The study of the ore-systems of Wetar Island aimed to:

- Determine the style of mineralisation,
- Document the sulphide mineral assemblages and associations, textures, paragenesis and zoning of the mineralisation through field mapping, analysis of drill core and reflected light microscopy.
- Investigate the barite deposits and their relationships to the sulphide mounds and host stratigraphy.
- Determine any relationships between Au, Ag, Hg and the barite.
- Map the extent of the hydrothermal alteration, determine the alteration assemblages and document any alteration zoning around sites of mineralisation.
- Ascertain formational depth of mineralisation.

This project was formulated to tackle these problems and formed part of an academic / industry based link between the School of Ocean and Earth Sciences, University of Southampton; the Department of Mineralogy, Natural History Museum, London and BHP-Billiton, formerly Billiton Mining. This study of the Wetar Island Au-Ag-Hg-Barite deposits forms part of ongoing research into the documentation and identification of VMS deposits displaying either *high* or *low-sulphidation* characteristics or in some cases, both. An analytical programme has been completed using material collected during detailed mapping and sampling of the open pits and associated drill core. Aims of the project also included:

- Determine the relative importance of the various geological reservoirs as sources for O, S, Sr and He, and by implication metals, in the hydrothermal system.
- Constrain fluid flow and mixing processes within the mound.

- Devise a genetic model for the geological / hydrothermal evolution of the deposits.
- Compare the results from Wetar Island to existing data from both modern and ancient systems to ascertain comparative mineralising systems.

1.6 THESIS LAYOUT

Following the brief introduction of this Chapter to the location of the study area and the importance of this study to current research concerning *high-sulphidation* VMS systems, Chapter 2 is a literature based review on the tectonic evolution of the Sunda / Banda arcs of Indonesia. Chapter 3 is an account of both regional and local geology of Wetar Island, Chapters 4, 5 and 6 document the hydrothermal alteration of the host volcanics, mineralisation of the Kali Kuning, Lerokis (Zones 4 and 5) and Meron deposits and fluid evolution of the system. Stable and radiogenic isotope systematics are examined in Chapters 7 and 8. Only pertinent discussion will be given at the end of each Chapter, discussion relating to comparative deposits / systems will be addressed within Chapter 9, thus providing an overall account encompassing all aspects of this study and will propose a genetic model with respect to both geological and hydrothermal evolution of the mineralised Wetar systems. Chapter 10 will give a summary, listing all of the conclusions of this study. Analytical techniques, results, geological maps, cross-sections and location maps are presented in the Appendices.

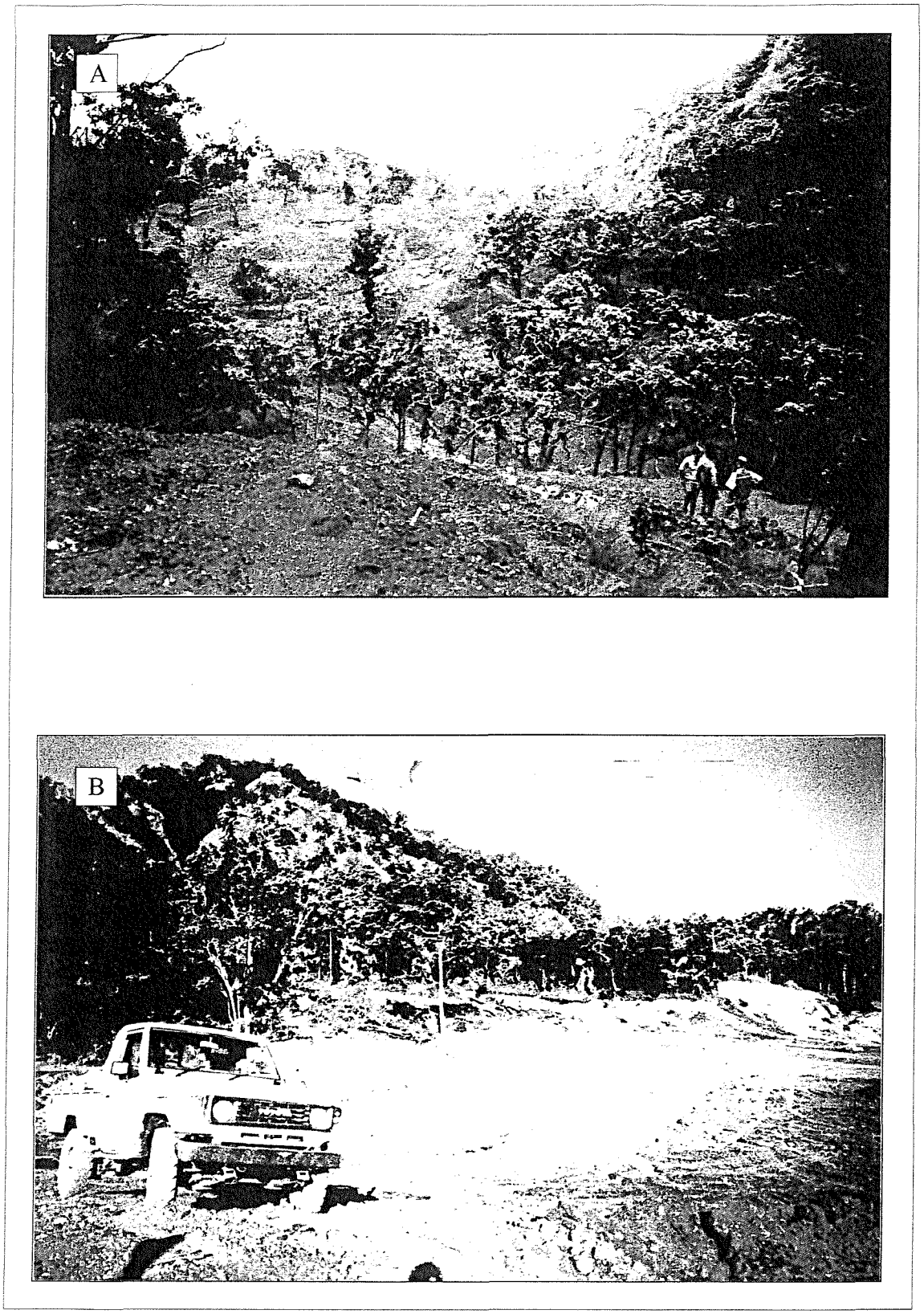


Figure 1.6. (A) Lerokis project area pre-mining, 1989; photo P. Ruxton. (B) Kali Kuning project area pre-mining, 1995; the top of the barite ore zone is shown in the centre and right of the field of view. Photo R. Herrington.

Chapter 2

TECTONIC EVOLUTION OF THE SUNDA AND BANDA ARCS

2.1. GENERAL EVOLUTION AND SUBDIVISION OF THE ARCS

The Sunda-Banda volcanic arc extends for some 3000 km and represents a zone of transition between subducted oceanic lithosphere lying to the west and a complex zone of continent-arc collision in the east, see Figure 2.1 (Hamilton, 1979; von der Borch, 1979; Karig et al., 1987; Audley-Charles, 1986, 1986b; Price and Audley-Charles, 1987; Masson et al., 1991; Richardson and Blundell, 1996). This zone of plate contact lies along the Java Trench west of 119° 45'E and continues into the Timor Trough (Masson, et al., 1991). The collision zone has been extensively studied using seismic surveys (Cardwell and Isacks, 1978; Audley-Charles, 1986; Masson et al., 1991 and references therein; Richardson and Blundell, 1996) and both gravity and magnetics (McBride, and Karig, 1987; Woodside et al., 1989). Seismic refraction surveys indicate that the Timor Trough - Tanimbar Trough (1200 km in length, up to 70 km wide and 2-3 km deep) is underlain by continental lithosphere (Figures 2.1 and 2.2) varying between 31-40 km in thickness from the west to the east (Audley-Charles, 1986).

Formation of the present day, fold and thrust belt in the Timor and Tanimbar region, began with the break-up of Gondwanaland and the development of the Australian passive margin. Development of early oceanic subduction began to the north of Australia culminating with the eventual collision of the Australian margin and maturing volcanic arc. Thus, the development of a collision complex / fold and thrust belt occurred part of which is exposed on Timor (Hughes et al., 1996; McCaffrey, 1996). Collision occurred over ~ 40 Ma, the final stages of which relate to the closure of the Tethys ocean which previously lay to the north of Australia, (Hall, 1996). Recent geodetic measurements by McCaffrey, (1996) suggest that the Timor collision zone has recently locked onto the northward moving Australian plate resulting in the cessation of subduction at the Timor Trough, (Figure 2.3). Ongoing volcanic activity to the east and west of Timor is related to the subduction of the Indian-Australian plate beneath the SE Asian plate at a present convergence rate of 7.5 cm y^{-1} (Masson et al., 1991).

Hamilton, (1979) subdivided the entire Sunda arc (SA) and Banda arc (BA) in to 4 segments based on the nature of subducted material, these four sections are illustrated in Figure 2.1. Stress distribution and seismotectonics formed the basis for a similar subdivision (Eva et al., 1988), whereas major and trace element geochemistry of arc volcanics also produce four similar segments (Wheller et al., 1987). Subduction of the 80-45 Ma Wharton Basin (part of the Indian Oceanic plate) below west Java has commenced at the Sunda Trench (segment 1 on Figure 2.1). This section of oceanic crust is bounded to the east by the Cretaceous-Early Tertiary subduction zone. In segment 2, subduction of 100-120 Ma oceanic crust below eastern Java, Bali and Lombok continues. To the east of this section (in segment 3), back-arc thrusts have developed behind the zone of subduction due to the continent-arc docking in the south in the region of Timor. Oceanic crust subducted in this zone has an age of 120-140 Ma and is among some of the oldest oceanic crust on earth. The islands of Adonara, Lomblen and Pantar, known as the (AP) segment (see Figure 2.2) form the eastern extremity of segment 3. Continuing to the east, the East Sunda arc (ESA) and Banda arc (BA) are separated by an inactive volcanic segment which consists of the islands of Alor, Atauro, Wetar and Romang. Abbott and Chamalaun, (1981) and Varekamp et al., (1989) suggest that volcanism ceased within this section of the Banda arc ~3-4 Ma, Silver et al., (1983) propose this inactive segment to be the foci of ongoing continent-arc collision where a subduction polarity change may be imminent. The remainder of the Banda arc (segment 4) continues to the east and curves around to the islands of Seram, Ambon and Buru with the Kai islands to the east occupying the region of maximum curvature of the Banda arc. As with the Timor trough, the Aru trough is regarded as the surface trace of past subduction and present arc-continent collision (Milsom et al., 1996). Other workers such Van Bemmelen, (1949) and Abbott and Chamalaun, (1981) have divided the East Sunda / Banda arc into an inner and outer arc, (see Figures 2.1, 2.2 and 2.3). The inner Banda arc consists of an array of islands surrounding the Banda sea, these islands are volcanic in origin and also include the volcanically inactive segment of the arc (Hamilton, 1979). The outer Banda arc in contrast is dominantly non-volcanic in origin (Abbott and Chamalaun, 1981; Silver et al., 1983; Breen et al., 1989). Timor, Moa, Sermata, Babar, the Tanimbar islands, the Kai islands to the east and Seram in the north are all part of this outer arc.

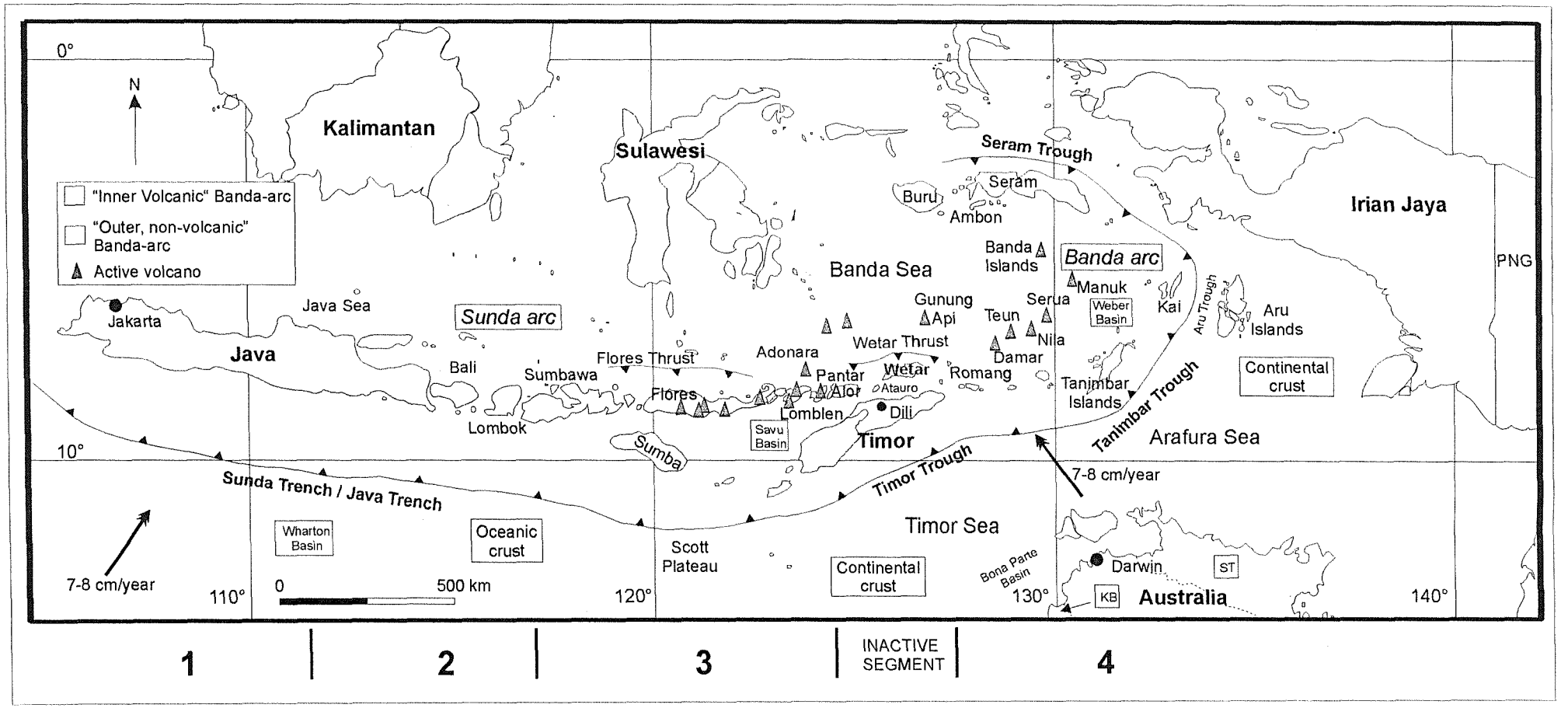


Figure 2.1. Principal geographic features of Eastern Indonesia, after Whitford et al., 1977; Hamilton, 1979; van Bergen et al., 1993; Masson et al., 1991; Snyder et al., 1996. 1-4 are subdivisions based on Hamilton, 1979, subdivision of the Banda arc into an outer and inner zone are illustrated and discussed in the text. Toothed lines indicate front of subduction zone, ST represents the Sturt Archaean block of the Australian mainland, KB represents part of the Kimberley Block, see text for explanation.

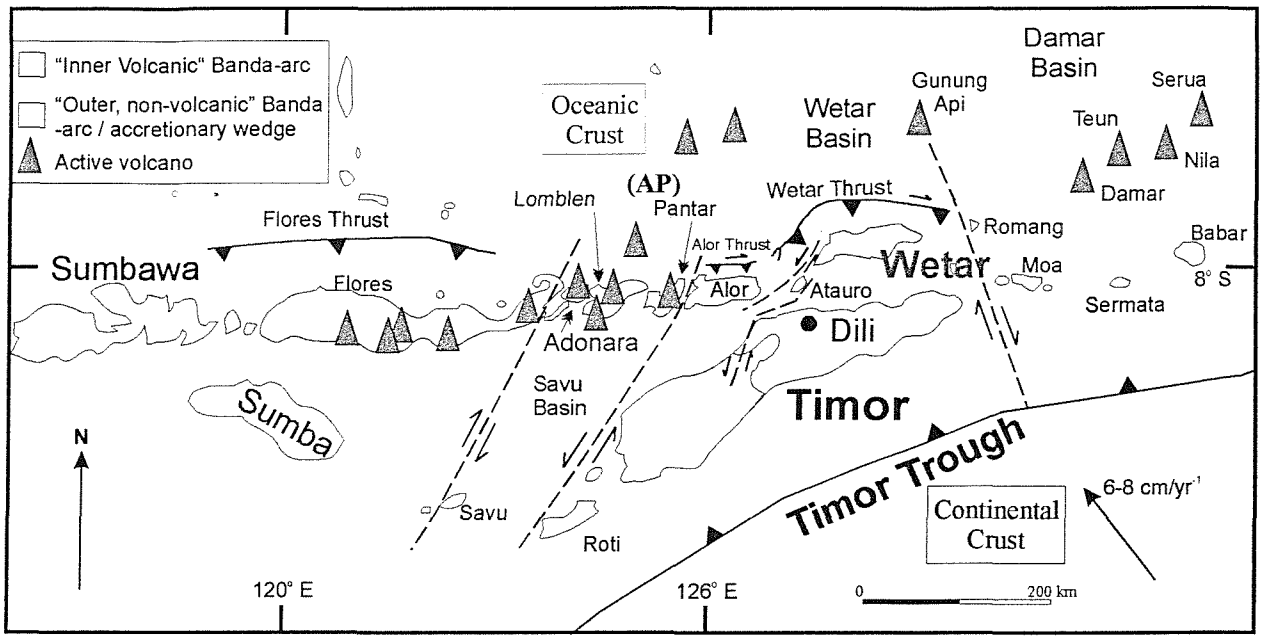


Figure 2.2. Principal tectonic and volcanic features of the Sumbawa to Serua section of the Banda-arc, Indonesia. After Hamilton, 1979, Varekamp, 1989, Breen and Silver, 1989 and Masson et al., 1991. The Banda arc is divided into an outer "non-volcanic" and inner "volcanic" arc. The extent of the Australian continental shelf is shown.

2.2 DETAILED EVOLUTION OF THE ARC

2.2.1 Australian continental shelf / margin

The Timor, Tanimbar, Aru and Seram Troughs (generally 1-2.5 km deep and less than 50 km across) separate the islands of the outer Banda arc from the Australian continental margin. In the area of the Banda Arc to the east, seismic reflection surveys mimic those of the Bouguer gravity contours, which may indicate the existence of the outer arc as a single geological unit prior to the present phase of arc-continent collision (Milsom et al., 1996). The age of initial collision of the continental margin with the arc is thought to be at ~ 3 Ma (Hamilton, 1979). Unconformable, Triassic-Recent marine sediments overlie the granite basement (see cross-section, Figure 2.3) and extensional faults cut both units. Continental crust of the Australian margin is thicker at the zone of collision than the Australian margin to the south, (Richardson and Blundell, 1996) thickness range between 31 and 40 km (Bowin, 1980). The slope of the Timor Trough in this region dips to the north at ~ 3.5°, at present the Timor collision complex overrides the Australian continental margin at this location with an orientation of SSW-NNE (Harris, 1992).

2.2.2 Timor Trough / zone of subduction

Seismic profiles of the Timor Trough suggest that the frontal section of the wedge (southern margin) is inactive as penetrative thrusts are absent; internal thickening of the wedge itself is taking place to accommodate crustal shortening within this region (Hughes et al., 1996). Horizontally bedded sediments are greater than 0.5 km in thickness and are present within the trough axis south of Timor indicating no recent convergence has taken place. Johnston and Bowin, (1981) have calculated that these overlying trough-fill sediments accumulated over the past 1.1 Ma, and are 3.8 km above the downgoing Australian plate to the east of Timor (Hughes et al., 1996). The Indian-Australian plate can be followed down to depths greater than 600 km based on seismic studies, dips of the subducting plate reach 60-70° in the eastern Sunda arc region at depths of 200 km but shallow off towards the eastern Banda arc (Cardwell and Isacks, 1978, McCaffrey, 1988, 1989).

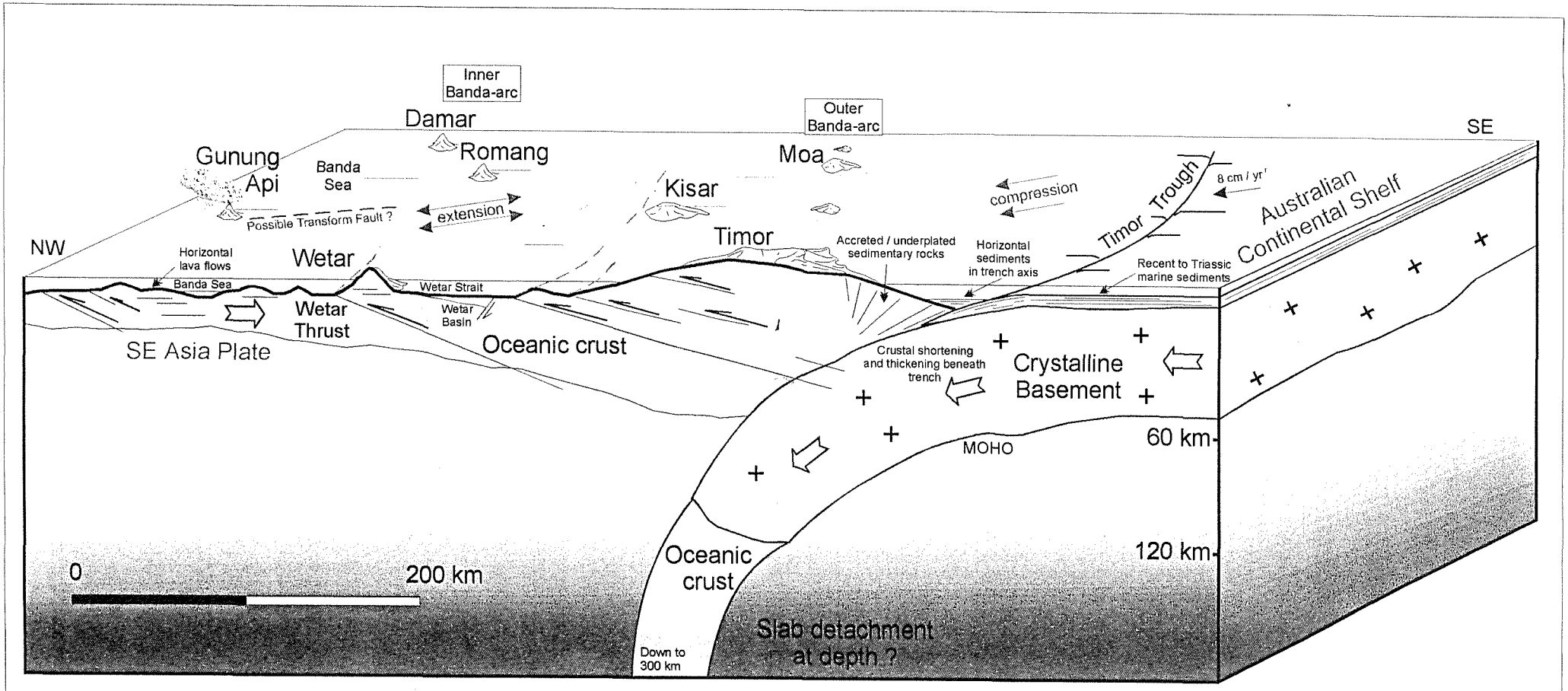


Figure 2.3. Simplified cross-section of the Banda Orogen based on geophysical data from Masson et al., 1991; Richardson and Blundell, 1996 and Snyder et al., 1996. The section illustrates the continent-arc collision of the Australian and SE Asian plates at the Timor section of the Banda arc. Timor (part of the "outer" non-volcanic Banda arc) was formerly an outlier of the Australian continental shelf and is now trapped between the volcanic "inner" Banda arc to the north and the Australian continental margin to the south. The collision zone is dominated by shallow, southward dipping faults structures which have accommodated crustal shortening and thickening within the zone of collision.

2.2.3 Forearc

The outer islands of the Banda arc are part of a wide forearc accretionary wedge which has been uplifted and widened since the subduction of the leading edge of the Australian continental margin to the south (Hamilton, 1979). Segments of the active arc presently occupy a forearc basin position and are active sites of post collisional extension (Harris, 1992). Seismicity in the forearc indicates a predominant regional stress pattern of N-S shortening and E-W extension, (McCaffrey, 1988) as the Savu and Weber Basins (Figure 2.1) are representative sites of this E-W extension (Harris, 1992). Forearc extension and trench migration around the indentation of Timor has resulted in the widening of the arc-trench gap by ~ 100 km adjacent to the Weber and Savu basins (Harris, 1992). The Weber Basin (to depths of 7000 m) comprise oceanic basement ranging in thickness between 7 and 10 km, proximal to the axis of extension. Overlying sediments average 1500 m in thickness and flanking extinct volcanic ridges also form prominent features in this region (Bowin et al., 1980). The horizontal floor of the Savu Basin (to depths of 3000 m) consist of ~2000 m of sediments, this area directly west of Timor represents a site of transcurrent faulting and thus forms the boundary between the Australian continental margin from subducting oceanic lithosphere, see Figure 2.2 (Eva et al., 1988). The basin is considered to be dominantly composed of oceanic crust (McBride and Karig, 1987; McCaffrey, 1989) and separates the island of Sumba from Timor. Sumba itself may be an uplifted section of forearc (Silver et al., 1985) currently resting on a thick section of crust termed the Sumba ridge (Silver et al., 1983). The Wetar Basin, south of Wetar has a horizontal base with water depths reaching 3000 m, seismic profiles indicate an extensional half-graben structure with deeper basin fill to the south indicating that it tilts northward (Masson et al., 1991). In the area around the island of Kisar, the forearc is only 15-20 km wide and contains only minor sediments. This indicates that it may have been previously a topographic high and thus did not act a centre of deposition in contrast to the Savu Basin (Snyder et al., 1996).

2.2.4 Collision complex / accretionary prism

A comprehensive review of the different models for the evolution of the Timor region is given in Richardson and Blundell, (1996). The island of Timor represents an

accretionary complex (Chamalaun and Grady, 1978: Barber and Brown, 1988) and can be subdivided into 3 distinct units (Audley-Charles, 1986b). The parautochthonous units are dominantly deepwater sediments (Permian to early Pliocene) which are folded and exhibit reverse faults and thrusts. The allochthon lacks penetrative deformation and contains some pre-Cretaceous metamorphic units but dominantly consists of strata similar to that of the parautochthon along with some shallow water deposits. Autochthonous units on Timor are post mid-Pliocene coral reefs and turbidites (Audley-Charles, 1986b). High-angle thrusts form the frontal portion of the collision complex as a result of imbrication, (Hughes et al., 1996) although the internal structure of the collision zone is complex the decollment itself is not clearly defined (Hughes et al., 1996). However, syn-orogenic duplex thrust sheets are suggested by lower crustal reflector geometries, (Snyder et al., 1996) both seismic velocity and gravity modelling indicate that the Timor profile ranges in thickness between 37 and 60 km (Woodside et al., 1989; Richardson and Blundell, 1996). The convergence rates and simple accretion of sediments since collision at 2.4Ma cannot account for this range of thickness alone (Richardson and Blundell, 1996) nor can accretion prior to the Pliocene collision event. It is suggested by Richardson and Blundell, (1996) that a micro-continental fragment or outlier of the former Australian continental margin dominates the material within the collision complex and this fragment collided with the subduction zone during the Tortonian at ~8 Ma. The resulting low-grade metamorphism at the leading edge of this parautochthon is recorded on Timor, Kisar and Moa (Snyder et al., 1996). Richardson and Blundell, (1996) further demonstrate that uplift of the Banda allochthon occurred as a result of underthrusting of this micro-continent. As a result, their interpretation is that accretion began in the late Miocene with the arrival of the Australian continental shelf at the site of collision at ~ 2.4 Ma (Piacenzian). The buoyant continental material which has subducted to depths of only ~ 100 km has now locked onto the collision complex and is now subsequently being pushed from the south by the Australian continent which is thus shortening and uplifting the collision zone on deep seated thrusts (see Figure 2.3). Audley-Charles (1986b) suggests that the Australian continental margin has overridden the Trench by some 240 km and that continental material extends at depth to the northern margin of the outer Banda arc. This material underlies the islands of Timor, Leti, Moa, Sermata, Babar, Tanimbar and Kai (Audley Charles, 1986 and references therein) see Figures 2.2 and 2.3.

Unsubducted Australian margin sediments within the Petrel sub-basin, part of the Bona-Parte Basin (>6 km in thickness) see Figure 2.1, are present some 500 km to the south between the Sturt and Kimberley Archaean blocks (Schlüter and Fritsch, 1985). The northward continuation of this basin may be indicated by the band of low Bouguer anomalies that underlie the region of Moa suggesting that a thick sedimentary Carboniferous-Jurassic basin may have underthrust the arc in the zone of collision (Snyder et al., 1996). At present, uplift rates are high in both the accretionary complex zone and associated islands and the inner volcanic arc. The islands of Timor, Buru, Seram and Kai have been the subject of microfaunal and palaeobathymetry studies providing data on vertical movement rates of the outer arc. De Smet et al., (1989) has proved that continent-arc collision has produced episodic and spasmodic uplift of the outer islands at rates of less than 50 cm/ka^{-1} in a million years to 500 cm/ka^{-1} in some hundreds of thousands of years. Audley-Charles, (1986b) estimated average uplift rates of 300 cm/ka^{-1} and 150 cm/ka^{-1} for the Pliocene and Quaternary in central Timor, Chappell and Veeh, (1978) calculated rates between 3 to 50 cm/ka^{-1} for reef terraces on Timor and Atauro. The results confirm that uplift rates differ greatly along the arc and illustrate that even in a compressive regime some islands experienced long episodes of submergence intermittent with rapid pulses of uplift during the Pliocene-Quaternary. Charlton, (1991) postulates decoupling of oceanic crust from the partially subducted Australian continental basement at the transition between the two could account for isostatic rebound of the collision complex and the outer Banda arc. Recent studies of mantle tomography suggest this may be the case (Wortel pers com, 2000). Since collision at ~2.4 Ma, the accretionary complex and the inner volcanic arc are being thrust northward over the floor of the Banda Sea.

2.2.5 Volcanic arc

The volcanic "inner" Banda arc is thought to be built upon sub-horizontal oceanic lava flows based on seismic reflection data (Bowin et al., 1980) and is likely to have experienced the same emergent history as the outer arc with fluctuating episodes of subsidence and uplift. Post 2.4 Ma (ie. after collision of the Australian margin with the outer Banda arc) uplift may have been substantially increased with

the development of the Wetar thrust and subsequent back arc thrusting aiding in the rapid exhumation of the Wetar volcanic edifice. Slab detachment (oceanic from continental) at depth under Timor may also have significant effects on uplift rates of the inner and outer Banda arcs, thus contributing to uplift rates (Wortel, pers com. 2000). The oceanic crust east of Wetar has a thickness of ~11 km (Bowin et al., 1980) however these thickness estimates are too sparse to characterise the entire region (Snyder et al., 1996). Seismic data from the Sunda arc, East Sunda arc and Banda arcs exhibit a well defined Benioff zone, however the Alor-Wetar segment lacks earthquake foci between depths of 50 and 250 km (McCaffrey, 1989). Within the Adonara-Pantar segment, seismic observations by Spence, (1986, 1987) and McCaffrey, et al., (1985) indicate strong downward slab pull and normal faulting. A complex zone of normal and strike-slip faults offset the inner Banda arc between the islands of Alor and Wetar to a distance of approximately 50 km, Figure 2.2. The northward displacement of Wetar and islands to the east from Atauro, relative to Alor and the islands to the west may be attributed to a north-trending left-lateral fault (Masson et al., 1991) or a large scale wrench fault (Breen and Silver, 1989) however there is no corresponding offset on the coast of Timor south of Atauro. This broad zone of faults which pass either side of the island of Atauro have a northerly trend off the west coast of Wetar (see Figure 2.2) changing to north-easterly off the coast of Timor (Masson et al., 1991). Data indicates that the volcanic arc is seismically more active in the east towards Damar, seismicity and southward dipping reflectors indicate active thrusts which penetrate both crust and upper mantle to depths of 100 km (Richardson and Blundell, 1996).

2.2.6 Backarc region

Present day seismic activity northwest of Wetar indicates a northeast-southwest trend which McCaffrey and Nabelek, (1984, 1986) and McCaffrey, (1988) attribute to complex association of both back-arc thrusting and strike-slip faulting. Breen et al., (1989) and Silver et al., (1983) also noted that back-arc thrusting in the south Banda Sea from Sumbawa to Wetar which is also closely associated with present day seismicity, however it is absent from the Adonara-Pantar segment. McCaffrey, (1989) suggests that continent-arc collision is resulting in a westward movement of the Adonara-Pantar section with subsequent eastward movement of the

Banda arc, this area of the arc is cut by a set of northeast-southwest trending cross-arc faults (Varekamp et al., 1989), see Figure 2.2. A north-south trending line of seamounts culminates at the active volcanic island of Gunung Api in the north, some 400 km above the Wadati-Benioff zone, (Cardwell and Isacks, 1978). This area is thought to represent a transform fault or zone of weakness thus allowing basaltic material to reach the surface (Snyder et al., 1996). Recent GPS data, (Genrich et al., 1994) seismicity and seismic reflection profiles (McCaffrey, 1988; Silver et al., 1983) indicates that the Wetar Thrust at the northern edge of the inactive segment of the "inner" Banda arc at present accommodates the majority of the 75 mm/a^{-1} convergence between the Australian margin and the Banda arc. The backarc thrusts north of Wetar and Flores are thought to represent a subduction polarity reversal due to the difficulty in subducting buoyant continental material, (Hamilton, 1979). Snyder et al., (1996) subsequently suggests that the Wetar Thrust is acting as a site of new development of subduction rather than overthrusting of the arc. This 350 km east-west trending thrust ends north of Romang and is associated with collision to the south, at present this zone is aiding uplift of the inner Banda arc and collision complex.

The backarc itself contains abundant seamounts trending east along the inner Banda arc towards Damar, seismic reflection data in the Banda Sea suggests a relationship with northeast trending ridges and faults. The Wetar and Damar basins (defined by positive gravity anomalies) were considered to be early Cretaceous in age becoming younger and shallower to the north (Chao-Shing and McCabe, 1986). However, recent dredging of seafloor samples and whole rock age dating proves that backarc rifting occurred from 6-3 Ma as multi-rift opening for the Wetar Basin and single-rift opening for the Damar Basin (Honthaas et al., 1998).

2.3 SUMMARY

The subduction of oceanic and continental material along the Timor trough has resulted in a complex zone dominated by compressional tectonics. Slab decoupling is suggested by Price and Audley-Charles (1987) to have commenced at about 3.5 Ma and may have assisted in producing extension within the volcanic arc region and back-arc however there is evidence that rifting occurred in the Wetar Basin between 6 and 3 Ma. Intra-arc, back-arc and post-arc rifts result from subduction cessation,

slowing of subduction or changes in slab configuration and are tectonically zones of extension favourable for the generation of VMS deposits (Sillitoe, 1982; Cathless et al., 1983; Sillitoe, 1999), see Figure 1.1, Chapter 1 and sections 3 and 4 on Figure 2.1. In contrast, compressive regimes are characterised by shallow dipping subducting slabs and are more favourable for the emplacement of porphyry deposits (Sillitoe, 1989, 1999), sections 1 and 2 on Figure 2.1.

The initiation of the Wetar thrust to the north of Wetar and may also have implications in the generation of the deposits preserved on the island.

Chapter 3

VOLCANIC AND STRUCTURAL SETTING OF THE DEPOSITS

3.1 INTRODUCTION

The East Sunda-Banda arc has been discussed in terms of tectonic evolution in Chapter 2 where subduction related volcanism has led to the generation of a chain of volcanic islands. These Banda arc volcanoes range from low-K tholeiitic in the NE to high-K calcalkaline in the SW (Jazek and Hutchinson, 1978; Whitford and Jazek, 1979; van Bergen et al., 1989; Vroon, 1992; de Hoog et al., 2001). Romang Island, located directly to the east of Wetar consists of an early andesitic to dacitic volcanic sequence followed by a dacitic to rhyodacitic succession (Garwin and Herryansyah, 1995). Wetar itself dominantly comprises submarine basaltic-andesite pillow lavas (Ruxton, 1995) intercalated with volcanoclastics progressively grading into felsic volcanics. Sediments and mudflows cap the stratigraphy (Sewell and Wheatley, 1994b). The island of Lirang, located SW of Wetar is composed dominantly of granodiorites and dacites (Heering, 1941).

This Chapter describes the structural setting and volcanic stratigraphy that hosts the ore deposits, subsequent Chapters give detailed descriptions of the mineralisation (sulphide mounds, barite deposits) and the associated alteration zones. Based on field mapping by the author and analysis of drill-core material, this study is focussed on the areas surrounding the sites of mineralisation at Kali Kuning, Lerokis and Meron. Principal objectives of the field mapping were:-

1) To map lithological contacts and to further update previous stratigraphic columns presented by mine geologists.
2) To collect a representative suite of samples for further laboratory based study.
3) Identify key field relationships between mineralisation and host arc volcanics.

3.2 PREVIOUS WORK

3.2.1 Structure

A photogeological study (Nash and Snodin, 1992) showed that structural elements of Wetar are dominated by prominent NNW-ENE normal faults along with subsidiary N-S and NNW structures. The Lerokis area (comprising six individual deposits, Zones 1 to 6) forms a topographically elevated NW orientated elliptical block that stands at a maximum elevation of 550 m, (Figure 3.1). This structure is bounded by these regional fault orientations which are commonly NW or NNW and are parallel to the Ilwaki-Lurang Lineament (ILL, Figure 3.2). The Arnau-Lihak Fault Zone (ALFZ) trends ENE from Arnau in the south to Lake Tihou where direction changes to a more NE trend paralleling the northern coast. The Lerokis area (Figure 3.1), Kali Kuning and Meron are thought to be part of a large arcuate feature, disrupted but convex to the north and masked by the Central Volcanic Complex to the south, see Figure 3.3. Nash and Snodin, (1992) suggest that these sites of mineralisation flank this large arcuate feature which may possibly be a caldera margin.

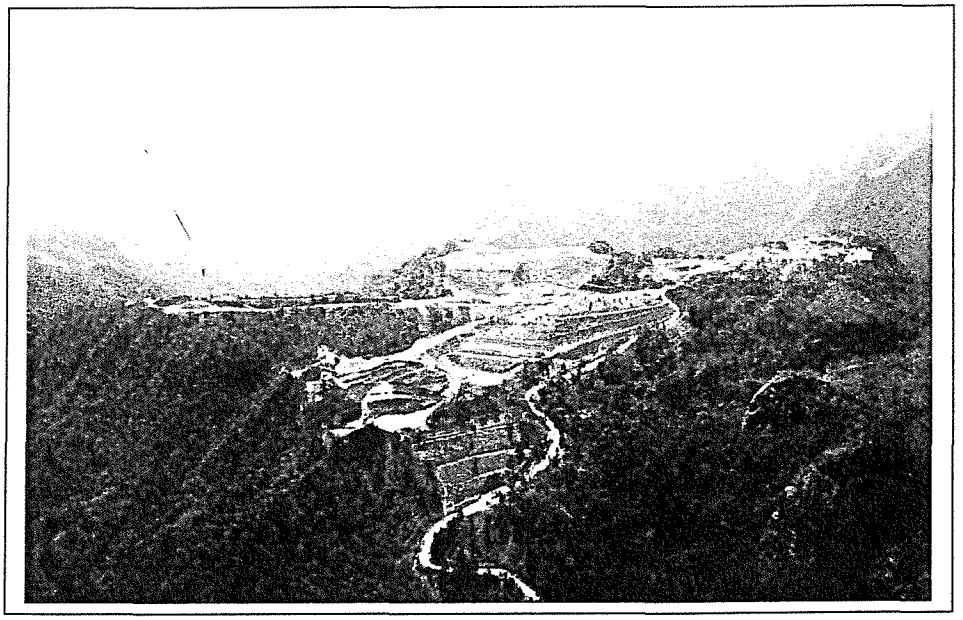


Figure 3.1. View approximately East of the Lerokis Mine area. The foreground at a slightly lower elevation, is Zone 6, Zones 1, 2 and 3 are central, Zone 5 is present far right.

3.2.2 Stratigraphy

A schematic cross-section of Wetar Island is given in Figure 3.2 illustrating principal stratigraphic units and geological relationships based on previous accounts; a simplified geological map of Wetar Island is illustrated in Figure 3.3. Subvolcanic diorites / dacites and rhyodacites are dated at ~12 Ma and are preserved to the south of the island (Abbott and Chamalaun, 1981). Dacitic lavas from the south east of the island are dated at ~ 5 Ma and contain volcanoclastic sediments and breccias which are in turn overlain by sediments and limestones (Heering, 1941, Herrington, 1993). Overlying this sequence are volcanoclastics which are dated at ~ 3 Ma (Abbott and Chamalaun, 1981) comprising andesites, basalts and conglomerates and thus record bimodal volcanism throughout the evolution of the Wetar Island edifice.

In the Western part of the island andesites and dacites are common and basalts are rare (De Jong, 1941), similar rocks are present in the East where rhyolites, dacites, keratophyres, andesites and basalts are recorded (Heering, 1941). Heering (1941) also describes granodiorite exposures at Tandjung Illipoi and along the Sau River with dolerites and rhyolites, see Figure 3.3. Also in the west of Wetar Island, andesitic to dacitic lava flows, breccias and tuffs are also intercalated with *globigerina* bearing limestones, a terrace is preserved in the southern part of the island at a high of 820m (Van Bemmelen, 1949).

3.3 PRESENT STUDY

3.3.1 Structure and Stratigraphy

The deposits of Kali Kuning, Lerokis and Meron are three of a number of identified mineralised zones on Wetar Island (see Table 3.1). The Kali Kunig, Lerokis and Meron deposits are located towards the north coast of the island, (Figure 3.4) where Au-Ag-Ba mineralisation crops out. Figure 3.4 illustrates that the majority of mineralised zones (outlined in Table 3.1) lie within the central part of the island bound to the west and east by extensive faulting that trend between the villages of Arnau and Numatang in the west and Ilwaki and Lurang in the east (Farmer and Clifford, 1993). There are however exceptions that include deposits located at J46,

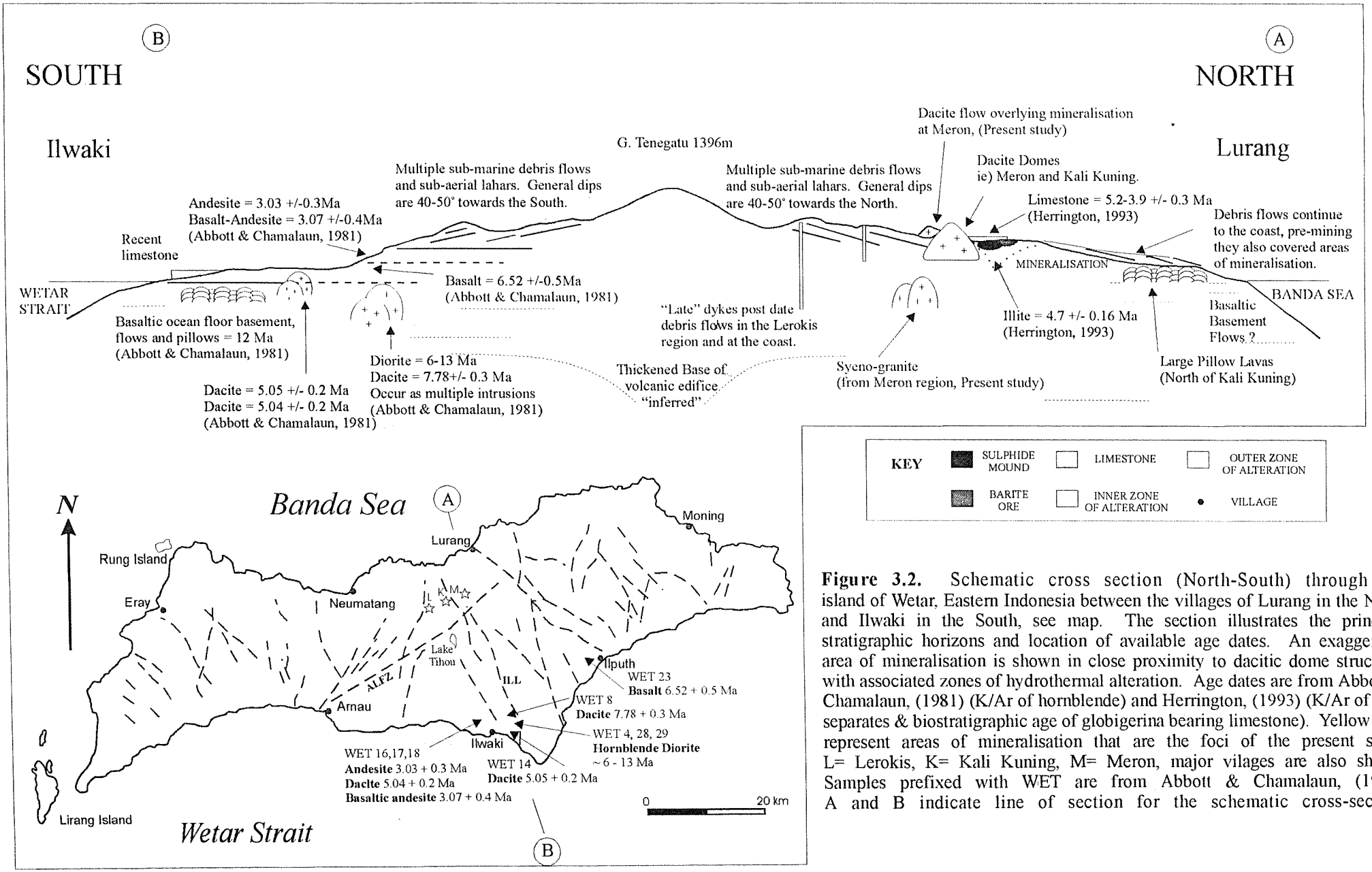


Figure 3.2. Schematic cross section (North-South) through the island of Wetar, Eastern Indonesia between the villages of Lurang in the North and Ilwaki in the South, see map. The section illustrates the principal stratigraphic horizons and location of available age dates. An exaggerated area of mineralisation is shown in close proximity to dacitic dome structures with associated zones of hydrothermal alteration. Age dates are from Abbott & Chamalaun, (1981) (K/Ar of hornblende) and Herrington, (1993) (K/Ar of illite separates & biostratigraphic age of globigerina bearing limestone). Yellow stars represent areas of mineralisation that are the foci of the present study, L= Lerokis, K= Kali Kuning, M= Meron, major vilages are also shown. Samples prefixed with WET are from Abbott & Chamalaun, (1981). A and B indicate line of section for the schematic cross-section.

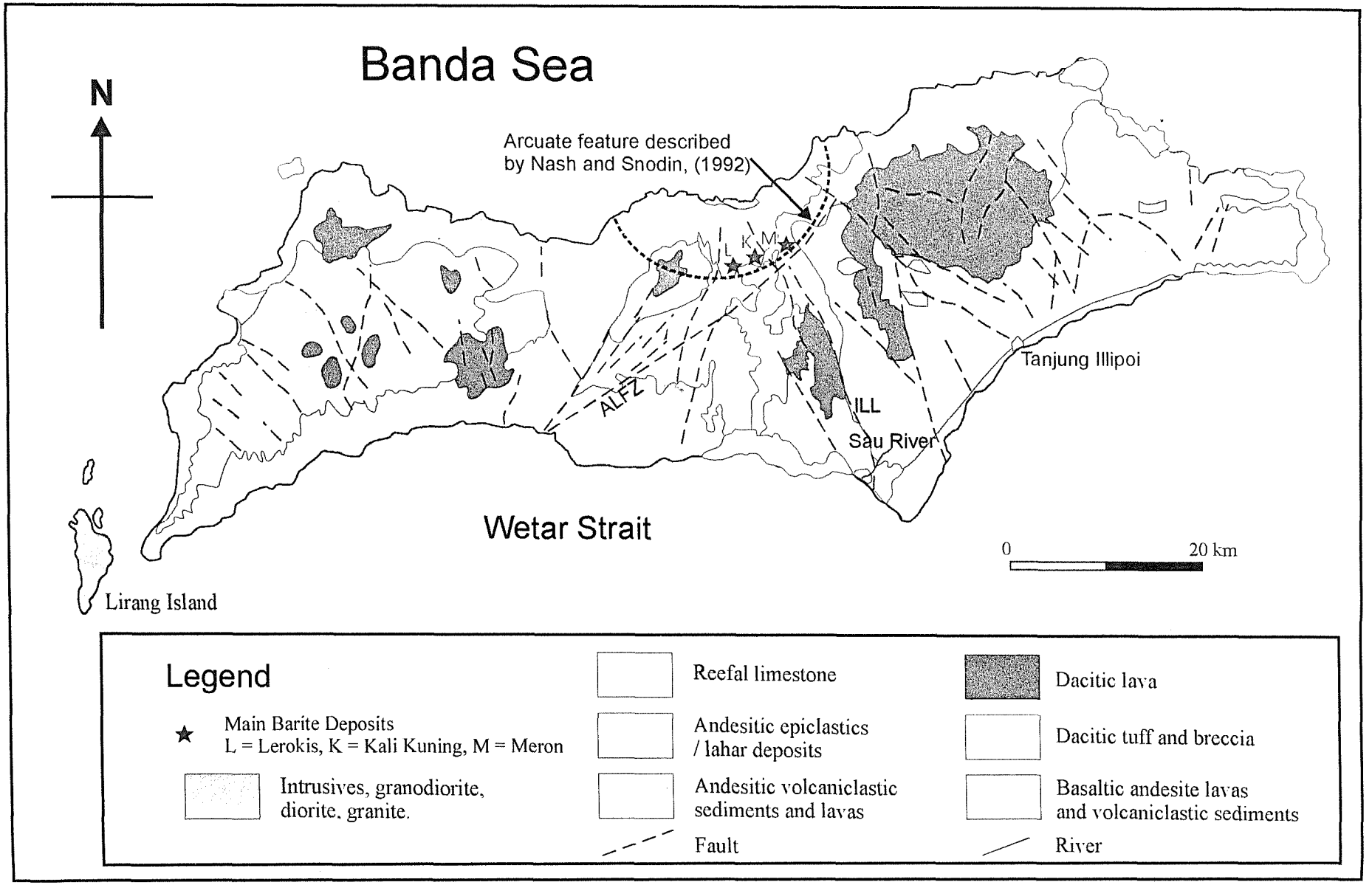


Figure 3.3. Simplified geological map of Wetar Island (after Nash and Snodin, 1992; Farmer and Clifford, 1993). Map shows principal mineralised areas, structural lineaments (drawn from aerial photos) and key geological units. Intrusives added from Burham et al., (1993).

Table 3.1. Key mineralogical, geological and alteration characteristics of the principle mineralised areas on Wetar Island, for locations see Figure 3.4.

Deposit / Prospect	Mineralogy	Wallrock alteration	Host Geology and Lithological controls	Comments	Reference
Kali Kuning 3	Massive Py mound with associated stockworks + Cpy, Sph, Ga, Cov, Dig, Ten, Tet. Overlying Baritic ore + Au, Ag, Hg.	Argillic: silicification + ill-chl-sm-kao.	Mafic, underlying basement, associted with vesicular flows and felsic intrusives. Overlying limestone / chert / gypsum / lahars / tuffs and debris flows. Associated with fault controlled basins.	Submarine formation, baritic sands onlap and overlie irregular massive sulphide lenses / mounds.	This study, Sewell, 1991, Carlile and Mitchell, 1994, Sewell and Wheatley, 1994a and b, Sillitoe, 1997, Sewell et al., 1991.
Lerokis 4	Baritic ore + Au, Ag, Hg.	Argillic: silicification + ill-chl-sm-kao, local advanced argillic: al-pyr-crys-dick.	Associated with fault controlled basins.	No sulphide mound observed. Baritic ores sit within an irregular shaped bowl.	This study, Sewell, 1991, Carlile and Mitchell, 1994, Sewell and Wheatley, 1994a and b.
Lerokis 5	Massive Py mound with associated stockworks + Cpy, Sph, Ga, Cov, Dig, Ten, Tet. Overlying Baritic ore + Au, Ag, Hg.	Argillic: silicification + ill-chl-sm-kao, local advanced argillic: al-pyr-crys-dick.	Associted with vesicular flows and felsic intrusives. Overlying lahars / tuffs and debris flows. Associated with fault controlled basins.	Submarine formation, baritic ores onlap and overlie irregular massive sulphide lenses / mounds.	This study, Sewell, 1991, Carlile and Mitchell, 1994, Sewell and Wheatley, 1994a and b, Sillitoe, 1997.
Meron	Massive Py mound at depth with overlying baritic ore + Au, Ag.	Argillic: silicification + ill-chl-sm-kao.	Dacite dome structures (both fresh and altered), mineralisation capped by extensive debris flows and dacitic flow.	Submarine formation, baritic ores onlap and overlie sulphide mounds.	This study, Budiono and Santoso, 1996, Clifford, 1993.
Baru Manu	Small massive Py mound with overlying barite ore. Sulphides ~1 m thick.	Pervasive clay, silicification.	Contained within a small depression with altered dacite. Overlain by fresh dacites and debris flows which interfinger in part.	Similar to Meron.	From mine cross section, Rena and Budiono, 1997, Hopgood et al., 1995b.
Gunung Botak	Vein Ba, Zn, Pb, Cu, As, Ag, Au + chalcodenic Qz.	Intermediate argillic: Hypogene sm-ill, local kao-al-pyr, supergene kao.	Located within an andesitic strato-volcano, associated with felsic breccias and flow-banded dacite / rhyodacite & diatremes. Overlying bedded tuffs. NE/SW sinistral faulting.	Late subaerial development, sub-economic.	Sillitoe, 1997, Booler, 1997.
W 75	Minor vein Ba + Sph, Ga, Ten, Cpy.	Silicification, sm-ill.	Located within an andesitic strato-volcano, associated with felsic breccias and flow-banded dacite / rhyodacite & diatremes. Overlying bedded tuffs.	Eastern area of Gunung Botak.	Booler, 1997.
Kali Kuning 1	Py, Ba, Au	Silicification.	Andesitic volcanic.	Similar to footwall of Kali Kuning 3.	Sewell, 1991.
Kali Kuning 2	Disseminated Py, Lim, Ja ± Ba.	Silicification + chl.	Dacitic volcanics, abundant faults / fractures.	Similar to footwall of Kali Kuning 3.	Sewell, 1991, Rena and Budiono, 1997.
Kali Kuning 4	Vein Py, Ba +/- cpy and chalcocite.	Silicification.	Tuffs, lapilli tuffs and breccias with extensive lahar cover. Rhyolitic domes and andesites.	Associated with NW-SE trending faults.	Sewell, 1991, Rena and Budiono, 1997.
J27 / 4	Minor Py.	Silicification.		Located on a shear sided ridge.	Sewell, 1991.
Kali Besar 1	Py, Lim, Ba.	Silicification and clay.	Dacitic volcanics, fractured.	Barite ore overly a clay siltstone.	Sewell, 1991.
Kali Besar 2	Py, Lim, Ba.	Silicification and clay.	Vesicular andesites trending ESE (pillows).		Sewell, 1991, Rena and Budiono, 1997.
Lerokis 1 (south)	Ba, Py.	Silicification, clay and jar.	Deposit contained within a small graben ~100m across.	Barite replaces host volcanics.	Sewell, 1991.
Lerokis 6	Ba, Py.	Silicification, clay and jar.	Intermediate volcanics and tuffs, associated with fault bounded grabens.	Gossanous baritic material overlies volcanics.	Sewell, 1991.
Kayu Lepa	Py and Ba veins and disseminations.	Fe-oxides + silicification.	Rhyodacites underlain by andesites.	Low assay results.	Rena and Budiono, 1997.
Kelapa Tiga	Py and Ba veins and disseminations +/- cpy.	Sericite, chl, silicification.	Vesicular andesites.	Low assay results.	Rena and Budiono, 1997.
Batu Kapal	Barite ore + sulphide mound, Py and Cpy.	Silicification + clay peripheral.	Mafic basement, associated with brecciated andesites. Barite rock in part above sand bodies.	Barite ores overly massive pyritic mound similar to Kali Kuning and Lerokis 5.	Hopgood et al., 1995.
Ilwaki	Ba, disseminated Sp, Ga, Ten, Cpy.	Silicification.	Breccias & flow banded porphyries.	Similar to Gunung Botak.	Sillitoe, 1997.
Batu Duri (J 91)	Barite sand, disseminated Sp, Ga, Ten, Cpy, coarse Ba rich rock.	Silicification, Fe-oxides.	Breccias & flow banded porphyries.	Similar to Gunung Botak and Ilwaki.	Sillitoe, 1997, Hopgood et al., 1995, Clifford and Santoso, 1992.
Pantai Merah	Small Barite ore resource (2-6 m)	Silicification/ silicified lst.	Overlying corraline limestone	Lst deposition post mineralisation.	Hopgood et al., 1995.
J 46	Qz, Ba, Fe oxide stockwork.	Moderate clay, illite / sm.	Brecciated dacite, andesite and associated dacite dyke.	Extensive lahar cover (50m).	Hopgood et al., 1995.
W 6	Small Barite ore + Cu oxides.	Silicification.	Occurs in small fault bounded basins, overlying dacites.	Similar to J 91.	Hopgood et al., 1995.
W 20	High Au + Base metal values.	Silicification.	Basaltic flows + diorite dyke.	Mineralisation assoc. with dykes.	Hopgood et al., 1995.
Kali Putih	Barite ore and 2 possible sulphide mounds.	Silicification, gossan, clay.	Andesites.	Similar to Lerokis and Kali Kuning.	Hopgood et al., 1995b.

Footnote to table 3.1: Abbreviations used within the table are listed in Appendix A, majority of information from unpublished internal company reports with additional information from this study.

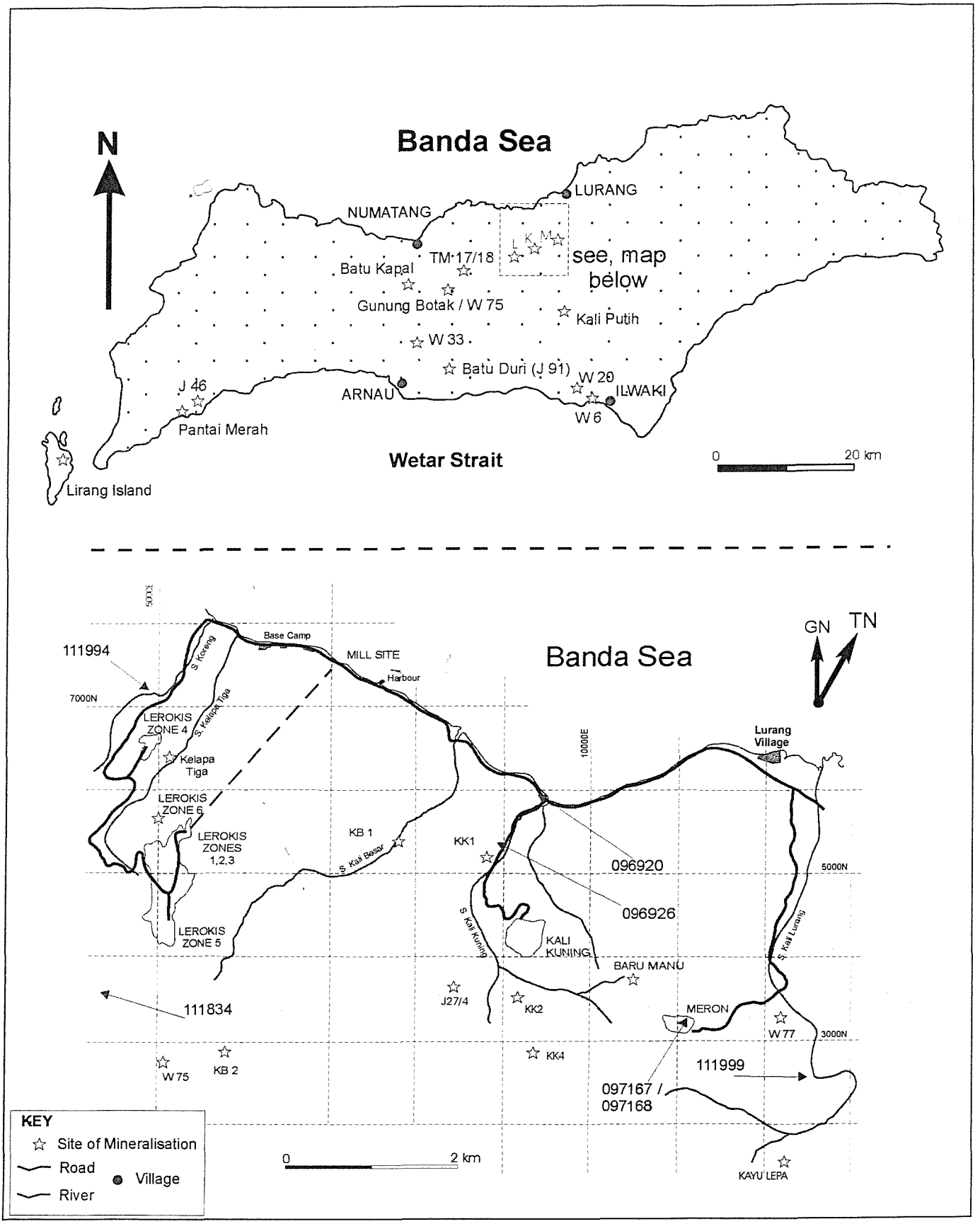


Figure 3.4. North Central Wetar, deposit location and study area. Yellow stars represent other areas of mineralisation within the area, refer to table 3.1 for descriptions. Blue stars and blue areas represent deposits in this study. Names prefixed with S are rivers, KB= Kali Besar, KK= Kali Kuning. Blue circles and names in capitals are villages. Sample locations for samples 096926, 096920, 111994, 097167, 111999 and 111834 are shown, see also map insert sheets 1 and 2. XRF data for these samples are given in chapter 4.

Pentai Merah and on neighbouring Lirang Island. The study area is characterised by rugged topography and reaches a maximum height of 650 m in the SW, aerial photographs of the Kali Kuning and Lerokis Zone 5 are shown in Figure 3.5A and B illustrating the surrounding topography. The associated zones of hydrothermal alteration that surround the centres of mineralisation are also shown. Alteration around these mineralised systems are extensive with hydrothermally altered host rocks covering an area measuring ~8 km E-W by ~4 km N-S. Due to the hydrothermal alteration around the deposits unaltered lithologies within the mapped area are rare; the alteration around the zones of mineralisation will be addressed in more detail in Chapter 4 whilst the deposits themselves (both sulphide mounds and barite ores) will be addressed in Chapter 5. Field mapping within the local area that surrounds the deposits of Kali Kuning, Lerokis and Meron has established the local stratigraphy which is summarised in Figure 3.6, see also the geological map of the area, (map insert sheets 1 and 2). The base of the stratigraphy comprises fine-grained andesitic flows which dip ~10°-028° (dip-dip direction) these are exposed along the coastal road on the north of the island (Figure 3.7A). The andesite consists of both simple and multiple twinned plagioclase phenocrysts along with pyroxene and minor amphibole (Figure 3.8A and B). A syeno-granite intrusive (sample 111999, for location see Figure 3.4) has been identified along the S Kali Lurang river in close proximity to the Meron deposit however its relationship to the andesite on the north coast at present is unclear. In thin section, quartz grains generally exhibit both a consertal texture and undulose extinction, plagioclase phenocrysts are partially or discontinuously zoned on both plagioclase and K-feldspar. Biotite is abundant and sphene occurs as an accessory phase (Figure 3.8C and D). Overlying the basal andesite and intrusives are a >450 m sequence of altered volcanic rocks which are the host to the Kali Kuning, Lerokis, and Meron mineralisation, termed the "mine-sequence" stratigraphy. Within this sequence, volcanic morphology and textures are preserved distally from the centres of mineralisation showing that they are laterally extensive. At the base of this sequence, large green chloritic altered andesitic pillow lavas are evident reaching diameters of between 1-2 m (Figure 3.7B). These contain abundant vesicles ranging in size from 1 mm up to 3-4 cm. The "mine sequence" is overlain unconformably by post-mineralisation lahars and debris flows (Figure 3.7C) which are geomorphologically controlled by the former palaeotopography.

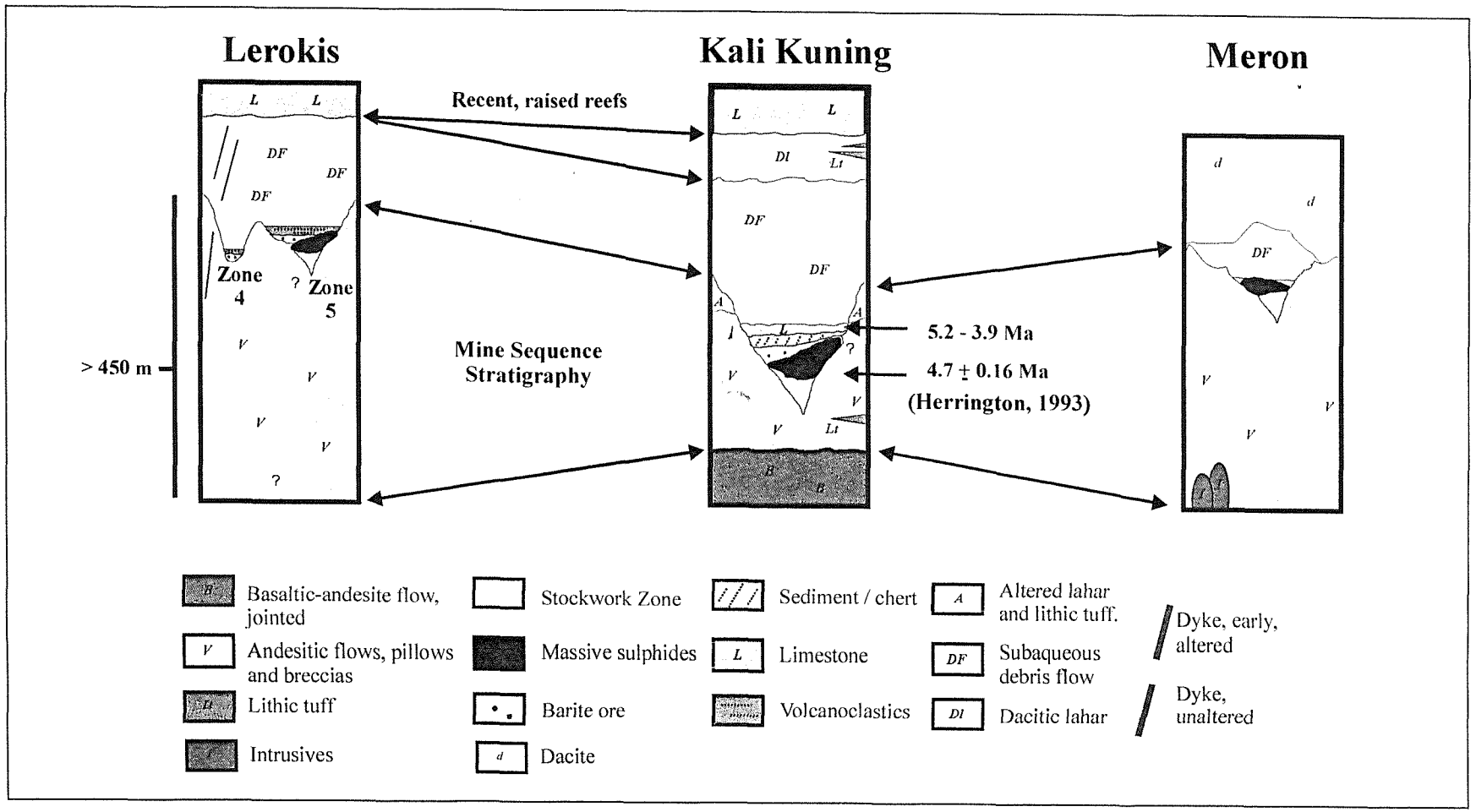
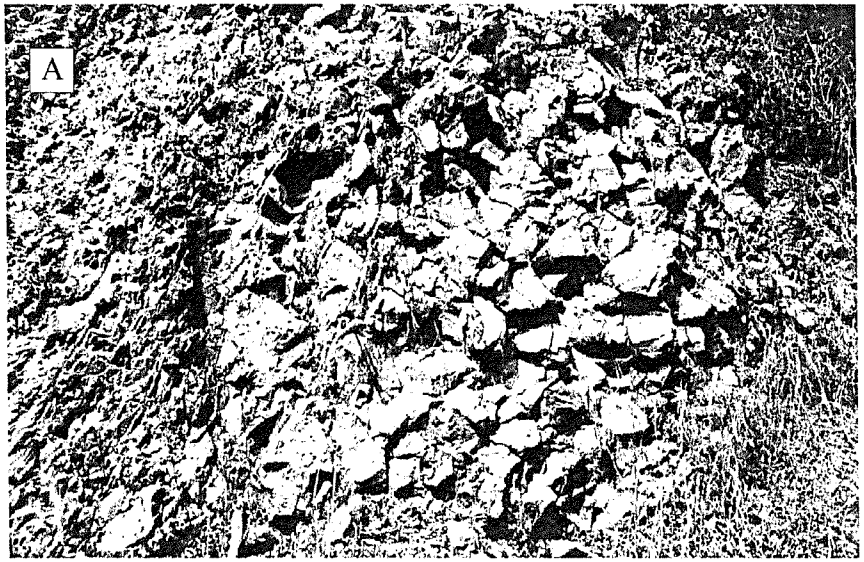


Figure 3.6. Schematic stratigraphy of the Lerokis, Kali Kuning and Meron areas based on field mapping (present study with additions from Ruxton, 1989 and Farmer and Clifford, 1993).





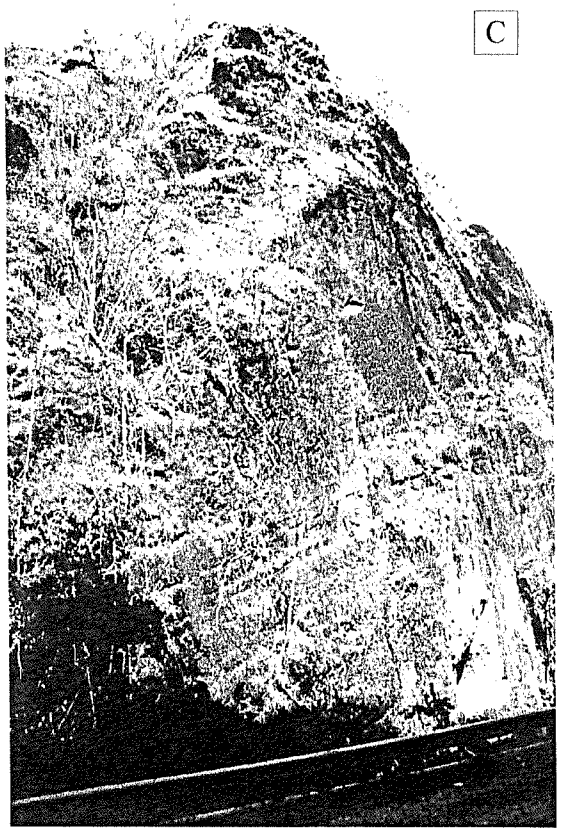


Figure 3.7. A) Columnar / regular jointing preserved within the andesitic feeder tube, north coast Wetar. Not all of the joints exhibit hexagonal outlines, the exposure is ~5 m high, individual columns are 30-50 cm in diameter, abundant vesicles are present. B) Large >1 m pillow structures on the Kali Kuning road section overlain by sub-aqueous debris flow, hammer is shown for scale. C) Sub-aqueous debris flow on the Kali Kuning road section exhibiting coarse grading (upward fining), height of section is approximately 30 m.

Figure 3.8

A-B. Coastal vesicular andesite, sample 096920 illustrating typically zoned phenocrysts of plagioclase feldspar. Both photomicrographs (XPL) include pyroxene and amphibole, field of view 4.5 mm.

C. Twinned and oscillatory zoned feldspars from the syeno-granite intrusion, (sample 111999) quartz and biotite, field of view 4.5 mm (XPL).

D. Same photomicrograph as C, (PPL), field of view 4.5 mm.

E. Sample 096926, lahar clast from post mineralisation debris flow, photomicrograph illustrates fine-grained nature of the groundmass, twinned feldspar and pyroxene (XPL), field of view 4.5 mm.

F. Spherulitic rhyolite, sample 111834 illustrating radiating fibres within spherules (XPL), field of view 4.5 mm.

G. Dacite sample 097167 (PPL) containing phenocrysts of plagioclase feldspar, quartz, amphibole and biotite, field of view 4.5 mm.

H. Dacite sample 097167 (XPL) illustrating simple and oscillatory zoning of plagioclase feldspar, field of view 2.5 mm.

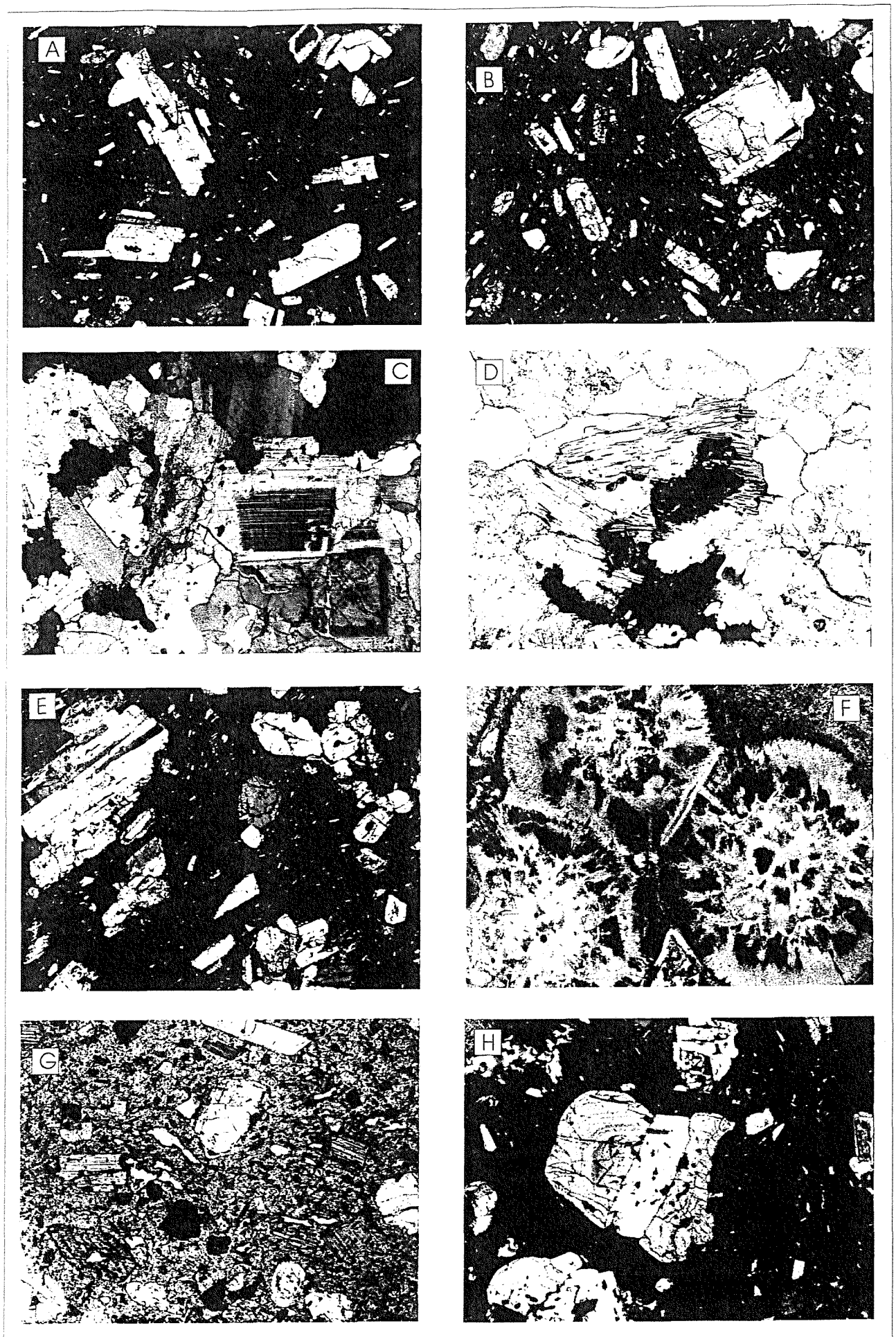


Figure 3.8. Photomicrographs of unaltered lithologies collected from the field area around the Kali Kuning and Lerokis zones of mineralisation. For brief thin section descriptions see opposite and Appendix B, see text for discussion.

These polymict debris flows contain altered mine sequence clasts at the base plus unaltered volcanic clasts presumably from outside of the mapped area. Sample 096926 (Figure 3.8E) can be seen in-situ in Figure 3.9A next to a large altered pillow structure along with abundant and intensely altered clasts, (for location, see Figure 3.4) this sample visually appears more mafic than other clasts and in thin section consists of a finer-grained groundmass than the coastal andesite. This stratigraphic unit dips towards the north (25°-340°) in the Kali Kuning river area in the north. Clasts within this unit vary from angular to rounded and are mostly matrix supported, clast sizes range from pebble sized fragments up to entire pillows of 1 m and greater in diameter. Later lahars and lithic tuffs overly the Kali Kuning area to the east, comprising of unaltered dacite clasts which are found in situ to the southeast at Meron, these clasts are absent from the other debris flows in the area, see geological map (insert sheet 1).

Reefal limestone crops out and is exposed along the north coastline indicative of rapid uplift of the island, these exposures rest on the debris flows and are offset by a series of sinistral NE-SW trending strike-slip faults. Post mineralisation dykes are evident in the NW corner of the mapped area with an orientation 80°-030°, one of which is offset by a NE-SW trending sinistral fault along the Kelapa Tiga river, the displacement is ~60 m. Spherulitic rhyolite (sample 111834, location 190) crops out approximately 1 km southwest of the Lerokis Zone 5 deposit, spherulites range in size up to a maximum of 5 mm in diameter and occur in clumps or compounds surrounded by glass (Figure 3.8F). In some instances the spherulites enclose microphenocrysts of plagioclase, radiating fibres are evident in all spherules. This lithology lies on a debris flow suggesting a stratigraphically young age, poor exposure does not allow any direction or thickness measurements. Alluvium is extensive throughout the study area and covers drainage channels and low-lying areas in close proximity to the coast.

3.3.2 Kali Kuning deposit geology

Kali Kuning is located within a small conical depression at a height of ~150 m and is surrounded to the east, south and west by hydrothermally altered volcanics (Figure 3.5A). In addition to mapping, three drillcores (KKD 031, KKD 049 and KKD 058) were examined to establish volcanic host stratigraphy below the mineralisation and to investigate potential feeder zones for the sulphide body and Au-Ag-bearing barite

ores. The location of these boreholes with those examined from Lerokis Zone 5 are illustrated in Chapter 4 in relation to sample locations and association with hydrothermal assemblages and zones of alteration. The study from Kali Kuing showed the sulphide body to be underlain by an extensive, silicified and intensely altered stockwork zone to depths of at least 250 m. A series of clay altered, vesicular and amigdale bearing lavas are present below and surrounding the deposit, amigdales and vesicles present are generally elongate, flattened or oval and range in size from a few mm up to 5 cm. Amigdales are more abundant towards the zone of mineralisation and are infilled with quartz ± pyrite cubes measuring up to 4 mm in diameter, generally at distal locations from mineralisation the vesicles are empty.

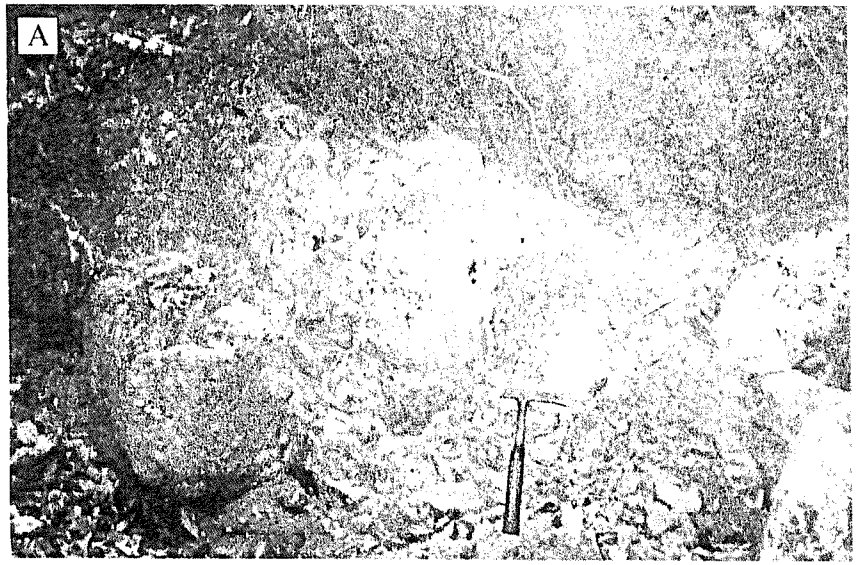
A large irregular shaped massive sulphide body of ~8 Mt (Clifford, 1993) has a thickness of ~80 m and appears to be plunging to the west, see Figure 3.5A. Sulphides are dominantly massive pyrite with minor chalcopyrite although banded pyrite-chalcopyrite mineralisation was collected from the top of the sulphide body. The upper parts of the massive sulphide are generally "blocky" in appearance and are comprised of ~99% pyrite. Unconsolidated barite ore lies in-situ on the massive sulphide body and can also be traced along the contact (to the north and the south) between the sulphide body and the altered rocks of the mine sequence. In places a thin skin of barite ore is still present "in-situ" on steeply dipping sulphide faces, at these locations the contact zone between the sulphides and barite is evident (ie. Location 84 at Kali Kuning, see map insert sheet 2A). Massive pyrite grades laterally into an unconsolidated, friable pyritic sand which subsequently grades into varying thickness' and colours of barite ore exhibiting varying degrees of cementation before contacting the intensely altered footwall volcanics.

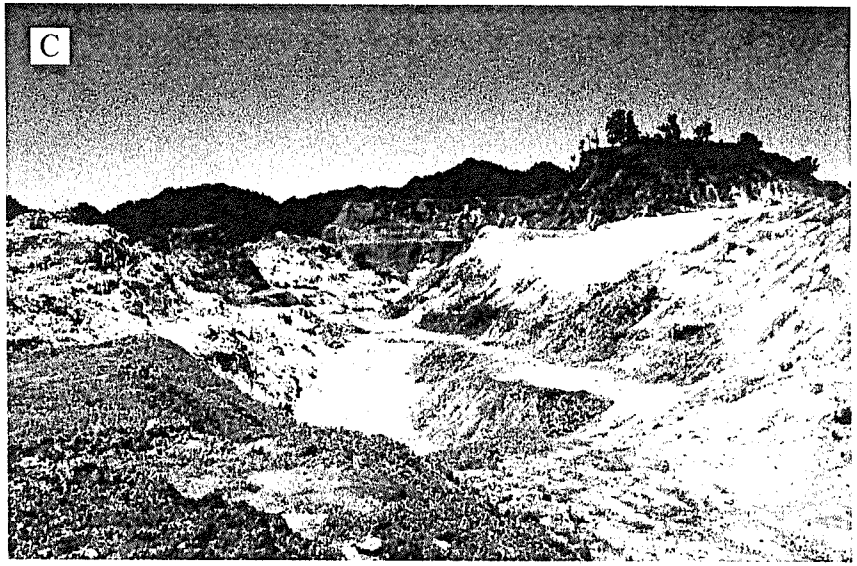
Overlying the sulphide mound rests a fine-grained purple chert (maximum thickness of 40 cm) which itself is overlain by a thin layer of fibrous gypsum (up to 15 cm). A fine-grained white, *Globigerina* bearing limestone caps the succession, (up to 2 m) the depth of deposition based on biostratigraphy is between 500-2000 m (Herrington, 1996) or >2 km based on rare benthic forams (Murray pers com, 1999, see Appendix B for a full list of planktonic and benthic assemblages). The association of chert, gypsum and limestone are illustrated in Figure 3.9B. The lateral continuation of each unit is poorly exposed as ~50 m of lahar / debris flow overlies the deposit directly to the east. The southern margin of the deposit itself is bounded by a fault trending approximately northwest, extensive hydrothermal breccias are preserved within this

area and are dominantly located at the margins of topographically higher areas. These structures have been previously described as dacite or rhyodacite domes (Ruxton, 1989) and are believed to form the direct footwall to mineralisation. In hand specimen these altered rocks still contain visible "free" quartz grains and distinguish them from the altered underlying andesites and basaltic-andesites. The flanks of the topographic high areas to the south and east of this zone consist of sub-rounded to angular clasts of up to 50 cm of footwall derived material within a fine grained kaolinised matrix. In contras, the immediate footwall to the mined barite ore preserves a unit of highly altered residual silica (see also Chapter 4).

3.3.3 Lerokis Zone 5 deposit geology

At a topographic height of 500 m, Lerokis Zone 5 is located ~2km due south of Lerokis Zone 4 and ~3.5 km due west of the Kali Kuning deposit (Figure 3.4) and is located on a topographically isolated ridge bounded by steep gradients to the east, south and west (Figure 3.5B). Intense hydrothermal alteration of host volcanics is evident again surrounding the deposit. Three drillcores (LKD 042, 043 and 044) were analysed from Lerokis Zone 5 to establish volcanic host stratigraphy and to investigate potential feeders zones for the sulphide body and Au-Ag-bearing barite ore. These investigations indicate the presence of a silicified stockwork of cross-cutting sulphide veins progressing with depth into a series of hydrothermally altered volcanics, dominantly amigdale and vesicle bearing lavas. The adjacent footwall to the mined barite ore comprises bodies of residual silica. At the centre of the ore zone a massive sulphide mound occurs as a single 4 Mt pyritic body, (Clifford, 1993). This mound is generally flat lying with a pronounced keel towards the south of the deposit. The massive sulphide mound consists dominantly of massive pyrite boulders giving a "blocky" appearance, surrounded by friable pyritic sand. Close to the keel of the sulphide body an extremely hard, siliceous unit is exposed which is part of the underlying stockwork zone. This area coincides with the intersection of two faults, (mapped prior to mining) trending NNW and W respectively. Two cemented Fe-oxide-barite structures are located at this intersection, proximal to the sulphide body and may represent fluid feeder conduits for the barite ore (see Chapter 5, mineralisation). In-situ barite ore is present at the south of the pit on steeply dipping north facing slopes and comprises of unconsolidated, grey





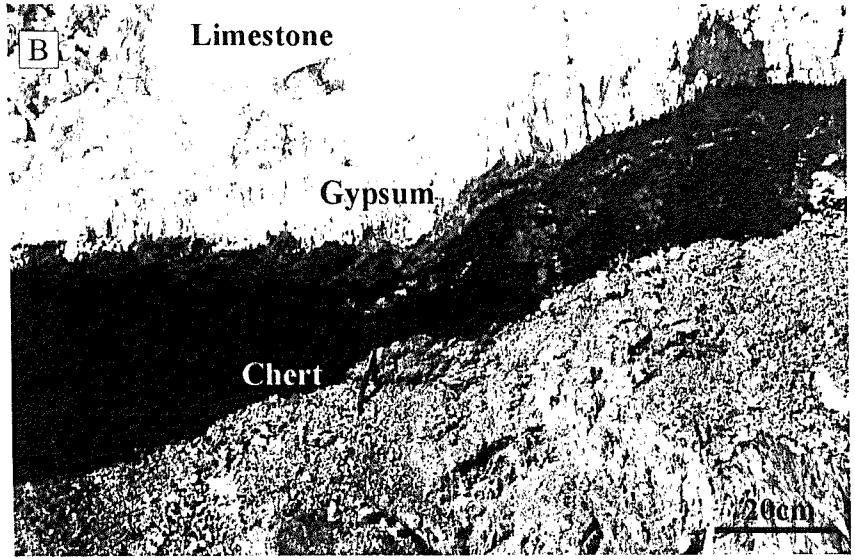


Figure 3.9. A) Polymict, sub-aqueous debris flow containing altered and unaltered clasts range in size from small pebbles to large boulders (including an andesitic pillow, bottom left). Clasts preserved are both angular and well-rounded and supported in a fine-grained mud. B) Chert, gypsum and limestone association from Kali Kuning. C) Overlying volcanoclastic sediment at Lerokis Zone 5, view approximately SE.

coloured, fine grained barite of general grain size ~1-2 mm. The morphology of the barite ore zone mimics to some extent the shape of the sulphide mound and appears to encase or envelope it. This feature however is not as evident as at the Kali Kuning deposit. A fine-grained volcanic sediment overlies the sulphide mound and fines-up in a series of 5-10 cm layers, (Figure 3.9C) this contact zone consists of a fine-grained reworked ~30 cm layer of pyrite, sediment and minor barite, a zone clearly indicative of marine reworking. In contrast to Kali Kuning there is no lahar or debris flow cover over the Zone 5 prospect.

3.3.4 Lerokis Zone 4 deposit geology

At Lerokis Zone 4, the deposit (Figure 3.10) occupies a small depression within an area of prominent topographic relief, (height of ~350 m). The deposit itself lies ~ 1.5 km inland from the coast (Figure 3.4) and contrasts to Zone 5 and Kali Kuning in that there is no sulphide mound present. Extensive silicification and hydrothermal alteration surrounds the ore-zone, jarosite veining is also present (varying in thickness up to 5 cm). As with Zone 5, the adjacent footwall to the barite ore preserves a highly altered residual silica unit and identifies the most intense areas of hydrothermal activity. No drill cores are available from this zone to establish the depth and extent of the underlying feeder zones.

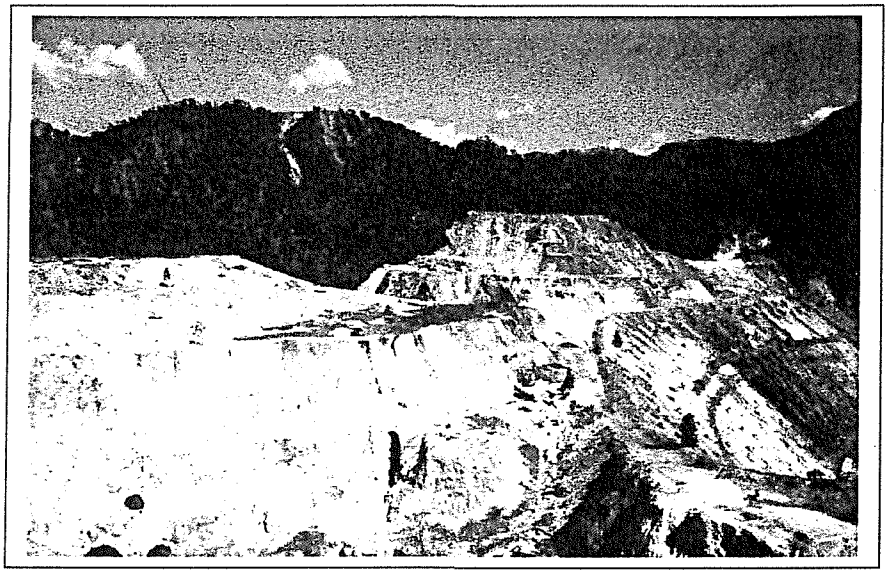


Figure 3.10. Lerokis Zone 4 deposit, post mining looking approximately south. The main barite ore zone was located bottom centre and bottom left of the photo. The deposit is void of a sulphide mound, present at Kali Kuning and Lerokis Zone 5 (Figure 3.5A and B). The alteration associated with Lerokis Zones 1, 2, 3 and 5 can be seen in the distance.

Approximately 0.5 km away from the centre of the deposit on the mine road, large vesicular, altered pillow lavas are present, these however are altered to a higher degree than those on the Kali Kuning mine road. Large pyritic veins are present up to a thickness of 3 cm, these veins exploit the gaps between individual pillows and minor barite veining is also present here.

In-situ barite ore is developed at the southern end of the pit on overlying hydrothermally altered host lithologies, chaotic bedding / slumping is present here indicating the barite has not been deposited in a simple basin. Two brown-orange cemented "Fe oxide-barite" pipe structures are present at the centre of the deposit (bottom of Figure 3.10) showing variations in both Fe and barite content. Both these structures are more "pipe like" than those preserved at Lerokis Zone 5. One individual barite vein, ~60 cm wide within the pipe structure and contains concentrated barite crystals of ~1-2.5 cm in diameter, the majority of barite crystal within the pipes are <1cm in diameter and are euhedral. The morphology of the barite ore appears to be confined to two individual lobes or small basins separated by a slightly raised area of topography. This may also be part of a dacite / rhyodacite dome structure which continues along the mine road to the south and would be consistent with findings from both Kali Kuning and Lerokis Zone 5 (see geological map, insert map sheet 1 and 2). Field investigation however did not identify the presence of "free" quartz grains within this altered host lithology as were evident at Kali Kuning and Lerokis Zone 5. No post-mineralisation lithological units overly this zone since the barite ore outcropped at the surface, the topographic highest areas surrounding the deposit are altered mine sequence volcanics.

3.3.5 Meron deposit geology

The Meron prospect, identified by Kavalieris and Sewell, (1986), (topographic height 300 m) exhibits dominantly altered and brecciated host lithologies. In-situ barite ore is poorly exposed but is present towards the south and east of the prospect, the lateral extent of the barite ore zone has been estimated at 350 m x 130 m x 9 m (Budiono and Santoso, 1996). A dacite flow overlies lahar in the north where dominant clasts are composed of basalt and andesite of varying sizes (small pebbles to large boulders up to 60 cm). The unaltered dacite flow continues toward the northwest and is also present overlying lahar at the Baru Manu prospect to a thickness of ~150 m (Figure

3.4 and map insert sheet 1). Along the eastern margin of the exposure however, hydrothermally altered dacites are exposed. Strongly zoned and twinned plagioclase feldspars are evident in thin section (sample 097167) with quartz, biotite and euhedral amphibole (Figure 3.8G and H).

Geological mine cross-sections indicate that the sulphide mound is generally flat lying and brecciated over its upper surfaces, the thickness of the pyrite mound reaches a maximum of 40 m. The associated barite ore zones are thin on the upper surfaces of the sulphide body but increase in thickness off the flanks of the mound and are therefore more similar to the Lerokis Zone 5 deposit than Kali Kuning. The barite ore zone is evident in the field within a small topographic depression bounded by faults, altered pillow lavas are inferred to underlie the Meron prospect at depth however were not located in the field. Hydrothermal breccias are abundant surrounding the ore zone as are post mineralisation lahars and debris flows.

3.4 DISCUSSION OF STRATIGRAPHY AND HOST GEOLOGY

Geological maps of the study area (map insert sheets 1 and 2 and cross sections, sheet 3) document the findings of the field mapping and illustrate the position of sample locations. Figure 3.11 also illustrates the key geological relationships around the four deposits. The basal basaltic-andesite pillow lavas and overlying lavas suggest that the stratigraphy is dipping only slightly toward the north and in the most part is flat lying; Sewell and Wheatley (1994b), suggested that Wetar is an ENE trending antiform illustrated by opposing dips in epiclastics units; field mapping by the author confirms that the dips of these debris flows (post-mineralisation) are indeed 30 to 40° however they are interpreted to record the underlying topography of the Wetar Island edifice. There is no evidence of folding in the area around Kali Kuning or Lerokis.

Table 3.1 presented a brief description of the abundant sites of mineralisation and their association with host lithology and structural controls. Dominantly, mineralisation is spatially related to felsic volcanics and breccias that overly basalts and andesites which are typical features of many VMS systems both modern and ancient (reviews in Sangster and Scott, 1976; Franklin et al., 1981; Lydon, 1988; Franklin, 1996). The numerous deposits located on Wetar (from the Kali Kuning / Lerokis area in the north to Batu Duri, W20 and W6 in the south, Figure 3.4) exhibit similar characteristics and imply that hydrothermal activity of a similar nature

commenced district wide and throughout the entire volcanic edifice. Host rocks surrounding the sites of mineralisation are predominantly silicified, the alteration assemblages and alteration characteristics will be addressed further in Chapter 4. Field mapping has identified similarities between all of the deposits although Lerokis Zone 4 is somewhat unusual in that there is no associated sulphide mound related to the barite mineralisation or it may be concealed at depth. The association of polymetallic sulphide mounds, host volcanics and tectonic environment suggest an affinity with subduction related arc / back-arc systems. However, the nature of the sulphide mounds and volcanic associations suggest some similarities to systems generated within tectonically different environments including ophiolite complexes and spreading ridges. Massive sulphide mounds are present at the margins of the dome structures and are associated with onlapping and overlying Au-Ag-Hg bearing baritic ores zones, both are related to underlying stockwork zones with varying amounts of mineralisation and alteration. The association of massive sulphides with flanking Au-Ag bearing baritic ore zones are somewhat unusual and will be addressed in more detail in Chapter 5. The sites of mineralisation show close associations with the NW/NNW trending dome structures, in particularly at Lerokis (Figure 3.11B) and suggests a strong structural control on their generation. These structures focused hydrothermal activity and subsequent mineralisation. Post mineralisation uplift has resulted in these domes now defining graben margins, former depressions and topographically lower areas between these domes acted as the principal sites for mineralisation. The presence of syeno-granite within the Meron area confirms the presence of intrusives located in the north of the island as well in the centre and south (Figure 3.3), this lithology is spatially located near to Meron and may therefore have implications on mineralisation. The nature of the volcanism and stratigraphy suggests a marine environment of deposition / formation.

Water depths during the life of the Wetar system suggest deep-water conditions initially with subsequent shallowing environments due to the extensive tectonic activity of the area. Sewell and Wheatley, (1994) suggest that mineralisation occurred < 600 m depth, given the age of mineralisation, 4.7 ± 0.16 Ma, (Herrington, 1993) an uplift rate of only 17 cm/ka^{-1} is calculated. This slow rate of uplift would lead to prolonged duration at shallow depths within the Banda sea, resulting in a greater duration and potential for wave erosion to erode the mineral deposits. At these

calculated rates, emergence would have occurred at ~ 1.3 Ma which would result in a further 1 Ma of exposure in subaerial conditions.

The *globigerina* bearing limestone that overlies mineralisation at Kali Kuning (200 m above sea level at present) yields a biostratigraphic age of between 5.2-3.9 Ma (Herrington, 1993). Based on planktonic / benthic assemblages, this lithological unit is likely to have formed at depths of at least 2000 m and possibly considerably deeper (Murray pers com. 1999). Calculations show that uplift rates of Wetar, based on these parameters are 42-57 cm/ka^{-1} which are consistent with those calculated for Timor in the outer arc (De Smet, 1989; Audley-Charles, 1986b) Chapter 2. These calculations however are based on movement over ~ 4-5 Ma, it is probable that Wetar experienced pulses of rapid uplift over shorter time spans as indicated by islands of the outer Banda arc where rates of 500 cm/ka^{-1} have been calculated (De Smet, 1989). Based on these uplift rates, the area of Kali Kuning would have emerged from the Banda Sea between 0.5 to 0.4 Ma. However, the central spine of Wetar (1500 m, present height) using an average uplift rate of ~ 50 cm/ka^{-1} indicates first emergence from the Banda Sea at ~ 3 Ma. Perhaps the last 40,000 years of uplift are the most important with emergence of the volcanic edifice occurring very recently. Considering the friable nature of the mineral deposits on Wetar and the amount of rainfall of between 1-3 m per year, (Heesterman, 1992) prolonged exposure of the deposits would result in complete erosion especially at Lerokis 4 where there is no stratigraphic cover. Depths of formation will be discussed further in relation to fluid inclusion microthermometry, Chapter 6 and in the discussion, Chapter 9.

3.5 SUMMARY

Mineralisation is spatially related to felsic volcanics and breccias that overly basalts and andesites, the deposits (massive sulphide mounds + Au bearing barite ores) are present at the margins of the dome structures related to NW/NNW trending fault structures. The barite ores onlap and overly the massive sulphide mounds and are underlain by extensive stockwork zones with varying amounts of mineralisation and alteration.

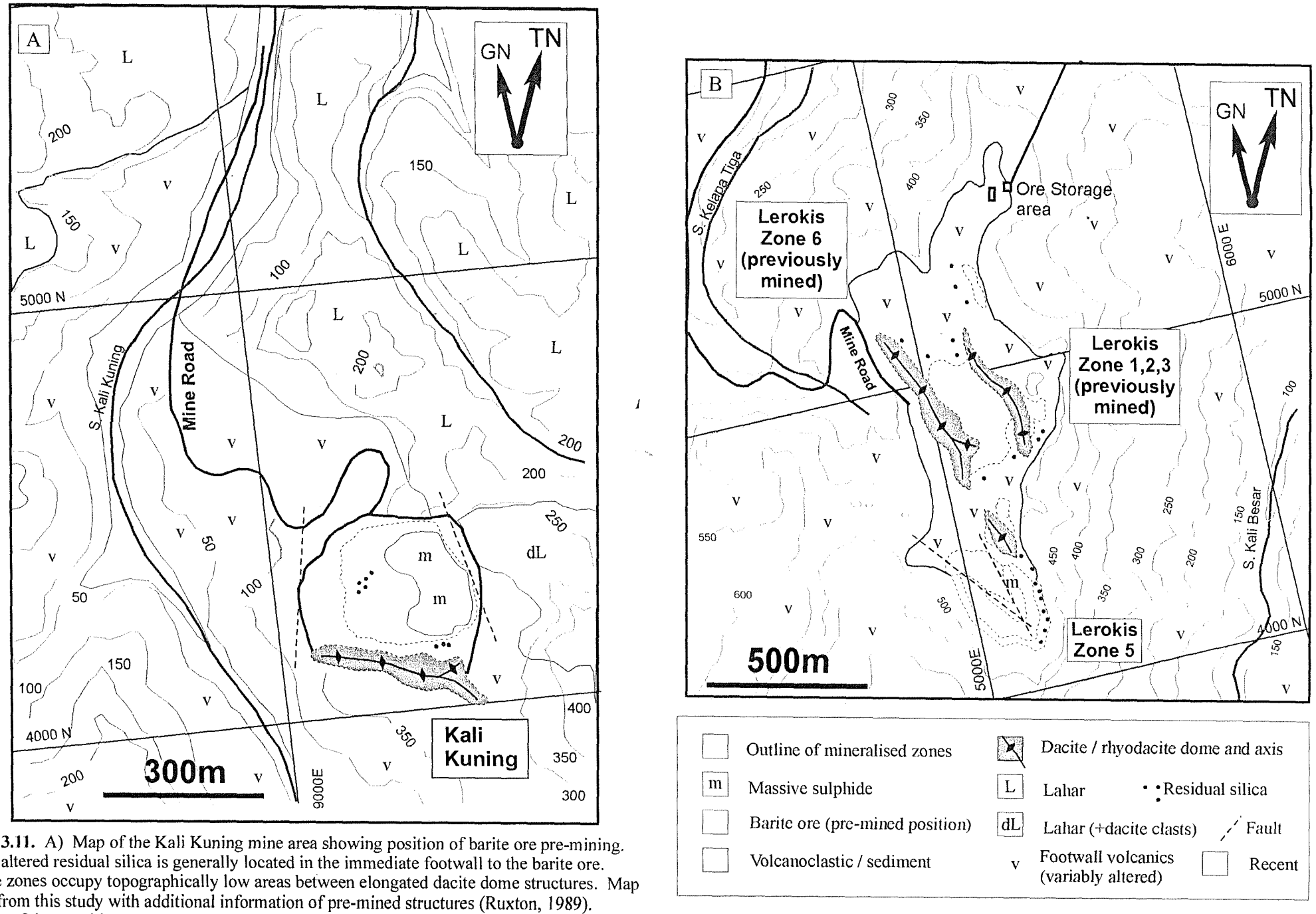


Figure 3.11. A) Map of the Kali Kuning mine area showing position of barite ore pre-mining. Highly altered residual silica is generally located in the immediate footwall to the barite ore. The ore zones occupy topographically low areas between elongated dacite dome structures. Map drawn from this study with additional information of pre-mined structures (Ruxton, 1989). B) Map of the Lerokis mine area.

Chapter 4

HYDROTHERMAL ALTERATION

4.1 INTRODUCTION

Mineralised systems during their formation produce characteristic alteration assemblages and haloes as a result of extensive fluid / rock interaction. This study employs X-ray diffraction (XRD) and Fourier Transform Infra-Red (FTIR) methods to:

1) Map the extent of the hydrothermal alteration around the ore deposits preserved at Kali Kuning, Lerokis Zone 4 and 5.
2) Characterise the alteration assemblages.

The techniques identify and characterise the alteration assemblages thus giving valuable information on the pH and temperature of the mineralising fluids.

In addition, selected samples from around the ore deposits with be analysed by XRF for major and trace element geochemistry, these samples will be compared to unaltered samples discussed in Chapter 3 thus further constraining the footwall volcanic stratigraphy to the mineralisation.

4.2 PREVIOUS WORK

Previous studies on Wetar Island, Herrington (1995) have revealed alteration zonation around the exploited ore deposits (Sewell and Wheatley, 1994b; Herrington, 1995). The reported alteration mineralogy includes kaolinite-illite-montmorillonite-sericite assemblages, (Sewell and Wheatley, 1994b) however chlorite-dickite-pyrophyllite-cristobalite-anatase and alunite are reported from other mineralised areas on Wetar (Herrington, 1995, 1996; Sillitoe, 1997; Booler, 1997).

Table 4.1. Alteration mineralogy of the Wetar Island deposits. Phases identified by XRD and FTIR study. (refer to Appendix C for alteration spectra and XRD traces).

Sample	Location	Deposit / Zone	XRD Results			FTIR Results		
			Major	Minor	Trace	Major	Minor	Trace
100118	64	Kali Kuning	op A	ja		n.d.		
100129	66	Kali Kuning	op A, qz					
111904	306	Kali Kuning	qz	ja		n.d.		
111907	309	Kali Kuning	op A, qz			n.d.		
111908	310	Kali Kuning	op A, qz			n.d.		
111910	312	Kali Kuning	op A, qz			n.d.		
111912	314	Kali Kuning	ja, goe	hem	sme	n.d.		
111914	316	Kali Kuning	chl		qz	n.d.		
111917	319	Kali Kuning	ja	op A	qz	op, qz		
111918	320	Kali Kuning	qz, trid			op, trid		
111919	321	Kali Kuning	qz, trid	ja	chl, ill	qz	ja	
111938	91	Kali Kuning	ill, sme			n.d.		
111939	231	Kali Kuning	n.d.			op	trid	
111941	300	Kali Kuning	op A			n.d.		
111945	301	Kali Kuning	op A			n.d.		
096853	74	Kali Kuning	op A, qz			n.d.		
096854	74	Kali Kuning	op A, goe		hem	n.d.		
096856	235	Kali Kuning	n.d.			qz, op		
096863	235	Kali Kuning	n.d.			op		
096865	55	Kali Kuning	op A, qz			n.d.		
096884	86	Kali Kuning	op A, qz			op A, qz		
096924	239	Kali Kuning	n.d.			qz		
096927	240	Kali Kuning	n.d.			qz		
097156	243	Kali Kuning	n.d.			ill	sme	
097157	244	Kali Kuning	n.d.			sme	ill	
097158	245	Kali Kuning	n.d.			op, qz	ill	
097159	246	Kali Kuning	n.d.			ill		
097160	303	Kali Kuning	op A	ill		n.d.		
097161	304	Kali Kuning	qz, op A	chl		n.d.		
097214	KKD058 @ 51m	Kali Kuning	ca	kao, sme	ill	ca		
097217	KKD058 @ 90m	Kali Kuning	ca	chl, sme	ill	ca	mont	
097220	KKD058 @ 92m	Kali Kuning	op A (qz)			op, trid	qz	
097223	KKD058 @ 125m	Kali Kuning	n.d.			chl, ill		
097226	KKD058 @ 160m	Kali Kuning	n.d.			qz, ill	mont	pyr
097231	KKD031 @ 37m	Kali Kuning	op A, qz			op, qz		
097232	KKD031 @ 39m	Kali Kuning	op A, qz			op, qz		
097234	KKD031 @ 43m	Kali Kuning	n.d.			qz	ill	alu, pyr
097235	KKD031 @ 46m	Kali Kuning	n.d.			ill, mont		
097236	KKD031 @ 50m	Kali Kuning	chl, sme		mg ca	mont	dick	
097237	KKD031 @ 56m	Kali Kuning	n.d.			chl, mont		
097239	KKD031 @ 70m	Kali Kuning	sme	chl		mont, chl	ill	
097240	KKD049 @ 5m	Kali Kuning	ba,	ill, sme	kao	ill, mont	ba	
097241	KKD049 @ 7m	Kali Kuning	n.d.			qz, op		
097243	KKD049 @ 21m	Kali Kuning	qz	ill, sme	kao	qz		alu
097245	KKD049 @ 26m	Kali Kuning	qz	trid	he	qz, op		
097249	KKD049 @ 57.5m	Kali Kuning	n.d.			ill, sme		
097253	KKD049 @ 62m	Kali Kuning	alu, ill			n.d.		
097259	KKD049 @ 73m	Kali Kuning	chl, ill	sme	mg ca	n.d.		
111923	171	Lerokis zone 5	qz, ill			n.d.		
111924	172	Lerokis zone 5	qz, op A			n.d.		
111926	174	Lerokis zone 5	qz	kao	ill	n.d.		
111927	175	Lerokis zone 5	qz, op A		kao	n.d.		
111928	176	Lerokis zone 5	kao			n.d.		
097029	LKD042 @ 68.5m	Lerokis zone 6	ill	kao		ill	mont	
097030	LKD042 @ 69m	Lerokis zone 7	ill, pyr			pyr	ill, mont	
097031	LKD042 @ 72m	Lerokis zone 8	ill	pyr	kao	ill, mont	kao	
097034	LKD042 @ 79.3m	Lerokis zone 9	kao, chl	ill	sme, he	kao, ill		mont

097046	LKD042 @ 141m	Lerokis zone 10	chl	ill		chl, ill	phy	
097063	LKD043 @ 44.9m	Lerokis zone 11	qz, ill	sme	sme, he	ill, mont	qz	
097071	LKD043 @ m	Lerokis zone 12	ill					
097072	LKD043 @ 57.4m	Lerokis zone 13	ill		kao	n.d.		
097077	LKD043 @ 57.4m	Lerokis zone 14	ill					
097078	LKD043 @ 72.5m	Lerokis zone 15	chl, ill			ill, chl		
097080	LKD043 @ 85m	Lerokis zone 16	ill	chl	kao	chl, ill		pyr
097093	LKD043 @ 116m	Lerokis zone 17	n.d.			kao, ill	chl	
097100	LKD043 @ 146m	Lerokis zone 18	chl	ill		chl	ill, mont	
097106	LKD043 @ 210m	Lerokis zone 19				chl		
097111	LKD044 @ 23.7m	Lerokis zone 20	n.d.			ill	kao	
097121	LKD044 @ 42m	Lerokis zone 21	n.d.			op, qz		
097130	LKD044 @ 85m	Lerokis zone 22	ill	kao, sme		ill	mont	
097134	LKD044 @ 99.5m	Lerokis zone 23	n.d.			kao, ill		mont
097201	305	Lerokis zone 5	qz, ill	op A, ja		n.d.		
097146	LKD044 @ 184m	Lerokis zone 6	n.d.			chl, kao	Ill	
097148	LKD044 @ 207m	Lerokis zone 7	n.d.			chl	mont	
099905	7	Lerokis zone 5	kao	ill		n.d.		
099910	11	Lerokis zone 5	ill, sme	ja		n.d.		
099913	13	Lerokis zone 5	op A			qz, op		
099926	26	Lerokis zone 5	op A (qz)			n.d.		
099932	24	Lerokis zone 5	kao	ill, sme	ja	n.d.		
099935	35	Lerokis zone 5	ill			ill		mont
099936	35	Lerokis zone 5	qz, ill	sme	goe	n.d.		
111929	216	Lerokis zone 4	op A			op, qz		
111932	218	Lerokis zone 4	op A			op, qz		
111933	215	Lerokis zone 4	ja			ja		
111934	217	Lerokis zone 4	op A			op	trid	
111935	136	Lerokis zone 4	op A					
111958	138	Lerokis zone 4	ill	ja	goe	ill		op A
111962	139	Lerokis zone 4	qz, ill	sme	chl	qz		alu
111965	140	Lerokis zone 4	op A			op	trid	
111966	141	Lerokis zone 4	op A, qz		ill	op, qz		
111969	143	Lerokis zone 4	op A, qz			op, qz		
111971	247	Lerokis zone 4	n.d.			op, qz		alu
111972	142	Lerokis zone 4	op A, qz			op, qz		
111973	248	Lerokis zone 4	n.d.			op, qz		
111978	249	Lerokis zone 4	n.d.			op, qz		
111983	153	Lerokis zone 4	op A		tri	op		
111985	154	Lerokis zone 4	chl	ill	sme	chl, kao	ill, mont	
111987	155	Lerokis zone 4	chl	ill	sme	ill	mont	
111991	157	Lerokis zone 4	chl	ill		chl, ill		dick
087072	162	Lerokis zone 4	n.d.			ill, mont		
096948	129	Lerokis zone 4	n.d.			ba		

Footnote: Sample location are given on Figures 4.2C, 4.3, 4.5, 4.6 and 4.8C.
n.d. = not determined, op A = opal A, ba= barite, qz = quartz, ill = illite, ja = jarosite, goe = goetite,
he = hematite, sme = smectite, kao = kaolinite, trid = tridymite, chl = chlorite, alu = alunite,
pyr = pyrophyllite, mont = montmorillonite, dick = dickite, mg ca = mg calcite.

4.3 SAMPLE SELECTION AND ANALYSIS

A total of one hundred and eleven altered samples collected from the footwall of the Kali Kuning, Lerokis Zones 4 and 5 orebodies and surrounding areas have been systematically analysed using FTIR / XRD methods. Results will determine alteration assemblages associated with mineralisation and identify zonation of alteration around the deposits. The methods used, analytical procedures and spectra are given in appendix C.

4.4 RESULTS

Diffractograms were interpreted qualitatively and the results are tabulated in Table 4.1 Field mapping around the ore deposits of Kali Kuning, Lerokis Zones 4 and 5 has identified intense zones of alteration around these systems related to mineralisation. Extensive gossanous areas surround all three systems as a product of sulphide oxidation, Figure 4.1 A-C.

Zones of alteration were identified and divided on the basis of major phases identified, these alteration zones attributed to the Wetar Island data are documented along with their associated mineral assemblages in Table 4.2 below. XRD analysis of twenty seven samples exhibited a broad symmetrical peak indicating an amorphous silica phase, these traces were matched to a standard / reference spectra and have been designated in this study as opal A. FTIR study of the same samples yielded spectra similar opal A / microcrystalline silica, see Appendix C.

Table 4.2. Classification of alteration zones, modified from Hedenquist, (1987); Thompson et al., (1999).

ALTERATION ZONE	MINERAL ASSEMBLAGE
Advanced Argillic	Quartz, dickite, pyrophyllite, alunite, residual silica.
Silicification/Quartz-sericite	Microcrystalline silica / opal A, quartz, cristobalite, trydimite, sericite.
Argillic	Quartz, illite, smectite, kaolinite.
Propylitic	Chlorite, smectite.

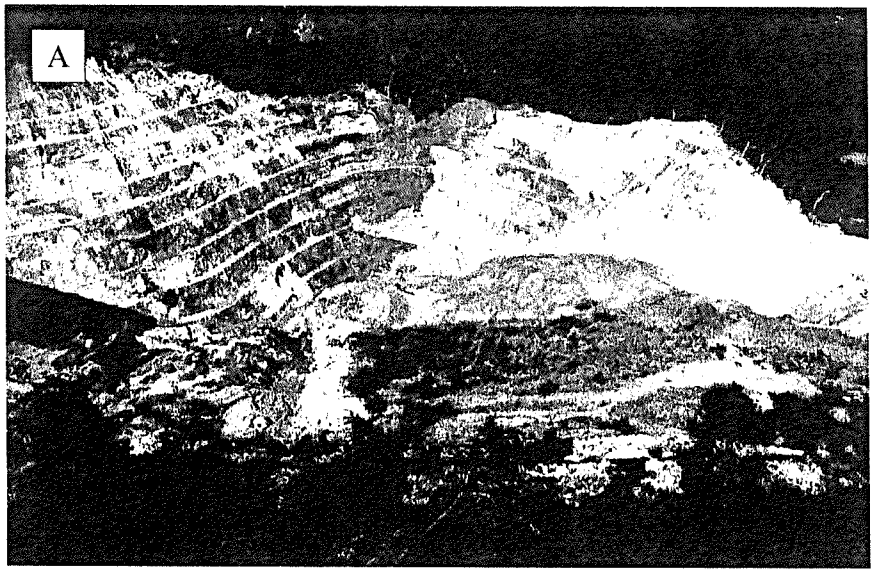






Figure 4.1. Extensive Gossan around the Wetar deposits. A) View approximately Southwest from the upper most exposure of the Kali Kuning sulphide mound toward the propylitic altered section of the footwall. B) View South of the Lerokis Zone 5 sulphide mound with surrounding altered footwall, height of the sulphides are ~12m. C) View East of the central part of the Lerokis Zone 4 deposit, note the author is present for scale on a fragment of fe-oxide/barite structure, right of centre. All three pictures show the position of the pre-mined barite ore deposits.

4.4.1 Kali Kuning

A broad zonation is evident around the massive sulphide and remaining barite ore, chloritic alteration is present (propylitic zone) in two areas of the footwall in the west of the pit and extending west and north (Figure 4.2A and 4.2C) and with increasing depth (Figure 4.3). The intensity of alteration increases towards the sulphide body where an illite-smectite assemblage is present (argillic zone) before passing in to a zone of intense silicification (quartz-sericite zone) closest to and surrounding the sulphide mound (Figure 4.2B and thin sections 4.4A and B). Figure 4.2C shows a geological plan of the Kali Kuning orebody with the alteration zones. The schematic corresponding cross-section, Figure 4.3 shows the location of the three boreholes beneath the orebody (KKD 031, 049 and 058) and illustrates that a systematic alteration pattern is present. Generally, with increasing depth, propylitic zones are observed comprising dominantly chlorite and quartz, sample 111914, location 316 illustrates this assemblage, see thin section (Figure 4.4C and D). Advanced argillic alteration is evident in core KKD 049 at a depth of 62 m by the presence of alunite which is present together with illite (determined by FTIR and XRD). Interestingly, intense silicification is present in close proximity to the inferred NNW trending fault interpreted to be the principal conduit for fluid flow and focus of mineralisation. The results indicate that the associated hydrothermal fluids have produced a zoned pattern of alteration around the Kali Kuning deposit. Hydrothermal breccias are more extensive to the south of the prospect where as residual silica is mapped within the footwall around locations 70 in the west and 56 in the south in close proximity to the sulphide / footwall contact (see Figure 4.2 and map insert sheet 2A).

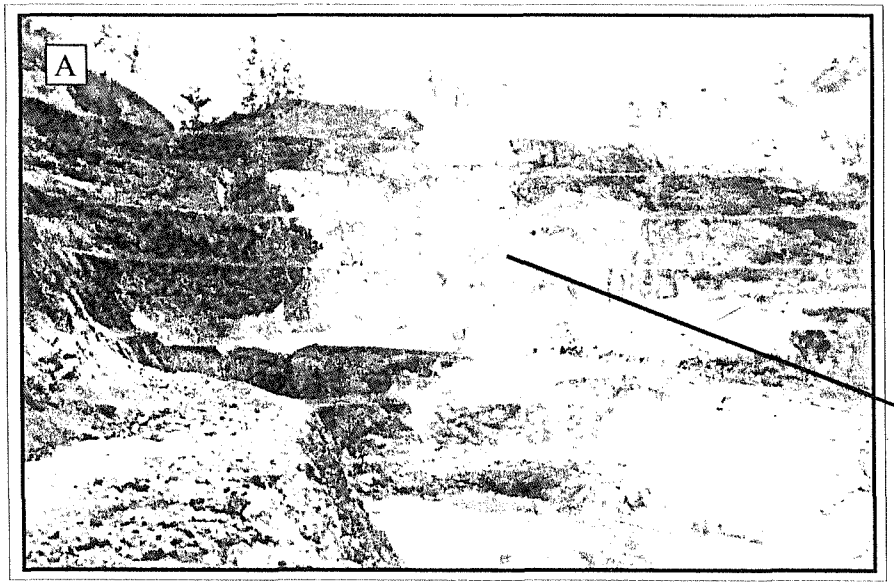
4.4.2 Lerokis Zone 5

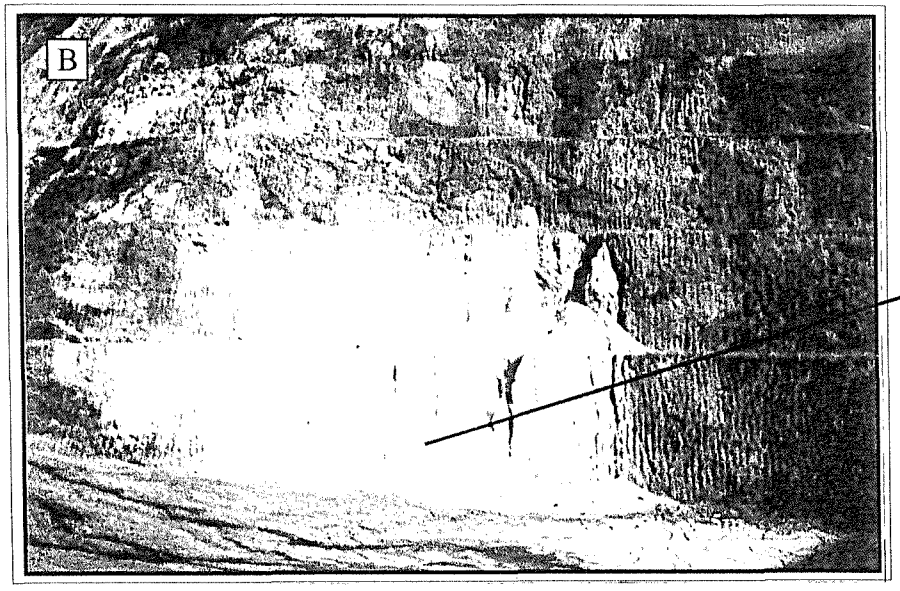
Alteration around the orebody is shown in Figure 4.5 and 4.6. The massive pyritic body is surrounded by intensely hydrothermally altered host volcanics, however zonation around this orebody is not as clear as the case for Kali Kuning. On Figure 4.5, areas of both silicification and extensive argillic alteration are evident, the argillic alteration is focussed around the margin of the sulphide body and the two cemented Fe-oxide barite structures. The outermost areas of the deposit exhibit argillic assemblages dominantly comprising quartz-kaolinite-illite, both XRD and FTIR

results suggest that kaolinite is more dominant here than at Kali Kuning. In cross-section, (Figure 4.6) quartz-illite-kaolinite alteration assemblages can be seen to dominate and (propylitic) chlorite alteration is present at depth. The three boreholes (LKD 042, 043 and 044) all show that alteration beneath the mineralisation become increasingly chloritic with depth, these deeper samples are brecciated generally and are associated with hematite and pyrite veining (Figure 4.7A). The most intense alteration is associated with the stockwork zone that directly underlies the sulphide mound, where rocks are white, fine grained but still preserve in some areas primary vesicles that are generally less than 1 cm (Figure 4.7B). Of important note is the presence of advanced argillic alteration assemblages within the LKD 042 stockwork zone where a zone of illite + pyrophyllite alteration is present immediately below the sulphide mound. The development of residual silica within the footwall is more prominent at than Kali Kuning and can be traced to some degree surrounding the entire zone (Figure 4.5). Sample 097104 (Figure 4.4E and F) contains micro-veinlets of muscovite cross-cutting chlorite-quartz altered footwall volcanics.

4.4.3 Lerokis Zone 4

The aerial photograph (Figure 4.8A) illustrates the intense alteration associated with mineralisation. The analysis of the collected samples confirms that of a previous study by Herrington, (1995) where a propylitic zone of alteration passes into an argillic zone (quartz-illite rich) before passing into a silicification zone (opal A-quartz). A small area of advanced argillic alteration is evident proximal to the centre of mineralisation and is expressed as a zone of residual silica (Figure 4.8B and C). With a slight increase in distance from the barite ore zone (~25 m), residual silica clasts are present but occur within a matrix of kaolinite, (Figure 4.7C). Figure 4.8C illustrates the results and their spatial relationship to the position of the barite ore, jarositic veins are also preserved proximal to the ore zone where they are up to 10 cm width (Figure 4.7D). At location 139, (sample 111962) fine-grained smectite alteration is evident in thin section (Figure 4.4G and H) and is also confirmed by XRD analysis. Bore-hole samples were unavailable from this Zone to test the alteration assemblages at depth. In more distal areas from the centres of mineralisation, the coastal andesite exhibits a chloritic margin, location 109, Figure 4.7E and thin section 4.7F).





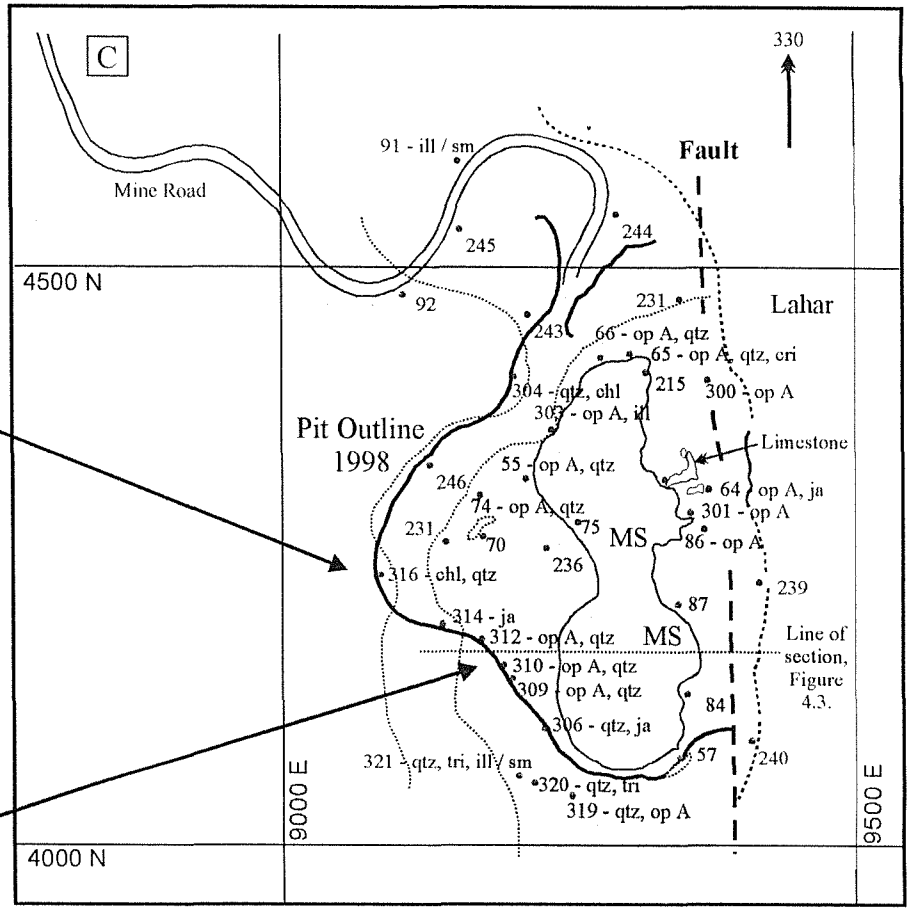


Figure 4.2. Alteration zonation around the Kali Kuning orebody.
A) Zone of propylitic alteration within the footwall, zone is ~ 25 m in width. B) Zone of more intense alteration in close proximity to the sulphide mound. C). Alteration zoning around the Kali Kuning orebody based on this study, grid interval = 500 m. Red spots indicate sample location, for sample description refer to table 4.1, for spectra refer to Appendix C, for key see Figure 4.3.

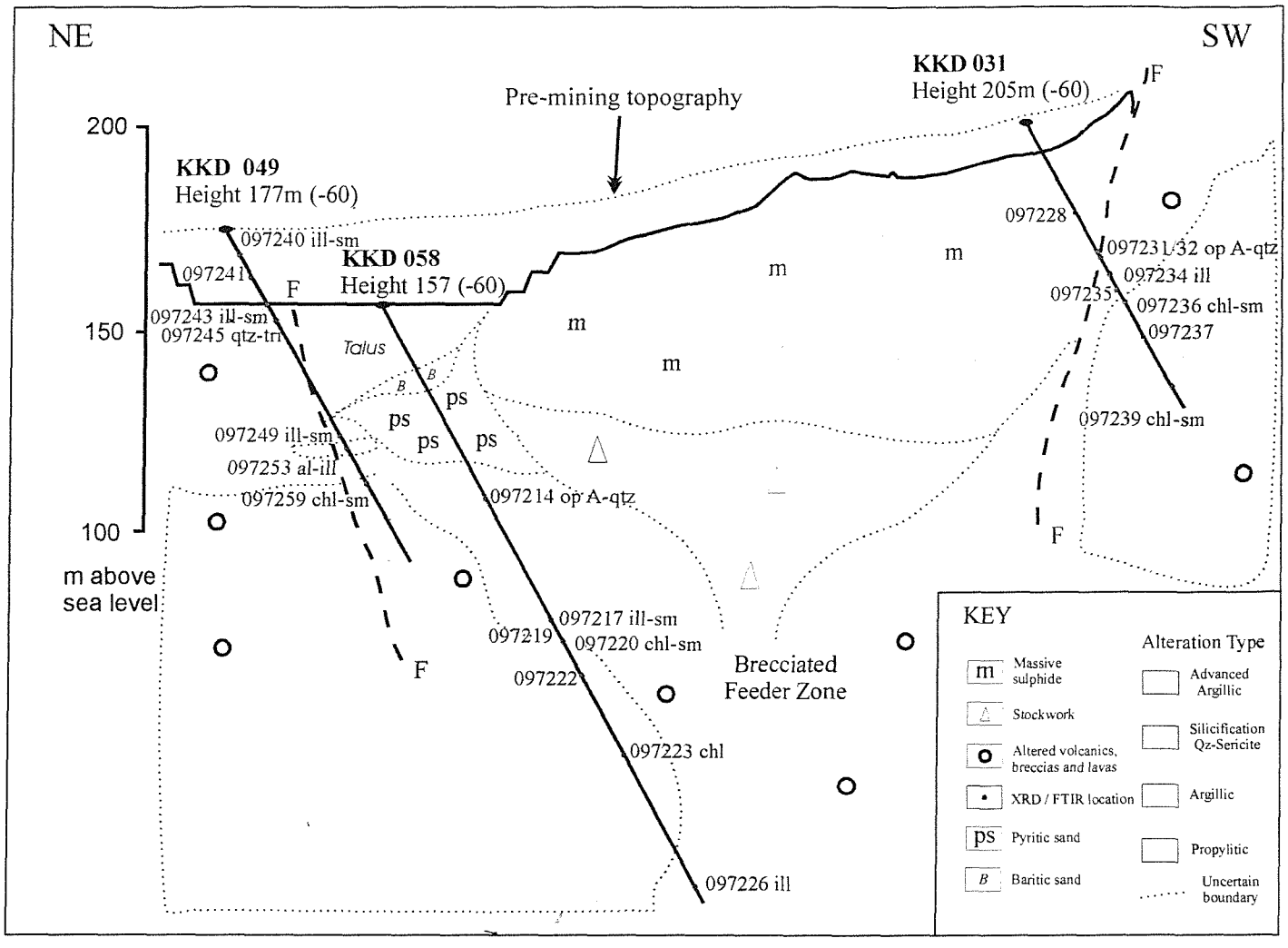


Figure 4.3. Cross section through the Kali Kuning orebody showing sample locations, propylitic alteration is dominant at depth and locations laterally away from the sulphide mound. Faults added from mine cross sections.

Figure 4.4

A. Fine-grained quartz alteration, (XPL) sample 111918 location 320 Kali Kuning, field of view 4.5 mm.

B. Fine-grained silicification of sample 111907, location 309. Vesicles are elongate and infilled with quartz (XPL), field of view 4.5 mm.

C. Propylitic alteration of vesicular footwall volcanics, Kali Kuning locatio 316. Vesicles are infilled with quartz and pyrite (not shown), field of view 4.5 mm (XPL).

D. Same photomicrograph as C, (PPL), field of view 4.5 mm.

E. Sample 097104, fine-grained chloritic alteration of stockwork volcanics and micro veinlets of sericite (PPL), field of view 4.5 mm.

F. Same as E, (XPL) field of view 2.5 mm.

G. Fine-grained smectite alteration of feldspars in sample 111962, field of view 4.5 mm (XPL).

H. Fine-grained smectite alteration, field of view 4.5 mm (PPL).

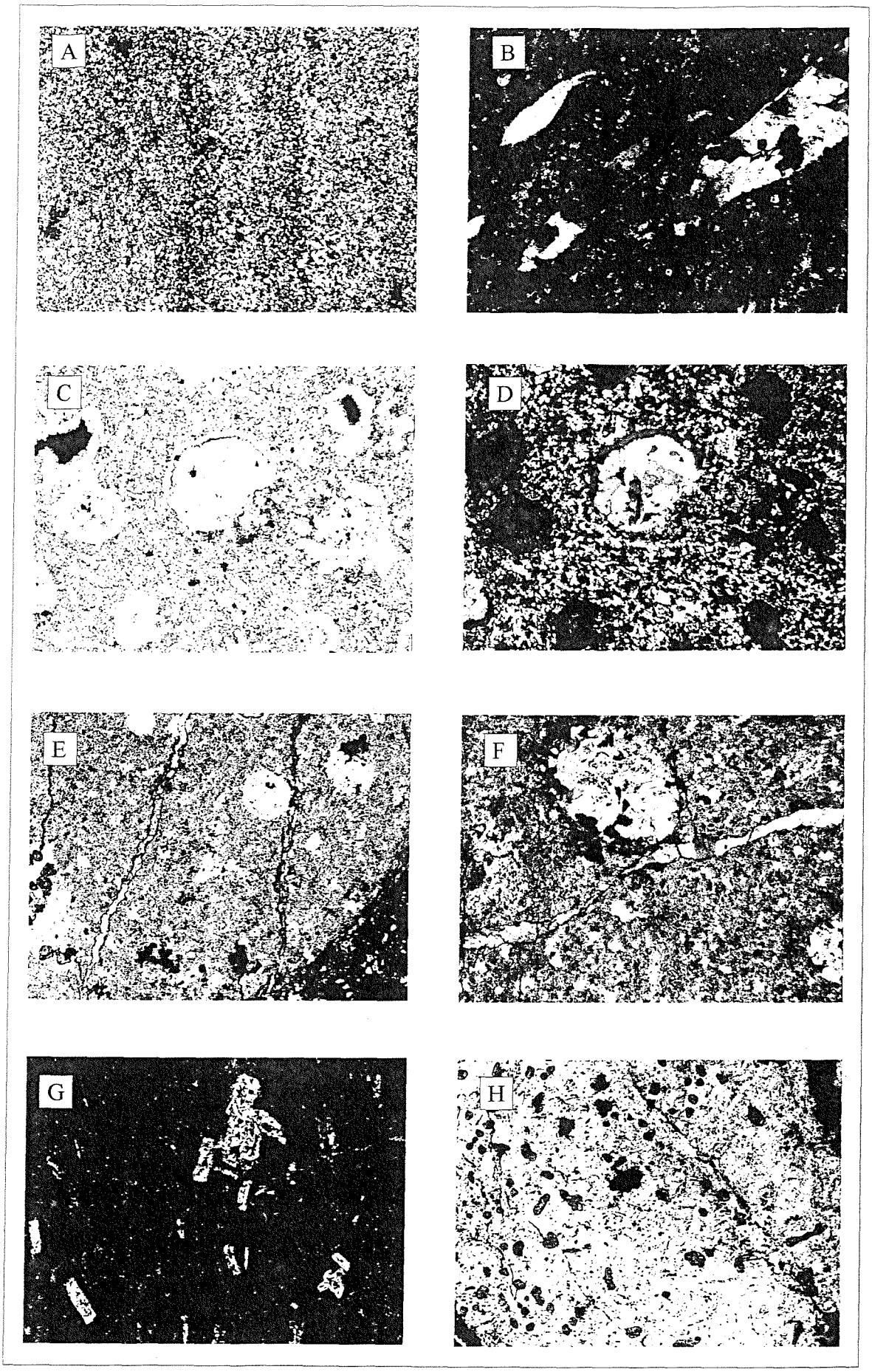


Figure 4.4. Thin section microphotographs of altered host volcanics.

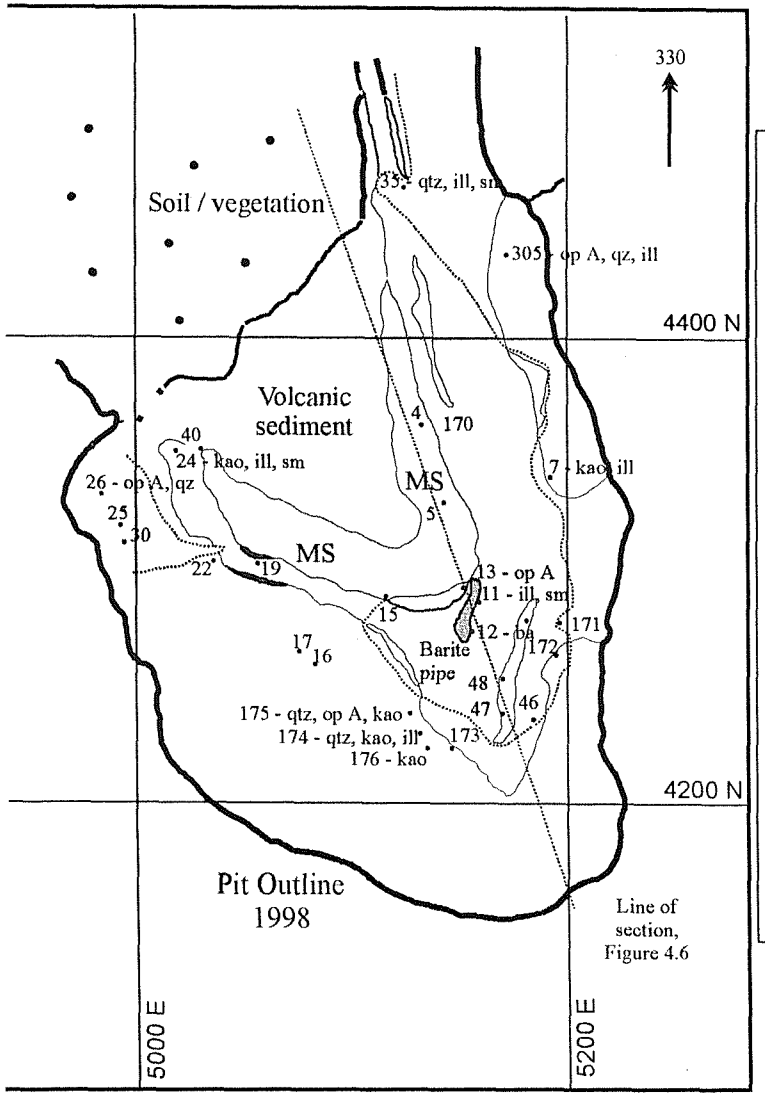


Figure 4.5. Alteration zonation around the Lerokis Zone 5 orebody, this study. Sample locations are given along with major alteration assemblages, MS = massive sulphide.

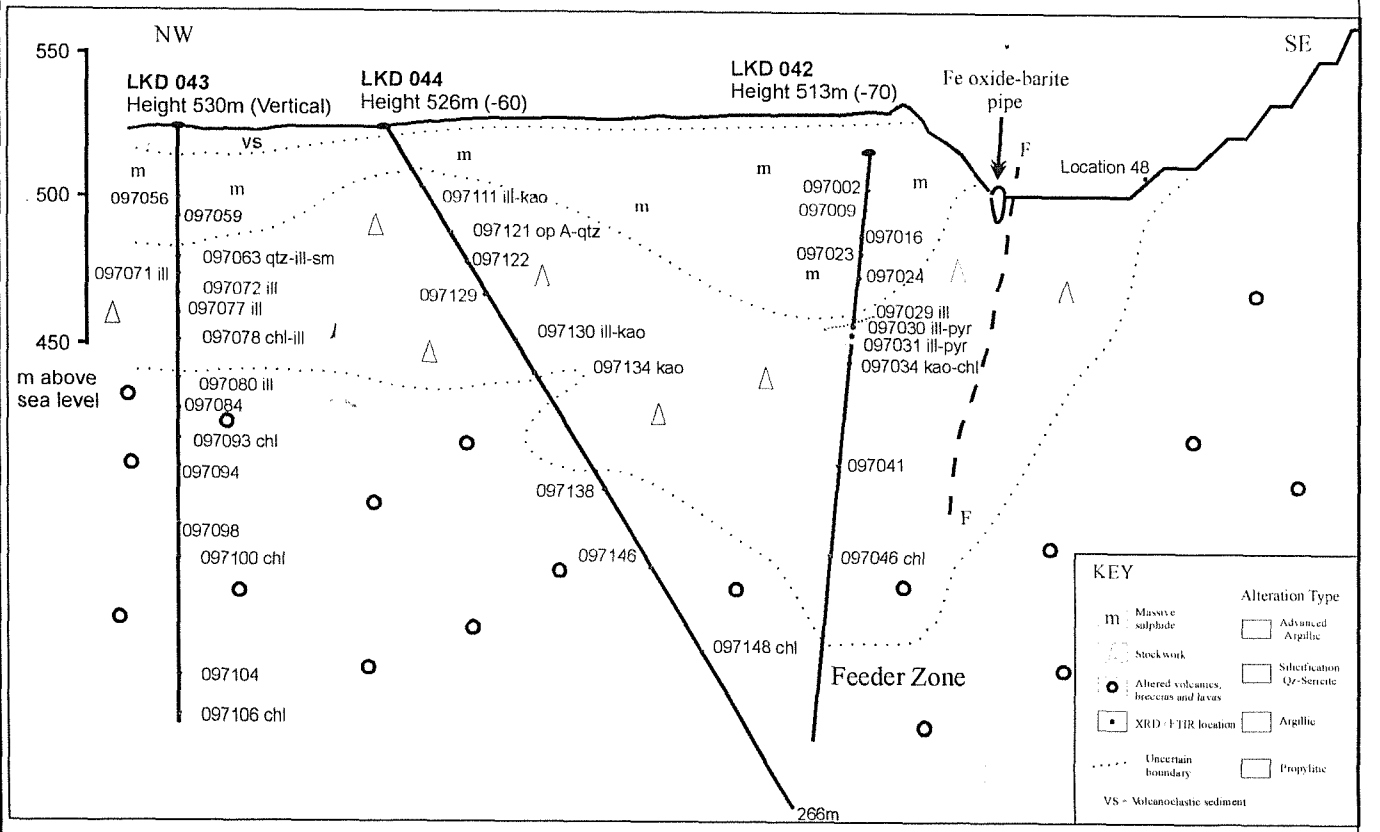


Figure 4.6. Cross section through the Lerokis Zone 5 orebody, the line of section is illustrated on Figure 4.5. Propylitic alteration assemblages are present at depth beneath the sulphide mound and are related to the feeder zone and underlying stockwork.

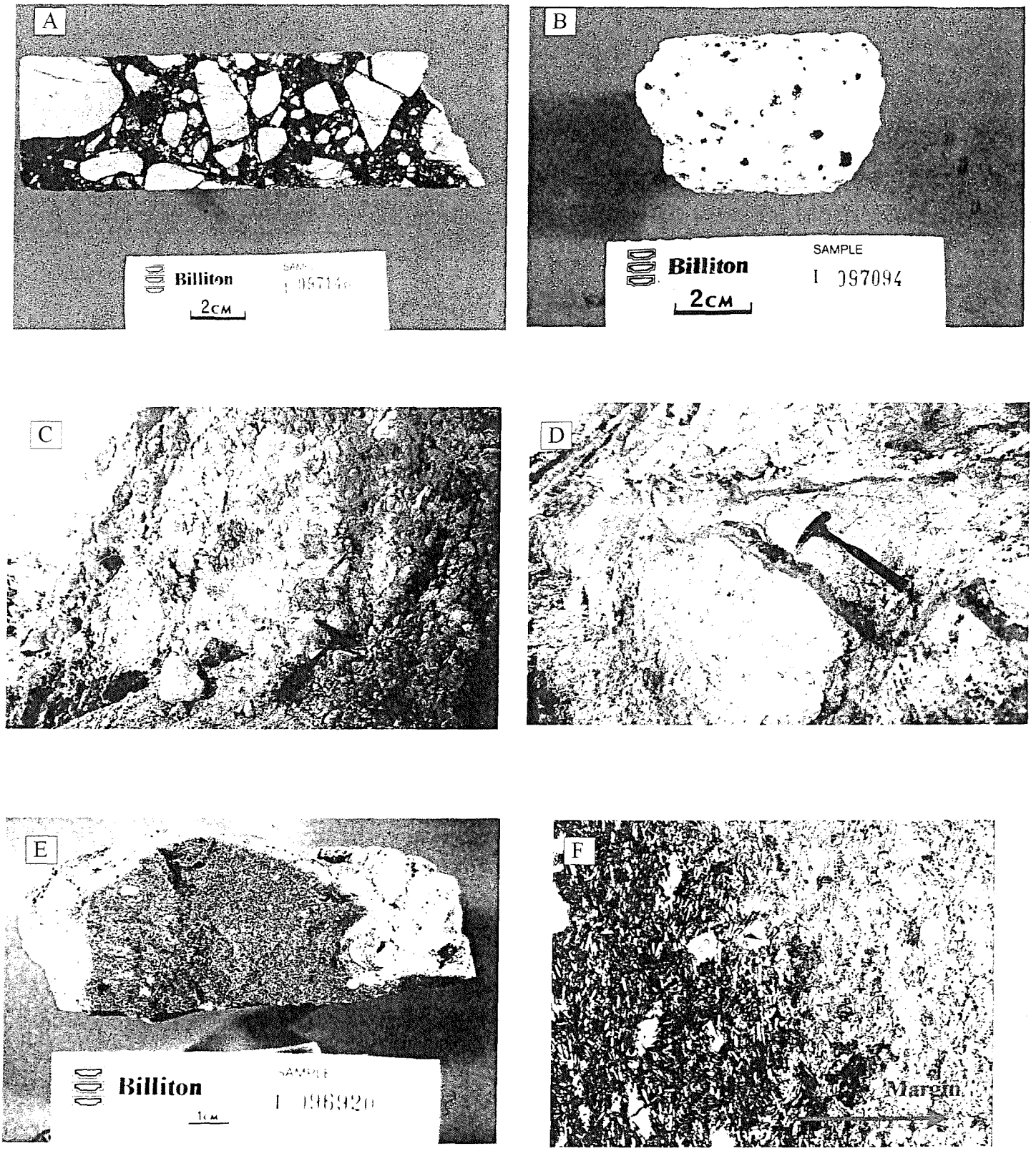
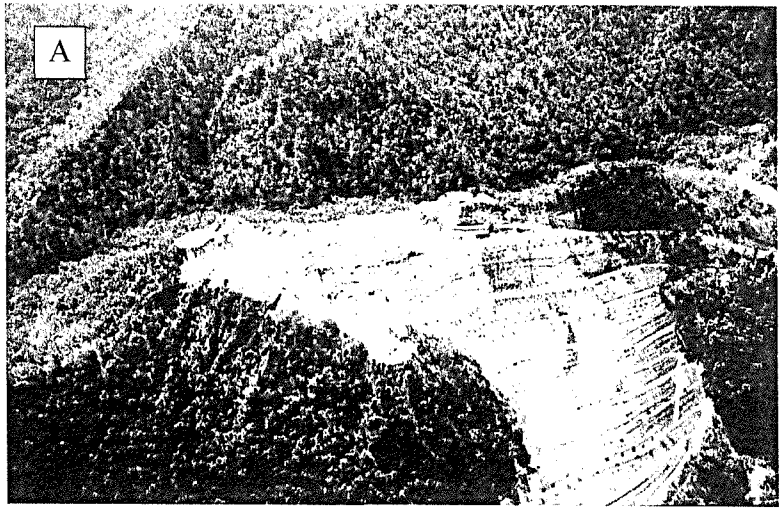
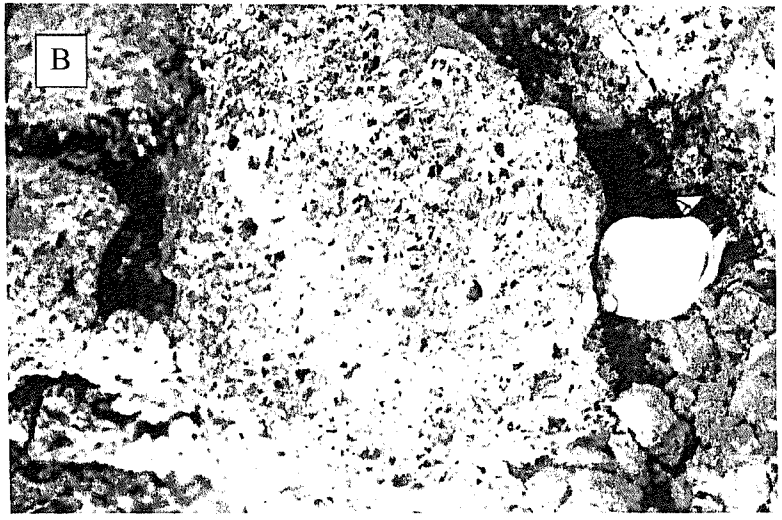


Figure 4.7. A) Brecciated, chloritic altered footwall volcanic from Lerokis Zone 5, sample 097146, see Figure 4.6 for location. B) Vesicular, intense altered footwall volcanic, Lerokis Zone 5, the majority of the vesicles are infilled with quartz. C) Residual silica from Lerokis Zone 4 surrounded by a kaolinite matrix. D) Jarosite vein from the Lerokis Zone 4 deposit, the vein is ~5cm in thickness. E) Vesicular coastal andesite, see Figure 3.4 for location. F) Chloritic altered margin of sample 096920, vesicles are empty, field of view on thin section photomicrograph is ~5mm.





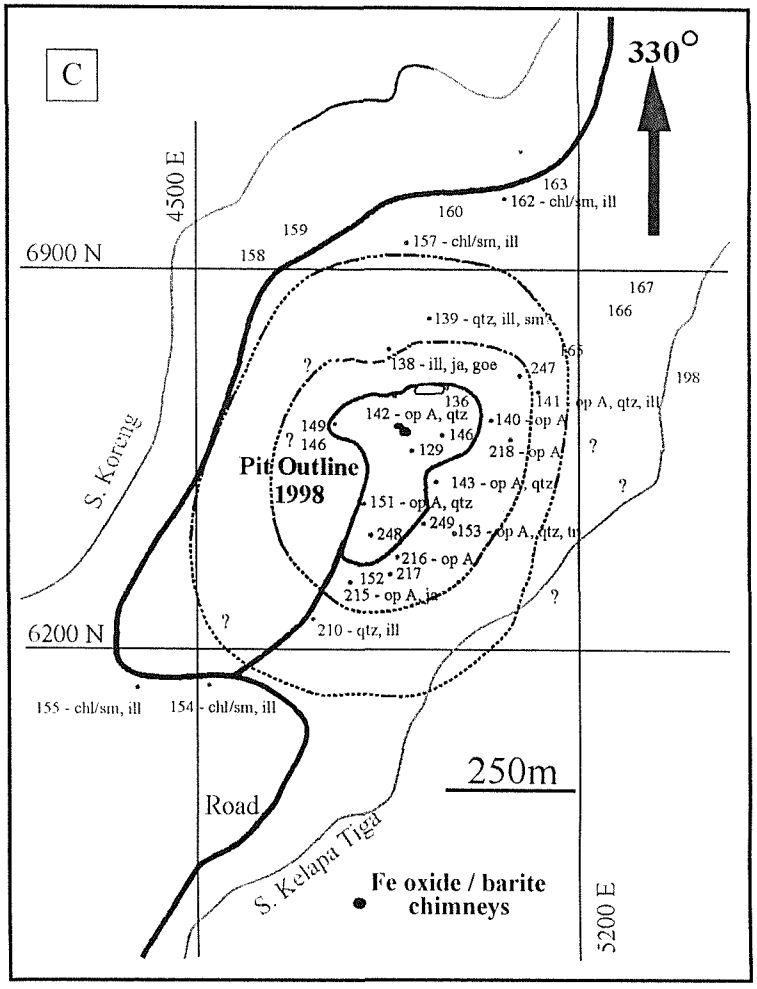


Figure 4.8. Alteration around the Lerokis Zone 4 orebody. A) Aerial view of Lerokis Zone 4, looking approximately Southeast. Extensive alteration around the deposit is evident. B) A sample of residual silica collected from the immediate footwall to the barite ore zone (sample 111935, location 136). C). Alteration zonation around he Zone 4 orebody based on this study. Same key as for Figures 4.2, 4.3, 4.5 and 4.6.

Figure 4.9 shows a cross-section through Lerokis Zone 4 and illustrates alteration spectra from this study in relation to defined alteration zoning.

4.5 ALTERATION GEOCHEMISTRY / PETROCHEMISTRY

Due to the intense hydrothermal alteration around the Wetar Island mineralisation, the identification of original protolith is extremely difficult. Therefore seven samples have been chosen from around the deposits for comparison to four unaltered samples already discussed in Chapter 3. Chosen samples were crushed and made into pressed powder discs and beads before analysis of major and trace elements by XRF at the University of Southampton. For techniques used and analytical conditions refer to Appendix C, results from the study are presented in Table 4.3.

The four unaltered samples all plot within the sub alkaline field of the SiO_2-total alkali plot, Figure 4.10A. The clast from the overlying debris flow at Kali Kuning (Figure 3.9A) plots within the basaltic-andesite field, the plot also confirms the presence of andesites located on the north coast and Lerokis road. The post-mineralisation dacite flow collected at Meron along with the other samples plot within the medium to high-K field of the K_2O-SiO_2 plot, Figure 4.10B.

The IUGS plutonic classification of the intrusive sample collected from the S Kali Lurang River section (Figure 4.10C) confirms the presence of high-level syeno-granite intrusives spatially related to the areas of principal mineralisation (Figure 3.4). The lahar clast collected from the Kali Kuning road section (096926) is more mafic than the other samples in the area, Table 4.3 and may record a lithology that underlies the mine sequence from elsewhere on the island.

Immobile elements considered to be unaffected by seafloor hydrothermal alteration include Al, Ti, Zr, Y, Nb and REE. These immobile trace elements are used to discriminate precursor lithology and magmatic affinity (Cann, 1970; Pearce and Cann, 1973; Winchester and Floyd, 1977; Maclean and Barrett, 1993). Plots of Ti vs. Zr, Nb/Y vs. Zr/TiO_2 and Zr vs. Y are given in Figures 4.11A and 4.11B. The Zr/TiO_2 vs. Nb/Y discrimination diagram illustrates that the Wetar Island altered host volcanics are dominantly andesites and andesite-basalts defining a group exhibiting wide ranges in both Zr/TiO_2 and Nb/Y (Figure 4.11A). The sample of residual silica

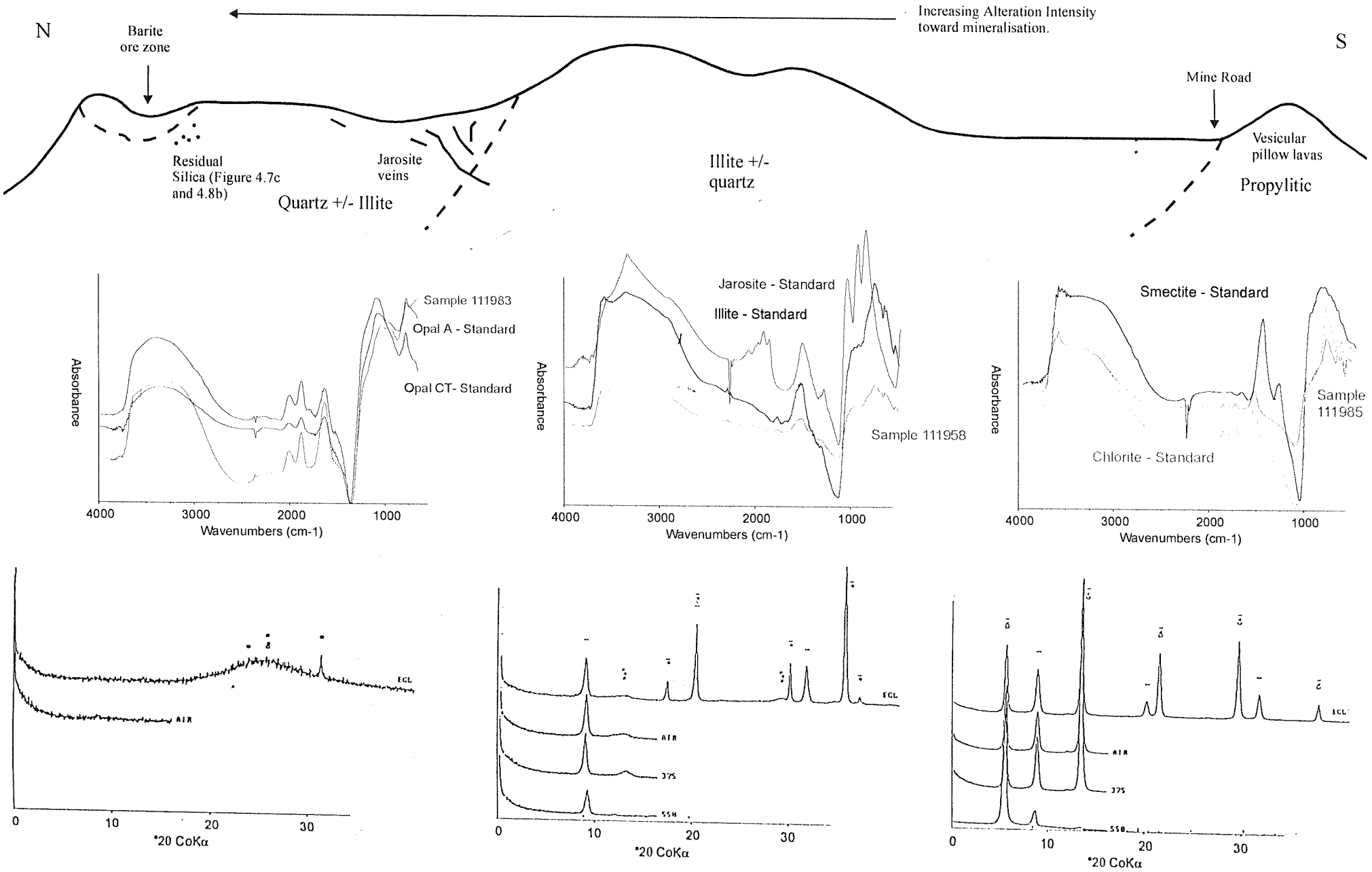


Figure 4.9. An idealized cross-section through the Lerokis Zone 4 ore body to illustrate key alteration zonation and associated FTIR spectra / XRD traces from this study.

Table 4.3. XRF data for unaltered and altered volcanics from Wetar Island.

Sample	096884	111001 Standard	097106	111994	096930	100129	097168	097167	096926	111935	096920	096927	111999	111914
Zone	KK		L5	-	KK	KK	Meron	Meron	-	L4	-	-	-	KK
Location	320		depth 210m	316	92	66	226	225	109	136	104	109	232	316
SiO2	76.879	52.872	68.06	62.839	65.312	96.811	69.341	68.43	54.109	99.179	59.888	76.906	76.154	66.865
TiO2	0.324	1.131	0.555	0.685	0.822	0.053	0.445	0.398	0.624	0.515	0.818	0.622	0.23	0.389
Al2O3	14.43	14.147	12.817	15.82	19.161	0.804	15.929	15.164	15.334	0.827	15.135	13.778	13.184	11.989
Fe2O3	1.777	13.998	9.929	6.069	1.567	1.405	3.492	3.906	7.188	0.252	10.277	4.063	2.392	11.324
MnO	0.027	0.217	0.096	0.173	0.01	0.005	0.052	0.08	0.156	0.005	0.157	0.052	0.035	0.041
MgO	1.027	4.724	5.856	1.785	0.396	0.04	1.573	1.394	3.375	0.043	3.273	0.313	0.449	10.085
CaO	0.945	9.714	0.165	4.995	0.17	0.083	2.986	3.631	7.162	0.036	7.546	0.113	2.423	0.072
Na2O	0.877	2.182	0.266	3.498	0.302	0.249	2.941	3.031	2.797	0.209	2.655	0.252	4.742	0.115
K2O	3.359	0.415	2.053	2.425	11.286	0.096	3.396	3.718	2.19	0.148	1.376	3.847	1.156	0.095
P2O5	0.02	0.09	0.05	0.17	0.02	0.01	0.1	0.1	0.11	0.01	0.07	0.02	0.04	0.03
SO3	0.11	0.11	0.21	0.11	0.14	0.1	0.13	0.14	0.14	0.13	0.13	0.12	0.11	0.27
CuO	n.d	n.d	n.d	n.d	n.d	n.d	n.d	n.d	n.d	n.d	n.d	n.d	n.d	n.d
BaO	n.d	n.d	n.d	n.d	n.d	n.d	n.d	n.d	n.d	n.d	n.d	n.d	n.d	n.d
ZnO	n.d	n.d	n.d	n.d	n.d	n.d	n.d	n.d	n.d	n.d	n.d	n.d	n.d	n.d
Sum	99.8	99.6	100.1	100.6	99.2	99.7	100.4	100	99.7	101.4	101.3	100.1	100.9	101.3

Element concentration data produced by Southampton's PW1400 XRF.
Concentrations expressed in wt%.

Sample	096884	111001 Standard	097106	111994	096930	100129	097168	097167	096926	111935	096920	096927	111999	111914
Rb	114.5	3.5	42.4	81.4	239.1	2.6	88.3	164.8	85.4	2.1	21.8	81.6	90.2	0.2
Sr	48.1	168	58.6	370.4	7.8	19.4	275.8	267.9	388.2	0.9	160.2	3.9	107.9	0.5
Y	43.3	22.9	21.7	32.6	19.5	0	24	27.3	30.4	10.5	23.3	13.7	17	8
Zr	176.3	43.5	90.9	133.2	77.6	39.5	171	153.7	127	67.1	71.2	59.7	118.2	42.7
Nb	9	2.9	5.8	10.4	5.5	5.3	21.1	18.5	11	4.9	5.3	4.2	7.4	4.1
Th	4.3	0	2.1	10.2	0	0	20.7	17.9	13.5	4.5	1.7	2.3	2.8	0
U	1.4	0	2	2.5	0	0	3.5	3.6	3.2	1.4	0	1	0.3	0.9
Pb	24.4	6	3.9	20	6.7	1365.9	30.2	29.3	21.6	50.7	9.9	11.3	16.5	56.4
Zn	506.4	97.4	1388.8	74.2	8	41	62.7	49.8	67.4	1.1	114.5	34	18.2	14.1
Ni	2.2	10.9	2.7	1.9	2.5	9.3	4.1	4.3	9.7	1.8	8.9	2.2	4.3	16.2
Ga	18	16.8	14.1	19.3	19.6	12.2	19.9	17.9	18.8	3.2	17.4	13.5	15.2	15.5
As	13.1	0.5	26.2	2.9	299.4	297.6	3.2	5.4	5.3	40.6	3.6	76.2	0	4.1
Cr	4.2	37.1	6.6	5.5	39.8	13.9	13.6	15.5	17	9.6	12.2	31.5	10.9	144.2
V	2	577.6	168.4	87.9	436.4	7.2	56.1	71.5	203.4	6.8	319.9	266.4	16.6	173.6
Ba	731.2	206.8	2086.3	658.6	676.4	831.8	810.8	688.6	1145.5	142.9	184.6	2130	484	22.2
La	16.6	3.2	2.7	29.5	8.1	0	29.1	35.8	38.6	0.4	3.6	3.5	11.9	2.8
Ce	29.5	4.7	5.6	52	13.7	9.3	49.6	52.1	57.5	0	12.3	5.7	16.7	0
MnO	269.4	2023.9	929.5	1598.5	144.6	90.9	525.5	796.4	1588.5	37	1497.1	511.1	362.5	363.6
TiO2	3311.9	10999.9	5494.4	6373.7	8685.8	428	4764.5	4546.2	6428.4	5648.6	8082.8	5896.9	2565.8	3854.1
Mo	0.5	1.6	13.6	0	1.8	699.4	0	0.4	0	54.9	0.4	1.1	1.8	21.3
Sn	0	3.4	0	0	0	0	1.6	0.8	0	0	0	0	0	0.9
Bi	1.2	1.9	2.1	1.4	2.2	111.3	1.5	0.7	1	33.7	1	5.5	2.4	2.7
Sb	4.9	0	0	0	114.5	4942.5	0	0	0	623.1	0	0	5.1	0
W	17.6	12.7	15.6	13.1	16.5	11.6	8.3	9.1	8.2	16	12.8	11	11	9.8

Element concentration data produced by Southampton's PW1400 XRF.
Concentrations expressed in ppm.

See also Appendix C for operating conditions.

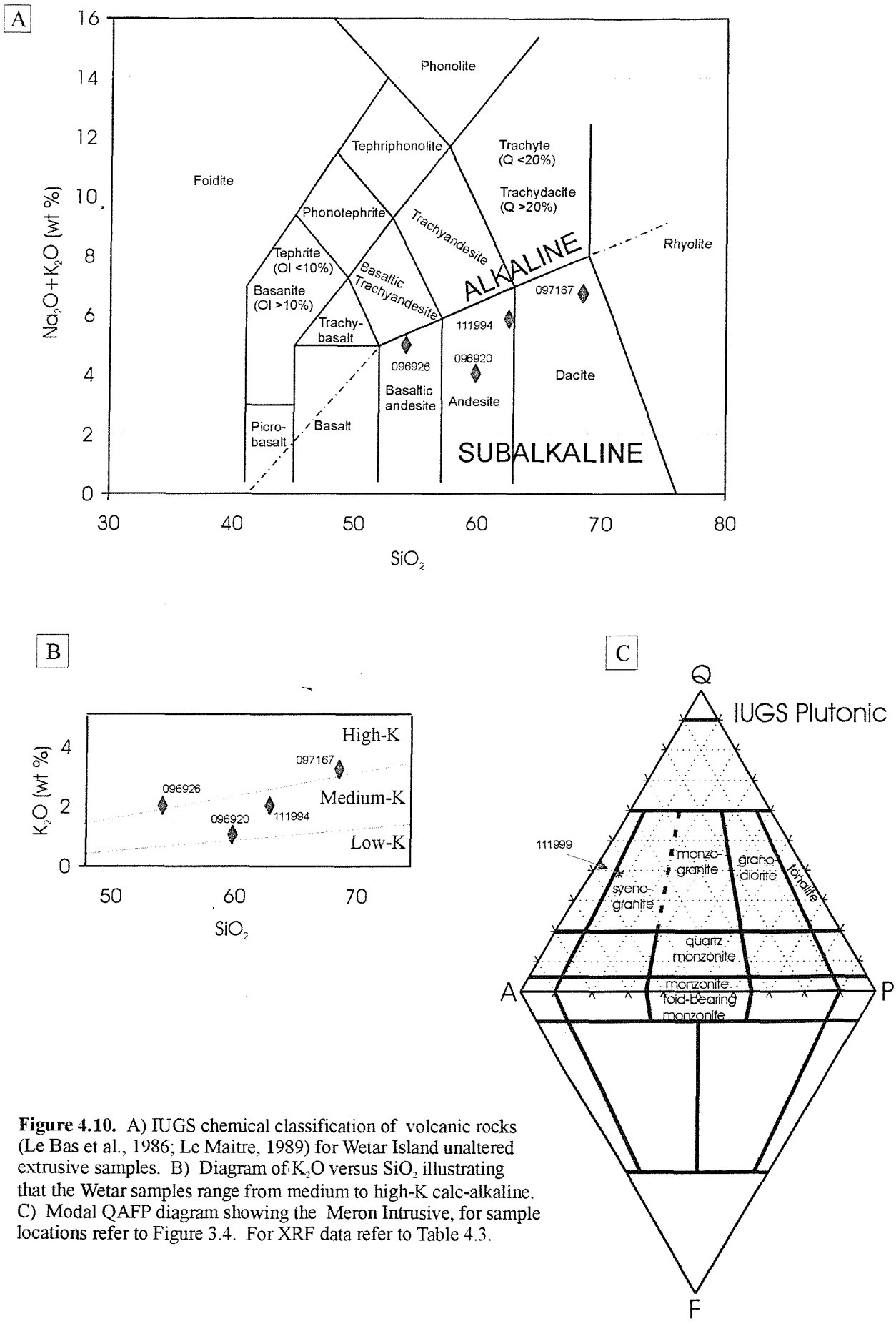
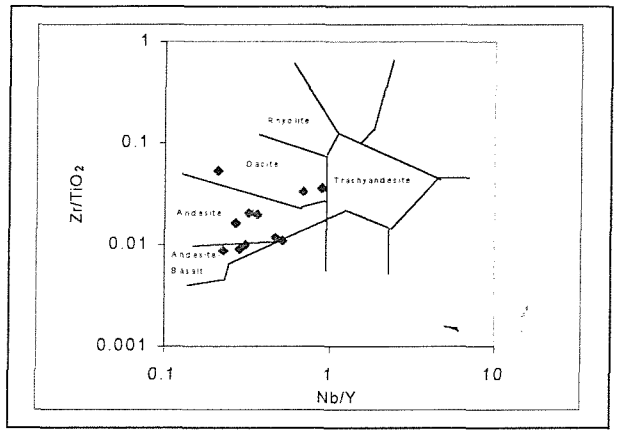


Figure 4.10. A) IUGS chemical classification of volcanic rocks (Le Bas et al., 1986; Le Maitre, 1989) for Wetar Island unaltered extrusive samples. B) Diagram of K_2O versus SiO_2 illustrating that the Wetar samples range from medium to high-K calc-alkaline. C) Modal QAFP diagram showing the Meron Intrusive, for sample locations refer to Figure 3.4. For XRF data refer to Table 4.3.

(111935, location 136) collected from the adjacent footwall to the barite ore zone at Lerokis Zone 4 plots on the boundary of the fields between andesite and basaltic-andesite, Figure 4.10A. This sample is characteristic of adjacent footwall to the barite ore in all of the mapped ore zones and is characterised by low TiO_2 (<0.5 wt%), high silica content (99.2 wt%) and high Ti/Zr ratio (84), Figure 4.12. Figure 4.11A also illustrates that similar values are preserved for the unaltered and altered post-mineralisation dacite flows collected from the Meron prospect, the altered sample 096884 from Kali Kuning (location 320, Figure 4.2C and map insert sheet 2A) also plots within this field.

A



B

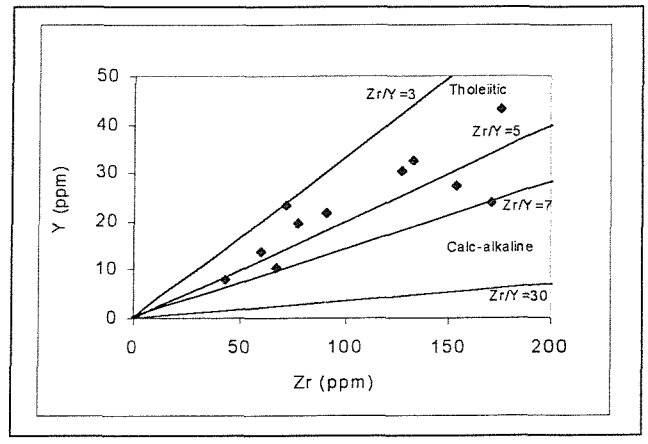


Figure 4.11. A) Discrimination diagram of Nb/Y vs. Zr/TiO_2 (after Winchester and Floyd, 1977) for altered samples from Wetar Island. Variations in immobile element ratios reflect primary geochemical variations. Red diamonds represent unaltered samples (visual criteria). B) Plot of Y vs. Zr for unaltered and altered volcanics showing the calc-alkaline and tholeiitic fields as defined by MacLean and Barrett (1993). Red diamonds represent unaltered samples, for whole-rock analytical data see Table 4.3 and Appendix C.

The brecciated sample (097106) from the Lerokis Zone 5 stockwork at a depth of 210 m below the sulphide mound (Figure 4.6) plots within the andesitic field and confirms the presence of andesite at depth within the footwall of this zone. Propylitic altered andesite pillow lavas have been mapped on the Lerokis road at a topographic height of 300 m, ~1.5 km to the NE and therefore confirms the lateral continuity of this unit throughout the area, (see also geological map, insert sheet 1). Sample 096927 (vesicular altered pillow flow, location 109) on the Kali Kuning road, 111914, location 316 and 096930, location 92 (both vesicular propylitic altered volcanics from

the Kali Kuning footwall, Figure 4.2C), all plot close to the boundary between the andesite and basaltic-andesite field. The proximity of sample 096927 to the andesite feeder tube located on the north coast (Figure 3.7A, Chapter 3) suggests that this coastal andesite (096920) is a feeder for this flow and that it extends into the footwall at Kali Kuning. Figure 4.11B illustrates that the majority of the altered samples are nearly all confined to the tholeiitic field on the Zr/Y plot thus suggesting they are co-magmatic. Both the unaltered and altered dacites from Meron plot outside the tholeiitic field with the altered sample lying on the boundary of the calc-alkaline field, Figure 4.11B. These two dacite samples (post mineralisation) plot away from the altered dacite collected from Kali Kuning (sample 096884).

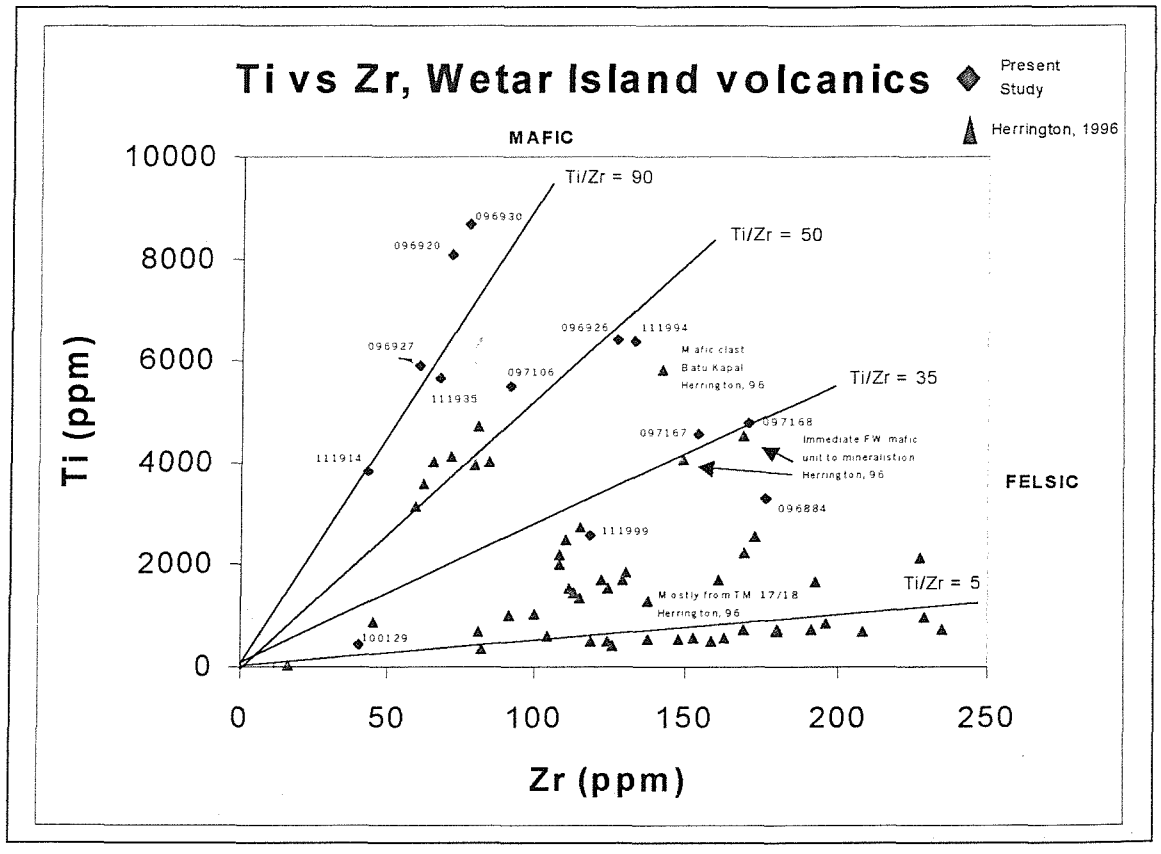


Figure 4.12. Discrimination diagram for Wetar Island whole rock samples based on Ti-Zr variations; after Pearce and Cann, (1973). Samples collected during the present study (blue diamonds) are shown in comparison to those collected by Herrington, (1996). Samples lying on a common line of regression suggest co-magmatic protoliths.

The lithogeochemistry defines at least 4 distinct groups within the Wetar Island volcanic stratigraphy hosting alteration, Figure 4.12. Mafic rocks lie on a line with a Ti/Zr ratio of ~90 and include the unaltered coastal andesite (sample 096920, Chapter

3, Figure 3.7A and Figure 4.7E). Four altered samples (111914, 111935, 096927 and 096930) also plot close to this line implying they are also mafic, confirmed also by Figure 4.11B. The intensely altered residual silica collected from the footwall of Lerokis Zone 4, (sample 111935, Figure 4.8B) also lies on this line suggesting that it was also originally a mafic rock. Other distinctive lithogeochemical groups are those with a Ti/Zr ratio of ~50 and include the unaltered basaltic-andesite (sample 096926) and andesite (111994). The altered sample 097106 (brecciated, propylitic altered volcanic from a depth of 210 m below the Lerokis Zone 5 sulphide mound, Figure 4.6) lies within this trend along with 7 samples collected by Herrington, (1996), Figure 4.12. These samples include footwall breccias from Lerokis Zone 4 and a lahar clast from Kali Kuning Zone 1 (KK1), see Figure 3.4, Chapter 3 for location. A sample collected by Kavalieris (1994) at W75 (for location see Figure 3.4) also plots along this trend and was suggested by the author to represent part of the original oceanic basement. The two dacite samples (097167 and 097168) collected from the post-mineralisation flow at Meron have a lower Ti/Zr ratio of ~35, these are consistent with the two samples collected by Herrington (1996) which are the immediate footwall unit to mineralisation at Kali Kuning. Interestingly, the altered dacite sample from Kali Kuning, location 320 (sample 096884) plots close to this trend and suggests that the topographically higher area to the SW of the massive sulphide mound is in fact the lower flank of an extremely altered dacite dome structure and confirms the association of mineralisation on the margins of dacite domes (Ruxton, 1989). The geochemically distinctive felsic suite at TM 17/18 (Herrington, 1996), (some 6 km south east of Lerokis, Figure 3.4) has a low Ti variation and a Ti/Zr ratio of ~5. Sample 100129, (location 66) collected from Kali Kuning also plots along this trend. The syeno-granite sample from the Meron area (111999) appears to lie almost on a trend with the altered dacite from Kali Kuning (096884), and may suggest that the underlying intrusives are feeding the dacite domes and that they are co-magmatic. The spatial presence of this lithology to sites of mineralisation suggets they may represent high-level intrusives responsible for supplying heat and volatiles to the hydrothermal system. The rocks at TM 17/18 have associated diaspore and alunite alteration associated with elevated Ba values, this is not the case for sample 100129 with Ba (832 ppm). Herrington, (1996) points out that highly acidic / oxidised fluids are needed to produce such an alteration assemblage. Collected samples are highly evolved, the petrology indicates the presence of late

alkali-feldspar and is tentatively attributed by the author to represent possible K-spar alteration related to the apex zone of a porphyry.

4.6 DISCUSSION OF ALTERATION

The alteration around the Wetar Island mineralisation is extensive and is zoned. Dominant alteration assemblages comprise of opal A (microcrystalline silica) and quartz proximal to mineralisation with illite-smectite and finally chlorite distal suggesting that the fluids are buffered by wallrock interaction. The footwall alteration beneath mineralised zones appears to be related to two hydrothermal fluid events, the first is related to sulphide mound development resulting in alteration patterns typical of many VMS systems (Franklin, 1996 and references therein). The second appears closely associated with the development of the baritic ore zones that flank the sulphide mounds resulting in intense footwall alteration adjacent to the barite ore and the deposition of advanced argillic mineral assemblages.

Field relationships during the study indicate that the residual silica in the adjacent footwall to the barite ore zones at each deposit is contemporaneous to the development of the barite ore itself (Figure 3.11). Fluids responsible are acidic based on the presence of kaolinite, pyrophyllite and native sulphur with the presence of trace alunite within the stockwork zone beneath the Lerokis Zone 5 sulphide body also indicating the role of a low pH fluid. Results indicate that each of the three deposits comprises local development of advanced argillic assemblages however they are only minor in abundance and quantity.

Previous work on alunite demonstrates it is diagnostic of acidic conditions (Leach and Erceg, 1992) and is stable at pH 2-3 but also over a broad temperature range (50 to >300°C). Illite however in most Philippine geothermal systems is indicative of temperatures > 230°C (Reyes, 1990). The scarcity of alunite as an alteration mineral therefore does not allow the environmental condition of formation to be determined, coarse grained tabular laths or pseudo rhombic crystals would suggest a magmatic origin (Rye et al., 1992). Alunite however is reported by Herrington, (1996), from the TM 17/18 prospect and from Batu Kapal thus confirming the presence of oxidising hydrothermal fluids at other sites of hydrothermal mineralisation on the island. On Wetar, alunite is associated with dickite and extensive hydrothermal brecciation

(Herrington, 1996). This study has proven that the minerals indicative of oxidised acidic fluids are associated with intense zones of hydrothermal brecciation, however the presence of alunite (at Kali Kuning) and pyrophyllite (at Lerokis Zone 5) are associated with illite in all instances. Illite co-exists with the Kaolin group minerals at fluid pH 4-5 however it also depends on temperature and fluid salinity (Hemley et al., 1980, Reyes 1990b). The geological characteristics and associated alteration suggest similarities with some Kuroko type ore deposits however kaolinite is not usually associated with Kuroko deposits. However when it is present in the core of alteration halos it is commonly found with pyrophyllite (Utada, 1980). Temperatures calculated from bulk oxygen isotope compositions of altered Kuroko host rocks (quartz – sericite zones) suggest fluid temperatures of between 260 and 320°C (Urabe et al., 1983), these temperatures are consistent with microthermetric data (Marutani and Takenouchi, 1978). These assemblages are typical of those in proximal locations to the stockwork zones that underlie the sulphide mounds at Lerokis Zone 5 and Kali Kuning, the emperatures of mineralisation will further be tested by fluid inclusion microthermometry in Chapter 6.

4.7 SUMMARY

A schematic section through a Wetar deposit (Figure 4.13) illustrates the findings of this Chapter. The alteration assemblages preserved on Wetar Island are typical for VMS systems (dominantly *low-sulphidation* assemblages) generated by seawater entrainment and heating at depth. In summary, the Wetar Island deposits are surrounded by a classic VMS style of alteration (chlorite-quartz) passing into restricted zones of advanced argillic assemblages (pyrophyllite, alunite and residual silica), proximal to sites of mineralisation typical if fluids are buffered by seawater / rock interation. The presence of pyrophyllite and alunite only occur as minor phases or as traces associated with illite and are found only beneath the ore-horizons. These alteration assemblages are consistent with the presence of low pH, oxidised fluids, not typically encountered in VMS systems and may suggest a magmatic component within the system (Figure 4.13).

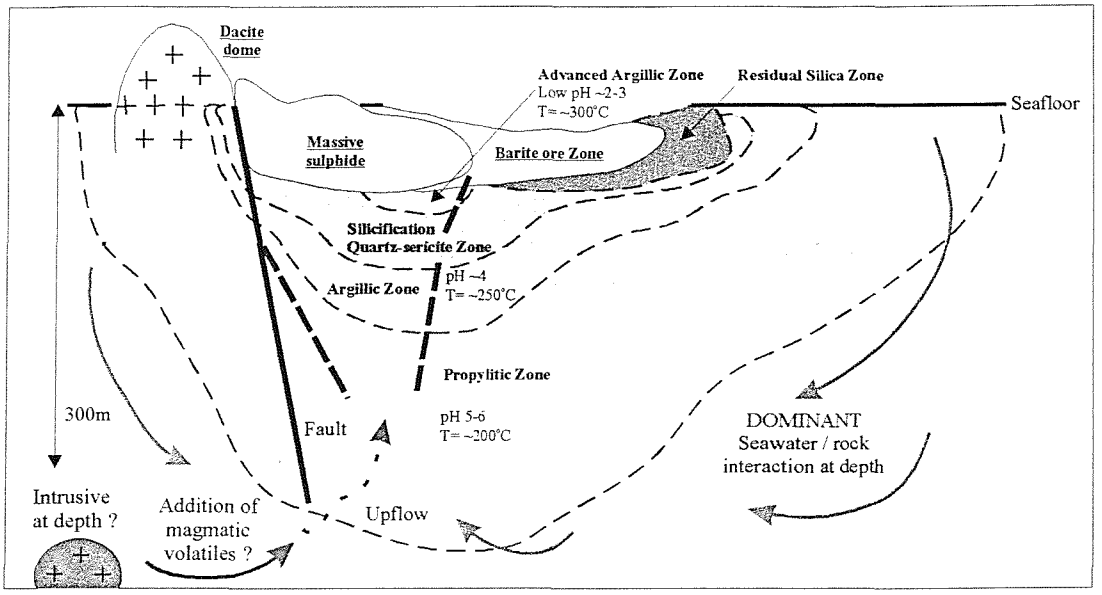


Figure 4.13. Schematic section through an idealized Wetar orebody showing the relationship between the massive sulphide, barite ore and underlying / surrounding pattern of hydrothermal alteration. The stockwork zones that underlie the orebodies (heavy dashed line) consist of all alteration zones. Temperatures and pH based on data from Leach and Erceg, (1990).

Chapter 5

ORE MINERALOGY, TEXTURES AND CHEMISTRY

5.1 INTRODUCTION

This Chapter describes in detail the ore mineralogy of the VMS deposits. Field observations along with optical microscopy, backscattered electron (BSE) imaging and electron-microprobe study are used to characterised the principal zones of mineralisation preserved on the Island. The study is particularly focussed on Kali Kuning, Lerokis Zones 4 and 5 with Meron, Gunung Botak and other sites of mineralisation located on Wetar discussed briefly in the text.

The principal objectives of the study were:-

1) To identify and describe the mineralogy, textures and associations of the Wetar Island deposits.
2) To determine the sulphide / sulphosalt assemblages and the paragenetic sequence of mineralisation.
3) To characterise the unique barite ore deposits with the aim of identifying cementing or inclusion phases and to identify any morphological variation within the barite sand deposits.

By careful examination of the above objectives, answers may be forthcoming to the following,

1) How extensive are the *high-sulphidation* sulphide assemblages and are they hypogene or supergene in origin?
2) Are the deposits on Wetar Island seafloor exhalative in origin or a sub-seafloor replacement types?
3) Where is the gold and what is its association with the deposits?

5.2 PREVIOUS WORK

Early field mapping on Wetar indicated the presence of volcanic hosted massive sulphide deposits (VMS) occuring proximal to rhyo-dacite dome structures and NE-SW trending faults (Ruxton, 1989), see also Chapter 3. Drilling indicated sulphide mounds have funnel or mushroom morphologies, oval in plan with associated onlapping baritic ore deposits containing significant reserves of both Au and Ag. Unpublished company petrological reports document a dominant assemblage of massive pyrite ± marcasite and chalcopyrite, (Ruxton, 1989; Herrington, 1993a,b). Pyrite present exhibits collomorphic textures in places (Fander, 1991). Covellite, digenite, bornite and sulphosalts are reported to rim brecciated massive pyrite, (Sewell and Wheatley, 1994) and enargite is also reported (de Ronde, 1995). Isopach maps based on drill-core data indiate that the barite ores vary in thickness with a maximum of 37 m at Lerokis, Zone 1C. Generally the barite ore zones thin as they onlap the sulphide mounds and exhibit grading and cross-bedding, the ore bodies are also confined to small fault-bounded basins (Sewell and Wheatley, 1994b).

Within the barite ore deposits, Sewell and Wheatley, (1994a, 1994b) report Au and Ag are concentrated in the lower parts of the deposits and are associated with jarositic and limonitic cements; Ag also appears to be associated with tetrahedrite and sulphosalts. Cerussite $PbCO_3$, plumbojarosite $PbFe_6^{3+}(SO_4)_4(OH)_{12}$ or anglesite, free grains of galena, arsenopyrite and dusserite $BaFe_3(AsO_4)_2(OH).5H_2O$ are present in minor amounts plus minor chalcopyrite, chalcocite, bornite, pyrite, pyrrhotite and secondary native Cu are also associated with the barite. The average Hg grade of the ore is 18 ppm and occurs as cinnabar, metacinnabarite (HgS), perroudite (AgHgClS) or tiemannite (HgSe) (De Roever, 1991). The barite ore at Lerokis Zone 4 contains occasional quartz crystals plus euhedral barite grains, sieving indicates that Au occurs only in the <50 μm fraction of the barite ore. In one instance Au is evident adhering to the margin of a barite grain and in another, to a concretion of jarositic material (Herrington, 1993). The barite also contains inclusions of acanthite (Ag_2S), galena, boulangerite ($Pb_5Sb_4S_{11}$), stibio-Luzonite (Cu_3SbS_4), tennantite, tetrahedrite, geocronite ($Pb_{14}(SbAs)_6S_{23}$) (Herrington, 1993, 1996) and is cemented in part by a series of oxides and arsenates. These include plumbojarosite, jarosite

$KF_3^{3+}(SO_4)_2(OH)_6$, mimetite $Pb_5(AsO_4)_3Cl$, arsendescloizite $PbZn(OH)(AsO_4)$, arsenbrackebuscite $Pb_2(FeZn)(AsO_4)_2.H_2O$ and chlorargyrite AgCl (Herrington, 1993b, 1995). At Lerokis Zone 4, the barite-oxide feeder structure contains collomorphic iron oxides and perroudite $Hg_5Ag_4S_5(ClIBr)_4$ as a cementing phase between tabular barite laths (Herrington, 1996).

5.3 SAMPLE SELECTION

A representative suite of samples was collected from Kali Kuning (KK3) and Lerokis Zones 4 and 5 to enable the mineralogical and textural characteristics of the barite and sulphide assemblages to be established. Following standard optical microscopic techniques, a further sub-set of samples where used for SEM and EPMA analysis to determine cementing phases within the barite ore. Sample locations are given on the geological maps (insert map sheet 2 and Figures 4.2C to 4.8 Chapter 4) see Appendix D for operating conditions and all the data.

5.4 FIELD RELATIONSHIPS

5.4.1 Sulphide Mounds

Pre-mining, no sulphide mounds were exposed at the surface (Figure 1.6 Chapter 1). The Wetar Island sulphide mounds at Kali Kuning and Lerokis Zone 5 have asymmetric geometries with dimensions of ~150 × 100 × 70 m and ~120 × 90 × 30 m respectively (Figure 5.1). Deposits are associated with faults (based on field mapping prior to mining, see also Chapter 3). The Lerokis Zone 5 mound has developed at the intersection of a northwest and westerly trending structure where a pronounced enlargement of the sulphide mound occurs at this intersection and may relate to the feeder zone for the sulphide mound, (see Figure 5.1B). The Kali Kuning sulphide mound is associated with a northwesterly trending fault. In plan, both the sulphide mounds have unusual shapes and are not simply oval (Sewell and Wheatley, 1994b), this is evident in the aerial photographs, (Figure 3.5, Chapter 3). Sulphide mounds at both Kali Kuning and Lerokis Zone 5 are dominantly massive pyrite (~

95% volume) with chalcopyrite and lesser amounts of sphalerite, galena and fahlore group sulphides. Extensive zones of alteration surround both deposits, see Chapter 4. The mounds have a blocky appearance (composed of blocky fragments) with globular clasts of massive pyrite ranging in diameter from a few cm up to boulders some 30 cm across (see Figure 5.2A-B). Banding of both pyrite and chalcopyrite occur on a cm scale in the upper parts of the Kali Kuning deposit, along with a cavity / void filled texture, (Figure 5.3A). This texture appears more frequently at the upper parts of the mounds (especially at Kali Kuning) and at mound margins, the same applies for the appearance of chalcopyrite. Covellite, digenite ($Cu_{1.8}S$) and bornite are present on external exposed faces of the massive pyrite (Figure 5.3B) and also as lining within large fractures that permeate through the sulphide mound and underlying stockwork (Figure 5.3C). Tabular, euhedral barite laths are associated with these sulphides and range in size up to 2 cm. Fine-grained pyritic sand marks the contact zone between the sulphide mounds and the barite ore and is preserved at both Kali Kuning and Lerokis Zone 5, this boundary or contact zone ranges in thickness between 0.2 and 2.5m. At Kali Kuning, this succession of massive sulphide, pyritic sand grading laterally into barite ore is present behind the sulphide mound at the contact zone between the mound and associated footwall. Talus / re-deposited sulphides occur marginal to the mounds where matrix supported angular fragments of massive sulphide are held in a fine-grained sulphide sand. The sulphide mounds are discordant to the host stratigraphy, this feature is evident at both Kali Kuning and Lerokis Zone 5 (Figures 5.4A-C). Minor evidence for sea-floor reworking is evident at Lerokis Zone 5 where a 30 cm zone of interbedded sulphide / volcanoclastic material overlies the massive sulphide mound, (see Figure 5.5A). The contact zone between sediment and sulphide is relatively flat lying, a feature easily evident in the field (Figures 5.5B and C). Mapping of the deposits has not identified any distinct evidence of metal zonations, the notable difference between the three ore zones was the lack of a sulphide mound associated with the Lerokis Zone 4 deposit. However pyritic veins and pyrite cubes have been identified in the surrounding footwall.

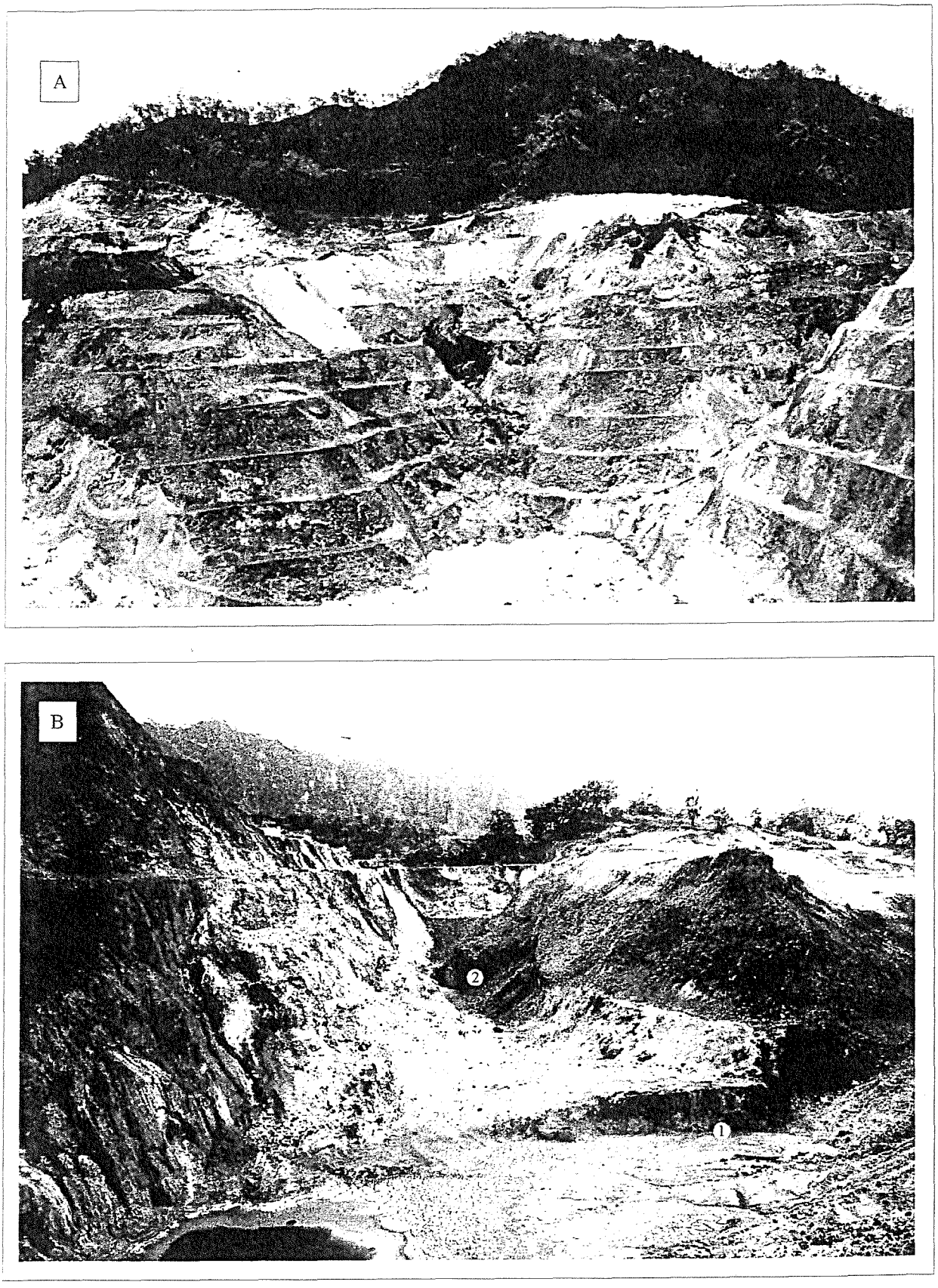
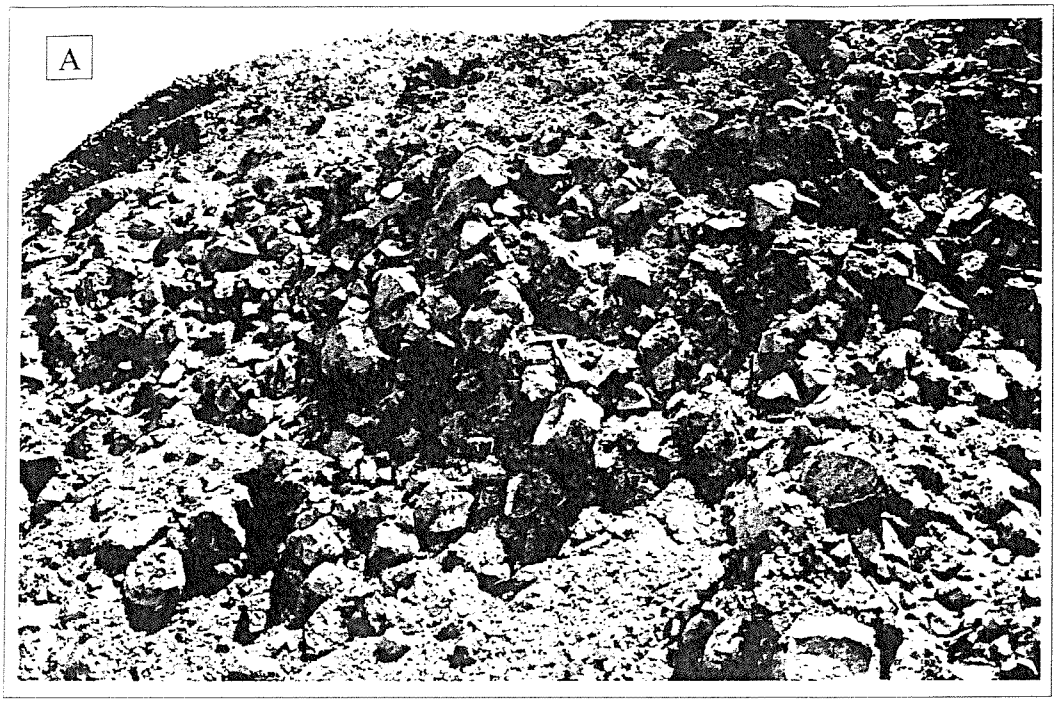


Figure 5.1. (A) Exposed sulphide mound at Kali Kuning (KK3), height of sulphide mound ~60 m, in-situ barite ore can be seen in the centre of the sulphide mound. (B) Exposed sulphide mound at Lerokis Zone 5. Possible feeder zones for baritic ore bodies (1 and 2) are shown in-situ, both are associated with intense zones of silicification. Extensive gossanous material surrounds the deposit. Height of the sulphide mound above the pit floor is ~15 m.



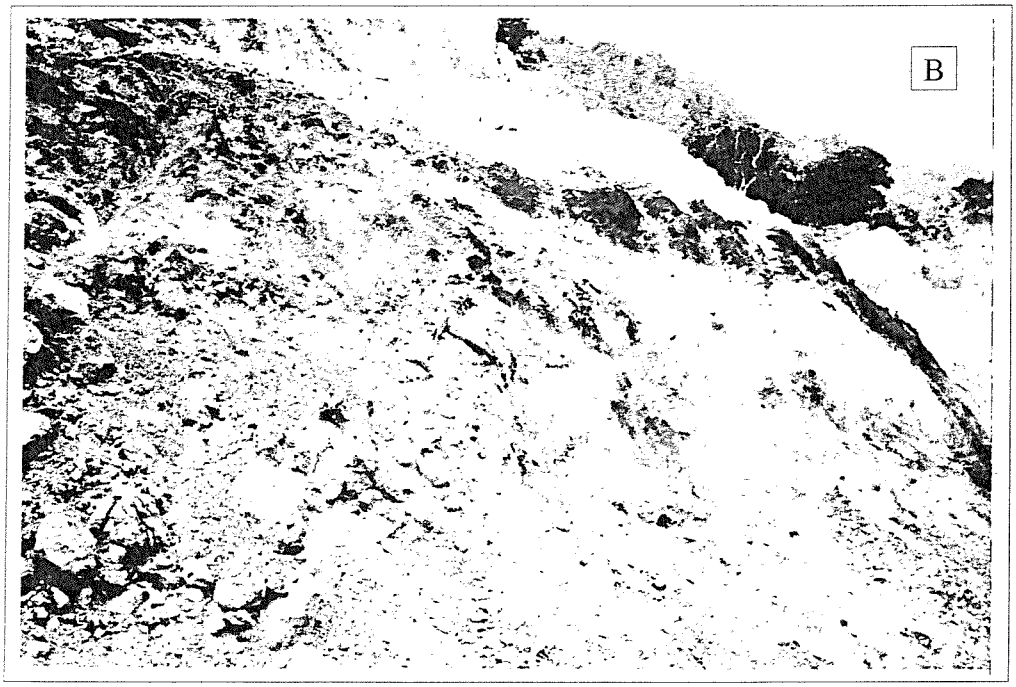


Figure 5.2. (A) Lerokis Zone 5 sulphide mound illustrating the "blocky" nature of the pyrite. Generalsizes range from a few cm up to 50 cm. hammer in the centre of the picture is for scale. (B) Massive, blocky sulphides at the upper part of the Kali Kuning sulphide mound, the overlying chert and *globigerina* bearing limestone are shown, hammer for scale.

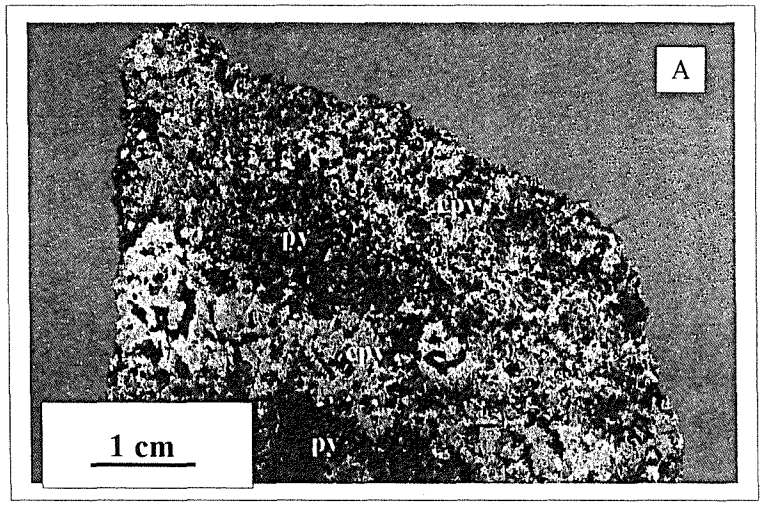
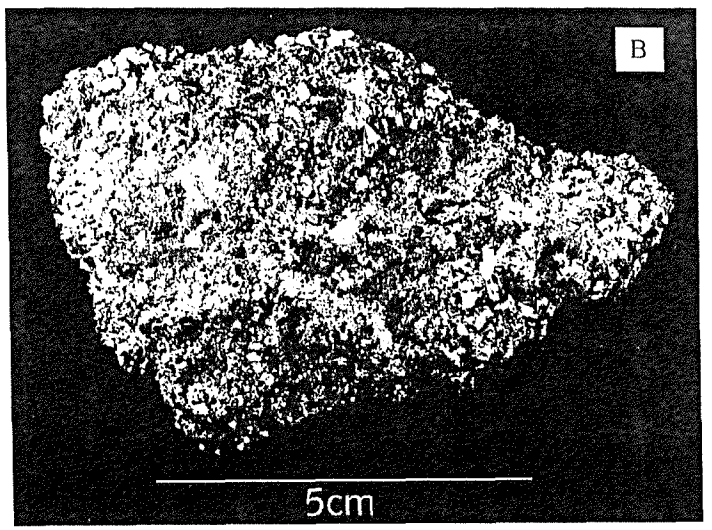
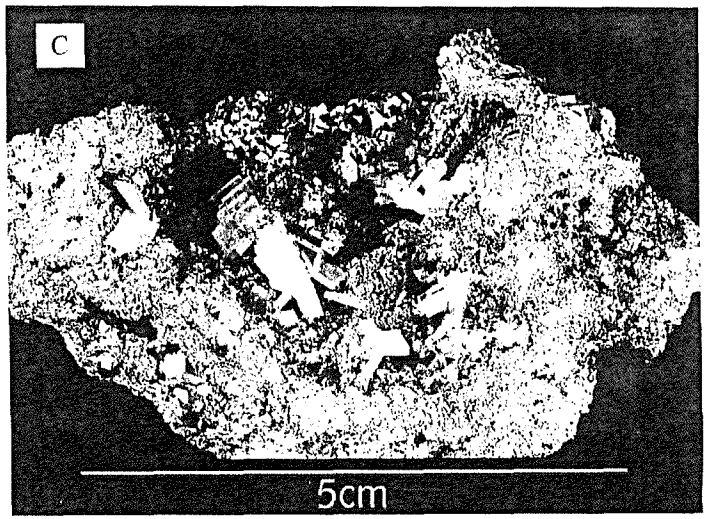


Figure 5.3. (A) Banded pyrite (py) and chalcopyrite (cpy) from the Kali Kuning massive sulphide mound, photo also illustrates the cavity / vuggy nature of the sulphides. (B) Massive pyrite from Kali Kuning. Sample shows cubic pyrite surrounded by bornite and covellite plus minor chalcopyrite. (C) Large vug / void infilled with covellite and tabular barite crystals surrounded by massive pyrite.









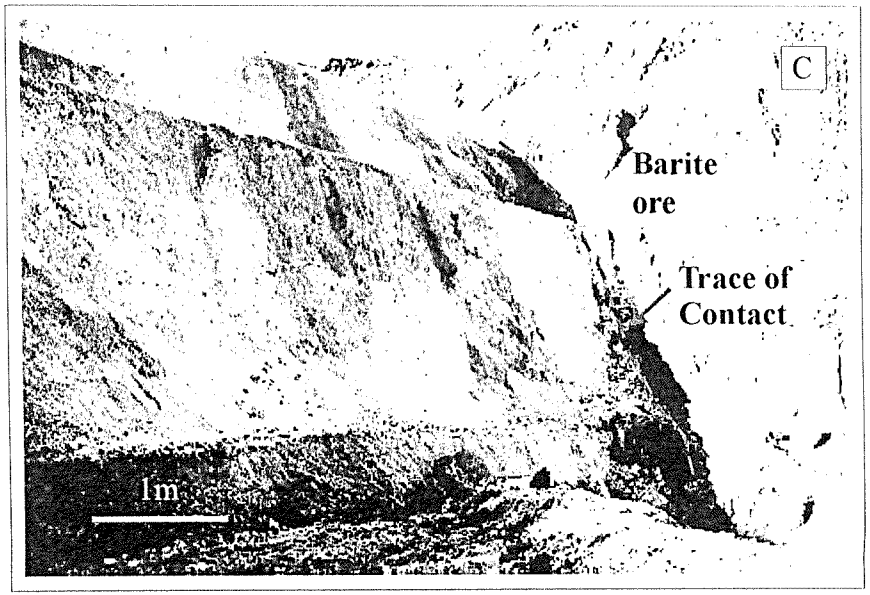
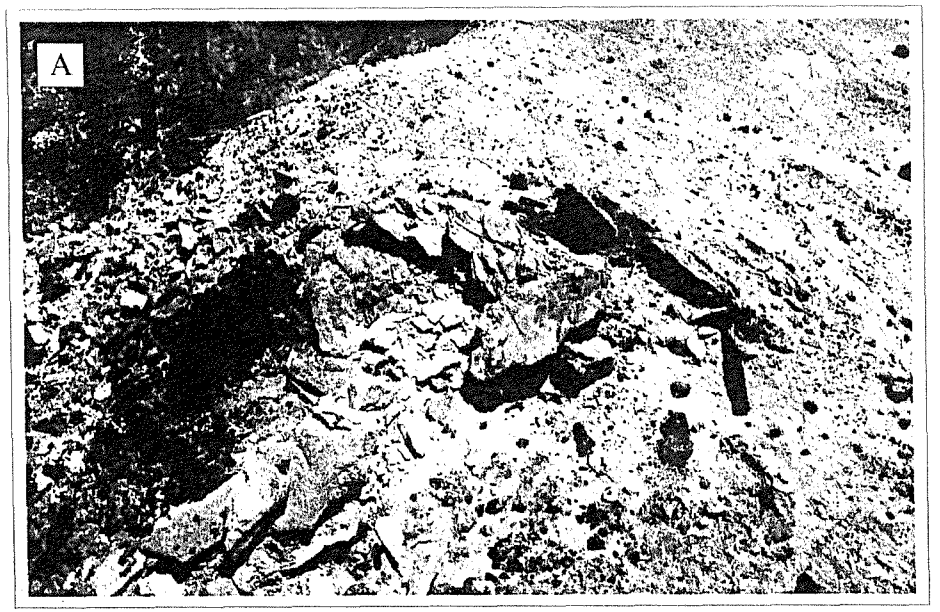
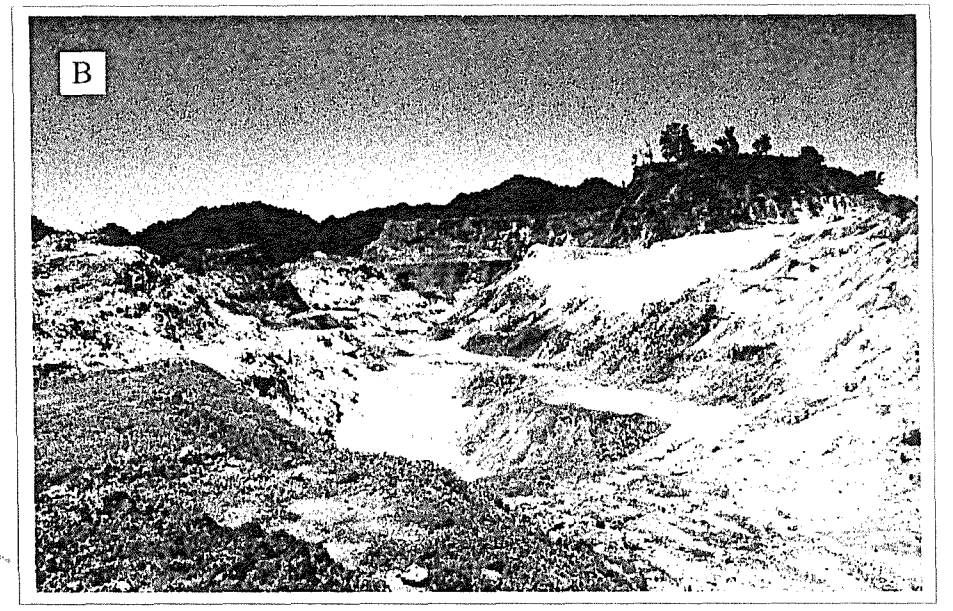


Figure 5.4. (A) Abrupt, curved contact between the Lerokis Zone 5 massive sulphides and the hydrothermally altered footwall. The contact zone is bounded by a thin zone of barite and pyritic sand, hammer for scale. (B) The base of the Kali Kuning massive sulphide, note the interfingering with the host volcanics. (C) Discordant nature of the contact between the Kali Kuning sulphide mound and the host stratigraphy, the contact dips at almost 70°, a thin layer of in-situ barite ore lies near the contact zone, a bag lies in the foreground for scale.





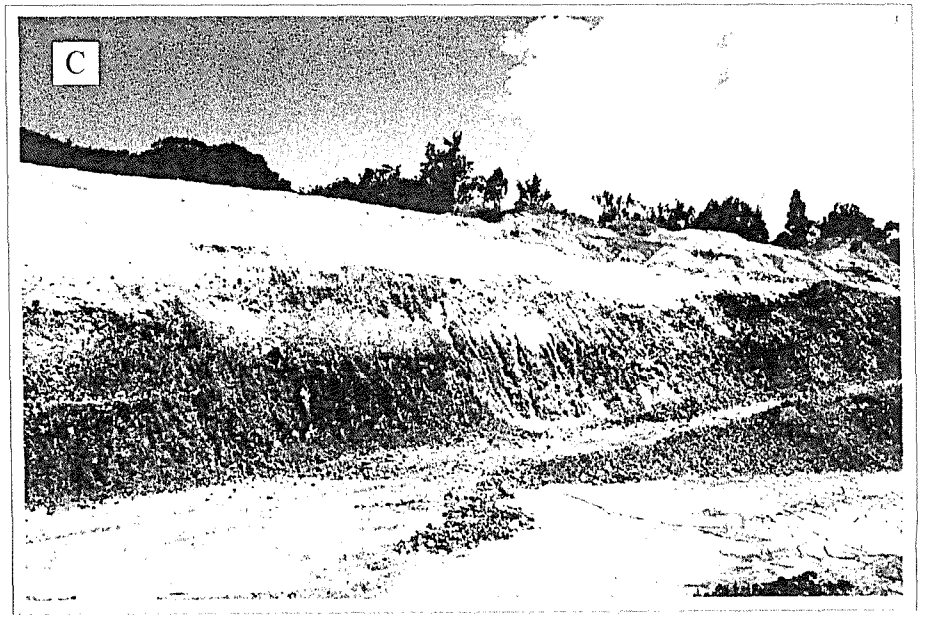


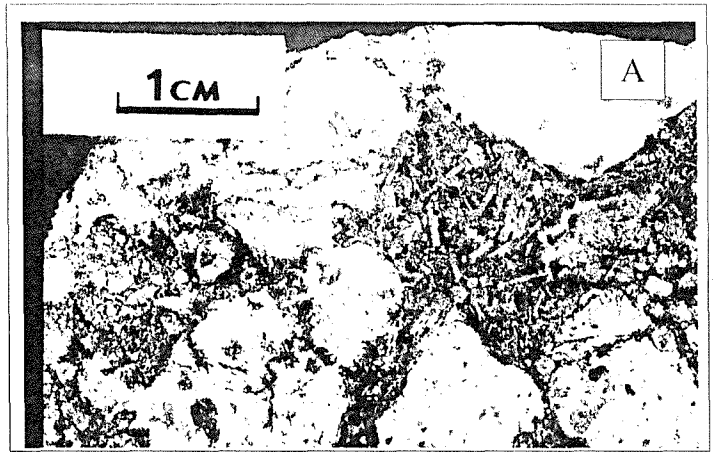
Figure 5.5. (A) Fine grained zone of interbedded sulphides and volcanoclastic sediment preserved above the massive pyrite mound of Lerokis Zone 5. (B) View towards the southeast of the same deposit, the overlying volcanoclastic sediment (pale yellow) can be seen towards the middle right overlying the massive sulphides. (C) Same features as B, looking west, the contact zone is relatively flat lying. Both massive sulphides and sediment thin toward the north.

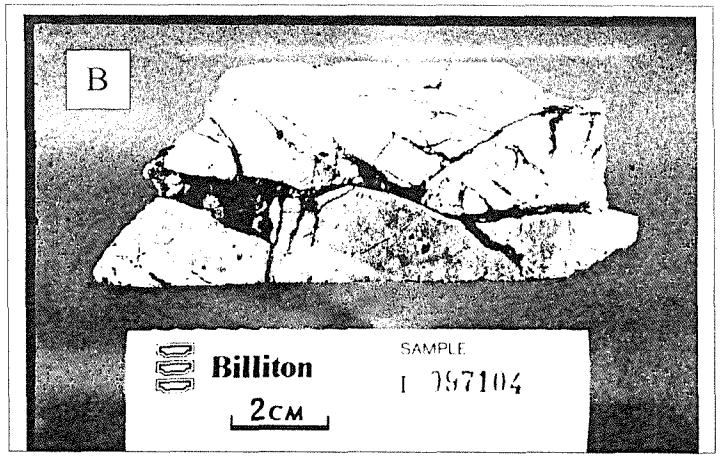
5.4.2 Stockwork Zones

The pyritic mounds are underlain by stockwork zones consisting of pyrite, chalcopyrite and sphalerite veins with lesser amounts of disseminated sulphides, which include galena. Pyrite is the most abundant sulphide within the stockwork accounting for >80% of all sulphides (Figure 5.6A). Stockworks reach depths of >210 m below the Lerokis Zone 5 deposit and > 150 m below Kali Kuning based on available core, sulphide veins present range from <1 mm up to 4 cm in width. Generally veinlets of chalcopyrite and sphalerite are < 0.5 cm in width, the latter are found more often at deeper locations (Figure 5.6B). Intense vein and disseminated mineralisation occurs within an extremely silicified zone immediately beneath the sulphide mound at Lerokis Zone 5 and appears to be related to the pre-mined fault intersection and probable "feeder zone" for the mineral deposits. This zone extends to the surface and makes an abrupt contact with the sulphide mound (see Figure 5.1B). The stockwork zone is hosted by and comprised of hydrothermally altered, silicified volcanics (vesicular in part), see also Chapter 4. Brecciated, angular host clasts are rimmed by sulphides and also contain sulphide disseminations < 1 mm (Figure 5.6C).
A late fracture network permeates throughout the stockwork and pyritic massive mounds and is infilled with a sulphide assemblage dominated by covellite, Fe-poor sphalerite and lesser amounts of tennantite-tetrahedrite. This characteristic sulphide assemblage is shown (Figure 5.6C). Barite laths are abundant and associated with this assemblage of sulphosalts.

5.4.3 Barite Deposits

Barite ore at Kali Kuning, Lerokis Zones 4 and 5 are ~60-90% barite and are cemented in some locations. Shapes of the deposits are highly variable, (see pre mined outlines on map insert sheets 2A-C). The deposits are "chaotic" in nature with variable degrees of cementation, generally they are friable deposits with evidence of slumping, (see Figure 5.7A-B). Individual barite crystals range in size up to a maximum of approximately 7 mm in length; generally they are between 2-4 mm. Cross-bedding and stratification are reported by Sewell & Wheatley, (1994b) however these features were evident pre-mining presumably in the "upper" parts of the





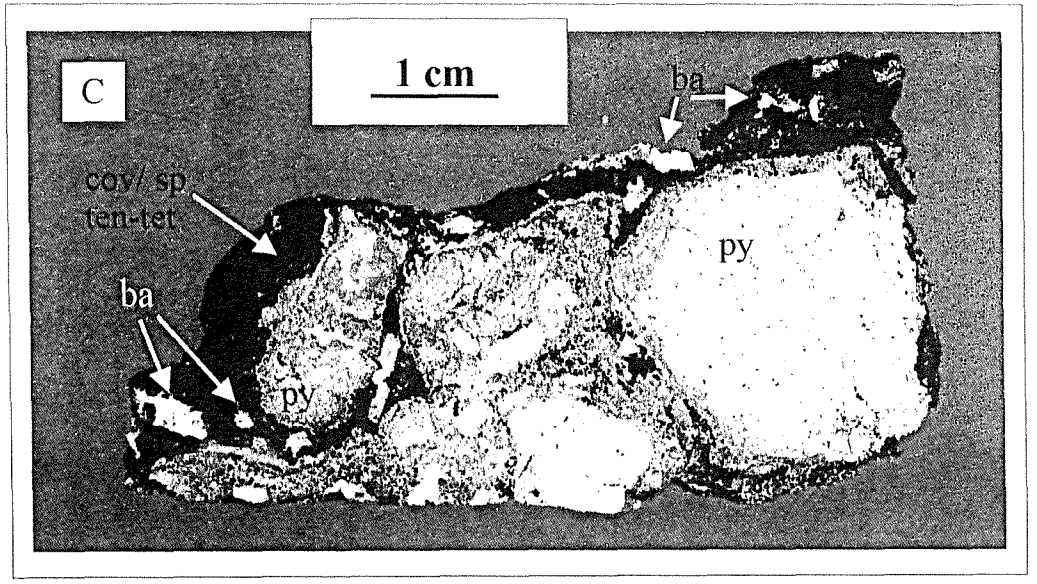


Figure 5.6. (A) Intense pyrite veining from Lerokis Zone 5 stockwork Zone. (B) Micro veinlets of chalcopyrite and sphalerite are associated with deeper areas of the stockwork. (D) Fracture fill assemblage collected from the Lerokis Zone 5 stockwork, depth 49.5 m below the massive sulphide mound. Euhedral barite laths are associated with the sulphosalt assemblage sulphides. Early pyrite rims surround the brecciated stockwork host volcanics, pyrite disseminations are also present within the brecciated hydrothermally altered fragments.

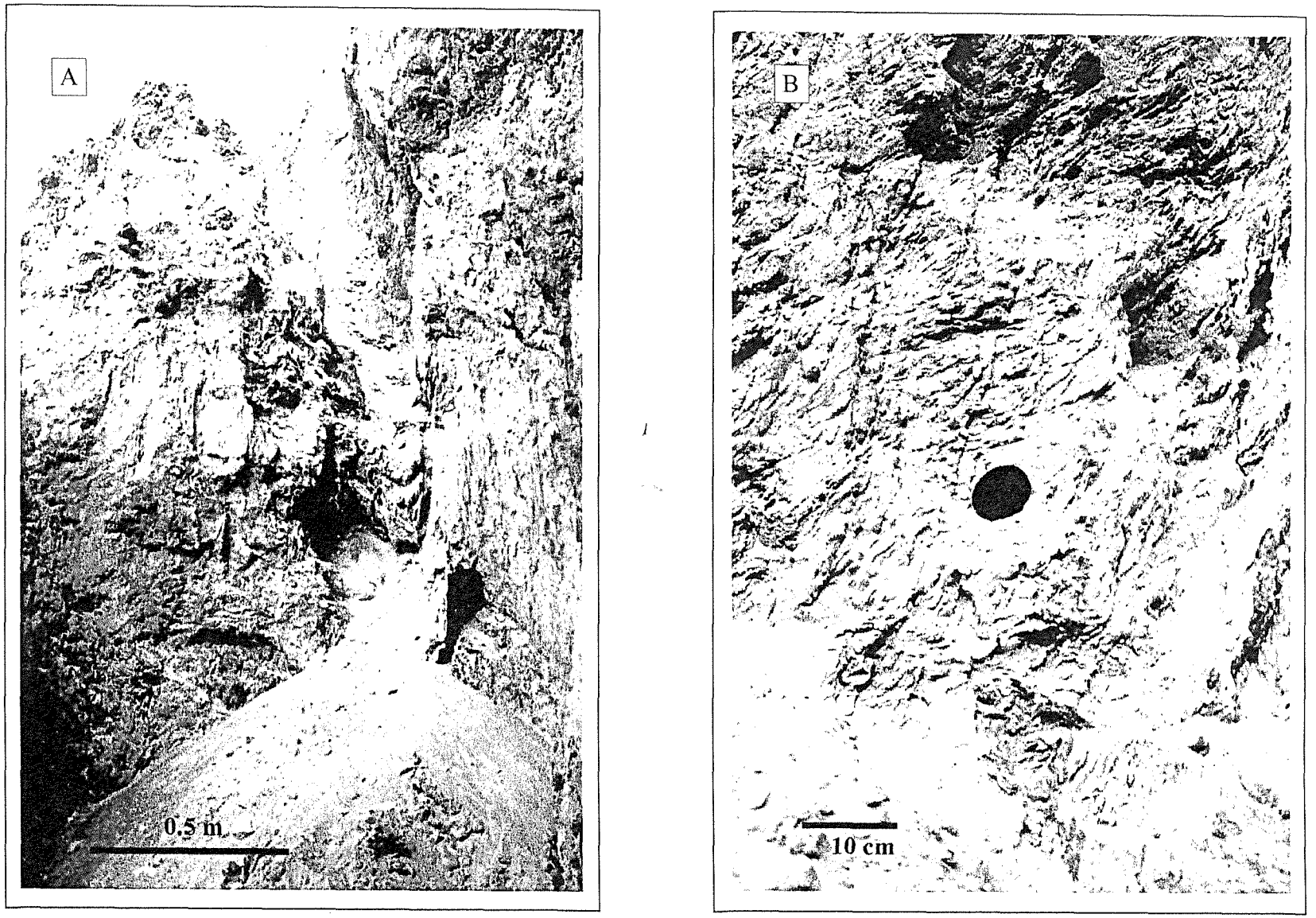
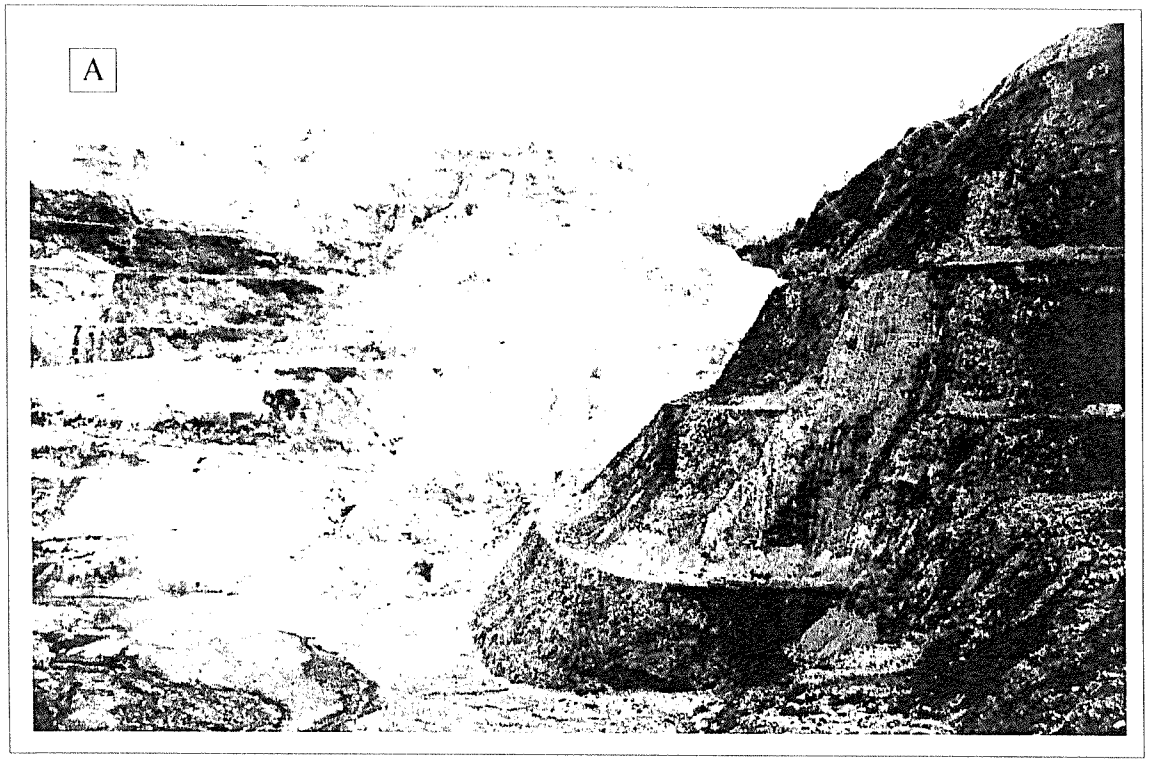


Figure 5.7. A-B, Lerokis Zone 4 (location 216). (A) Nature of barite ore deposits in the field, friable nature of these deposits results in development of scree. (B) Barite ore, close-up of (A), notice the chaotic nature of the deposit (evidence of slumping) and the fine, near vertical laminations (right edge of photo). Sample taken for petrological study (sample 111930).



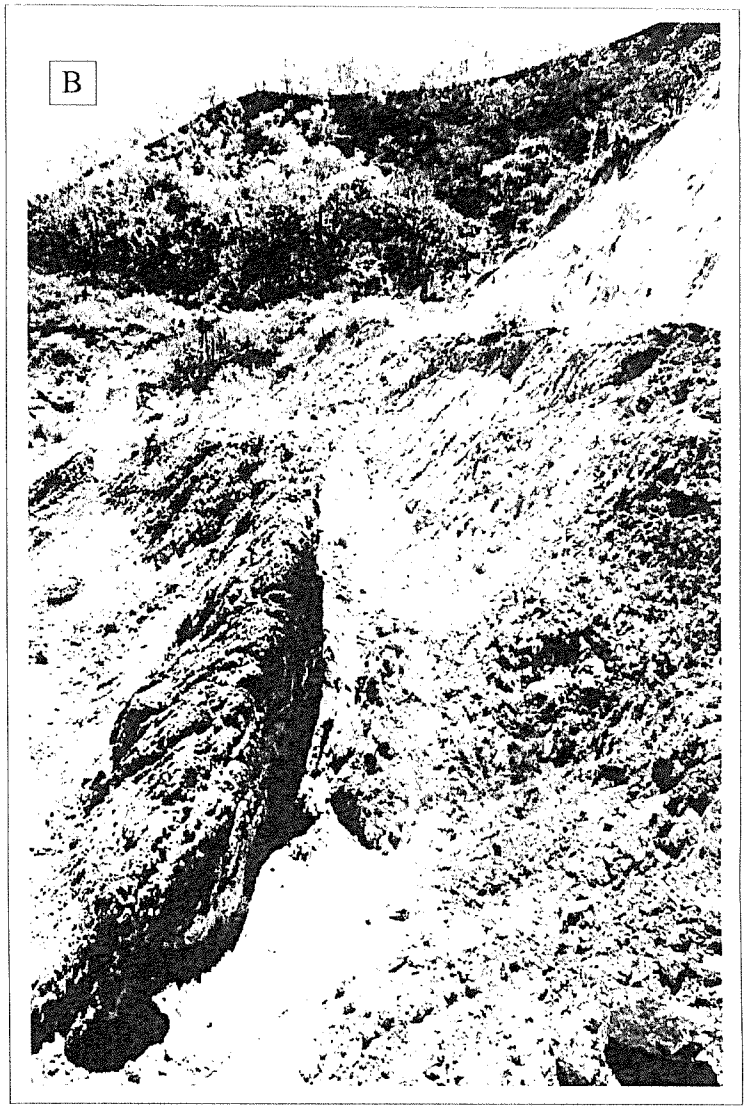


Figure 5.8. A-B, Kali Kuning sulphide mound. (A) Base of deposit looking approximately north. A thin "in-situ" layer of barite ore is evident (right of centre) on the surface of massive sulphide. The contact between the two is defined by a 10-30 cm zone of pyritic sand, see text for details. (B) View approximately northeast of the upper part of the sulphide mound in the region of the mound / footwall contact zone. A 50 cm zone of pyritic sand separates the massive sulphide (left) from the barite ore (right). The altered footwall is also present (upper right), see text for details.

deposits. Remaining in-situ barite ore exhibits variations in degree of cementation and colour especially at Kali Kuning in the area of the mound / footwall contact. This location of in-situ barite is important and suggests that the sands completely surround the sulphide mound as well as onlapping them. (Figure 5.8A-B and Figure 5.1A). The contact zone between the massive sulphide and barite is always comprised of pyritic sand, this is only between 10-30 cm in thickness at Kali Kuning (Figure 5.8B). The thickness of the pyritic sand is generally thicker at the footwall contact. The same feature is evident within Lerokis Zone 5 with the thin contact between the sulphides and footwall (~ 70 cm) containing 40 cm of pyritic sand and 30 cm of barite sand. At depth, barite also occurs as disseminated laths within stockwork zones (up to 1 cm), as vug fill within sulphide mounds, as laths associated with the *high-sulphidation* / sulphosalt fracture assemblage and as coatings on external mound faces. Vein barite occurs both proximal and distal to mineralisation with individual euhedral crystals measuring up to 5 cm (Figure 5.9).

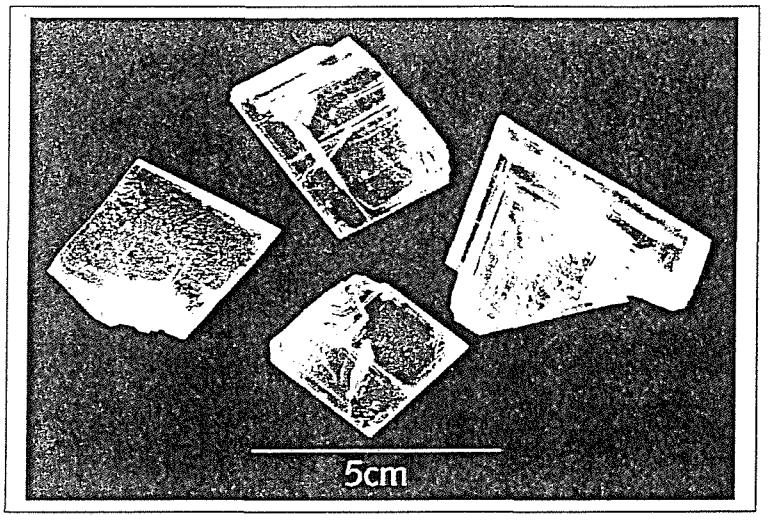


Figure 5.9. Large euhedral barite crystals collected from a 35cm wide barite vein from the Lerokis Road section, 300 m from the centre of mineralisation at Lerokis Zone 5, sample 099938, location 112, see map insert sheet 1.

5.4.4 Barite / Fe-oxide Feeder Structures

Cemented Fe-oxide / barite structures are preserved at Kali Kuning, Lerokis Zone 5 and Lerokis Zone 4 and may represent fluid feeder conduits for the baritic ore deposits. These structures, "pipe-like" in their nature (see Figure 5.10A-B) are located at both the base of, and central to the mined barite deposit at Lerokis Zone 4.

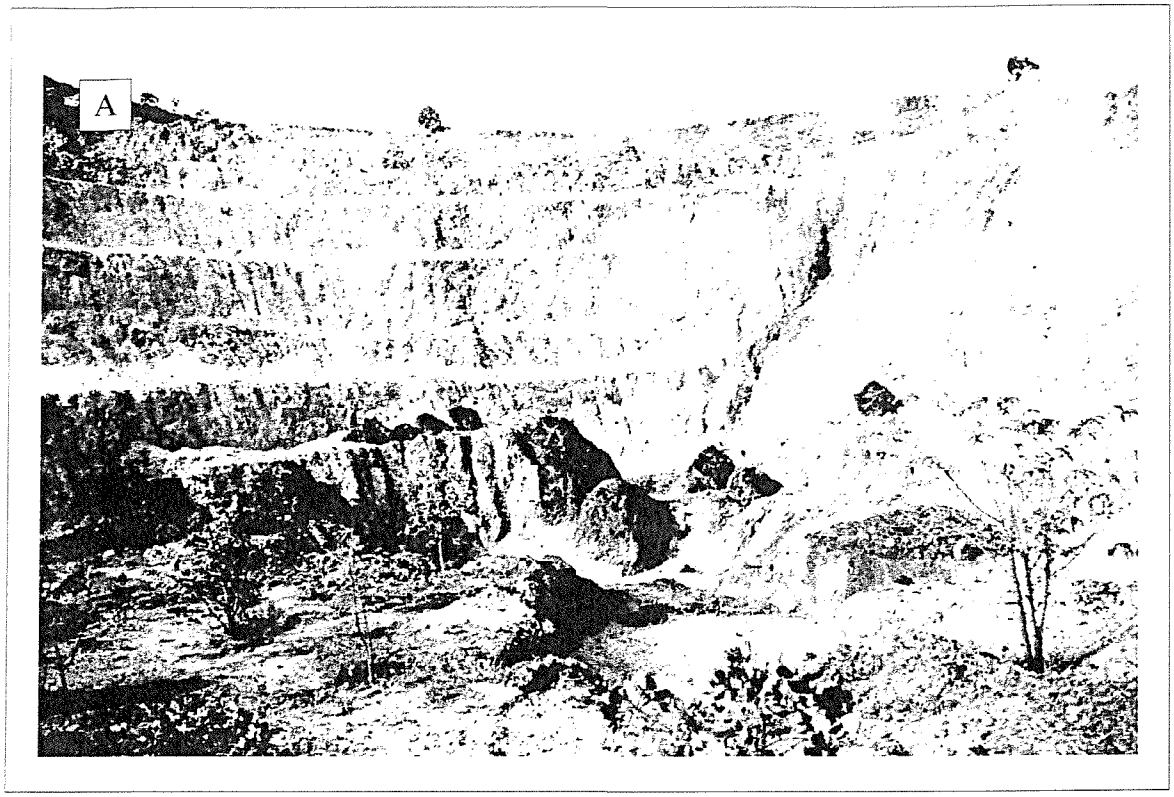




Figure 5.10. (A) Lerokis Zone 4, Wetar Island, Indonesia. Photo shows the two Fe-oxide / barite structures preserved at the centre of the deposit. The barite ore which surrounded the two structures has been removed, numerous fallen blocks of the oxide/barite material can be seen, see figure for scale. (B) Close-up of the two barite Fe-oxide "feeder structures", the structure in the foreground is approximately 1.5 m in height.

The structures preserved at Lerokis Zone 4 are 1-1.5 m in height and ~ 1.5 m at the exposed base. These structures are also present at Lerokis Zone 5 as two irregular structures (1 m × 12 m, see Figure 5.1B) and at Kali Kuning as one small feature (Figure 5.11). The material contains abundant anastomosing layers of concentrated barite ranging from a few mm up to 30 cm separated by layers of goethite and limonite, clasts of residual silica footwall material are also incorporated, (see Figure 5.12A). Banded Fe-oxides are present on a centimetre scale within the structure from Lerokis Zone 5, this is illustrated in (Figure 5.12B).

5.5 PETROGRAPHY AND MINERAL CHEMISTRY

5.5.1 Massive Sulphide Mounds

Mineral abundances in the specimens examined are grossly similar, with pyrite (98%) >> chalcopyrite > sphalerite > covellite / marcasite / tennantite and bornite. Tables 5.1 below presents relative abundances of sulphide phases of mineralised samples based on hand specimen identification. Results from optical examination of the sulphide phases and textures are given in Table 5.2.

Table 5.1. Relative abundance of sulphide minerals, in hand specimen:
* = < 5%, ** = 5-10%, *** = 10-25%, **** = 25-50%, ***** = >50%. Samples with a and b were collected from the same locality.

Mineral	**Pyrite** FeS_2	**Marcasite** FeS_2	**Chalcopyrite** $CuFeS_2$	**Sphalerite** (Zn, Fe)S	**Galena** PbS	**Fahlore Group** $Cu_{12}(As,Sb)_4S_{13}$	**Covellite** CuS	**Barite** $BaSO_4$
Sample								
097002	**	*	**	*		***	*	*
097104	**		**	****	***	***		
097009	*****	*	***	***	*			*
097016	****	**	**	**				**
097056	***	*	*****				***	
097059	*****		***			*		
097112	*****							
097122a	****		*	****	*	***	***	**
097122b	****			****	*	***	***	**
097129	*****							
097222	*****		**			*	*	
111943a	*****		****			*		
111943b	*****		****		*			*
096857	*****							
099917	*****							
099903	*****							

Table 5.2. Percentages of individual sulphide phases from the Kali Kuning and Lerokis Zone 5 massive sulphide mounds and related stockworks, Wetar Island.

Sample No.	Location	Sample Type	Total % sulphides in sample	py	cpy	ga	sph	cov	ten	Trace	Comments	Probe Study
096857	Kali Kuning loc. 75	Massive sulphide	100	99	1	-	-	-	-	cpy	Massive nature.	Yes
111943	Kali Kuning loc. 63	Massive sulphide	100	70	30	-	-	-	-	cov, sph,ten, bo	Porous, cavity filled texture.	
097222	Kali Kuning KKD 058 @ 90m	Stockwork vein & disseminated sulphides	10	80	-	-	20	-	-	ga, cov, ten	Associated with brecciated / silicified altered volcanics, ga and sph veins cut clasts and py veins.	
099917	Lerokis Zone 5 loc. 15	Massive sulphide	100	100	-	-	-	-	-	ma	Collomorphic and rythmic layering in py.	
099903	Lerokis Zone 5 loc. 5	Massive sulphide	100	100	-	-	-	-	-	-	Massive nature.	
097002	Lerokis Zone 5 LKD 042 @ 4.7 m	Talus sulphides	100	90	5	-	3	2	-		Clasts of sulphide within a sulphide mud.	
097009	Lerokis Zone 5 LKD 042 @ 22 m	Massive sulphide	100	95	5	-	-	-	-	-	Collomorphic layering in py.	Yes
097016	Lerokis Zone 5 LKD 042 @ 41 m	Massive sulphide	100	99	1	-	-	-	-	-	Brecciated massive ore.	
097056	Lerokis Zone 5 LKD 043 @ 33 m	Massive sulphide	95	95	5	-	-	-	-	ma	Brecciated massive ore, cavities & voids infilled with barite. Collomorphic banding in pyrite.	
097059	Lerokis Zone 5 LKD 043 @ 42 m	Massive sulphide	98	80	20	-	-	-	-	-	Brecciated massive ore, cavities & voids infilled with barite. Collomorphic banding in pyrite.	
097104	Lerokis Zone 5 LKD 043 @ 179 m	Stockwork vein & disseminated sulphides	25	20	5	5	70	-	-	-	Associated with brecciated / silicified volcanics and hematite veining.	
097122	Lerokis Zone 5 LKD 044 @ 50 m	Fracture-fill assemblage between brecciated host volcanic clasts	20	10	3	1	50	20	15	tet, bo, dig	Associated with brecciated / silicified volcanics, fracture assemblage contains tabular barite laths.	Yes
097129	Lerokis Zone 5 LKD 044 @ 77 m	Stockwork vein & disseminated sulphides	10	80	5	-	15	-	-	-	Associated with brecciated / silicified volcanics and hematite veining.	

Results are based on reflected light microscopy. py= pyrite, cpy= chalcopyrite, ga= galena, sph=sphalerite, cov= covellite, ten= tennantite bo= bornite, tet= tetrahedrite, dig= digenite, ma= marcasite. LKD 042 represents a drill core section and borehole number.

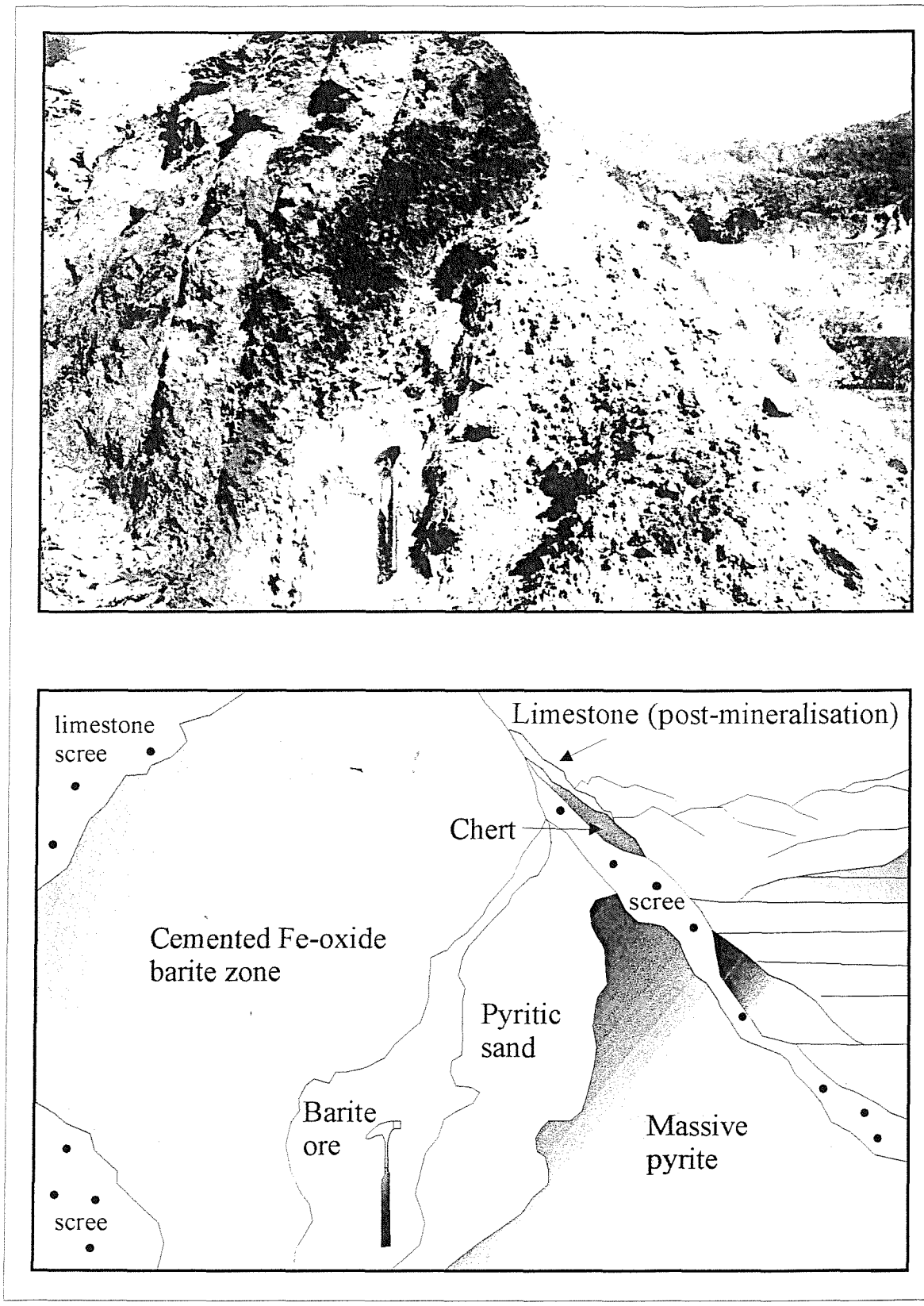
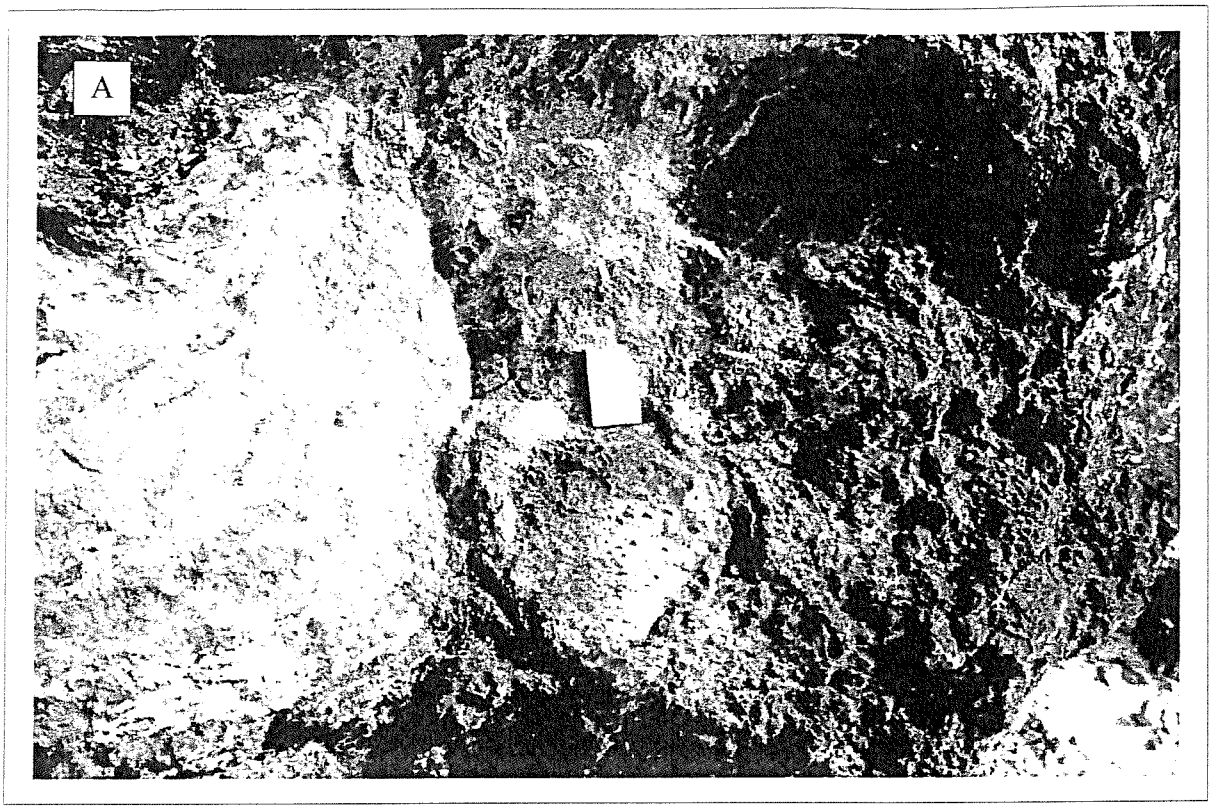


Figure 5.11. Preserved Fe-oxide / barite structure at Kali Kuning. The structure is not as linear or pipe like as at Lerokis Zone 4 however the succession of massive sulphide - pyritic sand - barite ore is the same as other localities within this deposit and at Lerokis Zone 5.



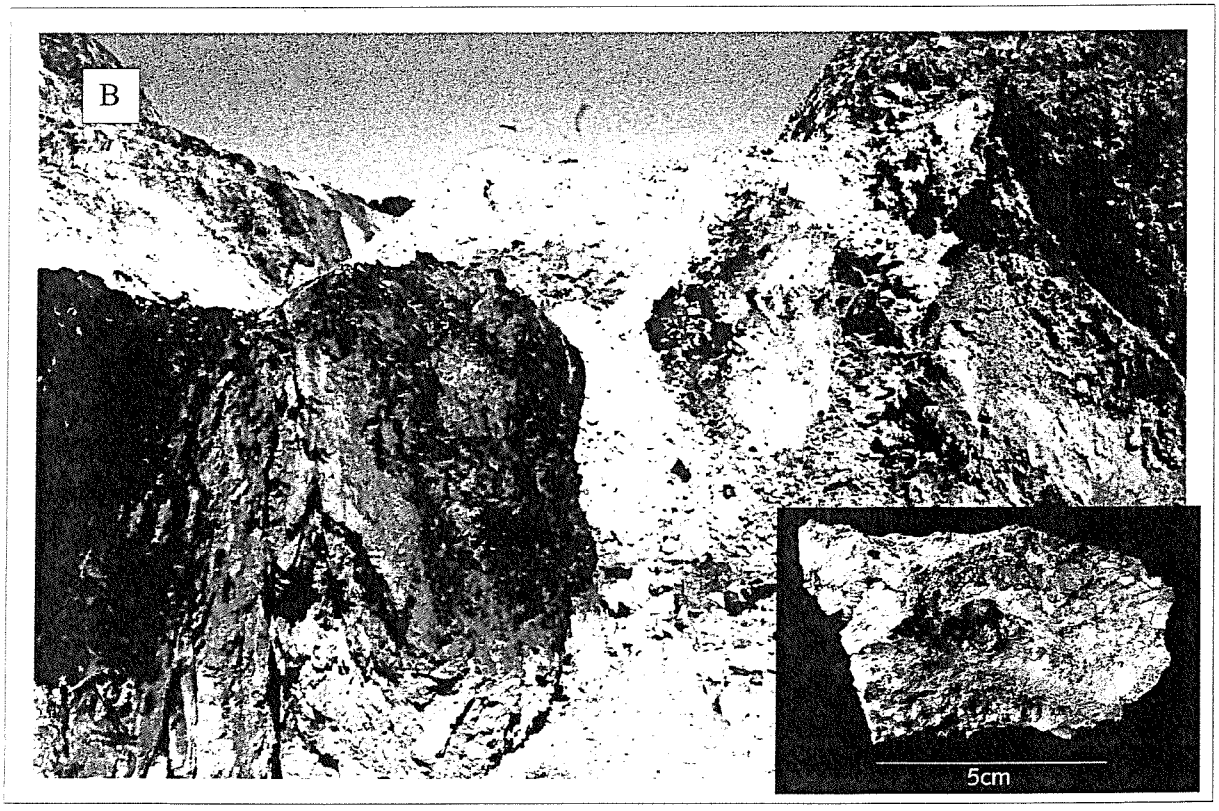


Figure 5.12. (A) Close-up of fe-oxide / barite structure, Lerokis Zone 4. A clast of footwall "residual silica" (10 cm in diameter) is present (centre) along with numerous anastomosing layers of barite and Fe-oxides. Barite is concentrated to the left. (B) View approximately west, Lerokis Zone 5, the Fe-oxide / barite structure is shown (hammer, bottom left for scale). The structure contacts the sulphide mound (right of centre), and delineates the feeder zone for this deposit, see also figure 5.1B. Banded goethite / limonite occurs on a cm scale here, see inset.

5.5.1.1 Pyrite

Pyrite is the dominant mineral and ubiquitous throughout the Kali Kuning and Lerokis Zone 5 orebodies. The massive pyrite (Figure 5.13A and B; 5.14A) contains abundant cavities / voids. Collomorphic (melnicovite) growth textures are observed in some samples within the pyrite (Figure 5.13C and D) and the preserved layers vary in thickness up to 3 mm in thickness. SEM backscattered images and microprobe data on pyritic samples indicate the pyrite within the sulphide mounds are arsenian (Table 5.3). Within the centre of the massive ore at Lerokis Zone 5 (22 m depth, LKD 042, sample 097009), zoning is evident as thin euhedral bands, (< 10μm) compositional variations range between 0.5 and 6.7 wt% As (n = 13). Towards the margin of the massive ore (099903), collomorphic zoning is dominant with compositional variations between 0.2 and 3.4 wt% As (n = 8). Both zoning features are illustrated in Figure 5.15. The microprobe traverse in Figure 5.15 illustrates that As is concentrated within the brighter layers or zones within the pyrite. The results are significantly higher than those discovered by De Roever and Besseling, (1991) who found up to 4 wt% As within a sample from Kali Kuning. The collomorphic textured pyrite tends to nucleate on and around massive euhedral pyrite grains which appear to act as cores (Figure 5.14B) however in the majority of samples collomorphic textured pyrite is surrounded by massive pyrite. Embayed textures are present in some pyrite samples (Figure 5.14C), the vugs / voids within the pyrite are commonly empty (5.14A) or infilled with barite (Figure 5.13D).

5.5.1.2 Marcasite

Marcasite occurs within massive pyrite samples as subhedral to anhedral inclusions (10-100 μm) and is present within most thin sections but only as a minor phase (Figure 5.13B). The presence of marcasite contrasts markedly to pyrite on the basis of optical chracteristics.

5.5.1.3 Chalcopyrite

Occasional banding of pyrite and chalcopyrite is evident as 1 cm bands in sample 111943 (Figure 5.3A; 5.14A). Field identification have shown that chalcopyrite is more prominant at the margins of the pyrite mounds, particularly in the

stratigraphically higher regions of the Kali Kuning deposit. This increase is also indicated in drill core specimens immediately beneath the mounds in the footwall, especially beneath the Lerokis Zone 5 deposit. Growth zones within pyrite contain thin chalcopyrite rims (Figure 5.13A) whereas late fractures and brecciated samples of massive pyrite are also commonly rimmed by chalcopyrite as anhedral masses (Figure 5.13C). Figure 5.13D illustrates that chalcopyrite can occur as vug / void fill within the sulphide mounds, in this instance it has co-precipitated with sphalerite. Replacement of pyrite is more common at the base of the mound at Lerokis Zone 5 (Figure 5.14C, depth of 42 m) at the contact with the underlying stockwork. No evidence of chalcopyrite disease has been identified in these samples.

5.5.1.4 Sphalerite

Within the massive ore, sphalerite occurs generally as subhedral to anhedral inclusions within pyrite characterised by a relatively high Fe content. A typical microprobe analysis shows the Fe content is ~ 6-9 wt% (n = 4), however when sphalerite is present it usually co-precipitates with chalcopyrite. Very thin veins occur in brecciated pyrite (< 2 mm) and within pyrite growth zone (Figure 5.13A). Larger voids may also be filled with sphalerite, (Figure 5.13D) at the base of the sulphide mound (Lerokis Zone 5) it is commonly associated with both tennantite and chalcopyrite (Figure 5.14D).

5.5.1.5 Tennantite

Intergrowth of tennantite as an anhedral phase occurs surrounding brecciated fragments of chalcopyrite, pyrite and sphalerite. Tiny, anhedral inclusions (<50 μm) are present within spahlerite and chalcopyrite. Inclusions of both sphalerite and chalcopyrite also occur within the tennantite, this phase is minor in abundance.

5.5.1.6 Barite

Fractures, growth zones and vugs may all be filled by barite (Figure 5.13A,D; 5.14C and D) where individual crystals reach up to 1 cm, barite also occurs as encrustations on the external surfaces of sulphides up to 2 cm (Figure 5.3C). In the majority of samples this phase occurs as interlocking masses of euhedral crystals.

5.5.1.7 Minor Phases

Several unusual phases have been identified from the massive sulphide mound at Lerokis Zone 5. Copiapite, $Fe^{2+}Fe^{3+}_4(SO_4)_6(OH)_2.20H_2O$ occurs as tiny (<3 mm) euhedral crystal concentrated in granular masses with red crystals (<3 mm) of Römerite $Fe^{2+}Fe^{3+}_2(SO_4)_4.14H_2O$ (see Figure 5.16). Both phases are intergrown with fine-grained barite and occur as encrustations on the surface of massive pyrite boulders, all phases were identified by XRD analysis, the traces are given in Appendix C.

5.5.2 Stockwork Zones

Mineral abundances in four of the specimens examined indicate pyrite > sphalerite > chalcopyrite >> covellite > galena / tennantite / tetrahedrite. Stockwork zones exhibit varying degrees of hydrothermal alteration (Chapter 4) and reach depths > 200 m below the sulphide mounds of Kali Kuning and Lerokis Zone 5. Sulphide phases generally tend to occur where brecciation is greatest.

5.5.2.1 Gold

Au was found in sample 097130 located at a depth of 85m below the Lerokis Zone 5 sulphide mound associated with intense clay alteration of the footwall volcanics, (for sample location see Figure 4.6, Chapter 4). The sample was found to be rich in illite (determined by XRD and FTIR) and located spatially close to underlying altered samples containing pyrophyllite. Microprobe analysis of this < 10 μm anhedral grain were as follows:

Sample	Type	Au	Fe	Pb	Hg
		Atomic%			
097029	Au	83.3	4.2	4.9	3.8

Only the one grain was evident in thin section.

Table 5.3. Representative electron microprobe analyses of Wetar Island sulphide phases from the Kali Kuning and Lerokis orebodie, Indonesia.

	Pyrite [1]		*Sphalerite* [2]	*Covellite* [3]	*Tetrahedrite* [4]	*Tennantite* [5]	
	wt%	*wt%*	*wt%*	*wt%*	*wt%*	*wt%*	*wt%*
Ag	0	0	0	0.165	0.006	0	0.047
Cd	0	0	0.438	0.009	0	0	0.07
S	48.01	52.287	31.587	30.808	25.158	26.56	31.233
Fe	44.367	46.014	0.028	0.039	2.195	0.114	0.038
Cu	0.034	0	0.314	63.048	38.556	41.236	45.798
Zn	0.038	0.017	64.72	0.208	5.216	8.297	0.164
As	6.613	0.598	0.026	0.067	7.017	17.792	15.911
Se	0.042	0.012	0	0.029	0.048	0.059	0.134
Sb	0	0.008	0.053	0.293	19.871	3.099	3.947
Pb	0	0	0	0	0	0	0
Total	99.104	98.936	97.166	94.666	98.067	97.157	97.342
	As rich	As poor				Zn rich	Zn poor

Analyses were undertaken at the Natural History Museum, London, using a Cameca SX50 analytical scanning electron microprobe, with an accelerating voltage of 15kV, 20nA and count time of 20 seconds, detection limits and full data set are given in Appendix D.

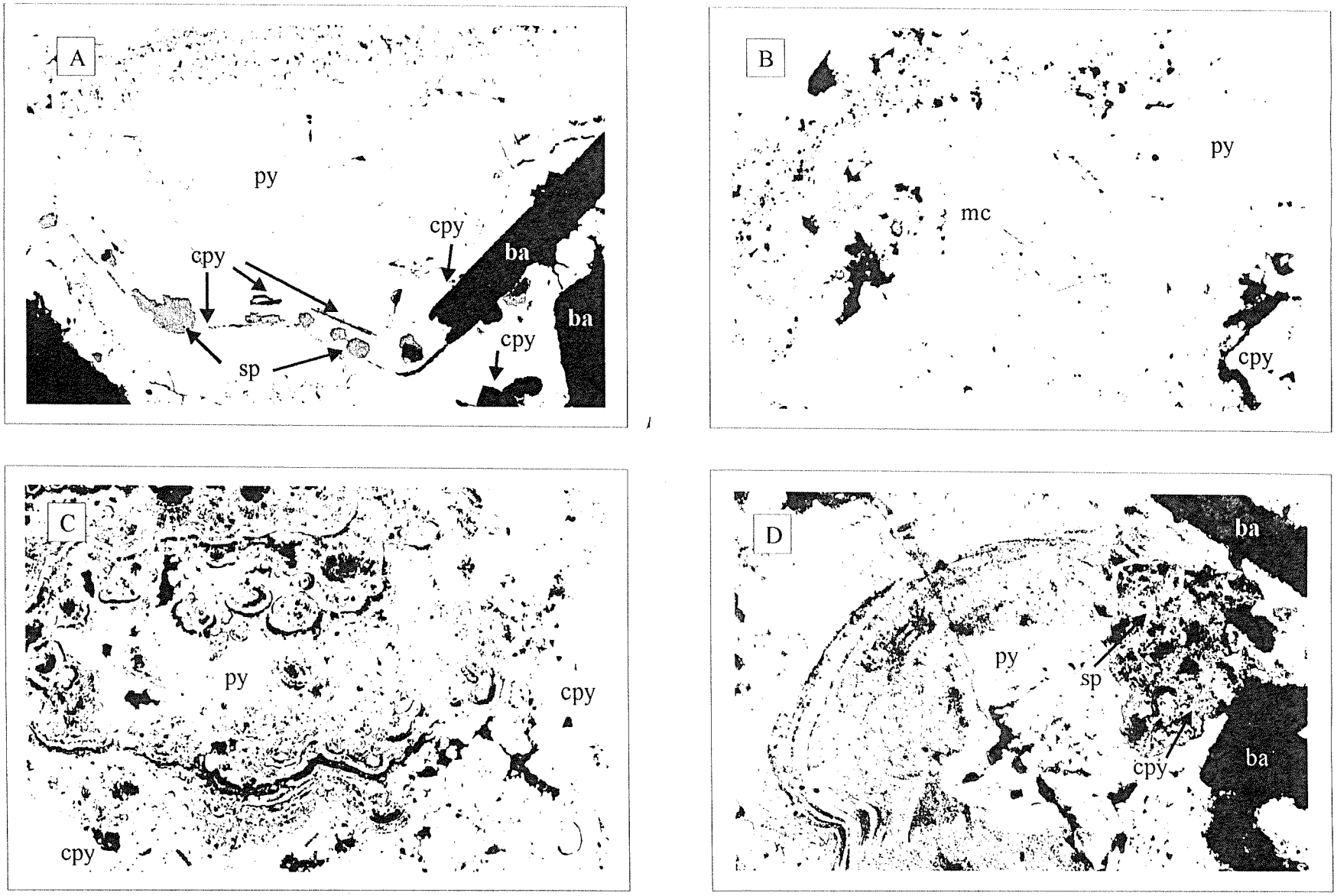


Figure 5.13. Reflected-light microphotographs of massive sulphide mound ore assemblages, A-B (sample 097009), C-D (sample 097056), both fromLerokis Zone 5. (A) Tabular lath of barite and sphalerite inclusions along a growth boundary of massive pyrite. Chalcopyrite is present as thin bands within the growth zones and as thin rims surrounding the sphalerite inclusions and barite laths. (B) Anhedral intergrowth of marcasite within massive pyrite, abundant voids / cavities are evident. (C) Collomorphic pyrite within massive pyrite exhibiting repeated overgrowths. (D) Rhythmic anastimosing collomorphic layers of pyrite overgrowing massive pyrite. The large cavity / void (right of centre) is infilled with a chalcopyrite / sphalerite intergrowth, others are infilled with barite. Minerals: py= pyrite, cpy= chalcopyrite, sp= sphalerite, ba= barite, mc= marcasite. Field of view (A-D) = 5mm.

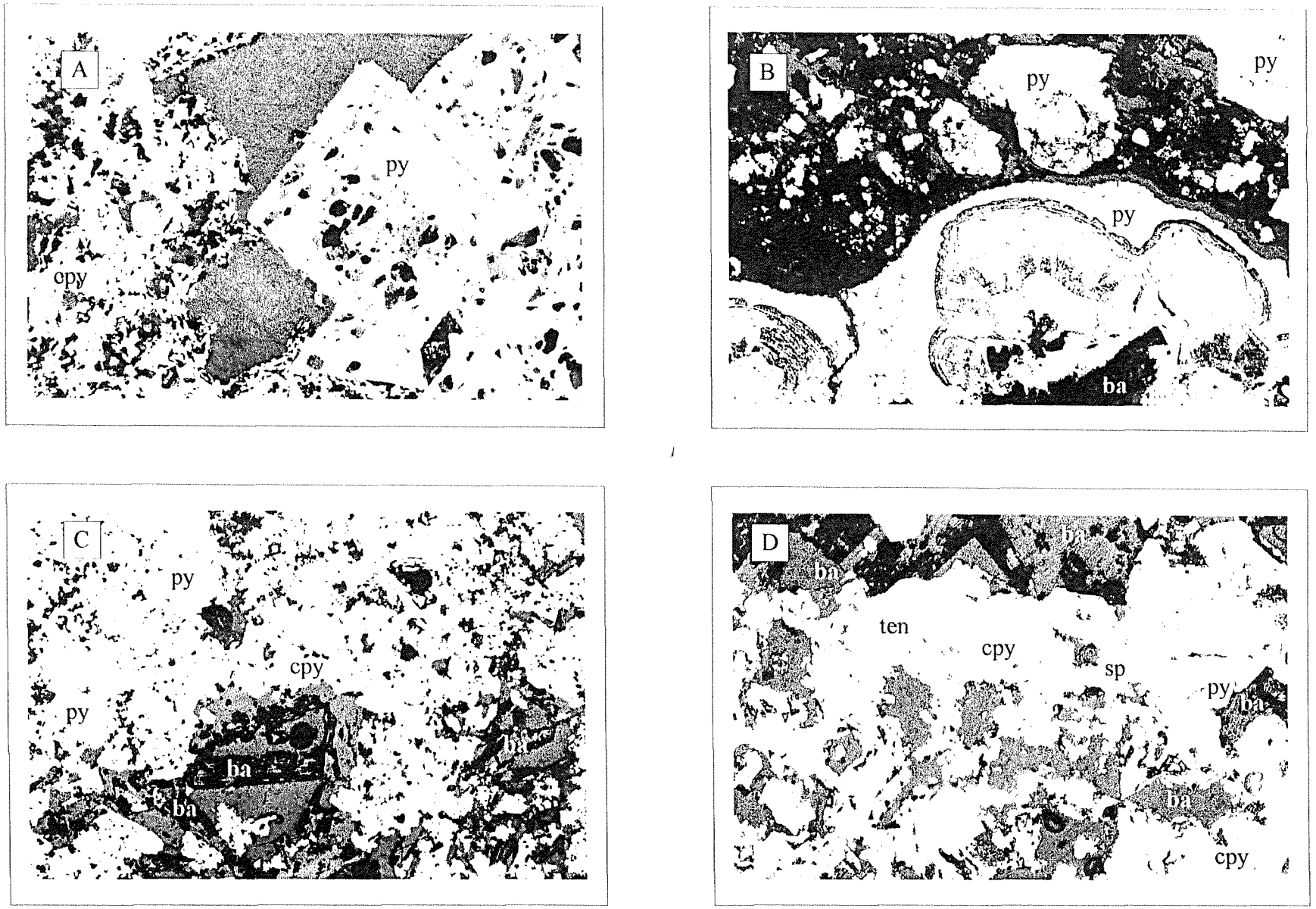


Figure 5.14. Reflected-light microphotographs of massive sulphide mound assemblages, A (sample 111943) from Kali Kuning, B (sample 097009); C (sample 097059); D (sample 097016), B-D are from Lerokis Zone 5. (A) Banded pyrite / chalcopyrite, (see hand specimen, figure 5.3A), field of view = 2.5mm. Euhedral pyrite are replaced and rimmed by chalcopyrite, both phases contain abundant voids / cavities which are empty. (B) Brecciated massive pyrite exhibits an early massive pyrite core (below centre) overgrown by collomorphic pyrite which is subsequently overgrown by massive pyrite before brecciation, field of view = 5mm. (C) Massive pyrite with chalcopyrite replacement, barite laths infill voids / cavities, field of view = 5mm. (D) Chalcopyrite, sphalerite, tennantite, pyrite, barite fracture-fill assemblage between two large clasts of brecciated massive pyrite (not in field of view), field of view = 5mm. Minerals: py= pyrite, ba= barite, ten= tennantite, sp= sphalerite, cpy= chalcopyrite.

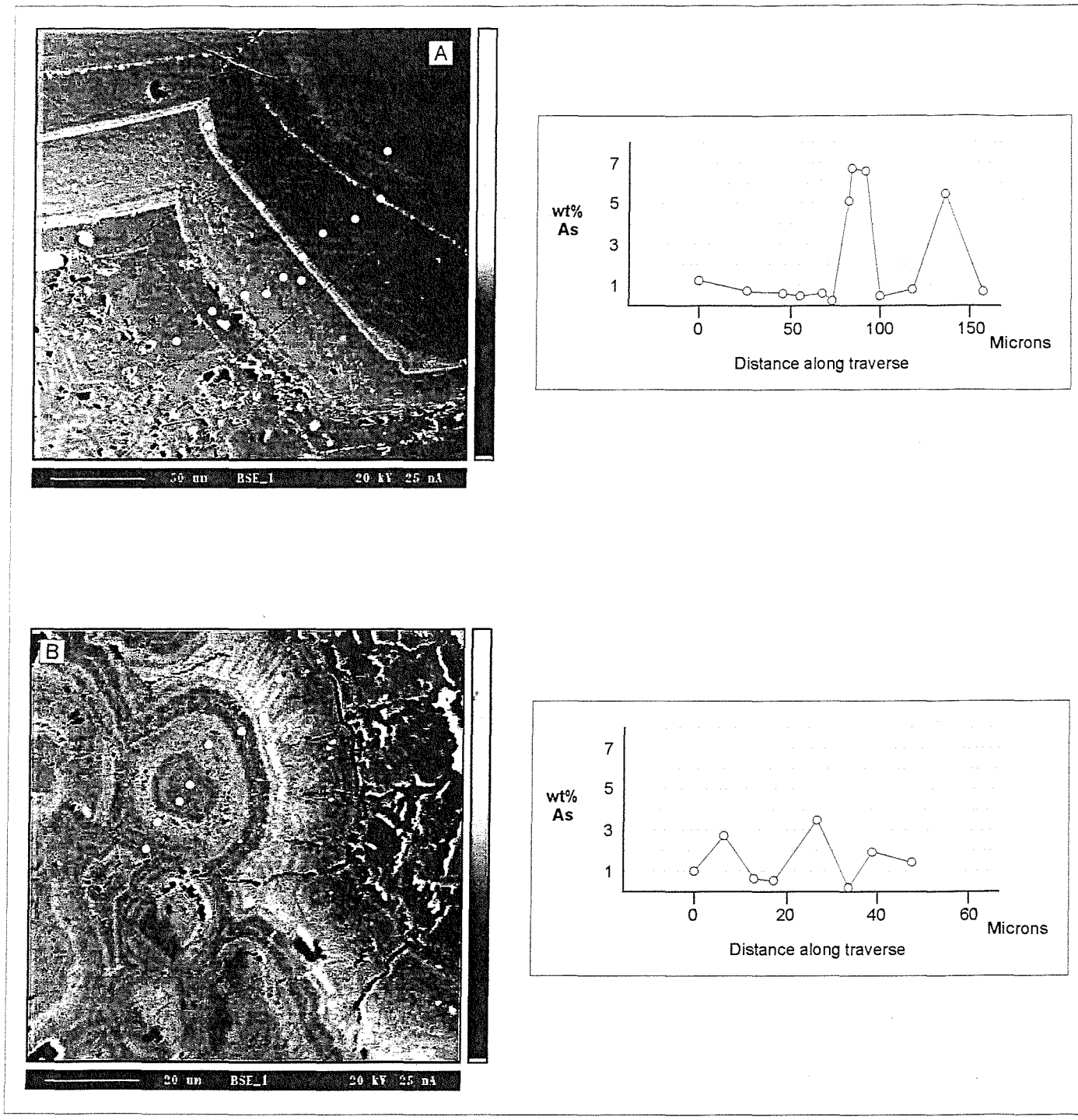


Figure 5.15. Back-scattered electron microphotographs of As zonation within massive pyrite samples from the Lerokis Zone 5 sulphide mound. Point locations are shown which correspond to the microprobe traverse, graphs illustrate the variation of As along each sample. A: sample 097009 illustrates <15 micron euhedral layers. B: sample 099903 illustrates concentric and collomorphic zoning.

Table 5.4. Representative electron microprobe analyses of barite sand cements and inclusion phases from the Kali Kuning and Lerokis orebodies, Wetar Island.

Cementing phases

	Mimetite	*Arsendescloizite*	*Karibibite/Schneiderhohnite?*	*Arsenbrackebuscite*		*Anglesite*	*Fe As phase?*
	Compound%	Compound%	Compound%	Compound%		Compound%	Compound%
Cl	2.094	0.204	0.005	0.058	0.033	0.021	0.013
SO_2	0.649	0.456	1.504	5.257	0.803	18.723	0.474
FeO	0.246	14.019	34.491	26.71	26.48	0.06	80.037
ZnO	0.126	0.068	0	0.123	0.047	0	0
As_2O_5	22.604	30.665	52.851	20.497	28.478	0	2.704
SeO_2	0.028	0.021	0.108	0.157	0.045	0	0
Ag_2O	0.788	0.149	0.068	0.087	0.025	0	0
PbO	73.046	50.645	0	26.597	30.175	58.186	0
Sb_2O_3	0.085	0.044	0.005	0.509	0.394	0.05	0.109
BaO	0.038	0	0.052	1.028	0.234	10.608	0.004
HgO	0	0	0	0	0	0	0.166
Bi_2O_3	0.149	0.33	0.105	0.009	0.233	0.198	0.396
Total	99.853	96.602	89.188	81.031	86.947	87.847	83.903
				Core	Rim		

Incusion phases.

	Bournonite	*Galena*	*Chalcopyrite*	*Argentite*	*Jordanite*	*Pyrite*	*Sphalerite*	*Moschellandsbergite*	*Bornite*
	wt%	wt%	wt%	wt%	wt%	wt%	wt%	wt%	wt%
Fe	0.052	0	29.068	1.255	0	44.858	6.119	0.44	7.148
S	19.356	13.736	34.315	12.004	17.935	51.641	32.613	0	30.455
Cu	12.781	0.024	34.618	0.062	0.03	0.226	0.234	0	62.208
Zn	0	0.158	0.071	0.013	0	0.178	56.282	0	0
As	1.831	0.068	0.1	0.055	11.123	1.419	0.002	0	0
Se	0.031	0.014	0.003	1.203	0.047	0.04	0.025	0.357	0.027
Sb	22.572	1.309	0.117	0	0.643	0.039	0.034	0.01	0
Pb	41.082	84.373	0	0	69.484	0	0	0	0
Hg	0	0	0.137	0.654	0	0	0.059	79.207	0.025
Ag	0.055	0.255	0	80.338	0.001	0.016	0	12.986	0.104
Ba	0.164	0.788	0.869	2.628	0.422	0.666	0.116	0.111	0.464
Total	97.924	100.73	99.298	98.212	99.685	99.083	95.484	93.111	100.431

Analyses were undertaken at the Natural History Museum, London, using a Cameca SX50 analytical scanning electron microprobe, with an accelerating voltage of 15kV, 20nA and count time of 20 seconds. Full data set and detection limits are given in Appendix D.

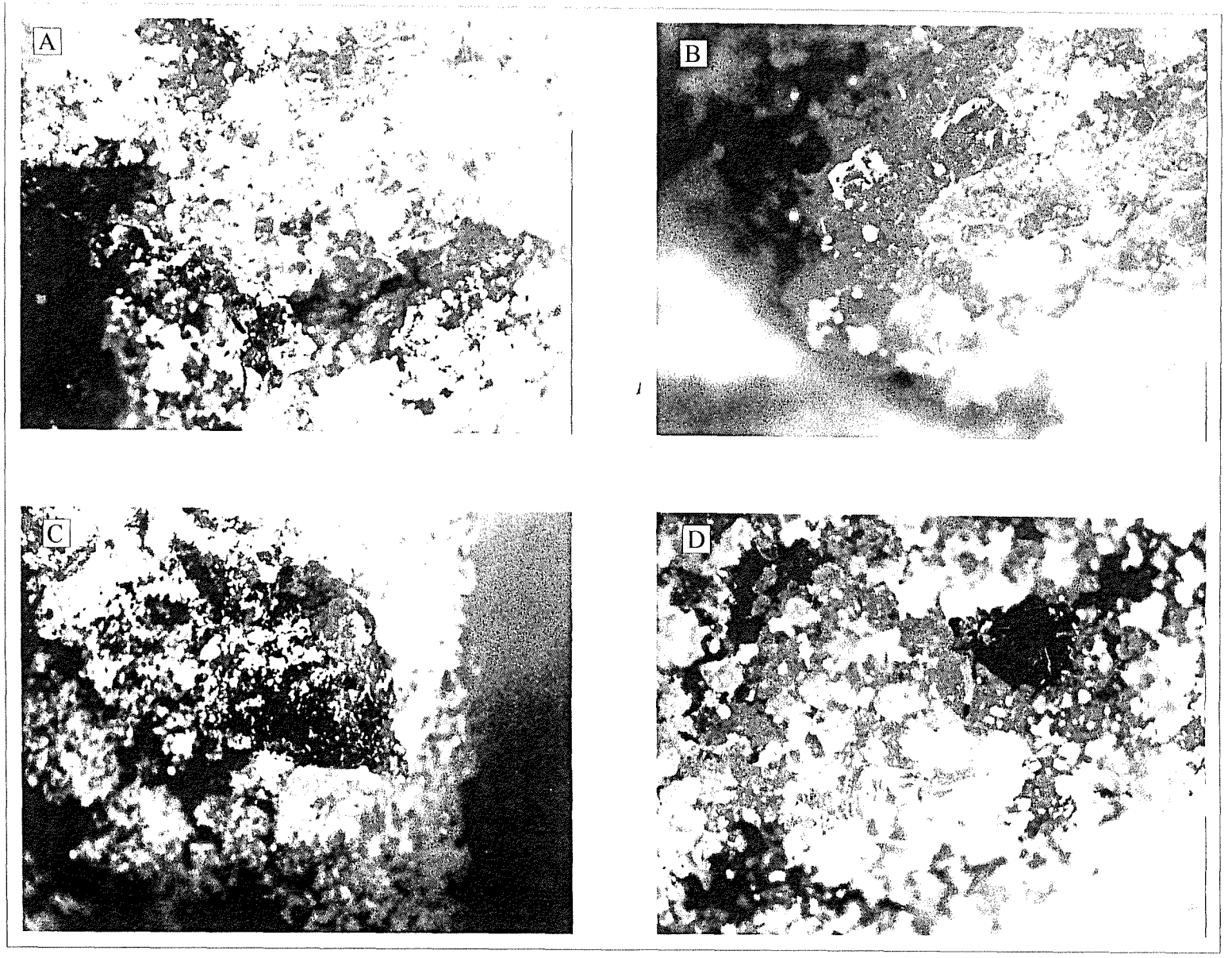


Figure 5.16. A-D, Copiapite and römerite crystals on barite ore, Lerokis Zone 5. (A) Crystals of copiapite (yellow) intergrown with römerite (dark red) and barite (clear / white), field of view = 5 mm. (B) Close-up of copiapite, tabular / bladed crystal faces are evident, field of view = 2 mm. (C) Close-up of römerite, field of view = 2 mm. (D) Fine intergrowth of all three phases, field of view = 2 mm. For XRD traces of each phase see Appendix C.

5.5.2.2 Pyrite

Disseminated pyrite is abundant (Figure 5.17A) and is generally euhedral to subhedral (usually <1 mm). Anhedral pyrite is present associated with intensely silicified volcanics, this feature is shown in Figure 5.17B. The brecciated, hydrothermally altered host volcanics are commonly rimmed with pyrite up to thicknesses of 5 mm. At the greatest depths within the stockwork, euhedral pyrite cubes are present up to sizes of 4 mm. Pyrite increases in abundance with stratigraphic height and is most abundant directly below the sulphide mounds at both Lerokis and Kali Kuning, veins exhibit multiple cross-cutting relationships, brecciation, fracturing and healing within single hand specimens. Veins can reach widths of 5cm in some locations.

5.5.2.3 Galena

Galena has only been identified in two samples (Table 5.2) and is more abundant in the sample at the greatest depth (179 m) below the sulphide mound at Lerokis. In hand specimen, galena can be identified associated with hematite veining as euhedral disseminations up to 5 mm in width. In thin section, galena is evident as being replaced by other sulphide phases (Figure 5.17C). Generally, the galena in this sample occurs at the margin of sphalerite and is surrounded by either chalcopyrite or tennantite.

5.5.2.4 Sphalerite

Deeper within the stockwork, sphalerite is present in close association with galena (5.17C) and also occurs as anhedral (<50 μm) disseminated inclusions within tennantite. In some samples, sphalerite is evident in association with chalcopyrite (Figure 5.17D). However, in the same sample, sphalerite can be seen surrounded by chalcopyrite or surrounding chalcopyrite (Figure 5.18A) and both phases occur as inclusions within each other. In contrast to this sphalerite, Fe-poor sphalerite (yellow in transmitted polarised light) is also present as a fracture fill sulphide and is always associated with covellite and fahlore minerals (Figure 5.19A-D). This sphalerite contrasts with that of the vein / inclusion type within the massive ore in terms of its Fe content. Compositionally, Fe content seldom increases over 0.05 wt% (n = 38) and is evident in thin section as a pale "honey" colour. Collomorphic textures are evident

when associated with covellite and fahlore group sulphides, this is absent when associated with pyrite and chalcopyrite.

5.5.2.5 Chalcopyrite

Occurs dominantly with sphalerite deeper within the stockwork system and replaces pyrite in the majority of samples. Rims of chalcopyrite surround sphalerite, galena and tennantite (Figure 5.17C) and occur as an interstitial phase between euhedral barite laths (Figure 5.17D). In some samples, chalcopyrite occurs as a patchy, irregular vuggy network surrounding other sulphide phases (Figure 5.18B). At the base of the Lerokis Zone 5 sulphide mound, chalcopyrite abundance increases, veins of pyrite that feed the sulphide mound are replaced and are cross-cut, (Figure 5.18C). Veins are not present at widths greater than 1 cm.

5.5.2.6 Fahlore minerals

Fahlore minerals, almost exclusively of tennantite composition are present within the stockwork zones as fracture-fill and are always associated with Fe-poor sphalerite and covellite (Figure 5.19A). The analysis suite (n = 25) indicates both a zinc rich and zinc poor variety (Table 5.4, Figure 5.19B). Compositionally, the Zn rich type has up to 8.3 wt% Zn, ~27 wt% S, ~19 wt% As and between 0.4 and 6.5 wt% Sb. This contrasts to the Zn poor type (0-1 wt% Zn), ~31 wt% S, ~17 wt% As and between 0.1 and 3.9 wt% Sb. In nearly all cases, the Zn poor variety exhibits a collomorphic texture and is surrounded or enclosed by the Zn rich variety, see Figure 5.19C and D. This phase also appears dominantly porous and may again explain low wt% analytical totals (Table 5.4). Tetrahedrite occurs as a minor phase as anhedral to subhedral inclusions (< 20 μm) within the Fe poor sphalerite. Zn is present at ~5 wt%, As ~7 wt% and Sb up to 19.8 wt%.

5.5.2.7 Covellite

Compositional variations (n = 25) range between 0.2 and 1.3 wt% As, low total wt% may be attributed to the fine-grained / porous nature of this phase. Covellite is associated closely to the tennantite and sphalerite particularly along micro-fractures in the latter where they are principal sites for replacement (Figure 5.19A-D). These phases also appear to be replacing an earlier cubic phase in 2 out of the four samples

(5.20A). Covellite is generally more massive when associated with Zn-rich tennantite (Figure 5.20B). In Figure 5.20C, the covellite that replaces the sphalerite along the micro-fractures can be seen to be cross-cut by later zone of zinc rich tennantite. Fragments of covellite with associated tennantite are present deeper within the system inside veins which are rimmed by coarse grained quartz (Figure 5.20D).

5.5.2.8 Barite

Barite laths of varying sizes are present throughout the stockwork zones of both Kali Kuning and Lerokis Zone 5. Sizes are present up to 2 cm and they are dominantly euhedral. When associated with the fracture-fill covellite, tennantite, Fe-poor assemblage (termed the *high-sulphidation* fracture fill assemblage) laths can reach 3cm. Sulphide inclusion phases are easily seen within larger crystals.

5.5.2.9 Silica phases

Amorphous silica is common in stockwork zones, especially in close proximity to the proposed feeder zones. Quartz is present infilling vesicles of the altered host andesites (Chapter 4) and may be present with or without pyrite (Figure 5.18D). Abundant chalcedonic quartz veins occur distal to all ore zones and exhibit traces of sulphide mineralisation, no hydrothermal quartz veins were identified during field mapping associated with mineralisation.

5.5.3 Barite Deposits

The Au-Ag-Hg bearing barite deposits have been described previously as barite sands (Sewell and Wheatley, 1994b and numerous company reports) due to the friable, unconsolidated nature of the deposits. However in some locations they are cemented and are compact. Due to the variable nature of this unit, the term "barite ore" or, "barite deposit" is preferred and used by the author.

Generally, these deposits consist dominantly of fine-grained euhedral barite, (< 5 mm) colours vary from location to location and generally they appear white, pale grey and yellow when friable and a range of orange, reds and browns when cemented. A detailed study of an in-situ lateral barite ore section was investigated at the sulphide

mound / footwall contact at the Kali Kuning deposit, Figure 5.21 (samples 096877-096880, location 84, see also Table 5.5). Other samples on Table 5.5 were analysed optically to identify differences within the barite ore from other location or deposits. Samples were divided in to a > 500 μm and < 500 μm fractions however generally they consisted of the same morphologies. The barites are dominantly euhedral, rectangular, rhombohedral and polyhedral crystals up to 3.5 mm in length, (Figure 5.22) forming interlocking masses. The 3 m section (Figure 5.21) illustrates that moving laterally from the massive sulphide mound, a 10-60 cm zone of pyritic sand (unconsolidated fine-grained pyrite) grades laterally in to variations of barite ore which are evident on the basis of colour alone, cementation also generally becomes greater towards the footwall contact. The results also indicate that there is a dramatic decrease in sulphide content and angularity of barite towards the footwall with a prominent increase in Fe-oxide content. Euhedral yellow crystals (< 2 mm) are present on the surface of barite laths at Lerokis Zone 4, Infra-Red analysis indicates these are crystals of dolomite (for XRD and IR traces see Appendix C). Texturally there does not appear to be any significant differences between the barite ore collected at varying distances or topographic height from the cemented Fe-oxide barite structure at the centre of Lerokis Zone 4 (Table 5.5).

The pyritic sands marks the boundary between the massive sulphide and barite ore and are dominantly composed of angular and irregular masses of pyrite. Euhedral pyrite cubes only occur in minor amounts, some samples contain fine-grained masses of barite which are "intermixed" with the pyrite. The pyritic sands are more extensive at the base of the sulphide mound at Kali Kuning than at location 84.

5.5.4 Barite Cementing Phases

A total of 117 analyses were carried out on 8 selected samples (see Figure 5.23A-H) to identify cementing phases present within the barite ores and to identify inclusion phases within the barite. Table 5.6 presents the results of the analyses with sample numbers and locations. Table 5.4 presents representative microprobe data for individual phases, all data is given in Appendix D, Tables 4-6. Back-scattered electron microphotographs (Figures 5.24- 5.27) illustrate features discussed in the text.

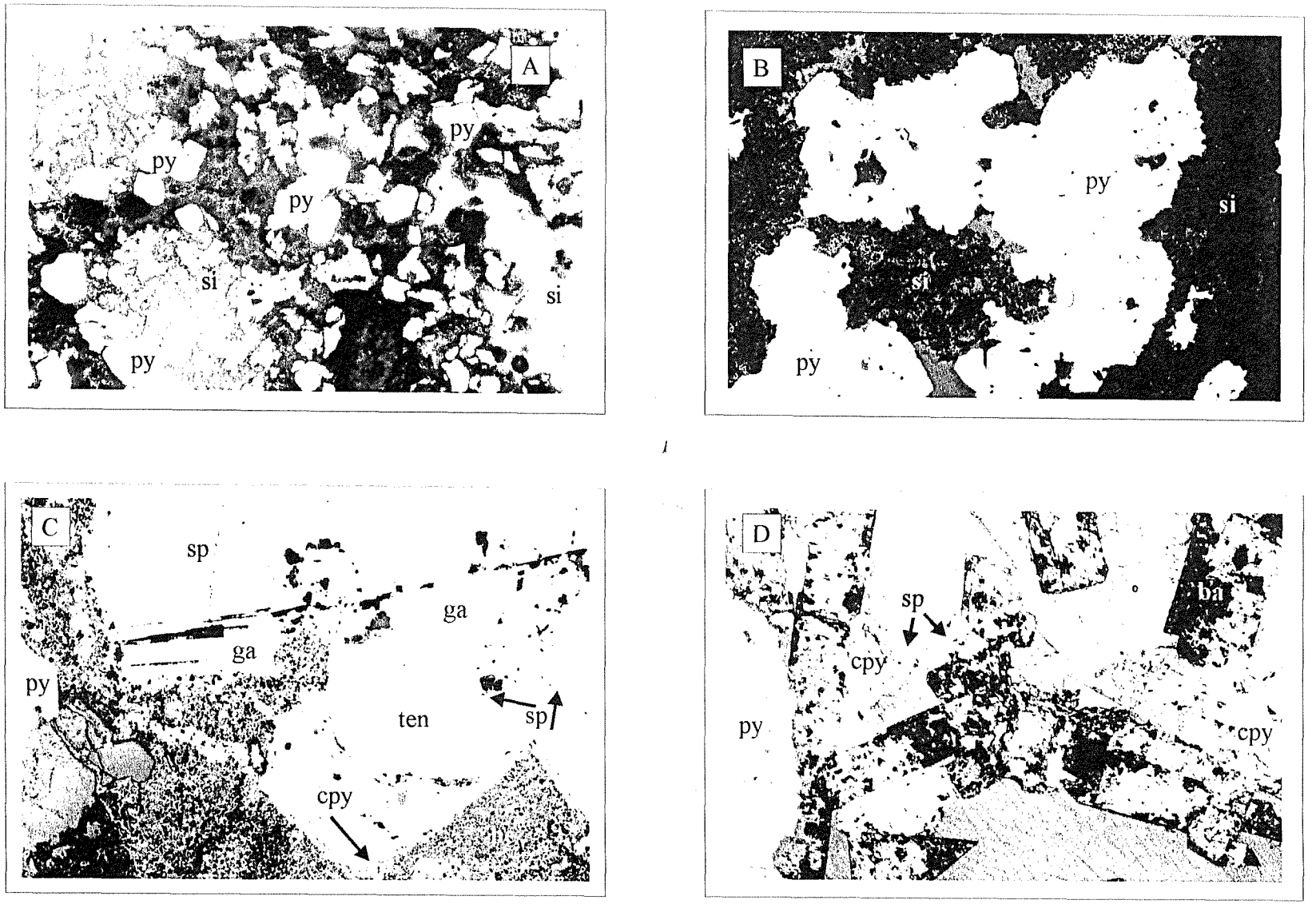


Figure 5.17. Reflected-light microphotographs of suphide assemblages, A, B and D (sample 097104), C (sample 097016), both from Lerokis Zone 5. (A) Abundant disseminated subhedral pyrite inclusions within silicified / clay altered brecciated host volcanics, field of view = 5mm. (B) Anhedral pyrite associated with intensely silicified volcanics, field of view = 2.5mm. (C) Vein-fill assemblage of sphalerite with overgrowth by galena and tennantite and thin chalcopyrite rims associated with hematite veining, field of view = 2.5mm. (D) Massive pyrite brecciated and infilled with tabular barite laths and a chalcopyrite / sphalerite assemblage, field of view = 5mm. Minerals: py= pyrite, cpy= chalcopyrite, sp= sphalerite, ba=barite, ten= tennantite, he= hematite.

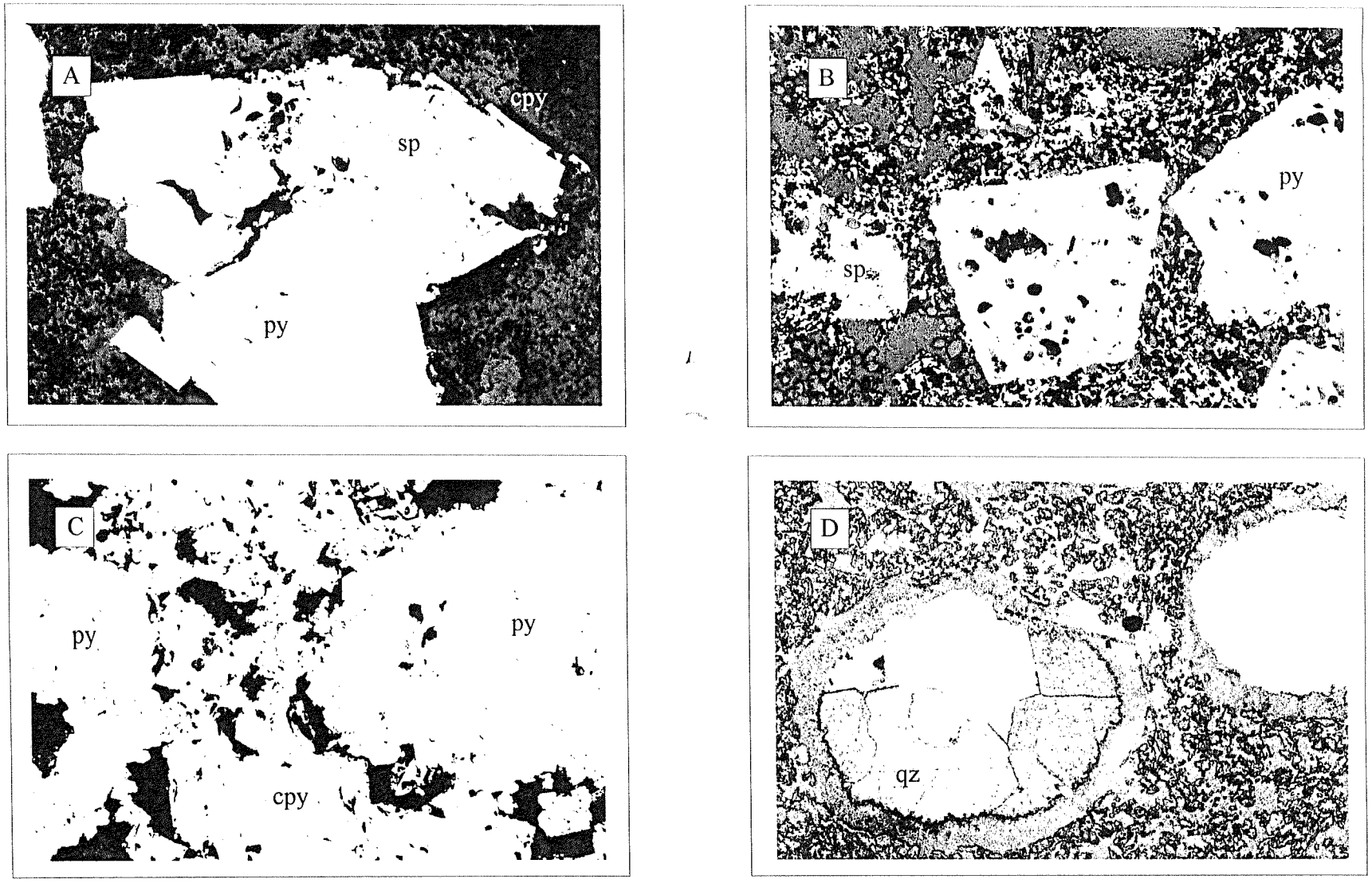


Figure 5.18. Reflected-ligh microphotographs of Wetar sulphide assemblages. (A) Sphalerite - chalcopyrite assemblage surrounding euhedral pyrite field of view 2.5mm. (B) Patchy, irregular network of chalcopyrite surrounding sphalerite and pyrite, field of view 2.5mm. (C) Chalcopyrite replacement of pyrite, field of view 5mm. (D) Quartz filling vesicles within altered host volcanics, field of view 5mm. Minerals: py= pyrite, cpy= chalcopyrite, sp= sphalerite, qz= quartz.

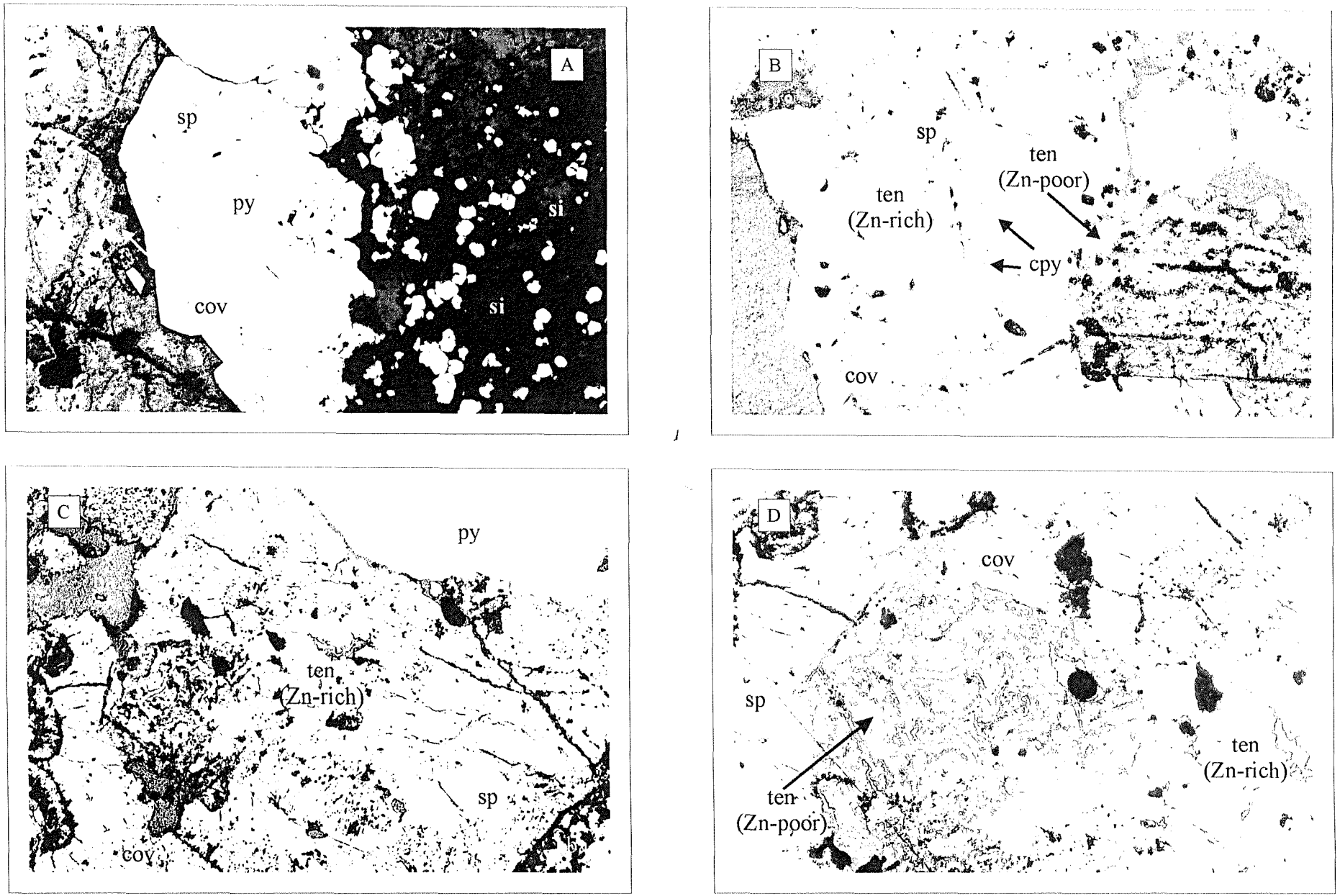


Figure 5.19. Reflected-light microphotographs of fracture-fill *high-sulphidation* sulphide assemblages, sample 097122 (for hand specimen see Figure 5.6C). (A) Fine-grained disseminated pyrite (right), associated with silicified / brecciated host volcanics, grades to a pyrite rim (centre) and *high-sulphdation* fracture-fill (left), field of view = 5mm. (B) Zinc-poor tennantite and covellite with overgrowth of zinc-rich tennantite, note the close relationship of covellite and Fe-poor sphalerite, field of view = 2.5mm. (C) Pyritic margin of brecciated host stockwork volcanics surrounded by *high-sulphidation* sulphide assemblage. Sphalerite contains abundant fractures which are principle sites for covellite replacement. Collomorphic texture is evident within the Fe-poor sphalerite (bottom left). The covellite replacement makes this texture more evident, field of view = 5mm. (D) Close-up of (C) illustrating the porous and collomorphic nature of the zinc-poor tennantite phase, field of view = 2.5mm. Minerals: py= pyrite, qz= quartz, ten= tennantite, cov= covellite, sp= sphalerite, ba= barite, si= silicified host volcanics.

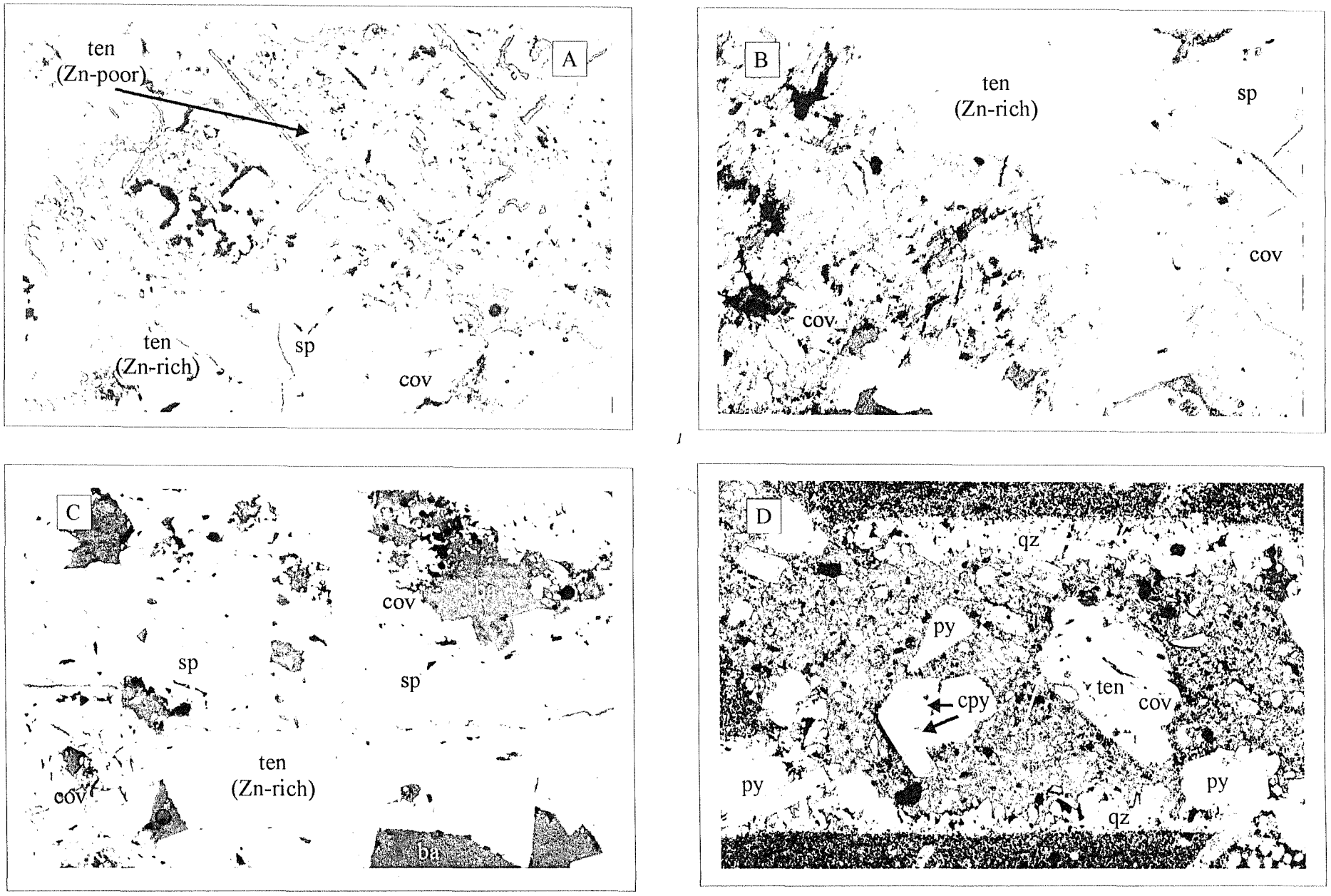


Figure 5.20. Reflected-light microphotographs of fracture-fill *high-sulphidation* sulphide assemblages (A-C) sample 097122 (for hand specimen see Figure 5.6C). (A) Zinc-poor tennantite and covellite replacive of an earlier cubic phase and surrounded by Fe-poor sphalerite / covellite (bottom) and zinc-rich tennantite (left), field of view = 2.5mm. (B) Zinc-rich tennantite separates two areas of covellite. The covellite associated with the Fe-poor sphalerite (right) is porous compared to that associated with the tennantite (left), the latter exhibiting stronger anisotropy, field of view = 2.5mm. (C) Zinc-rich tennantite cuts a former continuous zone of sphalerite and covellite. The covellite terminates at the contact with the tennantite therefore both phases predate the tennantite within the paragenesis, field of view = 2.5mm. (D) A deep stockwork vein (with coarse margin) contains covellite associated with tennantite, chalcopyrite, Fe-poor sphalerite and pyrite, field of view = 5mm. Minerals: py= pyrite, cpy= chalcopyrite, cov= covellite, ten= tennantite, sp= *sphalerite*, *ba= barite*, *qz= quartz.*

Table 5.5. Description and results of microscope analyses from barite ores and pyritic sands, Wetar Island, Indonesia. Data presents barite ore costituents, morphologies and abundances.

Sample	Description	Location	Size fraction	% Barite	Description / morphology	Comments	Probe Study
111975	White/yellow barite ore	Lerokis Zone 4 (location 146)	>500 um	99	90% of crystals are euhedral to sub-hedral rectangular, rhombohedral and polyhedral crystals up to 3.5 mm in length. Some minor cementing by jarositic material is evident. Numerous barite crystals are intergrown.	Sample collected 20m from the Ba-Fe oxide feeder structure at the centre of Lerokis Zone 4	Yes
			<500 um	99	The finer fraction is the same as the coarse fraction.		
111930	Yellow/grey barite ore	Lerokis Zone 4 (location 216)	>500 um	95	70% of the crystals are sub-hedral rectangular and rhombohedral crystals up to 2.5 mm. 20% are euhedral, rhomohedral and polyhedral . The remaining fraction is fine-grained, sugary masses of barite. Minor aggragates of sinterous looking material are present, some larger barite crystals have tiny (<1 mm) yellow dolomite crystals on there external faces.	Collected 120m from the Ba-Fe oxide feeder structure at the centre of Lerokis Zone 4. Sample collected @ a height of 1 5m.	Yes
			<500 um	90	The finer fraction is the same as the coarse fraction however there is an increase the sinterous material. The finest fraction are euhedral to anhedral fragments and shards.		
111983	Yellow/brown barite ore	Lerokis Zone 4 (location 152)	>500 um	99	90% of crystals are euhedral to sub-hedral rectangular, rhombohedral crystals up to 3.5 mm in length. Some minor cementing by jarositic material is evident. Numerous barite crystals are intergrown.	Collected 130m from the Ba-Fe oxide feeder structure at the centre of Lerokis Zone 4. Sample collected @ a the base of the pit.	Yes
			<500 um	98	The finer fraction is the same as the coarse fraction.		
096858	Black pyritic sand	Kali Kuning (location 75)	>500 um	0	Unusual, angular / fragmental massive pyrite, a few euhedral cubic pyrite faces are evident in places.	Sample collected at the base of the Kali Kuning pit. Not cemented	No
			<500 um	1	The fine fraction is as before however no euhedral faces are seen. Complete destruction of the massive pyrite in to angular / fragmented clusters.		
096890	Black pyritic sand	Kali Kuning (location 87)	>500 um	40	Sample dominated by anhedral masses of massive pyrite, numerous fine-grained masses of barite / pyrite are present accounting for 80% of the barite in the sample. The remaining fraction of barite is euhedral to anhedral, rectangular and rhombohedral crystals up to 2mm. Cubic faces are evident in some of the massive pyrite. One fragmented anhedral sphalerite mass was evident.	Sample collected at the top of the Kali Kuning mound at the sulphide / footwall contact.	No
			<500 um	60	Same as coarse fraction, 95% of barite occurs as fine-grained masses with pyrite, only minor individual crystals noted.		
096877	Grey/brown barite ore	Kali Kuning (location 84)	>500 um	90	65% of crystals are euhedral, rectangular, rhombohedral and polyhedral crystals up to 3 mm. Larger masses are comprised of fine-grained barite (euhedral to anhedral) with associated fine-grained sugary barite. Smaller euhedral to anhedral barites are also abundant. 5% pyrite is present with some fine-grained pyrite-barite masses	Sample collected at the top of the Kali Kuning mound at the sulphide / footwall contact.	No
			<500 um	99	Only 1% pyrite, barite nature as for coarse fraction, all clear barite contain sulphide inclusions. Fine-grained masses of barite exhibit Cu staining, smallest fragments/ shards are broken from larger crystals.		
096878	Grey barite ore	Kali Kuning (location 84)	>500 um	85	1% pyrite, 5% residual silica + Fe oxides. 50% of barites are euhedral rectangular, rhombohedral and polyhedral (minor) crystals up to 4 mm. Numerous fine-grained masses of euhedral rectangular and rhombohedral crystals are cemented by jarositic looking material. Some barites are intergrown, fine shards/fragments are abundant.	Sample collected at the top of the Kali Kuning mound at the sulphide / footwall contact.	No
			<500 um	97	Barite nature as for the coarse fraction, reduction in cementation and oxides.		
096879	White / grey barite ore	Kali Kuning (location 84)	>500 um	90	50% of crystals are euhedral, rectangular, rhomohedral and polyhedral crystals up to 3 mm. Smaller tabular crystals are cemented by and are associated with fine-grained sugary barite. Clear crystals contain sulphide inclusions. There are no free sulphides within the sample.	Sample collected at the top of the Kali Kuning mound at the sulphide / footwall contact. More competent sample, greater degree of cementation.	Yes
			<500 um	97	Nature of barites as for coarser fraction, less cementation and Fe-oxides.		
096880	Grey / green barite ore/ clay	Kali Kuning (location 84)	>500 um	99	Fine grained sugary looking barite, some have an external brown staining. No sulphides present or tabular crystals.	Sample collected at the top of the Kali Kuning mound at the sulphide / footwall contact.	No
			<500 um	80	Euhedral, rectangular, rhombohedral and polyhedral barite crystals . Abundant fine-grained masses of barite are present with some fine-clay material. No sulphides are present.		
099944	Orange/red/ yellow/white banded barite ore	Kali Kuning (location 50)	>500 um	30	Tabular, subhedral rectangular and rhombohedral crystals up to 1 mm. Barite occurs as disseminations and anastimosing layers within a white sinter and yellow jarositic fine-grained ground-mass material.	Sample collected at the top of the massive sulphide body under the limestone/chert contact.	Yes
			<500 um	40	Increase in barite, same features as for coarse fraction.		

Table 5.6. Description and results of SEM and Electron Microprobe analyses from cemented barite/Fe oxide structure and barite ore, Wetar Island, Indonesia. Data presents cementing phases present within the barite ores and inclusions present within barite laths.

Sample	Description	Location	Cementing Phases	Abundance %	Comments	Inclusion Phases	Comments
099923	Section of feeder pipe	Lerokis Zone 5 (location 19)	FeAs phase? Fe oxides Jarosite $KFe_3^{3+}(SO_4)_2(OH)_6$	10 70 20	Barite laths <2.5mm are euhedral to anhedral, rimmed and cemented by Jarosite and Fe oxides. Fe oxides are porous throughout, evidence that barite laths have been brecciated and re-cemented	Acanthite Ag_2S Sphalerite ZnS Chalcopyrite $CuFeS_2$ Galena PbS	Very few sulphide inclusions present. They are generally subhedral to anhedral <20υm. The acanthite inclusion is ~ 20υm and euhedral.
096948	Section of feeder pipe	Lerokis Zone 4 (location 129)	Fe oxides	100	Fe oxides are completely amorporous and porous throughout. They rim and cement subhedral to anhedral barite laths <2mm.	Chalcopyrite $CuFeS_2$ Jordanite $Pb_{14}(AsSb)_6S_{23}$ Galena PbS Pyrite FeS_2	Very few sulphide inclusions present, subhedral to anhedral <25υm.
111930	Yellow/brown barite ore	Lerokis Zone 4 (location 216)	Anglesite $PbSO_4$ Römerite $Fe^{2+}Fe_2^{3+}(SO_4)_4.14H_2O$ Silica SiO_2	5 60 35	Minor barite laths <1mm are present, all other barite broken in to euhedral to anhedral fragments, shards and laths. These are cemented in part by porous / amorphous Fe oxides.	Galena PbS Chalcopyrite $CuFeS_2$	Minor anhedral inclusions <15υm.
096879	White barite ore	Kali Kuning (location 84)	Anglesite $PbSO_4$	5	Euhedral barite laths <3mm are generally "not" cemented. In places anglesite cements barite laths anglesite pseudomorphs galena and is <150υm.	Argentite Ag_2S Pyrite FeS_2 Galena PbS	Anhedral sulphide inclusions <10υm. Galena incusions present within Anglesite.
111975	White/yellow barite ore	Lerokis Zone 4 (location 146)	No phases present	Na	Euhedral to subhedral barite laths <2mm have an interlocking nature in part (recrystallisation texture)	Galena PbS Bournonite $PbCuSbS_3$ Chalcopyrite $CuFeS_2$ Bornite Cu_5FeS_4 Sphalerite ZnS Acanthite Ag_2S	Numerous subhedral to anhedral inclusions <10υm.
099944	Orange/red/ yellow/white banded barite ore	Kali Kuning (location 50)	FeAs phase (no Pb) Römerite Jarosite Jasper SiO_2 Moschellandsbergite Ag_2Hg_3	20 10 60 9 1	FeAs phase occurs as a cementing phase, generally as <10υm euhedral to subhedral rhoms. Fe oxides are amorphous and porous throughout, jarosite rims barite which is rimmed by amorphous FeAs phase. Moschellandsbergite occurs as disseminations (<5υm) within the matrix Fe oxide.	Chalcopyrite $CuFeS_2$ Pyrite FeS_2	Minor subhedral to anhedral inclusions <200υm.
099911	Section of feeder pipe	Lerokis Zone 5 (location 12)	Fe Oxides (determined by SEM)	100	Fe oxides rim and cement euhedral to anhedral barite laths (<1mm). No probe data.	Pyrite FeS_2 Chalcopyrite $CuFeS_2$	Minor euhedral to anhedral inclsions <20um.
111983	Yellow/brown barite ore	Lerokis Zone 4 (location 152)	Mimetite $Pb_5(AsO_4)_3Cl$ Arsendescloizite $PbZn(OH)(AsO_4)$ Arsenbrackebuscite	30 50 20	Mimetite cements euhedral to anhedral barite laths (<2.5mm) and is amorphous, variations in Ag are evident. Arsendescloizite occurs as laths/needles (<20υm) at margins of amorphous arsendescloizite. FeAs phase occurs as amorphous cement and is zoned, cores are < As&Pb, more Sb&S.	Galena PbS Sphalerite ZnS	Very few anhedral inclusions <10um.

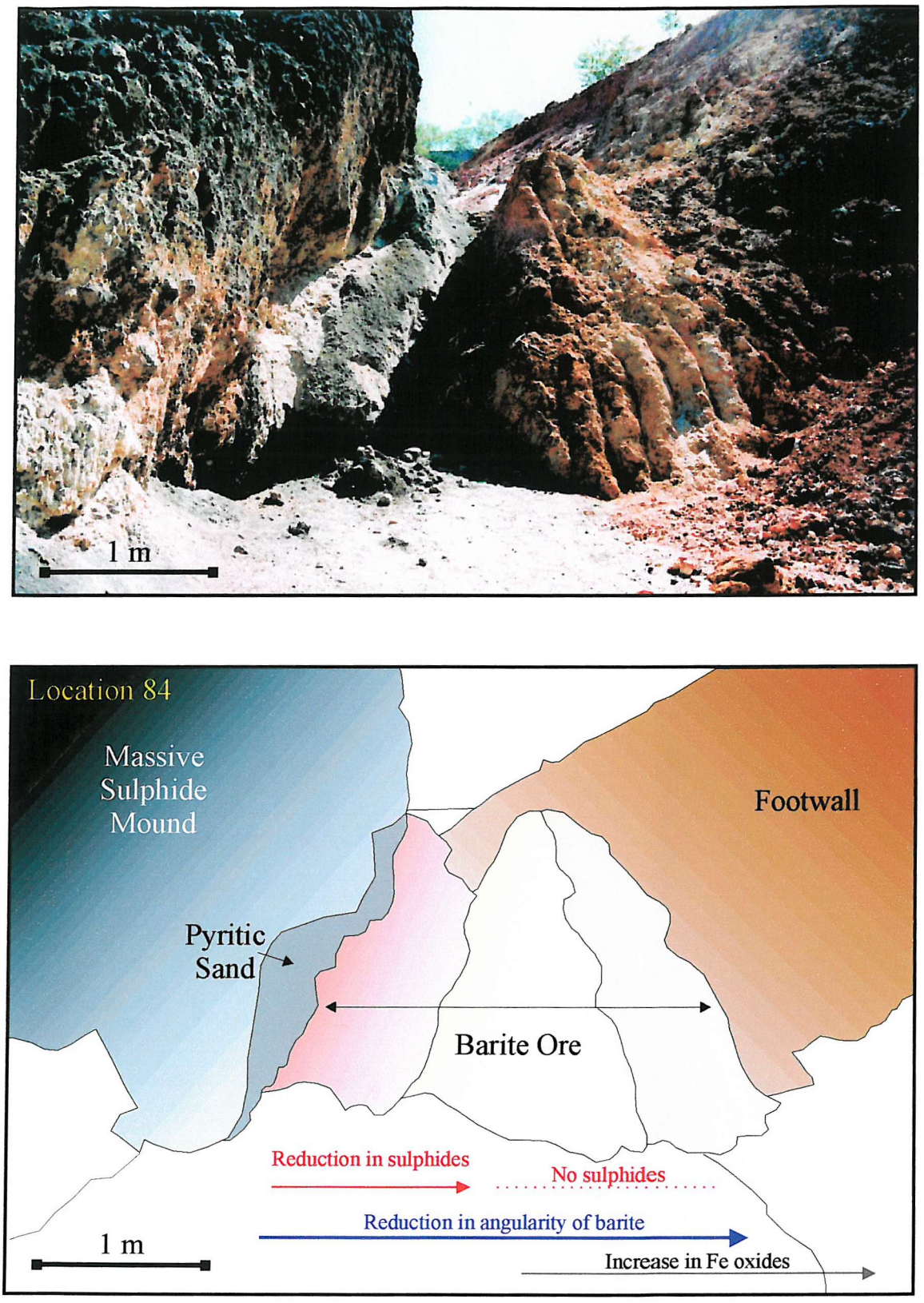
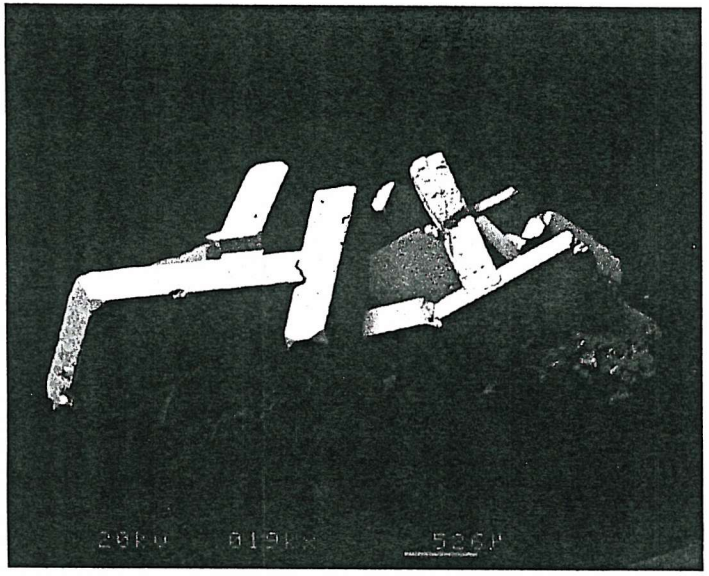
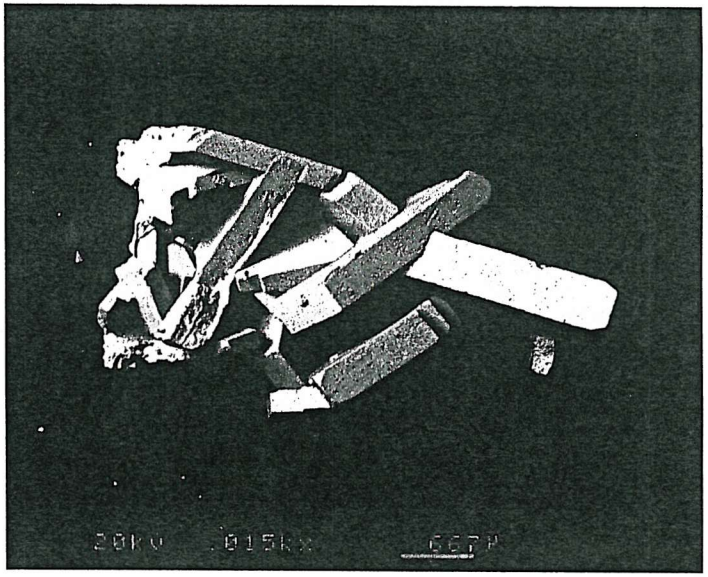


Figure 5.21. Detailed in-situ section of contact zone between massive sulphide mound, pyritic sand, barite ore and hydrothermally altered footwall, location 75 Kali Kuning. The section illustrates the results of a microscopic study of the pyritic and baritic ore. Samples were sieved into fractions > and < 500 microns. Results from the study are given in table 5.5. Generally, a reduction of sulphides and angularity of barite decrease towards the footwall of the deposit whilst there is a marked increase in Fe-oxides.





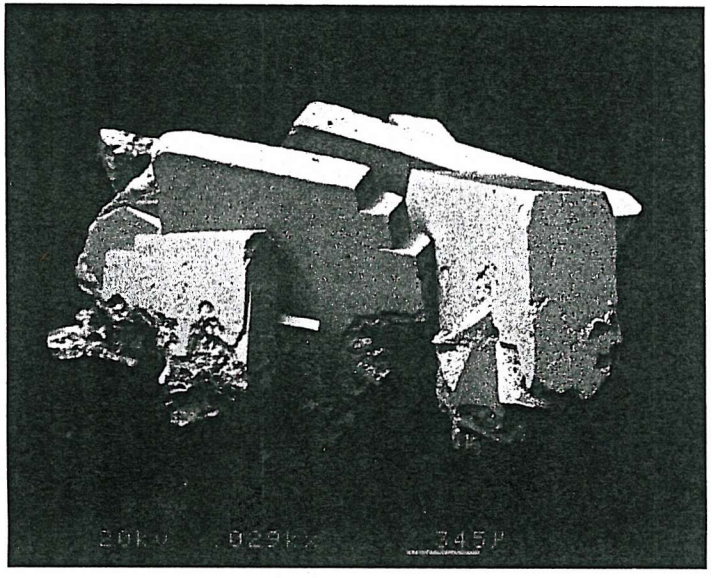


Figure 5.22. Rectangular, rhombohedral and polyhedral interlocking barite crystals from barite ore sample 096879, Kali Kuning. Scale bars are shown.

UNIVERSITY OF SOUTHAMPTON LIBRARY

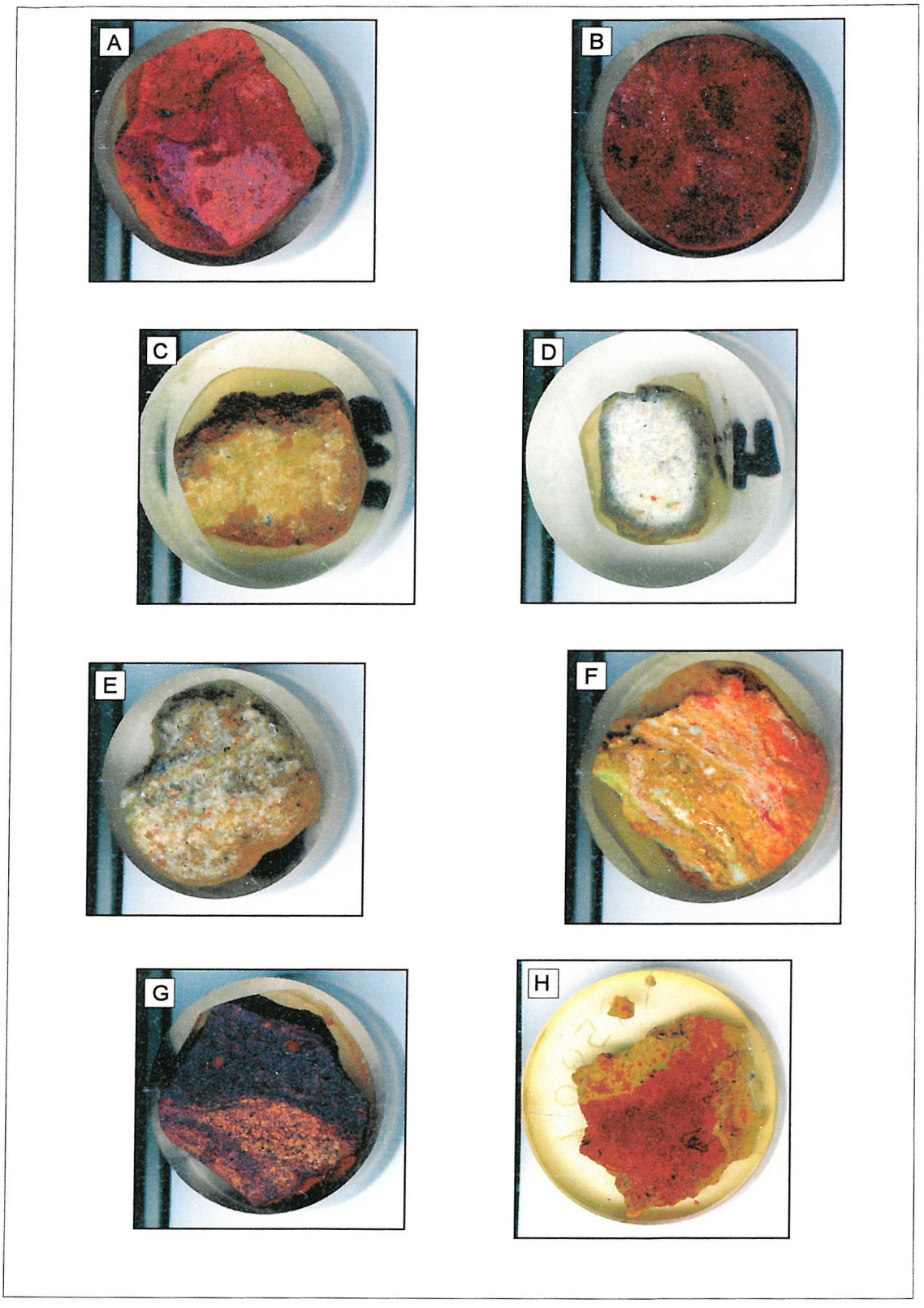


Figure 5.23. Baritic blocks for microprobe and SEM study to identify cementing phases and inclusion phases within the barite ore. (A) sample 099923, (B) 096948, (C) 111930, (D) 096879, (E) 111975, (F) 099944, (G) 099911, (H) 111983. For sample description, location and results of morphological study see Table 5.5, for results of inclusion phases and cements see Table 5.6, microprobe data is given in Appendix D.

Cementing phases comprise dominantly of zoned, collomorphic Fe-oxides and complex arsenates. For all phases, repeat analyses were performed. Anglesite is observed pseudomorphing galena (sample 096879) which cements both tabular laths of barite and brecciated fragments from within the Fe-oxide structure (Figure 5.24A-C). Arsendescloizite $PbZn(OH)(AsO_4)$, arsenbrackebuscite $Pb_2(FeZn)(AsO_4)_2.H_2O$ and mimetite $Pb_5(AsO_4)_3Cl$, are all found intergrown and cementing euhedral, tabular barite laths in sample 111983 (Figure 5.24D). Mimetite is the dominant cementing phase, microprobe analysis indicates a range between 0 and 0.9 compound% Ag_2O (n =6); generally this phase is amorphous (Figure 5.24D and 5.25A). Arsenbrackebuscite occurs within this sample as rhombic crystals (< 20 μm in size) and shows compositional zoning, the cores are < As and Pb (wt%) than margins and also > Sb and S than the margins (Figure 5.24D, 5.25A, 5.26 and Table 5.6). This phase also occurs as an amorphous cement, its porous nature yields low analytical totals. The cores of the zoned phase also yield low totals in comparison to the outer margins (Table 5.6). Arsendescloizite occurs as both an amorphous phase (Figure 5.24D) and needle like laths (< 20 μm) with no significant compositional difference, the needles are present at the margin of amorphous phase (Figure 5.25A and B). Wavelength dispersive element mapping was performed on this sample (111983) with the aim of mapping Ag distribution within the cementing phases. Figure 5.26 presents the X-ray maps and although these are only qualitative they illustrate that Ag and Pb are concentrated within mimetite. Fe is concentrated within arsenbrackebuscite and As within arsendescloizite. An iron-rich arsenate phase is present in (sample 099944) which may be either Karibibite $Fe_2^{3+}As_4^{3+}O_9$ or Schneiderhohnite $Fe_2{+}Fe_3^{3+}As_5^{3+}O_{13}$ (Figure 5.25C). This phase is also present as euhedral to subhedral rhombs (n =8) which are less than (< 10 μm) and therefore yield low analytical totals, compositionally this phase contains 33.7 to 34.2 compound % FeO and 49.9 and 52.8 compound % As_2O_5. Moschellandsbergite (Ag_2Hg_3) occurs as free, anhedral (<5 μm) grains within the Fe-oxide cement (sample 099944), see Figure 5.25D. This phase is only present in this sample, (n = 6) low totals account for the small size. The Hg bearing phase (Moscellandsbergite) occurs only at the stratigraphically highest point at Kali Kuning near to the overlying chert / limestone cover, the Ag bearing mimetite phase along with the majority of the complex

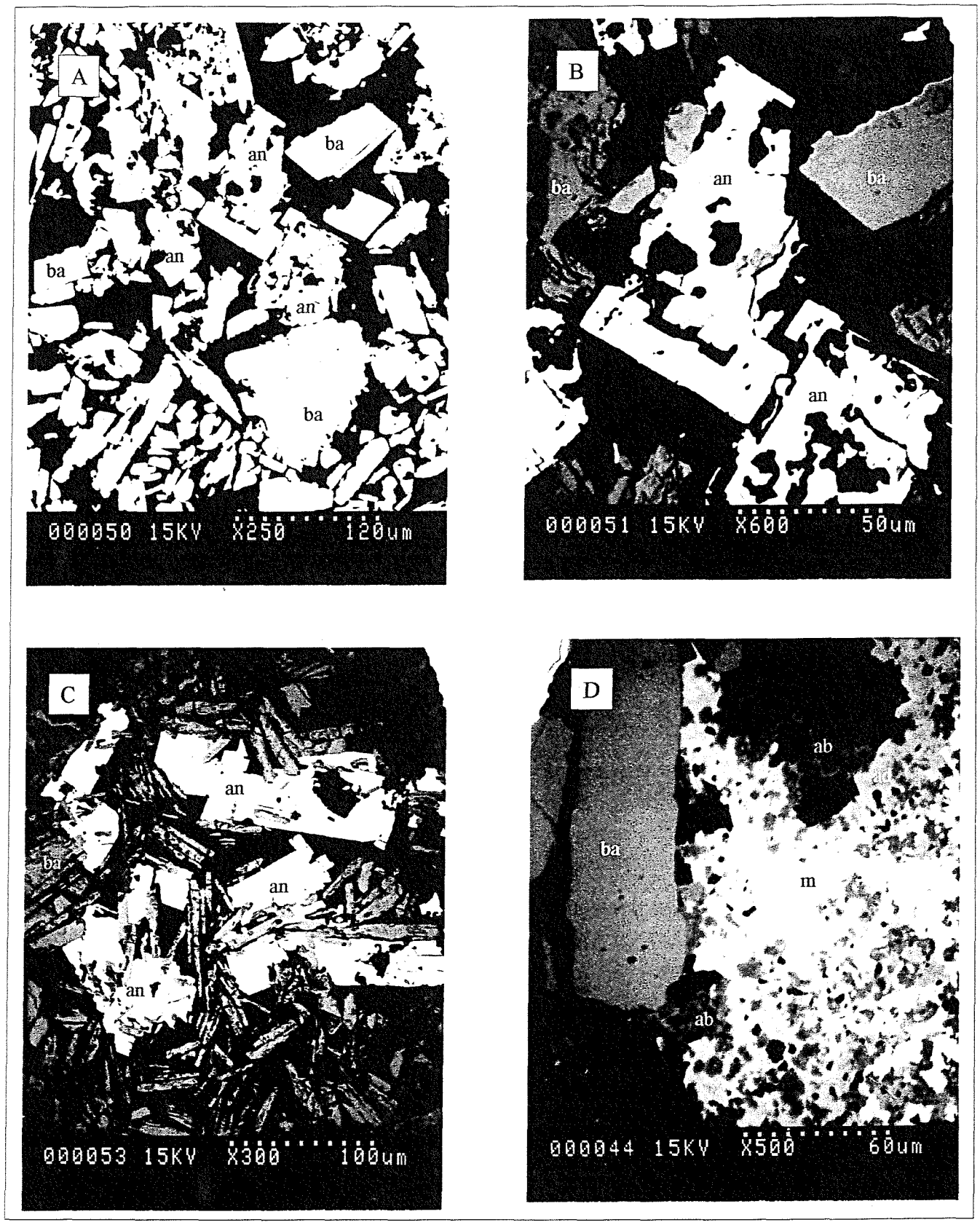


Figure 5.24. Back-scattered electron microphotographs of the Wetar Island barite ore, Indonesia. (A-C) Sample 096879, illustrating the secondary nature of anglesite (an) pseudomorphing cubic galena and cementing laths of barite (ba). (D) Sample 111983, a barite lath is cemented by mimetite (m), arsendescloizite (ad) and arsenbrackebuscite (ab). For samples used, location and descriptions see Table 5.5 and Figure 5.23. Scale bars are given on each photomicrograph, for all analytical data see Appendix D.

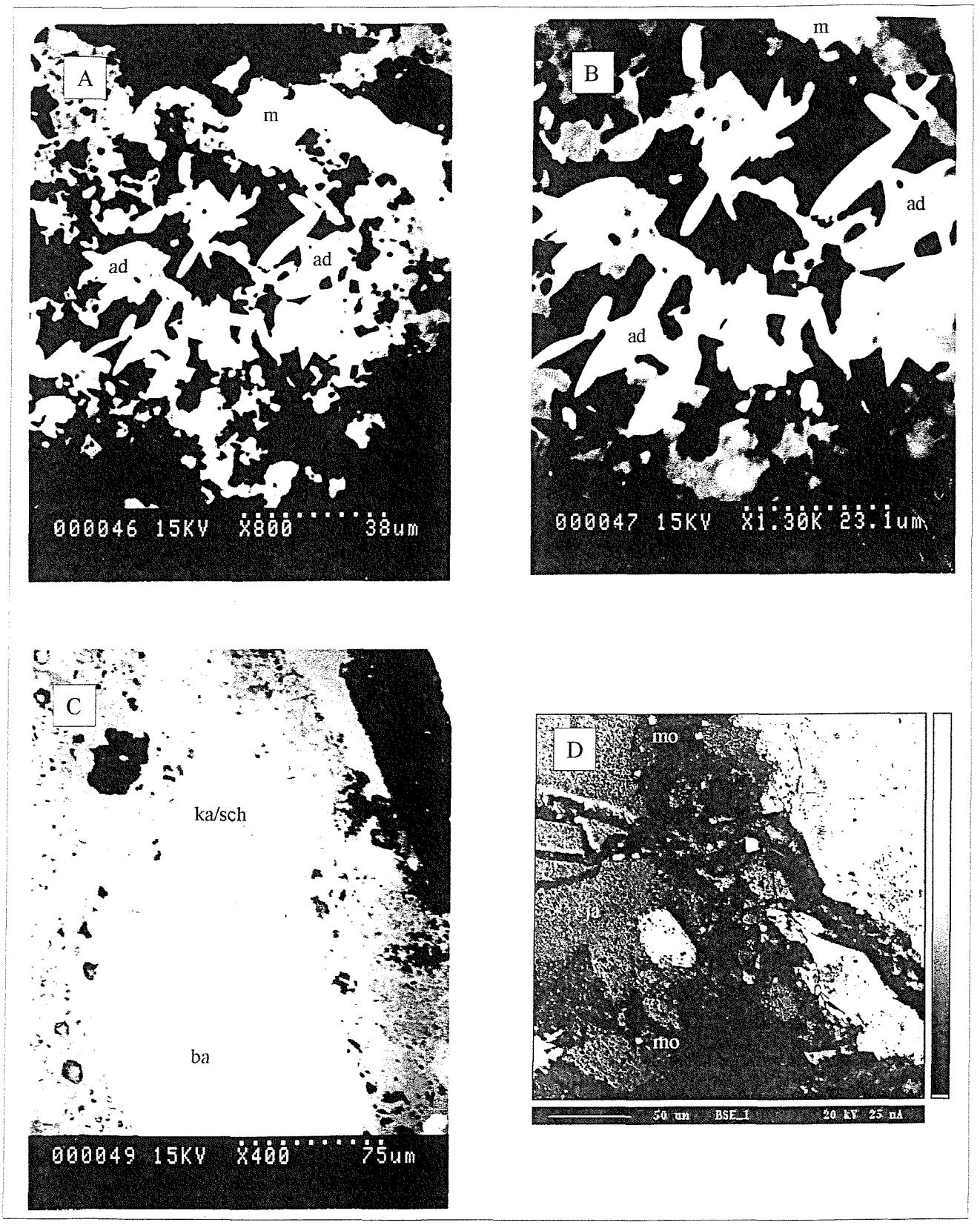


Figure 5.25. Back-scattered electron microphotographs of the Wetar Island barite ore, Indonesia. (A-B) Sample 111983, illustrating the needle like nature of the arsendescloizite (ad) phase, A also shows the association of mimetite. In both A and B, the zoning of the arsenbrackebuscite (ab) phase is evident. (C) Sample 099944 showing a barite lath rimmed by jarosite (ja) subsequently rimmed by karibibite or schneiderhohnite (ka/sch). (D) Sample 099944, moschelandsbergite (mo) occurs as subhedral to anhedral <10 micron phase associated with jarosite. For samples used, location and descriptions see Table 5.5 and Figure 5.23. Scale bars are given on each photomicrograph, for all analytical data see Appendix D.

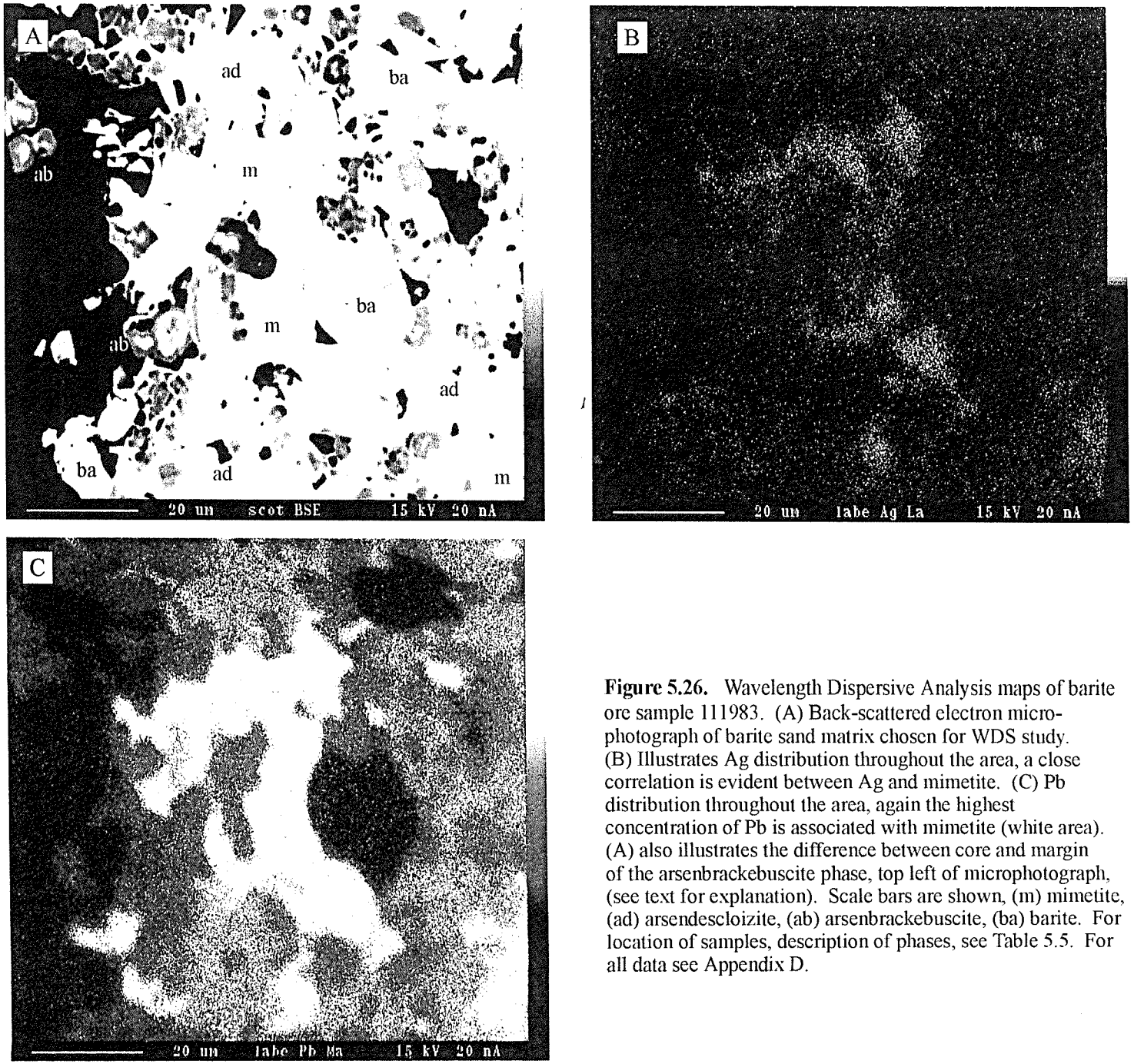


Figure 5.26. Wavelength Dispersive Analysis maps of barite ore sample 111983. (A) Back-scattered electron micro-photograph of barite sand matrix chosen for WDS study. (B) Illustrates Ag distribution throughout the area, a close correlation is evident between Ag and mimetite. (C) Pb distribution throughout the area, again the highest concentration of Pb is associated with mimetite (white area). (A) also illustrates the difference between core and margin of the arsenbrackebuscite phase, top left of microphotograph, (see text for explanation). Scale bars are shown, (m) mimetite, (ad) arsendescloizite, (ab) arsenbrackebuscite, (ba) barite. For location of samples, description of phases, see Table 5.5. For all data see Appendix D.

arsenates occur at the base of the Lerokis Zone 4 deposit. Sample 111975 contained no cementing phases with the barite laths occurring as interlocking structures (ie. Figure 5.22). The two samples of the cemented Fe-oxide barite structures contained dominantly Fe-oxides as cements, barite within these structures range in size from 2cm to ~1mm in diameter. Concentrations of barite occur as layers and disseminated barite is rare. Layers can reach up to 15 cm across in some sections (Figure 5.12A) and generally the barites are <2.5 mm and are brecciated. Within sample 099923 (location 19, Lerokis Zone 5) a minor FeAs phase has been identified rimming fragmented / brecciated barite. Microprobe analysis indicates this phase to be composed of 80 compound % FeO and ~ 3 compound % As_2O_5.

Of important note is the discovery of free grains of Au (sample 099944, see Figure 5.23) adhering to the margin of a barite laths, Figure 5.27. Grains are anhedral with sizes of ~ 15 μm x 10 μm and are located within barite ore collected from Kali Kuning, location 50 (insert sheet 1) in close proximity to the overlying chert / limestone. Microprobe analysis of this single grain are as follows:-

Sample	Type	Au	Fe	Pb	Hg
		Atomic%			
099944	Au	89.5	-	4.3	3.2



Figure 5.27. Anhedral, <20 μm Au grains adhering to the barite laths, barite ore sample 099944.

5.5.5 Inclusion Phases

Included phases within individual barite laths from the barite ores are numerous in some samples and rare in others. Dominant sulphide inclusions are pyrite and galena however seven other phases have been identified. An inclusion ratio of 10:1 is estimated between the samples of barite ore and within barite associated with the Fe-oxide feeder structures.

Inclusion phases identified are galena, chalcopyrite, argentite, barite, bournonite ($PbCuSbS_3$), bornite and sphalerite. Phases identified range from euhedral to anhedral but are dominantly the latter, size of inclusions are varied but are generally <50 μm in diameter. In Figure 5.28A (sample 096879) illustrates the anhedral nature of pyrite and galena inclusions within barite laths. The abundant nature of inclusions within some samples is evident in sample 111975 (Figure 5.28B).

Generally very few sulphide inclusions are present within barite associated with the Fe-oxide feeder structures, however the following have been identified: acanthite, (Figure 5.28C) sphalerite, chalcopyrite, galena, jordanite ($Pb_{14}(AsSb)_6S_{23}$) and pyrite. The inclusions within the Lerokis 5 Fe-oxide feeder structure (sample 099923) also comprise of arsenian pyrite (1.4 wt% As) and sphalerite (6.1 wt% Fe) which are comparable with sulphides from the massive sulphide ore and not the *high-sulphidation* assemblage. Phases present range from euhedral to anhedral but are dominantly subhedral to anhedral, size of inclusions are varied but are generally <25 μm in diameter. The most abundant inclusion phase within barite from the Fe-oxide structures are those of pyrite compared to chalcopyrite inclusions within the barite ore. The scarce nature of inclusions within barite associated with the Fe-oxide structures is illustrated in Figure 5.28D.

5.6 PARAGENESIS

Mineralisation on Wetar can be subdivided into paragenetic stages based on the three major components of the systems (sulphide mounds, stockworks and barite deposits) and cross-cutting relationships evident in both field and lab based study.

Figure 5.29 illustrates the mineral paragenesis in relation to the alteration around the ore deposits (Chapter 4).

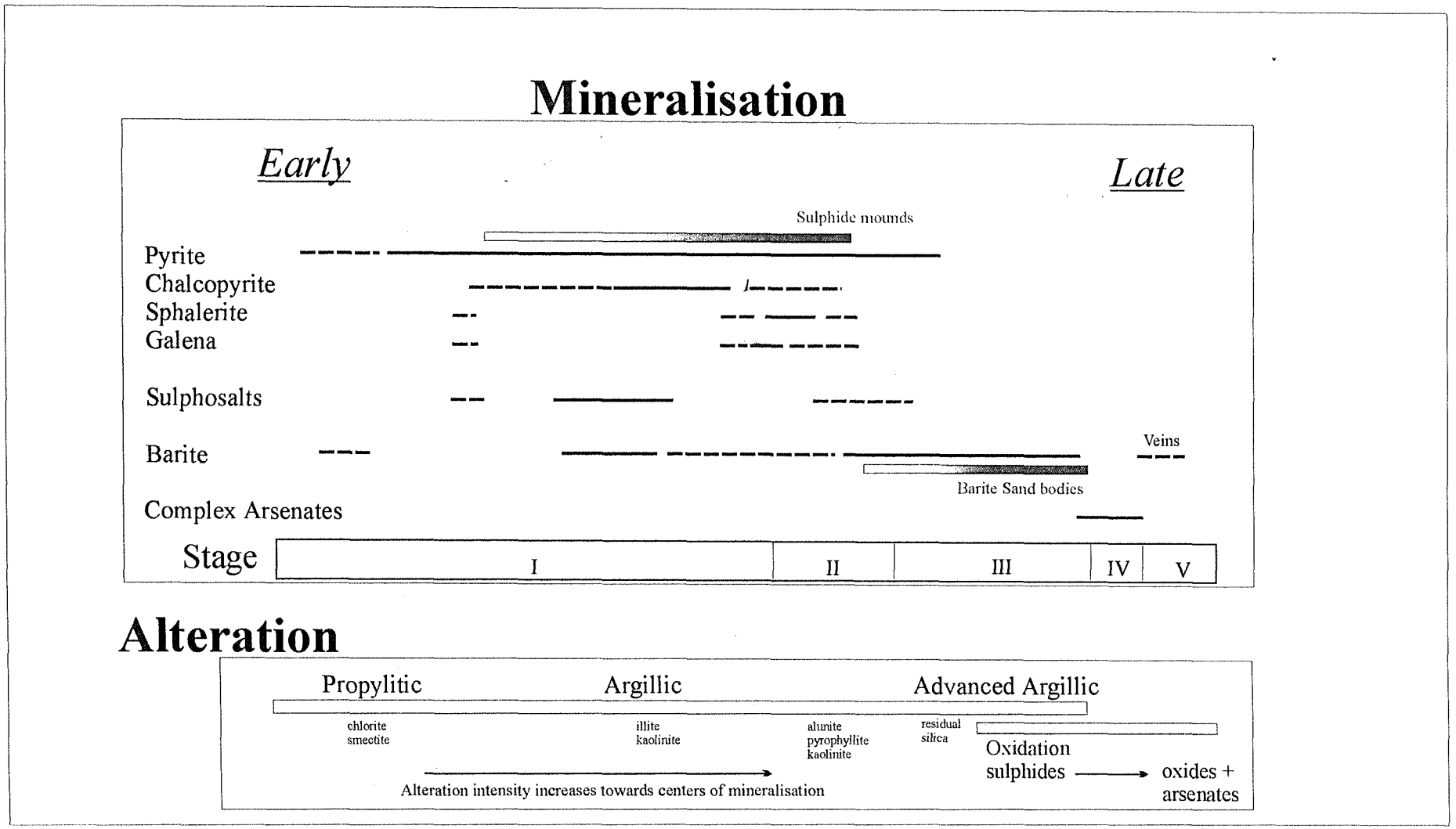


Figure 5.29. Paragenetic sequence of mineralisation based on the present study, paragenesis is shown in relation to hydrothermal alteration (Chapter 4). See text for description.

Stage I: An early pyrite stage consisting dominantly of disseminated cubic pyrite (euhehral to subhedral) < 1 mm in diameter, these pyrites are associated with brecciated host volcanics. The associated barite is euhedral and tabular in nature up to 4 mm in length. Brecciated host volcanics are rimmed with pyrite and re-cemented by pyrite deeper within the "roots" of the stockwork where veinlets of pyrite, galena, sphalerite and chalcopyrite are more abundant at depths of 100 m below the deposits and are associated with hematite. The mineral paragenetic order from oldest to youngest based on textural relationships is (1) pyrite, (2) sphalerite, (3) galena, (4) tennantite and (5) chalcopyrite.

The massive sulphide mound consists of generally ~99 % pyrite ± chalcopyrite and sphalerite. Massive pyrite forms both pyritohedron to anhedral masses, the pyrite contains abundant intergranular cavities and appears porous within deeper sections of the mound. Voids are infilled with barite and rarely chalcopyrite ± sphalerite. Chalcopyrite enrichment appears to have taken place at the base of the sulphide mound, at the margins and within the proximal footwall stockwork. Both collomorphic and euhedral growth zones are present within the massive pyrite, the collomorphic texture is less abundant towards the "feeder zone" for the sulphide mound at Lerokis Zone 5 which also contains less marcasite than the more massive ore.

Stage II: A second brecciation event opens stockwork fractures and also affects the sulphide mound, these voids and veins infill the sulphide mound, paragenetic order from oldest to youngest is (1) chalcopyrite / sphalerite intergrowth, (2) tennantite and (3) barite; no covellite is associated with this stage. Deeper fractures in the stockwork are dominantly infilled by *high-sulphidation* sulphides (covellite, digenite, bornite, tennantite-tetrahedrite and Fe-poor sphalerite). Tabular barite laths are also associated with this stage and are present up to 7 mm. The *high-sulphidation* sulphides also permeate through the sulphide mound to some degree. Figure 5.19A illustrates the relationship between paragenetic *stages I* and *II*, early disseminated pyrite is confined to silicified, brecciated host volcanics which are subsequently rimmed by and re-cemented by pyrite. After the second brecciation event, the fracture network is infilled by the *high-sulphidation* sulphide assemblage and the associated barite, this assemblage is not only confined below the sulphide mound in

the immediate footwall but also present at >170 m depth. Based on textural relationships the paragenetic order from oldest to youngest is as follows (1) Fe-poor sphalerite (2) covellite which appears porous and replaces sphalerite along micro-fractures (3) Zn-poor tennantite (4) Zn-rich tennantite ± tetrahedrite and covellite which is more massive and (5) barite. The Fe-poor sphalerite exhibits collomorphic textures in reflected light thin-section.

Stage III: Formation of the barite ore horizons, it is impossible to tell if they are the same barites as in *Stage II*, this event is related to the formation of the residual silica in the adjacent footwall (Ruxton, 1989 and this study, see also Chapter 4). The barite ores occur at the margins of the sulphide mounds, onlap them and even overlie them and are fed by feeder zones.

Stage IV: Cementation of the barite ores and oxidation of sulphides resulting in the formation of copiapite and römerite. Chert, gypsum and dolomite also develop post mineralisation as a result of waning hydrothermal activity.

Stage V: Late barite veins with individual crystals up to 5 cm develop both proximal and distal to mineralisation and coat external faces of the sulphide mounds (Figure 5.9).

5.7 DISCUSSION OF MINERALOGY

The association of seafloor sulphide mounds ± sulphosalts with flanking Au-Ag-Hg bearing, arsenate cemented baritic ore zones are unusual in relation to documented typical VMS systems however similar deposits are described throughout the central section of the island (Table 3.1, Chapter 3).

Mineral deposits contained along the Sunda and Banda arcs are low in quantity compared to other western Pacific island arcs eg. From Japan through the Philippines, PNG to New Zealand (review in Sillitoe, 1989). They include Kuroko type massive sulphides, epithermal vein systems, skarns and porphyry copper deposits. *High* and *low-sulphidation* epithermal systems are present at Milwah on the northern tip of Sumatera to Pelangan in the East Sunda Arc (Carlile and Mitchell, 1994; White et al., 1995). Between these systems are the *low–sulphidation* epithermal Au-Ag deposit at Ponkor, West Java (Milési et al., 1999) associated with quartz veins on the margin of a caldera, the Cirotan hybrid epithermal Au-Ag-Sn-W deposit (Milési et al., 1994)

and the Batu Hijau porphyry copper deposit, Sumbawa Island (Iriano and Clarke, 1995). There are no reported deposits with similar features to those at Kali Kuning / Lerokis.

The nature of the sulphide mounds, form and dominant mineralogy (pyrite + marcasite + chalcopyrite + sphalerite ± galena) indicate similarities with both modern and ancient VMS systems in varying tectonic environments. No significant metal zonation was evident within the mounds, in contrast to typical features of many VMS systems, especially the Kuroko deposits of Japan.

The sulphide mounds are arsenian in nature with collomorphic (melnicovite) and banding textures, similar textures are reported from many seafloor systems. The porous / void dominant texture, especially evident in the upper zone of the Kali Kuning deposit are similar to textures at Middle Valley (Duckworth et al., 1994) and Galapagos Rift (Knott et al., 1995). The formation of the sulphide mounds appears to have taken place at the seafloor as "replacement bodies". At Lerokis zone 5 the upper parts of the mound indicate minor evidence for local reworking with banding/stratification of sulphides within a 1 to 2 m thick volcanic sediment. Two prominent topographically high areas of sulphides occur on the Kali Kuning mound and may represent the basal remnants of former black smoker chimneys. These structures are absent from many fossil systems due to retrograde solubility of anhydrite and sulphides with ambient, oxidising seawater. Disintegration of these structures may occur over several thousand years (Halbach et al., 1998). At Lerokis Zone 5, a single pronounced feature occurs at the intersection between the two faults and again may represent a base of a former black smoker chimney. Mass wasting of sulphide mounds after phases of growth may be important in the sulphide textures preserved on Wetar. Cobbles of massive pyrite (up to 25 cm in diameter) are preserved especially at Lerokis Zone 5 and are re-cemented by pyrite. These features are also evident at the base of the Kali Kuning deposits thus forming talus deposits at the lower mound margin.

Enargite was reported as a sulphide phase associated with the sulphide mounds by de Ronde, (1995) and magnetite breccias are noted within the footwall of the Lerokis Zone 5 deposit (Herrington pers com. 2000). These features along with the presence of native sulphur at Kali Kuning (Chapters 3 and 4) all confirm an input of an

oxidising fluid associated with mineralisation. The presence of enargite or magnetite however during this study have not been substantiated.

Based on optical characteristics alone it is impossible to determine if the *high-sulphidation* assemblage is hypogene or supergene in origin, isotopic analysis may assist categorisation (Chapter 7). The Fe-poor sphalerite associated with the *high-sulphidation* fracture fill assemblage that permeates throught the stockwork and sulphide mounds crystalised under low aFes conditions. Enhanced Au values have been correlated with low FeS in both active and ancient VMS systems (Hannington and Scott, 1989; Herzig et al., 1993). The negative correlation between FeS and Au values is attributed to the influence of aFes, aS_2 and temperature which control gold deposition and the composition of sphalerite in the same setting (Hannington and Scott, 1989).

Vertical banding or zoning within the barite ores (Figure 5.21) is related to the nature of cementing phases which also relates to degree of cementation. Generally the Fe-oxides result in orange /yellow/browns colours, arsenate bearing phases are more typically pale yellow, grey or white.

Of important note is that no sulphide body was observed at Lerokis Zone 4, (Figure 5.10A and B) and suggests that the sulphide lenses and barite bodies are 2 completely different paragenetic stages. It could also imply that a sulphide mound may be concealed at depth, that total oxidation occurred of a former mound or that two separate fluids are involved, one forming the sulphide mounds, the second feeding the barite ore deposits. The field observation of barite ore occurring behind the sulphide mound at Kali Kuning as well as in front implies that these fluids percolate around the entire sulphide margin and again suggest that the baritic ore fluids are late stage in deposit development. This process may explain the presence of pyritic sand as an intervening horizon between the sulphide mound margin and the barite ore as the dense low pH fluids mechanically disintegrate the surface of the mound as the barite ore develops.

The presence of sulphide cobbles within the barite ore at Kali Kuning also indicates that wasting of the sulphide mound occurred during the formation of the baritic ore. At Lerokis Zone 5 the feeder structures to the barite ore deposit occur at the margin of the sulphide mound and suggests that these fluids could not pass through these relatively impermeable structures thus they exit at the sulphide mound margins.

Sample 100129, a vesicular sample collected from the highly altered footwall at Kali Kuning, (location 66) contained high levels of Sb (4943 ppm), Bi (111 ppm), Mo (699 ppm), As (298 ppm) and Pb (1366 ppm) compared to all other samples (see Table 4.3, Chapter 4) and may relate to incorporated arsenate phases that have been found to occur cementing the baritic ore. Microprobe study in this Chapter has revealed a close association between Pb and Ag with mimetite and high levels of As with the unusual arsenate phases. As with the sulphide phases exhibiting evidence of replacement, tiny quartz grains found in a barite ore sample from Lerokis Zone 4 (Herrington, 1995) may indicate replacement of the original host protolith (dacite / rhyodacite dome) with only the quartz phenocrysts surviving the intense, low pH alteration. The incorporation of residual silica clasts within the baritic ore and the feeder structures (up to 10 cm in diameter, see Figure 5.12A) indicates the replacive and destructive nature of the hydrothermal fluids. Au appears to be related to this acid leaching event associated with intense clay alteration of the footwall volcanics.

5.8 SUMMARY

The characteristics of the ore mineralogy are consistent with the alteration associations in that the generation of the system appears to be seawater dominated (Chapter 4) producing many features typical of modern and ancient VMS deposits. However, the presence of minor *high-sulphidation* ore characteristics coupled with minor advanced argillic alteration document the presence of acidic, oxidising fluids that are similar to those associated with *high-sulphidation* VMS systems. These characteristics coupled with a seafloor generation at varying depths suggest a magmatic contribution to deposit formation. The minor nature of these *high-sulphidation* characteristics may suggest a magmatic input within the Wetar hydrothermal system however the fluid is dominantly composed of Miocene seawater.

Chapter 6

FLUID INCLUSION STUDY

6.1 INTRODUCTION

In order to determine, the nature of the fluids at the time of mineral deposition, fluid inclusions from Wetar Island barites have been studied using microthermometry. Results will gain qualitative and quantitative data on the conditions (temperature, density and pressure) and nature (chemistry, salinity) of the mineralising fluids responsible for the formation of these deposits. Abundant literature describes microthermetric results from hydrothermal ore-deposits in both modern ocean-floor sites to preserved ancient systems.

This is the first detailed fluid inclusion study undertaken on samples collected from Wetar Island. A cursory study of barite and associated anhydrite suggested low temperatures of formation (<100°C) as no homogenisation bubbles were found within the inclusions however freezing data suggested salinities close to that of seawater (Sewell and Wheatley, 1994b).

The principal objectives of the study were:

1) Systematically study barite hosted fluid inclusions throughout the paragenesis to obtain P-V-T-X data.
2) Compare the results to the cursory study.
3) Use the microthermetric data to calculate pressure and thus further constrain depth of mineralisation

6.2 ANALYTICAL METHODS

Doubly polished fluid inclusion wafers (c. 20 mm in diameter) were prepared to a thickness of 100 μm. Microthermometry was performed on a Linkam THM600 heating / freezing stage at the University of Southampton. Techniques employed during the study are described by Roedder, (1984) and Shepherd et al., (1985) (see

also Appendix E). Abbreviations and nomenclature for phase changes during the microthermometry study follow those described by Shepherd et al., (1985). Repeat analysis of individual inclusions yielded a reproducibility of ± 0.2°C during freezing and ± 1.4°C during heating to homogenisation. Standards were used to calibrate the stage at temperatures of –56.6°, (CO_2) 0.0° (ice) and 306.8°C (sodium nitrate). Salinities were calculated from equivalent ice melting / freezing point depression temperatures using equation 6.1 for the NaCl-H_2O system (Bodnar, 1993).

$$\textbf{Salinity (wt\% NaCl)} = 1.78\theta - 0.0442\theta^2 + 0.000557\theta^3$$

(Equation 6.1)

Where θ is the final ice melting temperature in degrees Celsius.

Attempts were made to analyse inclusions that showed no evidence of necking-down or leakage. The progressive heating / cooling of individual inclusions were used to test for leakage, temperature was cycled at heating rates of 10°C min^{-1} to 1°C min^{-1} over key phase changes. As barite samples are to be used for the study, care will have to be taken during analysis as previous studies have proven that barite hosted inclusions are extremely susceptible to leaking and stretching even prior to reaching homogenisation (particularly if homogenisation temperature exceeds 250°C) (Ulrich and Bodnar, 1988). For this reason, all inclusions shall be observed continually during heating from room temperature to homogenisation.

6.3 SAMPLE SELECTION

A representative suite of eleven barite samples encompassing all stages of ore paragenesis from the mineralisation were analysed using microthermetric techniques. These included stockwork disseminations, barite ore, *high-sulphidation* associated barite, late vein barite and the possible feeder structures to the barite ore. The majority of analysed samples (7 out of 11) were collected from the Lerokis Zone 5 deposit. The abundant drill core from this site allows a more comprehensive view throughout the ore body and underlying system. The potential of this sample suite may allow recognition of depth variations within the Zone 5 system (with respect to

temperature and salinity) and thus may enable comparisons to be made with other hydrothermal systems.

6.4 NATURE AND OCCURRENCE

Optical examination indicates that >95% of all barite inclusions are associated with secondary and pseudo-secondary inclusion trails, <5% appear primary. Criteria for visually estimating degree of fill (F) and for subdivision of inclusions into primary (P), secondary (S) and pseudo-secondary (PS) types are outlined in Roedder, (1984) and Shepherd et al., (1985). The primary inclusions are generally larger the secondary or pseudo-secondary inclusions and range in size from 12 μm to 25 μm. these solitary bi-phase inclusions have been classed as type 1A (Figure 6.1A). Generally they are oval, rounded and even circular in some instances. Type 1B are two-phase liquid plus small amounts of vapour inclusions (L+V) and occur as pseudo-secondary and secondary trails (Figure 6.1B). Recognition of a few mono-phase (L) inclusions (by first and final ice melt phase changes) are present in sample 099938 and have been classed as Type 2 inclusions. These features are the only ones distinguishable optically between the 2 types before microthermometry. Abundant inclusions within the sample suite show evidence of decrepitation or leakage (Figures 6.1C and D).

The majority of analysed samples contain hundreds of inclusions, (Figure 6.1E) in some samples the inclusions are so abundant that it is impossible to unambiguously determine their origin with reference to primary, secondary or pseudo-secondary types. In contrast however, some samples (099917) exhibit barren areas which are almost completely void of inclusions, (Figure 6.1F). Sample 097106 (Figure 6.1G) contained more inclusions towards the crystal margin with a pronounced reduction towards the core. Degree of fill (F) within the two-phase inclusions (defined as the volumetric proportion of liquid relative to the total volume of the inclusion) are generally 0.9 or 0.95 (Figure 6.1H). Occasionally inclusions contain (F) values of 0.6, see also Figure 6.1H and later in the discussion (this Chapter). Biphase (L+V) inclusions of possibly primary origin are generally rare, pseudo-secondary trails are abundant and are parallel to crystal faces thus are controlled by crystal habit. Morphologies of inclusions are generally elongate or sub-rounded and rarely euhedral or angular, size varies between 3 and 20 μm. Cross-cutting secondary trails

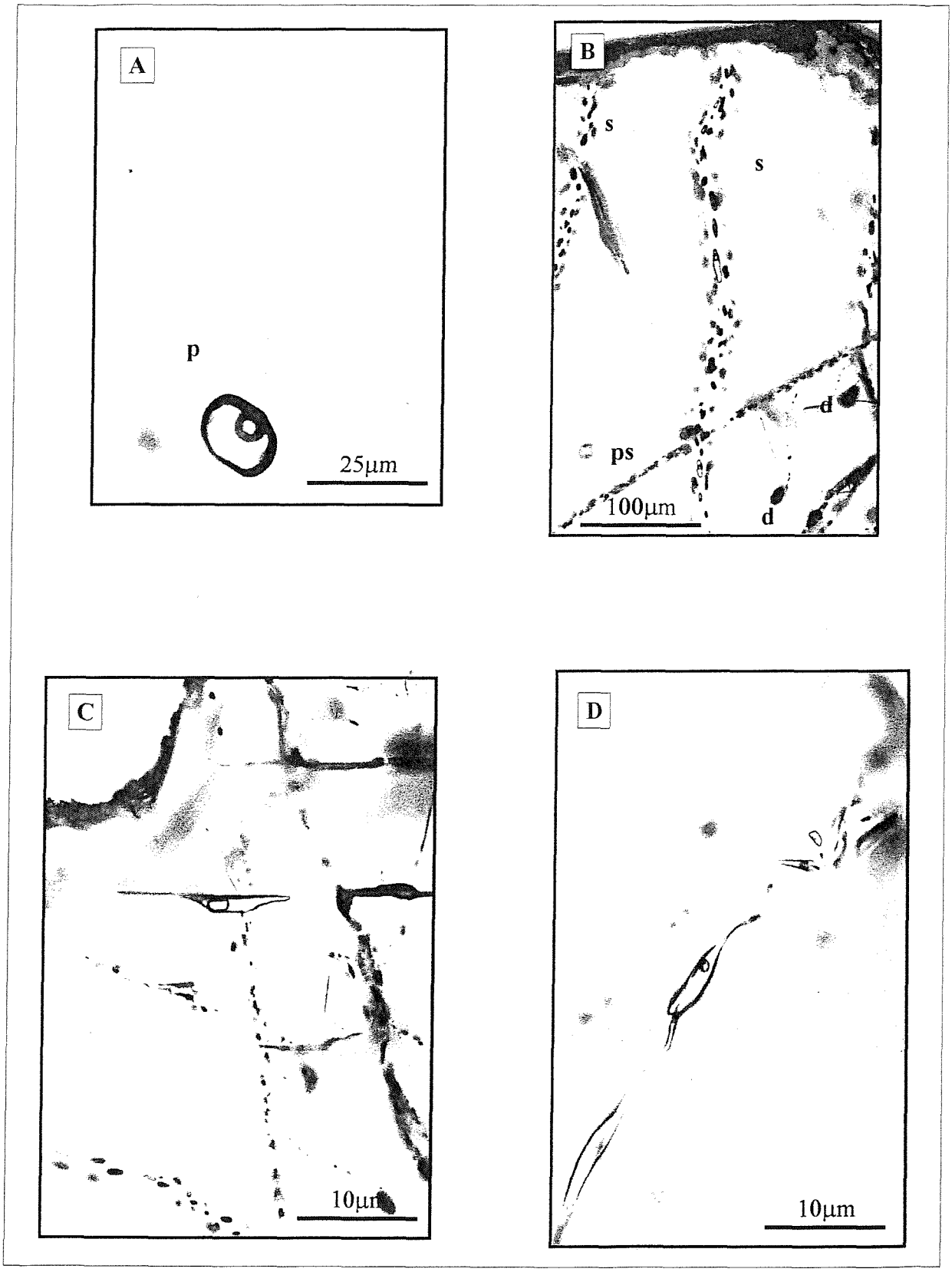


Figure 6.1. A-D, Photomicrographs of barite hosted fluid inclusions from Wetar Island. A) Possible two-phase primary fluid inclusion in sample 097106. B) Pseudo-secondary and secondary trails from sample 097084. C) Irregular two-phase inclusion in sample 099917 showing pre-heating evidence of necking. D) Two-phase fluid inclusion from sample 097106 after heating to178°C showing evidence of necking and leakage. d = decrepitated samples, p= primary, ps= pseudo-secondary, s= secondary trails.

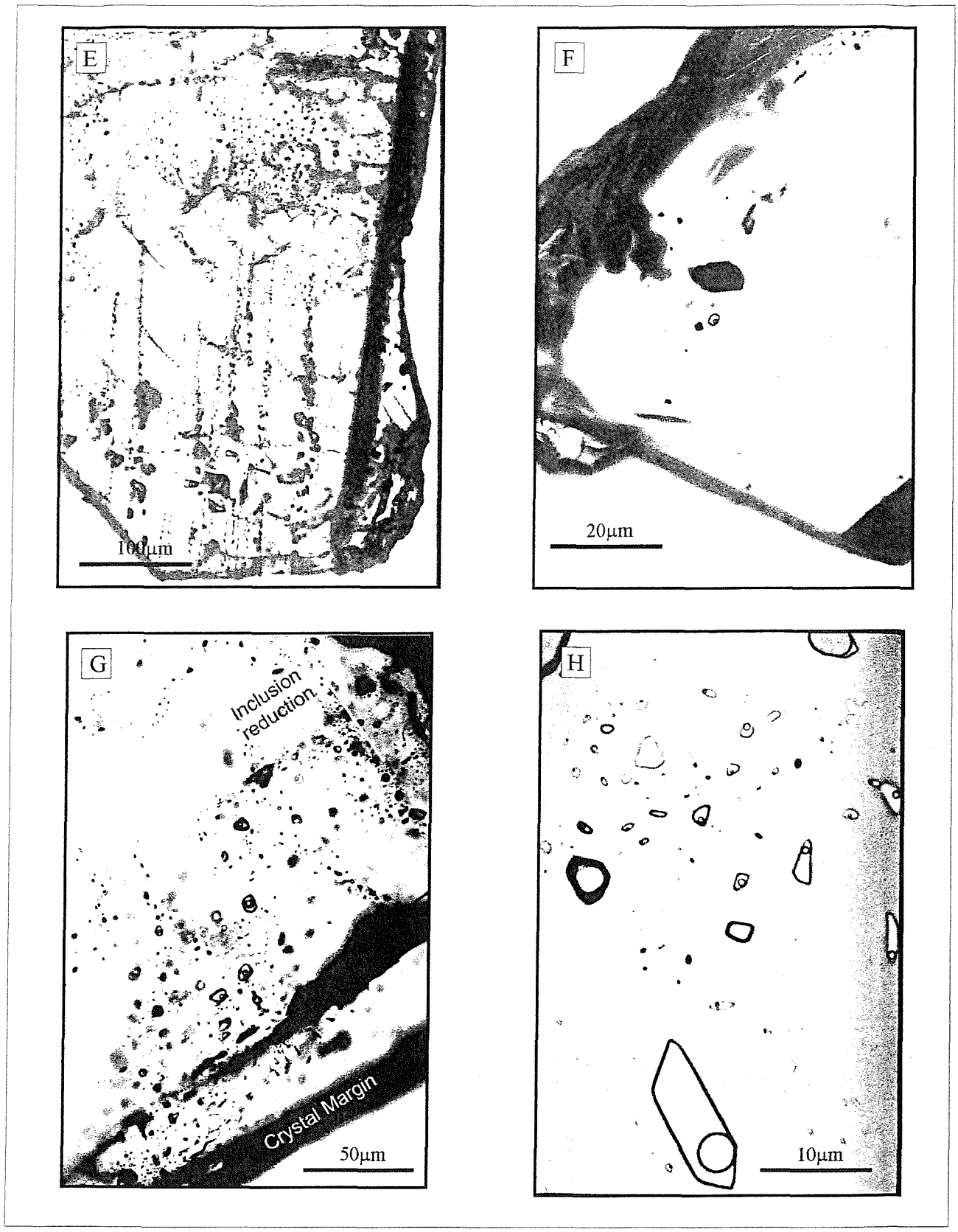


Figure 6.1 cont. E) Numerous 2 phase (L + V) inclusions, sample 111931. Abundant inclusion trails can be seen within the sample, field of view. F) Crystal margin of sample 099917 showing a barren area of fluid inclusions. A large (20μm) "black" decrepitated inclusion is evident. G) Abundant 2 phase inclusions evident, sample 097106. Note the reduction of inclusion towards the crystal core. H) Sample 096879 illustrating the dominance of 0.90 and 0.95 degree of fill. The sample does show variation in degree of fill (left centre and top right) see text for discussion.

are observed in some samples along microfractures which in some cases continue to crystal margins. Sizes and morphologies of these are identical in all aspects to pseudo-secondary trails.

Monophase aqueous inclusions have also been identified and are clear in appearance at room temperature. These inclusions vary in size from 8 to 15 μm, morphologies are sub-rounded rounded to euhedral / angular, >50% of all inclusions within the barite samples are decrepitated or "empty". The majority of empty inclusions are present within stockwork samples.

6.5 MICROTHERMOMETRY RESULTS

All calibrated data from the inclusion microthermometry are detailed in Appendix E, Table 6.1 tabulates a summary of the data from the present study. For all fluid inclusions (Figure 6.2A-D) the degree of fill (F) ranges from 0.6 to 0.95. Temperature of homogenisation (T_h) occurs between 144 to 314°C with a mode of 238°C (n=253); where 47 inclusions decrepitated before homogenisation. First ice melt temperatures (T_{fm}) occur between –20 and –24.4°C, (n=35) with final ice melting (T_{mice}) between –0.9 to –3.1°C, (mode –1.6) corresponding to salinities of 1.6 to 5.1 wt% NaCl (Bodnar, 1993) this suggests that salinities span both above and below the salinity of seawater, ~3.2 wt% NaCl (Biscoff and Rosenbauer, 1984). Figure 6.3 illustrates the microthermetric results of the inclusions when they are subdivided into Type 1A (possibly primary), 1B and Type 2 inclusions. Figure 6.3A illustrates the morphological characteristics of the various types and Figure 6.3B illustrates the differences in degree of fill (F) between Type 1A and 1B inclusions. 70% of analysed Type 1A inclusions decrepitated before homogenisation compared to only 13% from Type 1B, generally, these inclusions decrepitate between temperatures of 170 and 210°C. For both homogenisation and freezing data only a single fluid population is observed. Both type 1A and 1B have similar distributions, as do both secondary and pseudo-secondary inclusions. Wide ranges of homogenisation temperatures (T_h) are observed for both type the 1 inclusions, (Figure 6.3C) similar modes of occurrence of (T_{fm}) and (T_{mice}) are also noted (Figure 6.3D and E). Six mono-phase inclusions were identified in sample 099938 (barite vein, distal to mineralisation, Lerokis Zone 5). Salinity within these inclusions was great enough to visually see phase

Table 6.1. Microthermetric results and description of fluid inclusions hosted in barite samples from Wetar Island, Indonesia.

Sample	Description	Host	T_h (°C)				T_{Fm} (°C)				T_{mice} (°C)				wt%	Comments
			Range	*Av / mode*	*SD*	*n*	*Range*	*Av*	*SD*	*n*	*Range*	*Av*	*SD*	*n*	NaCl	
097106	Disseminated barite laths (<4mm) are associated with disseminated pyrite and brecciated silica/clay altered volcanics. Barite laths are euhedral, depth 210m.	ba	217-302	255 / 249	24.4	24	-20-21.8	-20.7	0.74	5	-1.8-3.1	-2.1	0.5	17	2.5-5.1 *mode 3.6*	Secondary L+V inclusion trails are abundant, some PS and P? inclusions. Reduction of inclusions toward crystal core.
096948	Euhedral barite laths (<6mm) associated with Fe oxides from the cemented structure, Lerokis Zone 4, location 129, central to barite ore deposit.	ba	197-309	240 / 256	28.8	20	—	-23	—	1	-0.9-2.4	-1.6	0.5	16	1.6-4.1 *mode 2.9*	Abundant PS and S trails.
097122	Euhedral barite laths (<6mm) intergrown with the high-sulphidation sulphide assemblage, Lerokis Zone 5, depth 49.5m below the massive sulphide mound.	ba	186-314	269 / 278	27.5	20	-22.1-22.5	-22.4	0.17	4	-1.9-2.8	-2.2	0.2	19	3.2-4.1 *mode 3.6*	Abundant PS and S trails associated with Fe-poor sphal ten, tet and cov.
111943	Vug / cavity filling euhedral barite (<5mm) from the banded cpy/py massive sulphide mound at Kali Kuning, location 63	ba	196-262	235 / 245	19.8	16	-22.1-22.8	-22.5	0.3	4	-1.4-2.3	-1.9	0.3	15	2.5-3.8 *mode 3*	Abundant PS and S trails.
097024	Vug filling barite within massive pyrite, Lerokis Zone 5, depth 59.8m. Barite is euhedral (<6mm).	ba	210-288	245 / 237	26.6	18	—	—	—		-1.6-2.4	-2.1	0.3	11	2.8-4.1 *mode 3.7*	Repeated heating showed that some inclusions were leaking on heating.
097084	Disseminated, euhedral barite laths, associated with silica / clay altered volcanics, depth 88.5m below the massive sulphide mound at Lerokis Zone 5.	ba	187-286	230 / 238	23	22	—	-21.4	—	1	-1-2.1	-1.8	0.3	16	1.7-3.6 *mode 3.2*	Numerous necked and decrepitated inclusions.
096879	Barite ore sample from Kali Kuning, location 84. Barites are euhedral (<5mm) & cemented by oxides and arsenates.	ba	209-289	242 / 232	22.7	21	-21-22.5	-21.9	0.9	2	-1-1.9	-1.6	0.2	17	1.7-3.2 *mode 3*	Abundant PS and S trails.
099938	Large vein barite crystals, upto 70mm collected from chloritized altered zone distal to Lerokis Zone 5, samples are post mineralisation, location 112.	ba	144-212	194 / 200	19.3	15	-22-24.4	-22.7	0.7	11	-1.4-2.7	-2.2	0.5	22	2.5-4.5 *mode 4.2*	Some Monophase L incusions, no V phase. Abundant PS bi-phase inclusions.
099917	External barite covering of massive py, Lerokis Zone 5,location 15, barite laths < 5mm.	ba	183-237	220 / 228	18.6	15	-20.4-21.8	-21.1	0.7	3	-1.6-2.6	-2.2	0.3	12	2.8-4.3 *mode 4.2*	Numerous necked and decrepitated inclusions, some barren areas within the sample.
111931	Barite ore sample from Lerokis Zone 4, location 217. Barites are euhedral (<5mm) & cemented by oxides and arsenates.	ba	189-267	228 / 237	59.8	17	—	-21.1	—	1	-1.1-2.1	-1.6	0.3	6	1.9-3.6	Abundant PS and S trails.
099939	Barite ore sample from Lerokis Zone 5, location 46. Barites are euhedral (<5mm). & cemented by oxides and arsenates.	ba	199-269	233 / 238	18.5	18	—	-22.6	—	1	-1.2-1.8	-1.6	0.2	17	2.1-3 *mode 3*	Abundant PS and S trails.

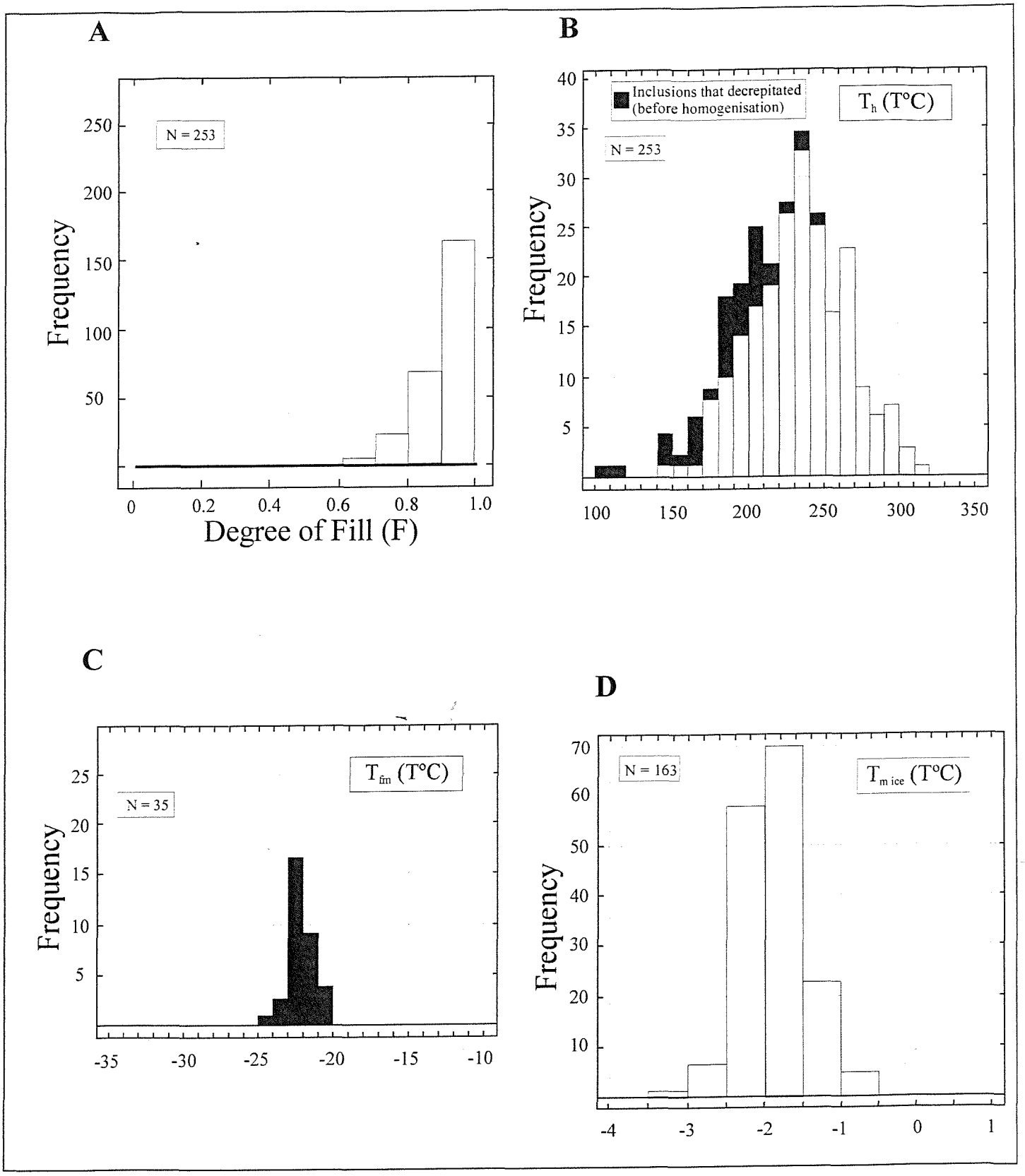


Figure 6.2. Microthermetric results for fluid inclusions in barite from Wetar Island (all data). **A.** Frequency histogram of degree of fill. **B.** Frequency histogram of homogenisation temperatures (T_h). **C.** Frequency histogram of first ice melting (T_{fm}). **D.** Frequency histogram of final ice melting (T_{mice}).

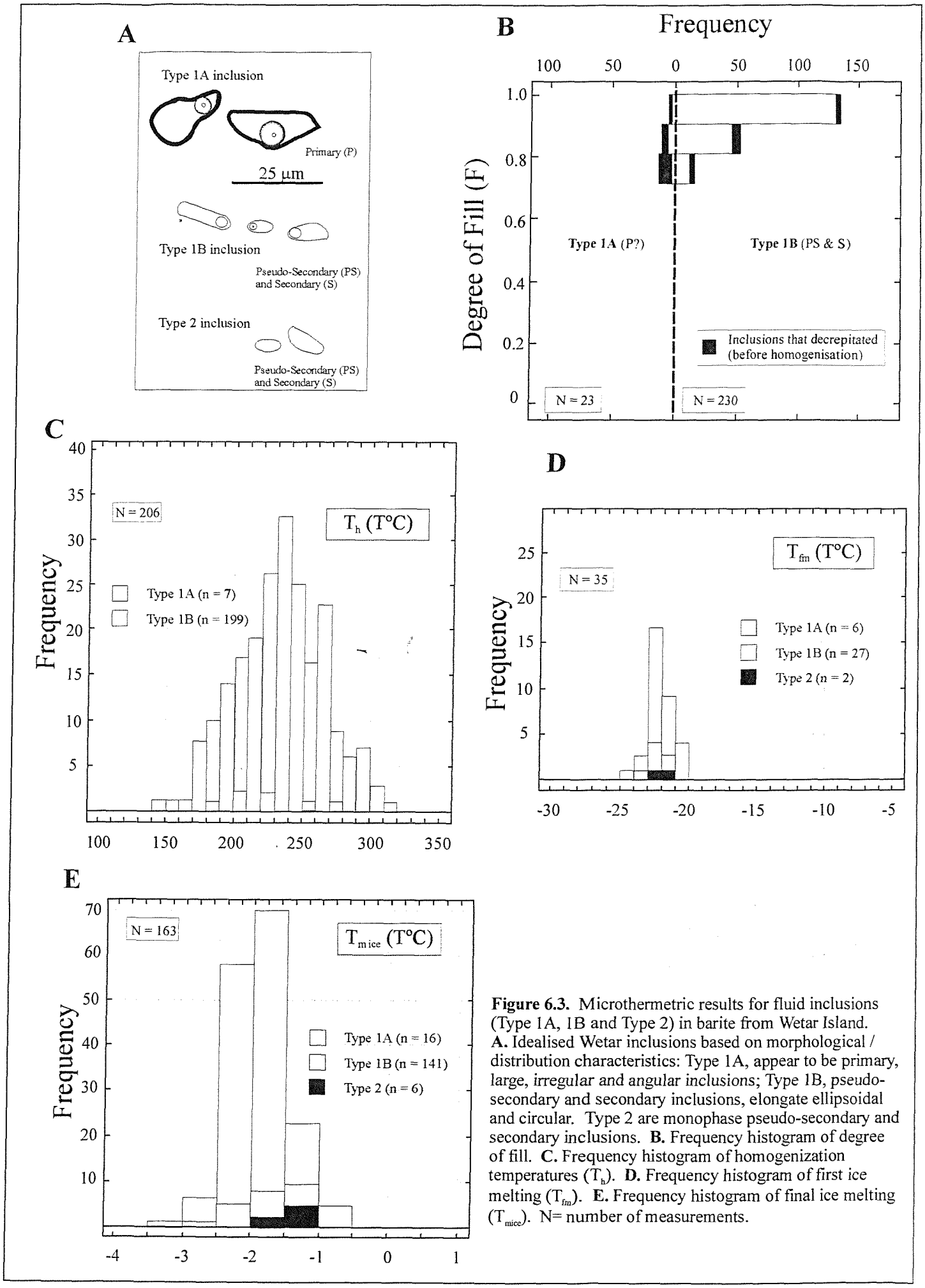


Figure 6.3. Microthermetric results for fluid inclusions (Type 1A, 1B and Type 2) in barite from Wetar Island. **A.** Idealised Wetar inclusions based on morphological / distribution characteristics: Type 1A, appear to be primary, large, irregular and angular inclusions; Type 1B, pseudo-secondary and secondary inclusions, elongate ellipsoidal and circular. Type 2 are monophase pseudo-secondary and secondary inclusions. **B.** Frequency histogram of degree of fill. **C.** Frequency histogram of homogenization temperatures (T_h). **D.** Frequency histogram of first ice melting (T_{fm}). **E.** Frequency histogram of final ice melting (T_{mice}). N= number of measurements.

Transformations however only two analyses were possible on first ice melting yielding results of –22 and –22.2°C. Final ice melting ranged between –1.4 to –1.7°C corresponding to salinities of 2.5 to 2.9 wt% NaCl. None of the inclusions contained daughter minerals and no other phases such as clathrates were observed upon cooling.

6.6.1 DISCUSSION

The results from the microthermetric data suggest that Type 1A and 1B inclusions are of the same generation, the size of inclusion is generally the only recognisable difference between them. The results also suggest that the larger inclusions with higher degrees of fill, (Figure 6.1H) are not in fact vapour dominated inclusions but that they have formed as an artefact of leakage since on heating these vapour rich inclusions they do not homogenise. Other inclusions show changing in degree of fill on heating, also due to leakage. The similarity of T_h and salinity ranges observed from both secondary and pseudo-secondary inclusions indicate no noticeable difference in the fluid salinity or temperature of formation throughout the crystallisation of the host mineral.

Ranges of (T_h), (T_{fm}) and (T_{mice}) are given for each sample in Table 6.1, the nature of sample occurrence and the statistical data are also tabulated. Figure 6.4A-C graphically illustrates these results as a series of frequency diagrams. Figure 6.4A illustrates that (T_h) ranges are wide for all samples, stockwork samples below the sulphide mound at Lerokis Zone 5 have a range between 187 to 302°C (mode of 249°C). Barite encrustations around massive pyrite samples at the mound surface, vug / cavity filling barite, samples from the Fe-oxide / feeder structure at Lerokis Zone 4 and barite ore samples all fall within this range. Temperature of homogenisation remains fairly consistent along inclusion trails within individual samples, (see Figure 6.4D).

At first appearance, no significant trend of depth vs (T_h) is observed within the Lerokis Zone 5 stockwork samples, (Figure 6.5A). At the greatest depth below the sulphide mound (210m) an average (T_h) of 255°C is recorded (mode of 249°C). At 88.5m the average has fallen to 230°C but increases to 245°C at 59.8 m before a reduction again to 233°C at the paleo-seafloor within the barite ore sample, (Figure 6.5A). This trend is not so obvious when using modal values, at 88.5 m the homogenisation temperature has fallen from 249°C to 238°C where it remains

constant over the proceeding 150 m into the barite ore. A reduction of only 11°C is noted compared to the reduction of 22°C when using the average values. Interestingly, the barite associated with the *high-sulphidation* sulphide assemblage (Chapter 5) has a (T_h) range of 186 to 314°C and an average of 269°C which is almost 15°C greater than that of the deepest stockwork sample. The recorded value is 29°C higher than the deepest stockwork sample when using the modal values. This sample (097122) also yielded the highest recorded homogenisation temperature of 314°C. Conversely, the data from the post-ore distal barite vein yields a lower (T_h) range than any of the other samples, ranges are between 144 and 212°C with an average of 194°C (mode of 200°C), Figure 6.4A and 6.5A. The association of vug filling barite within massive pyrite at Lerokis Zone 5 and the banded pyrite / chalcopyrite sample at Kali Kuning are remarkably similar. The Lerokis sample is from a depth of almost 60 m below the sulphide mound surface compared to the Kali Kuning sample which was collected in close proximity to overlying *globigerina* bearing limestone and would therefore represent a position close to the paleo-seafloor. Ranges of homogenisation are similar, 210 to 288°C (avg. 245°C) and 196 to 262°C (avg. 235°C) respectively. At present the deposits of Lerokis Zone 5 is some 250 m above Kali Kuning in elevation however the similarity between the two deposits (both in terms of their nature and similar microthermetric results) suggest near identical conditions of formation. The barite encrusted sulphide sample (099917) collected from the surface of the Lerokis Zone 5 mound is similar in range to that of the barite ore sample, also from Lerokis Zone 5, see Table 6.1.

Barite ore samples have been analysed from all three deposits, Lerokis Zones 4, 5 and Kali Kuning. Homogenisation ranges from 189 to 267°C (avg. 228°C), 199 to 269°C (avg. 233°C) and 209 to 289°C (avg. 242°C) are recorded respectively. The difference of only 14°C from the three averages (6°C from their modes) and similar ranges of homogenisation indicate that similar hydrothermal fluids are responsible for the generation of all three deposits. The baritic Fe-oxide "chimney" have (T_h) of 197 to 309°C and an average of 240°C) where as the surrounding barite ore (T_h) (average is 228°C). These results are consistent with the barite Fe-oxide "chimney" being a fluid feeder zone for the barite ore deposits.

The barren areas observed in some of the samples indicate that re-crystallisation of the host has occurred (Figure 6.1F). Re-crystallisation has removed any defects from the sample (including inclusions) indicating an early phase of slow growth followed

by more rapid growth. The alignment of inclusion trails parallel to crystal faces within the Wetar samples are also recorded in most hydrothermal systems, an example is recorded at 21°N EPR within anhydrite (Kusakabe et al., 1982).

Salinities within Wetar barite inclusions exhibit a narrow range of 1.6 to 5.1wt% NaCl equivalent for all inclusions, Table 6.1. Figure 6.4B and C illustrate that temperatures for F_m and F_{mice} have narrow ranges and no significant difference is evident throughout the Wetar system. As with the homogenisation data, salinity shows only a slight depth relationship, (Figure 6.5B) the barite ore deposit sample at Lerokis Zone 5 (099939) is less saline than seawater compared to the sulphide mound or stockwork related samples which overlap the seawater value of 3.2 wt% NaCl. The stratigraphic deepest sample (097106) at 210m below the sulphide mound yielded salinities of up to 5.1 wt% NaCl (significantly higher than the salinity of seawater). The results suggest that both higher and lower salinity fluids (with reference to seawater) have circulated within the hydrothermal system in the past, although no clear trends are noted. Groups of co-existing vapour and liquid rich inclusions would be indicative of boiling assemblages, however there is no evidence for this at either the Lerokis or Kali Kuning systems. Vapour rich inclusions within some of the Wetar samples have been proven to be artefacts induced by inclusion leakage. An inclusion within sample 097024 (0.7 degree of fill) was heated to homogenisation and then repeated 3 times to test for leakage. Initial T_h of 239°C increased to 247, 251 and 288°C after each subsequent heating indicating that the inclusion was in fact leaking before reaching homogenisation. Other samples tested with a large degree of fill thought to represent boiling assemblages also leak or decrepitate before homogenisation. The absence of boiling within the Wetar Island hydrothermal system will mean that a pressure correction will need to be applied to the homogenisation data due to the overlying / confining pressure of seawater. A plot of homogenisation temperature versus salinity is given in Figure 6.5C, results exhibit a fair degree of scatter and therefore individual trends are not easily discernable. Of interesting note is that the slightly lower temperature "post mineralisation" barite vein is slightly more saline than the majority of the data. There is also a slight suggestion that the *high-sulphidation* sulphide associated barite has a slightly higher T_h than the rest of the samples. Even though similar T_h and salinity data of this sample compared to the other barite samples within the system are observed, the sulphide mineral assemblage

association (covellite, Fe-poor sphalerite, tennantite-tetrahedrite) occuring as a fracture fill permeating throughout the stockwork zone and mound are unusual for VMS systems. Stable and radiogenic isotopes (Chapters 7 and 8) may give more information on these fluids. Observations made from the Wetar samples suggest two distinct hydrothermal events are recorded. An early, high temperature hydrothermal system, (300 to 350°C) like those documented from modern seafloor sites (Table 6.2) precipitated pyritic dominated sulphide mounds at or just below the seafloor. Trapping temperatures in anhydrite from TAG indicate a difference of only 10°C less than the measured black smoker fluids that exit the mound and only 12°C difference within white smoker systems (Edmond et al., 1995). Similarities between trapping temperatures in sulphides (21°N EPR, Styrt et al., 1981; Lebel and Oudin, 1982) and sulphates (13°N EPR, Nehlig, 1991; 21°N EPR, Styrt et al., 1981; Lebel and Oudin, 1982; Southern Juan de Fuca Ridge, Brett et al., 1987) are all in agreement with measured vent fluids. These results and sulphide hosted inclusions in ancient samples suggest that temperatures exceeded 300°C throughout the Wetar hydrothermal system and were responsible for the deposition of the sulphide mounds. It is also likely that during this early phase of mineralisation, sulphide rich chimneys may have vented black smoker fluids into the Banda Sea. A change in the hydrothermal fluids to sulphate rich, acidic with lower temperatures occurred (average 275°C) post pyrite mound formation and precipitated abundant barite and thus generating the barite ores, these fluids are similar in temperature to those currently venting from white smokers (Table 6.2). Modern sites record the presence of both black and white smokers occurring together in the same hydrothermal system, eg. JADE (Lüders et al., 2001) TAG (Tivey et al., 1998) and Vai Lili, Lau Basin (Herzig et al., 1993). The white smokers venting in the Kremlin area (TAG) are 60-90°C cooler than venting black smokers but are considerably more acidic (Tivey et al., 1998). Precipitation of Fe-sulphide within the mound accounts for low Fe, H_2S and pH (Edmond et al., 1995), changes from black to white smoker fluids are attributed to mixing the former with seawater, conductive cooling and precipitation within the mound (Tivey et al., 1998). These more acidic fluids are responsible for the generation of the barite ore and may also produce the observed *high-sulphidation* style alteration assemblages and the associated footwall residual silica that are present at all of the mineralised zones (Chapter 4). If a condensed vapour is contributing to the barite ore, then higher temperatures are expected at depth and are possibly related to a buried intrusion.

Table 6.2. Published fluid inclusion studies of selected modern and ancient systems, for location of individual deposits see Figure 1.2, Chapter 1.

DEPOSIT and References	FLUID INCLUSION DATA		FLUID Temp °C	COMMENTS
	Homog. Temp °C	Salinity wt% NaCl		
Modern Sea Floor Systems				
TAG 1, Mid Atlantic Ridge 26°N (Edmond et al., 1995); (Rona et al., 1993)			366	Venting Black smoker at 3670m depth. pH of fluid 3.4.
			273 - 301	Venting White smoker, pH 3.
(Peterson et al., 2000); (Tivey et al., 2000)	301 – 358 311 - 362	1.9 – 6.2 1.2 – 5.1		Proposed upflow zone at TAG 1 an hosted inclusion, authors suggest higher T at depth.
TAG 4 (Peterson et al., 2000)	191 - 364	2.8 – 3.7		Venting White smokers and qz hosted inclusions.
Kremlin, TAG 2 (Peterson et al., 2000); (Tivey et al., 1998)	242 – 349 255 - 342	 1.4 – 5.1		(an) and (qz) hosted inclusions. (an) hosted inclusions.
TAG 5 (Peterson et al., 2000); (Tivey et al., 1998)	234 - 357 168 - 309	 3.2 – 4		(an) and (qz) hosted inclusions. (an) hosted inclusions.
Broken Spur (James et al., 1995)			357 - 366	Venting Black smoker.
Lucky Strike 37°N (Langmuir et al., 1997); (Von-Damm et al., 2000)			150 - 333	Venting Black smokers. At the Sintra site, both low temperature diffuse flow and higher temperature focused flow occur together.
Menez Gwen 37°N (Charlou et al., 2000)			285	Clear venting fluids.
Oceanographer Transform (Vanko et al., 1992)	>340 150 - 400	40 3 - 8		Gabbroic (qz) hosted inclusions, calcium rich. (L) dominated secondary inclusions.
South West Indian Ridge (Kelly & Früh-Green, 2001)	333 – 418 255 – 418 369 – 401 190 - 465	32 – 51 32 – 47 1.4 – 4.5 1.4 – 18.0		(L) dominated to (V) rich brine inclusions. Halite bearing inclusions. Secondary (V) dominated inclusions (ap). (L) dominated inclusions (pl, ap, qz)
21°N EPR (Von-Damm et al., 1985)	179 – 354	2.9 – 3.8	 260 - 350	(an) hosted inclusions. Active vent fluid, pH 3.4.
13°N EPR			347 - 380	PH of fluids are 3.1 – 3.7.
White Lady, North Fiji Basin (Ishibashi et al., 1994)			265	Venting fluid from an anhydrite chimney, depth of 1840m.
Vai Lili, Lau Basin (Lecuyer et al., 1999); (Fouquet et al., 1993); (Herzig et al., 1993)	290 - 344 225 – 280 320 - 280 - 148 - 261	30 5 4.7 3.2	- 320 – 342 250 - 320 -	(an) hosted inclusions. (ba) hosted inclusions. (sp) hosted inclusions. Present day vent temperature, black smoker. Present day vent temperature, white smoker. Barite hosted inclusions, vent fluid pH 2.
Hine Hina, Lau Basin (Lecuyer et al., 1999); (Marignac et al., 1995)	170 - 230 190 - 230	1.6 – 2.6 -	-	(ba) hosted inclusions. Higher Th recorded in the core of the chimney.
White Church, Lau Basin (Lecuyer et al., 1999); (Marignac et al., 1995); (Herzig et al., 1993)	203 – 262 210 - 260	3.2 – 5.3 -	-	? (sp) hosted inclusions, cores exhibit lower Th. Numerous sp and ba rich chimneys.
Satanic Mills, Roman Ruins and Roger Ruins			Up to 268	Venting black smokers.

sites (Binns et al., 1997, 1996)				
Onsen site, DESMOS caldera, East Manus Basin (Gamo et al., 1997)			88 & 120	Venting White smokers, low pH fluids (2.08). Depth of 1926m, similar fluids associated with sub-aerial volcanic activity.
Franklin Seamount, Western Woodlark Basin (Binns et al., 1993); (Binns & Scott 1991)	184 – 244 200 - 240	3.4 – 5.8 -	- -	2mm euhedral barite laths from 2m sulphate spire, depth 2100m
JADE, Okinawa Trough (Marumo and Hattori, 1999); (Halbach et al., 1989); (Hou et al., 1999); (Lüders et al., 2001)	139 – 230 200 – 360 220 - 392	4 – 5.2 2 – 15 4 – 7.5	320 220	Venting Black smoker. Venting White smoker. (ba) hosted inclusions. (sp) hosted inclusions, variation due to phase separation at depth. (qz) hosted inclusions.
Suiyo Seamount, Sumisu Rift, Izu Bonin Arc (Tsunogai et al., 1994)			310	12 high temperature chimneys venting fluids.
Central Hill, Escanaba Trough (Zierenberg et al., 1993)			108 - 207	2 vent sites are 275m apart, pH of fluids are 5.4.
Guaymas Basin, Gulf of California (Von-Damm et al., 1985)			250 - 308	
Bent Hill, Middle Valley, Juan de Fuca Ridge (Goodfellow and Franklin., 1993); (Ames et al., 1993)			184 - 274	(an) chimney. At the Dead Dog vent field, ~ 20 vents emit fluids up to 276°C.
Ancient				
Kuroko, Japan (Pisutha-Arnond and Ohmoto, 1983)	200 - 330			Highest temperatures associated with yellow ore formation.
Hellyer, Tasmania (Zaw et al., 1995, 1996)	165 - 320	8 - 11	-	Stockwork hosted primary inclusions, no evidence of boiling. <1 mole% CO2.
Tharsis, Mt Lyell, Tasmania (Zaw et al., 2001)	120 – 160 160 – 260 230 – 240 140 - 190	8 - 12 6 - 34 6 - 14		Interpreted to have formed at <500m. 2 and 3 phase inclusions are recorded. (sp) hosted inclusions. (fl) hosted inclusions. (to) hosted inclusions. (wo) hosted inclusions.
Mt Chalmers, Queensland (Zaw et al., 2000)	160 - 268	5 - 10		(qz) hosted primary inclusions, no evidence of boiling. <1 mole% CO2.
Yaman Kasy, Urals (Herrington et al., 1998)	> 350 < 100	3.5		No evidence of boiling, cooler Th in ba from the outer zone of chimneys.
Eskay Creek, Canada (Sherlock et al., 1999)	< 200	2.6 – 10.7		Thought to be similar to the Jade deposits

Table 6.2 footnote: All values are reported in °C, fluid temperature refers to data collected from actively venting hydrothermal sites. (L) = liquid, (V) = vapour, ap = apatite, pl = plagioclase, an = anhydrite, qz = quartz, ba = barite, sp = sphalerite, fl = flourite, to = topaz, w = woodhousite.

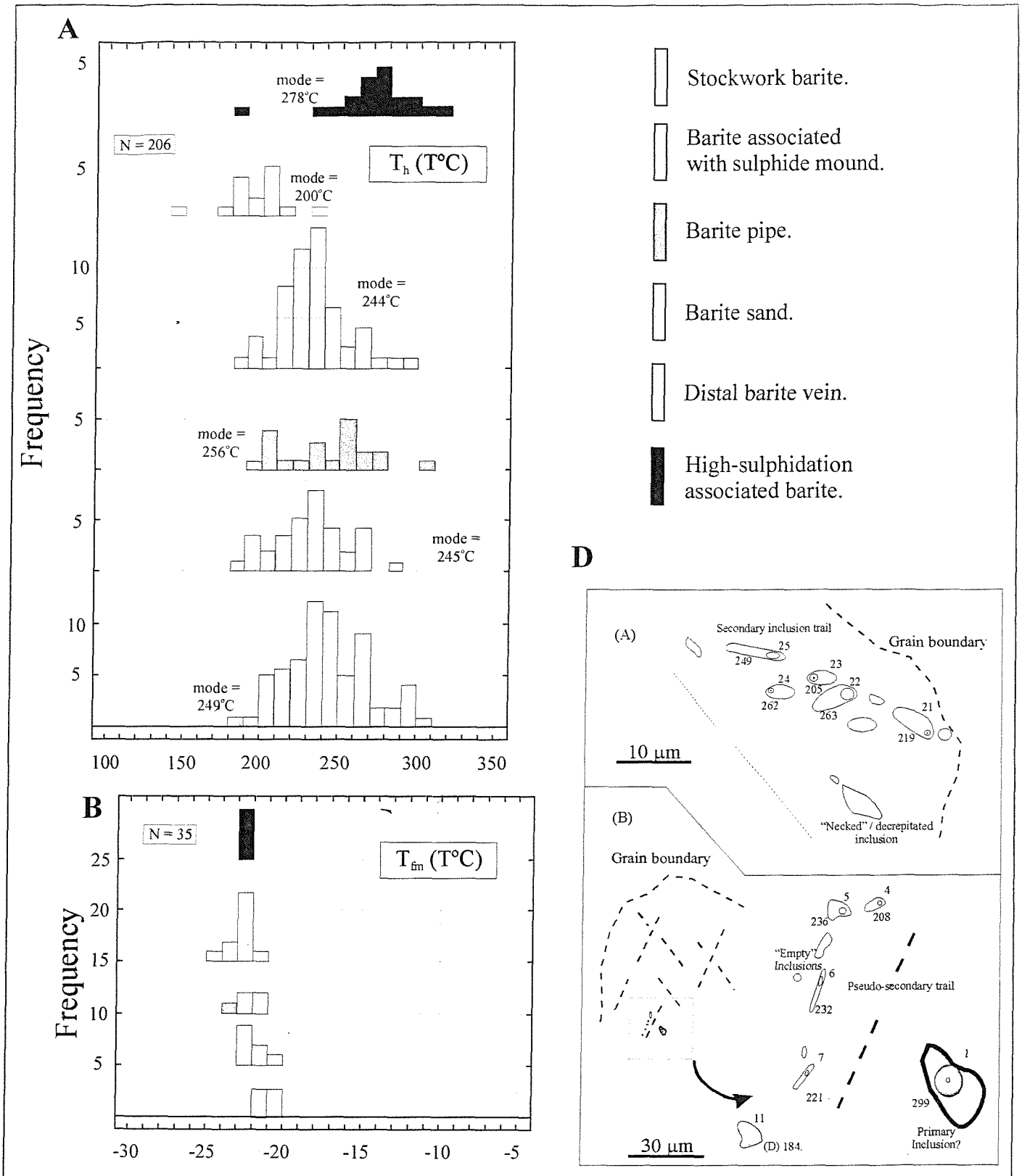


Figure 6.4. Microthermetric results for fluid inclusions in barite from Wetar Island (data divided into different occurrence associated with the deposits). **A.** Frequency histogram of homogenization temperatures (T_h). **B.** Frequency histogram of first ice melting (T_{fm}). **C.** Frequency histogram of final ice melting (T_{mice}). **D.** Representative line drawings of aqueous fluid inclusions in Wetar Island barite. (A) secondary inclusion trail (sample *097106*). (B) pseudo-secondary and possibly a primary inclusion (sample *096879*). Single-digit and two-digit numbers are reference numbers for individual inclusions; three-digit numbers are homogenisation temperatures (T_h) for these inclusions. Where preceded by "D" it indicates decrepitation temperature N= number of measurements.

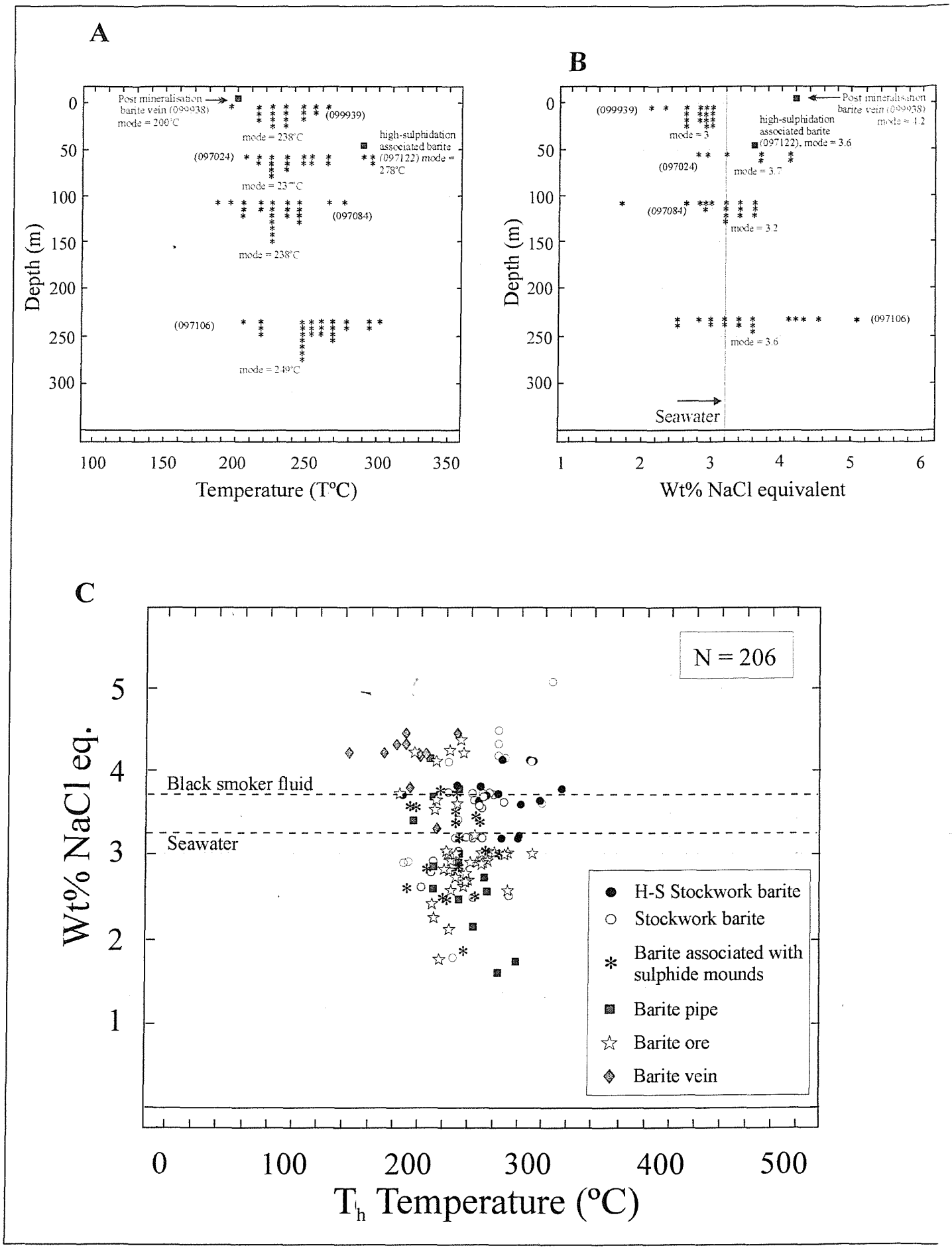


Figure 6.5. **A.** Homogenisation temperatures for barite fluid inclusion and corresponding depths of host samples, Lerokis Zone 5 only. **B.** Salinities for barite fluid inclusions and corresponding depths of host samples, Lerokis Zone 5 only, salinity of seawater is shown for reference. Only the modes from the high-sulphidation assemblage are shown on the plots for clarity, modes from the other samples are shown for reference. **C.** Homogenisation temperature T_h versus NaCl variation of inclusions from Wetar Island.

Phase separation at depth produces high salinity brines, lower salinities than seawater are a result of phase separation by boiling or condensation of seawater derived fluids and / or by mixing of hydrothermal seawater with phase separated brines (Tivey et al., 1998 and references therein). No saline brines have been observed at Wetar like those at Vai Lili, Lau Basin or at JADE. The results from these sites and the presence of low salinity fluids (less than seawater) observed within the inclusions suggest that Wetar also had a brine phase resulting from sub or supercritical phase separation at depth. This has led to the generation of the observed salinity range, however in this instance the brine phase did not reach the seafloor. Samples collected deeper within the hydrothermal system, particularly associated with the *high-sulphidation* sulphide assemblages may preserve this brine phase. The 2 phase boundary of seawater coincides with that of the 3.2 wt% NaCl in the H_2O system. At depths of 3 km, the critical point is ~ 400°C (Bischoff and Rosenbauer, 1984), a temperature much higher than those recorded in the barite samples therefore the phase boundary is encountered at lower temperatures than the critical point. This would result in subcritical phase separation forming a pure water vapour and a saline liquid phase.

6.6.2 Depth of formation and Pressure Estimates

Based on geological evidence (Chapter 3), the *globigerina* bearing limestone that caps the mineralisation at Kali Kuning is the best indicator of water depth. The assemblages preserved (including *Favocassidulina*) and the benthic:planktonic ratios indicate that formation occurred at least 2000 m and possibly considerably deeper (Murray pers com, 1999). As there is a lack of evidence suggesting that boiling occured within the system, a deep environment during deposit formation is highly plausible. These results contradict those of Sewell and Wheatley, (1994) who propose that mineralisation occurred at depths of < 600 m. Geological relationships suggest that the deposits formed at, or just below the paleo-seafloor so only hydrostatic confining pressure is acting. Assuming that the formation of the limestone occurred at depths of between 2 and 2.5 km, both prior to this and during mineralisation, it is likely that the deposit formed at greater depths. Hydrothermal activity within the area may have proceeded through waning stages for some considerable length of time prior to deposition of the limestone. We know from the tectonics of the region (Chapter 2), uplift can be rapid and also occur in pulses with uplift values as high as 500 cm/ka^{-1}

(de Smet, 1989), post 4.7 Ma. the deposits may have transgressed substantially to a shallower position before the deposition of the limestone. Based on a minimum depth estimate of 2250m and a maximum estimate of 3000 m, the confining pressure equates to a homogenisation temperature correction of +23°C and +40°C (Potter, 1977), see also Figure 6.6A. The depth estimates concur with current known depths of the Wetar Basin, directly to the south of Wetar they reach 3000m, with depths as great as 7000 m in the Weber Basin to the east (Chapter 2). Therefore these estimates are geologically plausible.

The pressure–temperature diagram, Figure 6.6A utilises the minimum and maximum depth estimates. The average degree of fill (F) for the Wetar inclusions is 0.9 (90% L, 10%V), the average salinity is 3.2 wt% NaCl therefore the density of the inclusions ~ 0.92 gcm^{-3} based on data in Shepherd et al., (1985). The temperature correction to the homogenisation data based on these parameters are consistent with the values given in Potter, (1977). If the maximum correction is applied, the Wetar Island average homogenisation temperature will be **275°C.**

Depth of mineralisation may have important implications in the generation of these systems as both shallow and deeper water conditions are recorded on deposits with similar sulphide-barite associations (JADE and Madneuli deposits). Depth may also have an importance especially in the transport of precious metals where in particular shallow water can allow boiling of hydrothermal fluids and precipitation of Au above the zone of boiling ie. Juan de Fuca Ridge (Hannington et al., 1999). Volcanic facies are not depth specific (Huston and Cas, 2000) as pillow lavas can occur in all water depths and vesicular lavas are not indicative of shallow waters. The limestone unit is by far the most important lithology in terms of estimating depth of formation for the Wetar Island deposits, the relationship with the underlying sulphides suggests that the sulphides formed at or extremely near to the palaeo-seafloor. The minor evidence of reworking above the Lerokis Zone 5 deposit does not necessarily suggest shallow water conditions as ocean currents in deep water have recently been documented on the slopes of the Kermadec Arc volcanoes at depths up to 1500 m (Wright, in press).

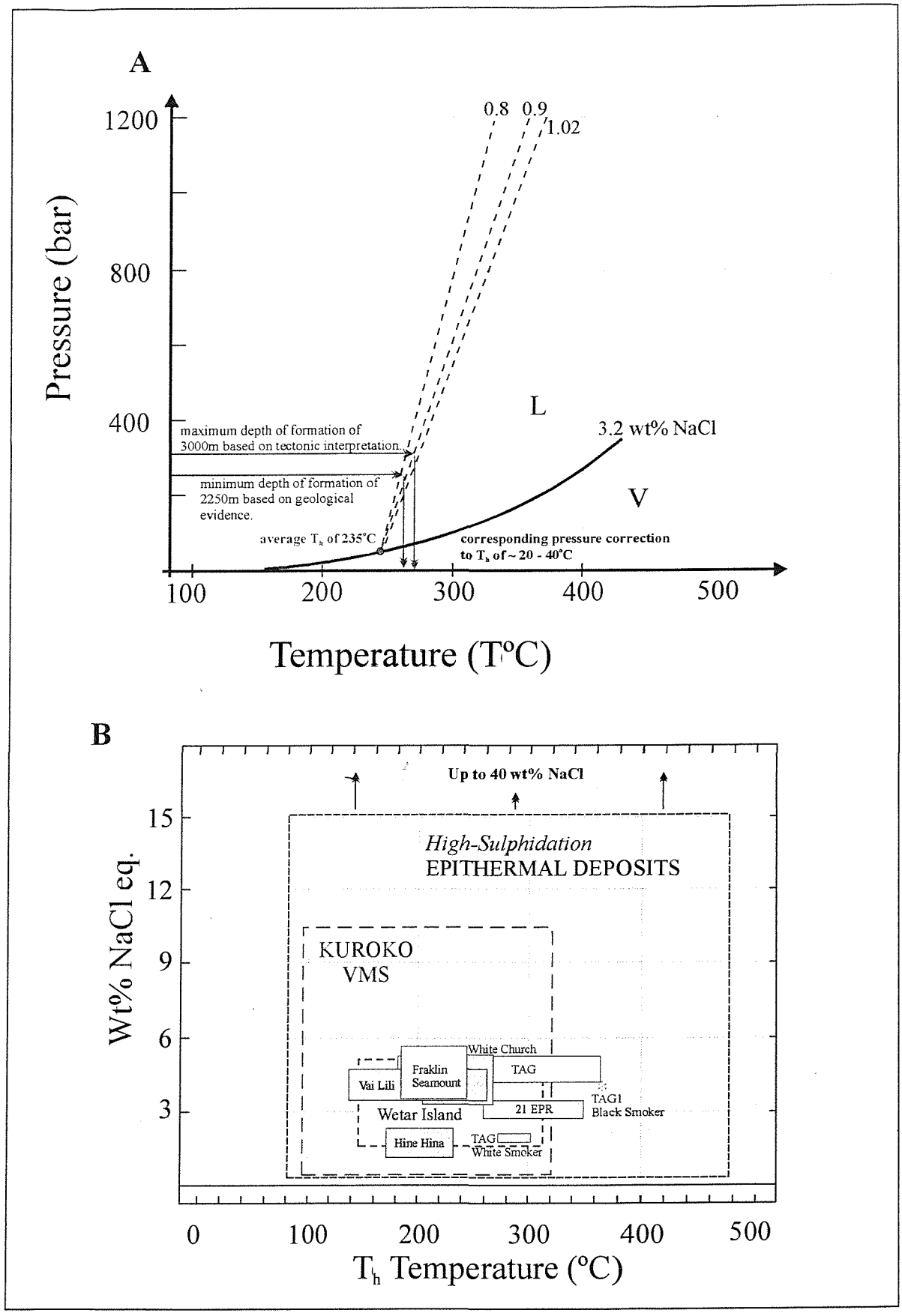


Figure 6.6. A. Pressure-temperature diagram for the H_2O-NaCl system, a temperature correction is based on geological evidence from the overlying *globigerina* bearing limestone at Kali Kuning, see text for explanation. Using a minimum depth estimate of 2250 m and a maximum of 3000 m, a pressure correction to the T_h data corresponds to ~20 - 40°C. An average homogenisation temperature of 235°C and density of 0.92 gcm^{-3} have been used, the liquid -vapour curve for 3.2 wt% NaCl is shown, modified from Shepherd et al., (1985).
B. Homogenisation temperature T_h versus NaCl variation of inclusions from Wetar Island, Kuroko VMS deposits, selected seafloor systems and *high-sulphidation* epithermal deposits, data from Roedder 1984; Arribas 1995; Hedenquist and Lowenstern, 1994, see text.

6.7 SUMMARY

The temperatures of homogenisation are consistent with those presented in Chapter 4 based on alteration mineral assemblages. A plot of homogenisation temperature versus salinity, (Figure 6.6B) indicates that the data from Wetar Island lies within the data fields for both Kuroko VMS systems and high-sulphidation epithermal deposits (data from Roedder, 1984; Hedenquist and Lowenstern, 1994; Arribas, 1995). Comparisons of the Wetar Island deposits to VMS and epithermal systems based on previous Chapters (geology, alteration and mineralogy) have proven that the deposits preserved at Wetar are unusual and whilst the deposits show many characteristics typical of seafloor VMS deposits, there are features similar to those in sub-aerial *high-sulphidation* epithermal systems. The observed low salinity fluids within the Wetar samples may therefore be meteoric derived however geological relationships do suggest a deep marine environment. Stable and Radiogenic isotopes (Chapters 7 and 8) will be used to better identify marine or meteoric fluid input within the hydrothermal system responsible for the Wetar mineralisation.

In summary, the Wetar fluid data (moderate temperature and dilute, low salinity) is similar to that of venting white smoker fluids on active ridges and collected samples from White Church sites, Lau Basin; TAG (Kremlin area). Further comparison to other systems outlined in Table 6.2 will be addressed in Chapter 9.

Chapter 7

STABLE ISOTOPES

7.1 INTRODUCTION

This chapter presents and reviews the results of a detailed sulphur and oxygen isotope investigation of the Wetar Island Au-Ag-Ba deposits. The study aims to provide information on source fluid reservoirs (Sasaki, 1974), temperature of sulphide deposition, constraints on mechanisms of mineral precipitation or physiochemical conditions (Taylor, 1987). Study of the Wetar Island alteration and mineralogical associations (Chapters 4 and 5) indicates features both typical to VMS systems with some characteristics of *high-sulphidation* conditions. The deposits preserved on Wetar may therefore be an example of a VMS system with a component of magmatic / igneous contribution to the mineralising hydrothermal fluids.

Stable isotope systematics (sulphur and oxygen) will be used primarily to test for the presence and contribution of a magmatic component in to the system. The results will be compared to previously published Wetar data (de Ronde, 1995), data from other ancient systems as well as actively forming deposits (VMS and *high-sulphidation* VMS).

Principal objectives of the study are therefore:-

1) To determine the source of sulphur and oxygen in the deposits.
2) To test if the *high-sulphidation* assemblage is hypogene or supergene in origin.
3) To test for magmatic fluid involvement in the formation of these deposits.

All isotopic analyses were performed at the Isotope Community Support Facility, Scottish Universities Environmental Research Centre (SUERC), East Kilbride, Scotland. Funding for which was through a successful NERC facilities grant.

7.2 SULPHUR ISOTOPES

The $\delta^{34}S$ ratios of sulphides in most volcanic dominated sea-floor hydrothermal systems, on sediment-free mid-ocean ridges and back-arc spreading centres, fall within a narrow range of values close to that of magmatic sulphur $\delta^{34}S$ 0‰ (Sakai et al., 1984) and + 4 to 5‰ respectively (Alt et al., 1993; Shanks and Seyfried, 1987; Herzig et al., 1998). Incorporation of sulphur into the hydrothermal system from the leaching of a basaltic source involves a negligible effect on isotopic signature such that the fluid H_2S will have a value close to the value of MORB due to the reduced nature and relatively high temperature of the deep system (Shanks et al., 1995). $\delta^{34}S$ ratios of oceanic island arc andesites contrast to basaltic dominated mid-ocean ridge systems with values ranging between +5 and +7‰ (Ueda and Saki, 1984). The observed enrichment in $\delta^{34}S$ is attributed to subduction zone recycling of hydrated oceanic crust and sediments containing sulphate from seawater (Alt, 1994, Alt et al., 1993). However, recent sulphide and barite data from sediment free systems including the Hine Hina Hydrothermal Field, Lau Basin and from the crater of a fore-arc sea-mount near Lihir Island, Papua New Guinea record much lower values of $\delta^{34}S$ (Herzig 1994, 1998). The Hine Hina sulphides record light $\delta^{34}S$ values of -4.9‰ for pyrite, -5.7‰ for sphalerite + chalcopyrite and -3.4‰ for a chalcopyrite separate whereas barite analyses show relatively light sulphate at +16‰. $\delta^{34}S$ data for alunite collected from the crater near Lihir Island are +7‰ with the reported sulphides averaging -5.3‰. (Herzig 1994) thus the isotopic compositions of the sulphides at Hine Hina and Lihir show a dramatic decrease in $\delta^{34}S$ from the normally reported values. A unique $\delta^{34}S$ depleted source of probable magmatic origin is proposed (Herzig 1994, 1998) in these systems due to the association of advanced argillic alteration mineral assemblages and the absence of biogenic sulphur. Isotopically light values of $\delta^{34}S$ in such systems may be produced principally in three ways, by the fractionation of sulphur between reduced and oxidised species as a result of large shifts in oxidation state by 1) boiling, 2) direct incorporation of a magmatic volatile phase or by 3) biogenic reduction of seawater sulphate (Herzig et al., 1998).

7.3 PREVIOUS WORK

A preliminary $\delta^{34}S$ study by de Ronde, (1995) on sulphides and sulphates is shown on Figure 7.1. The exact location of analysed sulphide/sulphate samples from the Lerokis, Kali Kuning and Meron VMS orebodies are uncertain, however the $\delta^{34}S$ results from sulphides and sulphates show signatures similar to Kuroko deposits with $\delta^{34}S$ of between 0-10°/$_{oo}$ for sulphides and 15-25°/$_{oo}$ for barite. de Ronde, (1995) interprets these $\delta^{34}S$ results as being almost identical to those for Kuroko barite, a mean value of ~ 22 °/$_{oo}$ for both systems is consistent with the value of Miocene seawater suggesting a seawater origin for ore deposit sulphate. One $\delta^{34}S$ value of barite at ~15/$_{oo}$ contrasts to the majority of the barite data as does the isotopically light value of enargite at 0/$_{oo}$.

7.4 PRESENT STUDY

7.4.1 Sample selection

Fifty four samples (comprising 29 sulphides, 25 sulphates including 23 barite samples, 1 gypsum and 1 native sulphur) from the deposits of Kali Kuning, Lerokis Zones 4 and 5 were analysed for sulphur isotopes. Sulphides were selected from all stages of the mineral paragenesis and included early disseminated pyrite from altered host volcanics, disseminated pyrite and pyritic veins from mineralised stockwork zones, sulphide mounds and late stage *high-sulphidation* fracture-fill sulphides which permeate through and below the massive pyritic mounds. Analysis of individual mineral phases present within the *high-sulphidation* assemblage was not possible due to the nature of the fine-grained intergrowth, (Figure 5.19, Chapter 5) therefore a bulk covellite-sphalerite-tennantite sample was analysed.

Sulphate samples (barite) were chosen to encompass all types within the mineralised systems, including disseminated laths from deep stockwork zones and barite associated with the sulphide mounds (vug/void hosted and as encrustations). The barite deposits themselves were sub-divided into barite feeder structures, barite ore deposits and baritic veins. One sample of post mineralisation gypsum and one sample of native sulphur (from Kali Kuning) were also analysed.

7.4.2 Results

All samples analysed are reported in Table 7.1 and Appendix F; a summary is given in Table 7.2 outlining ranges and mean values. The sulphur data are presented as a series of histograms in Figures 7.2 and 7.3. Sample preparation techniques are given in Appendix F, as are analytical techniques. Sulphur isotopic results are reported as per mil (‰) values relative to Vienna Canyon Diablo Troilite (V-CDT). Reproducibility of standards yielded results of –4.51 ± 0.18‰ (1σ n = 4) for CP1, 17.0 ± 0.14‰ (1σ n = 5) for NBS 123 and –29.9 ± 0.9‰ (1σ n = 3) for IAEA-S-3. The ratio of standards to analysed samples during the study is approximately 1:5, the reproducibility of samples analysed by repeat analysis during the study was 0.01‰ for sample 097122 and 0.8‰ for sample 097219 and 2.9‰ for sample 099938. The variability of reproducibility in natural samples is probably a reflection of variable isotopic homogeneity in the samples. It is clear however from the standard data that technique reproducibility is ± 0.2‰ or better.

The Wetar Island $\delta^{34}S$ sulphide data vary between +3.3 and +11.7‰ (mean, 8.0‰ and standard deviation of 1.9‰, n=29) whereas the $\delta^{34}S$ barite data vary between +22.4 and +31.0‰ (mean, 24.8‰ and standard deviation of 2.1‰, n=23). The sulphide data demonstrates a near normal distribution (see Figure 7.2) in contrast to the barite data which is skewed towards relatively isotopically lighter values, native sulphur and post mineralisation gypsum from Kali Kuning deposit yielded $\delta^{34}S$ values of +15.8‰ and +12.8‰ respectively (see Figure 7.2). Figure 7.3 reveals differences within the $\delta^{34}S$ values when the data is dissected in to individual deposits and paragenetic stages.

The sulphide mound sulphides range in $\delta^{34}S$ from +6.2 to +11.7‰ (mean, 8.7‰ and standard deviation of 1.7‰, n=13) whereas sulphide mound sulphates range in $\delta^{34}S$ from +22.7‰ and +24.7‰ (n=5). The histograms in Figure 7.3 illustrate that the Kali Kuning mound sulphides are isotopically heavy with respect to $\delta^{34}S$ than the Lerokis Zone 5 mound sulphides whereas the sulphates associated with both sulphide mounds exhibit similar $\delta^{34}S$ isotopic values. Chalcopyrite separates analysed from the Kali Kuning and Lerokis Zone 5 sulphide mounds yielded results of 10.25 and 7.44‰ respectively, again, the sample from Kali Kuning is isotopically heavy with respect to

$\delta^{34}S$ compared to that of Lerokis Zone 5. The shift of ~2.5‰ for the chalcopyrite samples is consistent with the shift also exhibited by the mean values for the sulphide mounds of 9.98‰ and 7.26‰. The pyritic sands, which surround the massive sulphide mounds at the Kali Kuning and Lerokis Zone 5 deposits were analysed and yielded results of $\delta^{34}S$ of +11.7‰ and +8.5‰, these results are similar to their associated sulphide mounds. These pyritic sands also contain barite (see also Chapter 5), the sample from Kali Kuning returned a result of +25.3‰.

Stockwork sulphides range between +3.3 and +9‰ at Lerokis Zone 5 and are isotopically similar to the overlying sulphide mound with respect to $\delta^{34}S$ (mean, +6.7‰ and standard deviation of 1.8‰, n=10). $\delta^{34}S$ results from disseminated low-Fe sphalerite and the bulk sphalerite-tennantite-covellite sample (*high-sulphidation* sulphide assemblage, 097122) are +4.3 / +6.1‰ and +6.9‰ respectively, Table 7.1 and Figure 7.3. Stockwork sulphates are isotopically heavier than the sulphide mound sulphates and range in $\delta^{34}S$ from +25.0 to +28.1‰ (n=4).

The barite results from the Au bearing barite deposits themselves exhibit a range of $\delta^{34}S$ values between +22.4 to +26.9‰ (mean, +24.3‰ and standard deviation of 1.9‰, n=8). The histograms indicate the barite deposits at Lerokis Zone 4 (where no sulphide body is present) are slightly isotopically heavier with respect to $\delta^{34}S$ than those at Kali Kuning and Lerokis Zone 5. $\delta^{34}S$ data from the cemented barite pipe structures fall within a narrow range, the samples from Lerokis Zone 4 and 5 yielded results of +24.6‰ and +24.5‰ respectively. The barite veins, (099938, location 112) distal to the Lerokis Zone 5 mineralisation are isotopically heavy when compared to all other barite from the mineralisation. This value recorded in this sample is similar with that from a proximal vein collected at Lerokis Zone 5 (sample 099333, location 30, Figure 4.5 and insert map 2A), the three samples exhibit a range of values between +27.8 and +31.03‰. A pyritic vein (cross cutting chloritic altered pillow lavas approximately 0.5 km from Lerokis Zone 4, sample 111997, location 162) yielded a result of +7.25‰, disseminated pyrite from the Kali Kuning footwall yielded results of +7.6‰ and +8.4‰.

Table 7.1. $\delta^{34}S$ and $\delta^{18}O$ data of sulphides and sulphates, Wetar Island.

Sample	Zone	Location	Sample Type	Mineral	$\delta^{34}S_{V\text{-}CDT}$	$\delta^{18}O_{V\text{-}CDT}$
096876	KK	84	Sulphide Mound	pyrite	11.7	
096877	KK	84	Barite ore	barite	24.2	
096878	KK	84	Barite ore	barite	27.0	
096879	KK	84	Barite ore	barite	23.7	10.9
096888	KK	87	Barite ore	barite	23.1	
096889	KK	87	Barite ore	barite	22.4	
096890	KK	87	Pyritic sand	pyrite	11.6	
096889	KK	87	Barite ore	barite	22.4	
111943	KK	215	Sulphide Mound	pyrite	9.3	
111943	KK	215	Sulphide Mound	chalcopyrite	10.3	
111943	KK	215	Barite associated with sulphides	barite	22.8	
100134	KK	69	Sulphide Mound	pyrite	8.4	
096890	KK	87	Barite associated with pyrite sands	barite	25.3	
100133	KK	69	Barite ore	barite		9.1
096857	KK	75	Sulphide Mound	pyrite	10.4	
097169	KK	74	*Native sulphur*	sulphur	15.6	
111914	KK	316	Vein/disseminated pyrite (within propylitic altered zone of footwall)	pyrite	9.9	
097219	KK	*	Vein/disseminated stockwork sulphides	pyrite	8.4 / 7.6	
097228	KK	*	Sulphide Mound	pyrite	10.8	
111942	KK	92	*Small sulphide mound, located on the Kali Kuning road*	pyrite	8.5	
100103	KK	50	Post mineralisation sulphate	gypsum	12.8	13.3
096948	L4	129	Cemented Baritic feeder structure	barite	24.6	8.7 / 9.4
111979	L4	149	Barite ore	barite	25.2	6.5
111931	L4	217	*Barite ore*	*barite*	26.3	7.7
099902	L5	4	Sulphide Mound	pyrite	6.9	
099917	L5	15	Sulphide Mound	pyrite	6.3	
099917	L5	15	Barite associated with sulphides	barite	24.2	8.4
099923	L5	19	Cemented Baritic feeder structure	barite	24.5	7.8
099939	L5	46	Barite ore	barite	23.9	6.8
099933	L5	30	Barite vein, proximal to sulphide mound	barite	27.8	10.6
099938	L5	112	Barite vein, distal to sulphide mound	barite	31 / 28.1	11.3
111997	L5	162	Pyrite vein, distal to sulphide mound	pyrite	7.3	
097106	L5	*	Disseminated stockwork sulphides	pyrite	3.3	
097106	L5	*	Disseminated stockwork barite	barite	27.5	7.7
097104	L5	*	Disseminated stockwork sulphides	sphalerite	6.1	
097098	L5	*	Disseminated stockwork sulphides	pyrite	6.7	
097098	L5	*	Disseminated stockwork barite	barite	25.0	8.9
097084	L5	*	Disseminated stockwork sulphides	pyrite	9.0	
097084	L5	*	Disseminated stockwork sulphides	sphalerite	4.3	
097084	L5	*	Disseminated stockwork barite	barite	27.0	8.6 / 7.7
097059	L5	*	Sulphide Mound	pyrite	8.0	
097059	L5	*	Sulphide Mound	chalcopyrite	7.4	
097059	L5	*	Barite associated with sulphides	barite	22.7	5.8
099929	L5	40	Pyritic sand	pyrite	8.6	
097122	L5	*	Stockwork sulphides	pyrite	8.02 / 8.01	
097122	L5	*	Stockwork sulphides (high-sulphidation assemblage)	cov-spha-ten	6.9	
097122	L5	*	Barite associated with the high-sulphidation sulphides	barite	28.1	8.6
097138	L5	*	Stockwork sulphides	pyrite	7.3	
097041	L5	*	Stockwork sulphides	pyrite	6.6	
097024	L5	*	Stockwork sulphides	pyrite	8.6	
097024	L5	*	Barite associated with sulphides	barite	24.6	11.3
097023	L5	*	Sulphide Mound	pyrite	7.5	
097023	L5	*	Barite associated with sulphides	barite	24.4	
097009	L5	*	Sulphide Mound	pyrite	7.4	

Footnote: For all data and analytical techniques, refer to Appendix F, KK = Kali Kuning, L5 = Lerokis Zone 5, L4 = Lerokis Zone 4, sample locations are on insert map sheet 2A to C and Figures 4.2 to 4.8. Samples with * notation are from drill core beneath Kali Kining and Lerokis Zone 5, refer to Figures 4.3 and 4.6 for locations.

Table 7.2. Summary statistics of $\delta^{34}S$ and $\delta^{18}O$ data.

Sample	N	$\delta^{34}S_{V\text{-}CDT}$ Range	$\delta^{34}S_{V\text{-}CDT}$ Mean	$\delta^{34}S_{V\text{-}CDT}$ Std. Dev.
Kali Kuning				
Sulphide Mounds	7	8.4 - 11.7	9.9	1.22
Stockwork Zone sulphides	3	7.6 - 9.9	8.8	1.16
Barite Ore	4	22.4 - 27.0	24.3	1.94
Lerokis Zone 5				
Sulphide Mounds	6	6.3 - 8.0	7.3	0.6
Stockwork Zone sulphides	10	3.3 - 9.0	6.7	1.79
Stockwork Zone (barite)	6	22.7 - 28.1	25.8	2.06
Barite Ore	1	23.9	-	-
Lerokis Zone 4				
Barite Ore	2	25.2 - 26.3	25.7	-

Sample	N	$\delta^{18}O_{V\text{-}CDT}$ Range	$\delta^{18}O_{V\text{-}CDT}$ Mean	$\delta^{18}O_{V\text{-}CDT}$ Std. Dev.
Kali Kuning				
Barite Ore	2	9.1-10.9	10.0	-
Lerokis Zone 5				
Stockwork Zone (barite)	5	7.7-8.9	8.3	0.56
Barite Ore	1	6.8	-	-
Lerokis Zone 4				
Barite Ore	2	6.5-7.7	7.1	-

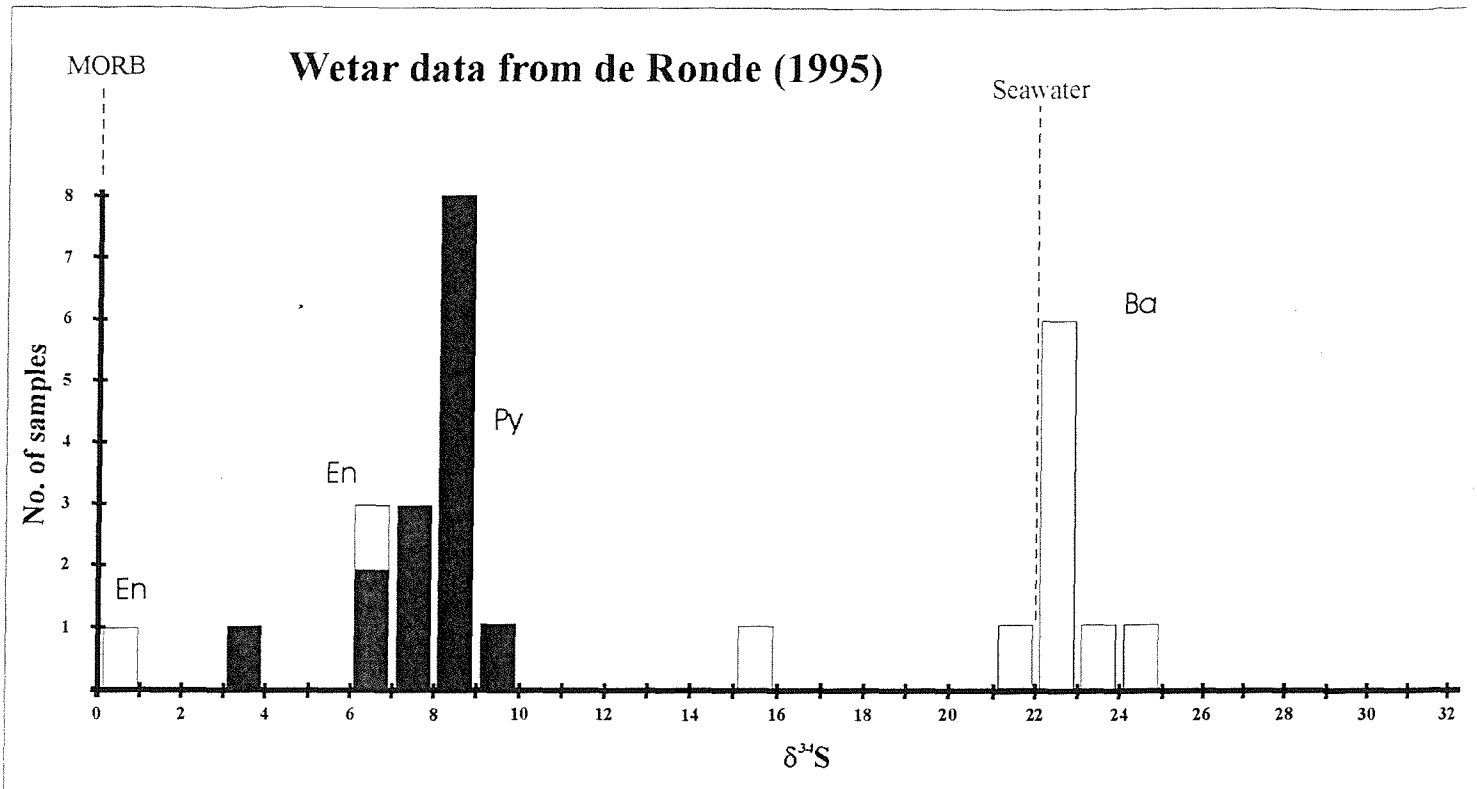


Figure 7.1. Sulphur isotopic compositions of sulphides and sulphates from Wetar Island, Indonesia, data from de Ronde, 1995. The values for MORB and modern day seawater are indicated. En= enargite, Py= pyrite, Ba= barite.

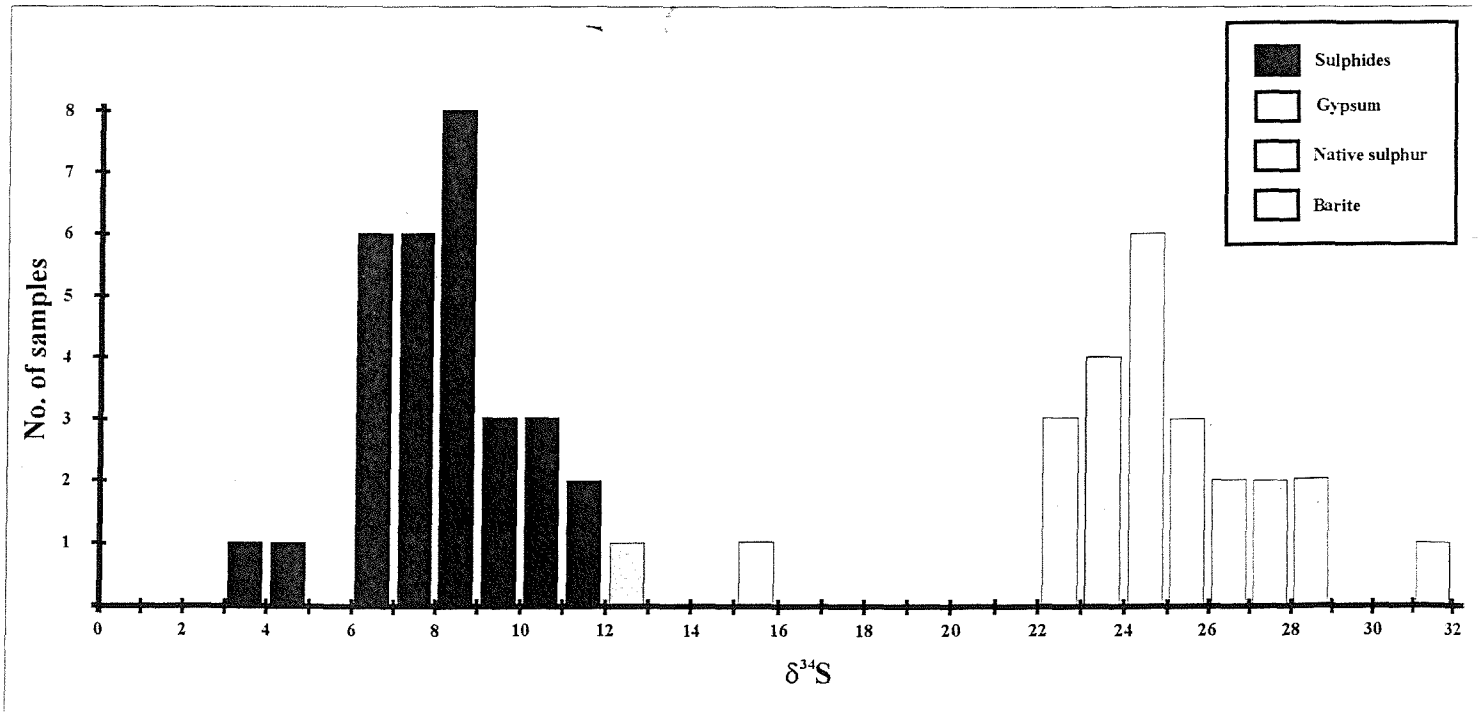


Figure 7.2. Sulphur isotopic compositions of sulphides and sulphates and native sulphur from the Kali Kuning, Lerokis Zone 5 and Lerokis Zone 4 sulphide-barite deposits Wetar Island, Indonesia.

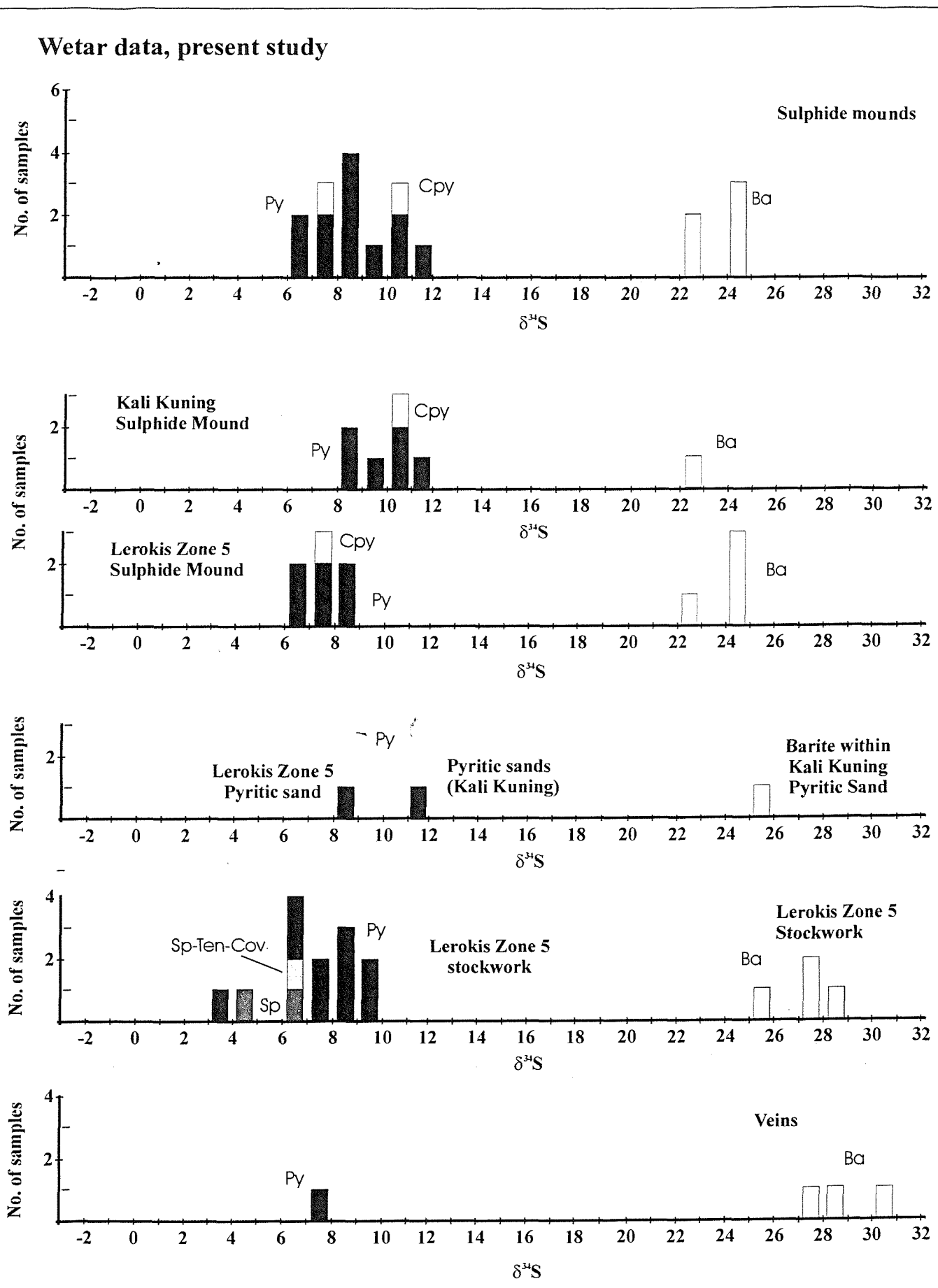


Figure 7.3. Comparison of sulphur isotope data from the Kali Kuning, Lerokis Zone 5 and Lerokis Zone 4 sulphide-barite deposits, Wetar Island, Indonesia. Py = pyrite, Sp = sphalerite, Sp-Ten-Cov = sphalerite, tennantite, covellite assemblage, Ba = barite.

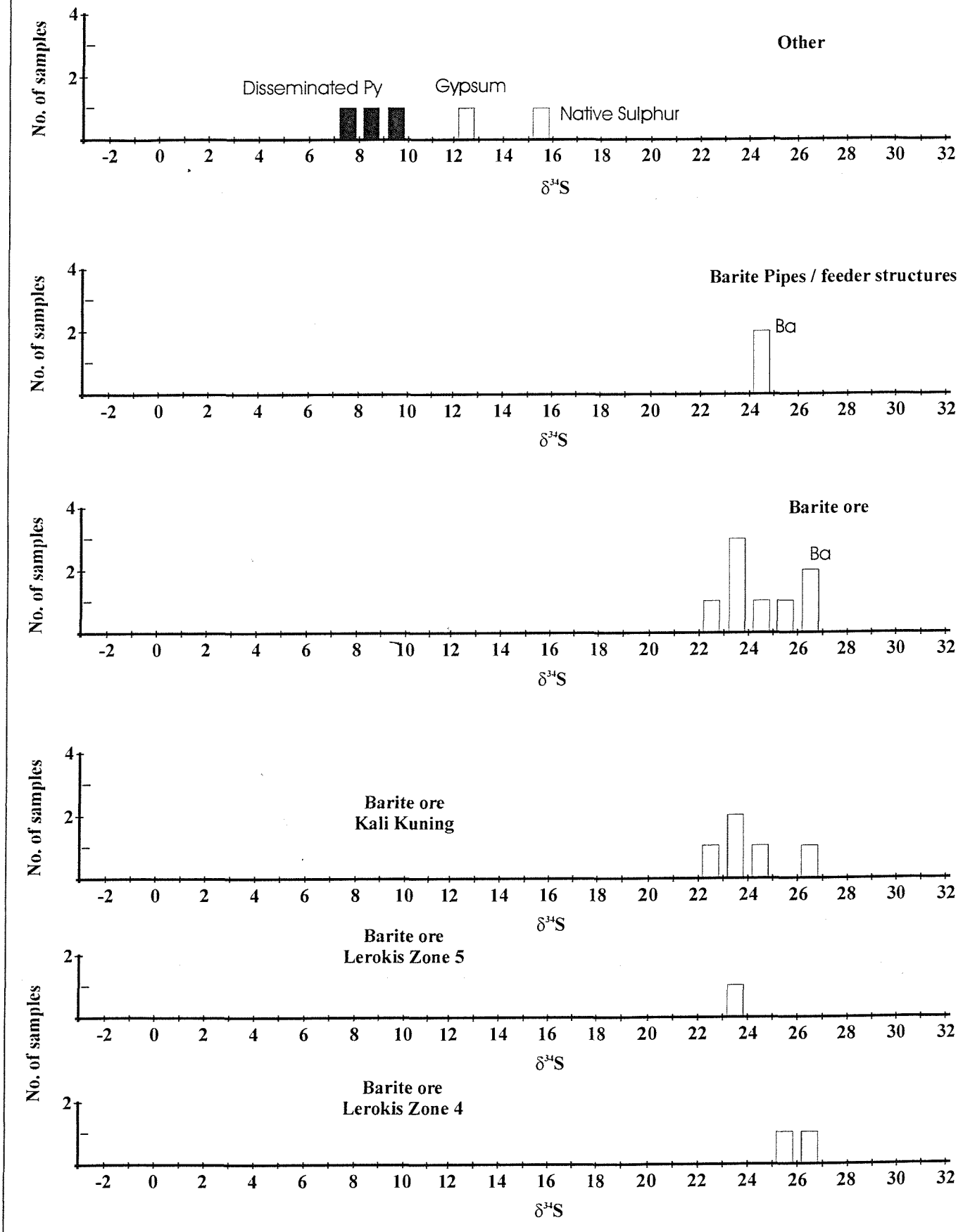


Figure 7.3. cont. Comparison of sulphur isotope data from the Kali Kuning, Lerokis Zone 5 and Lerokis Zone 4 sulphide-barite deposits, Wetar Island, Indonesia.

7.5 OXYGEN ISOTOPES

A number of VMS deposits have been studied using oxygen isotopes (reviews in de Ronde, 1995). Many of these systems (including Kuroko deposits) and active seafloor vents yield isotopic compositions in between those of seawater and magmatic water. Magmatic waters have well defined O-isotope compositions of between ~ +5.5 to +10‰ as do ocean waters at +0.5 to –1.0‰, meteoric waters are generally < 0‰ (Sheppard, 1986).

No previous oxygen work has been done on Wetar Island samples.

7.6 PRESENT STUDY

7.6.1 Sample selection

Nineteen representive samples were collected from the deposits of Kali Kuning, Lerokis Zones 4 and 5 for oxygen isotopic study of the Wetar Island mineralisation, the sample suite analysed consisted of samples used during the sulphur study. Eighteen barite samples were analysed for oxygen isotopes with one sample of post mineralisation gypsum from the Kali Kuning deposit. Sample preparation techniques are given in Appendix F.

7.6.2 Results

The sulphate oxygen data is presented as a series of histograms in Figures 7.4 and 7.5, the location of the samples and all results are reported in Table 7.1.

$\delta^{18}O$ sulphate data vary between +5.8 and +11.3‰ (mean, 8.5‰ and standard deviation of 1.6‰, n=18), the sample of post mineralisation gypsum from Kali Kuning yielded a distinct $\delta^{18}O$ value of 13.3‰ (Figure 7.4). The histograms in Figure 7.5 illustrate differences within the oxygen values when the data is dissected into individual deposits and paragenetic stages.

Barite $\delta^{18}O$ values associated with Lerokis Zone 5 sulphide mound range from +5.8 to +11.3‰ (n=3) with stockwork zone barite data falling within a narrow range (+7.7 to

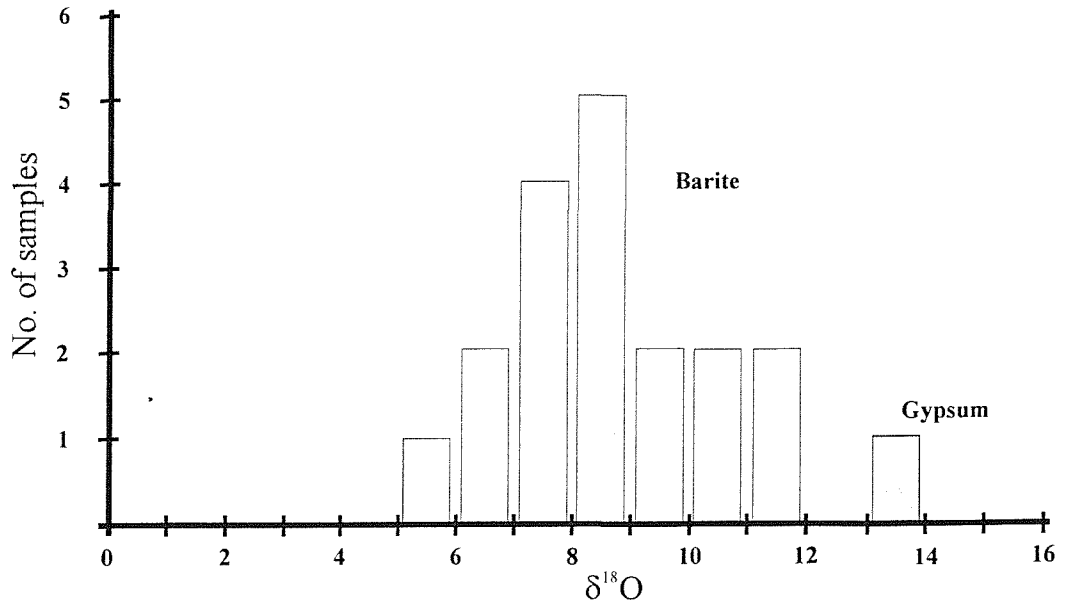


Figure 7.4. Oxygen isotope compositions of sulphates from the Kali Kuning, Lerokis Zone 5 and Lerokis Zone 4 sulphide-barite deposits, Wetar Island, Indonesia.

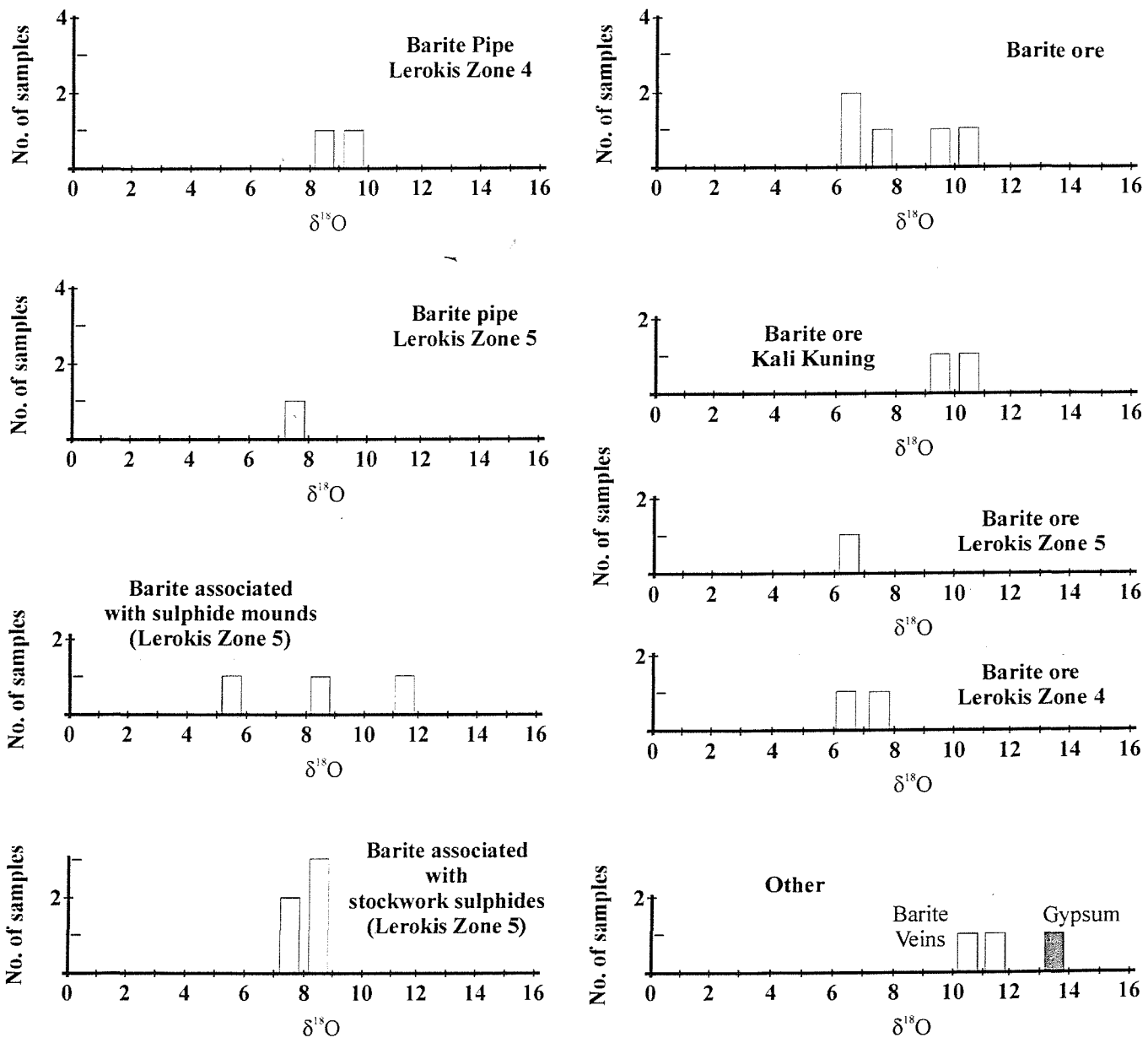


Figure 7.5. Comparison of oxygen isotope data of from the Kali Kuning, Lerokis Zone 5 and Lerokis Zone 4 sulphide-barite deposits, Wetar Island, Indonesia.

+8.9‰, n=5). The barite deposits themselves exhibit a range of $\delta^{18}O$ values between +6.5 to +10.9‰, Table 7.2 and the histograms indicate that the barite from the Kali Kuning barite ore deposits are slightly isotopically heavy with respect to $\delta^{18}O$ than those at Lerokis Zone 4 and 5. Barite analysed from the cemented possible feeder structures also fall within a narrow range, Lerokis Zone 4 and 5 yielded results of 8.7 / 9.4 and 7.8‰ respectively. These barite veins are isotopically heavy compared to all other barite from the mineralisation with respect to $\delta^{18}O$, the measured values were 10.5 and 11.3‰

7.7.1 DISCUSSION OF ISOTOPIC DATA

The sulphur data from the present study (Figures 7.1 and 7.2) compares to that of de Ronde, (1995) illustrating similar sulphide modal values however the enargite sample (~ 0‰) and the isotopically light barite sample (~15‰) contrast to the data from the present study.

The pyritic sands from Kali Kuning and Lerokis Zone 5 have consistent $\delta^{34}S$ ranges reported from their associated mounds, (Figure 7.3) consistent with the theory that the pyritic sands are mechanically derived from the surface of the sulphide mounds. The conclusion that the pyritic sands are formed by the generation of the barite ore deposits is based on field observation that the pyritic sand forms the contact zone between the sulphide mound and barite ore zones. This similarity of data is evident at Lerokis Zone 5 between the pyritic sand (8.55 ‰) and the adjacent sulphide mound value of 8.57‰, at Kali Kuning the sulphide mound yielded a value of 11.69‰ with the pyritic sand at 11.55‰. The lateral succession at Kali Kuning of the sulphide mound, pyritic sands, barite ore and hydrothermally altered footwall volcanics has been discussed in Chapters 3 and 5 (geology and mineralogy) and is shown in Figure 7.6 along with the isotopic sample locations. The results from the barite analysis across this contact zone (23.65 to 26.98‰) illustrates that there is no systematic lateral variation from the sulphide mound to the footwall (Figure 7.6). Anhedral barite crystals from within the pyritic sand at this location yielded a result of 25.25‰ which is consistent within the range of data for the barite ore. The data suggests a correlation between barite in the pyritic sands and the barite ore itself, this again suggests that the fluids from which the barite ore

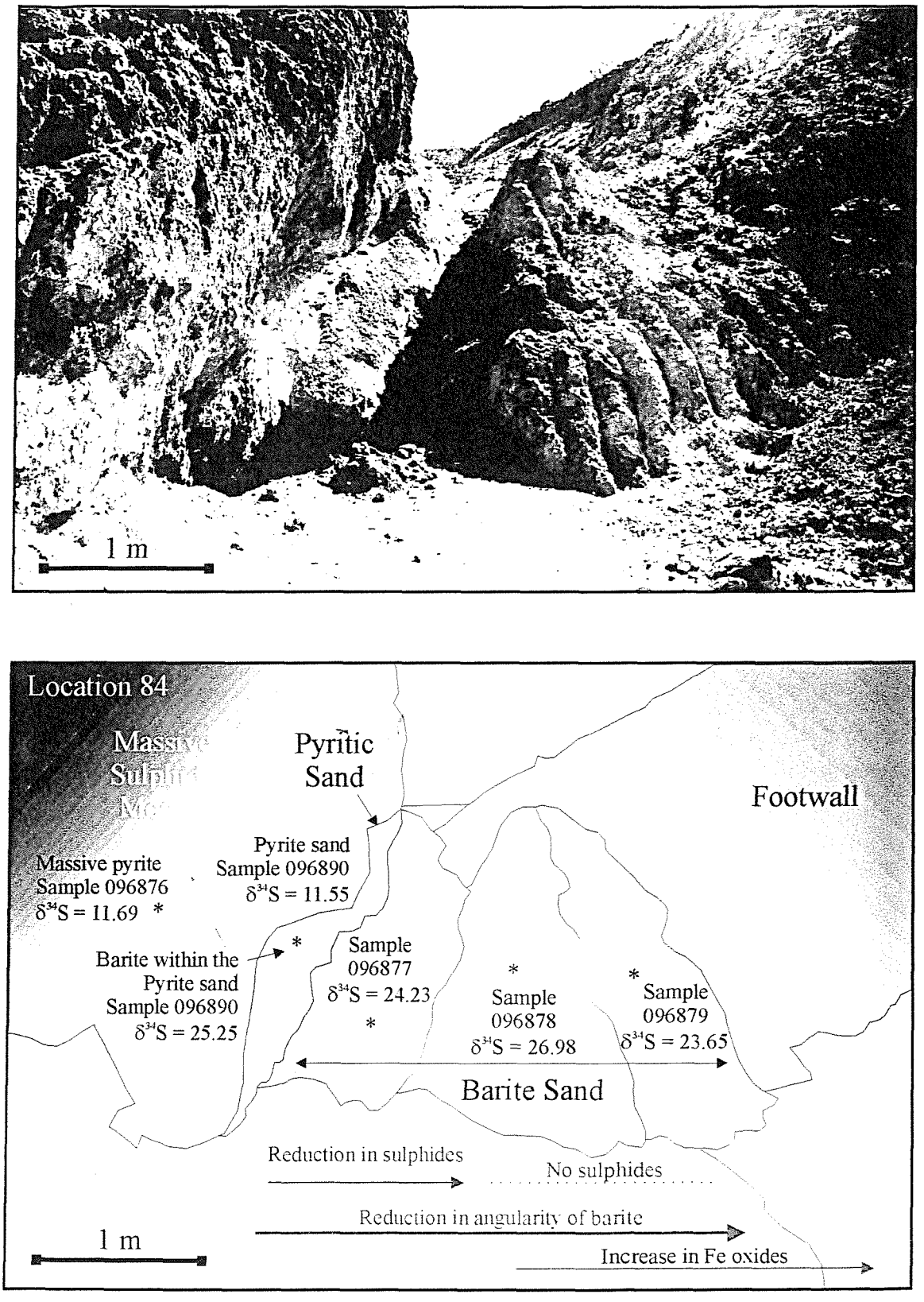


Figure 7.6. Detailed in-situ section of contact zone between massive sulphide mound, pyritic sand, barite sand and hydrothermally altered footwall, location 84, Kali Kuning. The section is discussed in more detail in chapter 5. $\delta^{34}S$ study of sulphide and sulphate phases are discussed in the text, results are shown along with sample location denoted by *. No systematic lateral variation in $\delta^{34}S$ values are recorded.

precipitated is responsible for the generation of the pyritic sands. The similarity of the sulphide data from both the underlying stockwork zones and overlying sulphide mounds (exhibited at both Kali Kuning and Lerokis 5) suggests a common source of sulphur for each deposit. This feature is also observed at TAG, where the data from TAG 2 (Kremlin area), TAG 4 and 5 are all coincident with a wider range observed at TAG1 (Peterson et al., 2000). Even over greater distances sulphide ranges can be similar as recorded from 11 and 13°N, EPR (Bluth and Ohmoto, 1988) however at 21°N, the average of the sulphides is lighter by ~2‰ (Woodruff and Shanks, 1988). In contrast, sulphides values can be varied as is evident at the White Church, Vai Lili and Hine Hina sites in the Lau Basin. (Herzig et al., 1998).

Abadi, (1996) suggests that the Cu enrichment at Wetar and the *high-sulphidation* sulphide assemblage are supergene in origin. The barite analysed from this assemblage (sample 097122) yielded a $\delta^{34}S$ value of +28‰ which is isotopically heavy than the majority of barite, the only heavier values recorded are those from the distal barite veins. Values close to those exhibited by the sulphides would be expected if this assemblage were a result of oxidation and weathering of the hypogene massive sulphide mound since oxidation results in limited fractionation. Data from Barite Hill confirm these results, a supergene barite sample yielded a value of 9.9‰ (where sulphides range between +1 to +5.3‰) compared to hypogene barite (+26‰ average), Clarke et al., (1999). These results are consistent with the postulation that the *high-sulphidation* assemblage preserved at Wetar Island are hypogene in origin. The distal barite veins are interpreted to be associated with the waning stages of hydrothermal activity and it is conceivable that a reduction in temperature could thus yield the observed heavy $\delta^{34}S$ values; the barite oxygen data is similarly consistent in that this sample is also isotopically heavy with respect to $\delta^{18}O$ as a result of increased fractionation. The fluid inclusion homogenisation temperatures (Chapter 6) confirm these results and which also record a lower temperature than the rest of the barite associated with mineralisation. The majority of the sulphate data ranges between 22 and 25‰ and suggests derivation from Miocene seawater sulphate (22‰, Claypool et al., 1980). Values greater than Miocene Seawater may suggest precipitation took place within a restricted basin where reduction of seawater sulphate will result in sulphate in the residual fluid being progressively enriched in $\delta^{34}S$ resulting in the range of values observed. The barite sample from the Lerokis Zone 5 barite deposit lies within the range of data recorded from the Kali Kuning deposit, (Figure 7.3)

however, the barite collected from the Lerokis Zone 4 deposit is heavier with respect to $\delta^{34}S$ and could suggest lower temperature of formation. Modal homogenisation temperatures from the three deposits (Chapter 6) do not support this theory as these barite ores all record similar temperatures. The isotopic data in concert with microthermometry confirms that the cemented barite-Fe oxide structures preserved within the deposits are in fact the fluid conduits for the barite ore deposits. The isotopic data from these structures with respect to both S and O are consistent with the surrounding barite ore-deposit data suggesting that they share a common source. The consistency between the vug / cavity filling barite within the sulphide mounds and the barite from the surrounding barite ore suggests these are derived from the same fluid. The fluid inclusion microthermetric data from these same samples (Chapter 6) also suggest they are of the same generation, infilling voids during the generation of the barite ores. Post mineralisation gypsum, $\delta^{34}S$ = 12.8‰ indicates derivation from oxidised sulphides and has not formed from seawater, the occurrence of native sulphur (Figure 7.7) with $\delta^{34}S$ of +15.8‰, must be a result of oxidation on the seafloor. The Wetar Island sulphur data contrasts to the fracture and vesicle filling native sulphur at the DESMOS site, East Manus Basin, where a range of –5.9 to –6.8‰ is reported Gemmell et al., (1999). These values are isotopically lighter than those reported from Hine Hina, (-2.4 to –4.8‰), the absence of biogenic sulphur and boiling within the system indicates a depleted $\delta^{34}S$ source of probable magmatic origin in these cases. On the basis of one result it is not possible to be definite in the interpretation of what is an unusual occurrence at Wetar.

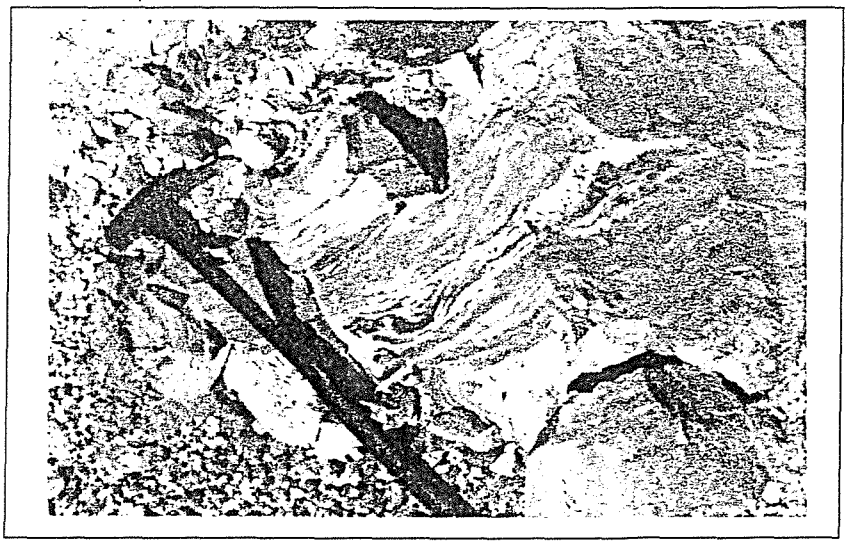


Figure 7.7. Native sulphur collected from the Kali Kuning deposit footwall, sample 097159, location 74, see map insert sheet 2A and Figure 4.2.

7.7.2 Isotopic Variations with Depth

Figure 7.8 shows an isotopic depth profile through the Lerokis 5 orebody, the data shows a slight depth/sample relationship is observed from the sulphide $\delta^{34}S$ data. The isotopically lightest value (+3.3‰) occurs at the greatest depth, similar observations are also recorded in a stratigraphic depth versus $\delta^{34}S$ profile from the Gossan Hill deposit where a 1.5‰ variation with depth over a 320 m section is evident. Lighter values are present and occurring at depth (Sharpe and Gemmell, 2000). In contrast to these results, there appears no significant correlation between $\delta^{34}S$ and depth for the Wetar sulphate data. At TAG, heavier values are observed at depth progressively becoming lighter toward the surface (Peterson et al., 2000), similar to data from Cyprus (Alt 1994). Deep seated sulphate reduction is proposed for generating the heavier values at depth (Chiba et al., 1998, Peterson et al., 2000). No significant trends are observed with the Oxygen data and depth, see Figure 7.8.

7.7.3 Isotopic Geothermometers

The temperature dependency of isotope fractionation between differing co-precipitated phases enables pairs of sulphur bearing compounds to be used as geothermometers (Ohmoto and Rye 1979). This technique was applied throughout the Wetar system principally to sulphate-sulphide pairs (dominantly barite-pyrite), to test if both phases were in equilibrium with the mineralising hydrothermal fluid. Temperature (°C) was calculated using the following equations.

Mineral Pair (T in Kelvin; $\Delta = \delta^{34}S_A - \delta^{34}S_B$)

Sulphates-pyrite

$$T = \frac{2.16\times10^3}{(\Delta - 6 \pm 0.5)^{1/2}} \qquad (T < 350^\circ C) \qquad (1.1)$$

Pyrite-sphalerite

$$T = \frac{(0.55 \pm 0.04)\times10^3}{\Delta^{1/2}} \qquad (1.2)$$

Sulphates-chalcopyrite

$$T = \frac{2.30\times10^3}{(\Delta - 6 \pm 0.5)^{1/2}} \qquad (T < 350^\circ C) \qquad (1.3)$$

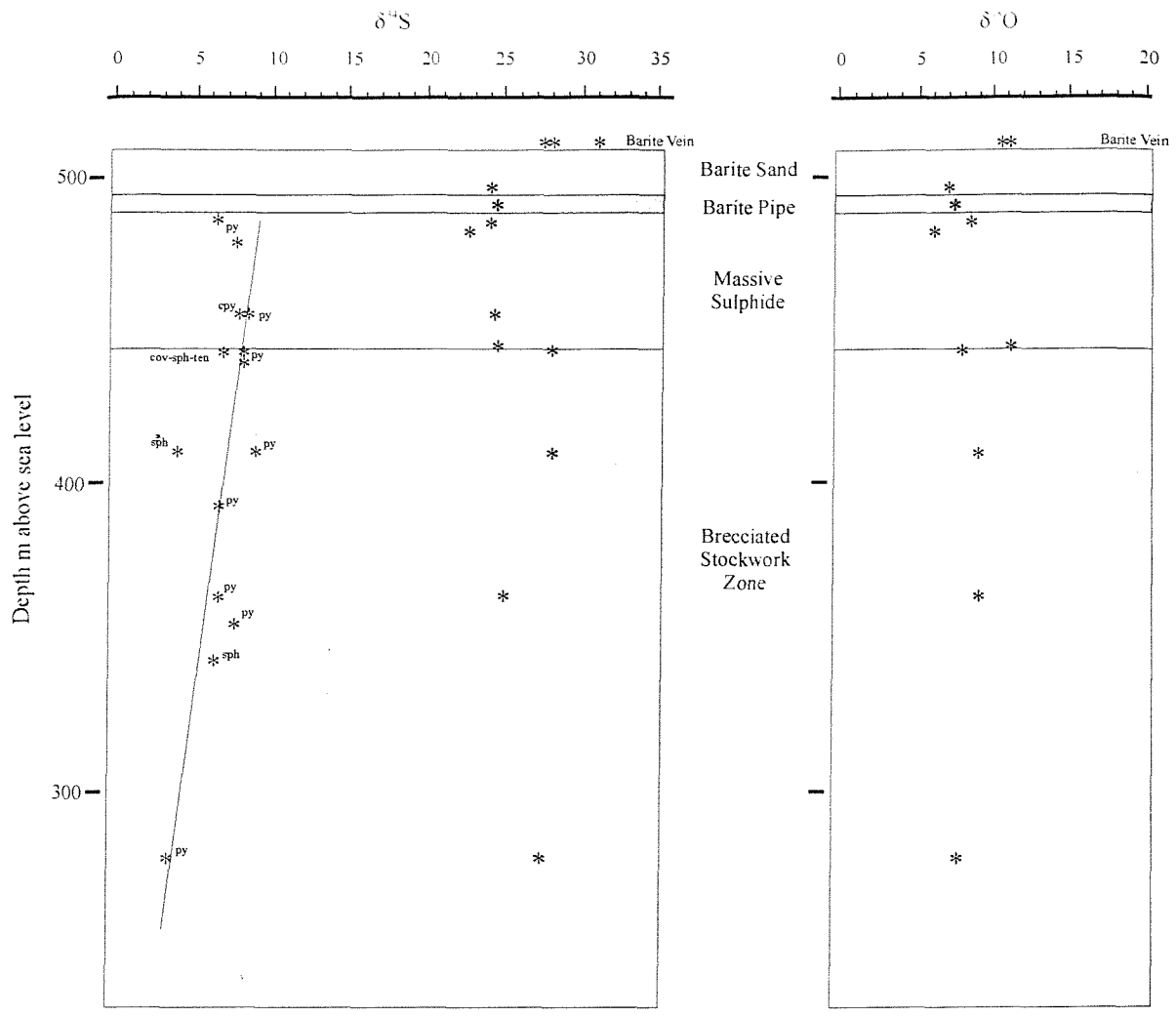


Figure 7.8. Plot of measured barite $\delta^{18}O$ and $\delta^{34}S$ for sulphides and sulphates versus depth for the Lerokis Zone 5 orebody, Wetar island, Indonesia. The Diagram is constructed from 3 drill hole intercepts, a slight increase from light to heavier $\delta^{34}S$ values is noted for the sulphide data.

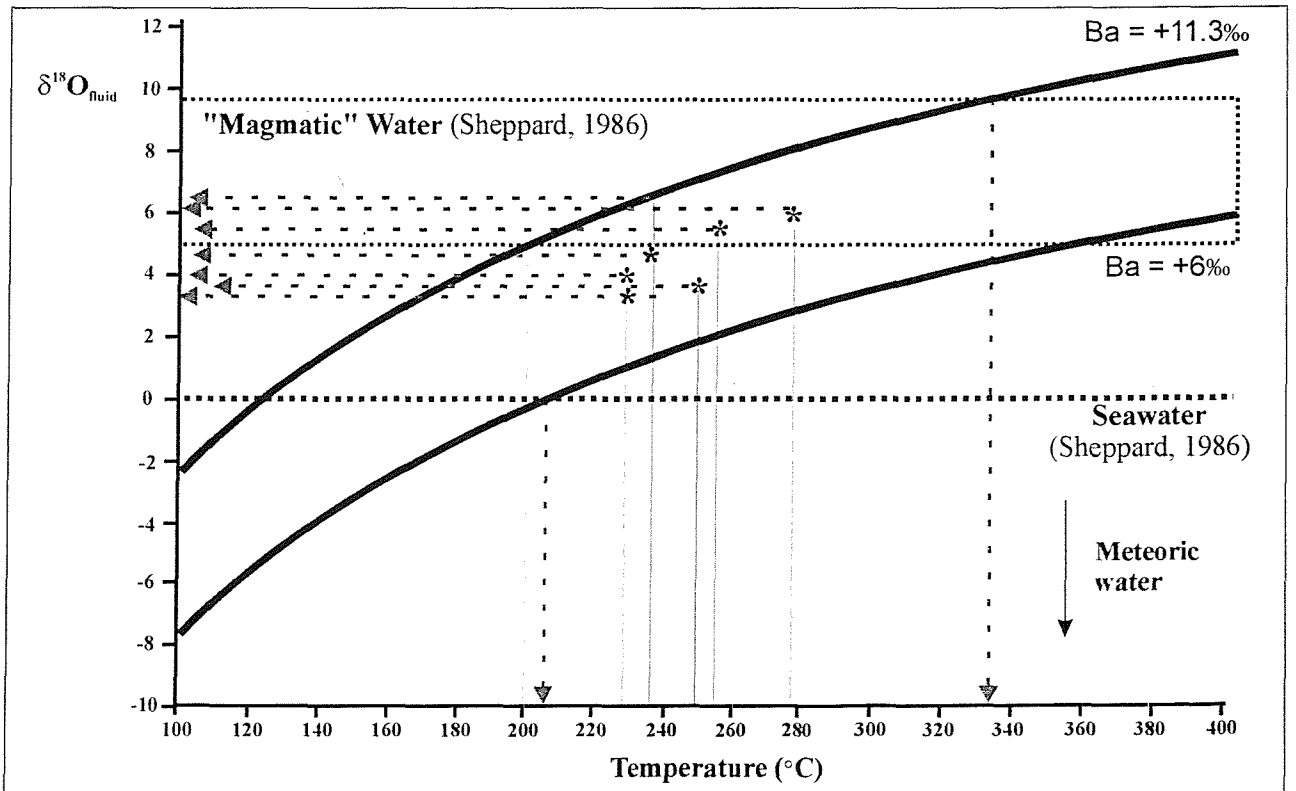


Figure 7.9. Calculated fluid $\delta^{18}O$ versus temperature for barite from Wetar Island, Indonesia. Plot shows extreme measured barite $\delta^{18}O$ values and ranges of surface / magmatic waters (Sheppard, 1986). Curves are plotted using ba-H_2O(1M NaCl) = (2.64 106 / T^2) - 5.3 (Robinson and Kusakabe, 1975). Red lines are plotted with reference to modal homogenisation temperatures, microthermetric result from Chapter 6.

Pyrite-chalcopyrite

$$T = \frac{(0.67 \pm 0.04 \times 10^3}{\Delta^{1\cdot 2}} \qquad (1.4)$$

Ohmoto and Rye (1979)

Calculated temperatures are reported in Table 7.3, this method demonstrates that the Wetar Island sulphate/sulphide pairs and co-existing sulphide pairs are dominantly out of isotopic equilibrium with each other as calculated temperatures of –21°C and > 400°C are geologically unrealistic in seafloor VMS hydrothermal systems. $\delta^{34}S$ values of pyrite and chalcopyrite separates from the banded sample at Kali Kuning (Figure 5.3A, Chapter 5) indicate that sulphide pairs within the system are also out of isotopic equilibrium as the chalcopyrite separate is heavier with respect to $\delta^{34}S$ than the pyrite. This feature is also observed in chalcopyrite separates from Snakepit, (Butler et al., 1998, Duckworth et al., 1995) which are also isotopically heavier with respect to $\delta^{34}S$ than the Fe sulphides. In the deepest part of the Wetar stockwork system (sample 097106) at 210 m below the Lerokis Zone 5 sulphide mound, a disseminated barite/pyrite sample yield a calculated temperature of 233°C and is therefore interpreted to be in equilibrium based on temperatures of modern seafloor systems, Table 7.3 however this may also be coincidence. The calculated temperature of 233°C for this sample is in agreement with microthermetric analysis of fluid inclusions from this barite sample where a modal homogenisation temperature of 249°C are recorded (range from 217 – 302°C). Isotopic disequilibrium is common in many hydrothermal systems and is reported from samples at mounds and inactive chimneys at 21°N EPR. (Bluth and Ohmoto, 1988, Zierenberg et al., 1984) from sulphides on the Escanaba Trough, Gorda Ridge (Zierenberg et al., 1993) and pyrite and pyrrhotite at the Archean Gossan Hill deposit (Sharpe and Gemmell, 2000). The *high-sulphidation* fracture-fill assemblage from the Lerokis Zone 5 stockwork contains euhedral barite laths, the calculated temperature of 302°C is based on this euhedral barite and pyrite that rims the silicified, brecciated host volcanics. These temperatures are confirmed by microthermetric data (modal homogenisation temperature of 278°C) however it is unlikely that the barite and pyrite are in equilibrium based on textural observations (Chapter 5).

Table 7.3. Calculated temperatures using sulphur isotopic geothermometers.

Sample No	Location	Mineral Pair	Temp °C	Equation used	Comments	Fluid Inclusion Temp °C
097106	Lerokis Zone 5: Drill core LKD 043 @210m depth	$27.5_{ba} - 3.33_{py}$	233	1.1	Disseminated ba & py deep within the stockwork zone: Possibly in isotopic equilibrium.	249
097098	Lerokis Zone 5: Drill core LKD 043 @139m depth	$25_{ba} - 6.7_{py}$	342	1.1	Temperature too high for isotopic equilibrium.	-
097084	Lerokis Zone 5: Drill core LKD 043 @88.5m depth	$27.02_{ba} - 5.82_{py}$ $27.02_{ba} - 9.03_{py}$ $5.82_{py} - 4.26_{sp}$ $9.03_{py} - 4.26_{sp}$	281 351 167 -21	1.1 1.1 1.2 1.2	Low yield for $\delta^{34}S_{SULPHIDE}$ = 27% Repeat yield = 90% – More reliable $\delta^{34}S_{SULPHIDE}$ Value. Pyrite and sphalerite clearly not in isotopic equilibrium.	238
097024	Lerokis Zone 5: Drill core LKD 042 @59.8m depth	$24.6_{ba} - 8.57_{py}$	409	1.1	Temperature too high for isotopic equilibrium.	237
097023	Lerokis Zone 5: Drill core LKD 042 @55m depth	$24.4_{ba} - 7.52_{py}$	381	1.1	Temperature too high for isotopic equilibrium.	-
097122	Lerokis Zone 5: Drill core LKD 044 @49.5m depth	$28.1_{ba} - 8.01_{py}$	302	1.1	Barite and pyrite unlikely to be in isotopic equilibrium based on mineralogical observation.	278
097059	Lerokis Zone 5: Drill core LKD 043 @41.9m depth	$22.7_{ba} - 8.01_{py}$ $22.7_{ba} - 7.44_{cp}$ $8.01_{py} - 7.44_{cp}$	460 457 614	1.1 1.3 1.4	Temperature too high for isotopic equilibrium.	-
099917	Lerokis Zone 5: From the massive sulphide mound	$24.2_{ba} - 6.26_{py}$	352	1.1	Temperature too high for isotopic equilibrium.	228
111943	Kali Kuning: From the massive sulphide mound	$22.78_{ba} - 9.52_{py}$ $27.5_{ba} - 10.25_{cp}$ $9.52_{py} - 10.25_{cp}$	529 532 *	1.1 1.2 --	Temperature too high for isotopic equilibrium.	245
100134	Kali Kuning: From the massive sulphide mound	$24_{ba} - 11.69_{py}$	587	1.1	Temperature too high for isotopic equilibrium.	-

Footnote:
ba = barite, py = pyrite, cp = chalcopyrite, sp = sphalerite, * temperatures were not calculated for the pyrite / chalcopyrite pair from sample 111943 due to chalcopyrite recording a $\delta^{34}S$ value > than pyrite, see text for discussion. Fluid inclusion temperatures are modal values, see Chapter 6.

7.7.4 Sources of Sulphur and Oxygen

The mean value of the sulphides from this study at +8 $^{o}/_{oo}$ are only slightly heavier than the reported range of Banda Island arc values of $\delta^{34}S$ +5 and +7 $^{o}/_{oo}$ (de Hoog et al., 2001) suggesting derivation of sulphur by leaching from the underlying host volcanics. The frequency histogram, Figure 7.2 illustrates a unimodal distribution, this is consistent with either a single homogeneous source of sulphur or an extremely well mixed reservoir of dual sources, namely arc rocks combined with Miocene seawater sulphate. Heavier $\delta^{34}S$ values found in sulphides indicate a larger component of reduced seawater sulphate in the hydrothermal fluids, a value of +6‰ would indicate a seawater/basalt mix of ~ 30/70, (Herzig et al., 1998) sulphates would typically have a value of contemporaneous seawater (+21‰). The Wetar sulphides extreme value of (+12‰) with an underlying host rock sulphur value of +4‰ (data from de Hoog et al., 2001) indicates a shift of ~8‰ and also suggests a ~30/70 mix of reduced seawater sulphate within the hydrothermal fluid compared to that of the underlying basaltic basement. The higher $\delta^{34}S$ values of Indonesian arc lavas are enriched compared to MORB and OIB sources, de Hoog et al., (2001) and suggests an input of slab derived material (sediments rather than altered oceanic crust) in the generation of these arc lavas.

The disseminated sulphides collected from 210 m within the stockwork yielded the lightest $\delta^{34}S$ value of 3.3‰. These are therefore lighter than the Banda arc basalt sulphur values and may suggest a magmatic contribution to the hydrothermal system as does lighter sulphur values in the Lau Basin (Herzig et al., 1998) and East Manus Basin (Gemmell et al., 1999) with respect to magmatic sulphur. Lighter values of Wetar barite than Miocene seawater are reported by de Ronde, (1995). Similar observations reported from the Sonne Field, Indian Ridge where barite values are less than modern seawater (+16.5 to +20.1‰). Halbach et al., (1995) attribute these results to admixture of magmatic sulphur and suggest a magmatic component in the hydrothermal system. The light value of the barite and enargite outliers from the de Ronde data may back up these arguments however their geological location and context are unknown.

Equation (1.5) was used to model measured $\delta^{18}O$ from barites against the original fluids they would have been in isotopic equilibrium with over a range of temperatures. The extreme measured values of +6 and +11.3‰ are plotted on Figure 7.9.

$$\therefore \Delta_{ba-H2O(1MNaCl)} = (2.64 \times 10^6 / T^2) - 5.3 \quad (1.5)$$

(Robinson and Kusakabe, 1975)

For a $\delta^{18}O$ measured value of +11.3‰, the system would have temperatures <340°C if in equilibrium with original fluid of magmatic origin, these temperatures are recorded in many VMS systems particularly in the generation of sulphide mounds (Ohmoto and Skinner, 1983, Von Damm, 1990). If the $\delta^{18}O$ measured value was +6‰, equilibrium with an original fluid of a magmatic origin would involve temperatures >400C, unrealistic for VMS systems. Modal homogenisation temperatures of the analysed samples (Chapter 6) have been plotted on Figure 7.9, the results indicate $\delta^{18}O$ of initial fluid between ~3.5 and ~6.5‰ interpreted as a seawater / magmatic mix.

7.8 SUMMARY

The isotope variation in the Wetar samples are due to variations in the H_2S of the end member fluids, varying sub surface mixing between igneous leached sulphur from the host arc volcanics and sulphate reduction from Miocene seawater sulphate. A mean value of +24.8‰ for all sulphate sulphur data from the Wetar Island barite strongly suggests a dominant derivation from Miocene seawater sulphate (22‰), sulphide sulphur values suggest derivation from the underlying arc volcanics. The data is similar that of many modern and ancient deposits with a dominant seawater influence, key similarities and deposits will be addressed in Chapter 9.

The stable isotopes study has confirmed that the cemented Fe oxide-barite structures are fluid conduits for barite ore and that the pyrite sands are derived from the surface of the sulphide mounds. The hydrothermal system is seawater dominant with perhaps a minor indication of a magmatic input.

Chapter 8

RADIOGENIC ISOTOPES

8.1 INTRODUCTION

Previous Chapters have established that the deposits preserved on Wetar Island are similar to typical VMS systems with minor *high-sulphidation* mineralogy. The associated alteration suggests a direct input of magmatic volatiles into the generation of the mineralisation eg. (Lau Basin, Herzig et al., 1998, Manus Basin, Gemmell et al., 1999). Helium and strontium isotopes were chosen to:-

1) Better define fluid sources and
2) Confirm the role of mantle-derived fluids and those derived from footwall volcanics and seawater.

Although preliminary K/Ar data was available for stockwork illite samples at Lerokis, a programme of Ar/Ar dating is applied to test the ages of the host volcanics, intrusive and alteration.

8.2 HELIUM

8.2.1 PREVIOUS WORK

The application of noble gases to identify fluid reservoirs by analysis of fluids trapped in hydrothermal mineral is relatively new (Stuart et al., 1994, 1995, 1999; Jean-Baptiste and Fouquet, 1996; Hu, et al., 1998; Burnard et al., 1999). Studies have illustrated that helium trapped within fluid inclusions entrained within sulphide phases provide information on palaeofluids and their sources (Stuart et al., 1994, 1995) and the mantle contributions to the hydrothermal system can be resolved (Stuart et al., 1994; Burnard et al., 1999). Primordial ^{3}He is virtually absent from "surface" derived fluids whereas ^{36}Ar is virtually absent from deeper "mantle" sources. Marine or meteoric fluids are characterised by atmospheric He and Ar isotope compositions ($^{3}He/^{4}He = 1.39\times10^{-6} = 1R_a$; $^{40}Ar/^{36}Ar = 295.5$), mantle derived rocks from the upper

mantle also have characteristic signatures ($^3He/^4He$ = 1-1.3×10^{-5} = 7-9R_a; $^{40}Ar/^{36}Ar$ = >40,000 (Burnard et al., 1999 and references therein). Therefore combining He and Ar analysis enables the discrimination of both mantle and surface derived components within the hydrothermal system (Burnard et al., 1999). Helium isotopic study of sulphides from the East Pacific Rise 13°N (Jean-Baptiste and Fouquet, 1996); 21°N and both 26°N (TAG) and 23°N (Snakepit) from the Mid-Atlantic Ridge (Stuart et al., 1994) confirmed that the $^3He/^4He$ ratio of sulphide phases analysed was almost indistinguishable from the value recorded from the hydrothermal fluid and are also close to local basaltic values. These results illustrate that sulphide mineral phases precipitated in equilibrium with the end-member fluids retain the helium isotopic ratios of their original fluids (Stuart et al, 1994).

8.3 HELIUM RATIOS

8.3.1 Circum-Pacific arcs

The circum-Pacific island arcs are active sites of subduction where altered oceanic crust returns to the mantle. In eleven of twelve circum-Pacific volcanic arcs, $^3He/^4He$ ratios are similar to MORB as they are dominated by primordial ^3He released from the mantle wedge above the subducting oceanic slab, with the exception of the Banda arc (see Figure 8.1). Arc volcanics derived from re-melted subducting oceanic crust yield lower $^3He/^4He$ ratios (~2 R_A or less) due to radiogenic ^4He production from U, Th decay, no significant primordial ^3He would be retained (Lupton and Craig, 1975). As radiogenic He has almost no ^3He (R/R_A ~ 0.02) the dominant source of helium in volcanic arcs is mantle (MORB), He with R/R_A = 8, (Hilton and Craig, 1989). The fraction of He derived from the mantle X_M, corresponds to the He ratio where most arcs have a ratio of 7.5 to 8 R_A with a general mean of ~7.5 R_A (the fraction of He derived from the mantle X_M = ~94%). The similarity of MOR basalts with volcanic gases and phenocrysts indicate the presence of primordial ^3He released from the mantle wedge (Poreda and Craig, 1989). The results illustrate that the subducted oceanic crust does not significantly contribute to the upwelling magma even though the subduction drives arc volcanism (Hilton and Craig, 1989).

8.3.2 Sunda and Banda arcs

Helium isotope ratios of phenocryst-bearing lavas (Hilton and Craig, 1989; Hilton et al., 1992) and geothermal gases and fluids (Hilton and Craig, 1989; Poreda and Craig, 1989) illustrate a complex transition zone from primordial helium (in the Sunda arc) to radiogenic helium emissions in the Banda arc. The transition zone appears to be centred west of the "inactive" segment of the Banda arc between east Flores and Pantar, see inset, Figure 8.1. $^3He/^4He$ ratios of R/R_A = 5.7-8.2 from western Java to central Flores are similar to previously studied circum-Pacific arcs (Poreda and Craig, 1989). These ratios, when compared to mean MORB (R/R_A = 8±1) and crustal, radiogenic He (R/R_A = <0.02) correspond to a MORB (helium) fraction of 70-100% (where R_A = $^3He/^4He$ ratio of air) (Hilton and Craig, 1989). The $^3He/^4He$ ratios of summit fumaroles and lavas from the Banda arc have $^3He/^4He$ ratios of R/R_A = 1.6-1.1 indicating a radiogenic derived helium component amounting to >80% (Poreda and Craig, 1989; Hilton and Craig, 1989).

The abrupt reduction in the $^3He/^4He$ ratio occurs in the region of Keli Mutu (6.0 R_A) on central Flores (east Sunda arc). This location is bounded to the west and east (Iya and Egon) by radiogenic helium values of 2 and 1.3 R_A indicating the influence of subducted continental material in the generation of volcanism as far west as Iya (Hilton et al., 1992). The pattern of $^3He/^4He$ ratios east of Flores is synonymous, Lewotolo (3.5 R_A) situated on Lomblen and Batu Tara ((4.5 R_A) ~ 50 km north of Lomblen island) are bounded to the west and east by Boleng and Sirung (1.4 R_A and 1.0 R_A) (Hilton et al., 1992). Directly south of Lewotolo on the southern coast of Lomblen, three lavas from Werung all have R/R_A ratios < 1 with one sample as low as 0.0075 R_A. Samples from the volcanically "inactive" section of the Banda arc (representing the collision zone between the Australian continental margin and the arc), have a narrow range in R/R_A from 3.9 R_A on Kisu (located in the straits of Pantar) to 1.0 R_A for Romang, located only ~55 km east of the present study area. As a result of tectonics in the region of Wetar, low R_A values may also be expected.

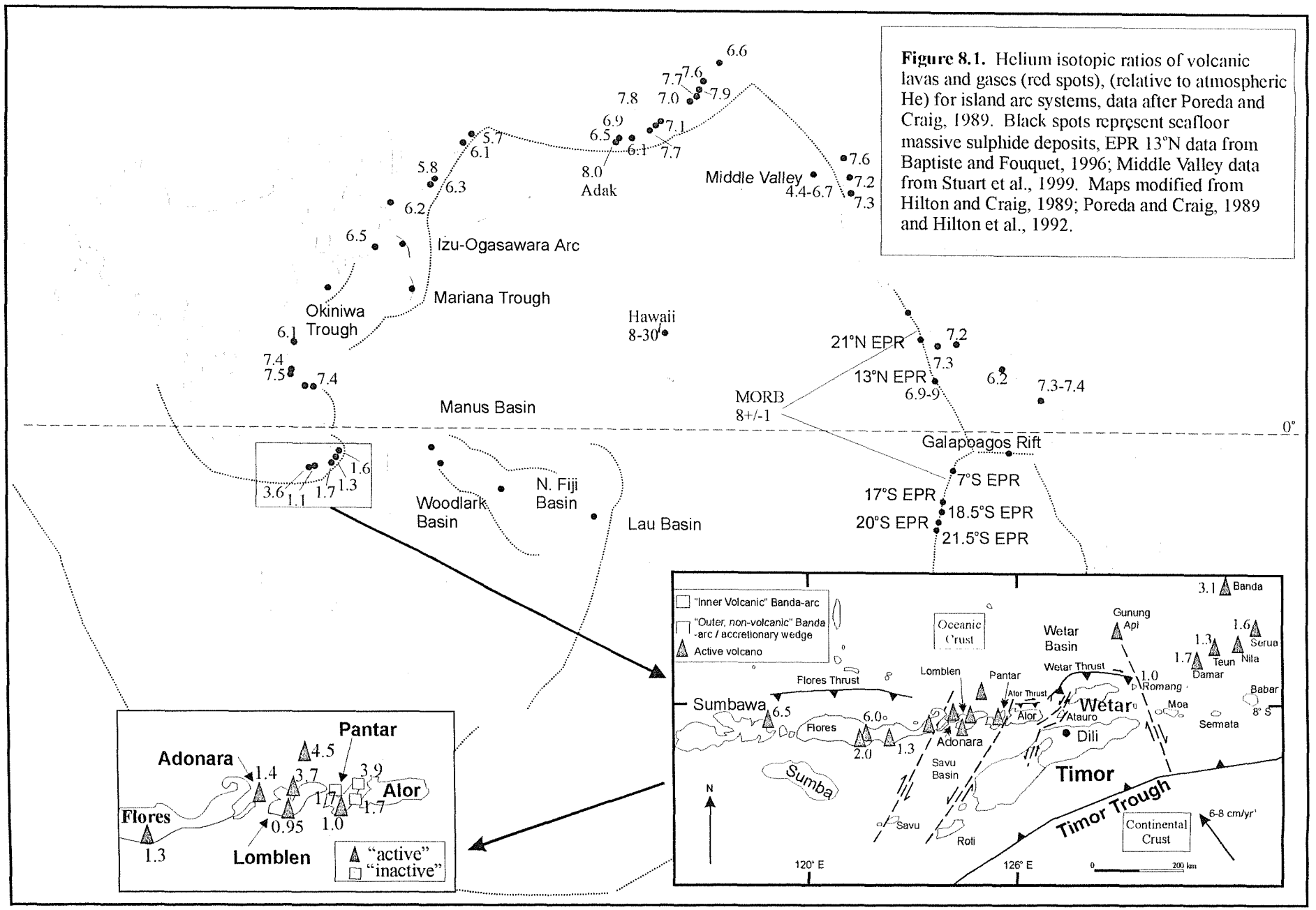


Figure 8.1. Helium isotopic ratios of volcanic lavas and gases (red spots), (relative to atmospheric He) for island arc systems, data after Poreda and Craig, 1989. Black spots represent seafloor massive sulphide deposits, EPR 13°N data from Baptiste and Fouquet, 1996; Middle Valley data from Stuart et al., 1999. Maps modified from Hilton and Craig, 1989; Poreda and Craig, 1989 and Hilton et al., 1992.

8.4 SAMPLE SELECTION

Eight samples were chosen for the study, five pyrite samples (from the massive sulphide ore bodies and stockwork zones) one from the *high-sulphidation* assemblage which is present as a "fracture-fill" network within the stockwork of Lerokis Zone 5 (Chapter 5) and two samples from the barite ore deposits.

8.5 ANALYTICAL TECHNIQUES

The technique employed for helium and argon analysis follows that described by Stuart et al., (1995) and Burnard et al., (1999), see also Appendix F. Sample sizes were generally 1-2 g, each sample was crushed once, experience shows that repeat crushes are not necessary. All analytical work was carried out at the University of Manchester on an MAP 215 mass spectrometer. Isotopic measurements were made for ^{3}He, ^{4}He, ^{36}Ar and ^{40}Ar. Procedural blanks used during analysis are given in the footnote of Table 8.1.

8.6 RESULTS

The results of the helium analyses of the present study are given in Table 8.1. The $^{3}He/^{4}He$ ratios of the Wetar sulphides and sulphates are relatively uniform, R/R_A 0.57-1.46 (n=8), the $^{40}Ar/^{36}Ar$ data is confined to a narrow range between 290 and 317 (where atmospheric $^{40}Ar/^{36}Ar$ =295.5). The $^{3}He/^{4}He$ ratio of helium released during analysis yields an average of R/R_A = 1.09. The *high-sulphidation* sulphide assemblage collected from the Lerokis Zone 5 stockwork (covellite, tennantite, Fe-poor sphalerite) had the lowest $^{3}He/^{4}He$ ($R/R_A \sim 0.57$), Ar was not analysed for due to technical difficulties. The Wetar sulphides have extremely confined ranges in terms of both $^{3}He/^{4}He$ and $^{40}Ar/^{36}Ar$ ratios, 0.57-1.33 (n=5) and 289.9-316 respectively. Sulphates also have a confined range for the two samples analysed, $^{3}He/^{4}He$ = 1.12-1.46 (n=2) and $^{40}Ar/^{36}Ar$ = 307.5-309.1. Interestingly, the amount of ^{4}He released for the two sulphate samples is also very similar (1.37 and 1.47), the $\delta^{34}S$ of these samples are also similar with variation of less than $2^{o}/_{oo}$.

Table 8.1. Noble gas compositions of fluids trapped in sulphides and sulphates from the Wetar Island deposits, Indonesia.

Sample	Description	Location	Sample weight g	^{4}He mL STP $x10^{-9}$	$^{40}Ar/^{36}Ar$	$^{3}He/^{4}He$ Rc/Ra	Depth m	$\delta^{34}S$
097106	Disseminated pyrite from stockwork	Lerokis Zone 5	1.63	29.5 ± 0.26	310 ± 12	1.19 ± 0.04	210	3.3
099902	Pyrite from massive sulphide mound	Lerokis Zone 5 location 4	2.01	16.1 ± 0.14	316 ± 12	1.17 ± 0.05	surface	6.9
097059	Pyrite from massive sulphide mound	Lerokis Zone 5	1.23	9.89 ± 0.09	292.6 ± 11	0.98 ± 0.05	surface	8
097098	Disseminated and vein pyrite from stockwork	Lerokis Zone 5	1.65	55.6 ± 0.49	289.9 ± 11	1.33 ± 0.05	139	6.7
097122	Fracture fill *high-sulphidation* sulphide assemblage from stockwork	Lerokis Zone 5	1.45	21.1 ± 0.19	a	0.57 ± 0.03	59	6.9
111979	Barite from barite sand deposit	Lerokis Zone 4 location 149	1.93	1.37 ± 0.01	307.5 ± 12	1.12 ± 0.2	surface	25.2
097084	Disseminated stockwork barite	Lerokis Zone 5	2.74	1.47 ± 0.04	309.1 ± 12	1.46 ± 0.25	89	27
096857	Pyrite from massive sulphide mound	Kali Kuning location 75	1.92	1.55 ± 0.03	298.7 ± 11	0.86 ± 0.29	surface	10.4

Footnote: Errors are quoted at 1s confidence, a: Argon not analysed due to technical difficulties. $d^{34}S$ data from present study (chapter 7). *High-sulphidation* assemblage = fine intergrowth of covellite, Fe-poor sphalerite, tennantite. Rc/Ra = the air-corrected $^{3}He/^{4}He$ ratio, depths are quoted in metres below the palaeo-seafloor surface assuming that the upper parts of the sulphide mounds were at, or at close proximity to the seafloor. Each sample was crushed once, procedural blanks are $2.15x10^{-11}$ - $2.5x10^{-10}$ ml STP ^{4}He, 2.2-2.4$x10^{-10}$ ml STP ^{20}Ne and $5.1x10^{-10}$ - $4.8x10^{-9}$ ml STP ^{40}Ar.

8.7 DISCUSSION

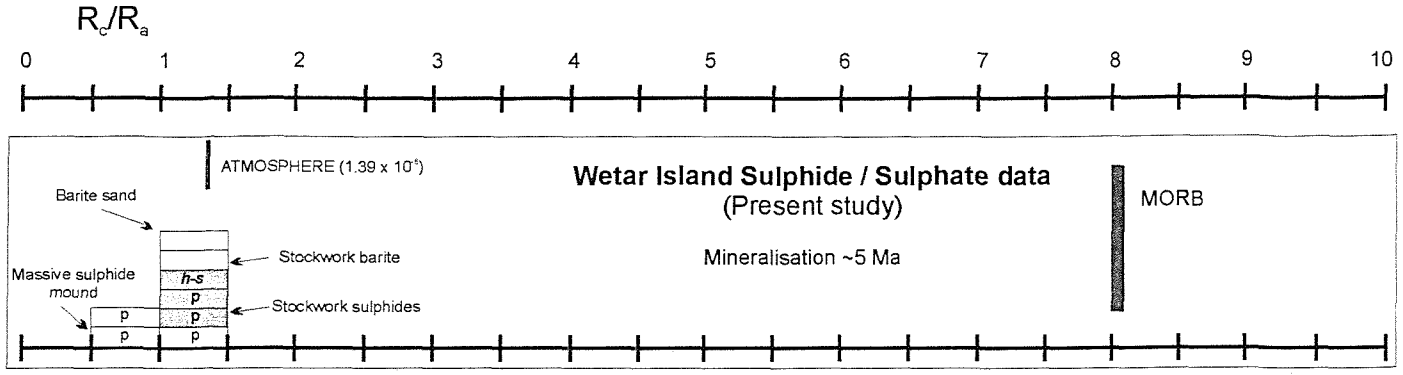
8.7.1 Evolution of the arc

The Wetar Island helium data is consistent with published Banda arc data and implies a significant crustal component in the generation of both arc edifice and mineralisation. These results also support the view that subducted Australian continental material has underthrust the Banda arc beneath the Timor region (see Chapter 2, Tectonic Evolution). A histogram of the Wetar sulphide / sulphate data is presented on Figure 8.2, helium data of selected modern and ancient VMS systems are shown for comparative purposes.

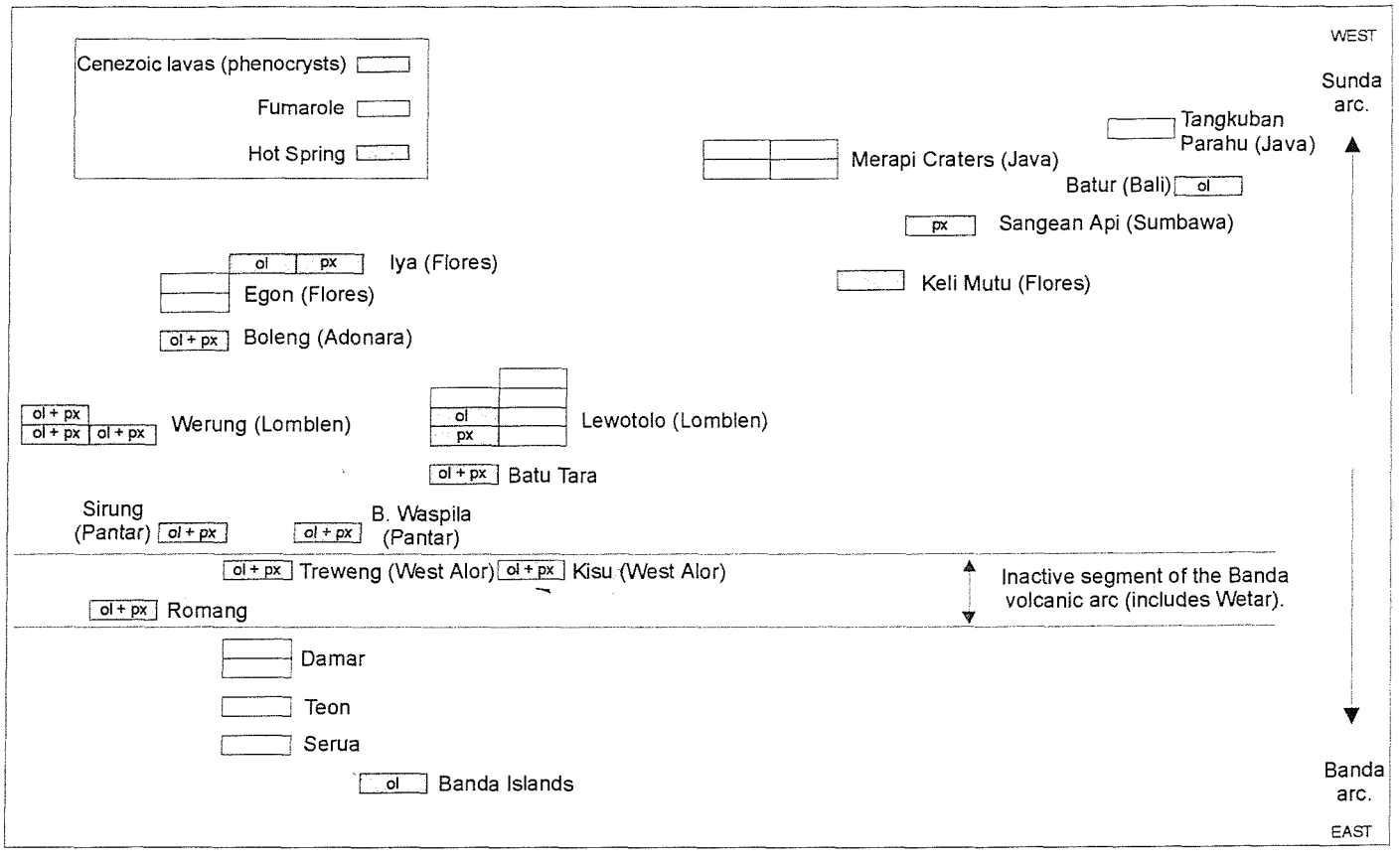
Hilton et al., (1992) eluded to the uncertainty of helium ratios from samples collected on islands from the "inactive" segment of the Banda arc due to the absence of geochronological data. An important factor may be that no account can be made for radiogenic ingrowth of ^{4}He in the samples which will lower the ^{3}He/^{4}He ratios. At Tangkuban Parahu (West Java) Ra values are ~ 8, moving east along the arc helium ratios become more radiogenic towards the Banda arc and the volcanically inactive segment in the region of Pantar and Alor (Figure 8.2).

8.7.2 Hydrothermal system

Studies from other seafloor hydrothermal sites illustrate that sulphide phases typically show ^{3}He/^{4}He ratios close to both local basalts and end-member fluids as steady state hydrothermal circulation extracts helium from underlying hosts (Stuart et al., 1994). By analogy, the Wetar sulphides (R/R_A 0.5-1.4) should represent underlying basaltic values. The values for Wetar (~1 Ra) are representative of ratios at the time of eruption and generation of ore deposits and are consistent with ratios from the nearest island of Romang (measured basaltic phenocrysts, also 1 Ra (Hilton et al., 1992)) see Figure 8.1. No depth related variation in the ^{3}He/^{4}He ratio is observed in the Wetar samples, nor any significant correlation between ^{3}He/^{4}He and δ^{34}S, this apparent lack of correlation between both ^{3}He/^{4}He and δ^{34}S may be attributed to the small sample set and relatively confined range of data with respect to the ^{3}He/^{4}He ratios. The ^{3}He/^{4}He ratios of the Wetar sulphides and sulphates are relatively uniform R/R_A 0.5-1.4 (n=8) indicating that there is unequivocally a mantle volatile input into



Sunda / Banda arc data



Mid Ocean Ridges

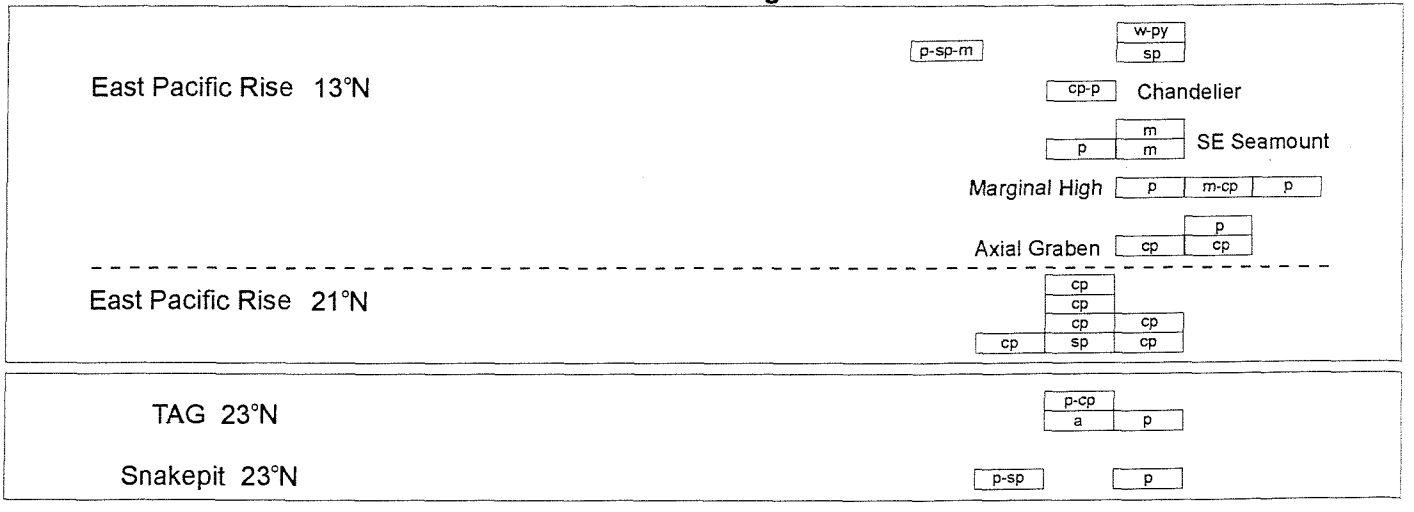


Figure 8.2. Histogram summarising the range in $^3He/^4He$ for Wetar Island sulphide and whole sulphate data compared to published helium data. Wetar data this study, Banda arc data after Hilton et al., 1992; Hilton and Craig, 1989; Poreda and Craig, 1989. EPR data from Lupten et al., 1980; Stuart et al., 1994 and 1995; Baptiste and Fouquet, 1996. Middle valley data from Stuart et al., 1994. TAG and Snakepit data from Rudnicki and Elderfield, 1992. p= pyrite; h-s= high sulphidation sulphide assemblage (covellite, Fe-poor sphalerite, tennantite); ol= olivine; px= pyroxene; w= wurtzite; m= marcasite; cp= chalcopyrite; sp= sphalerite; a= anhydrite.

the system where data exceeds values >1 R/R_A). The Wetar $^{40}Ar/^{36}Ar$ data is confined to a narrow range between 290 and 317 which are essentially atmospheric values ($^{40}Ar/^{36}Ar$ = 295.5) and similar to the range for surface waters and seawater ($^{40}Ar/^{36}Ar$ = 295.5-320). The similarity of the data from the two sulphate samples suggest they precipitated from a similar fluid even though they are from different ore zones (Lerokis 4 and 5). The range of data for the Wetar samples must be due to a mixing of MORB (8 R/R_A) and a crustal endmember substantially reducing the R/R_A value. The % of mantle helium can be calculated using the formula below:

$$\textbf{\% mantle He} = \textbf{(R-Rc)/(Rm-Rc)} \times \textbf{100}$$

where R_C= crustal $^3He/^4He$ ratio of 0.01-0.05 R_A, Rm= mantle $^3He/^4He$ ratio of 8 R_A

Calculated mantle helium input into the generation of the Wetar Island sulphides and by analogy, the host volcanics only amounts to 5.6-16.4%. The U and Th contents are low in our case due to the young age of the deposits therefore the lowering of the $^3He/^4He$ ratio is due to radiogenic ingrowth, we can discount atmospheric He on the basis that F^4He ratio:

ie) $(^4He/^{36}Ar)_{sample} / (^4He/^{36}Ar)_{air}$ which should be >>0.165 (air value).

Calculated F values for the Wetar samples are between 94 and 223 which are significantly higher than the value of air therefore the radiogenic values observed are not a result of atmospheric helium

The Wetar data contrasts to systems such as those at mid-ocean ridges which have a mantle (igneous) helium input of 100% if their calculated values are 8 R_A. This is because no contaminant has been involved during subduction to modify the $^3He/^4He$ ratio. Noble gas study from fluid inclusions in sulphides at the EPR, 13°N illustrate direct addition of magmatic volatiles into the hydrothermal system and R/R_A of 6.9-9 (Stuart et al., 1995; Jean-Baptiste and Fouquet, 1996) as does the data from TAG and Snakepit (Rudniki and Elderfield, 1992) see also Figure 8.2. Sulphides R/R_A of 4.4-6.7 at the Bent Hill site (Middle Valley) are dominated by basalt derived He (Stuart et al., 1999) although there is quite a spread of values as a result of sediment contribution.

At the Manus Basin, the range of data is extremely wide (~1 R/Ra up to ~15) with a cluster of data around 12. The lower mantle has R/Ra of ~35 measured in OIB, (eg. Kurz et al., 1983), suggesting helium derivation from a deeper source / mantle plume.

8.8 STRONTIUM ISOTOPES

8.8.1 PREVIOUS WORK

The whole-rock strontium data along the Sunda-Banda arcs is consistent with the helium data in that the Banda arc lavas (east of Flores) are displaced towards more radiogenic ratios indicating a contribution from crustal material / sediment from the subducted Australian craton (Whitford and Jazek, 1979), see Figure 8.3. Strontium ratios of samples from the NE Banda arc (Banda Archipelago) range between $^{87}Sr/^{86}Sr$ = 0.7045-0.7055 for low-K tholeiitic rock types and are typical ratios for arc signatures (Vroon et al., 1993). Towards Wetar in the SW (Nila, Teon and Damar), rock types are high-K calc-alkaline with strontium ratios between $^{87}Sr/^{86}Sr$ = 0.7065-0.7083. The limited range of Manuk $^{87}Sr/^{86}Sr$ = 0.7051-0.7055, contrast to the large range of Serua $^{87}Sr/^{86}Sr$ = 0.7075-0.7095; see also Figure 8.3. The large within-suite Sr variation is also present at Nila, Teon and Romang, this is also the case for Nd isotopic ratios however Pb isotopic variations are limited (Vroon et al., 1993). The Banda arc as a whole illustrates a systematic increase of potassium from Ambon to Romang (Whitford and Jazek, 1979) and both $^{87}Sr/^{86}Sr$ and Pb isotopic ratios from the NE to the SW whereas $^{143}Nd/^{144}Nd$ ratios decrease (Magaritz et al., 1978; Whitford and Jazek, 1979; Whitford et al., 1981; Vroon et al., 1993). Andesites and rhyodacites from Romang have Sr ratios of $^{87}Sr/^{86}Sr$ = 0.70852-0.70926 coupled with low $^{143}Nd/^{144}Nd$ = 0.51243-0.51245 ratios. The radiogenic Sr ratios from other presently non-volcanic islands of the Banda arc include Alor (0.7077) and Atauro (0.7066-0.7082) and Maupura (0.70908) (Whitford et al., 1977). The Sr ratio of a dredged 0.4 Ma high-Mg basalt sample from a seamount off the north coast of Wetar yielded a ratio of $^{87}Sr/^{86}Sr$ = 0.7074 and $^{143}Nd/^{144}Nd$ = 0.5125, comparable to the data from Nila, Teon and Damar (Morris et al., 1984). Sr-Nd data from McCulloch et al.,

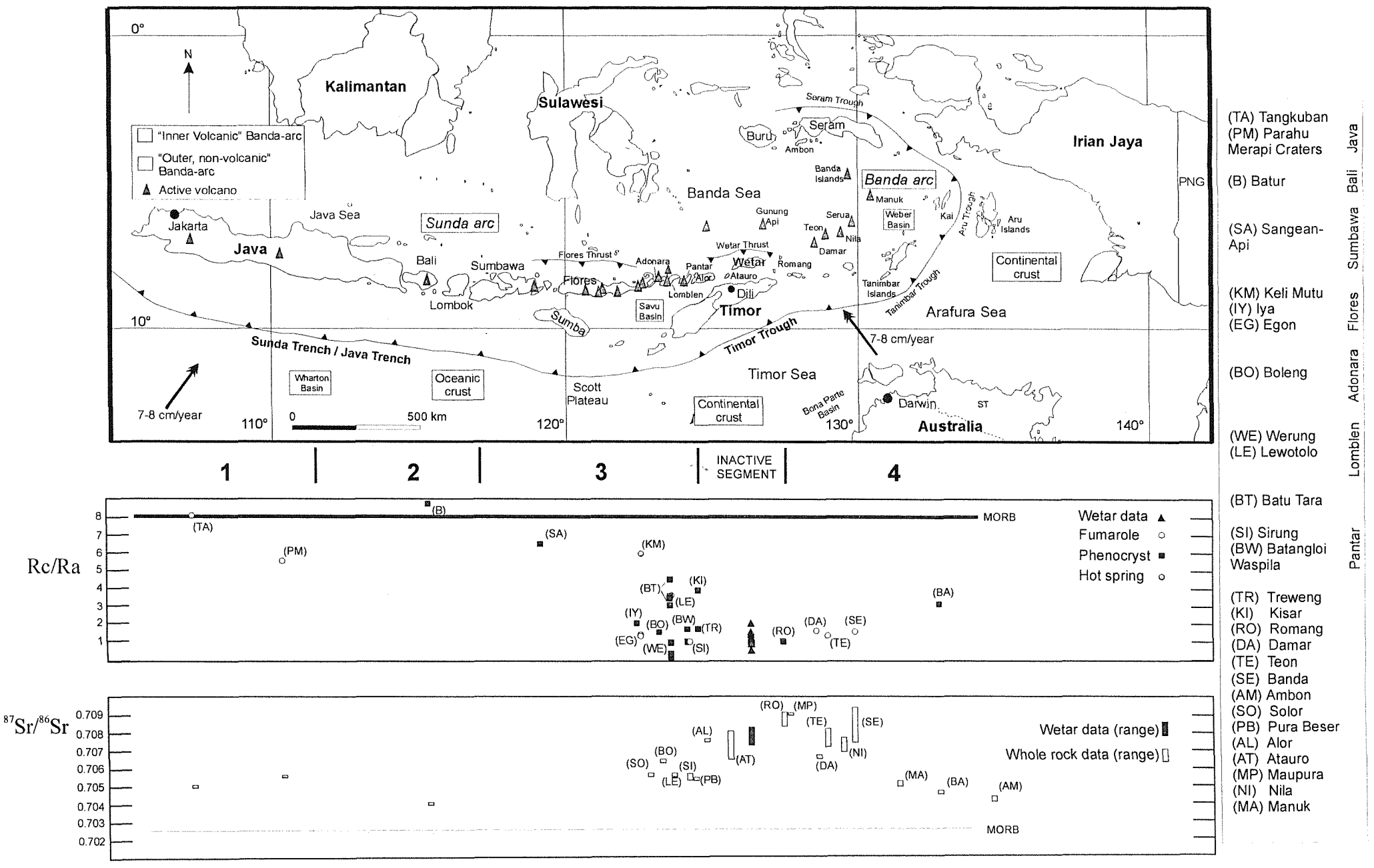


Figure 8.3. Principal geographic features of eastern indonesia after Hamilton, 1979; Whitford et al., 1977; van Bergen et al., 1993; Masson et al., 1991; Snyder et al., 1996. 1-4 are subdivisions based on Hamilton, 1979 and are discussed in Chapter 2. $^{3}He/^{4}He$ and $^{87}Sr/^{86}Sr$ ratios from the Sunda and Banda arcs are shown in relation to the subdivions of the arcs. Helium isotope ratios (reported relative to atmospheric helium [$1.39x10^{-6}$] following the procedure and assumptions of Craig et al., (1978) of sulphides and sulphates are shown (present study). Other data from phenocryst-bearing lavas (Hilton and Craig, 1989; Hilton et al., 1992) and geothermal gases and fluids (Hilton and Craig, 1989; Poreda and Craig 1989). Ra is the atmospheric $^{3}He/^{4}He$ value and Rc is the air-corrected value. The lowermost plot profiles the $^{87}Sr/^{86}Sr$ ratios for whole-rock data (present study) and for Cenezoic lavas and phenocrysts (Whitford et al., 1977; Whitford and Jazek, 1977, 1979; Margaritz et al., 1978; Varekamp et al., 1989; Vroon et al., 1993, 1996, 2000).

(1982) shows that Wetar Island samples data encompass that of the entire data for the Banda arc.

8.9 SAMPLE SELECTION

A representative suite of twelve rocks from around the ore deposits have been analysed for $^{87}Sr/^{86}Sr$ ratios, the same samples were used as for the XRF study (Chapter 4). Rock powders for Sr isotope study follow the procedure of Taylor and Nesbitt, (1998), for analytical technique see Appendix F. Sixteen barite samples and one sample of post mineralisation gypsum were chosen for analysis following the procedure of Cooper, (1995), for sample preparation and sample running see Appendix F.

8.10 RESULTS

Data from the whole rock and sulphate data are presented in Table 8.2 and Figure 8.4. Whole rock strontium data from both unaltered and hydrothermally altered volcanics yield a range between $^{87}Sr/^{86}Sr$ 0.70747 to 0.71166 (n=13). At the Kali Kuning zone of Ba-Au-Ag mineralisation, distal propylitic alteration of host volcanics yields a $^{87}Sr/^{86}Sr$ result of (0.70747), $^{87}Sr/^{86}Sr$ increases with alteration intensity as the centre of mineralisation is approached with the advanced argillic core comprising of a zone of residual silica ($^{87}Sr/^{86}Sr$ 0.70819). The least radiogenic strontium ratio was found in a sample of hydrothermally altered andesite from the Kali Kuning footwall, $^{87}Sr/^{86}Sr$ 0.707466 whereas the most radiogenic samples were the post mineralisation dacites collected from the Meron deposit. The intrusive syeno-granite sample yielded a $^{87}Sr/^{86}Sr$ ratio of 0.70803, all results are relative to 0.710245 ± 12, NBS 987. There appears no systematic variation in $^{87}Sr/^{86}Sr$ ratios between the analysed sulphate data (Figure 8.4), the barites range between $^{87}Sr/^{86}Sr$ 0.70747 to 0.70880 (n=16). The post mineralisation gypsum yielded a result of $^{87}Sr/^{86}Sr$ 0.70791, two samples collected at the Batu Kapal prospect (Figure 3.4), (Herrington, 1995) yielded results of $^{87}Sr/^{86}Sr$ 0.70815 and $^{87}Sr/^{86}Sr$ 0.70644.

Table 8.2. Strontium results from the Wetar Island whole-rock and sulphate samples.

Sample No	Sample Comments	$^{87}Sr/^{86}Sr$	(2SE) +/-	Comments
096920	Unaltered coastal basalt, loc. 104	0.707733	17	
096920	Unaltered coastal basalt, loc. 104	0.707729	18	
096920	Unaltered coastal basalt, loc. 104	0.707745	17	
096884	Altered volcanic (Kali Kuning, loc. 320)	0.708336	21	
097168	Altered dacite (Meron, loc. 226)	0.711656	20	
097167	Unaltered dacite (Meron, loc. 225)	0.711068	12	
111914	Altered volcanic (Kali Kuning, loc 316)	0.707466	17	
097106	Brecciated/altered stockwork volcanic (LKD043 @210m)	0.707722	7	
100129	Vesicular, clay altered volcanic (Kali Kuning, loc. 66)	0.70789	9	
111935	Hydrothermal vuggy residual silica (Lerokis 4, loc. 139)	0.708188	23	
111999	Syeno-granite (Meron area, loc. 232)	0.708031	25	
096927	Vesicular, clay altered volcanic (Kali Kuning road, loc. 109)	——		sample fail
096930	Vesicular, clay altered volcanic (Kali Kuning road, loc. 92)	-----		sample fail
111994	Unaltered basalt-andesite (Kali Kuning, loc. 316)	0.707814	7	
096926	Unaltered basalt-andesite (loc. 109) clast from debris flow	0.707484	9	

Sample No	Sample Comments	$^{87}Sr/^{86}Sr$	(2SE) +/-	Comments
097122	barite (disemminated stockwork), LKD 044, Lerokis 5 @ 49.5m	0.708356	7	
099933	barite vein, proximal to sulphide mound (Lerokis 5, loc 30)	0.708804	8	
097098	*barite (disemminated stockwork), LKD 043, Lerokis 5 @ 179m*	0.70836	7	
097059	barite (associated with sulphide mound, LKD 043, Lerokis 5 @ 35m	0.708091	8	
099923	barite pipe structure (Lerokis 5, loc 19)	0.708303	8	
097024	barite (associated with sulphide mound), LKD 042, Lerokis 5 @ 59.8 m	0.708727	7	
111943	barite associated with sulphides (Kali Kuning, loc. 215)	0.707638	7	
099939	barite ore (Lerokis 5, loc 46)	0.708356	8	
111931	barite ore (Lerokis 4, loc.217)	0.707741	8	
096948	barite pipe structure (Lerokis 4, loc 129)	0.708012	8	
097106	barite (disemminated stockwork), LKD 043, Lerokis 5 @ 210m	0.708065	8	
099938	barite vein, distal to sulphide mound (Lerokis 5, loc.112)	0.707862	8	
099917	barite associated with sulphides (Lerokis 5, loc 15)	0.70829	7	
097084	barite (disemminated stockwork), LKD 043, Lerokis 5 @ 88.5m	0.708542	8	
111979	barite ore (Lerokis 4, loc 149)	0.708269	7	
096879	barite ore (Kali Kuning, loc 84)	0.707732	7	
NBS 987	Standard	0.710243	7	
NBS 987	Standard	0.710232	8	
100103	gypsum, post-mineralisation (Kali Kuning, loc. 50)	0.709086	7	

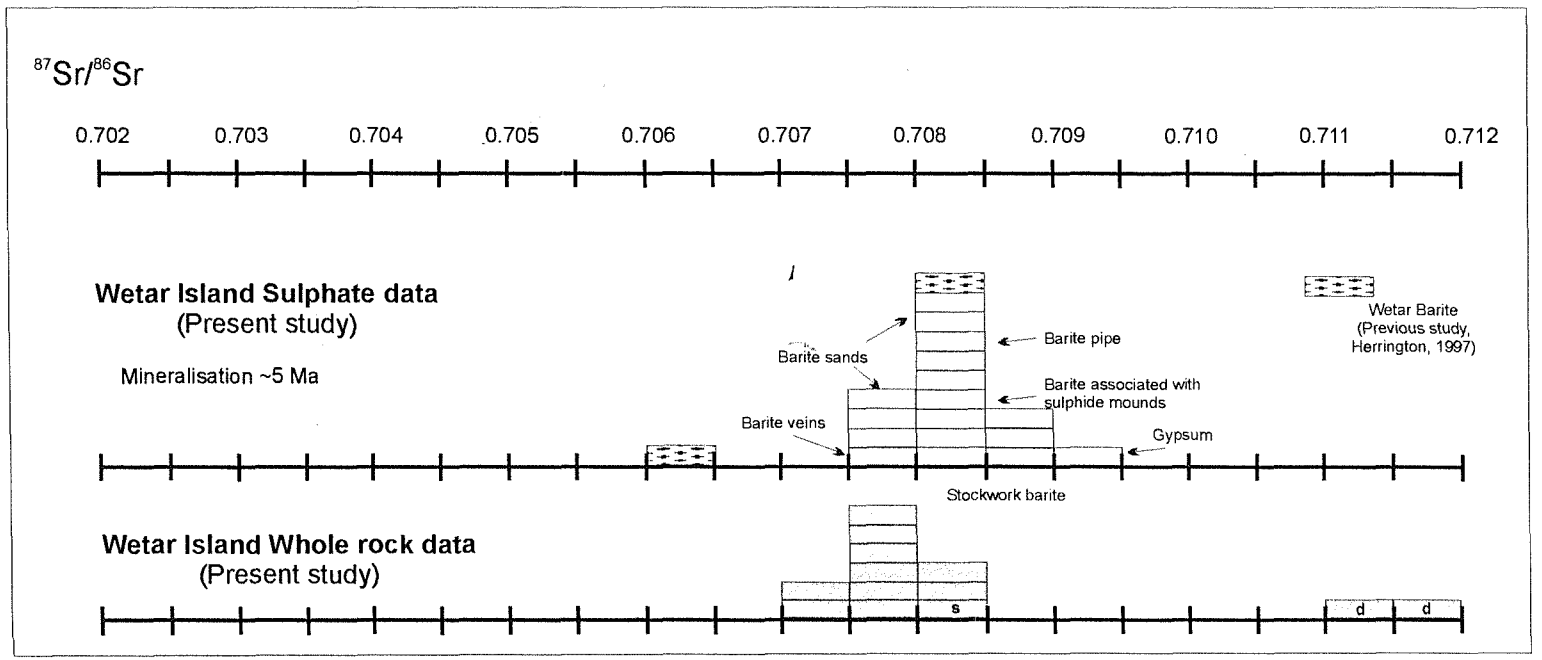


Figure 8.4. Histogram summarising the range in $^{87}Sr/^{86}Sr$ for Wetar Island barites and whole rock data. Wetar data this study and Herrington 1997, s= syeno-granite; d= dacite.

8.11 DISCUSSION

8.11.1 Arc and petrogenetic evolution of Strontium

A strontium, helium study on dredged basalts from the Woodlark basin indicated that $^{87}Sr/^{86}Sr$ ratios increased geographically from ocean ridge values at the Woodlark Spreading Centre (0.7025-0.7029) to ratios of between (0.7035-0.7039) at the Solomon Islands fore-arc (Trull et al., 1990). $^{3}He/^{4}He$ ratios are more radiogenic in the fore-arc (6.9 ± 0.2Ra) than at the spreading centre, (8.2-9.3Ra) both sets of results suggest that subduction contributes melts or fluids to magma genesis (Trull et al., 1990). Parsons, (1981) suggested that in this location (Woodlark Spreading centre) an area which experiences a high input of crustal material into the mantle via subduction; the eruption of lavas with values typical of mid-ocean ridges indicates limited lateral mantle convection or derivation from mantle diapirs originating at depths unaffected by lithospheric input. The variations exhibited in strontium ratios along the length of Sunda-Banda arcs are similar to other circum Pacific Island arcs which also involve contamination of source magmas (reviews in Vroon et al., 1993; Faure, 2001). Strontium isotopic ratios of volcanics from the Sunda and Banda arcs vary in relation to zones of subduction, 1-4 (see Figure 8.3). The trend of increasing radiogenic ratios is clearly evident at the collision zone between the Australian continental margin and the Banda arc and is focussed at the volcanically "inactive zone" of the Banda arc, north of Timor (Wheller et al., 1987; Whitford, 1975 and Varekamp et al., 1989). Strontium concentrations within andesitic lavas reported by Whitford et al., (1977) and Whitford and Jazek, (1979) show variations along the Banda arc from Solor in the West, Figure 8.5. This figure illustrates that a more complex pattern of along arc Sr concentrations than postulated by Faure, (2001) particularly between the islands of Pantar and Wetar.

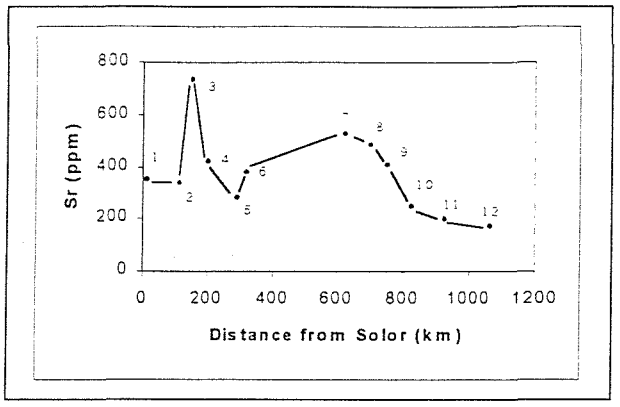


Figure 8.5. Sr concentrations of Banda arc andesitic volcanics from Solor to Banda (modified from Faure 2001, sources: Whitford et al., 1977 and Whitford and Jazek, 1979). 1. Solor; 2. Pantar; 3. Pura Beser; 4. Alor; 5. Atauro; 6. Wetar; 7. Damar; 8. Teun; 9. Nila; 10. Serua; 11. Manuk; 12. Banda.

The $^{87}Sr/^{86}Sr$ ratios from the Banda arc (Whitford et al., 1977; and Whitford and Jazek, 1979) suggest that lavas form colinear clusters that define mixing lines which extrapolate to MORB-like values, see Figure 8.6. The unaltered Wetar Island lavas along with those from Atauro and Pura Beser deviate from the Damar-Manu-Banda array (Figure 8.6) as well as exhibiting a more complex pattern of Sr concentrations in Figure 8.5 (dependent on fractionation). A wide range of $^{87}Sr/^{86}Sr$ ratios are illustrated in Figure 8.6 for Wetar, Atauro and Serua, the wide range for Wetar is attributed to the presence of the post mineralisation dacite sample which yielded an extremely radiogenic $^{87}Sr/^{86}Sr$ value of 0.711068, the two samples of andesite from Wetar Island cluster close to the data from Teun and Nila.

The large isotopic range of Wetar Island samples are similar to large in-suite ranges evident at Damar, Teon, Nila and Serua; see histograms, Figure 8.7. The high $^{87}Sr/^{86}Sr$ ratios evident from this study and corresponding low $^{143}Nd/^{144}Nd$ ratios (Abbot and Chamalaun, 1981; McCulloch et al., 1982) are interpreted by Vroon et al., (1993) as almost pure SCM (subducted continental material) melts. Thus producing acidic melts on Wetar and rhyodacites on Romang which are associated with basaltic andesites, both having Sr signatures representative of a SCM component ($^{87}Sr/^{86}Sr$ = 0.7084-0.7092).

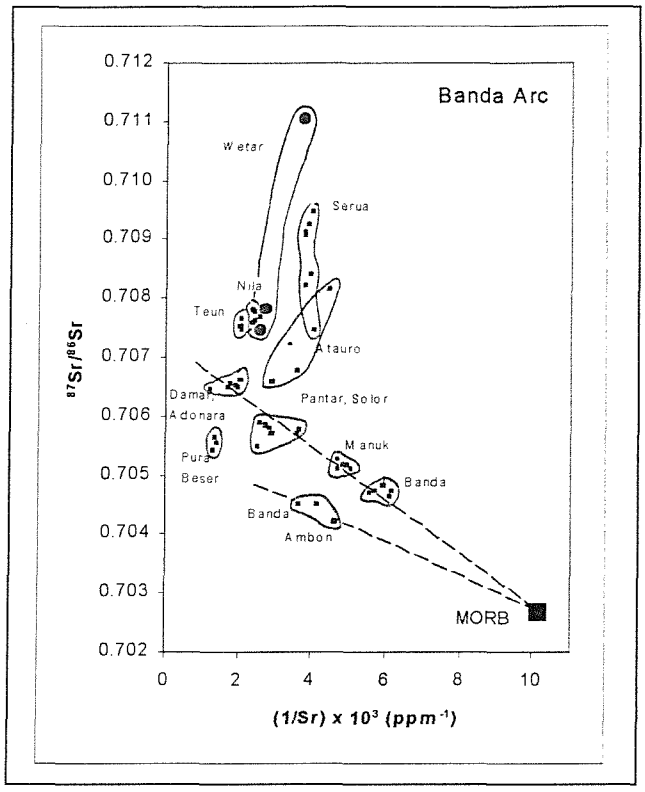


Figure 8.6. Sr-isotope mixing diagram for the calc-alkaline lavas of the Banda arc. The islands of Damar, Manuk and the Banda Islands form colinear clusters that define a mixing line which extrapolates to MORB-like values $^{87}Sr/^{86}Sr$ = ~0.7029 and Sr ~100 ppm. One sample from Banda and the Island of Ambon define a separate mixing line. Deviation of data from these arrays are caused by additions of varying amounts of sediment / crustal component in the mantle wedge (modified from Faure 2001, sources: Whitford et al., 1977 and Whitford and Jazek, 1979). The unaltered Wetar Island lavas from this study are shown for comparison (red data points).

Sr-Nd mixing models by Vroon et al., (1993) indicate sediment addition of up to 5% to generate the volcanic isotopic signatures present on these islands and values > 5% for Romang. The radiogenic post mineralisation dacite flows at Meron ($^{87}Sr/^{86}Sr$ = 0.71107-0.71166) must also involve a > 5% contribution. End-member sediment isotopic ratios used for modelling SCM input in to magma generation in the Banda arc is discussed in Vroon et al., (1993), Vroon et al., (1995). They argue that the terrigenous fraction obducted during subduction is representative of previously subducted crust and or sediments involved in magma genesis where 70% of subducted sediments bypass accretionary prisms (Von Huene and Scholl, 1991). The provenance regions of these sediments thus controls the compositions of the resultant volcanics. The correlation between the trace element ratios (K/Rb, Ba/Th, Ba/La and La/Th) of Banda arc volcanics and those from local sediments also indicate that

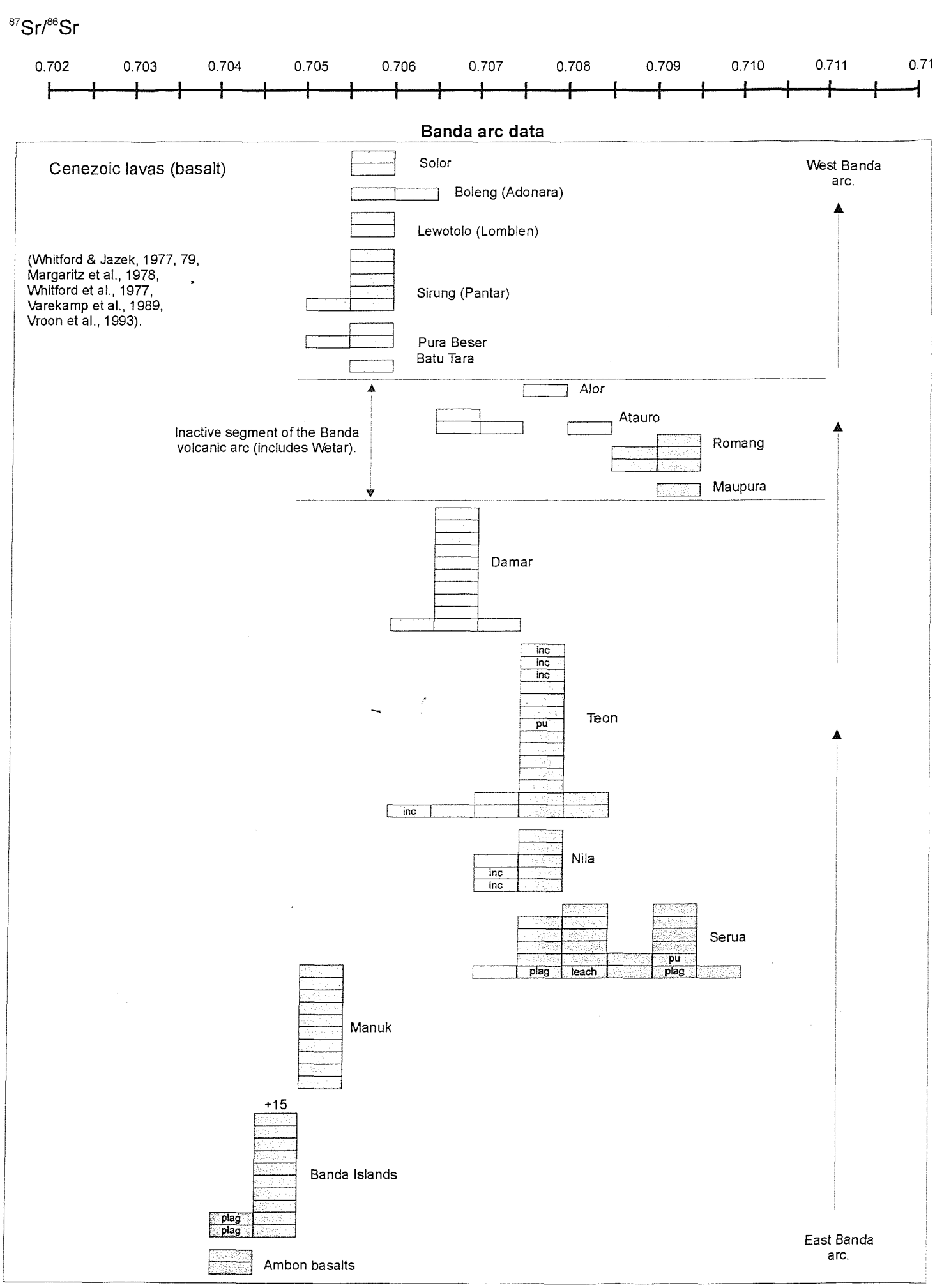


Figure 8.7. Histogram summarising the range in $^{87}Sr/^{86}Sr$ for published whole rock data for the Banda arc, data after Whitford & Jazek, 1977, 79; Margaritz et al., 1978; Whitford et al., Varekamp et al., 1989 and Vroon et al., 1993. plag= plagioclase phenocryst; pu= pumice; inc= inclusion.

sediments subducted are involved in magma genesis and thus determine the trace-element signatures of the volcanics (Vroon et al., 1995).

8.11.2 Hydrothermal Evolution

The Wetar Island hydrothermal barite samples exhibit a range of $^{87}Sr/^{86}Sr$ ratios that are higher than the underlying host volcanics (Figure 8.4). The Sr values are considered to be mixtures between Miocene seawater ($^{87}Sr/^{86}Sr$ = 0.7088, the value estimated for Miocene seawater, Farrell and Holland, 1983 and references therein) and hydrothermal fluids. In Figure 8.8 a trend between Sr and alteration intensity is evident. With progressive alteration, Sr ratios approach the value of Miocene seawater however the sample of residual silica (111935) shows a divergence from this trend line and may reflect that fluids closest to alteration have a greater hydrothermal component than seawater. The barite ore sample from Batu Kapal (Herrington, 1995) is consistent with the present study in that they exhibit Sr ratios similar to seawater. The stockwork sample collected by Herrington contrasts to the rest of the data yielding a ratio of $^{87}Sr/^{86}Sr$ 0.70644 suggesting a deeper magmatic / igneous influence, this result is lower than the unaltered mineralisation hosting volcanics (Table 8.2 and Figure 8.4). The majority of the barite data is similar to the value of Miocene seawater

This data is consistent with those of the Miocene Kuroko deposits where sulphate values < seawater (Kusakabe and Chiba, 1983; Farrell and Holland 1983). Barite morphologies outlined in Chapter 5, Figure 5.22 are similar to those studied by Shikazono, (1994) from Kuroko and Mariana deposits, the author attributes these morphologies as a result of recrystallisation. Seawater interaction with host rocks consisting of radiogenic $^{87}Sr/^{86}Sr$ ratios prior to precipitation may also have an affecton the Sr values, radiogenic values of volcanics are recorded throughout the Banda arc (Whitford et al., 1977; Whitford and Jazek, 1979).

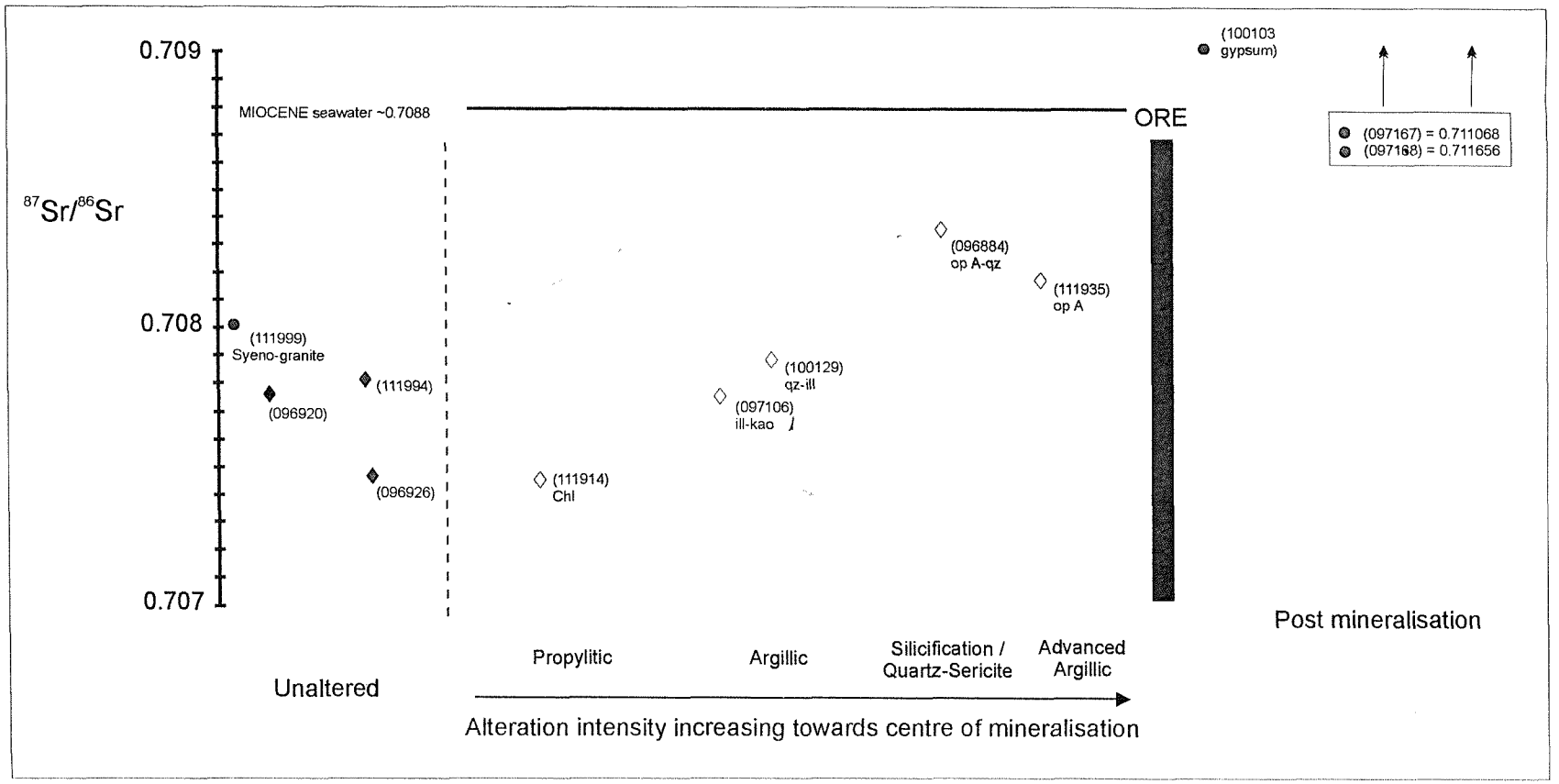


Figure 8.8. Six figure numbers refer to samples, hydrothermally altered samples have been assigned to an alteration assemblage / zone as a result of XRD and FTIR study (see chapter 4). Major phases identified are: chl= chlorite; ill= illite; kao= kaolinite; qz= quartz; op A= opal A. Value of Miocene seawater from Farrell and Holland, (1983).

8.12 ARGON

8.12.1 PREVIOUS WORK

K/Ar dates for fresh volcanics on the island have been presented in Chapter 3, Figure 3.2 however no other previous Argon work has been undertaken on samples from the island.

8.13 PRESENT STUDY

8.13.1 SAMPLE SELECTION

Three further samples have been chosen to better constrain age of mineralisation on Wetar Island, these age determinations will better define volcanic / mineralogical events of the Lerokis area. The three samples are located by references to a grid on topographic maps (see Figure 3.4 for sample locations): (1) sample 111999 collected from the Kali Lurang river in the Meron area. (2) sample 097167 from a post mineralisation capping dacite flow at Meron, topographic height of 300 m. (3) sample 056896, a fine-grained illite sample collected from the hydrothermally altered footwall volcanics at Lerokis at a depth of 26 m below the mineralisation (collected by Herrington, 1993). The volcanic and intrusive samples were disaggregated by light crushing, individual biotite grains (2-5 mm in length) were hand picked and cleaned in deionised water.

8.13.2 ANALYTICAL TECHNIQUES

The samples were irradiated at the Ford reactor, University of Michigan (irradiation MN15) with a fast neutron fluence of approximately 10^{18}n cm^{-2}. Hb3gr monitors (t= 1072 ± 11Ma) were used to determine the irradiation parameters J = 0.017093 ± 0.000026. Noble gas extraction and analytical technique (step heating) follows that of Kendrick et al., (2001), samples were analysed at the University of Manchester, UK. Due to the fine-grained nature of the illite sample, recoil loss of ^{39}Ar is likely, the sample was encapsulated in a quartz vial prior to irradiation. The recoil ^{39}Ar gas was analysed using a UV laser to drill into the tube. The recoil ^{39}Ar was only 5% of the

total ^{39}Ar released from the sample and was re-combined in the total age calculation. The Ar-Ar dating method has been used instead of conventional K-Ar due to the advantages outlined in McDougal and Harrison, (1999).

8.13.3 RESULTS

Samples used are given in Table 8.3, $^{40}Ar/^{39}Ar$ data are also given as amounts of Cl, K and ^{40}Ar, additional information is presented in Appendix F. $^{40}Ar/^{36}$ vs. $^{39}Ar/^{36}$ correlation diagrams and Age vs. %K released are given in Figure 8.9. The age obtained from the illite sample at 4.52 ± 0.22 Ma is within error of the K/Ar age of the same sample (4.7 ± 0.16 Ma). The age of the syeno-granite intrusion and dacite flow are 4.72 ± 0.22 Ma (Zanclian) and 2.4 ± 0.28 Ma (Piacenzian) respectively.

8.14 DISCUSSION

The data indicates that the spatially related syeno-granite intrusion (proximal to the Meron prospect) to the mineralisation are the same age and therefore implies that this intrusive may be responsible for supplying heat to the hydrothermal system. The Ar/Ar age date confirms that previously recorded by K/Ar (Herrington, 1993) and indicates mineralisation of the Lerokis deposit occurred between 4.7 and 4.5 Ma. The dates from both studies are within error of each other. The post mineralisation dacite flow indicates that volcanism continued up until at least 2.4 Ma, this is also the age given for the collision and accretion of the Australian continental margin with the outer Banda arc in the region of Timor (Richardson and Blundell, 1996). The sample may record a period of extension within the inner Banda arc as a direct result of compressional tectonics to the south in the outer arc. These dacites are also radiogenic in terms of their $^{87}Sr/^{86}Sr$ ratios (0.7111 and 0.7117) and may reflect significant contributions of continental material to magma generation. The age dates from the present study are shown schematically on the cross-section, Figure 8.10 with all other age dates from the Island. The sample of dacite also indicates that the debris flow that overlies the Meron deposit also occurred pre 2.4 Ma.

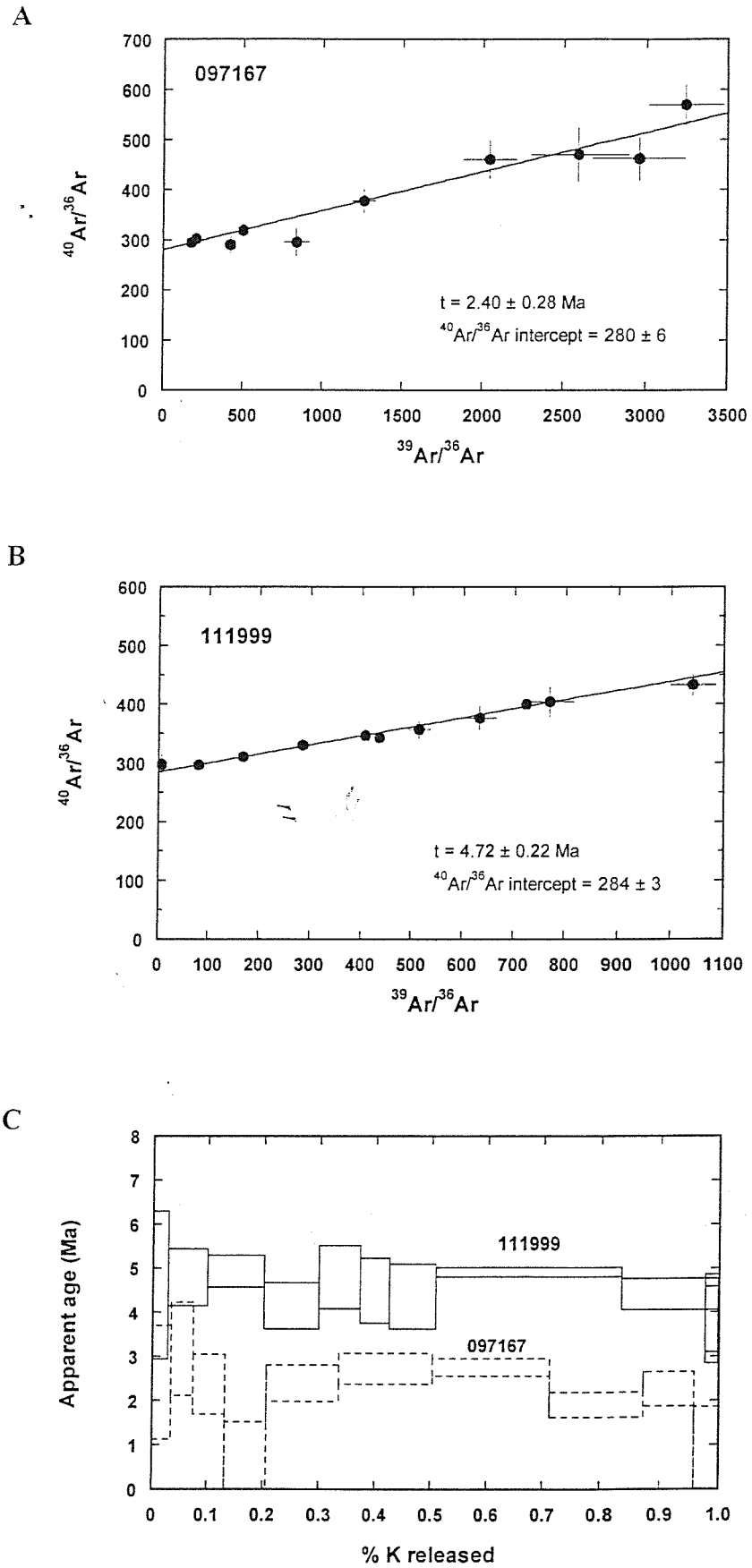


Figure 8.9. $^{40}Ar/36$ v. $^{39}Ar/36$ correlation diagrams for A, (sample 097167; post mineralisation dacitic flow overlying the Meron prospect) and B, (sample 111999; syeno-granite intrusion) biotite grains were sampled in each case. Diagram C shows Age v. % K released during the stepped heating process.

D

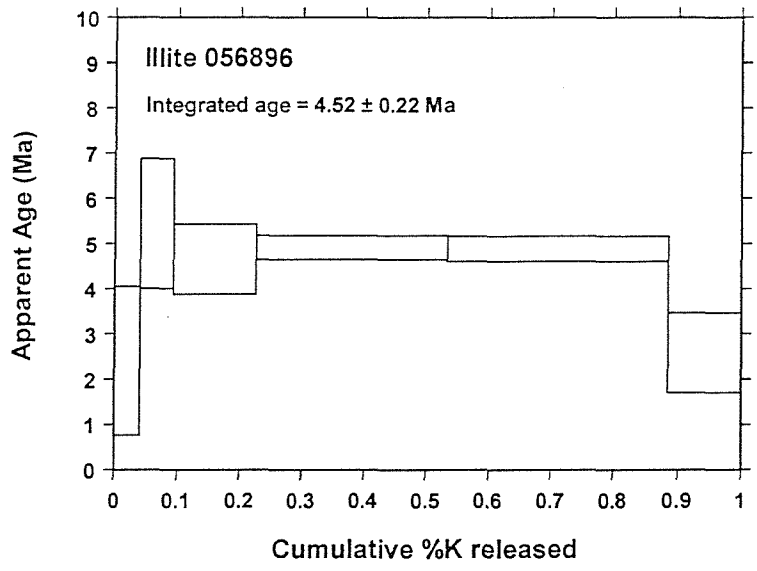


Figure 8.9. cont. Age v. % K released during the stepped heating process for sample 056896; <2μ illite separate from the Lerokis footwall, LKD 034 at a depth of 26 m, collected by Herrington, 1993 (see text for discussion). Sample 111999 was collected from the river S. Kali Lurang in the Meron area, sample 097167 was collected from Meron, elevation 300 m.

Table 8.3. Stepped heating Ar/Ar data for biotite grains and illite seperates (<2μ), Wetar Island, Indonesia.

Sample No	Location	Sample Type	Weight (mg)	Cl ppm	K Wt%	$^{40}Ar^*$ x 10^{-6} cc/g	Age (Ma)
111999	Meron area	Biotite	12	2288 ± 6	7.35 ± 0.01	1.35 ± 0.4	4.72 ± 0.22
097167	Meron	Biotite	11	9404±7.1	8.73 ± 0.01	0.75 ± 1.2	2.40 ± 0 .28
056896	Lerokis	Illite	9.1	13.88 ± 0.90	7.90 ± 0.01	1.38 ± 0.05	4.52 ± 0.22

1 σ errors are quoted. Amounts of Cl and K obtained from measured $^{38}Ar_{Cl}$ and $^{39}Ar_K$ using the Hb3 gr monitor and the parameters of α = 0.542 ± 0.01, β = 4.37 ± 0.03 and J = 0.017093 ± 0.000026. Samples were irradiated at the Ford Reactor, University of Michigan with fast neutron fluence ~10^{18}ncm^{-2}. Analytical technique follows that of Kendrick et al., 2001, samples were analysed at the University of Manchester, United Kingdom. Analytical data for each sample is given in Appendix F.

8.15 SUMMARY

The strontium and helium isotopic data support the sulphur data in that an increased involvement of subducted continental material (continental crust and or detrital sediments derived from continental crust) have aided the generation of the volcanic lavas. Similarly with the sulphur and oxygen data, sulphate $^{87}Sr/^{86}Sr$ ratios indicate no systematic variations with samples or depth and thus indicate contrasting seawater influence throughout the mineralising systems. Increasing Sr ratios towards centres of mineralisation correspond with Ca depletion.

Chapter 9

DISCUSSION / GENETIC MODEL

The following discussion attempts to draw on the information presented in this study of the mineralisation, hydrothermal alteration, hosting volcanic stratigraphy, isotopic and fluid evolution which have affected the Wetar Island deposits in order to establish a model of formation.

The preceding Chapters have documented a system characterised by:

1) An unusual hydrothermal system.
2) Unusual part of an arc environment.
3) Unusual volcanics.

9.1 HOST VOLCANIC STRATIGRAPHY

The Wetar Island deposits are associated with lavas that range in composition from basalt, basaltic-andesites, andesites to felsic dacites and rhyodacites thus recording stages of bimodal volcanism throughout the evolution of the Wetar edifice. These lithologies within modern systems, in varying abundances are present in the southern Lau Basin (Fouquet et al., 1993; Herzig et al., 1993); Manus Basin (Parr et al., 1995, Binns et al., 1995); Okinawa Trough (Halbach et al., 1993); Woodlark Basin (Binns et al., 1993; Scott and Binns, 1995) and the Kermadec island arc (de Ronde et al., 2000) which contrast to basalt dominated ocean ridge systems, Mariana Trough (Macdougall et al., 1987; Hawkins et al., 1990), North Fiji Basin (Bendel et al., 1993) and Mid Atlantic Ridge (Rona et al., 1993).

Unaltered sperulitic rhyolite collected from the Lerokis Zone 5 area, (Figure 3.4 for location) records late felsic volcanism within the deposit area, this was the major host lithology drilled in the rifted back-arc of the Manus Basin (Roberts pers com, 2001). The association of mineralisation at the margins of dacite and rhyodacite dome structures has been documented by this study and by previous workers (Ruxton, 1989; Herrington, 1993, 1995; Sewell and Wheatley, 1994b) a typical feature of many VMS systems, ie. Kuroko deposits (Ohmoto, 1978); Madneuli (Migineishvili, 2000); Gacun

(Hou et al., 2000) and Cerattepe (O'Brien and Hodgson, 1994, Herrington pers com. 2001).

Sewell and Wheatley, (1994b) suggested that mineralisation on Wetar Island may have occurred within a seafloor caldera. The Brothers Volcano, southern Kermadec frontal arc exhibits a caldera structure (3-3.5 km in diameter) associated with basalts, dacite domes and sulphide mineralisation (de Ronde, et al., 2000), at the Perubar VMS deposit, Central Peru, Polliand and Fontboté, (2000) speculate that these deposits were emplaced in an intracaldera incipient depression prior to a major caldera collapse. If the same processes are responsible for the formation of the Wetar deposits, then a considerable amount of the Wetar edifice may have been lost to the Banda sea to the north.

Many of the Kuroko type massive sulphide deposits have been proposed by Hodgson and Lydon, (1977) to have been generated in resurgent calderas as a result of enhanced permeability and radial fractures thus promoting the development of convective hydrothermal systems. The large Kuroko deposits (Koaska, Hanoaka, Shakanai and Matsuki) all lie within small calderas, 2-3 km in diameter near to the summit or flanks of volcanoes (Nakajima, 1993), if the Wetar deposits are related to calderas then a diameter of 3 km may be sufficient in size to contain the deposits located within the Kali Kuning, Lerokis and Meron area. The association of felsic volcanics at Wetar overlying older arc crust is very similar to the situation at PACMANUS, Binns et al., (1995), the sediment free nature of the Wetar stratigraphy however contrasts to the deposits at Jade (Binns et al., 1995).

9.2 HYDROTHERMAL ALTERATION

Field relationships during the study indicate that the residual silica in the adjacent footwall to the barite ore zones at each deposit is contemporaneous to the development of the barite ore itself. Fluids responsible are acidic and oxidised based on the presence of advanced argillic assemblages including kaolinite, pyrophyllite and native sulphur, Au appears related to this event. The presence of trace alunite within the stockwork zone beneath the Lerokis Zone 5 sulphide body also indicates the role of a low pH fluid. These assemblages however are only local in development with

typical alteration features more akin to the majority of VMS systems; consistent with seawater dominated fluid, black smoker type fluidss have a pH of ~3.

However, VMS systems may also preserve local mineralogical associations intermediate between sericite-chlorite and advanced argillic. For example, the Late Proterozoic Barite Hill deposit, Carolina Slate Belt has widespread sericitic and silicic alteration associated with sulphide and barite mineralisation and is proposed to be analogous to Kuroko style deposits (Clarke et al., 1999). Australian Zn rich VMS systems are sericitic dominant and also display intense inner zones of silicification (microcrystalline silica dominant) around the ore zones (Henty, Callaghan, 2001; Hellyer, Gemmell and Fulton, 2001) and are comparable to Wetar. Surrounding the intensely altered inner zones, alteration passes into dominantly sericite-pyrite zones, some of these VMS systems however preserve the presence of *high-sulphidation* alteration minerals such as pyrophyllite. The Eskay Creek precious metal rich VMS deposit is proposed to have had a magmatic influence during its formation, alteration within host rhyolite is dominated by K-feldspar and moderate silicification (Sherlock et al., 1999).

The polymetallic orebody at Lagoa Salgada, Iberian Pyrite Belt, Portugal is underlain by a tectonised zone of kaolinite and surrounded by sericite-chlorite altered stockwork zone of host tuffs and volcanics (Oliveira et al., 1998). The core of the stockwork zone includes pyrophyllite (Relvas et al., 1994), ore zones typically within the IPB are underlain by chloritic and sericitic alteration halos (Carvalho, 1979; Barriga, 1990).

Other systems where massive sulphides are surrounded by or have associations of advance argillic alteration include Undu, Morne Bossa, Grand Bois, deposits of the Pontid belt of Northeastern Turkey, the Bousquet Camp and Boliden (Sillitoe et al., 1993 and references therein). The development of advanced argillic alteration around the Wetar deposits are only local in development and relatively minor in abundance, similar associations are present at the Las Cruces deposit, IBP (Knight, pers com, 2001) and the Cerattepe deposit, Turkey, where proximal zones to mineralisation are kaolinite rich with local areas of advanced argillic alteration (O'Brien and Hodgson, 1994; Herrington pers com. 2001).

Kuroko type deposits with alteration similarities to Wetar include the Miamishiraoi barite deposit with an underlying footwall dickite-illite-montmorillonite-kaolinite assemblage. Chlorite-montmorillonite assemblages are present at distal locations (Marumo and Fujinuki, 1993) and pyrophyllite is also present (Marumo, 1989).

Numerous other Kuroko deposits of the Green Tuff region of Japan exhibit similar alteration patterns to those identified around the Wetar deposits. At the Uwamuki and Kosaka deposits, quartz and sericite cores are surrounded by chloritic and kaolinite rich margins (Urabe et al., 1983). Kaolinite however is not common around Kuroko deposits and when it is present it is associated with pyrophyllite (Urabe, 1974) as identified at Wetar.

Modern seafloor systems with alteration assemblages comparable to those identified at Wetar include the Hine Hina, Vai Lili and White Church deposits, Lau Basin, (Herzig et al., 1993). SuSu Knolls, East Manus Basin (Binns et al., 1997) and the Onsen hydrothemal site, (Gamo et al., 1997), DESMOS caldera, (Gemmell et al., 1999) all exhibit similarities however the extent of advanced argillic alteration at these sites are unknown as they are surface samples. Minor kaolinite and alunite are reported from Conical Seamount associated with illite-smectite-chlorite, sericite and silicification (Herzig et al., 1999, 2000). At the Jade site, Okinawa Trough, assemblages of kaolinite, mixed layer chlorite/montmorillonite are present with varying amounts of native sulphur and barite (Halbach et al., 1993; Marumo and Hattori, 1999).

At TAG, dominant alteration assemblages comprise quartz, paragonite, chlorite and kaolinite (Hannington et al., 1998; Teagle et al., 1998a and b) which in may instances are similar to assemblages at Wetar, however advanced argillic assemblages are not reported suggesting a difference in fluid pH or a reduced magmatic influence.

9.3 MINERALISATION AND STYLE OF DEPOSITS

The association of seafloor sulphide mounds ± sulphosalts with flanking Au-Ag-Hg bearing, arsenate cemented baritic ore zones preserved on Wetar are unusual. Similar deposits are described throughout the central section of the island (Table 3.1, Chapter 3) however in contrast to these unusual VMS deposits, *low-sulphidation* epithermal vein systems are present at Gunung Botak, associated with chalcedonic quartz veins (Sillitoe, 1997) representing a more recent phase of mineralisation.

Barite mounds are however reported in the Jade hydrothermal field, (depth 1350-1600 m) Parr et al., (1995); Binns et al., (1995); (Lüders et al., (2001). Distinctive Au-Ag-barite deposits associated with polymetallic sulphides are present on at least 6 frontal andesitic cones that are part of Izu-Ogasawara arc (Ishibashi and Urabe, 1995) and

barite lenses are reported overlying vein and disseminated sulphides at the Madneuli Cu-Au deposit, Georgia (Migineishvili, 2000) where the author suggests formational depths of <200m based on hosting lithofacies. These deposits are associated with subduction related Upper Cretaceous bimodal volcanics, (Migineishvili, 2000). Other ancient deposits that preserve sulphide-barite mineralisation similar to Wetar include the Minamishiraoi Kuroko type barite deposit, (Marumo and Fujinuki, 1993). These deposits are hosted by Middle Miocene andesitic to felsic lavas associated with barite ore horizons overlying barite bearing silicified breccias (a feature within adjacent footwall zones at the Wetar deposits) containing disseminated sulphides and sulphosalts. The Barite Hill deposit, South Carolina, USA is hosted by Late Proterozoic, felsic volcanoclastics and intrusives (Clarke et al., 1999; Seal II et al., 2001). Clarke et al., (1999) suggest that sulphide-barite associations are an ancient analogue of those preserved on Wetar, the association of Au-Ag rich zones with siliceous barite in the Main pit area is extremely similar to the mineralogical association at Wetar.

The Late Triassic Gacun VMS deposit, China is hosted within dacitic / rhyolitic lavas overlying mafic volcanics. The deposit comprises massive sulphide sheets with underlying stockwork zones, large quantities of barite and barite beds occur at the top of or between the massive sulphides (Hou et al., 2000). These mineralogical associations in concert with a sericite-quartz-chlorite alteration assemblages and bimodal volcanism are similar to Wetar. The Cerattepe deposit, Turkey is also interesting in its similarities to the Wetar deposits, mineralisation occurs at the margin of brecciated felsic domes comprising massive sulphide mounds with associated barite rich gossanous zones.

The form and nature of the polymetallic massive sulphide mounds preserved at Kali Kuning and Lerikis Zone 5 (Pyrite, marcasite, chalcopyrite) have similarities to many modern and ancient systems associated with varying tectonic environments (convergent and divergent margins). The simple sulphide mound mineralogy have similarities with those located in modern systems including the slow spreading mid-ocean ridge deposits of TAG (Rona et al., 1993; Mills and Elderfield, 1995; Hannington et al., 1998; Peterson et al., 2000), Snake Pit (Fouquet et al., 1993) Broken Spur (Duckworth et al., 1995; Butler et al., 1998) and the fast spreading deposits of the East Pacific Rise (Hekinian et al., 1993) and the Sonne Field, Central Indian Ridge (Halbach et al, 1995, 1998). Deposits with similar mineralogical

features associated with subduction related arc and back-arc environments include the Franklin Seamount, Western Woodlark Basin (Binns et al., 1993; Scott and Binns, 1995); PACMANUS / DESMOS deposits, East Manus Basin (Binns and Scott, 1993; Parr et al., 1995; Binns et al., 1995; Moss and Scott, 2001); Lau Basin (Fouquet et al., 1993; Herzig et al., 1993); JADE, Okinawa Trough (Halbach et al., 1989, 1993). At the JADE site, angular sulphide boulders are similar to features particularly at the Lerokis Zone 5 deposits, blocky / porous pyritic mounds are also reported on the E Galapagos Rift (Embley et al., 1988) and at Mine Gallen, Quebec (Watkinson et al., 1990). Recent seafloor discoveries include Conical Seamount which represents a site of mineralisation within a fore-arc environment (New Ireand) related to the Tabar-Feni island chain (Herzig et al., 2000), Au is associated with disseminated sulphides and chalcedonic quartz veins which contrast to features at Wetar. The Brothers hydrothermal system, Southern Kermadec Arc (de Ronde et al., 2000) preserves massive pyrite breccias and pyrite rich stockworks therefore exhibiting some mineralogical similarities with features at Wetar.

Ancient systems with similarities to the Wetar Island mineralisation include the VMS deposits of the Kuroko District, Japan, (Ohmoto and Skinner, 1983; Ohmoto et al., 1983; Nakajima, 1993) and ophiolite hosted systems (Hannington et al., 1998 and the review in Galley and Koski, 1999). The Wetar deposits are located in close proximity to each other and are similar to Kuroko style VMS deposits in that numerous clusters of small deposits or groups appear within a single area, these all represent single hydrothermal fluid conduits for solutions reaching the seafloor. Australian systems are reviewed in (Large et al., 2001) documenting many mineralogical similarities identified during this study. The porous, massive pyrite mounds exhibited at some of the Cyprus – type deposits are also extremely similar to mound morphology characteristics at Wetar. In particular, the pyrite breccias, nodular / globular / conglomeratic pyrite, talus debris (ie. Mathiati, Lydon, 1984) and fine grained sandy pyrite (ie. Kalavasos, Constantinou, 1973) overlying more competent porous massive pyrite. The coarse granular, globular features of these deposits and at Wetar are also present at the margins of the TAG hydrothermal mound (Hannington et al., 1998). However, the minor abundance of lead and zinc at the Wetar sites of mineralisation is also a feature of some Cyprus deposits, at Mathiati, late stage Fe-poor sphalerite is present filling cavities along with chalcedonic silica.

Enargite was reported as a sulphide phase associated with the Wetar sulphide mounds by de Ronde, (1995), magnetite breccia is noted within the footwall of the Lerokis Zone 5 deposit (Herrington pers com. 2000). These features along with the presence of native sulphur at Kali Kuning (Chapters 3 and 4) all confirm an input of an oxidising fluid associated with mineralisation. The presence although of enargite and magnetite during this study have not been substantiated. Sulphosalt assemblages are present within the mineral paragenesis as part of a fracture-fill assemblage that permeates through the sulphide mound (Chapter 5), sulphosalts are documented and reported from many Kuroko VMS deposits however in generally they are rare in base metal deposits genetically related to the Green Tuff Volcanism (Matsukuma et al., 1974). Sulphosalts occur generally located towards the middle and upper zones of black-ore horizons associated with colloform pyrite, sphalerite, galena and tetrahderite and abundant barite (Matsukuma et al., 1974); again, similar to features at Wetar. Hypogene sulphosalts are reported from the deposits of Yokata, Tashiro, Kurosawa (Yamaoka and Asakura, 1974) and the Shakanai deposit (Nishiyama, 1974). Interestingly, the presence of VMS deposits on Wetar + baritic ore, or just the presence of the latter and the presence of epithermal vein deposits occurring within a single district has remarkable similarities with southwestern Hokkaido, Japan (Shimizu et al., 1998). The Minamishiraoi barite deposit is similar to Wetar in terms of host geology and alteration and association of barite deposits, however the lack of a sulphide mound is similar to Lerokis Zone 4. The deposit is located within an area ~5 km from the Shiraoi sulphur-iron deposit, an area also containing abundant epithermal deposits (Marumo and Fujinuki, 1993) and in this respect is similar to the Kali Kuning and Lerokis area in general.

Au grades at Wetar are low in comparison to other modern systems such as the Lau Basin and Manus Basin systems (Herzig and Hannington, 2000) however the Au at Wetar is associated with the barite deposits and not the sulphides. At the East Manus Basin however, Au is associated with tennantite and chalcopyrite as inclusions (Moss and Scott, 2001); in ancient systems, Au rich VMS's consist of sulphosalts and Pb / Zn generally associated with Au: eg. Horne, Bousquet, Eskay Creek and Roseberry (Hannington., 1999).

The Fe-poor sphalerite associated with the *high-sulphidation* fracture fill assemblage that permeates throught the stockwork and sulphide mounds crystalised under low aFes conditions. Enhanced Au values have been correlated with low FeS in both

active and ancient VMS systems (Hannington and Scott, 1989; Herzig et al., 1993). The correlation between FeS and Au values is attributed to the influence of aFes, aS_2 and temperature which control gold deposition and the composition of sphalerite in the same setting (Hannington and Scott, 1989).

9.4 FLUID COMPOSITION

The salinities of the Wetar barite hosted inclusions fall within the measured mid-ocean ridge fluids (~0.2- ~7 wt% NaCl), (Von Damm, 1990; Butterfield and Massoth, 1994; Von Damm et al., 1995). They are also similar to those measured within anhydrite from TAG, (Tivey et al., 1998), 21°N EPR (Lebel and Oudin, 1982), 13°N EPR (Nehlig, 1991) and the Southern Juan de Fuca Ridge (Brett et al., 1987). The dominant sulphate mineral present at active vents from the fast-spreading 21°N East Pacific Rise is anhydrite (Styrt et al., 1981), measured exit temperatures range between 260 to 350°C (Kusakabe et al., 1982) whereas homogenisation temperatures from anhydrite range between 179 and 354°C. The maximum fluid inclusion temperature was 10-20°C higher than the measured exit temperature suggesting that measured temperatures of active vents are not necessarily the maximum temperature of the hydrothermal system. Salinities recorded are 2.9-3.8 wt% NaCl (Styrt et al., 1981; Kusakabe et al., 1982).

The Wetar Island fluid inclusion homogenisation range (144 to 314°C, avg, 235°C) is substantially less than the 366°C venting black smoker fluids at the TAG-1 site (Slow spreading TAG system, Mid Atlantic Ridge). However, they are vary similar to white smoker fluids which range between 273-301°C, (Edmond et al., 1995) especially when allowing for a maximum pressure correction of 40°C, based on a formational depth of ~ 3 km. The TAG salinity average is 4.3 wt% NaCl for anhydrite hosted inclusions and 5 wt% for quartz (Peterson et al., 2000). From the proposed upflow zone at TAG-1 confined homogenisation temperatures are 301-358°C, therefore Wetar has a range more comparable to the area of low heat flow (TAG-4) and those of venting white smokers in the Kremlin area (Thompson et al., 1988). To the north of TAG at Broken Spur, black smokers vent fluids at 357-366°C (James et al., 1995) and are similar to those at TAG-1. At Lucky Strike, both low and high temperature fluids occur together, 150-333°C (Von-Damm et al., 2000), the barite rich nature of this system distinguishes it from TAG, Snake Pit and Broken Spur.

At the mature back-arc spreading centre of the North Fiji Basin, the highest fluid temperature venting from the anhydrite chimney "White Lady" was recorded at 265°C (Ishibashi et al., 1994) , the chimneys of Kaiyo and LHOS (150 m southwest of White Lady) yielded temperatures of 290 and 230°C respectively. Small fluctuations in chemical composition between the two sites is attributed to sub-seafloor, fluid-rock interaction after phase segregation. Inclusion studies from propagating back-arc rifts in the Lau Basin include those from anhydrite hosted inclusions at Vai Lili. The data indicates a high salinity fluid (30 wt% NaCl) and temperatures of 290-344°C (Lecuyer, 1999), these results are consistent with present day temperatures at the active vent of 342°C, (Fouquet et al., 1993) however present day salinities reach only 4.7 wt% NaCl. The results contrast to those of a barite sample from the same location with salinities of less than 3.2 wt% NaCl and temperatutures of 148 to 261°C. Lecuyer, (1999). These results indicate that Vai Lili is the first oceanic hydrothermal system where high-salinity brines have reached the seafloor. Sphalerite hosted inclusions from the JADE hydrothermal field (Central Okinawa Trough) record salinities of 2-15 wt% NaCl and temperatures of between 270-360°C, see Table 6.2 (Lüders et al., 2001). These results are higher than those recorded at Wetar Island, the authors attribute the varying salinities as a result of phase separation at deeper levels where the resulting brine favoured the transport of the associated *high-sulphidation* sulphide assemblages (tetrahedrite-tennantite and enargite). Barite from the same site records lower temperatures of formation (150-200°C). From an active black smoker chimney at JADE, fluids are discharging at a maximum temperature of 320°C (Marumo and Hattori, 1999), inclusion data ranges between 200 to 354°C with a salinity of 3.7-6.5 wt% NaCl. Lüders et al., (2001) suggest that the low salinity vapour phase that separated from the brine at depth, ascended, condensed and mixed resulting in a lower salinity liquid than seawater, this process may also explain the salinity variations recorded in the Wetar samples. At Hine Hina, barite hosted inclusions have homogenisation temperatures of 170-230°C and salinities of 1.6 to 2.6 wt% NaCl, at White Church, homogenisation temperatures range between 203 to 262°C with corresponding salinities of 3.2 to 5.3 wt% NaCl (Lecuyer et al., 1999). These published results are very similar to the Wetar Island data from this study. Fluid temperatures however are higher than those at the East Manus Basin, Onsen venting site, (DESMOS caldera) where white smoker fluids exit hydrothermal vents with temperatures of 88° and 120°C at a depth of ~1900 m (Gamo et al., 1997) and a

pH of 2.08. The East Manus Basin data are comparable to inclusion and vent fluids from the Lau Basin where fluids are also acidic, pH 2 (Fouquet et al., 1991). The fluids at DESMOS are cooler than Wetar but the low pH fluids must be present at Wetar to account for the associated alteration assemblage and occurence of native sulphur and residual silica (see also Chapter 4). Au-rich inactive barite-silica chimneys from the summit caldera, Franklin seamount, Western Woodlark Basin have slightly cooler homogenisation temperatures than Wetar of between 184 to 244°C and salinities slightly more saline than seawater, 3.4-5.8 wt% NaCl (Binns et al., 1993). Similar ranges are also recorded from a barite spire at Axial Seamount (Hannington and Scott, 1998). Venting fluids up to 310°C are present on the Suiyo seamount, Izu-Bonin arc (Tsunogai et al., 1994) whereas numerous extinct barite-silica chimneys (depth of 1500-1600m) are present on the central ridge of the Sumisu Rift, Izu Bonin Arc (Urabe and Kusakabe, 1990).

Extensive local footwall development of amorphous silica proximal to the Wetar sulphide mineralisation feeder zones suggest lower temperatures occurred during waning stages of hydrothermal activity or precipitation occurred as a result of cooling fluids. The average homogenisation temperature from sample 099938 (distal barite vein) is 194°C and may record this hydrothermal stage. The occurrence of amorphous silica with barite hosted one-phase liquid dominanced fluid inclusions on the Sumisu rift also indicates low formational temperatures which preclude nucleation of a bubble on cooling (Urabe and Kusakabe, 1990). At Green Seamount, opal-barite rocks are present at the periphery of sulphide deposits, formation is thought to have been at temperatures of ~100°C during waning stages of activity (Alt, 1988), overlying chert layers from Kuroko deposits yield formational temperatures of 110 ± 30°C (Tsutsumi and Ohmoto, 1983). Silica supersaturation sufficient for precipitation of amorphous silica at 150°C requires an initial fluid in equilibrium with quartz at deeper levels to have temperatures of at least 243°C (adiabatic cooling) to 280°C (conductive cooling) (Fournier, 1985).

The salinities of 5 major Kuroko deposits (Kosaka, Fukazawa, Shakanai, Furutobe and Matsumine) have constant salinity ranges of between 3.5 to 6 wt% NaCl, formation of black ore minerals occurred at temperatures between ~200 to 330°C. Following formation of yellow ore minerals occurred at a thermal maximum of 330° ± 50°C after which temperatures again dropped to 260° ± 50°C (Pisutha-Arnond and Ohmoto, 1983). At Wetar, no convincing evidence exists to suggest that the fluids

have boiled, this is the same for Kuroko systems (Pisutha-Arnond and Ohmoto, 1983). Barites in Kuroko deposits generally show wide homogenisation ranges and varying L/V ratios due to stretching, leakage or necking down (Pisutha-Arnond and Ohmoto, 1983 and references therein). The larger, vapour rich barite hosted inclusions in the Wetar samples are similar to those identified in Kuroko ores, however the nature of these are more likely due to leakage of the liquid phase rather than boiling of the hydrothermal fluid at the time of entrapment. Decrepitation of inclusions can occur during overheating by later and higher temperature periods of mineralisation and has been documented in both sphalerite and quartz (Bodnar and Bethke, 1984). The Minamishiraoi deposit has already been shown to exhibit features similar to those on Wetar, (section 9.2 and 9.3) temperatures of quartz veins within the silicified barite breccia zone records temperatures of 230-250°C (data taken from Marumo et al., 1995) thus recording similar fluid temperatures to those at Wetar. Interestingly, the neighbouring island of Romang exhibits quartz veins with inclusions of moderate salinity (1.4-4.4 wt% NaCl) and temperatures of homogenisation around 200°C (Lawless, 1991). These veins are attributed to sub-aerial epithermal systems and have no relationship to VMS style mineralisation, these results may be similar to mineralisation reported at Gunung Botak by Sillitoe, (1998).

Other ancient VMS systems where fluid inclusions preserve similar fluids (temperatures and salinities) to those at Wetar Island include the Australian and Tasmanian deposits of Mt Chalmers (Zaw et al., 2000) Tharsis and Hellyer (Zaw et al., 1995, 1996, 2001). The Eskay Creek deposit, British Columbia, Canada documents an unusual *high-sulphidation* mineral assemblage combined with many typical VMS characteristics. The fluid data from Eskay Creek (Sherlock et al., 1998) exhibits homogenisation temperatures lower than those at Wetar but records higher salinities.

9.5 DEPTH AND TIMING OF MINERALISATION

Depth of mineralisation may have important implications in the generation of these systems, as outlined in section 9.3 *high-sulphidation* VMS deposits can form in both shallow and deeper water conditions. These contrasting depths are recorded at deposits with similar sulphide-barite associations (ie. JADE and Madneuli deposits).

Depth may also have an importance especially in the transport of precious metals where in particular shallow water can allow boiling of hydrothermal fluids and precipitation of Au above the zone of boiling ie. Juan de Fuca Ridge (Hannington et al., 1999). Volcanic facies are not depth specific (Huston and Cas, 2000) as pillow lavas can occur in all water depths and vesicular lavas are not indicative of shallow waters, the limestone unit overlying the Kali Kuning deposit is by far the most important lithology in terms of estimating depth of formation for the Wetar Island deposits, the relationship with the underlying sulphides suggests that the sulphides formed at or extremely near to the palaeo-seafloor and that water depths were between 600- 2000 m (Herrington, 1995) however Murray (pers com. 1999) suggests deeper conditions of deposition. The minor evidence of reworking above the Lerokis Zone 5 deposit does not necessarily suggest shallow water conditions as ocean currents in deep water have recently been documented on the slopes of the Kermadec Arc volcanoes at depths up to 1500 m (Wright, in press). The study has further constrained the age of mineralisation at ~4.7 Ma and has also illustrated that volcanism continued post collision between the Australian margin and the outer Banda arc. It had been suggested by Abbott and Chamalaun, (1981) that no volcanic activity occurred within the inner Banda arc post 3 Ma however the dacites at Meron record active volcanism at 2.4 Ma.

9.6 ISOTOPES

Mineralogical and alteration associations at Wetar suggests a magmatic component involved in deposit formation however this is not compounded by the isotopic data (Chapter 7). At Broke Spur, 29°N, Mid Atlantic Ridge, $\delta^{34}S$ values of –0.8 to +2.4 are reported for sulphides which are significantly lower than those from the fast spreading East Pacific Rise (Duckworth et al., 1995) and values from Wetar. Anhydrite has a value of +19.3‰, similar to that of modern seawater of +21‰ (Rees et al., 1978). The values at TAG are similar to those of Wetar but with narrower ranges of both sulphate and sulphides (+4.4 to +8.2‰, average 6.5‰ for bulk sulphides) (Peterson et al., 2000). Both systems are heavier with respect to $\delta^{34}S$ than those of other sediment starved ridges (Shanks et al, 1995), at 12° 43'N EPR the sulphides from the axial region are slightly heavier than those from the off-axial sites

(Fouquet et al., 1996) but are generally lighter than the range of sulphides recorded at Wetar. Within the Sonne Field, Indian Ridge, massive sulphides from 270 km north of the Rodriguez Tripple Junction close to the medium spreading rift axis, inactive sulphides record values of +1.9 to +3.7‰ and are typical of basalt hosted ridge deposits (Halbach et al., 1995). Values < than modern seawater for barite (+16.5 to +20.1‰) the authors attribute to admixture of magmatic sulphur.

The sample of native sulphur from the footwall of the Kali Kuning deposit recorded a value higher than the sulphide phases and suggests oxidation of pre-existing sulphides (Chapter 7). The value contrasts to the isotopically light values recorded at the DESMOS site, East Manus Basin, where fracture and vesicle filling native sulphur have a range of –5.9 to –6.8‰ Gemmell et al., (1999). Similar isotopically light values are also reported from Hine Hina (-2.4 to –4.8‰), (Herzig et al., 1998) and the Brothers hydrothermal system (de Ronde et al., 2000). The absence of biogenic sulphur and boiling within the system indicates a depleted $\delta^{34}S$ source of probable magmatic origin. At the Onsen Site, East Manus Basin, acidic <2.1 pH sulphate rich fluids are vigorously venting at the DESMOS caldera with low δD (H_2O) and $\delta^{34}S$ (H_2S) values of –8.1 and –5.6‰ respectively (Gamo et al., 1997). The authors suggest incorporation of magmatic fluid and disproportionation of the exsolved SO_2. These fluids are similar to acid-sulphate hot springs associated with subaerial volcanic activity and the generation of *high-sulphidation* epithermal deposits (Heald et al., 1987, Hedenquist, 1987). At Conical Seamount, a shallow submarine volcano south of Lihir within the New Ireland Fore-arc, PNG, sulphides reported range from –0.2 to –8.6‰ (average 3.2, n=14), $\delta^{34}S$ of alunite is +7‰, both sets of results indicate a magmatic contribution to the hydrothermal system, the disproportionation of magmatic SO_2 into H_2S and $H_2SO_4^{2-}$ forms acid sulphate alteration assemblages (Herzig et al., 1999). Similar magmatic contributions are present at site 876 from the outer fore-arc basement high of the Izu-Bonin arc at a water depth of 3082 m, light $\delta^{34}S$ value of sulphides (-2 to –5.5‰) and sulphate (12.5‰) (Alt et al., 1998) contrast to the data observed at Wetar. The sulphide values reported at Vali Lili (7.2-10.9‰) (Hezig et al., 1998) are similar to the Wetar data however the sulphides are dominantly chalcopyrite and sphalerite which contrast to the pyrite dominated sulphide mounds at Wetar Island.

At the Sumisu rift, Izu-Bonin arc, barite from a barite/amorphous silica chimney yielded $\delta^{34}S$ and $\delta^{18}O$ values of +21.7- +22.3‰ and 8.8-10.3‰ respectively (Urabe and Kusakabe, 1990), these values suggest a significant seawater component in the hydrothermal system and are more similar to values recorded on Wetar Island.

A review of Phanerozoic Kuroko deposit isotopic data is given by Sasaki (1974), approximate ranges of variation of $\delta^{34}S$ are as follows: pyrite, -6 to +8‰ (dominantly +3 to +8‰); chalcopyrite, +2 to +7‰; sphalerite, +3.5 to +7‰; galena, 0 to +3.5‰; gypsum and anhydrite, +21 to +23‰ and barite, +22 to +25‰. The majority of Kuroko sulphates are uniform (+22 to +23‰) however some are isotopically heavy (up to +27‰), these samples usually tend to have heavier $\delta^{18}O$ values which can be proved to be as a result of bacterial reduction (Sasaki, 1974). The same relationship is evident at Wetar where the barite veins are isotopically heavy with respect to both sulphur and oxygen. Marumo et al., (1995) suggests that isotopic data from the Minamishiraoi deposit indicates a seawater dominated system with minor mixing of magmatic water. At Eskay Creek, the precious metal rich VMS deposit is suggested to be like the Jade deposit (Sherlock et al., 1999), values of $\delta^{34}S$ for sulphides and sulphates are –3.3 to 12.2‰ and 21.7 to 29.3‰ respectively. The average of –0.4‰ for the sulphides is suggested to represent a deep seated igneous source, excluding one low $\delta^{34}S$ value, the sulphate data, average of 24‰ is ~ 5-6‰ higher than Jurassic seawater (18-19‰), (Claypool, 1980) suggesting a dominant seawater source of sulphate. The sulphate range of data is similar to that recorded from Wetar, however the sulphate average is only ~3‰ higher than Miocene seawater, again suggesting a dominant seawater influence. The Barite Hill deposit records $\delta^{34}S$ values from +1 to 5.3‰ for massive sulphides however disseminated pyrite in volcanoclastics yield ranges from –12.8 to +3‰ and are attributed to a seafloor biogenic origin in a restricted basin (Clarke et al., 1999). The presence however of dominantly serecitic alteration coupled abundant sediments (greywackes, silts and shales) contrast to features preserved at Wetar.

The strontium and helium data from the study records the input of subducted sediment within the generation of the arc lavas that now host the mineralisation. These radiogeneic results have made the identification of a magmatic component within the hydrothermal system difficult to trace where as the addition of mineralogical and alteration associations have aided this interpretation.

9.7. SUMMARY

The Wetar data from this study has identified a minor magmatic component involved with mineralisation, consistent with the local / minor presence of advanced *high-sulphidation* alteration / mineralogical associations. The study of the Wetar deposits has documented an unusual VMS system, although I propose that there is no exact analogue to these deposits the study has indicated many similarities to numerous other systems. Modern deposits with perhaps the most similarities to the deposits at Wetar include Vai Lili (Lau Basin) and Jade deposit (Okinawa Trough) especially in terms of mineralogy and alteration, the key contrast to many of the many modern sites are the isotopic values, these differences are attributed to the tectonic association and associated arc lava contamination (Chapter 2 and 8). Similar ancient analogues are Barite Hill, Cerattepe and the Kuroko Minamishiraoi deposits. Submarine VMS deposits are considered part of a continuum between VMS, epithermal and porphyry copper deposits (Sillitoe et al., 1996; Hannington et al., 1999; Hannington and Herzig, 2000) where interplay between seawater, magmatic fluid and meteoric waters at varying depths of formation result in mineralisation and in some instances generate hybrid deposits with overlapping features. Wetar can be considered as a hybrid VMS deposit or *high-sulphidation* VMS deposit however the *high-sulphidation* mineralogy / alteration does not occur in appreciable amounts.

9.8 GENETIC MODEL

The model integrates the information presented in this study based on local geological mapping, alteration and ore mineralogy, fluid evolution and both radiogenic and stable isotope systematics.

9.8.1 TECTONIC, MAGMATIC AND GEOLOGICAL EVOLUTION

The tectono-magmatic / geological evolution of the Wetar Island system is illustrated in Figure 9.1 as a series of 3-D diagrams. In this broadly compressional tectonic regime caused by the NE movement of the Australian shelf towards the Eurasian plate ($7.5cm^{-1}/yr$), subduction has occurred along the Java trench / Timor Trough, south of Timor. Between 12 and 5 Ma, the process of subduction resulted in the generation of seafloor basaltic-andesite volcanism (tholeiitic to calc-alkaline) due to extensive rifting, the formation of the "outer volcanic" Banda arc and the early evolution of the Wetar edifice (see inset picture on Figure 9.1, stage 1). Extensive rifting within the oceanic crust resulted in voluminous seafloor volcanism and the building of rhyo-dacite domes during periods of bimodal volcanism. Nascent hydrothermal activity occurred as a result of vast quantities of cold seawater being drawn down to deep crustal levels due to fault initiation and extension, see Figure 9.1; stage 1. The thin nature of the oceanic crust in this region (~11 km and Bowin et al., 1980) resulted in the emplacement of a shallow magmatic source or may have enabled high-level emplacement of plutons thus providing a substantial heat engine / reservoir. Syeno-granite intrusives spatially close to the Meron prospect (dated at 4.7 Ma) records this phase of igneous activity, geochemically these intrusives are co-magmatic with the dacite dome structures mapped at Kali Kuning. Petrographic and geochemical analyses of the host statigraphy confirm the presence of a basalt-andesite unit underlying the mineralisation, vesicular andesitic feeder channels and pillow lavas are present along the north coast and show evidence of weak propylitic alteration related to distal hydrothermal alteration. At ~4.7 Ma, focused hydrothermal fluid flow discharged along major fault intersections and at the margins of the rhyo-dacite dome structures, Figure 9.1; stage 2. The construction of massive sulphide mounds and barite ore zones occurred at the seafloor with the generation of associated underlying stockwork zones coupled with extensive hydrothermal alteration of the

host volcanic stratigraphy (Figure 9.1, stage 2). Post mineralisation gypsum and chert covered the deposits during the waning stages of hydrothermal activity as a result of sulphide oxidation on the seafloor. *Globigerina* bearing limestones proceeded to cover the gypsum and chert after cessation of hydrothermal activity. The planktonic:benthic ratio within this unit and presence of *Favocassidulina* indicate open oceanic conditions and depths >2000 m at the time of formation (Murray pers com, 1999). Both rapid and sporadic uplift of both the "inner" and "outer" Banda arcs may be related to slab detachment (oceanic from continental) at depth, post locking between the Australian continental margin and the outer arc at Timor (~2.4Ma, Richardson and Blundell, 1996). This tectonic environment could be the key to generating sudden and massive extension within the inner arc region (Wortel pers com. 2000) and the generation of post mineralisation dacitic flows observed at Meron and spherulitic rhyolites SW of Lerokis. The dacitic flows are extremely radiogenic in their $^{87}Sr/^{86}Sr$ ratios and record an igneous phase of activity strongly contaminated by sediment or continental derived material from the subducting slab to the south. This contamination is widespread and is recorded in volcanic lavas along the entire length of the Banda arc, however, contamination is greatest in the region of Wetar, Romang and to the east at Serua (see Chapter 8). Episodes of extension within volcanoplutonic arcs are excellent tectonic settings for base and precious metal mineralisation (Mitchell and Bell, 1973), in many instances resulting in Au mineralisation (Sillitoe, 1989). Rapid exhumation of the Wetar edifice continued and shallow marine conditions reworked locally the upper parts of the deposits producing minor cross-bedding structures within the barite sands (noted pre-mining). Sulphides are also reworked at the upper margin of the Lerokis zone 5 deposit where they still remain in-situ with volcanoclastic sediment. Based on calculated uplift rates, the Wetar edifice emerged from the Banda Sea at ~ 3 Ma, sub-aerial lahars generated along the central spine of Wetar and developed into extensive sub-aqueous debris flows, these units (up to 250 m in thickness in the Kali Kuning area) covered mineralised areas and filled topographic depressions, (see Figure 9.1; stage 3). Continued volcanism led to the generation of tuffs that are intercalated with these mass flows. Dips of the debris flow units range from flat lying to 50°, continued uplift post collision (2.4 Ma) of the Australian continental margin with the "outer" Banda arc has left the deposits some 250 m above present sea level.

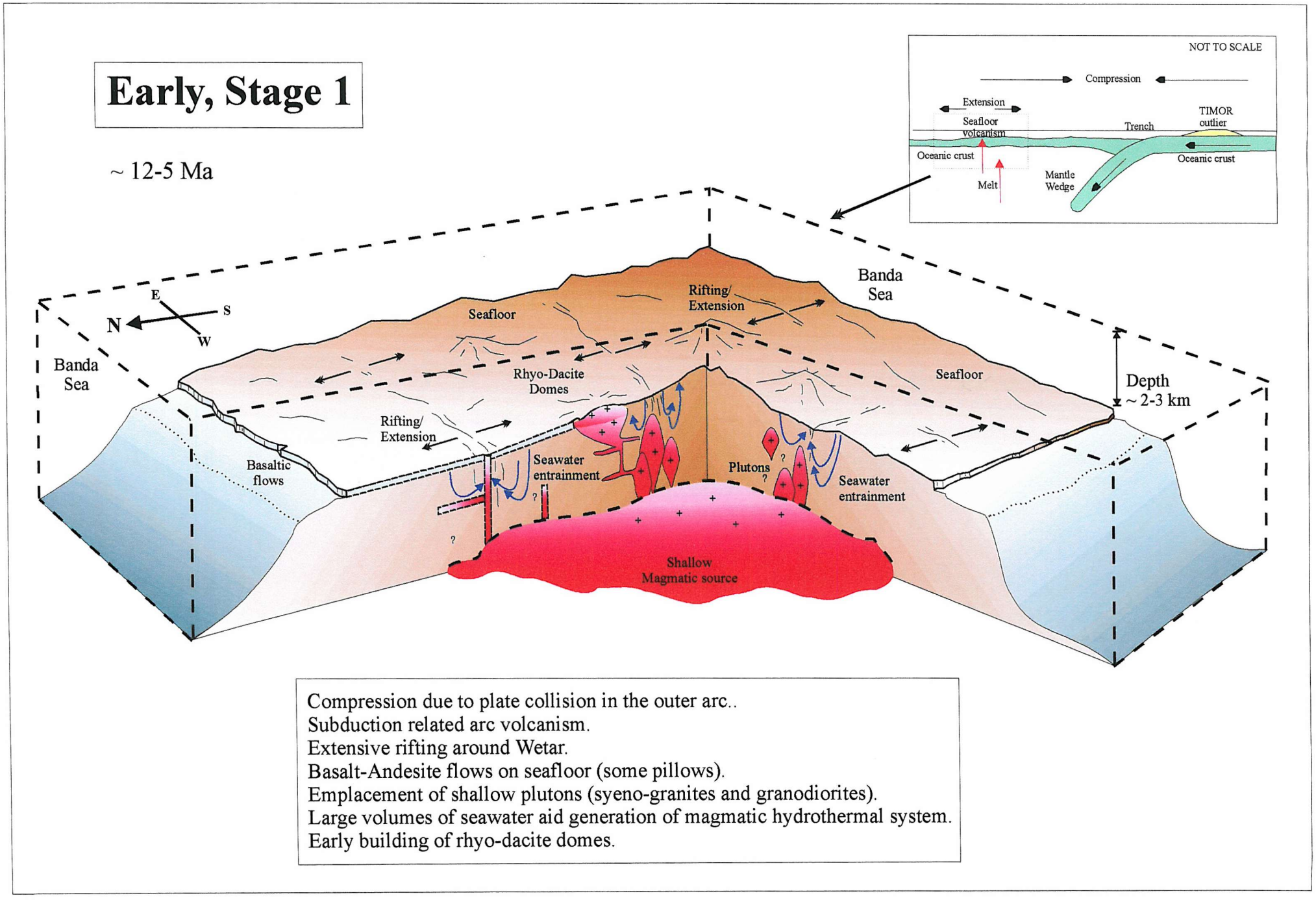
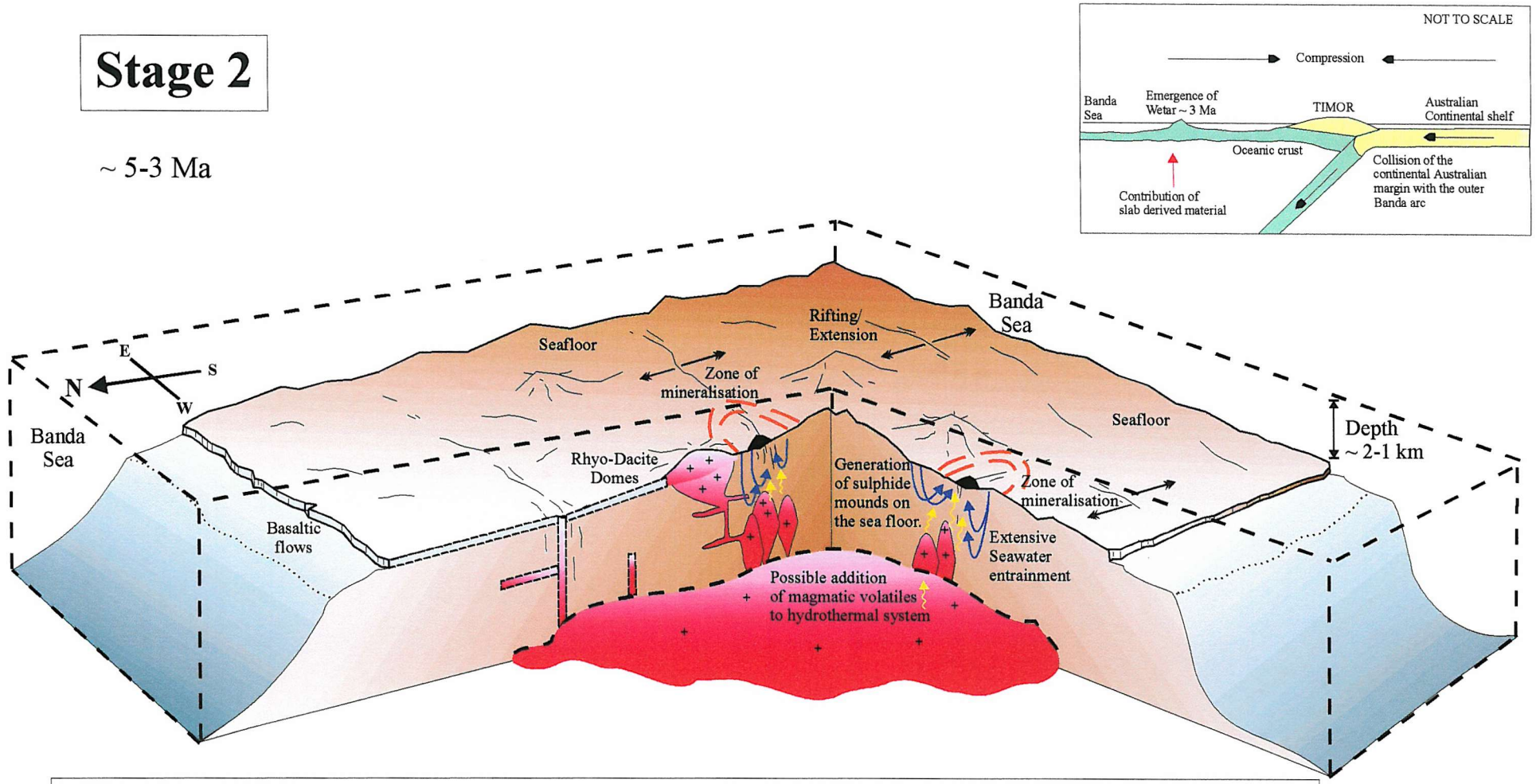


Figure 9.1. 3D evolution model of the Wetar Island ore deposits.



Focused fluid flow along major faults and at margins of dome structures.
Nascent mineralisation develops with subsequent generation of ore-deposits (c.f. with mineralisation model, Figure 9.2).
Minor addition of magmatic volatiles into hydrothermal system.
Associated hydrothermal alteration of host protoliths.
Rapid uplift of arc-edifice (related to slab detachment at depth and collision of the Australian margin with the outer arc).
Central Wetar emerges from the Banda Sea at ~ 3 Ma.
Shallow sea reworking of ore-deposits.
Post-mineralisation capping of deposits by volcanoclastics and sediments.

Figure 9.1. continued.

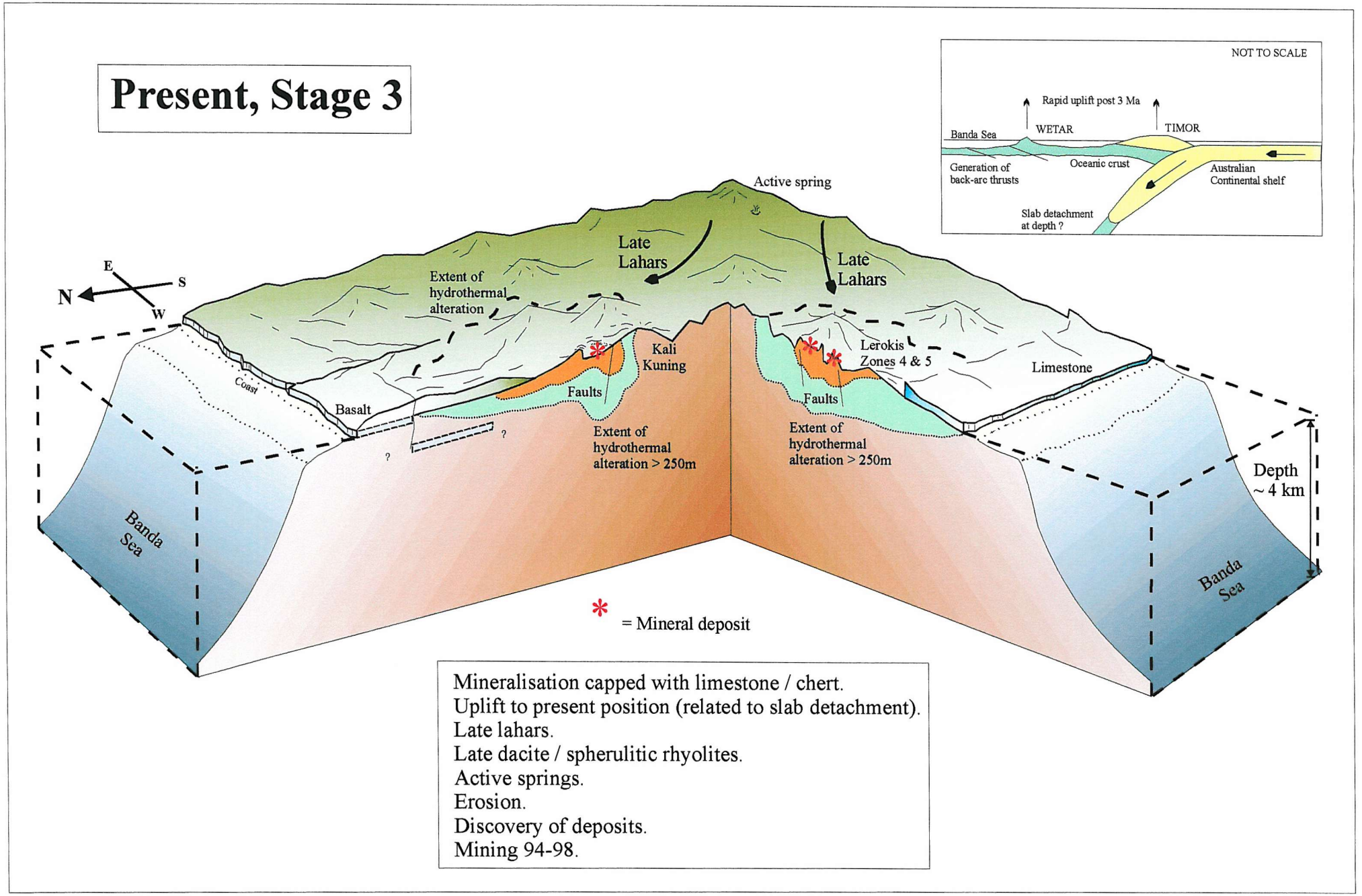


Figure 9.1. continued.

9.8.2 ORE-DEPOSIT EVOLUTION

Features of deposit evolution are illustrated in Figure 9.2 A-H. An early influx and downflow of cold seawater is promoted by fault initiation due to extensional tectonics within the developing island arc. At considerable depth the seawater is heated by intrusives and returns to the surface, leaching metals from the underlying basalts and basaltic-andesites, see Figure 9.1; stage 1 and Figure 9.2A. The dominance of Miocene seawater throughout the mineralisation has been confirmed by isotopic analysis. δ34S ratios of early disseminated stockwork sulphides reflect the host volcanic values as sulphur is leached through fluid / rock interaction, the hydrothermal system continues to develop thus resulting in extensive stockwork zones developing around fault intersections, thus providing a foci for mineralisation (Figure 9.2B and C). Continuation of hydrothermal activity results in the subsequent development of sulphide mounds as sulphur is leached from the underlying volcanics, these pyritic mounds develop at, or just below the sediment / sea-water interface and continue to grow from the base (Figure 9.2D and E). This interpretation is based fact that there is no evidence of exhalative style sulphides with intercalated sediments; chimney features are absent from the Wetar sulphide mounds suggesting they have been removed by recrystallisation of the sulphide mound or by mass wasting on the seafloor. This process explains the talus type features exposed at the base of the Kali Kuning sulphide mound. Pyrite / chalcopyrite are rapidly precipitated above the fluid conduit as the rapidly ascending hydrothermal plume vents into open water. The growth of the massive sulphide mound occurs at the seafloor, as hydrothermal plumes are buoyant and vent fluid velocities are high in many cases, phases may be lost to the ocean due to plume dissipation as a result of turbulence or slow moving currents. Pb and Zn may remain entrained within the hydrothermal plume due to slow precipitation and saturation (Solomon, 1979) especially if fluid temperature falls below 250°C. This may be the reason why Wetar has no Pb / Zn outer zone that many VMS's have as either vent velocity remains to high or currents sweep the plume away. Both $^{3}He/^{4}He$ and $\delta^{34}S$ values from the stockwork zones and sulphide mounds coupled with $^{87}Sr/^{86}Sr$ ratios of unaltered host volcanics reflect arc lava contamination and an input of sediment / continental derived material from the subducting Australian margin to the south. Post sulphide development, barium-rich, low pH fluids enter the

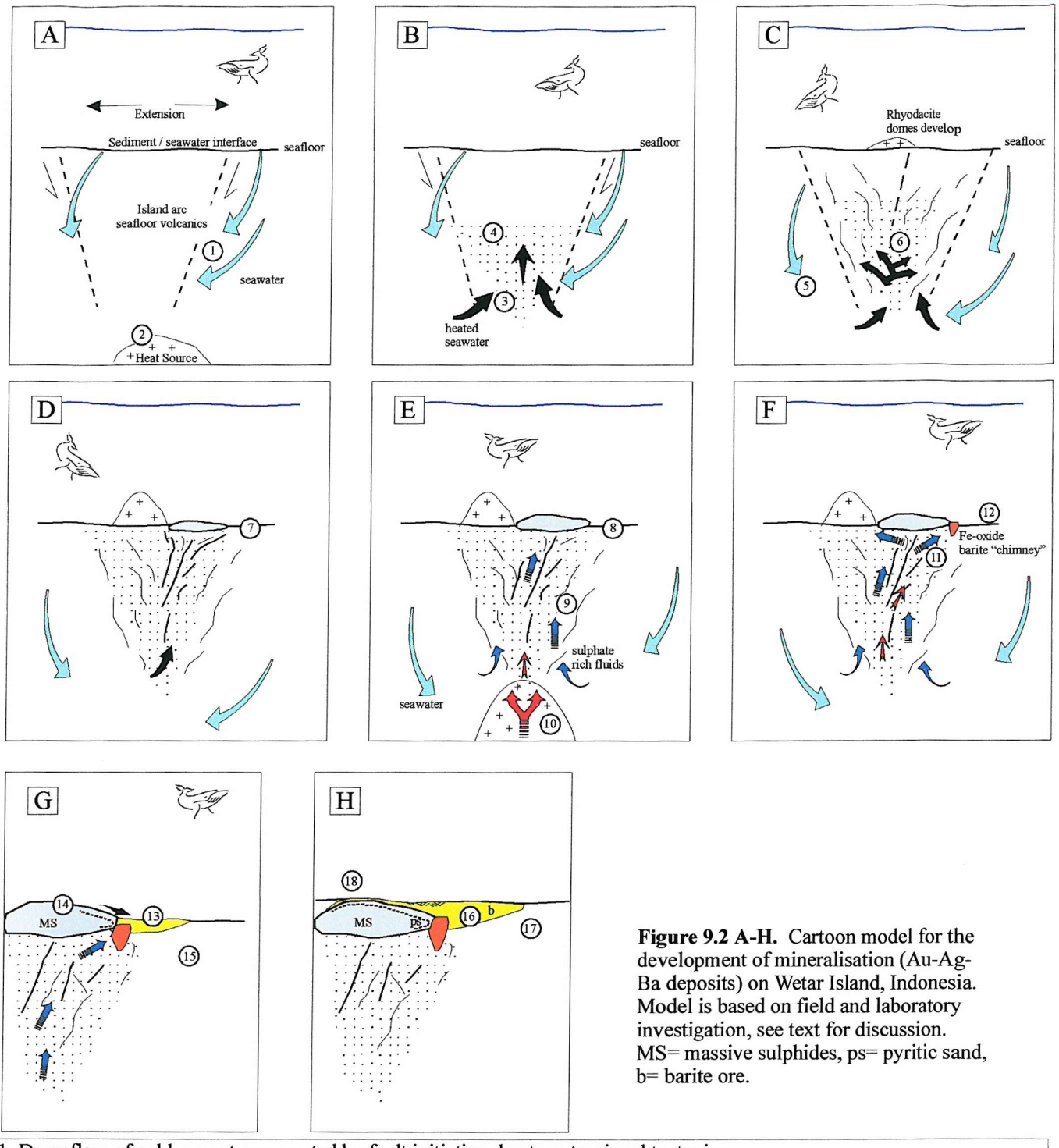


Figure 9.2 A-H. Cartoon model for the development of mineralisation (Au-Ag-Ba deposits) on Wetar Island, Indonesia. Model is based on field and laboratory investigation, see text for discussion. MS= massive sulphides, ps= pyritic sand, b= barite ore.

1 Downflow of cold seawater promoted by fault initiation due to extensional tectonics.
2 At considerable depth the seawater is heated.
3 Heated seawater returns to surface leaching metals from volcanic host lithologies: nascent hydrothermal convection.
4 Early precipitation of disseminated sulphides.
5 Hydrothermal system continues to develop with influx of large volumes of seawater.
6 Stockwork zones begin to develop.
7 Fault intersections provide a focus for mineralisation: development of sulphide mounds.
8 Sulphide mounds continue to grow from the base.
9 Late, barium-rich fluids enter the hydrothermal system, post sulphide precipitation. The fluids become progressively sulphide deficient as they exit or discharge onto the seafloor.
10 Minor input of magmatic volatiles enter the system at depth.
11 Barium-rich fluid (+/- magmatic volatiles) cannot pass through the sulphide mound: fluid exits at mound margin.
12 Development of Fe-oxide / barite "chimney" structures and early development of barite ore zones.
13 Possible ponding of dense, barium fluid, conductively cooled fluids undergo significant lowering of pH.
14 Barium-rich fluid begins to onlap the sulphide mounds and mechanically disintegrate the surface: development of the pyritic sands.
15 Acidic alteration occurs in the immediate footwall beneath barite ore zones, Au is related to this event..
16 Barite ores continue to develop which subsequently develops pyritic sands that interfinger with each other.
17 Residual silica develops in the immediate footwall to the barite ore, evident in all ore zones.
18 Uplift: shallower sea develops local reworking at the tops of sulphide mounds and produces some cross-lamination in the barite ore. Late oxidation: sulphides form oxides and arsenates; deposits are then covered by sediments / lahars.

hydrothermal system, $^{3}He/^{4}He$ ratios suggest a minor magmatic input / volatiles released from the underlying melt, see Figure 9.1, stage 2 and 9.2E. Significant lowering of the fluid pH occurs due to conductive cooling, these fluids exploit the same fluid conduits as the earlier sulphide rich hydrothermal fluids and discharge at temperatures of ~275°C and salinities of both above and below that of seawater which are typical ranges observed on seafloor white smoker systems and suggest phase separation at depth. These fluids may be sulphide poor due to extensive sulphide precipitation and replacement of the host stratigraphy prior to fluid discharge. It is plausible that these late fluids may be responsible for the *high-sulphidation* sulphide assemblage and associated advanced argillic alteration, typical features of many epithermal systems overlying porphyries which contain a contribution of magmatic volatiles (Figure 9.1, stage 2 and Figure 9.2E). The spatial field relationships between the sulphide mounds and barite feeder structures indicate that the impermeable nature (to a large degree) of the sulphide mounds restrict fluid flow and thus results in these late fluids having to exit at the mound margins with the development of the Fe-oxide / barite chimney structures and early development of barite ore zones, Figure 9.2F. This feature is clearly the case in Lerokis Zone 5 (Figures 5.1B and 5.12B). Barite that infiltrates the base of the pyritic mound fills any voids or fractures present, building of pressure below the sulphide mound causes brecciation of the hosting volcanics. Alteration assemblages within the stockwork zones suggest that the fluids are oxidised, the development of the barite ore zones at the margins of the sulphide mounds subsequently destroy the footwall host volcanics resulting in the development of adjacent residual silica and advanced argillic alteration assemblages in the immediate footwall (Figure 9.2G). Au is present within the stockwork zones beneath the sulphide mounds related to clay alteration assemblages and within the barite ores as free grains adhering to barite lath margins. As these barium-rich fluids begin to onlap the sulphide mounds, they mechanically destroy the surface of the sulphide mound leading to development of coarse pyritic sands and talus deposits. The barite ores continue to develop and thus subsequently develop interfingering of both barite and fine-grained pyritic material, (evident at Kali Kuning) cobbles of massive sulphide are also found within the barite ore particularly in the stratigraphically lower areas of the sulphide mound suggesting mass wasting of the sulphide mound is occurring at the same time as barite ore development. The field observation of barite ore occurring behind the sulphide mound at Kali Kuning as well as in front implies

that these fluids percolate around the entire sulphide margin and again suggest that the baritic ore fluids are late stage in deposit development. Clasts of residual silica (derived from the footwall) are incorporated within the cemented Fe-oxide barite feeder structure at Lerokis Zone 5, this intense alteration is also found in all deposits adjacent to and underlying the barite ore indicating partial replacement of the host volcanics by progressive acidic destruction. The incorporation of footwall clasts within the barite- Fe oxide structures, the similar microthermetric / isotopic data of barite from these features and the surrounding barite ores imply that these are the fluid feeder conduits for the deposits.

It may also be a possibility that the sulphide and barite ore development occurred with some degree of overlap, therefore both black and white smoker chimneys may have at some point vented together as are observed at the TAG and JADE deposits. The development of vertical layering within the barite ore based on colour observation in the field (evident at the sulphide mound / footwall contact zone at Kali Kuning, see Figure 7.6) are related to cementing phases and degree of oxidation. Generally the orange / brown coloured barite zones contain abundant Fe-oxides compared to white and yellow varieties containing a greater abundance of arsenates. Interestingly, no sulphide mound was present at Lerokis Zone 4, these may have been completely destroyed and replaced by the barite bodies or by analogy with Zone 5 and Kali Kuning; a sulphide body hidden at depth.

Uplift from depths of > 2 km (based on overlying limestone at Kali Kuning) to a shallower environment occurred post 3.9 Ma based on the upper limit constrained by the microfaunal assemblage. The development of complex-arsenate phases, which now cement the re-crystallised barite laths are possibly the result of oxidation of sulphides on the periphery of the sulphide mounds. This hypothesis is supported by the presence of anglesite pseudomorphs which occur as a cementing phase within the barite ore. Anglesite pseudomorphs are also present as cementing phases within the barite sands at Lerokis Zone 4, (where no sulphide mound was present) clearly indicative that sulphides are involved in mineral paragenesis at all deposits.

The fine-grained tabular nature of barite within the barite sand deposits suggests late recrystallisation perhaps related to the formation of the barite sand cementing phases, present day hydrothermal activity is still ongoing with hot springs present at Ilwaki.

Chapter 10

CONCLUSIONS

- Wetar Island is located in the eastern inner Banda Arc where back arc thrusting has initiated to accommodate collision between the Australian continental margin and the outer Banda Arc.

- Centres of mineralisation at Kali Kuning (KK3), Lerokis and Meron occur within hydrothermally altered volcanics and breccias and are spatially marginal to rhyodacite domes that overly tholeiitic ocean floor basalts and extensive andesitic flows. Orebodies occur within the same stratigraphic horizon at different heights related to regional fault trends. Extensive (> 200m) post-mineralisation lahars and sub-aqueous debris flows cover much of the deposits. Post-mineralisation lithologies also include *globigerina* bearing limestones, cherts, tuffs, volcanoclastic sediments, dacites and spherulitic rhyolites.

- Calculated uplift rates based on the overlying *globigerina* bearing limestone are in the order of 42-57 cm/ka^{-1} which are consistent with uplift rates from other areas of the Banda arc.

- Zones of advanced argillic alteration and residula silica are located proximal to the ore zones and within the immediate footwall, propylitic zones are present laterally and at increasing depth reflecting mixing of highly acidic fluid and Miocene seawater adjacent to upflow zones. The dominant alteration assemblage around the deposits is comprised of illite-kaolinite-smectite assemblages.

- Lithogeochemistry defines at least for distinct volcanic groups within the Wetar Island volcanic stratigraphy.

- The Au-Ag-Hg bearing barite deposits onlap and are adjacent to the massive sulphide mounds at Kali Kuning and Lerokis Zone 5, they completely surround the massive pyritic mound at Kali Kuning however no sulphide mound is associated with the barite ore at Lerokis Zone 4. The barite deposits are late stage in formation compared to the sulphide mounds, their generation has mechanically destroyed the margins of the pyrite mounds at both Kali Kuning and Lerokis Zone 5 thus forming the intervening pyritic sands.

- Massive sulphide mounds are asymmetric and are dominantly pyrite. The pyrite is arsenian, (up to 6.7wt% As) chalcopyrite is present in minor amounts but more abundant at mound margins, marcasite occurs in some samples however sphalerite and galena are rare to absent. No other vertical or lateral mineralogical zonation is observed.

- Massive sulphide mounds are discordant features that are structurally controlled, only minor evidence suggests upper sections of the mounds were at or on the seafloor. Features within the underlying stockwork suggest partial replacement of the host volcanics. Brecciated massive sulphides and talus deposits occur in lower parts of the Kali Kuning deposit and at mound margins through mass-wasting of the sulphide mound.

- Stockwork zones underlie sulphide mounds to depths greater than 250 m, a pyrite, chalcopyrite, Fe-poor sphalerite, tennantite, barite assemblage is observed, galena is present as a minor phase. Intense zones of brecciated host volcanics are present where sulphide veining is most prominent. Chalcopyrite is more abundant within the feeder zone under Lerokis Zone 5.

- The barite deposits are cemented by a series of complex arsenate phases including arsendescloizite, mimetite, karibibite or schneiderhöhnite plus anglesite and amorphous Fe-oxides, Ag is closely associated with mimetite. Colour variation within the barite ore corresponds to cementing phases and degree of oxidation.

- Linear and pipe-like cemented barite Fe-oxide structures are evident at Kali Kuning, Lerokis Zone 4 and 5 microthermetric and isotopic data indicates that these are hydrothermal fluid feeders conduits for the barite deposits.

- Barite ores formed by precipitation from a seawater dominated fluid at temperatures of ~ 275°C. Fluid inclusions in barite from the ores show no evidence of boiling, the data indicates similarities to seafloor white smokers.

- *High-sulphidation* sulphide assemblages (covellite, chalcocite, tennantite-tetrahedrite, bornite, enargite, Fe-poor sphalerite) fill a fracture network that permeates through the massive pyrite mounds and underlying stockworks. These are relatively minor in abundance. Isotopic data on co-genetic barite associated with these sulphides indicate that they are of hypogene origin and not due to supergene enrichment.

- Stable isotopes suggest hydrothermal fluids are dominantly composed of Miocene seawater, the sulphide mounds are derived by leaching of sulphur from the underlying volcanics.

- Stable and radiogenic isotopes confirm that mineralisation hosting volcanics and younger volcanics indicate contamination from subucted continental material derived from the Australian margin to the south. Along arc variations in isotopic ratios confirm that the most contamination occurs in the area of the Banda Arc in the Wetar region.

- $^{40}Ar/^{39}Ar$ dating of biotite grains from a syeno-granite intrusion from the Meron area yielded a Zanclian age of 4.72 Ma ±0.22 which is consistent with syn-volcanic mineralisation. A hydrothermally altered illite sample from the footwall of the Lerokis deposit gave an $^{40}Ar/^{39}Ar$ age of 4.52 Ma ±0.22 which is consistent with that of the published K-Ar age of 4.7 Ma ±0.16 (Herrington, 1993).

- Biotites from an overlying dacitic flow at Meron yielded a Piacenzian age of 2.4 Ma ±0.28 thus indicating that volcanism continued on the island post locking between the continental margin of Australia and the outer non-volcanic arc. These post mineralisation dacites record this collision event, Sr values are radiogenic and record a strong sediment / continental signature within the volcanics. Mineralisation hosting volcanics are also modified by subduction related contaminants.

- Syeno-granite intrusives feed dacite domes and supply heat to the mineralising system.

- The Wetar Island deposits are an unusual VMS hybrid type involving two separate stages of mineralisation, stable and radiogenic isotopes confirm a minor magmatic contribution to mineralisation.

FUTURE WORK / RECOMMENDATIONS

- Attempt Ar/Ar dating of K-bearing, barite ore cementing phases ie) plumbojarosite to assess whether oxide assemblages are contemporaneous with the footwall alteration assemblages.

- Use the same whole rock sample set analysed for Strontium to test for Nd and O, this may allow modelling the role of subducted slab, continental material and sediments in arc lava generation.

- Obtain footwall illite separates from Lerokis Zone 4 and Kali Kuning to see if they are contemporaneous with the age of mineralisation at Lerokis Zone 5.

- Follow up on other mineralised sites on Wetar where *high-sulphidation* alteration is indicated to assess the relationship to intrusive bodies.

- Undertake a regional study of the island to better establish the geological framework of the host volcanic suite.

- Separate alunite for isotopic and dating studies to assess whether hypogene / supergene and its relationship to magmatic volatiles.

- Assess arc terrains and associated rifts for rhyodacite domes that overly mafic volcanics for the presence of sulphide-barite mineralsistion where footwall volcanics show evidence of advanced argillic alteration.

- Explore for deposits in arc environments where evidence of a change in subucted material occurs or arc reversal.

- Investigate hydrothermal alteration effects on felsic volcanism and contrast to mafic volcanism.

References

Abadi, P.S., 1996, Mine planning at Kali Kuning pit, PT. Prima Lirang Mining, Indonesia: Internal Unpublished Company Report, p. 8.

Abbott, M.J., and Chamalaun, F,H., 1981, Geochronology of some Banda ac volcanics: In Geology and Tectonics of Eastern Indonesia, (eds) Barber, A.J., Indonesia. Geological. Research And Development. Centre. Spec. Publ. 2, p. 253-268, Bandung.

Alt, J.C., 1988, The chemistry and sulfur isotope composition of massive sulfide and associated deposits on Green Seamount, eastern Pacific: Economic Geology v. 83, p.1026-1033.

Alt, J.C., and Teagle, D.A.H., 1998, Probing the TAG hydrothermal mound and stockwork: Oxygen-isotopic profiles from deep ocean drilling: in Herzig, P.M., Humphries, S.E., Miller, D.J., and Zierenberg, R.A.,ed.,Proceedings of the Ocean Drilling Program, Scientific results, v. 158 (21), p. 285-295.

Alt, J.C., Teagle, D.A.H., Brewer, T., Shanks III, and Haliday, A., Alteration and mineralization of an oceanic forearc and the ophiolite-ocean crust analogy: Journal of Geophysical Research, v. 103, B6, p. 12365-12380.

Alt, J.C., 1994, A sulfur isotopic profile through the Troodos ophiolite, Cyprus, Primary composition and the effects of seawater hydrothermal alteration: Geochimica et Cosmochimica Acta, v. 58, p. 1825-1840.

Alt, J.C., Shanks III, W.C., and Jackson, M.C., 1993, The geochemistry of sulfur in the Mariana Island Arc and back-arc trough: Earth and Planetary Science Letters 119, p. 477-494.

Arehart, G.B., Chryssoulis, S.L., and Kesler, S.E., 1993, Gold and arsenic in iron sulphides from sedimented-hosted disseminated gold deposits: Implications for depositional processes: Economic Geology, 88, p. 171-185.

Arribas, (Jr) A., 1995, Characteristics of high-sulphidation epithermal deposits and their relationship to magmatic fluid: In Magmas, Fluids and Ore Deposits ed., Thompson J.F.H. Min. Assoc. of Canada, Short Course Series, p. 419-454.

Asadi, H.H., Voncken, J.H.L., and Hale, M., 1999, Invisible gold at Zarshuran, Iran: Economic Geology, 94, p. 1367-1374.

Audley-Charles, M.G., 1986, Timor-Tanimbar Trough, the foreland basin of the evolving Banda orogen: Special Publication, Int. Association Sediment. 8, p. 91-102.

Audley-Charles, M.G., 1986b, Rates of Neogene and Quaternary tectonic movements in the southern Banda Arc based on micropalaeontology: Journal of the Geological Society, London, 143, p. 161-175.

Barber, A.J., and Brown, K., 1988, Mud diapirism, the origin of melanges in accretionary complexes? : Geology Today, May, p. 89-94.

Barriga, F.J.A.S.,1990, Metallogesis in the Iberian pyrite belt: In Dallmeyer, R.D., and Martinez Garcia, eds., Pre-Mesozoic Geology of Iberia: Berlin, Springer-Verlag, p. 369-379

Bendel, V., Auzende, J.M., Lagabrielle, Y., Grimaud, D., Fouquet, Y., and Urade, T., 1993, The White Lady hydrothermal site in the north Fiji Basin, Economic Geology, 88, p. 2237-2249.

Binns, R.A., Scott, S.D., Bogdanov, Y.A., Lisitzin, A.P., Gordeev, V.V, Gurvich, E.G., Finlayson, E.J., Boyd, T., Dotter, L.E., Wheller, G.E. and Muravyev, K.G., 1993, Hydrothermal Oxide and Gold-Rich Sulfate Deposits of Franklin Seamount, Western Woodlark Basin, Papua New Guinea: Economic Geology v. 88, p. 2122-2153.

Binns, R.A., Parr, J.M., Scott, S.D., Gemmell, J.B., and Herzig, P.M, 1995, PACMANUS: An active seafloor hydrothermal field on siliceous volcanic rocks in the eastern Manus Basin, Papua New Guinea: In PACRIM 95, p. 49-54.

Binns, R.A., and Scott, S.D., 1993, Actively forming polymetallic sulfide deposits associated with felsic volcanic rocks in the Eastern back-arc basin, Papua New Guinea: Economic Geology 88, p. 2226.

Binns, R.A., Scott, S.D., Gemmell, J.B., and Crook, K.A.W., 1997, The SuSu Knolls hydrothermal field, Eatern Manus Basin, PNG: Abstracts from the American Geophysical Union Fall conference, 1997, San Fransisco EOS Transactions AGU, v.78, no. 46

Bischoff, J.L., and Rosenbauer, R.L., 1984, The critical point and two-phase boundary of seawater, 200-500°C: Earth and Planetary Science Letters, 68, p. 172-180.

Bluth, G.J., and Ohmoto, H., 1988, Sulfide-Sulfate chimneys on the East Pacific Rise, 11 and 13N latitudes, part II, Sulfur Isotopes: Canadian Mineralogist, v.26, p. 505-515.

Bodnar, 1993, Revised equation and table for determining the freezing point depression of H2O-NaCl solutions: Geochima et Cosmochima Acta, 57, p. 683-684.

Booler, J., 1997, Gunung Botak prospect, Wetar Island, results of 1996 work program: Unpublished Company Report, p.18.

Bowin, C., Purdey, G.M., Johnson, C., Shor, G., Lawver, L., Hartono, H.M.S., and Jazek, P., 1980, Arc-continent collision in the Banda Sea region: AAPG Bulletin, 64, p. 868-915.

Brathwaite, 1999, Hydrothermal fluid mixing and boiling in the Waihi epithermal gold-silver deposit, New Zealand: Mineral Deposits, Processes to Processing, Stanley et al., (eds) Balkema, Rotterdam, p. 25-28.

Breen, N.A, and Silver, E.A., 1989, The Wetar back arc thrust belt, eastern Indonesia, The effect of accretion against an irregularly shaped arc: Tectonics, 8, 1, p. 85-98.

Budino, J., and Santoso, I., 1996, PT Prima Lirang Mining, Meron Resource Calculation, February, 1996: Unpublished Company Report, p.13.

Burnard, P.G., Hu, R., Turner, G., and Bi, X.W., 1999, Mantle, crustal and atmospheric noble gases in Ailaosham Gold deposits, Yunnan Province, China: Geochimica et Cosmochimica Acta, Vol, 63, p. 1595-1604.

Butler, I.B., Fallick, A.E., Nesbitt, R.W., 1998, Mineralogy, sulphur isotope geochemistry and the development of sulphide structures at Broken Spur hydrothermal vent site, 2910'N, Mid-Atlantic Ridge: Journal of the Geological Society, London, v. 155, p. 773-785.

Butterfield, D.A., and Massoth, G.L., 1994, Geochemistry of north Cleft segment veny fluids, temporal changes in chlorinity and their possible relation to recent volcanism: Journal of Geophys Research 99, p. 4951-4968.

Cann, J.R., 1970, Rb, Sr, Y, Zr and Nb in some Ocean floor basalts: Earth and Planetary Science Letters, v. 10, p. 7-11.

Callaghan, T., 2001, Geology and host-rock alteration of the Henty and Mount Julia gold deposits, Western Tasmaina: Economic Geology, v. 96, p. 1073-1088

Campbell, A.R., and Larson, P. B., 1998, Isotope applications in hydrothermal systems, Society of Economic Geologists Review; v. 10, p. 173-193.

Cardwell, R.K., and Isacks B.L., 1978, Geometry of the subducted lithosphere beneath the Banda Sea in eastern Indonesia from seismicity and fault plane solutions: Journal of Geophysical Research, 87, p. 2825-2838.

Carlile, J.C., and Mitchell, A.H.G., 1994, Magmatic arcs and associated gold and copper mineralisation in Indonesia: Journal of Geochemical Exploration, 50, p. 91-142.

Carvalho, D., 1979, Geologa, metalogenia e metodologia da investigação de sulfuretos polimetálicos do sul de Potugal: Comunicações Serviços Geológicos Portugal, Lisboa, v. 65, p. 169-191

Cathless, L.M., Guber, A.L., Lenagh, T.C., and Dudas, F.O., 1983, Kuroko-type massive sulfide deposits of Japan, Products of an aborted island-arc: Economic Geology Monograph 5, p. 96-114.

Chamalaun, F.H., and Grady, A.E., 1978, The tectonic development of Timor, a new model and its implications for petroleum exploration: Australian Petroleum Exploration Association Journal, 18, p. 102-108.

Chappel, J.A., and Veeh, H.H., 1978, Late Quaternary movements and sea-level changes at Timor and Atauro islands: Bulletin Geological Society America, 89, p. 356-368.

Charlton, T.R., 1991, Postcollision extension in arc-continent collision zones, eastern Indonesia: Geology, 19, 28-31.

Chao-Shing L., and McCabe, R., 1986, The Banda-Celebes-Sulu basin, a trapped piece of Cretaceous-Eocene oceanic crust?: Nature, 322, p. 51-54.

Chiba, H., Uchiyama, N., and Teagle, D.A.H., 1998, Stable isotope study of anhydrite and sulfide minerals at the TAG hydrothermal mound, Mid-Atlantic Ridge, 26°N[1]: in Herzig, P.M., Humphries, S.E., Miller, D.J., and Zierenberg, R.A.,ed.,Proceedings of the Ocean Drilling Program, Scientific results, v. 158 (6), p. 85-90.

Clarke, S.H.B., Gray, K.J., and Back, J.M., 1999, Geology of the Barite Hill Gold-Silver Deposit in the Southern Carolina Slate Belt: Economic Geology, v. 94, 8, p. 1329-1347.

Clifford, M.J., 1993, Meron prospect outline drilling, September – December, v. 1of 6, Unpublished Company Report, p.28.

Claypool, G.E., Hosler, W.T., Kaplan, I.R., Sakai, H., and Zak, I., 1980, The age curves of sulfur and oxygen isotopes in marine sulfate and their mutual interpretation: Chemical Geology, 28, p. 199-260.

Cooper, M., 1995, Lau Basin Hydrothermal Vent Fluids, Neodymium Isotopic Compositions from Hydrothermal Fluids, unpublished laboratory rpt, IFREMER, centre de Brest

Costantinou, G., 1973, Geology, geochemistry and genesis of Cyprus sulphide deposits: Economic Geology, 68, p. 843-858.

Dejong, J.D., 1941, Geological investigations in West Wetar, Lirang and Solor: *in:* Geological Expedition Lesser Sunda Islands under leadership of H.A. Brouwer, Vol 3. Noord Holland, Amsterdam, p. 241-380.

De Hoog, J.C.M., Taylor, B.E., and van Bergen, M.J., 2001, Sulfur isotope systematics of basaltic lava from Indonesia, implications for the sulfur cycle in subduction zones: Earth and Planetary Science Letters 189, p. 237-252.

De Roever, E.W.F, 1991, Characterisation of the mercury bearing phases in the main ore types of the Lerokis gold-silver deposit, Indonesia, PLM report: Internal Unpublished Company Report, p. 26.

De Roever, E.W.F., and Besseling, A.J., 1991, Mineralogical investigation of gold-bearing copper ore from Kali kuning and Lerokis, Indonesia: Internal Unpublished Company Report, OD/91/24 p. 13.

de Ronde, C.E.J., 1995, Fluid chemistry and isotopic characteristics of seafloor hydrothermal systems and associated VMS deposits: Potential for Magmatic Contribution: In Magmas, Fluids and Ore Deposits Ed Thompson J.F.H. Min. Assoc. Canada, Short Course Series, p. 479-509.

de Ronde, C., Hannington, M., Stoffers, P., Wright, I., Gennerich, H.H., Browne, P., and Herzig, P., 2000, Massive sulfide mineralisation associated with a frontal arc volcano: Brothers hydrothermal system, Southern Kermadec Arc, New Zealand: In Volcanic Environments and Massive Sulfide Deposits Conference, Tasmania, Australia, p. 37-38.

De Smet, M.E.M., Fortuin, A.R., Tjokrosapoetro, S., and Van Hinte, J.E., 1989, Late Cenezoic vertical movements of the non-volcanic islands in the Banda Arc area: Netherlands Journal of Sea Research, 24, p. 263-275.

Duckworth, R.C., Fallick, A.E., and Rickard, D., 1994, Mineralogy and sulphur composition of the Middle Valley Massive Sulfide Deposit, Northern Juan de Fuca Ridge: Proceedings of the Ocean Drilling Program, Scientific Results, v. 139, p. 373-386.

Edmond, J.M., Campbell, A.C., Palmer, M.R., German, C.R., Klinkhammer, G.P., Edmonds, N.H., Elderfield, H., Thompson, G., and Rona, P., 1995, Time series studies of vent fluids from the TAG and MARK sites: Mid Atlantic Ridge: a new solution chemistry model and mechanisms for Cu/Zn zonation in massive sulfide ore bodies: In Parson, L.M., Walker, C.L., and Dixon, D.R., eds, Hydrothermal Vents and Processes, Geological Society Special Publication, London, 87, p. 77-86.

Embley, R.W., Jonasson, I.R., Perfit, M.R., Franklin, J.M., Tivey, M.A., Malahoff, A., Smith, M.F., and Francis, T.J.G., 1988, Sibmersible investigation of an extinct hydrothermal system on the Galapagos Ridge, sulfide mounds, stockwork zone and differentiated lavas: Canadian Mineralogist, 26, p. 517-539.

Eva, C., Cattaneo, M., and Merlanti, F., 1988, Seismotectonics of the central segment of the Indonesian arc: Tectonophysics, 146, p. 241-249.

Fander, H.W., 1991, *Copper mineralogy and grain size relationships from Kali Kuning*: Unpublished Internal Company report, PLM, p. 2.

Farmer, C., and Clifford, M., 1993, Exploration status, Wetar Island, Indonesia: Unpublished Company Report, p.11.

Farrell, C., Holland, H.D., and Petersen, U., 1978, The isotopic composition of strontium in barites and anhydrites from Kuroko deposits: Mining Geology, v. 28, p. 281-291.

Faure, G., 2001, Origin of Igneous Rock – The Isotopic Evidence: Springer Verlag, p. 496.

Fouquet, Y., von Stakelberg, U., Charlou, J.L., Erzinger, J., Herzig, P.M., Mühe, R., and Wiedicke, M., 1993, Metallogenesis in back-arc environments, the Lau Basin example: Economic Geology 88, p. 2154-2181.

Fouquet, Y., von Stakelberg, U., Charlou, J.L., Donoval, J.L., Erzinger, J., Foucher, J.P., Herzig, P.M., Muhe, R., Soakai, S., Wiedicke, M., and Whitechurch, H., 1991, Hydrothermal activity and metallogenesis in the Lau back-arc basin: Nature, 338, p. 778.

Fournier, R.O., 1985, The behavior of silica in hydrothermal solutions: in Geology and Geochemistry of Epithermal systems, Berger, B.R., and Bethke, P.M., eds., Reviews in Economic Geology, 2, p. 45-61.

Franklin, J.M., 1996, Volcanic-associated massive sulfide base metals: In Geology of Canadian Deposits Types, Eckstrand, O.R,., Sinclair, W.D., and Thorpe, R.I., eds Geological Survey of Canada, Geology of Canada, 8, p. 158-813.

Franklin, J.M., Hannington, M.D., Jonasson, I.R., and Barrie, C.T., 1998, Arc-related volcanogenic massive sulphide deposits: In: Metallogeny of Volcanic Arcs, B.C. Geological Survey Short Course Notes, Open File 1998-8, section N.

Franklin, J.M., Lydon, J.W., and Sangster, D.F., 1981, Volcanic-associated massive sulfide deposits, Economic Geology 75th Anniversary Volume, p. 485-627.

Franklin, J.M., 1996, Volcanic-associated massive sulphide base metals: In Geology of Canadian Mineral Deposit Types, Geological Survey of Canada 8, p. 158-183.

Galley, A.G., Koski, R.A., 1999, Setting and characteristics of ophiolite-hosted volcanogenic massive sulfide deposits: Reviews in Economic Geology, v. 8, p. 221-246.

Gamberi, F., Marani, M.P., Parr, J.M., and Binns, R A., 1999, Sub-seafloor minerisation at the Panarea shallow-water platform, Aeolian volcanic arc, Italy: Mineral Deposits: Processes to Processing, Stanley et al. eds, Balkema, Rotterdam, p. 499-502

Gamo, T., Okamura, K., Charlou, J., Urabe, T., Auzende, J., Ishibashi, J., Shitashima, K., and Chiba, H., 1997, Acidic and sulfate-rich hydrothermal fluids from the Manus back-arc basin, Papua New Guinea: Geology, v. 25, n. 2, p. 139-142.

Garwin, S.L., and Herryansyah, 1995, Geological setting, style and exploration of gold-silver mineralisation on Romang Island, Indonesia: Ashton Group Report, Indonesia, p. 258-274.

Gemmell, J.B., Binns, R.A., and Parr, J.M., 1999, Submarine, high sulphidation alteration within DESMOS caldera, Manus basin, PNG: In Mineral Deposits: Processes to Processing, Stanley et al., (eds), Balkema, Rotterdam.

Gemmell, J.B., and Fulton, R., 2001, Geology, genesis, and exploration implications of the footwall and hanging-wall alteration associated with the Hellyer volcanic-hosted massive sulfide deposit, Tasmania, Australia: Economic Geology, v. 96, p. 1003-1035

Gemmell, J.B., and Sharpe, R., 1998, Detailed sulfur-isotope investigation of the TAG hydrothermal mound and stockwork zone, 26°N, Mid-Atlantic Ridge: in Herzig, P.M., Humphries, S.E., Miller, D.J., and Zierenberg, R.A.,ed.,Proceedings of the Ocean Drilling Program, Scientific results, v. 158 (5), p. 71-84.

Genrich, J., Bock, Y., McCaffrey, R., Calais, E., Stevens, C., et al., 1994, Kinematics of the eastern Indonesian island arc estimated by global positioning system measurements: EOS Abstracts, 75, p. 162.

Goodfellow, W.D., and Franklin, J.M., 1993, Geology, mineralogy and chemistry of sediment-hosted clastic massive sulfides in shallow core, Middle Valley, Northern Juan de Fuca Ridge: Economic Geology, v. 88, p.2037-2069.

Halbach, P., Blum, N., Münch, U., Plüger, W., Garbe-Schönberg, D., and Zimmer, M., 1998, Formation and decay of a modern massive sulphide deposit in the Indian Ocean: Mineralium Deposita, 33, p. 302-309.

Halbach, P., Wahsner, M., Kaselitz, L., Sakai, H., and Hein, U., 1989, The Jade hydrothermal field in the Okinawa Trough-first discovery of massive sulphides in an intercontinental back-arc basin: Proceedings of the 6th International Symposium on Water-Rock-Interaction, p. 279-283.

Halbach, P., Pracejus, B., and Marten, A., 1993, Geology and mineralogy of massive sulphide ores from the Central Okinawa Trough, Japan: Economic Geology, 88, p. 2210-2225.

Hall, R., 1996, Reconstructing Cenezoic SE Asia, *in* Hall, R., and Blundell, D., ed., Tectonic evolution of southeast Asia: Geological Society Special Publication No. 106, p. 153-184.

Hamilton, W., 1979, Tectonics of the Indonesian region: U.S. Geological Survey, Professional Paper 1078, p. 1-345.

Hannington, M.D., and Herzig, P.M., 2000, Submarine epithermal deposits and the VMS-epithermal transition: a new exploration target: In Volcanic Environments and Massive Sulfide Deposits Conference, Tasmania, Australia, p. 75-77.

Hannington, M.D., Poulsen, K.H., Thompson, J.F.H., and Sillitoe, R.H., 1999, Volcanogenic Gold in the Massive Sulfide Environment, In Volcanic-Associated Massive Sulfide Deposits, Processes and Examples in Modern and Ancient Settings: Reviews in Economic Geology, v.8, p. 325-356.

Hannington, M.D., Galley, A.G., Herzig, P.M., and Petersen, S., 1998, Comparison of the TAG mound and stockwork complex with Cyprus-type massive sulfide deposits: in Herzig, P.M., Humphries, S.E., Miller, D.J., and Zierenberg, R.A.,ed.,Proceedings of the Ocean Drilling Program, Scientific results, v. 158 (4), p. 389-415.

Hannington, M.D., 1997, The porphyry-epithermal-VMS transition: Lessons from the Iskut River area, British Columbia, and Modern Island Arcs: Economic Geology Commentary, SEG Newsletter, No 29, p.12-13.

Hannington, M.D., and Scott, S.D., 1989, Sulfidation equilibria as guides to gold mineralization in volcanogenic massive sulfides, Evidence from sulfide mineralogy and the composition of sphalerite: Economic Geology, v. 84, p. 1978-1995.

Hannington, M.D., and Scott, S.D., 1989, Gold mineralization in volcanogenic massive sulfides: Economic Geology Monograph 6, p. 491.

Harris, R.A., 1992, Peri-collisional extension and the formation of Oman-type ophiolites in the Banda arc and Brooks Range, *in* Parson, L.M., Murton, B.J., and Browning, P., ed., Ophiolites and their Modern Oceanic Analogues: Geological Society Special Publication No. 60, p. 301-325.

Hatfield, R., and Budiono, J., 1995, PT Prima Lirang Mining, Lerokis – Kali Kuning Deep Drilling Programme, May – October: Internal Unpublished Company Report, 12/93/01 p. 1-10

Hawkins, J., Lonsdale, P.F., Macdougall, J.D., and Vope, A.M., 1990, Petrology of the axial ridge of the Mariana Trough back arc spreading center: Earth and Planetary Science Letters, 100, p. 226-250

Hayba, D.O., Bethke, P.M., Heald, P., and Foley, N.K., 1985, Geologic, mineralogic and geochemical characteristics of volcanic hosted epitherma precious metal deposits: Reviews in Economic geology 2, p. 129-167.

Heald, P., Foley, N.K. and Hayba, D.O., 1987, Comparative anatomy of volcanic hosted epithermal deposits: Acid sulphate and adularia-sericite types; Economic Geology, v. 82, p. 1-26.

Hedenquist, J.W., 1987, Mineralisation associated with volcanic-related hydrothermal systems in the circum-Pacific Basin: In Trans. of the fourth Circum-Pacific Energy and Min. Resources Conf. *A.A.P.G.* p. 513-524.

Hedenquist, J.W., and Lowenstern, J.B., 1994, The role of magmas in the formation of hydrothermal ore deposits: Nature, v. 370, p. 519-527.

Heering, J., 1941, Geological investigations in East Wetar, Alor and Poera Besar, *In*: Geological Expedition Lessre Sunda Islands under leadership of H.A. Brouwer, Vol 4. Noord Holland, Amsterdam, p. 125.

Heesterman, L.J.L., 1992, The Regional Geology of Wetar: Unpublished Company Report, p.30.

Hekinian, R., Francheteau, J., Renard, V., Ballard, R.D., Choukroune, P., Cheminée, J.L., Albarède, F., Minster, J.F., Marty, J.C., and Boulègue, J., 1983, Intense hydrothermal activity at the axis of the East Pacific Rise near 13°N; submersible witnesses the growth of a sulfide chimney. Marine Geophys. Research, 6, p. 1-14.

Hemley, J.J., Montoya, J.W., Marinenko, J.W., and Luce, R.W., 1980, Equilibria in the system Al2O3-SiO2-H2O and some general implications for alteration / mineralization processes: Economic Geology 75, p. 210-228.

Herrington, R.J., 1993, Interim Petrological Report for the Billiton Companies in Indonesia: Internal Unpublished Company Report, 12/93/01 p. 1-17.

Herrington, R.J., 1993b, Interim Report for the Billiton Companies in Indonesia: Internal Unpublished Company Report, 12/93/05 p. 1-22.

Herrington, R.J., 1995a, Geochemical Report for the Billiton Companies in Indonesia: unpubl. Rpt. 12-95-03, p. 12.

Herrington, R.J., 1995b, Mineralogical note on the Wetar barite sand unit for the Billiton Companies in Indonesia: Internal Unpublished Company Report, 12/95/04 p. 1-4.

Herrington, R.J., 1996, Geochemical and Petrological Report for the Billiton Companies in Indonesia: Internal Unpublished Company Report, 12/96/02 p. 1-17.

Herrington, R.J., and First, D., 1996, Massive sulphide and barite-gold mineralisation on Wetar Island, Indonesia, VMS or high-sulphidation mineralisation?: GAC/AGC Program with abstracts, Vol, 21, p. A44.

Herrington, R.J., Maslenikov, V., Spiro, B., Zaykov, V., and Little, C.T.S., 1998, Ancient vent chimney structures in the Silurian massive sulfides of the Urals: In Mills, R.A., and Harrison, K., eds, Modern Ocean Floor Processes and the Geological Record, Geological Society, London, Special Publication 148, p. 241-257.

Herzig, P.M., Hannington, M.D., Fouquet, Y., von Stackelberg, U., and Peterson, S., 1993, Gold-rich polymetallic sulfides from the Lau back arc and implications for the geochemistry of gold in sea-floor hydrothetmal systems of the southwest Pacific: Economic Geology, v. 88, p. 2182-2209.

Herzig, P.M., Hannington, M.D., McInnes, B., Stoffers, P., Villinger, H., Seifert, R., Binns, R., Liebe, T., & Scientific Party R/V Sonne Cruise SO-94, 1994, Submarine volcanism and hydrothermal venting studied in Papua New Guinea: Eos 75, p.513-516.

Herzig, P.M., Peterson, S., and Hannington, M.D., 1998, Geochemistry and sulfur-isotopic composition of the TAG hydrothermal mound, Mid-Atlantic Ridge, 26°N: in Herzig, P.M., Humphries, S.E., Miller, D.J., and Zierenberg, R.A.,ed.,Proceedings of the Ocean Drilling Program, Scientific results, v. 158 (4), p. 47-70.

Herzig, P.M., Hannington, M.D., and Arribas Jr, A., 1998, Sulphur isotopic compositions of precipitates from the Lau back-arc: Implications for magmatic contributions to seafloor hydrothermal systems. Mineralium Deposita 33, p. 226-237.

Herzig, P.M., 1997, Present-day Submarine Hydrothermal Systems, An Up-date: SEC Neves Corvo Field Conference, Lisbon, Portugal, May 11-14, p. 23.

Herzig, P.M., Petersen, S., Hannington, M.D., 1999, Epithermal-type gold minerisation at Conical Seamount: a shallow submarine volcano south of Lihir Island (Papua New Guinea): In Mineral Deposits, Processes to Processing, Stanley et al., eds, Balkema, Rotterdam, p.527-530.

Herzig, P.M., and Hannington, M.D., 2000, Polymetallic massive sulfides and gold mineralization at Mid-Ocean Ridges and in Subduction-related environments: In Handbook of Marine Mineral Deposits, Cronan, D.S., eds, CRC Press, p. 347-368.

Herzig, P.M., Petersen, S., Hannington, M.D., Jonasson, I.R., 2000, Conical seamount: a submarine analog of the Ladolam epithermal gold deposit on Lihir Island, Papua New Guinea?: Volcanic Enviroments and Massive Sulfides, Tasmania, Australia, November, p. 83-84.

Hilton, D.R., and Craig, H., 1989, A helium isotope transect along the Indonesian archipelago: Nature, 342, p. 906-908.

Hilton, D.R., Hoogewerff, J.A., van Bergen, M.J., and Hammerschmidt, K., 1992, Mapping magma sources in the east Sunda-Banda arcs, Indonesia: Constraints from helium isotopes: Geochimica et Cosmochimica Acta, Vol, 56, p. 851-859.

Hodgson, C.J., and Lydon, J.W., 1977, Geological setting of the volcanogenic massive sulphide deposits and the active hydrothermal systems: Some implications for exploration: Canadian Inst. Mining Metall. Bulletin., v. 70, no. 786, p. 95-106.

Honthaas, C., Réhault, J., Maury, R.C., Bellon, H., Hémond, C., Malod, J., Cornée, J., Villeneuve, M., Cotton, J., Burhanuddin, S., Guillou, H., and Arnaud, N., 1998, A Neogene back-arc origin for the Banda Sea basins, geochemical and geochronological constraints from the Banda ridges (East Indonesia): Tectonophysics, 298, p. 297-317

Hopgood, D., Santoso, I., Caswell, M., Budiono, J., and Hatfield, R., 1995, Quartarly exploration report, Wetar Island, Fourth quarter: Unpublished Company Report, p.15.

Hou, Z., Deng, J., Sun, H., and Song, S., 1999, Volcanogenic massive sulfide deposits in China, Setting, Feature and Style: Exploration Mining Geology, v. 8, 3 and 4, p. 149-175.

Hu, R., Burnard, P.G., Turner, G., and Bi, X., 1998, Helium and Argon isotope systematics in fluid inclusions of Machangqing copper deposit in west Yunnan province, China: Chemical Geology, 146, p. 55-63.

Hughes, B.D., Baxter, K., Clarke, R.A., and Snyder, D.B., 1996, Detailed processing of seismic reflection data from the frontal part of the Timor trough accretionary wedge, eastern Indonesia, *in* Hall, R., and Blundell, D., eds., Tectonic evolution of southeast Asia: Geological Society Special Publication No. 106, p. 75-83.

Huston, D.L., and Cas, R., 2000, Shallow water volcanic-hosted massive sulfide deposits: how common are they? In Volcanic Environments and Massive Sulfide Deposits Conference, Tasmania, Australia, p. 93-95.

Irianto, B., and Clarke, G.H., 1995, The Batu Hijau porphyry copper – gold deposit, Sumbawa Island, Indonesia. PACRIM.

Ishibashi, J., Grimaud, D., N, Y., Auzende, J., Urabe, T., 1994, Fluctuation of chemical compositions of the phase-separated hydrothermal fluid from the North Fiji Basin Ridge: Marine Geology, 116, p. 215-226.

Ishibashi, J., and Urabe, T., 1995, Hydrothermal activity related to arc-backarc magmatism in the Western Pacific: In Taylor B. (Ed), Backarc Basins: Tectonics and Magmatism, Plenum Press, New York, p. 451-495.

James, R., Elderfield, H., and Palmer, M.R., 1995, The chemistry of vent fluids from the Broken Spur site, 29°N Mid Atlantic Ridge: Geochemica et Cosmochimica Acta, 59, p. 651-659.

Jazek, P.A., and Hutchinson, C.S., 1978, Banda arc of eastern Indonesia, Petrography and geochemistry of the volcanic rocks: Bull. Volc., 41, p. 586-608.

Jean-Baptiste, P., and Fouquet, Y., 1996, Abundances and isotopic compositions of helium in hydrothermal sulfides from the East Pacific Rise at 13°N: Geochimica et Cosmochimica Acta, Vol, 60, p. 87-93.

Johnston, C.R., and Bowin, C., 1981, Crustal reaction resulting from the mid-Pliocene to Recent continent-island arc collision in the Timor region: Australian Bureau of Mineral Resources Journal of Geology and Geophysics, 6, p. 223-243.

Karig, D.E., Barber, A.J., Charlton, T.R., Klemperer, S., and Hussong, D.M., 1987, Nature and distribution of deformation across the Banda Arc-Australian collision zone at Timor: Bulletin Geological Society America, 98, p.18-32.

Katili, J.A., 1975, Volcanism and plate tectonics in the Indonesian island arcs: Tectonophysics, 26, p. 165-188.

Kavalieris, I., 1986, Report on geochemical investigation of W2, W5 and Meron prospects and the lake Tihou and W81 drainage area, Wetar: Unpublished Internal Company Report.

Kavalieris, I., 1994, Cu-Au porphyry potential of Wetar Island: Unpublished Company Report, p. 8.

Kendrick, M.A., Burgess, R., Pattrick, R.A.D., and Turner, G., 2001, Halogen and Ar-Ar age determinations of inclusions within quartz veins from porphyry copper deposits using complementary noble gas extraction techniques: Chemical Geolgy, 177, p. 351-370.

Kelly, D. S., and Früh-Green, G. L., 2001, Volatile line of descent in submarine plutonic environments: Insights from stable isotope and fluid inclusion analyses: Geochemica et Cosmochimica Acta, v. 65, n. 19, p. 3325-3346.

Knott, R., Fallick, A.E., Rickard, D., and Bäcker, H., 1995, Mineralogy and sulphur isotope characteristics of a massive sulphide boulder, Galapagos Rift, 85°55'W: From Parson, L.M., Walker, C.L., and Dixon, D.R., (eds), Hydrothermal Vents and Processes, Geological Society Special Publication No 87, p. 207-222.

Koepnick, R.B., Burke, W.H., Denison, R.E., Hetherington, E.A., Nelson, H.F., Otto, J.B., and Waite, L.E., 1985, Construction of the seawater $^{87}Sr/^{86}Sr$ curve for the Cenezoic and Cretaceous: Supporting data: Chemical Geology, 58, p. 55-81.

Koski, R.A., 1995, The making of a metal deposit: Nature, v. 377, p. 697-680.

Kusakabe, M., and Chiba, H., 1979, Oxygen isotope geothermometry applicable to sulphate minerals from the Kuroko Deposits: Mining Geology, 29(4), p. 257-264.

Kusakabe, M., Chiba, H., and Ohmoto, H., 1982, Stable isotopes and fluid inclusion study of anhydrite from the East Pacific Rise at 21°N: Geochemical Journal, v. 16, p. 89-95.

Kusakabe, M., and Chiba, H., 1983, Oxygen and sulfur isotope composition of barite and anhydrite from the Fukazawa Deposit, Japan: Economic Geology, Monograph 5, p. 202-301.

Langmuir, C., Humphris, S., Forari, D., Van Dover, C., Von Damm, K., Tivey, M.K., Colodner, D., Charlou, J.L., Desonie, D., Wilson, C., Fouquet, Y., Klinkhammer, G., and Bougault, H., 1997, Hydrothermal vents near a mantle hot spot: The Lucky Strike vent field at 37N on the Mid Atlantic Ridge: Earth and Planetary Science Letters 148, p. 69-91.

Large, R.R., 2000, The significance of hybrid deposits in the continuum of VHMS-epithermal and porphyry systems: an example from the Mt Read Volcanics: In Volcanic Environments and Massive Sulfide Deposits Conference, Tasmania, Australia, p. 113.

Large, R.R., Mcphie, J., Gemmell, J.B., Hermann, W., and Davidson, G.J., 2001, The Spectrum of Ore Deposit Types, Volcanic Environments, Alteration Halos, and Related Exploration Vectors in Submarine Volcanic Successions: Some Examples from Australia: Economic Geology, v. 96, 5, p. 913-939.

Lawless, J.L., 1991, Petrology Report on six samples from Romang Island: Ashton Group KRTA Report, Indonesia, p.

Leach and Erceg, 1990. The Wafi River high sulphur epithermal gold deposit, Papua New Guinea, in, Pacific Rim Congress '90, AIMM, p. 450-456.

Lebel, L., and Oudin, E., 1982, Fluid inclusion studies of deep sea hydrothermal sulfide deposits on the East Pacific Rise near 21N: Chemical Geology, v. 37, p. 129-136.

Lécuyer, C., Dubois, M., Marignac, C., Gruan, G., Fouquet, Y., and Ramboz, C., 1999, Phase seperation and fluid mixing in subseafloor back arc hydrothermal systems: A microthermetric and oxygen isotope study of fluid inclusions in the barite-sulfide chimneys of the Lou Basin: Journal of Geophysical Research, v. 104, p. 17911-17927.

Li, B., and Manuel, O.K., 1994, A noble gas technique for the identification of mantle and crustal materials and its application to the Kuroko deposits: Geochemical Journal, 28, p. 47-69.

Luders, V., Pracejus, B., and Halbach, P., 2001, Fluid inclusion and sulfur isotope studies in probable modern analogue Kuroko-type ores from the JADE hydrothermal field (Central Okinawa Trough, Japan): Chemical Geology, 173, p. 45-58.

Lupton, J.E., and Craig, H., 1975, Excess ^{3}He in oceanic basalts; evidence for terrestrial primordeal helium: Earth and Planetary Science Letters: 26, p. 133-139.

Lupton, J.E., Klinkhammer, G.P., Normark, W.R., Haymon, R., Macdonald, K.C., Weiss, R.F., and Craig, H., 1980, Helium-3 and manganese at the 21 N East Pacific Rise hydrothermal site: Earth and Planetary Science Letters, v. 50, p. 115-127.

Lydon, J.W., 1984, Some observations on the morphology and ore textures of volcanogenic sulphide deposits of Cyprus: Geol Surv Can Pap 84-1A, p. 601-610.

Lydon, 1988.Volcanogenic Massive Sulphide deposits, In: Ore Deposit Models, edited by Roberts and Sheahan, Geoscience Canada Reprint Series 3, 1988.

Macdonald, A.J., Lewis, P.D., Thompson, J.F.H., Nadaraju, G., Bartsch, R.D., Bridge, D.J., Rhys, D.A., Roth, T., Kaip, A., Godwin, C.I. and Sinclair, A.J., 1996, Metallogeny of an Early to Middle Jurassic Arc, Iskut River Area, Northwestern British Columbia: Economic Geology. Vol. 91, p. 1098-1114.

Macdougal, J.D., Volpe, A., and Hawkins, J.W., 1987, An arc like component in Mariana Trough basalts: Transactions American Geophysical Union 68, p. 1531.

MacLean, W.H., and Barrett, T.J., 1993, Lithogeochemical techniques using immobile elements: Journal of Geochemical Exploration, v. 48, p. 109-133.

Magaritz, M., Whitford, D.J., and James, D.E., 1978, Oxygen isotopes and the origin of high andesites: Earth and Planetary Science Letters, 40, p. 220-230.

Marani, M.P., Gamberi, F., Savelli, C., 1997, Shallow-water polymetallic sulfide deposits in the Aeolian island arc: Geology, 25, p. 815-818.

Marignac, C., Lécuyer, C., Dubois, M., Fouquet, Y., and Ramboz, C., 1995, Fluid mixing and unmixing in deep-sea hydrothermal systems, the barite-sulphide chimneys of the Lau Basin: Terra Abstracts, 7, 1, p. 211-212.

Marumo, K., and Fujinuku, T., 1993, Mineralization and hydrothermal alteration of the Minamishiraoi Kuroko-type barite deposit, Hokkaido: Bulletin of the Geological Survey of Japan, v. 44 (2/3/4), p. 127-145.

Marumo, K., and Hattori, K.H., 1999, Seafloor hydrothermal alteration at Jade in the back-arc Okinawa Trough, Mineralogy, geochemistry and isotope characteristics: Geochemica et Cosmochimica Acta, v. 63, n. 18, p. 2785-2804.

Marumo, K., 1989, Genesis of kaolin minerals and pyrophyllite in Kuroko deposits of Japan, Implications for the origins of the hydrothermal fluids from minerlogical and stable isotope data: Geochimica et Cossmochimica Acta, v53, p. 2915-2924.

Marumo, K., Longstaffe, F.J., and Matsubaya, O., 1995, Stable isotope geochemistry of clay minerals from fossil and active hydrothermal systems, southwestern Hokkaido, Japan: Geochimica et Cossmochimica Acta, v59, p. 2245-2559.

Marutani, M., and Takenouchi, S., 1978, Fluid inclusion study of stockwork siliceous orebodies of Kuroko deposits at the Kosaka mine, Akita, Japan: Mining Geology, v. 28, p. 349-360.

Masson, D.G., Milsom, J., Barber, A.J., Sikumbang, N., and Dwiyanto, B., 1991, Recent tectonics around the island of Timor, eastern Indonesia: Marine and Petroleum Geology, Vol. 8, p. 35-49.

Matsukuma, T., Niitsuma, H., Yui, S., and Wada, F., 1974, Rare minerals from Kuroko ores of the Uwamuki deposits of the Kosaka mine, Akita Prefacture, Japan: Mining Geology Special Issue, No. 6, p. 349-361.

McBride, J.H., and Karig, D.E., 1987, Crustal structure of the outer Banda arc, new free-air gravity evidence: Tectonophysics, 140, p. 265-273.

McCaffrey, R., 1988, Active tectonics of the eastern Sunda and Banda arcs: Journal of Geophysical Research, 93, p. 15163-15182.

McCaffrey, R., 1989, Seismological constraints and speculations on Banda arc tectonics: Netherlands Journal of Sea Research, 24, p. 141-152.

McCaffrey, R., 1996, Slip partitioning at convergent plate boundaries of SE Asia: *In* Hall, R., and Blundell, D., ed., Tectonic Evolution of Southeast Asia: Geological Society Special Publication 106, p. 3-18.

McCaffrey, R., and Nabelek, J., 1984, The geometry of back-arc thrusting along the eastern Sunda arc, Indonesia, constraints from earthquake and gravity data: Journal of Geophysical Research, 89, p. 6171-6179.

McCaffrey, R., and Nabelek, J., 1986, Seismological evidence for shallow thrusting north of the Timor trough: Geophys . J. R. Astr. Soc. 85, p. 365-381.

McCaffrey, R., and Nabelek, J., 1987, Earthquakes, gravity and the origin of the Bali Basin, an example of a nascent continental fold and thrust belt: Journal of Geophysical Research, 92, p. 441-460.

McCaffrey, R., Molnar, P., Roecker, S.W., and Joyodiwiyo, Y.S., 1985, Microearthquake seismicity and fault plane solutions related to arc-continent collision in the eastern Sunda Arc, Indonesia: Journal of Geophysical Research 90, p. 4511-4528.

McCulloch, M.T., Compston, W., Abbott, M., Chivas, A., Foster, J.J., and Nelson, D.R., 1982, Neodymium, strontium, lead and oxygen isotopic and trace element constraints on magma genesis in the Banda island arc, Wetar: Research School of Earth Sciences Annual Report, p. 236-238.

McDougal, I., and Harrison, T.M., 1999, Geochronology and Thermochronology by the 40Ar/39Ar Method: New York Oxford University Press, p. 269.

Migineishvili, R., 2000, Formation of a volcanic-hosted massive sulfide in a shallow water setting: the Madneuli Cu-Au deposit, Georgia: In Volcanic Environments and Massive Sulfide Deposits Conference, Tasmania, Australia, p. 123-125.

Milési, J.P., Marcoux, E., Sitorus, T., Simandjuntak, M., Leroy, J., and Bailly, L., 1999, Ponkor (west Java, Indonesia): a Pliocene supergene-enriched epithermal Au-Ag-(Mn) deposit: Mineralium Deposits, 34, p. 131-149.

Milési, J.P., Marcoux, E., and Nehlig, P., 1994, Cirotan, West Java, Indonesia, A 1.7Ma Hybrid Epithermal Au-Ag-Sn-W Deposit: Economic Geology 89, p. 227-246.

Mills, R.A., and Elderfield, H., 1995, Hydrothermal activity and the geochemistry of metalliferous sediments. In Humphris, S.E, Zierenberg, R.A., Mullineaux, L.S., Thomson, R.E eds. Seafloor hydrothermal systems, physical, chemical biological and geological interations: American Geophysical Monograph 91, p. 392-407.

Minniti, M., and Bonavia, F.F., 1984, Copper-ore grade hydrothermal mineralisation discovered in a seamount in the Tyrrhenian Sea (Mediterranean): Is the mineralisation related to porphyry-coppers or to base metal lodes?: Marine Geology, v. 59, p. 271-282.

Milsom, J., Kaye, S., and Sardjono., 1996, Extension, collision and curvature in the eastern Banda arc, *in* Hall, R., and Blundell, D., ed., Tectonic evolution of southeast Asia: Geological Society Special Publication No. 106, p. 85-94.

Morris, J.D., Gill, J.B., Schwartz, D., and Silver, E.A., 1984, Late Miocene to recent Banda sea volcanism, III, Isotopic compositions: EOS Transactions, AGU, 65, p. 1135.

Moss, R., and Scott, S.D., 2001, Gold content of Eastern Manus Basin Volcanic Rocks, Implications for enrichment in associated Hydrothermal precipitates: Economic Geology, v. 19, p. 91-107.

Nakajima, T., 1993, Reconstruction of the depositional circumstances of the Kuroko deposits in the Hokuroko basin: Bulletin of the Geological Survey of Japan, v. 44 (2/3/4), p. 251-282.

Nash, C., and Snodin, S., 1992, Photogeological study of Wetar Island, Indonesia: unpubl. Rpt. PLM 023J/92.

Nehlig, P., Salinity of oceanic hydrothermal fluids, a fluid inclusion study: Earth and Planetary Science Letters 102, p. 310-325.

Nishiyama, T., 1974, Minor elements in some sulphide minerals from the Kuroko Deposits of the Shakanai mine: Mining Geology Special Issue, No. 6, p. 371-376.

O'Brien, N., and Hodgson, C.J., 1994, The Cerattepe Cu-Au deposit; an unusual zone of copper sulphide enrichment of uncertain origin: GAC MAC Program with abstracts, 19, p. 83.

Ohmoto,H., 1978, Submarine calderas: A key to the formation of the volcanogenic massive sulfide deposits: Mining Geology, v. 28, p. 219-232.

Ohmoto,H., and Rye, R.O., 1979, Isotopes of Sulfur and Carbon: In Geochemistry of Hydrothermal Ore Deposits, 2nd ed., Barnes, H.L., J., Wiley, New York, p. 509-567.

Ohmoto, H., and Skinner, B.J., 1983, The Kuroko and related volcanogenic massive sulfide deposits: Introduction and summary of new findings: Economic Geology Monograph 5, p. 1-8.

Ohmoto, H., Mizukami, M., Drummond, S.E., Eldridge, C.S., Pisutha-Arnond, V., and Lenagh, T.C., 1983, Chemical processes of Kuroko formation: Economic Geology, v. 5, p. 570-604.

Oliveira, V., Matos, J., Bengala, M., Silva, N., Sousa, P., and Torres, L., 1998, Geology and geophysics as successful tools in the discovery of the Lagoa Salgada Orebody (Sado Tertiary Basin- Iberian Pyrite Belt), Grândola, Portugal: Mineralium Deposita, v.33, p. 170-187.

Parr, J.M., Murao, S., and Binns, R.A., 1995, A comparison of massive sulfide deposits forming at the PACMANUS (Manus Basin, PNG) and Jade (Okinawa Trough, South China Sea) seafloor hydrothermal fields: In PACRIM 95, p. 453-458.

Parsons, B., 1981, The rates of plate creation and consumption: Journal of Royal Astrological Society, 67, p. 437-448.

Pearce, J.A., and Cann, J.R., 1973, Tectonic setting of basic volcanic rocks determined using trace element analysis: Earth and Planetary Science Letters, v. 19, p. 290-300.

Peterson, S., Herzig, P.M., and Hannington, M.D., 2000, Third dimension of a presently forming VMS deposit, TAG hydrothermal mound, Mid-Atlantic Ridge, 26N: Mineralium Deposita, 35, p. 233-259.

Pisutha-Arnond, V., and Ohmoto, H., 1983, Thermal history, and chemical and isotopic compositions of the ore-forming fluids responsible for the Kuroko Massive Sulfide Deposits in the Hokuroko District of Japan: Economic Geology, Monograph 5, p.523-558

Platt, J., 1996, A review of ore reserves / resources and mining geology for PT Prima Lirang Mining, Wetar Island, Indonesia, as at 29 February: Unpublished Company Report, p. 43

Polliand, M., and Fontboté, L., 2000, The Perubar Ba-Pb-Zn VHMS deposit, Central Peru: a possible Andean Kuroko-type equivalent in a shallow water caldera: In Volcanic Environments and Massive Sulfide Deposits Conference, Tasmania, Australia, p. 159-161.

Poreda, R., and Craig, H., 1989, Helium isotope ratios in circum-Pacific volcanic arcs: Nature, 338, p. 473-478.

Potter, R.W., 1977, Pressure correction for fluid inclusions homogenisation temperatures based on the volumetric properties of the system NaCl-H2O: Journal Res US, Geological Survey Monograph 5, p. 603-607.

Price, N.J., and Audley-Charles, M.G., 1987, Tectonic collision processes after plate rupture: Tectonophysics, 140, p. 121-129.

Rees, C.E., Jenkins, W.J., and Monster, J., 1978, The sulfur isotopic composition of ocean water sulfate: Geochimica et Cossmochimica Acta, v42, p. 377-381.

Relvas, J.M.R.S., Barriga, F.J.A.S., Bernardino, F.B.C.P., Oliveira, V.M.S., Matos, J.X., 1994, Ore zone hydrothermal alteration in drill hole IGM-LS1, at Lagoa Selada, Grandola, Portugal: A first report on pyrophyllite in a central stockwork: Boletín de la Sociedad Espanola de Mineralogía, 17-1, p. 157-158.

Reyes, A.G., 1990, Petrology of Philippine geothermal systems and the application of alteration mineralogy to their assessment: Journal of Volcanology and Geothermal Research., v. 43, p. 279-309.

Richardson, A.N., and Blundell, D.J., 1996, Continental collision in the Banda arc, *in* Hall, R., and Blundell, D., ed., Tectonic evolution of southeast Asia: Geological Society Special Publication No. 106, p. 47-60.

Robinson, B.W., and Kusakabe, M., 1975, Quantitative preparation of sulfur dioxide, for 34S/32S analysis from sulfides by combustion with cuprous oxide: Anal. Chem., 47, p. 1179-1181.

Roedder, E., 1984, Fluid Inclusions: Reviews in Mineralogy, Mineralogical Society America, no. 12.

Roth, T., Thompson, J.F.H., and Barrett, T.J., 1999, The precious Metal Rich Eskay Creek Deposit, Northwestern British Columbia, in Processes and Examples in Modern and Ancient Settings (eds) Barrie, C.T., and Hannington, M.D.,: Reviews in Economic Geology, v. 8, p. 357-373.

Rona, P.A., Hannington, M.D., Raman, C.V., Thompson, G., Tivey, M.K., Humphris, S.E., Lalou, C., and Peterson, S., 1993, Active and relict sea-floor hydrothermal mineralization at the TAG hydrothermal Field: Economic Geology 88, p. 1989-2017.

Rudnicki, M.D., and Elderfield, H., 1992, Helium, radon and manganese at the TAG and Snakepit hydrothermal vent fields, 26 and 23 N, Mid-Atlantic Ridge: Earth and Planetary Science Letters, v. 113, p. 307-321.

Ruxton, P.A., 1989, A geological model for the Lerokis project, Indonesia: Billiton Australia, The Metals Division of the Shell Company of Australia, Internal unpublished company report, p. 29.

Rye, R.O., Bethke, P.M., and Wassermann, M.D., 1992, The stable isotope geochemistry of acid sulfate alteration: Economic Geology 87, p. 225-238.

Sangster, D.F., and Scott, S.D., 1976, Precambrian stratabound massive Cu-Zn-Pb sulfide ores in North America, In: Wolfe, K.H. (eds) Handbook of Stratabound and Stratiform Ore Deposits, Vol 7, Elsevier, p. 129-222.

Sakai, H., des Marais, D.J., Ueda, A., and Moore, J.G., 1984, Concentrations and isotope ratios of carbon, nitrogen and sulfur in ocean-floor basalts: Geochimica et Cosmochimica Acta 48, p. 2433-2441.

Sasaki, A., 1974, Isotopic data of Kuroko deposits: Mining Geology Special Issue, No. 6, p. 389-397.

Schlüter, H.U., and Fritsch, J.,1985, Geology and tectonics of the Banda arc beween Tanimbar Island and Aru Island, Indonesia: results of the R/V Sonne Cruise SO-16, Geologisches Jahrbuch Reihe E, 30, p. 3-41.

Scott, S.D., and Binns, R.A., 1995, Hydrothermal processes and contrasting styles of mineralization in the western Woodlark and eastern Manus Basins of the western Pacific. In Parson, L.M., Walker, C.L., and Dixon, D.R eds, Hydrothermal Vents and Processes, Geological Society Special Publication 87, p. 191-205.

Seal II, R.R., Ayuso, R.A., Foley, N.K., and Clarke, S.H.B., 2001, Sulfur and lead isotope geochemistry of hypogene mineralisation at the Barite Hill Gold Deposit, Carolina Slate Belt, southeastern United States: a window into and through regional metamorphism: Mineralium Deposita, v. 36, 2, p. 137-149.

Sewell, D.M., 1991a, Prospects and anomalies defined in the Lerokis mine area: Internal unpublished company report, p. 30.
Sewell, D.M., 1991b, PT Prima Lirang Mining, RC and diamond drilling, sampling and mapping, Lerokis Zone 1 South and Zone 5: Internal unpublished company report, p. 23.

Sewell, D.M., Tarmizi, S., and van der Vegt, R., 1991, PT Prima Lirang Mining, RC and diamond drilling, sampling and mapping, Kali Kuning (KK3) prospect: Internal unpublished company report, p. 27.

Sewell, D.M., and Wheatley, C.J.V., 1994a, Intergrated exploration success for gold at Wetar, Indonesia: Jornal of Geochemical Exploration, 50, p. 337-350.

Sewell, D.M., and Wheatley, C.J.V., 1994b, The Lerokis and Kali Kuning submarine exhalative gold-silver-barite deposits, Wetar Island, Malaku, Indonesia: Jornal of Geochemical Exploration, 50, p. 351-370.

Shanks, III W.C., Bohlke, J.K., & Seal, R.R., 1995, Stable Isotopes in Mid-Ocean Ridge hydrothermal systems: Interactions between Fluids, Minerals & Organisms: In Seafloor Hydrothermal systems: Physical, Chemical, Biological and Geological interactions. Geophys. Mon. 91, Amer. Geophys.l Union, p. 195-221.

Shanks, W.C. III., Seyfried, W.E. Jr., 1987, Stable isotope studies of vent fluids and chimney materials, southern Juan de Fuca Ridge. Sodium metasomatism and seawater sulfate reduction: Journal of Geophysical Research 92, p. 11387-11399.

Sharpe, R., and Gemmell, J.B., 2000, Sulfur isotopic characteristics of the Archean Cu-Zn Gossan Hill deposit, Western Australia: Mineralium Deposita, v. 35, p. 533-550.

Shepherd , T., Rankin, A.H., Alderton, D.H.M., 1985, A practical guide to fluid inclusion studies: London, Blackie, 239 p.

Sheppard, S.M.F., 1986, Characterisation and isotopic variations in natural waters: In Stable Isotopes in High-temperature Geological Processes, Valley, J.W., Taylor, H.P., and O'Neil, J.R., eds, Reviews in Mineralogy 16, Mineralogical Society of America, Washington, D.C., p. 165-183.

Sherlock, R.L., Roth, T., Spooner, E.T.C., and Bray, C.J., 1999, Origins of the Eskay Creek precious metal-rich volcanogenic massive sulfide deposit: Fluid inclusion and stable isotope evidence: Economic Geology, v. 94, p. 803-824.

Shikazono, N., 1994, Precipitation mechanisms of barite in sulfate-sulfide deposits in back-arc basins: Geochimica et Cosmochimica Acta, v. 58, 10, p. 2203-2213.

Shimzu, T., Matseueda, H., Ishiyama, D., and Matsubaya, O., 1998, Genesis of Epithermal Au-Ag Mineralisation of the Koryu Mine, Hokkaido, Japan: Economic Geology, v. 93, p.303-325.

Sillitoe, R.H., 1989, Gold Deposits in Western Pacific Island Arcs: The Magmatic Connection: Economic Geology Monograph 6, p. 274-291.

Sillitoe, R.H., Hannington, M.D., and Thompson, J.F.H., 1996, High Sulfidation in the Volcanogenic Massive Sulfide Environment: Economic Geology, v.91, p. 204-212.

Sillitoe, R. H., 1997, Comments on the geology and exploration potential of the Gunung Botak prospect, Wetar Island, Indonesia: Internal unpublished company report for PT Gencor, p. 8.

Sillitoe, R.H., 1999, VMS and porphyry copper deposits, Products of discrete tectono-magmatic settings: In Mineral Deposits, Processes to Processing, Stanley et al., eds, Balkema, Rotterdam, p. 7-10.

Silver, E.A., Reed, D., McCaffrey, R., and Joyodiwiryo,Y., 1983, Back-arc thrusting in the eastern Sunda arc, Indonesia, a consequence of arc-continent collision: Journal of Geophysical Research, 88, p. 7429-7448.

Silver, E.A., Gill, J.B., Schwartz, D., Prasetyo, H., and Duncan, R.A., 1985, Evidence for a submerged and displaced continental borderland, north Banda Sea, Indonesia: Geology, 13, p. 687-691.

Snyder, D.B., Milsom, J., and Prasetyo, H., 1996, Geophysical evidence for local indentor tectonics in the Banda arc east of Timor, *in* Hall, R., and Blundell, D., ed., Tectonic evolution of southeast Asia: Geological Society Special Publication No. 106, p. 61-73.

Spence, W., 1986, The 1977 Sumba earthquake series, evidence for slab pull force acting at a subduction zone: Journal of Geophysical Research 91, p. 7225-7239.

Stoffers, P., and 21 others, 1999: Geology, v. 27, p. 931-934.

Stuart, F.M., Turner, G, Duckworth, R.C., and Fallick, A.E., 1994, Helium isotopes as tracers of trapped hydrothermal fluids in ocean-floor sulphides: Geology, v. 22, p. 823-826.

Stuart, F.M., Harrop, P.J., Knott, R., Fallick, A.E., Turner, G., Fouquet, Y., and Rickard, D., 1995, Noble gas isotopes in 25 000 years of hydrothermal fluids from 13°N on the East Pacific Rise: From Parson, L.M., Walker, C.L., and Dixon, D.R., (eds), Hydrothermal Vents and Processes, Geological Society Special Publication No 87, p. 133-143.

Stuart, F.M., Ellam, R.M., and Duckworth, R.C., 1999, Metal sources in the Middle Valley massive sulphide deposit, northern Juan de Fuca Ridge: Pb isotope constraints: Chemical Geology, 153, p. 213-225.

Styrt, M.M., Brackmann, A.J., Holland, H.D., Clarke, B.C., Pisutha-Arnond, V., Eldridge, C.S., and Ohmoto, H., 1981, The mineralogy and isotopic composition of sulfur in hydrothermal sulfide/sulfate deposits on the East Pacific Rise, 21°N latitude: Earth and Planetary Science Letters, 53, p. 382-390.

Suryantoko, 1997, Copper Resources Update, Lerokis – Kali Kuning – Meron: Unpublished Company Report, PLM 08, p. 27.

Taylor, R.N., and Nesbitt, R.W., 1998, Isotopic characteristics of subduction fluids in an intra-oceanic setting, Izu-Bonin Arc, Japan: Earth and Planetary Science Letters, 164, p. 79-98.

Taylor, B.E., 1987, Stable isotope geochemistry of ore-forming fluids, in Kyser, T.K., eds., Stable isotope chemistry of low temperature fluids: Mineralogical Association of Canada, v. 13, p. 337-445.

Taylor, D., and Van Leeuwen, T., 1980, Porphyry-type deposits in southeast Asia: Mining Geology Special Issue, No. 8, p. 95-116.

Teagle, D.A.H., Alt, J.C., Chiba, H., and Halliday, A.N., 1998a, Dissecting an active hydrothermal deposit, The strontium and oxygen isotopic anatomy of the TAG hydrothermal mound-Anhydrite[1]: in Herzig, P.M., Humphries, S.E., Miller, D.J., and Zierenberg, R.A.,ed.,Proceedings of the Ocean Drilling Program, Scientific results, v. 158 (11), p. 129-141.

Teagle, D.A.H., Alt, J.C., Humphries, S.E., and Halliday, A.N., 1998b, Dissecting an active hydrothermal deposit, The strontium and oxygen isotopic anatomy of the TAG hydrothermal mound-Whole rock and silicate minerals[1]: in Herzig, P.M., Humphries, S.E., Miller, D.J., and Zierenberg, R.A.,ed.,Proceedings of the Ocean Drilling Program, Scientific results, v. 158 (22), p. 297-309.

Tivey, M.K., Mills, R., and Teagle, D., 1998, Temperature and salinity of fluid inclusions in anhydrite as indicators of seawater entrainment and heating in the TAG active mound. In Herzig, P.M., Humphris, S.E., and Miller, J eds: Proc ODP 158, Scientific Results, p. 179-190.

Tokunaga, M., and Honma, H., 1974, Fluid inclusion in the minerals from some Kuroko deposits: Mining Geology Special Issue, No. 6, p. 385-388.

Trull, T.W., Perfit, M.R., and Kurz, M.D., 1990, He and Sr constraints on subduction contributions to Woodlark Basin Volcanism, Solomon Islands: Geochimica et Cosmochimica Acta, Vol, 54, p. 441-453.

Tsunogai, U., Ihibashi, J., wakita, H., Gamo, T., Watanabe, K., Kajimura, T., Kanayama, S., and Sakai, H., 1994, Peculiar features of Suiyo Seamount hydrothermal fluids, Izu-Bonin Arc, Differences from subaerial volcanism: Earth and Planetary Science Letters, 126, p. 289-301.

Tsutsumi, M., and Ohmoto, H., 1983, A preliminary oxygen isotope study of Tetsusekiei ores associated with the Kuroko deposits in the Hokuroko district, Japan: Economic Geology Monograph 5, p. 433-438.

Tufar, W., 1992, Paragenesis of complex massive sulfide ores from the Tyrrhenian Sea: Osterreichischen Geologischen Gesellschaft Mitteilungen, v. 84, p. 265-300.

Turner, G., and Stuart, F.M., 1992, Helium/heat ratios and deposition temperatures of sulphides from the ocean floor: Nature, v. 357, p. 581-583.

Ueda, A., and Sakai, H., 1984, Sulfur isotope study of Quaternary volcanic rocks from the Japanese Island Arc: Geochimica et Cosmochimica Acta 48, p. 1837-1848.

Ulrich, M.R., and Bodnar, R.J., 1988, Systematics of stretching of fluid inclusions II: In Barite at 1ATM confining pressure: Economic Geology v. 83, p. 1037-1046.

Urabe, T., and Kusakabe, M., 1990, Barite silica chimneys from the Sumisu Rift, Izu-Bonin Arc, possible analogue to hematitic chert associated with Kuroko deposits: Earth and Planetary Science Letters, 100, p. 283-290.

Urabe, T., Scott, S.D., and Hattori, K., 1983, A comparison of footwall-rock alteration and geothermal systems beneath some Japanese and Canadian volcanogenic massive sulfide deposits: Economic Geology Monograph 5, p. 345-364.

Utada, M., 1980, Hydrothermal alteration related to igneous activity in Cretaceous and Neogene formations of Japan: Society of Mining Geologists Japan Special Issue 8, p. 67-83.

Van Bemmelen, R.W., 1949, The geology of Indonesia and adjacent archipelagos: Government Printing Office, The Hague.

Van Bergen, M.J., Erfan, R.D., Siriwana, T., Suharyono, K., Poorter, R.P.E., Varekamp, J.C., Vroon, P.Z., and Wirakusumah, A.D., 1989, Spatial geochemical variations of arc volcanism around the Banad Sea: Netherlands Journal Sea Research, 24, p. 313-322.

Vanko, D.A., Griffith, D., and Erickson, C.L., 1992, Calcium-rich brines and other hydrothermal fluid inclusions from plutonic rocks, Oceanographer Transform, Mid-Atlantic Ridge: Geochemica et Cosmochimica Acta, v. 56, p. 35-47.

Varekamp, J.C., Van Bergen, M.J., Vroon, P.Z., Poorter, R.P.E., Wirakusumah, A.D., Erfan, R., Suharyono, K., and Sriwana, T., 1989, Volcanism and tectonics in the eastern Sunda arc, Indonesia: Netherlands Journal of Sea Research, 24, (2/3), p. 303-312.

Von Damm, K.L., 1995, Controls on the chemistry and temporal varaibility of seafloor hydrotrhermal fluids: In Seafloor Interactions, Humphris, S.E., eds, AGU Geophysical Monograph 91, p. 222.

Von Damm, 1990, Seafloor hydrothermal activity, Black smoker chemistry and chimneys: Annu Rev Earth Planetary Science 18, p. 173-204.

Von der Borch, C.C., 1979, Continental-island arc collision in the Banda Sea: Tectonophysics, 54, p. 169-193.

Von Huene, R., and Scholl, D.W., 1991, Observations at convergent margins concerning sediment subduction, subduction erosion and the growth of continental crust: Reviews in Geophysics, 29, p. 279-316.

Vroon, P.Z., 1992, Subduction of continental material in the Banda-arc, Eastern Indonesia, Sr-Nd-Pb isotope and trace-element evidence from volcanics and sediments. PhD Thesis, Univ. Utrecht, p.205.

Vroon, P.Z., Lowry, D., van Bergen, M.J., Boyce, A.J., and Mattey, D.P., 2001, Oxygen isotope systematics of the Banda Arc: Low d18O despite involvement of subducted continental material in magma genesis: Geochemica et Cosmochima Acta,

Vroon, P.Z., van Bergen, M.J., White, W.M., and Varekamp, J.C., 1993, Sr-Nd-Pb Isotope systematics of the Banda arc, Indonesia: Combined subduction and assimilation of continental material: Journal of Geophysical Research, Vol, 98, B12, p. 22349-22366.

Vroon, P.Z., van Bergen, M.J., Klaver, G.J., and White, W.M., 1995, Strontium, neodymium, and lead isotopic and trace-element signatures of the East Indonesia sediments, Provenance and implications for Banda Arc magma genesis: Geochimica et Cosmochimica Acta, v. 59, 12, p. 2573-2598.

Watkinson, D.H., McEwen, J., and Jonasson, I.R., 1990, Mine Gallen, Noranda, Quebec: Geology of an Archean Massive Sulphide Mound: In The Northwestern Quebec Polymetallic Belt: A summary of 60 years of mining exploration, The Canadian Institute of Mining and Metallurgy, Special v. 43.

Wheller, G.E., Varne, R., Foden, J.D., and Abbott, M.J., 1987, Geochemistry of Quaternary volcanism in the Sunda-Banda arc, Indonesia, and three-component genesis of island-arc basaltic magmas: Journal of Volcanology and Geothermal Research, 32, p. 137-160.

White, N. C., and Hedenquist, J.W., 1995, Epithermal Gold Deposits: Styles, characteristics and exploration: Economic Geology, SEG Newsletter, No 23.

White, N.C., Leake, M.J., McCaughey, S.N., and Parris, B.W., 1995, Epithermal gold deposits of the southwestern Pacific: Journal of Geochemical Exploration, 54, p. 87-136.

Whitford, D.J., 1975, Strontium isotopic studies of the volcanic rocks of the Sunda arc, Indonesia, and their petrogenetic implications: Geochimica Cosmochimica Acta, 39, p. 1287-1302.

Whitford, D.J., Compston, W., Nicholls, I.A., Abbott, M.J., 1977, Geochemistry of late-Cenozoic lavas from eastern Indonesia: Role of subducted sediments in petrogenesis: Geology, 5, p. 571-575.

Whitford, D.J., and Jazek, P.A., 1979, Origin of late-Cenozoic lavas from the Banda arc, Indonesia; Trace element and Sr Isotope evidence: Contributions to Mineralogy and Petrology, 68, p. 141-150.

Whitford, D.J., White, W.M., and Jazek, P.A, 1981, Neodymium isotopic composition of Quaternary island arc lavas from Indonesia: Geochemica Cosmochima Acta, 45, p. 989-995.

Winchester, J.A., and Floyd, P.A., 1977, Geochemical discrimination of different magma series and their different products using immobile elements: Chemical Geology v. 20, p. 325-343.

Woodruff, L.G., and Shanks, W.C. III., 1988, Sulfur isotope study of chimney minerals and hydrothermal fluids from 21N East Pacific Rise, hydrotheraml sulfur sources and disequilibrium sulfate reduction: Journal of Geophysiscal Research 93, p. 4562-4572.

Woodside, J.M., Jongsma, D., Thommeret, M., Strang van Hees, G., and Puntodewo, 1989, Gravity and magnetic field measurements in the eastern Banda Sea: Netherlands Journal of Sea Research, 24, (2/3), p. 185-203.

Yamaoka, K., and Asakura, E., 1974, Metallic ore minerals and associated clay minerals from the Kuroko deposits in the Nishi-Aizu District, Fukushima Prefecture, Japan: Mining Geology Special Issue, No. 6, p. 363-370.

Zaw, K., Huston, D.L., Gemmell, J.B., Hunns, S.R., Large, R.R., Ryan, C.G., and Mernagh, T.P, 2001, Microthermometry and geochemistry of ore fluids bearing on the genesis of volcanic-hosted massive sulphide deposits, Water depth and source of metals: Faculade de Ciências do Porto, Departmento de Geologia, Memória 7, PhD Dissertation, Univer. Utrecht. , p. 463-466.

Zaw, K., Gemmell, J.B., Hunns, S.R., Large, R.R., Ryan, C.G., Mernagh, T.P., 1995, Compositions of fluid inclusions from Hellyer and Mt Chalmers deposits, Implications for source of VHMS ore-forming fluids: Proceeding of Pacrim Conference 95, Aukland, New Zealand 19-22, p. 633-668.

Zaw, K., Gemmell, J.B., S.R., Large, R.R., Mernagh, T.P., and Ryan, C.G., 1996, Evolution and source of ore fluids in the footwall stringer zone, Hellyer VHMS deposit, western Tasmania. Constraints from fluid inclusion microthermometry and geochemistry: Ore Geology Review 10, p. 251-278.

Zaw, K., Hunns, S.R., Large, R.R., Gemmell, J.B., Ryan, C.G., and Mernagh, T.P., 2000, Geochemistry of fluid inclusions from the Mt Chalmers VHMS deposit, Australia, Implications for ore genesis: Abstract, 31st International Geological Congress, 6-17 August, Rio de Janiero, Brazil.

Zierenberg, R.A., Shanks, W.C. III., and Bischoff, J.L., 1984, massive sulfide deposits at 21N, East Pacific Rise, chemical composition, stable isotopes and phase equilibria: Greological Society of America Bulletin 95, p. 922-929.

APPENDIX A

LIST OF ABBREVIATIONS

Terms used and not explained in the text

BSE	- Back-scattered electron
CDT	- Canyon diablo troilite
FTIR	- Fourier transform infrared
HREE	- Heavy rare earth elements
LILE	- Large ion lithophile elements
LOI	- Loss on ignition
MOHO	- Mohorovičič discontinuity
REE	- Rare earth elements
SEM	- Scanning electron microscope
SMOW	- Standard mean ocean water
TIMS	- Thermal ionisation mass spectrometry
XRD	- X-ray diffraction
XRF	- X-ray flourescence
MORB	- Mid Ocean Ridge Basalt
MOR	- Mid Ocean Ridge
PPL	- Plane polarized Light

Appendix A: Samples used during study.

Sample	Location	Deposit / Zone	Comment	Type of Study
100118	64	Kali Kuning	Hydrothermally Altered Volcanic	XRD / FTIR
100129	66	Kali Kuning	Hydrothermally Altered Volcanic	XRD / FTIR
111834	190	Lerokis area	Felsic Volcanic	TS
111904	306	Kali Kuning	Hydrothermally Altered Volcanic	XRD / FTIR
111907	309	Kali Kuning	Hydrothermally Altered Volcanic	XRD / FTIR / TS
111908	310	Kali Kuning	Hydrothermally Altered Volcanic	XRD / FTIR
111910	312	Kali Kuning	Hydrothermally Altered Volcanic	XRD / FTIR
111912	314	Kali Kuning	Hydrothermally Altered Volcanic	XRD / FTIR
111914	316	Kali Kuning	Hydrothermally Altered Volcanic	XRD / FTIR / TS XRF
111917	319	Kali Kuning	Hydrothermally Altered Volcanic	XRD / FTIR
111918	320	Kali Kuning	Hydrothermally Altered Volcanic	XRD / FTIR / TS
111919	321	Kali Kuning	Hydrothermally Altered Volcanic	XRD / FTIR
111938	91	Kali Kuning	Hydrothermally Altered Volcanic	XRD / FTIR
111939	231	Kali Kuning	Hydrothermally Altered Volcanic	XRD / FTIR
111941	300	Kali Kuning	Hydrothermally Altered Volcanic	XRD / FTIR
111945	301	Kali Kuning	Hydrothermally Altered Volcanic	XRD / FTIR
111999	232	Meron Area	Intrusive	TS
096853	74	Kali Kuning	Hydrothermally Altered Volcanic	XRD / FTIR
096854	74	Kali Kuning	Hydrothermally Altered Volcanic	XRD / FTIR
096856	235	Kali Kuning	Hydrothermally Altered Volcanic	XRD / FTIR
096863	235	Kali Kuning	Hydrothermally Altered Volcanic	XRD / FTIR
096865	55	Kali Kuning	Hydrothermally Altered Volcanic	XRD / FTIR
096884	320	Kali Kuning	Hydrothermally Altered Volcanic	XRD / FTIR / XRF
096920	104	Coatal Road	Mafic Volcanic	TS / XRF
096924	239	Kali Kuning	Hydrothermally Altered Volcanic	XRD / FTIR
096926	109	Kali Kuning area	Lahar Clast	TS / XRF
096927	240	Kali Kuning	Hydrothermally Altered Volcanic	XRD / FTIR
096930	92	Kali Kuning	Hydrothermally Altered Volcanic	XRF
097156	243	Kali Kuning	Hydrothermally Altered Volcanic	XRD / FTIR
097157	244	Kali Kuning	Hydrothermally Altered Volcanic	XRD / FTIR
097158	245	Kali Kuning	Hydrothermally Altered Volcanic	XRD / FTIR
097159	246	Kali Kuning	Hydrothermally Altered Volcanic	XRD / FTIR
097160	303	Kali Kuning	Hydrothermally Altered Volcanic	XRD / FTIR
097161	304	Kali Kuning	Hydrothermally Altered Volcanic	XRD / FTIR
097167	225	Meron Area	Dacite	TS / XRF
097168	226	Meron Area	Dacite	XRF
097214	KKD058 @ 51m	Kali Kuning	Hydrothermally Altered Volcanic	XRD / FTIR
097217	KKD058 @ 90m	Kali Kuning	Hydrothermally Altered Volcanic	XRD / FTIR
097220	KKD058 @ 92m	Kali Kuning	Hydrothermally Altered Volcanic	XRD / FTIR
097223	KKD058 @ 125m	Kali Kuning	Hydrothermally Altered Volcanic	XRD / FTIR
097226	KKD058 @ 160m	Kali Kuning	Hydrothermally Altered Volcanic	XRD / FTIR
097231	KKD031 @ 37m	Kali Kuning	Hydrothermally Altered Volcanic	XRD / FTIR
097232	KKD031 @ 39m	Kali Kuning	Hydrothermally Altered Volcanic	XRD / FTIR
097234	KKD031 @ 43m	Kali Kuning	Hydrothermally Altered Volcanic	XRD / FTIR
097235	KKD031 @ 46m	Kali Kuning	Hydrothermally Altered Volcanic	XRD / FTIR
097236	KKD031 @ 50m	Kali Kuning	Hydrothermally Altered Volcanic	XRD / FTIR
097237	KKD031 @ 56m	Kali Kuning	Hydrothermally Altered Volcanic	XRD / FTIR
097239	KKD031 @ 70m	Kali Kuning	Hydrothermally Altered Volcanic	XRD / FTIR
097240	KKD049 @ 5m	Kali Kuning	Hydrothermally Altered Volcanic	XRD / FTIR
097241	KKD049 @ 7m	Kali Kuning	Hydrothermally Altered Volcanic	XRD / FTIR
097243	KKD049 @ 21m	Kali Kuning	Hydrothermally Altered Volcanic	XRD / FTIR
097245	KKD049 @ 26m	Kali Kuning	Hydrothermally Altered Volcanic	XRD / FTIR
097249	KKD049 @ 57.5m	Kali Kuning	Hydrothermally Altered Volcanic	XRD / FTIR
097253	KKD049 @ 62m	Kali Kuning	Hydrothermally Altered Volcanic	XRD / FTIR
097259	KKD049 @ 73m	Kali Kuning	Hydrothermally Altered Volcanic	XRD / FTIR
111923	171	Lerokis zone 5	Hydrothermally Altered Volcanic	XRD / FTIR
111924	172	Lerokis zone 5	Hydrothermally Altered Volcanic	XRD / FTIR

111926	174	Lerokis zone 5	Hydrothermally Altered Volcanic	XRD / FTIR
111927	175	Lerokis zone 5	Hydrothermally Altered Volcanic	XRD / FTIR
111928	176	Lerokis zone 5	Hydrothermally Altered Volcanic	XRD / FTIR
097029	LKD042 @ 68.5m	Lerokis zone 5	Hydrothermally Altered Volcanic	XRD / FTIR
097030	LKD042 @ 69m	Lerokis zone 5	Hydrothermally Altered Volcanic	XRD / FTIR
097031	LKD042 @ 72m	Lerokis zone 5	Hydrothermally Altered Volcanic	XRD / FTIR
097034	LKD042 @ 79.3m	Lerokis zone 5	Hydrothermally Altered Volcanic	XRD / FTIR
097046	LKD042 @ 141m	Lerokis zone 5	Hydrothermally Altered Volcanic	XRD / FTIR
097063	LKD043 @ 44.9m	Lerokis zone 5	Hydrothermally Altered Volcanic	XRD / FTIR
097071	LKD043 @ m	Lerokis zone 5	Hydrothermally Altered Volcanic	XRD / FTIR
097072	LKD043 @ 57.4m	Lerokis zone 5	Hydrothermally Altered Volcanic	XRD / FTIR
097077	LKD043 @ 57.4m	Lerokis zone 5	Hydrothermally Altered Volcanic	XRD / FTIR
097078	LKD043 @ 72.5m	Lerokis zone 5	Hydrothermally Altered Volcanic	XRD / FTIR
097080	LKD043 @ 85m	Lerokis zone 5	Hydrothermally Altered Volcanic	XRD / FTIR
097093	LKD043 @ 116m	Lerokis zone 5	Hydrothermally Altered Volcanic	XRD / FTIR
097100	LKD043 @ 146m	Lerokis zone 5	Hydrothermally Altered Volcanic	XRD / FTIR
097104	LKD043 @ 196m	Lerokis zone 5	Hydrothermally Altered Volcanic	TS
097106	LKD043 @ 210m	Lerokis zone 5	Hydrothermally Altered Volcanic	XRD / FTIR / XRF
097111	LKD044 @ 23.7m	Lerokis zone 5	Hydrothermally Altered Volcanic	XRD / FTIR
097121	LKD044 @ 42m	Lerokis zone 5	Hydrothermally Altered Volcanic	XRD / FTIR
097130	LKD044 @ 85m	Lerokis zone 5	Hydrothermally Altered Volcanic	XRD / FTIR
097134	LKD044 @ 99.5m	Lerokis zone 5	Hydrothermally Altered Volcanic	XRD / FTIR
097201	305	Lerokis zone 5	Hydrothermally Altered Volcanic	XRD / FTIR
097146	LKD044 @ 184m	Lerokis zone 5	Hydrothermally Altered Volcanic	XRD / FTIR
097148	LKD044 @ 207m	Lerokis zone 5	Hydrothermally Altered Volcanic	XRD / FTIR
099905	7	Lerokis zone 5	Hydrothermally Altered Volcanic	XRD / FTIR
099910	11	Lerokis zone 5	Hydrothermally Altered Volcanic	XRD / FTIR
099913	13	Lerokis zone 5	Hydrothermally Altered Volcanic	XRD / FTIR
099926	26	Lerokis zone 5	Hydrothermally Altered Volcanic	XRD / FTIR
099932	24	Lerokis zone 5	Hydrothermally Altered Volcanic	XRD / FTIR
099935	35	Lerokis zone 5	Hydrothermally Altered Volcanic	XRD / FTIR
099936	35	Lerokis zone 5	Hydrothermally Altered Volcanic	XRD / FTIR
111929	216	Lerokis zone 4	Hydrothermally Altered Volcanic	XRD / FTIR
111932	218	Lerokis zone 4	Hydrothermally Altered Volcanic	XRD / FTIR
111933	215	Lerokis zone 4	Hydrothermally Altered Volcanic	XRD / FTIR
111934	217	Lerokis zone 4	Hydrothermally Altered Volcanic	XRD / FTIR
111935	136	Lerokis zone 4	Hydrothermally Altered Volcanic	XRD / FTIR/ XRF
111958	138	Lerokis zone 4	Hydrothermally Altered Volcanic	XRD / FTIR
111962	139	Lerokis zone 4	Hydrothermally Altered Volcanic	XRD / FTIR / TS
111965	140	Lerokis zone 4	Hydrothermally Altered Volcanic	XRD / FTIR
111966	141	Lerokis zone 4	Hydrothermally Altered Volcanic	XRD / FTIR
111969	143	Lerokis zone 4	Hydrothermally Altered Volcanic	XRD / FTIR
111971	247	Lerokis zone 4	Hydrothermally Altered Volcanic	XRD / FTIR
111972	142	Lerokis zone 4	Hydrothermally Altered Volcanic	XRD / FTIR
111973	248	Lerokis zone 4	Hydrothermally Altered Volcanic	XRD / FTIR
111978	249	Lerokis zone 4	Hydrothermally Altered Volcanic	XRD / FTIR
111983	153	Lerokis zone 4	Hydrothermally Altered Volcanic	XRD / FTIR
111985	154	Lerokis zone 4	Hydrothermally Altered Volcanic	XRD / FTIR
111987	155	Lerokis zone 4	Hydrothermally Altered Volcanic	XRD / FTIR
111991	157	Lerokis zone 4	Hydrothermally Altered Volcanic	XRD / FTIR
111994	316	Lerokis zone 4 area	Hydrothermally Altered Volcanic	XRF
087072	162	Lerokis zone 4	Hydrothermally Altered Volcanic	XRD / FTIR
096948	129	Lerokis zone 4	Hydrothermally Altered Volcanic	XRD / FTIR
096857	75	Kali Kuning	Sulphides	RLTS / EM / He
111943	63	Kali Kuning	Sulphides	RLTS
097222	KKD 058 @ 90m	Kali Kuning	Sulphides	RLTS
099917	15	Lerokis zone 5	Sulphides	RLTS
099903	5	Lerokis zone 5	Sulphides	RLTS / EM
097002	LKD 042 @ 4.7 m	Lerokis zone 5	Sulphides	RLTS / He
097009	LKD 042 @ 22 m	Lerokis zone 5	Sulphides	RLTS / EM
097016	LKD 042 @ 41 m	Lerokis zone 5	Sulphides	RLTS
097056	LKD 043 @ 33 m	Lerokis zone 5	Sulphides	RLTS
097059	LKD 043 @ 42 m	Lerokis zone 5	Sulphides	RLTS / He

097104	LKD 043 @ 179 m	Lerokis zone 5	Sulphides	RLTS
097122	LKD 044 @ 50 m	Lerokis zone 5	Sulphides	RLTS / EM
097129	LKD 044 @ 77 m	Lerokis zone 5	Sulphides	RLTS
111975	146	Lerokis zone 4	Barite	OS/ SEM / EM
111930	216	Lerokis zone 4	Barite	OS/ SEM / EM
111983	152	Lerokis zone 4	Barite	OS
096858	75	Kali Kuning	Pyrite sand	OS
096890	87	Kali Kuning	Pyrite sand	OS
096877	84	Kali Kuning	Barite	OS
096878	84	Kali Kuning	Barite	OS
096879	84	Kali Kuning	Barite	OS / SEM / EM
096880	84	Kali Kuning	Barite	OS
099944	50	Kali Kuning	Barite	OS / SEM / EM
099911	12	Lerokis zone 5	Oxide / barite pipe	SEM / EM
099923	19	Lerokis zone 5	Oxide / barite pipe	SEM / EM
096948	129	Lerokis zone 4	Oxide / barite pipe	SEM / EM / FI
097106	LKD043 @ 210m	Lerokis zone 5	Barite	FI / He
097122	LKD044 @ 50m	Lerokis zone 4	Barite	FI / He
111943	63	Lerokis zone 4	Barite	FI
111979	149	Lerokis zone 4	Barite	He
097024	LKD043 @ 210m	Lerokis zone 5	Barite	FI
097084	LKD043 @ 210m	Lerokis zone 5	Barite	FI / He
096879	84	Kali Kuning	Barite	FI
099938	112	Lerokis zone 5	Barite	FI
099917	15	Lerokis zone 5	Barite	FI
111931	217	Lerokis zone 4	Barite	FI
099939	46	Lerokis zone 5	Barite	FI

For S, O and Sr samples used, refer to Tables 7.1 and 8.2. TS = Thin Section, RLTS = Reflected Ligh thin section
OS = Optical study, EM = electron Microprobe, FI = Fluid Inclusion, He = Helium, XRD = X Ray Diffraction
FTIR = Fourier Transform Infra red, XRF = X ray flourescence

APPENDIX B

Location 52 Sample 099950

Planktonic assemblage includes:

Orbulia universa
Globigerinoides conglobatus
Globigerinoides sacculifer
Globorotalia menardiform group
Sphaeroidinella dehiscens

Benthic assemblage includes:

Cibicidoides
Globocassidulina
Favocassidulina
Fontbotia
Pleurostomella
Stilostomella
Uvigerina

Planktonic:Benthic = >99 : < 1

The planktonic forms are tropical. *Sphaeroidinella dehiscens* is a deep water form which occurs deeper than 500m.

The rare benthic forms are mainly deep water character.
The types of recent *Favocassidulina* were from >2000m, it is present in the Miocene of the Pacific Ocean at this depth.

The planktonic:benthic ratio is indicative of open ocean conditions, probably >2000m as the benthic forms are so rare.

Conclusion:
All the evidence points to this being a deep water deposit – a true biogenic ooze. It is impossible to determine the depth precisely because there are no depth indicator species (most are tied to water masses or to food supply). However, it is likely to be from at least 2000m and possible considerably deeper.

John Murray
Feb. 1999

APPENDIX C

APPENDIX C. X-RAY FLOURESCENCE

SAMPLE PREPARATION

Major and trace element concentrations were determined by XRF analysis using fused glass discs and pressed powder pellets respectively.

- Whole-rock samples were crushed using a hydraulic rock-splitter,
- the fine material was then ground in case-hardened purified steel pot within a TEMA® mill.

Crushing apparatus was thoroughly cleaned after each sample to avoid any sample contamination.

Fused discs

- Samples were calcined overnight in porcelain crucibles at temperatures of ~970°C.
- Accurately weighed portions of this were then mixed with flux in a ratio of 5:1, the flux used was Spectroflux® 100B containing lithium tetraborate.

Pressed pellets

- Use ~10 g of fine sample powder,
- the non-calcined sample powder was mixed with~ 8 drops of polyvinyl aldehyde (PVA) binder,
- A 12 tonne pressure was applied to each sample to form the disc.

SAMPLE RUNNING

Samples were run on a Phillips PW1400 automated sequential wavelength dispersive X-ray Flourescence spectrometer which used a 3kW Rhodium anode side window X-ray tube at Southampton University.

GENERAL METHODOLOGY

Elements can be measured at concentrations ranging from approximately 1 ppm through to 100 %.

Major Elements: Majors are normally determined on a fused bead using a borate flux that is chosen to be most suitable to dissolve the sample. Where there is sufficient sample for produce a bead and a powder pellet then a 5:1 dilution is normally chosen to produce bead. Where material is in limited supply, then major and trace element data may be determined on a 2:1 bead. Additionally, for rock compositions that are difficult to form homogeneous solid-solutions high dilution factors may be used (e.g. 10:1, 20:1, 50:1, 100:1 etc.).

Trace Elements: Since the concentration of trace elements is low their contribution to enhancement effects is negligible and therefore only absorption needs to be compensated for. The scattered radiation method is used to compensate for matrix variations between samples and this is well-established procedure.

Detection Limits:

Table 1: Detection Limits in routine XRF analysis at Southampton using a Rh anode X-ray tube.

Element	X-Ray	Possible interferences*	L.L.D. (ppm) **
As	As L		6
Ba	Ba L	Ce, high As	10
Bi	Bi L	W	5
Br	Br K		30
Ce	Ce L		10
Cl	Cl K		50
Cr	Cr K	V	4
Cu	Cu K	Cu from the tube	3
Ga	Ga K		1.5
I	I K		4
La	La K		5
Mo	Mo K		5
Ni	Ni K		1.5
Nb	Nb K	Y	1.5
P	P K		30
Pb	Pb L	Bi	1.5
Rb	Rb K	high U	1.5
S	S K		50
Sb	Sb Kα		5
Sn	Sn K		4
Sr	Sr K		1.5
Th	Th L	High Pb	2
U	U	High Rb	3
V	V K		4
W	W L	High Zn, Ga	8
Y	Y K	Rb	1.5
Zn	Zn K		1.5
Zr	Zr K	Sr	1.5

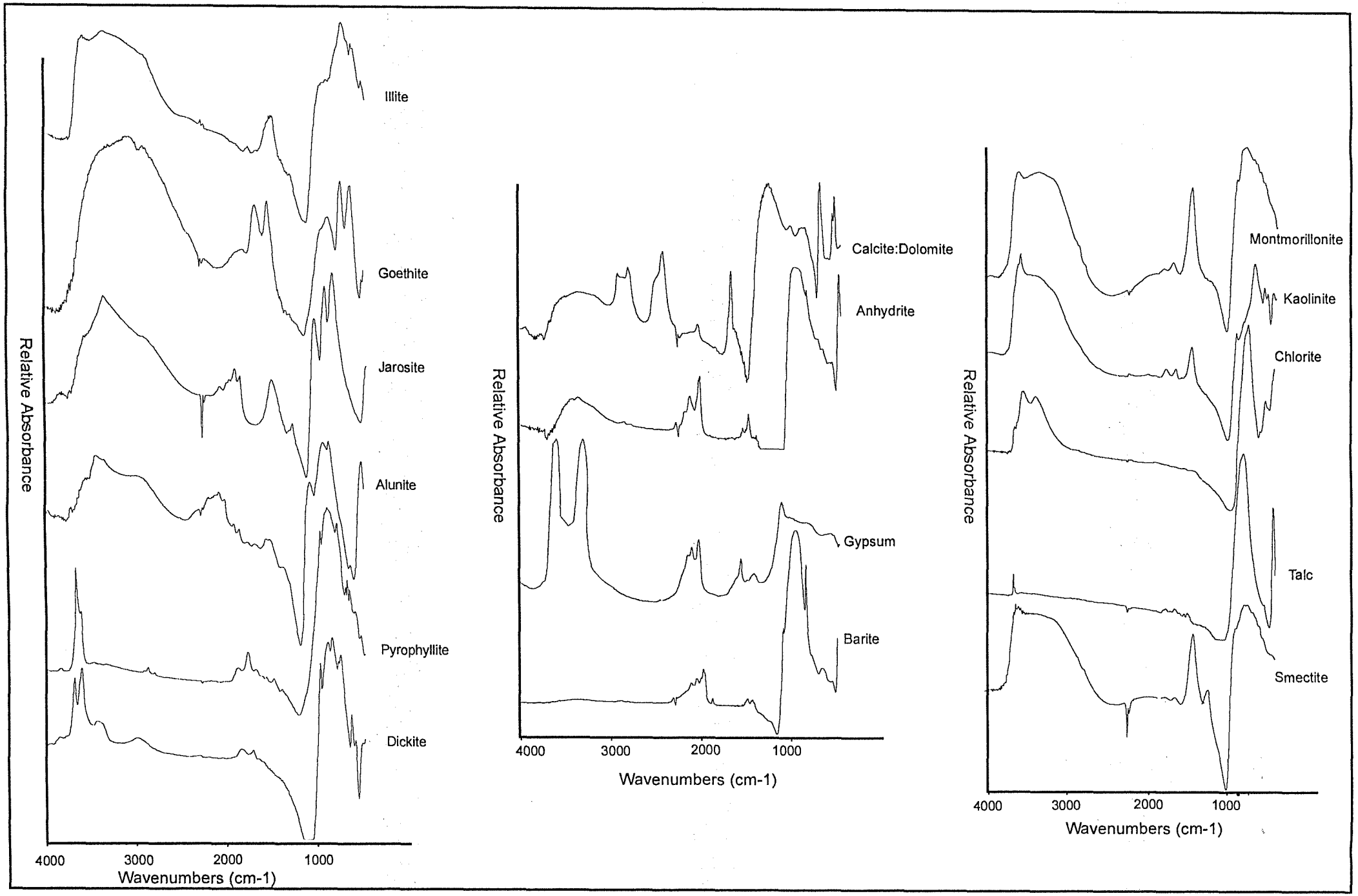
Footnote:

The detection limits are calculated assuming a count-time of 100 seconds on the background.

* Note that most of these interferences are already dealt with automatically.

**Better DLs may be obtained by using longer count times.

Appendix C.						
XRF analysis						
Sample	**Crucible**	**Crucible**	**Crucible +**	**Crucible + dry**	**Crucible + ignited**	**LOI**
	code	**weight (g)**	**sample weight (g)**	**sample weight (g)**	**sample weight (g)**	**in weight %**
097167	D11	16.7601	19.1748	19.1675	19.1010	11.23%
097168	20	10.3387	12.4532	12.3970	12.3369	6.40%
096884	4	15.1502	17.1389	17.0911	17.0284	8.32%
111914	25	11.0368	13.2858	13.2789	13.1475	7.41%
096920	8	15.4226	17.4682	17.4526	17.4207	8.87%
100129	29	17.8744	19.9550	19.8549	19.7772	9.87%
096926	14	15.8075	18.1255	18.1182	18.0934	10.29%
111001	3	15.2358	17.5820	17.5778	17.5715	10.08%
111994	9	15.2334	17.3087	17.3008	17.2560	8.95%
096930	7	14.6314	16.6662	16.6372	16.5737	8.37%
096927	1	15.9925	18.1950	18.1857	18.1312	9.92%
111999	E3	14.4244	16.5342	16.5306	16.5255	8.68%
111935	ZZ3	16.7188	19.0734	19.0726	19.0675	10.97%
097106	16	15.7620	17.8441	17.8399	17.7026	9.32%



Appendix C. Representative FTIR spectra used to determine alteration zones at Wetar Island.

APPENDIC C. X-RAY DIFFRACTION

The mineralogy of the altered volcanics around the Wetar deposits were determined using the Phillips PW1390 diffracter at the University of Southampton.

SAMPLE PREPARATION

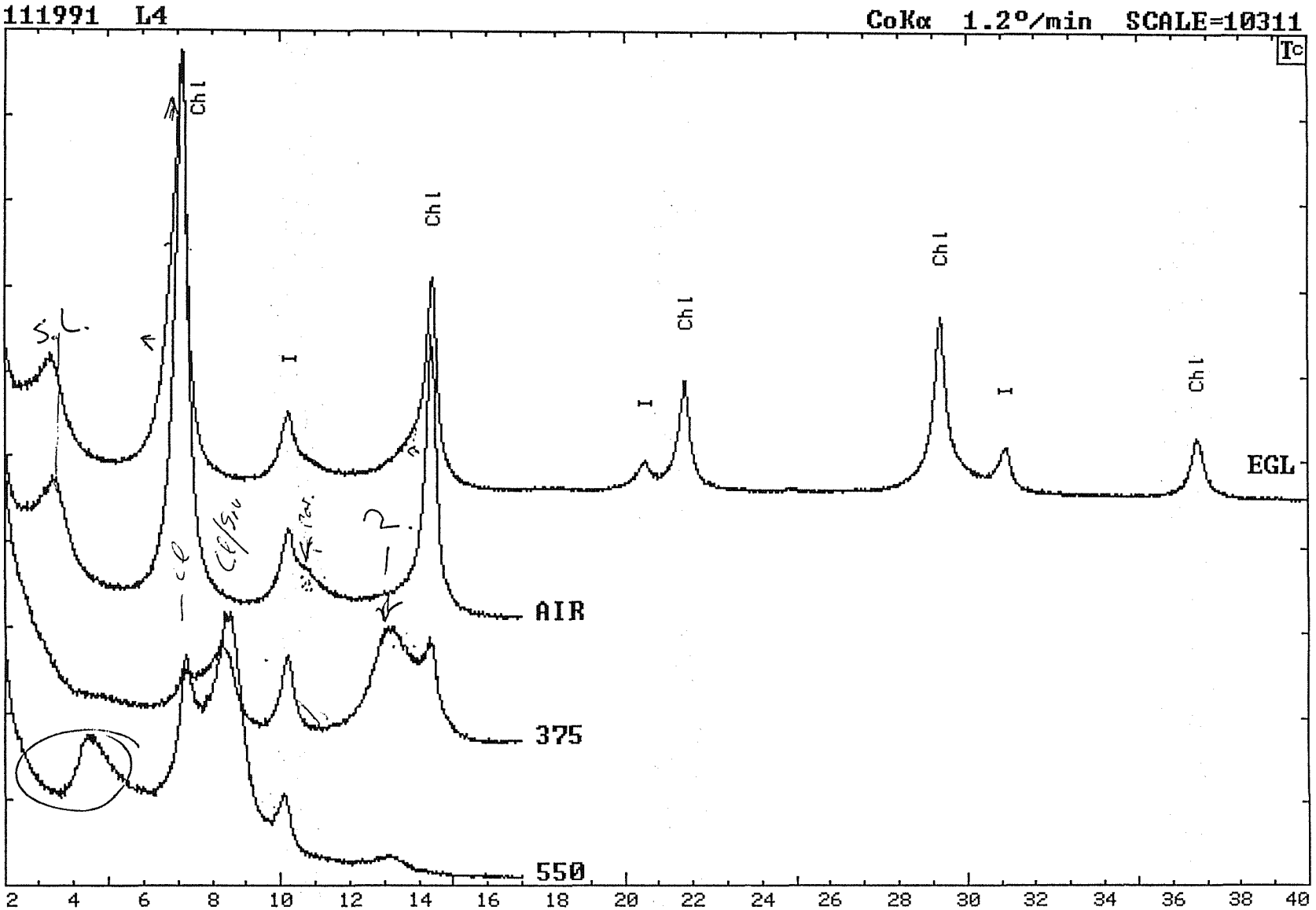
The crushed rock samples were rolled with a metal roller then dispersed in distilled water and placed into the ultrasonic bath for 45 minutes to liberate clay and alteration minerals from the rock into suspension. Calgon was then added to keep clay minerals in suspension whilst larger or denser mineral phases settled out during a period of approximately 30 seconds. Samples were then decanted, the coarser fractions were discarded and the remaining < 2μm clay fraction was centrifuged at 750 rpm for 3.3 minutes. The sample were decanted again, this time keeping the coarse fraction, Mg chloride was then added to counter affect the calgon by saturating expandable clays with Mg. The remaining clay fraction was centrifuged at 3,000 rpm, the clear water was discarded and the clay samples were then smeared onto glass slides. The samples were run through XRD in an air dried state and glycolated. This vapour pressure method involved leaving the slide in a sealed container with warm glycerol (42°C). The glycerol vapour is absorbed by the clay mineral modifying the crystal structure slightly thus changing the XRD trace. The clays were also analysed immediately after heating to 350° and 550°C, this was done to note any transformations in the clay minerals. The mineralogy of the orientated clay samples (dry and glycolated) was determined by using CuK alpha radiation and a graphite monochrometer.

FTIR Method

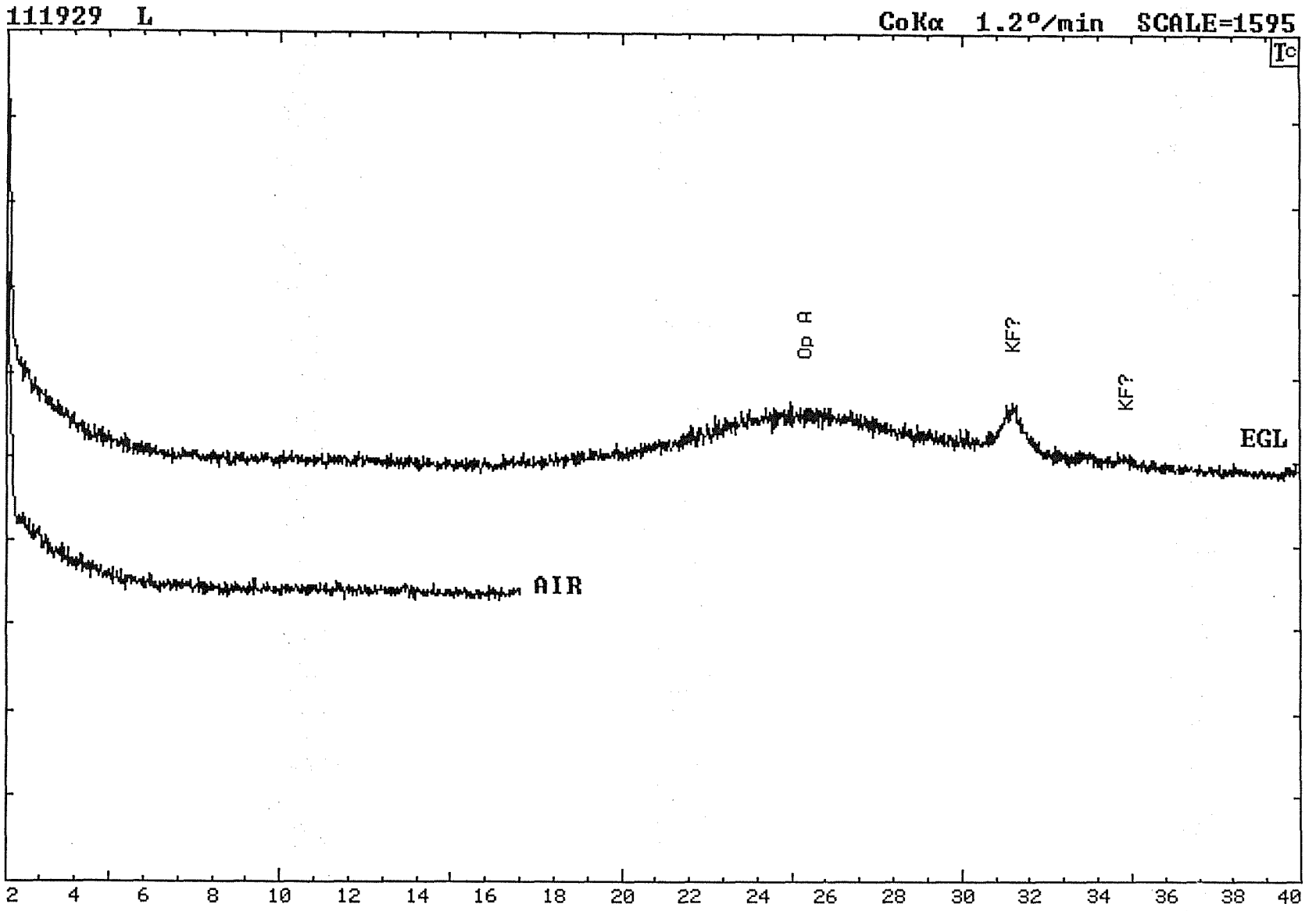
Fourier transform infrared spectroscopy (FTIR) is an analytical technique used to identify organic (and in some cases inorganic) materials. The FTIR technique measures the range of wavelengths in the infrared region that are absorbed by a material being analysed. These infrared absorption bands identify molecular components and structures. Absorption bands in the range of 4000 - 1500 wavenumbers are typically due to functional groups (e.g. -OH, C=O, N-H, CH3, etc.). The region between 1500 - 400 wavenumbers is referred to as the fingerprint region. Sample preparation involved liberating a minute amount of altered specimen with a set of sharp tweezers.

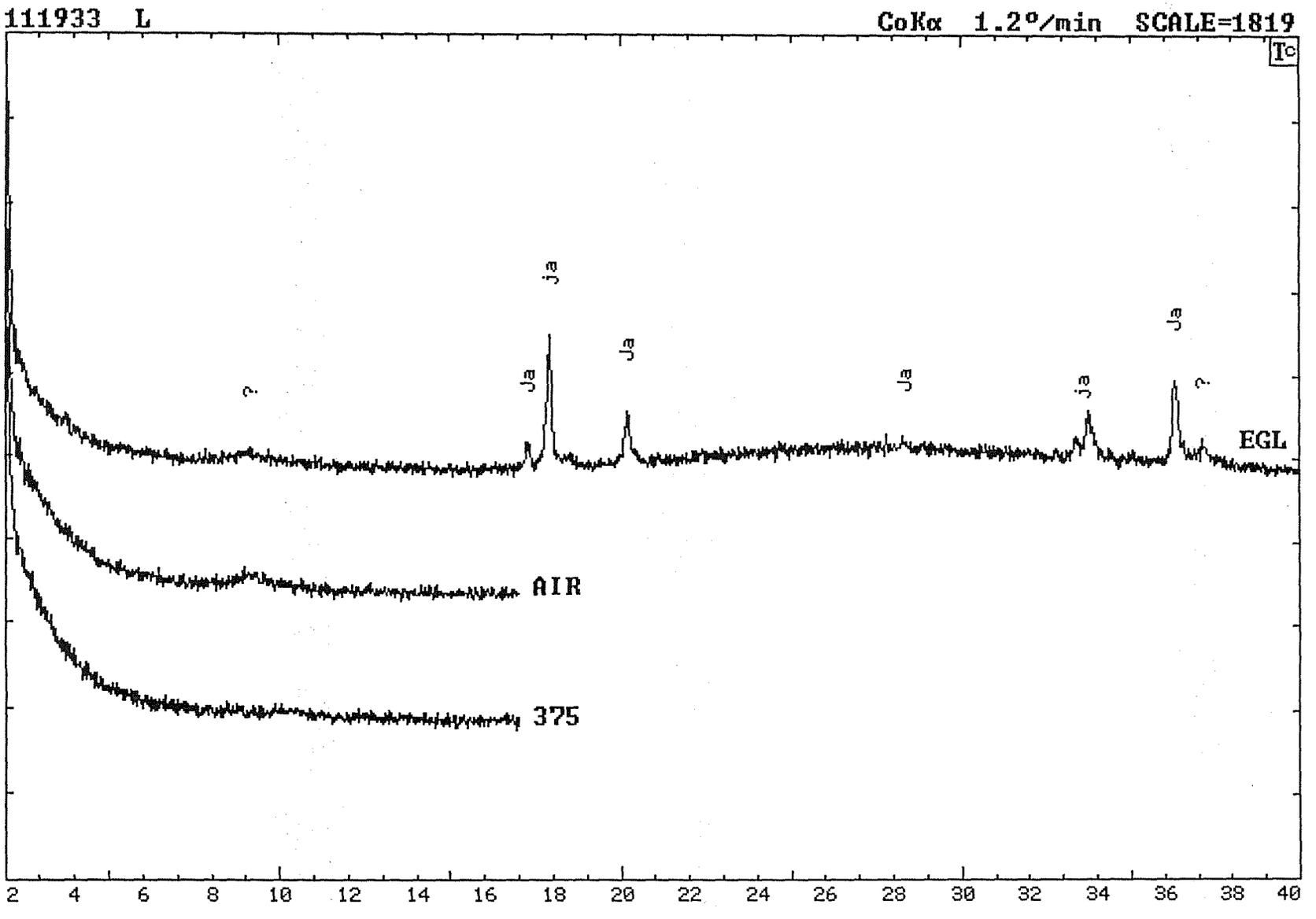
All samples were analysed at the University of Southampton. Concentration of a compound can be determined by establishing a standard curve of known concentrations. The technique was used to supplement the XRD study.

? Re Kun.

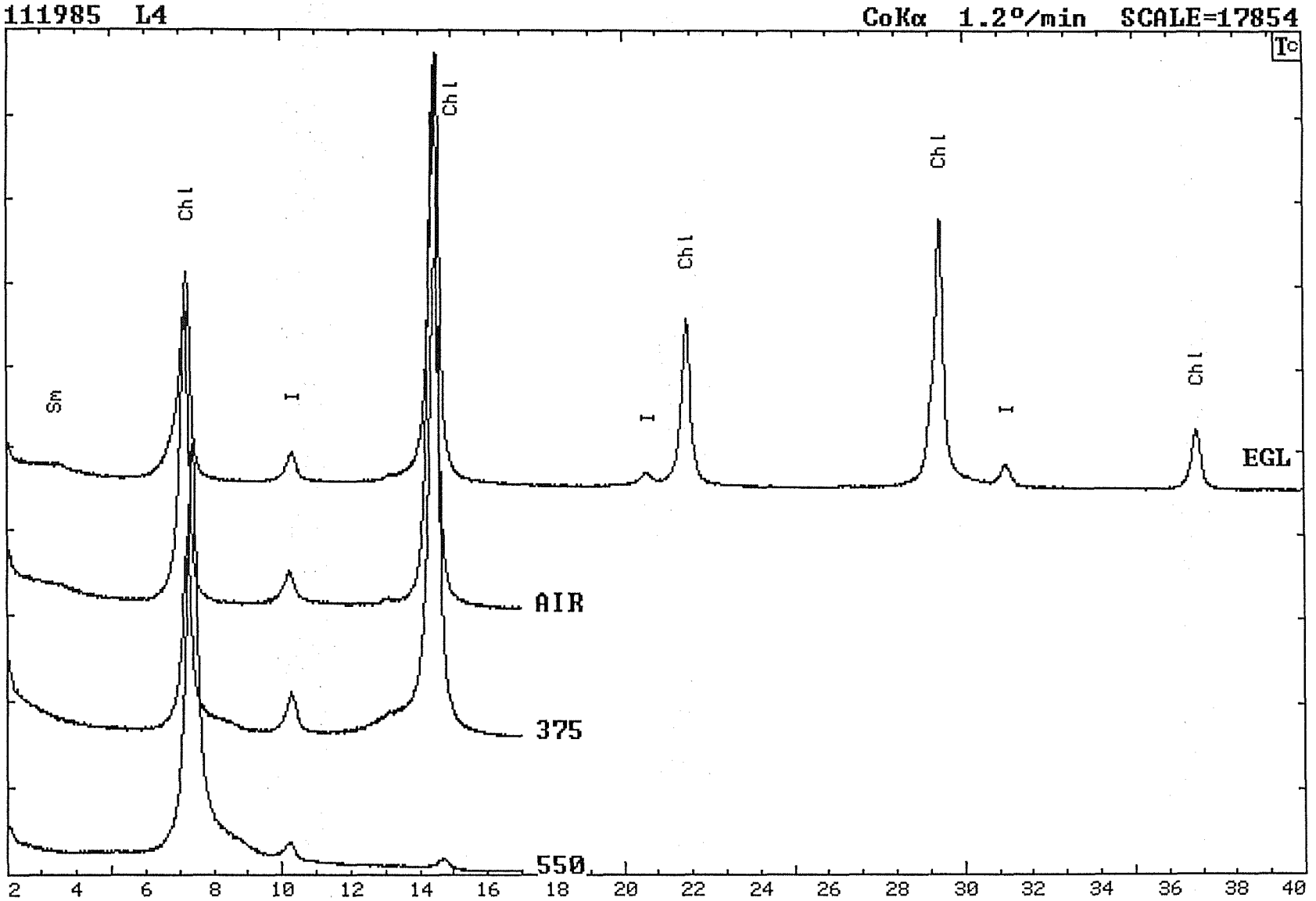


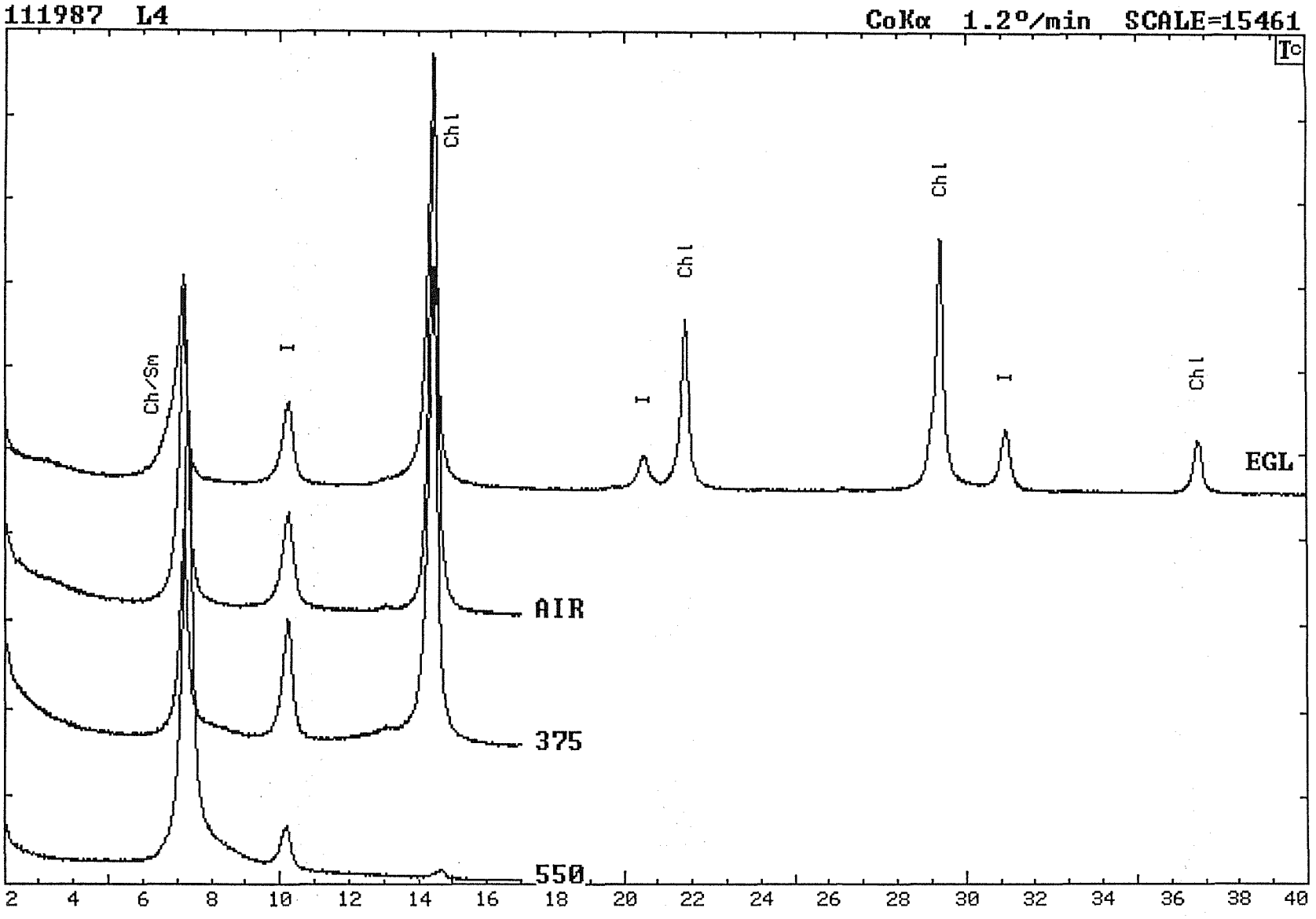
not heated sample.

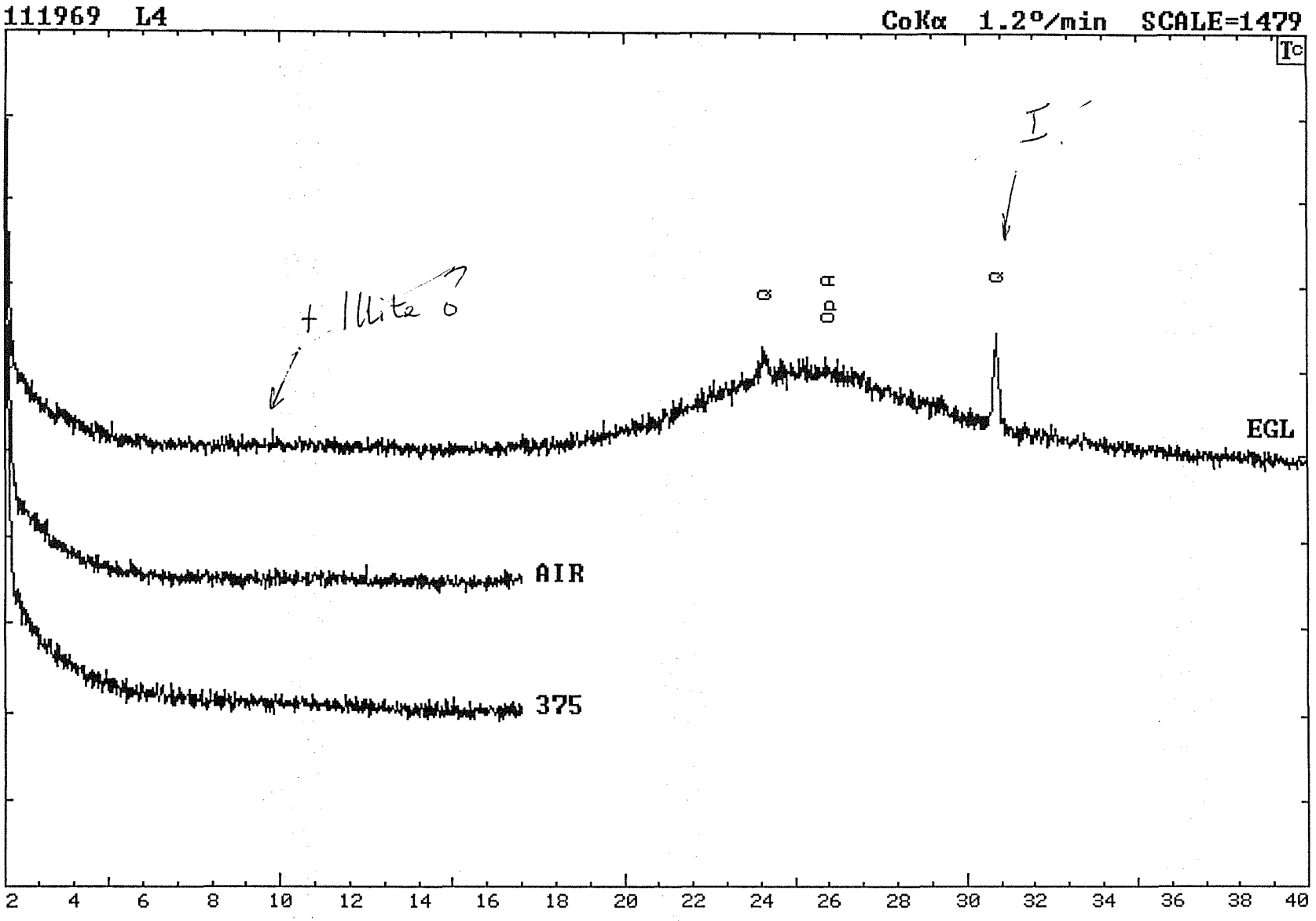

111929 L
CoKα 1.2°/min SCALE=1595
Tc
Op A
KF?
KF?
EGL
AIR
2 4 6 8 10 12 14 16 18 20 22 24 26 28 30 32 34 36 38 40

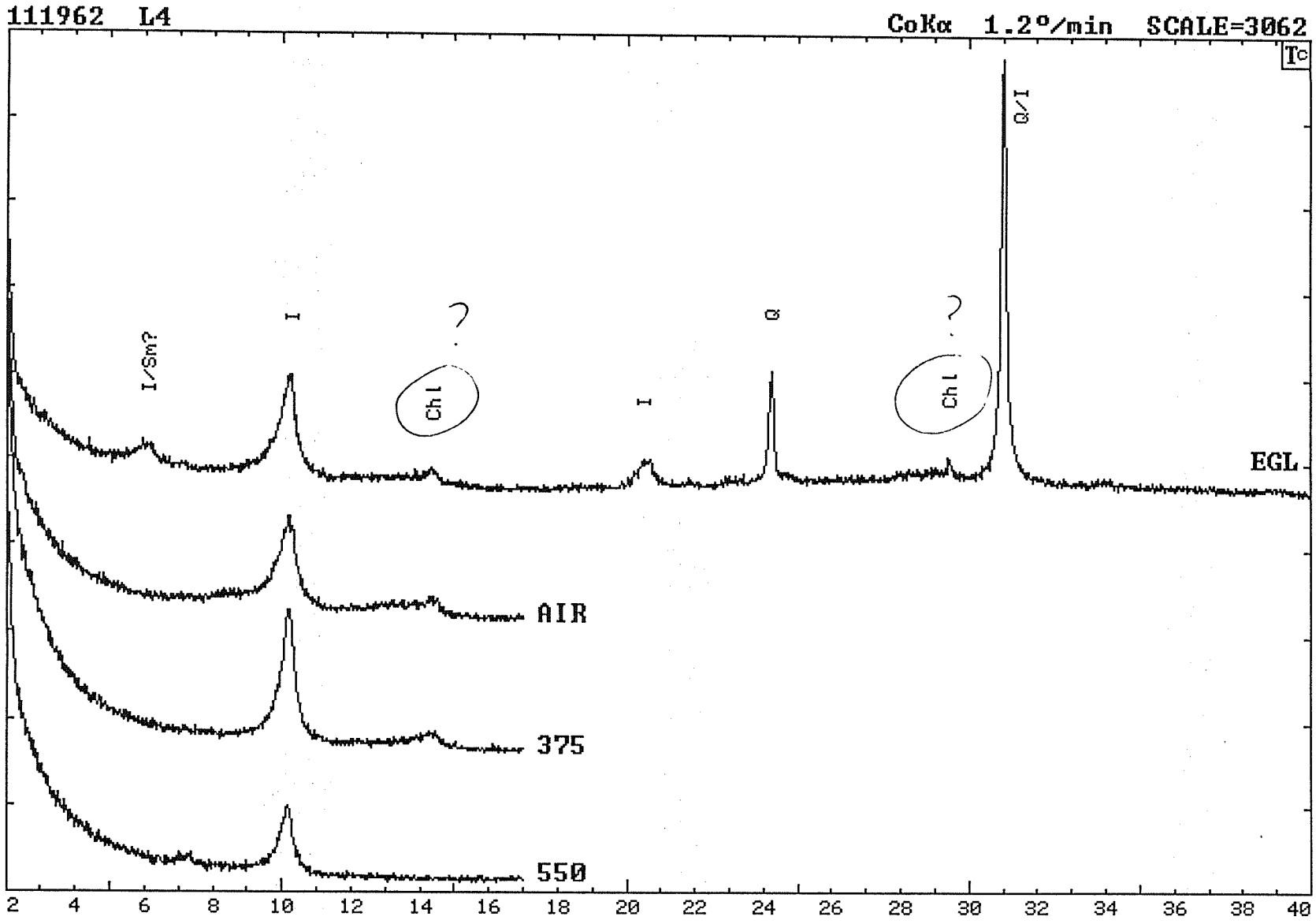

111933 L
CoKα 1.2°/min SCALE=1819
Tc
?
Ja
Ja
Ja
Ja
Ja
?
EGL
AIR
375
2 4 6 8 10 12 14 16 18 20 22 24 26 28 30 32 34 36 38 40

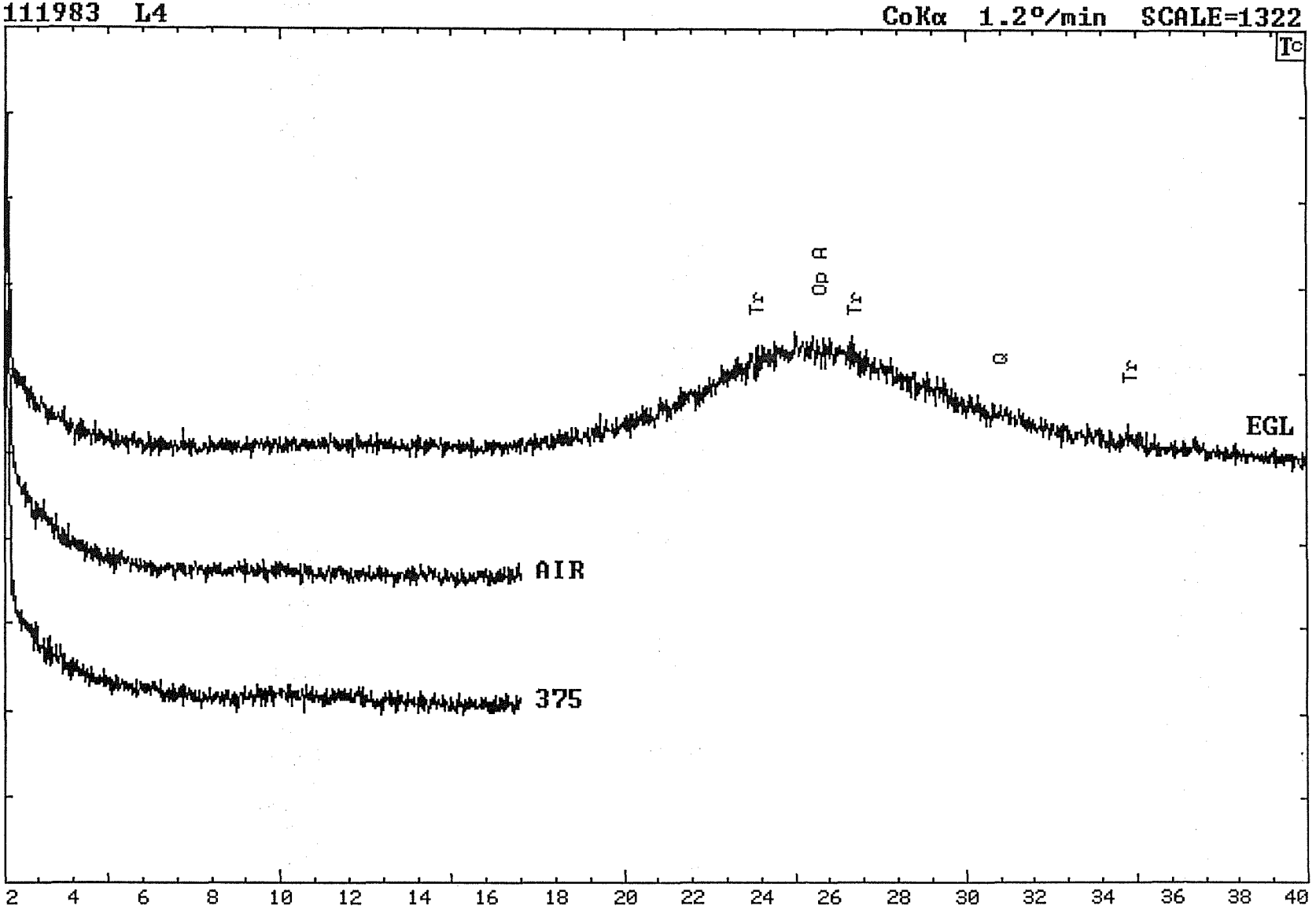
Loc 154

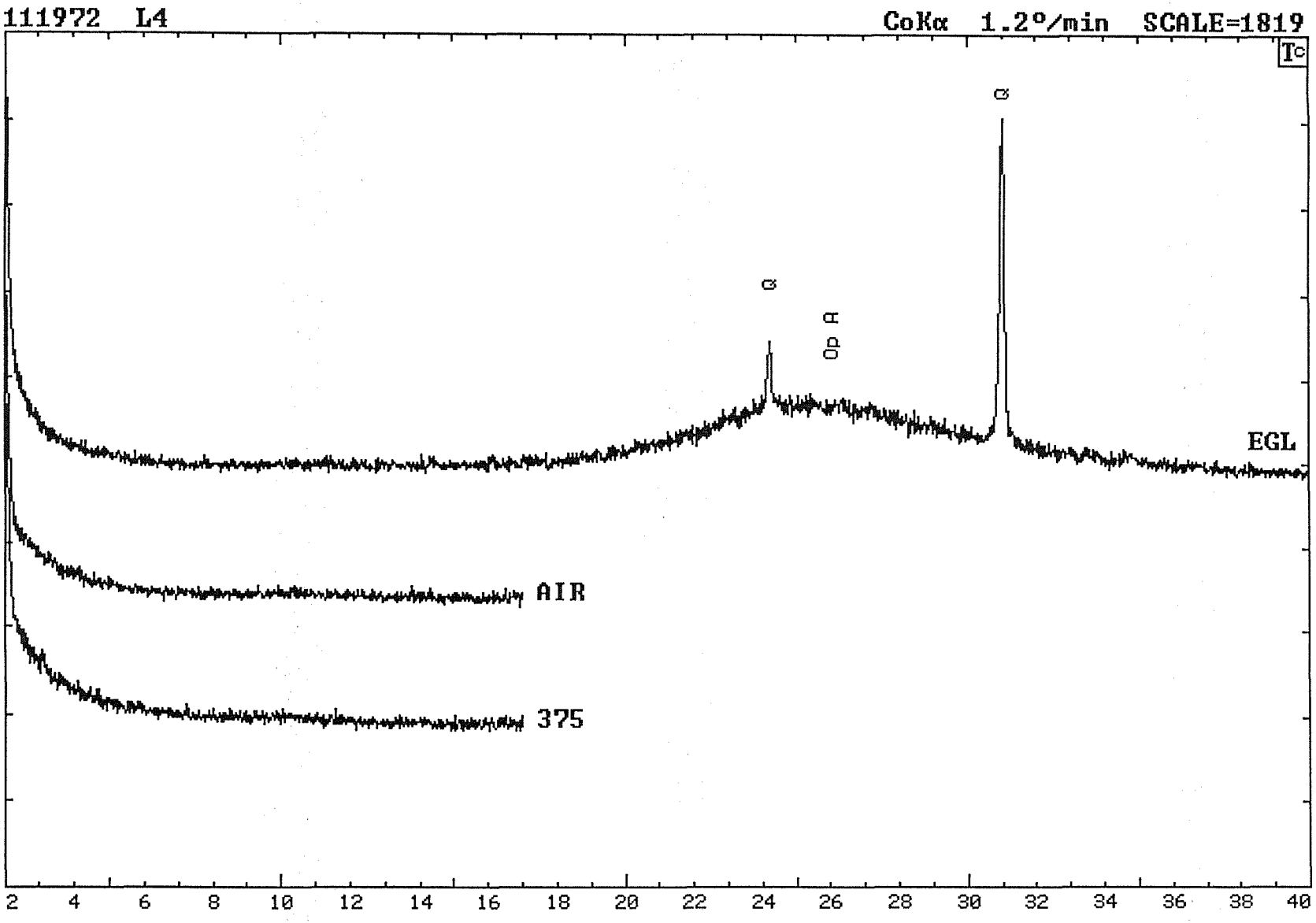

111985 L4
CoKα 1.2°/min SCALE=17854
Tc
Chl
Chl
Chl
Chl
Sm
I
I
I
EGL
AIR
375
550
2 4 6 8 10 12 14 16 18 20 22 24 26 28 30 32 34 36 38 40

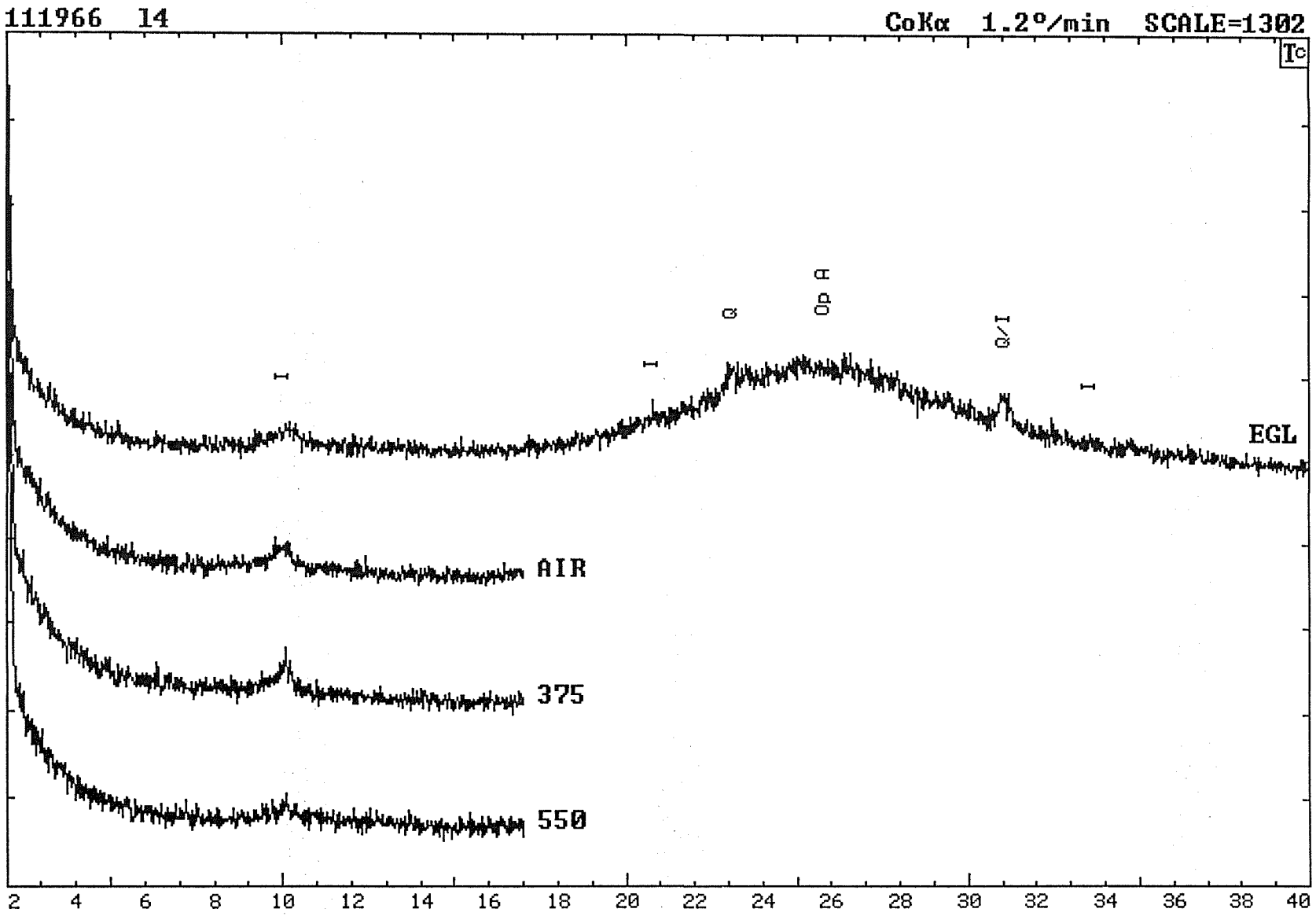

111987 L4
CoKα 1.2°/min SCALE=15461
Tc
Ch/Sm
I
Chl
I
Chl
Chl
I
Chl
EGL
AIR
375
550
2 4 6 8 10 12 14 16 18 20 22 24 26 28 30 32 34 36 38 40

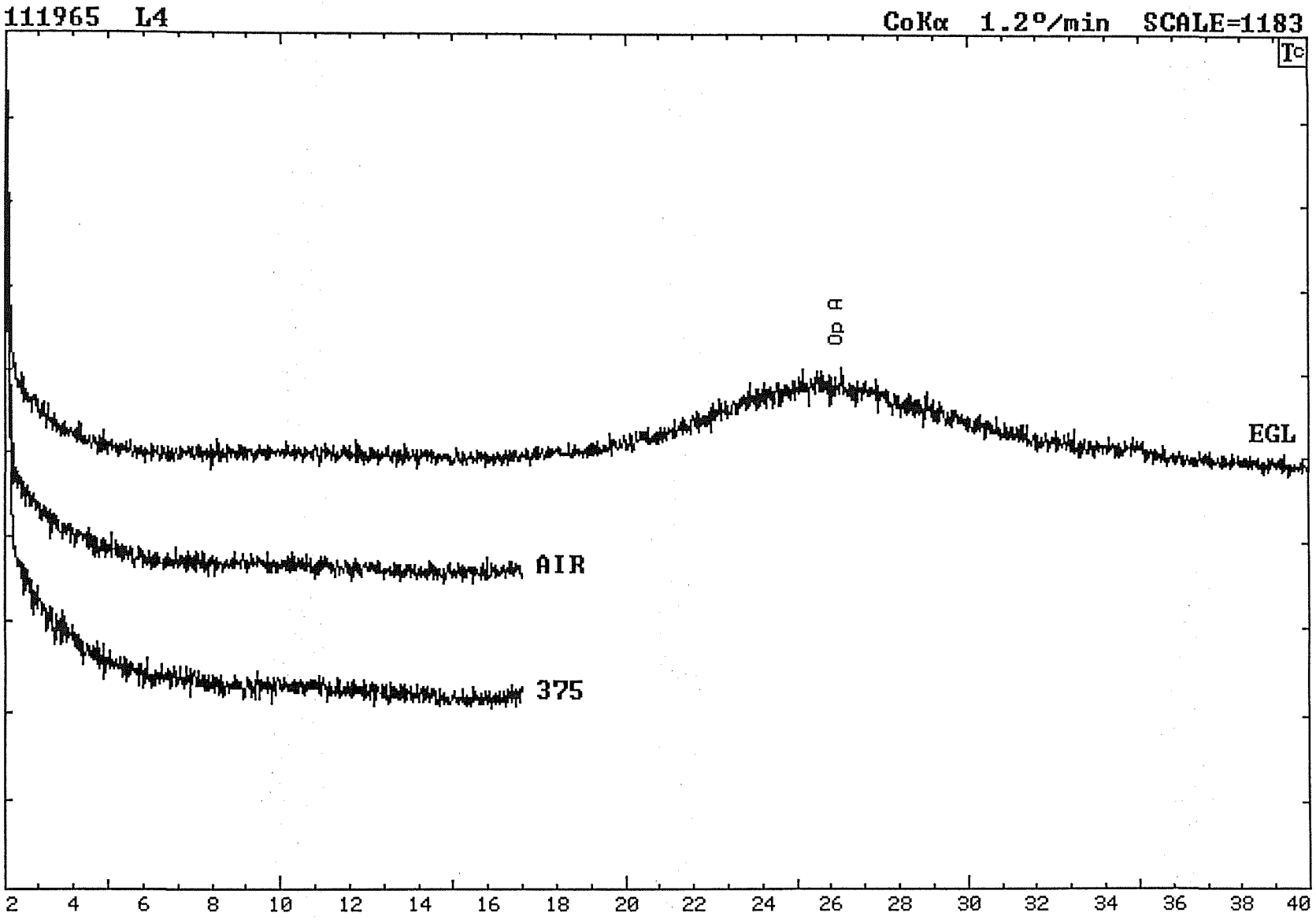

111969 L4
CoKα 1.2°/min SCALE=1479
Tc
I
+ Illite ?
α
αβ α
α
EGL
AIR
375
2 4 6 8 10 12 14 16 18 20 22 24 26 28 30 32 34 36 38 40

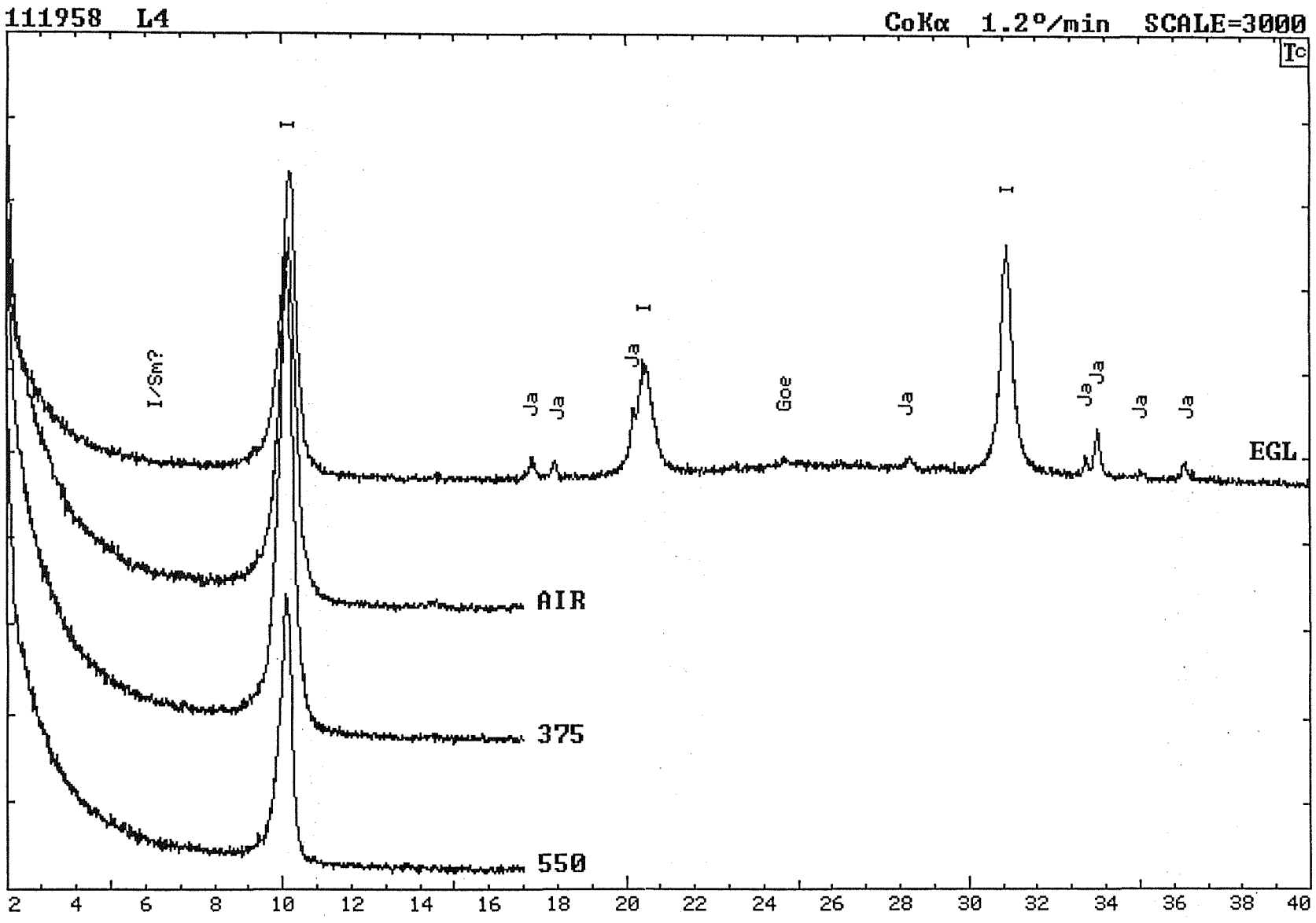

111962 L4
CoKα 1.2°/min SCALE=3062
Tc
I/Sm?
I
Chl ?
I
Q
Chl ?
Q/I
EGL
AIR
375
550
2 4 6 8 10 12 14 16 18 20 22 24 26 28 30 32 34 36 38 40


111983 L4
CoKα 1.2°/min SCALE=1322
Tc
Tr
Op A
Tr
α
Tr
EGL
AIR
375
2 4 6 8 10 12 14 16 18 20 22 24 26 28 30 32 34 36 38 40

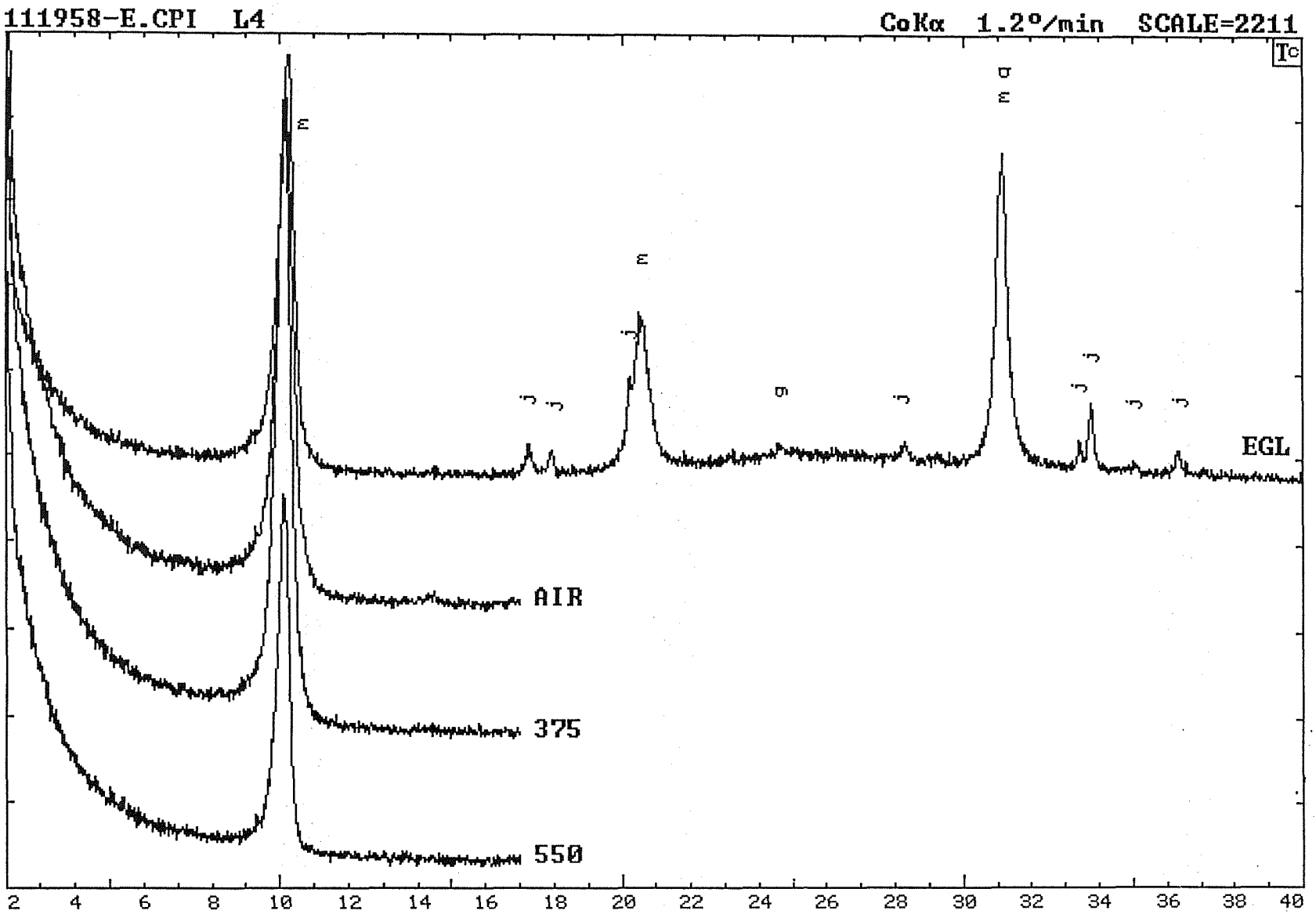

111972 L4
CoKα 1.2°/min SCALE=1819
Tc
α
Op A
α
EGL
AIR
375
2 4 6 8 10 12 14 16 18 20 22 24 26 28 30 32 34 36 38 40


111966 14
CoKα 1.2°/min SCALE=1302
Tc
I
I
Q
Qp A
Q/I
I
EGL
AIR
375
550
2 4 6 8 10 12 14 16 18 20 22 24 26 28 30 32 34 36 38 40

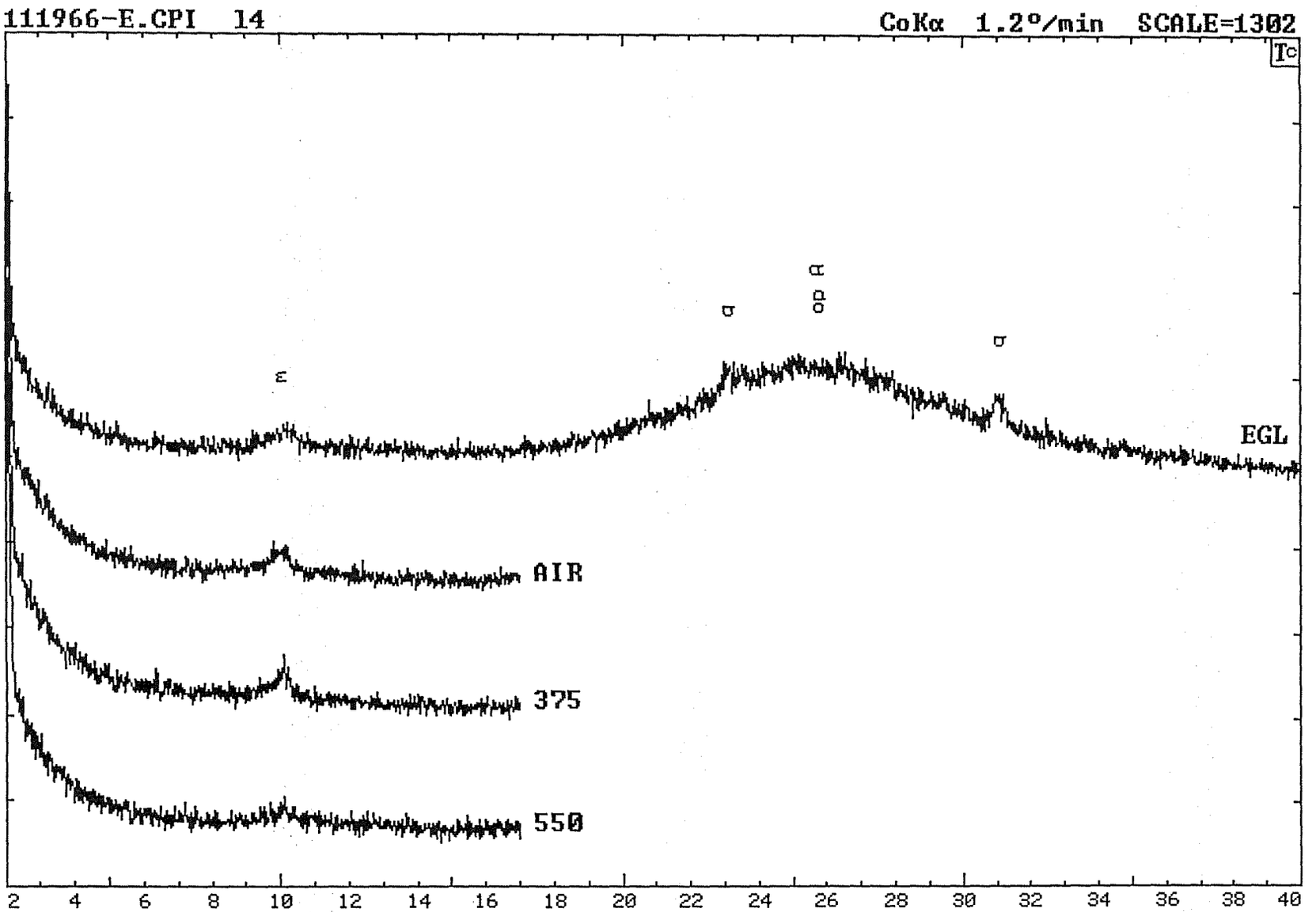

111965 L4
CoKα 1.2°/min SCALE=1183
Tc
Op a
EGL
AIR
375
2 4 6 8 10 12 14 16 18 20 22 24 26 28 30 32 34 36 38 40

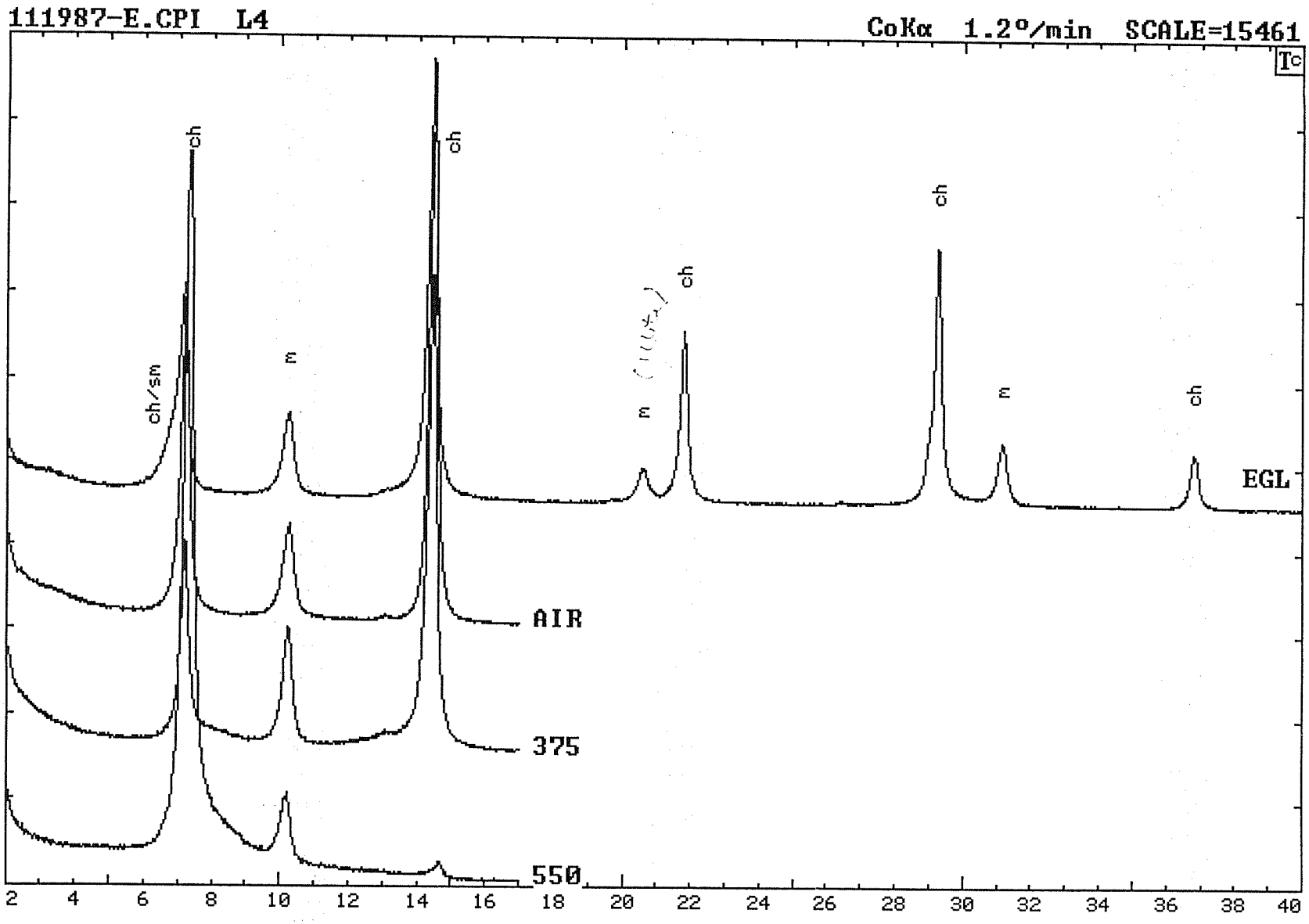

111958 L4
CoKα 1.2°/min SCALE=3000
Tc
I/Sm?
I
Ja
Ja
I
Ja
Goe
Ja
I
Ja
Ja
Ja
Ja
EGL
AIR
375
550
2
4
6
8
10
12
14
16
18
20
22
24
26
28
30
32
34
36
38
40

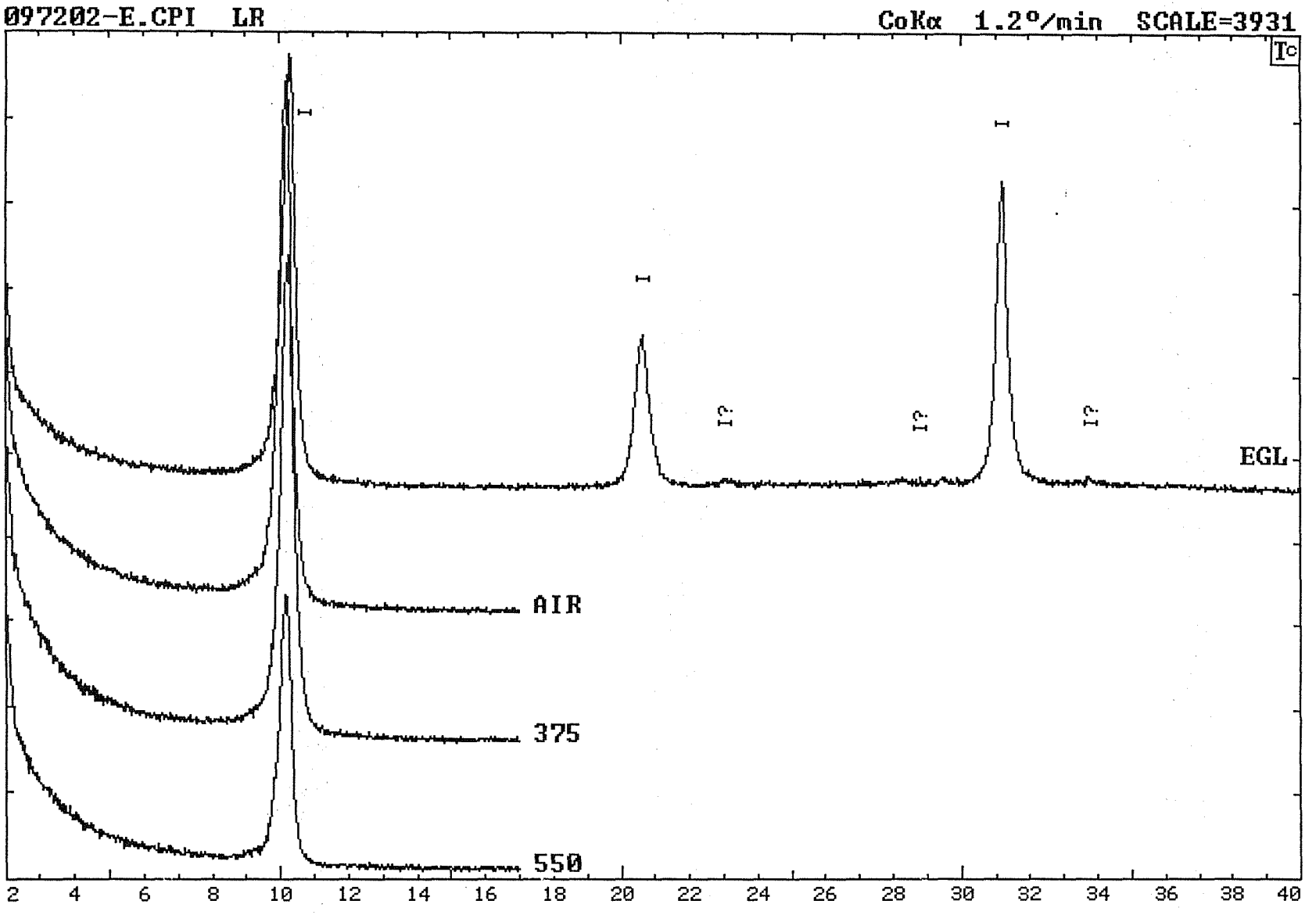
Gossanous

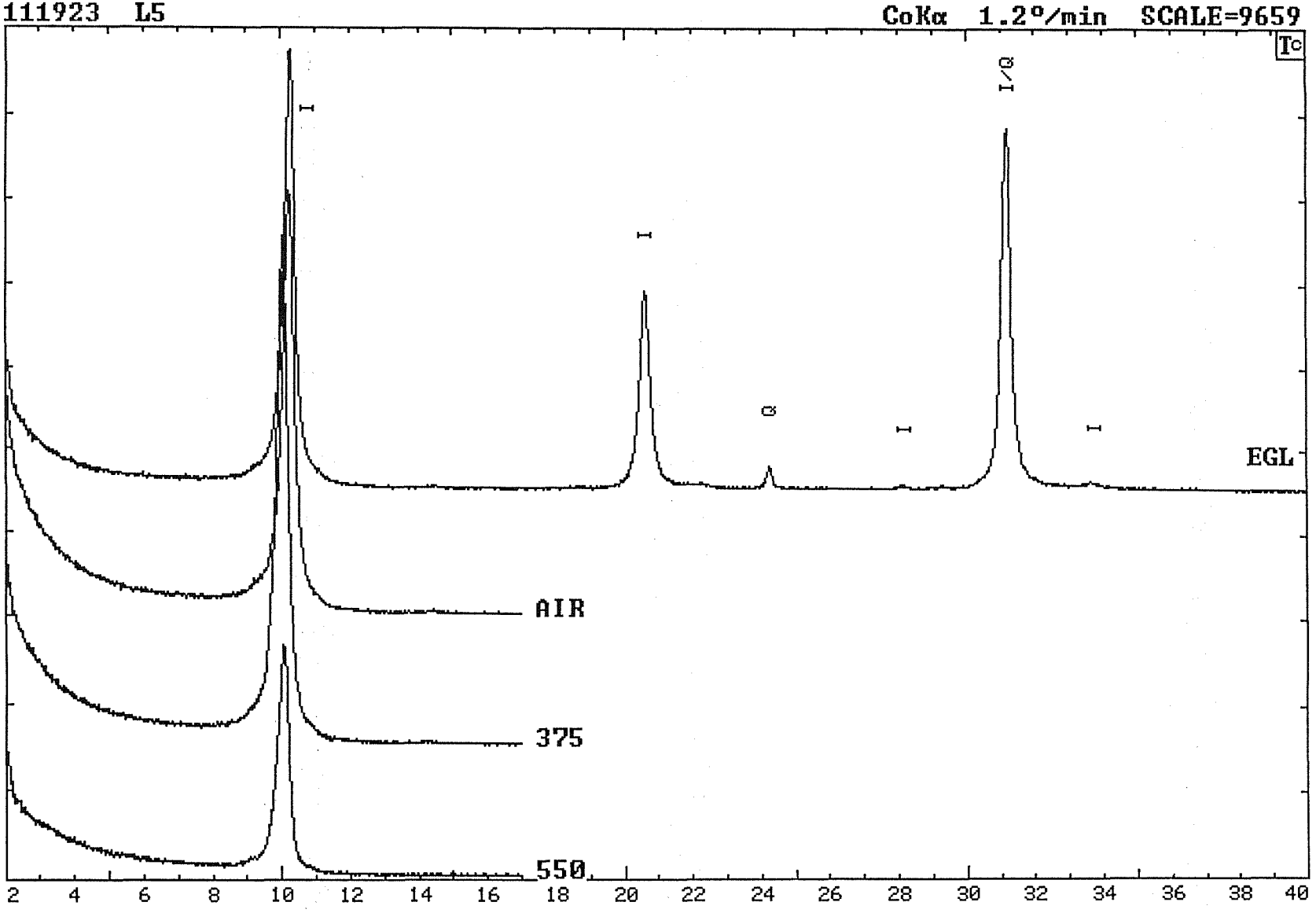

111958-E.CPI L4
CoKα 1.2°/min SCALE=2211
Tc
EGL
AIR
375
550
2 4 6 8 10 12 14 16 18 20 22 24 26 28 30 32 34 36 38 40

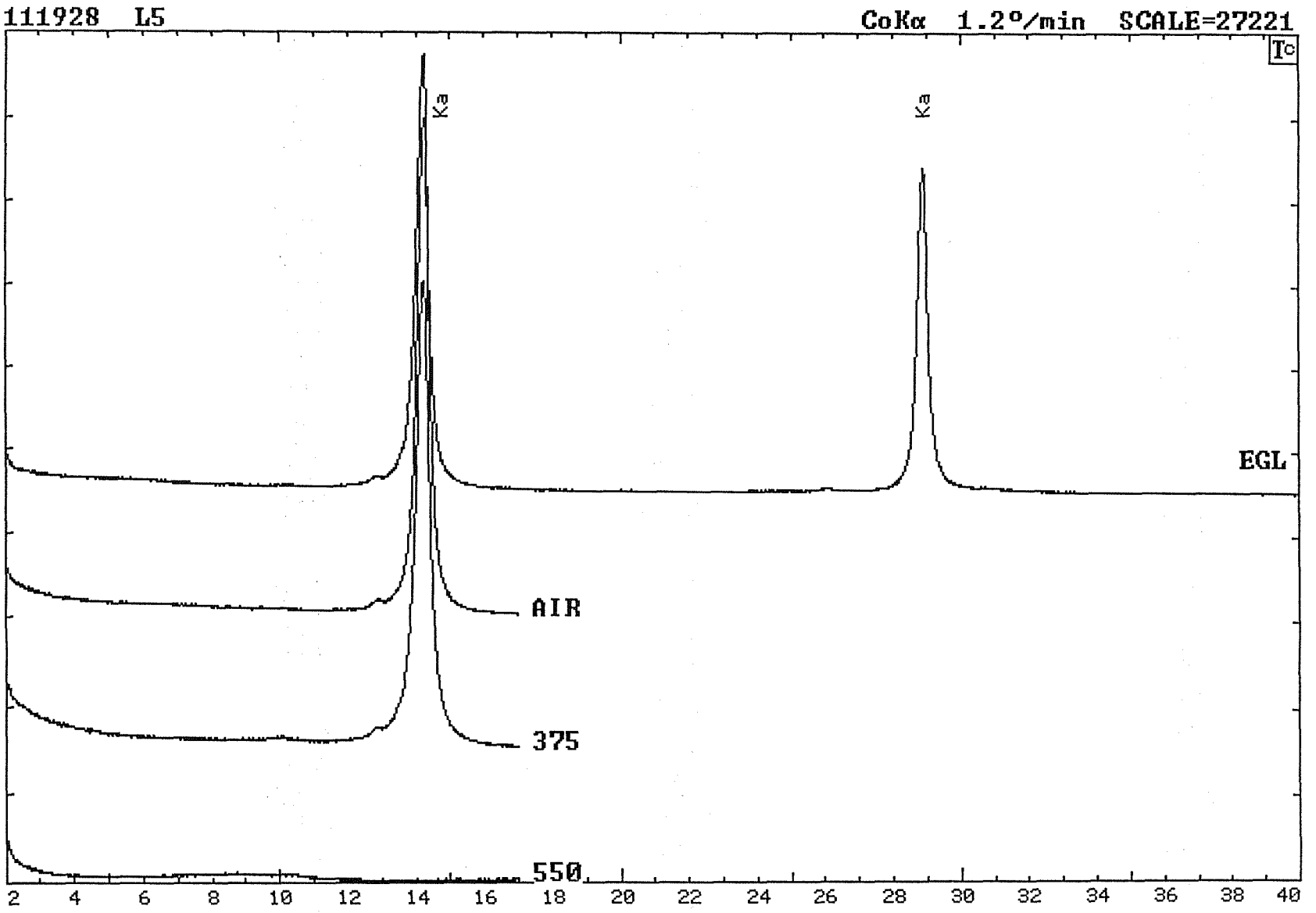
6044N/4962E

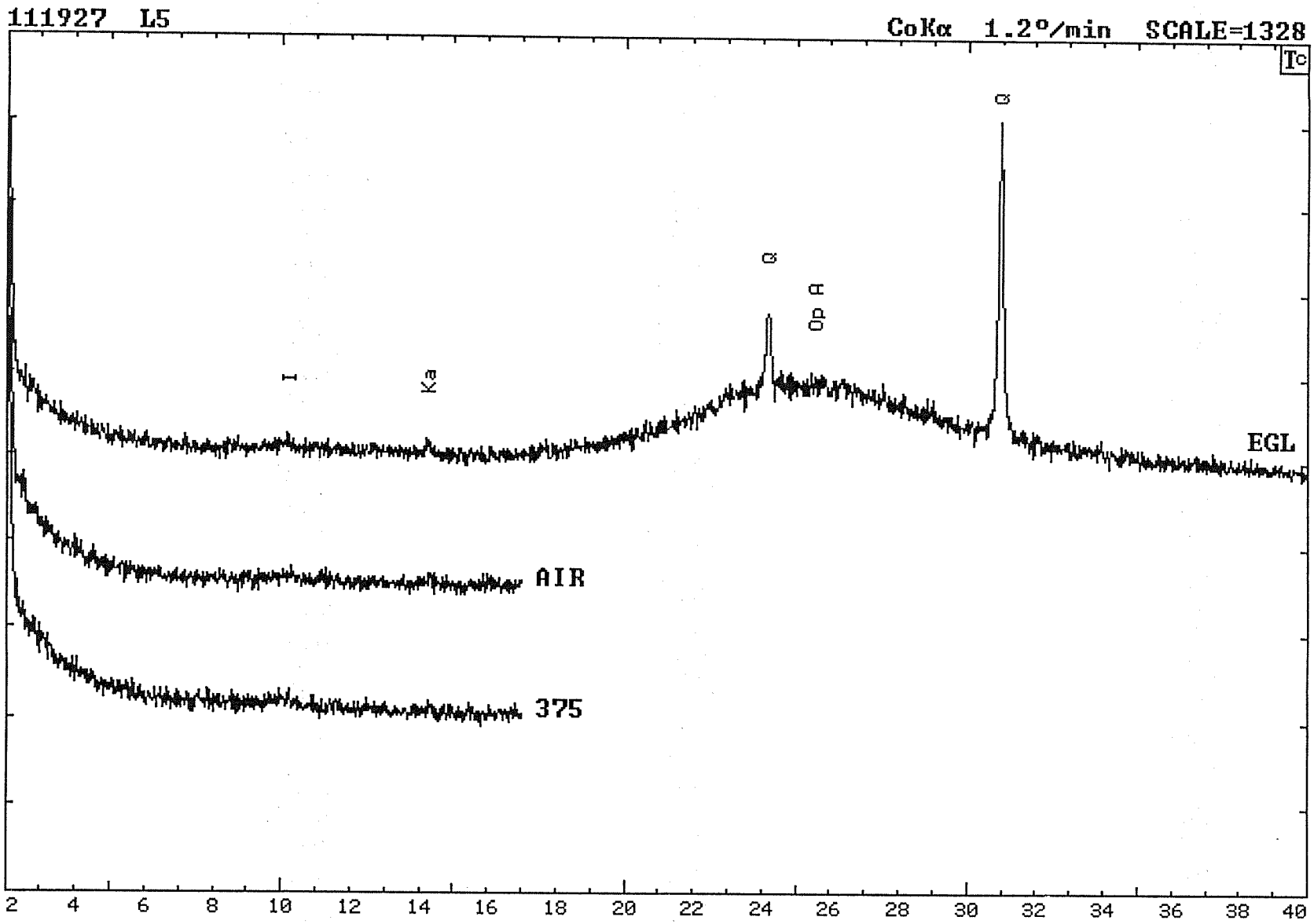

111966-E.CPI 14
CoKα 1.2°/min SCALE=1302
Tc
ε
α
αα
α
EGL
AIR
375
550
2 4 6 8 10 12 14 16 18 20 22 24 26 28 30 32 34 36 38 40


111987-E.CPI L4
CoKα 1.2°/min SCALE=15461
Tc
ch/sm
ch
m
ch
m (111)
ch
ch
m
ch
EGL
AIR
375
550
2 4 6 8 10 12 14 16 18 20 22 24 26 28 30 32 34 36 38 40

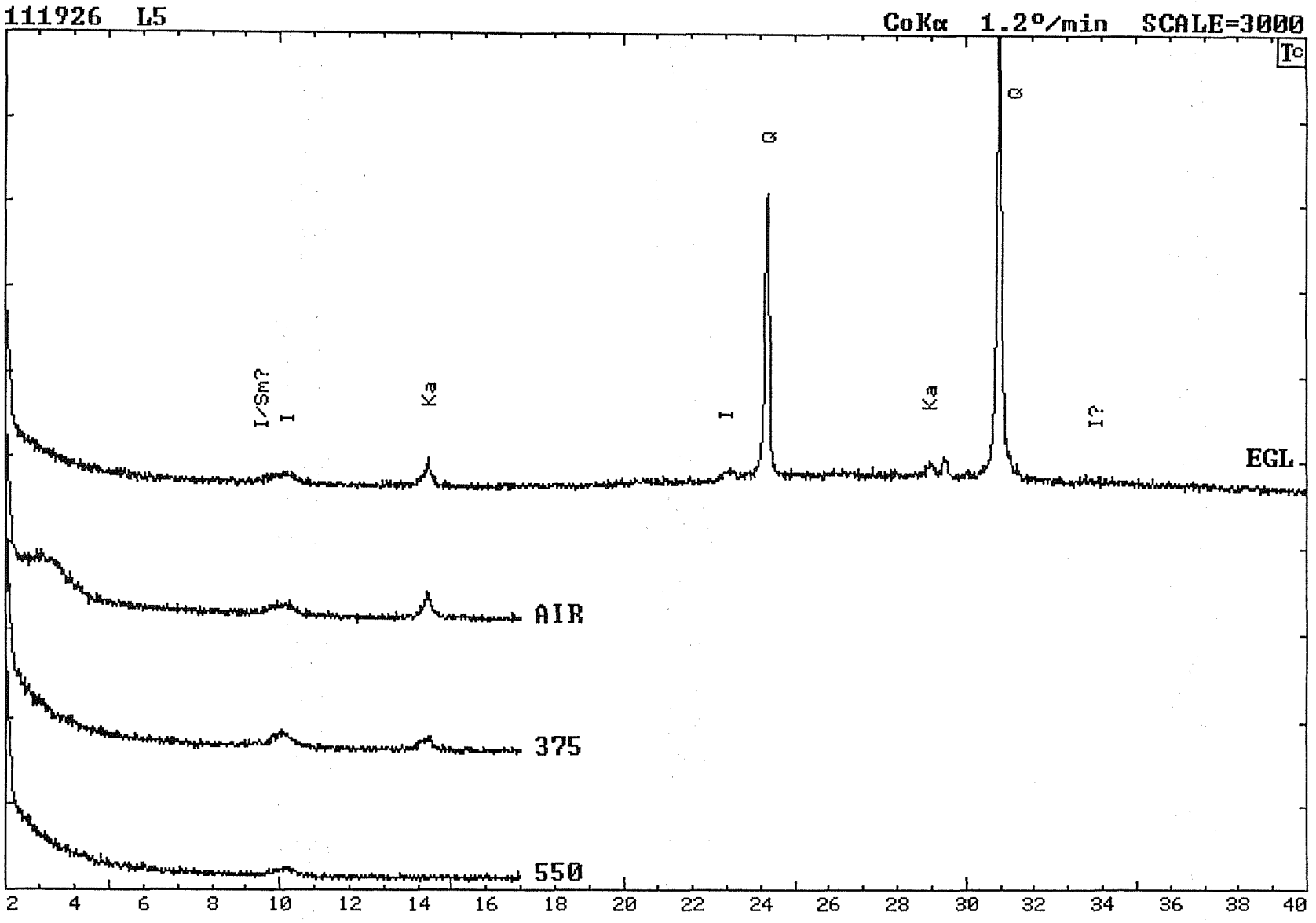

097202-E.CPI LR
CoKα 1.2°/min SCALE=3931
Tc
I
I
I
I?
I?
I?
EGL
AIR
375
550
2 4 6 8 10 12 14 16 18 20 22 24 26 28 30 32 34 36 38 40

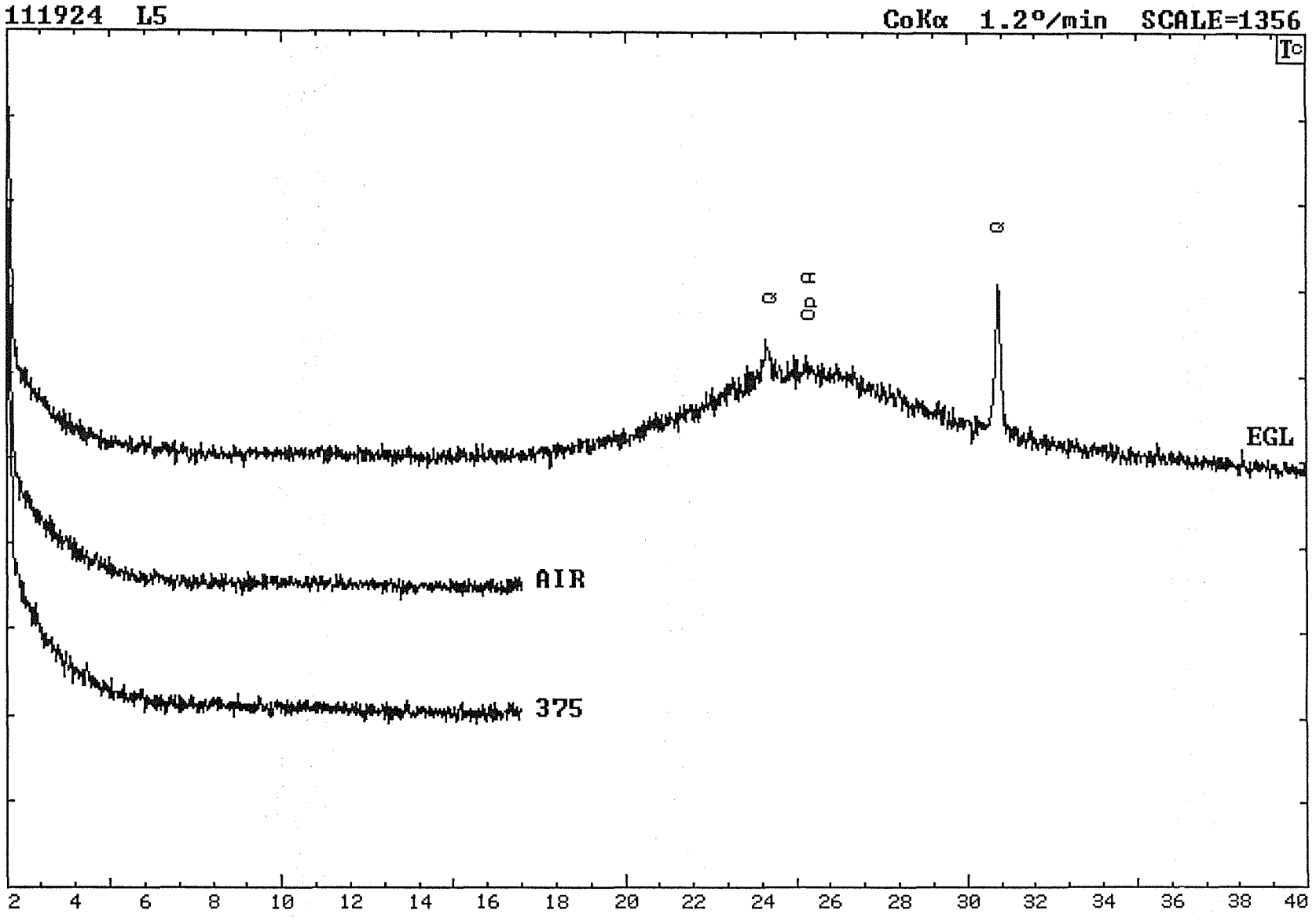

111923 L5
CoKα 1.2°/min SCALE=9659
Tc
I
I
Q
I
I/Q
I
EGL
AIR
375
550
2 4 6 8 10 12 14 16 18 20 22 24 26 28 30 32 34 36 38 40

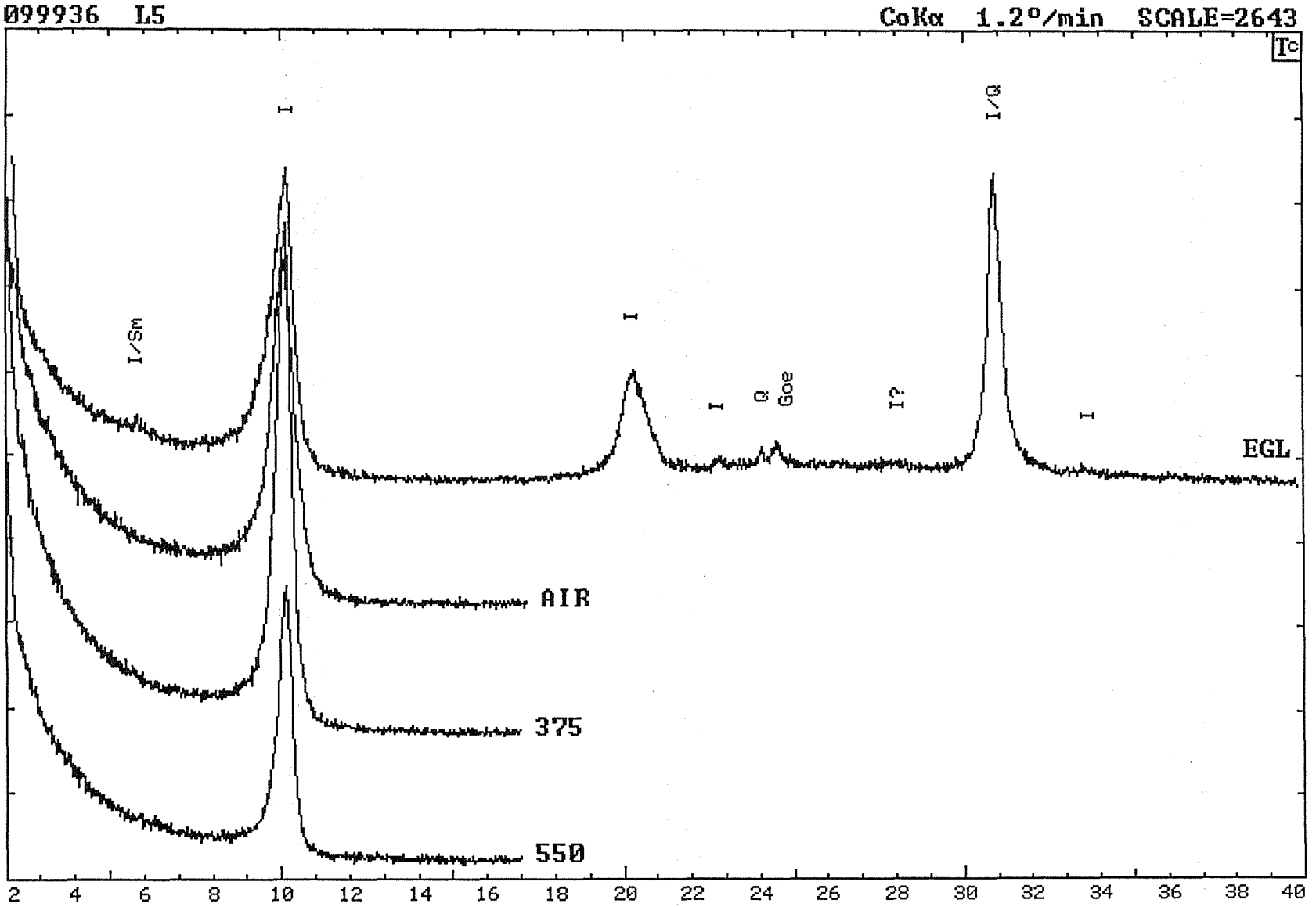

111928 L5
CoKα 1.2°/min SCALE=27221
Tc
Ka
Ka
EGL
AIR
375
550
2 4 6 8 10 12 14 16 18 20 22 24 26 28 30 32 34 36 38 40


111927 L5
CoKα 1.2°/min SCALE=1328
Tc
I
Ka
Q
Op A
Q
EGL
AIR
375
2 4 6 8 10 12 14 16 18 20 22 24 26 28 30 32 34 36 38 40

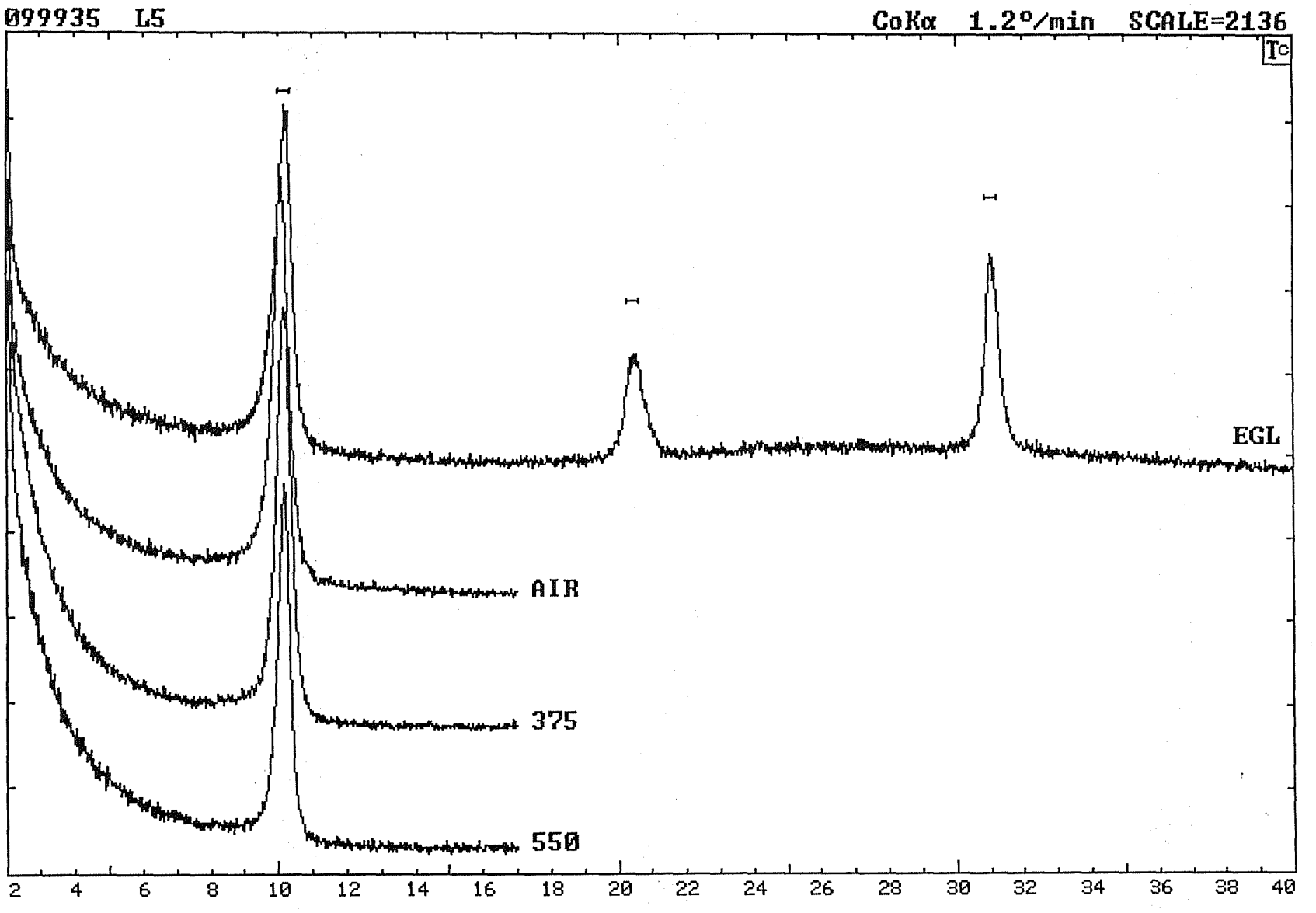
Loc. 174

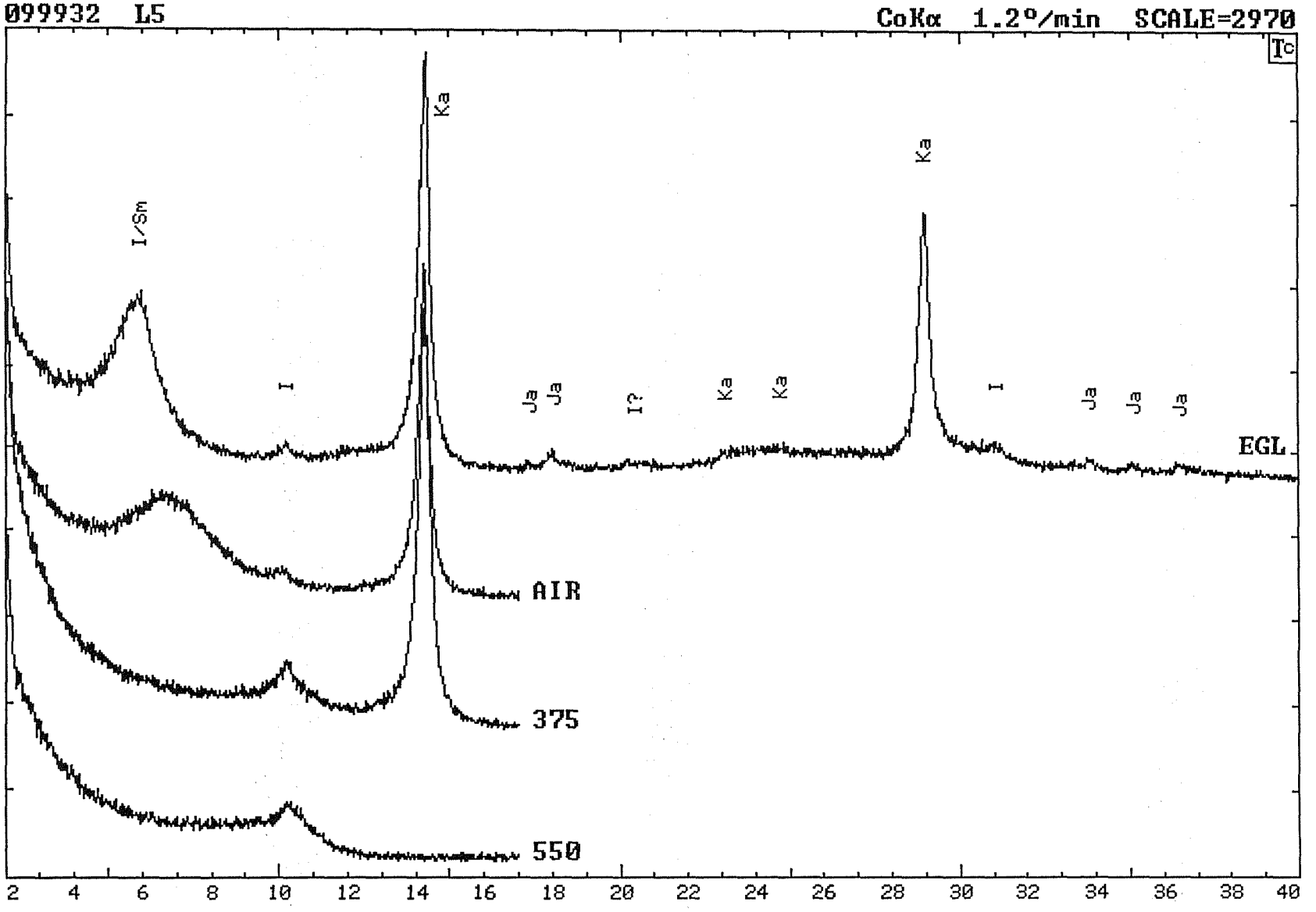

111926 L5
CoKα 1.2°/min SCALE=3000
Tc
I/Sm?
I
Ka
I
Q
Ka
Q
I?
EGL
AIR
375
550
2
4
6
8
10
12
14
16
18
20
22
24
26
28
30
32
34
36
38
40

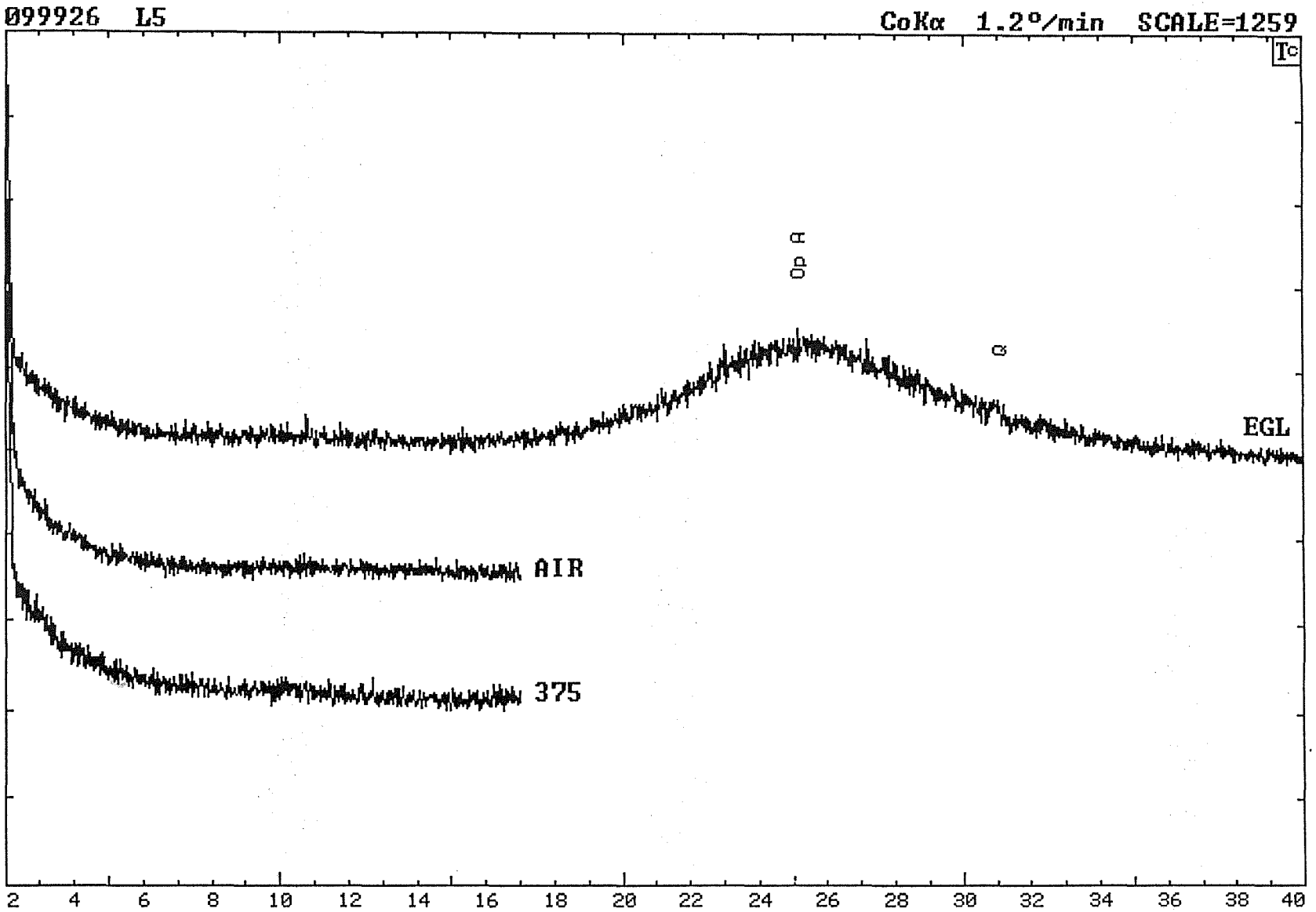

111924 L5
CoKα 1.2°/min SCALE=1356
Tc
α
Op A
α
EGL
AIR
375
2 4 6 8 10 12 14 16 18 20 22 24 26 28 30 32 34 36 38 40

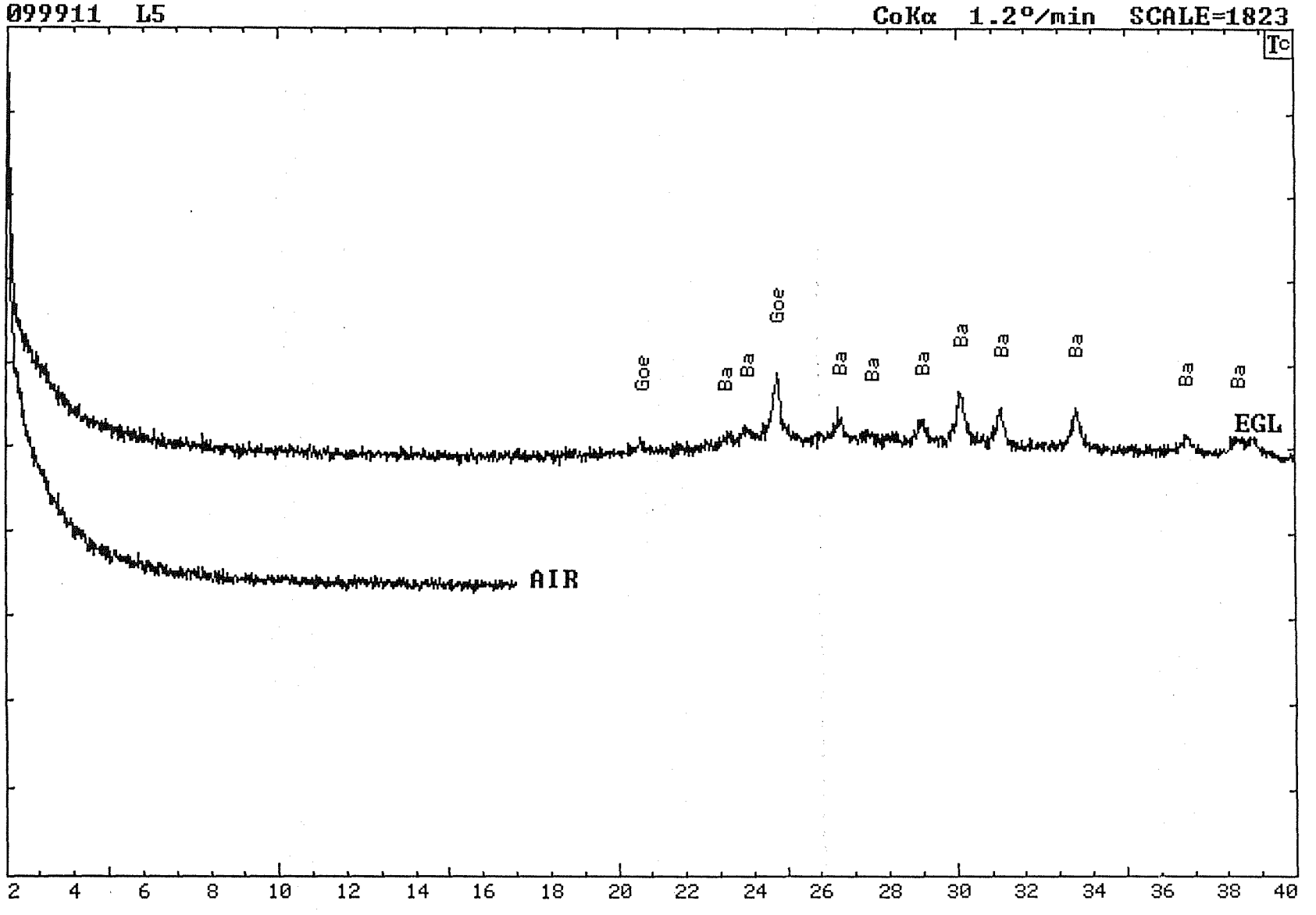

099936 L5
CoKα 1.2°/min SCALE=2643
Tc
I
I/Sm
I
I
Q
Goe
I?
I/Q
I
EGL
AIR
375
550
2
4
6
8
10
12
14
16
18
20
22
24
26
28
30
32
34
36
38
40

Co. 35

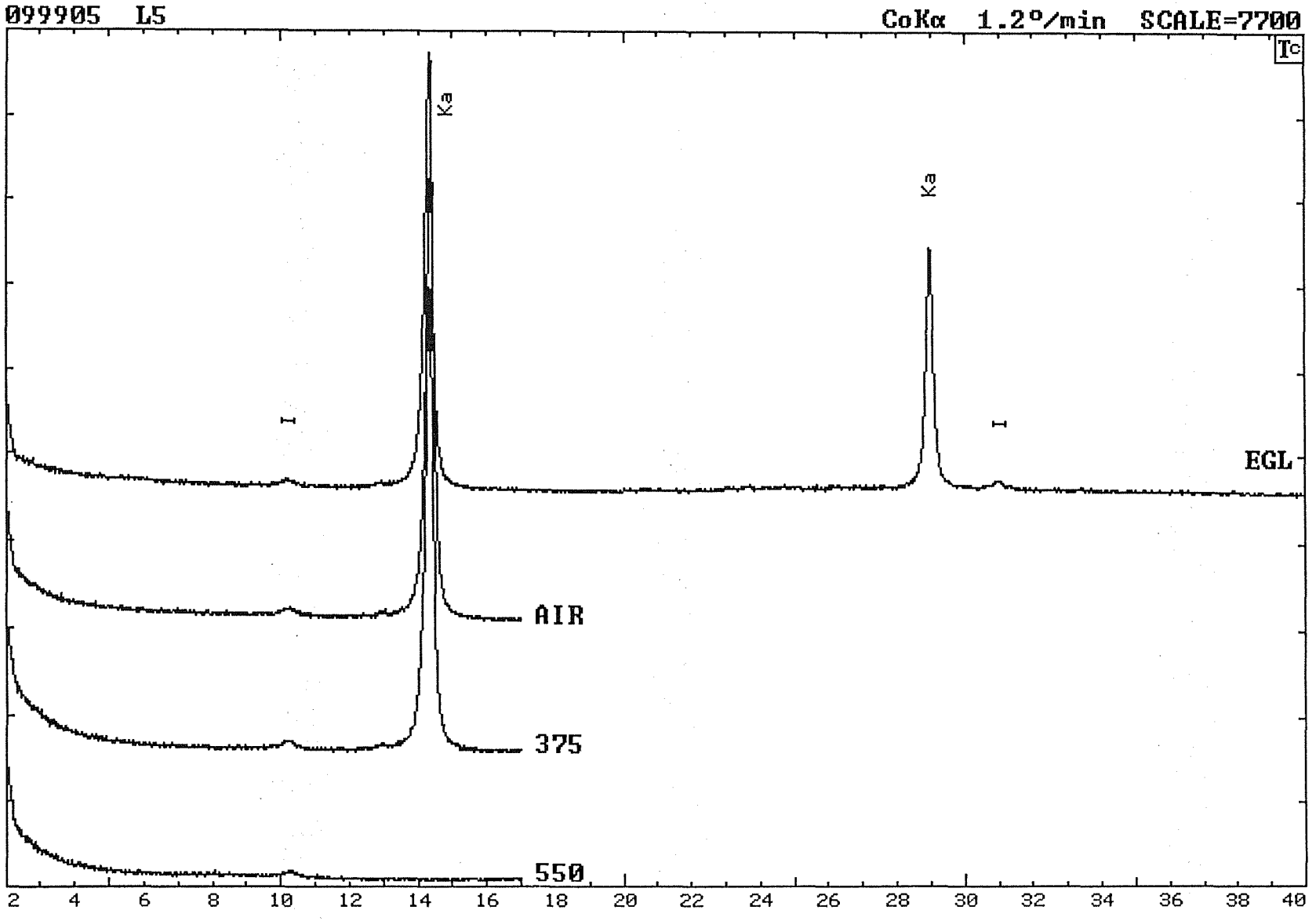

099935 L5
CoKα 1.2°/min SCALE=2136
Tc
EGL
AIR
375
550
2 4 6 8 10 12 14 16 18 20 22 24 26 28 30 32 34 36 38 40

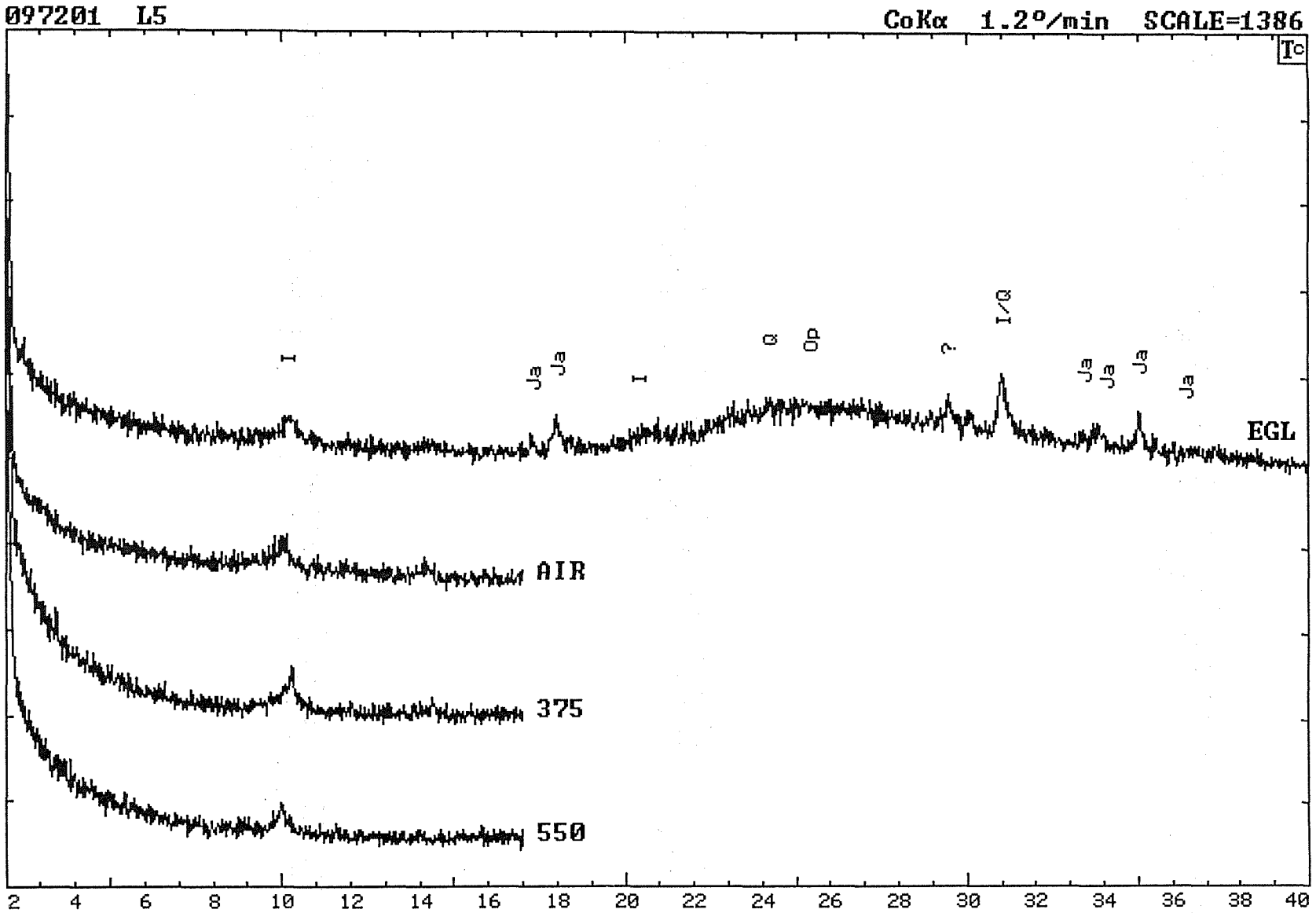

099932 L5
CoKα 1.2°/min SCALE=2970
Tc
I/Sm
I
Ka
Ja
Ja
I?
Ka
Ka
Ka
I
Ja
Ja
Ja
EGL
AIR
375
550
2
4
6
8
10
12
14
16
18
20
22
24
26
28
30
32
34
36
38
40

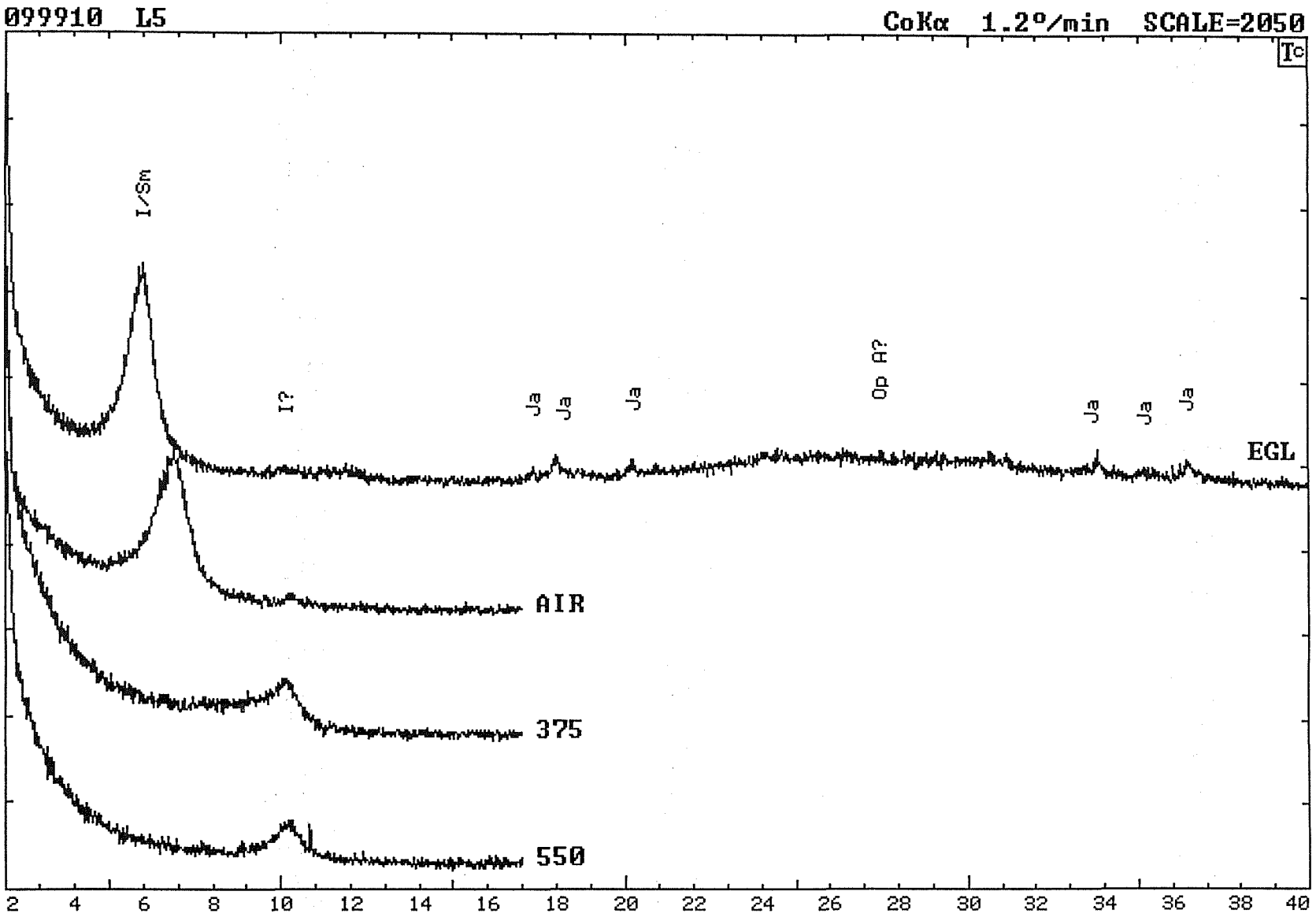

099926 L5
CoKα 1.2°/min SCALE=1259
Tc
Op α
α
EGL
AIR
375
2 4 6 8 10 12 14 16 18 20 22 24 26 28 30 32 34 36 38 40

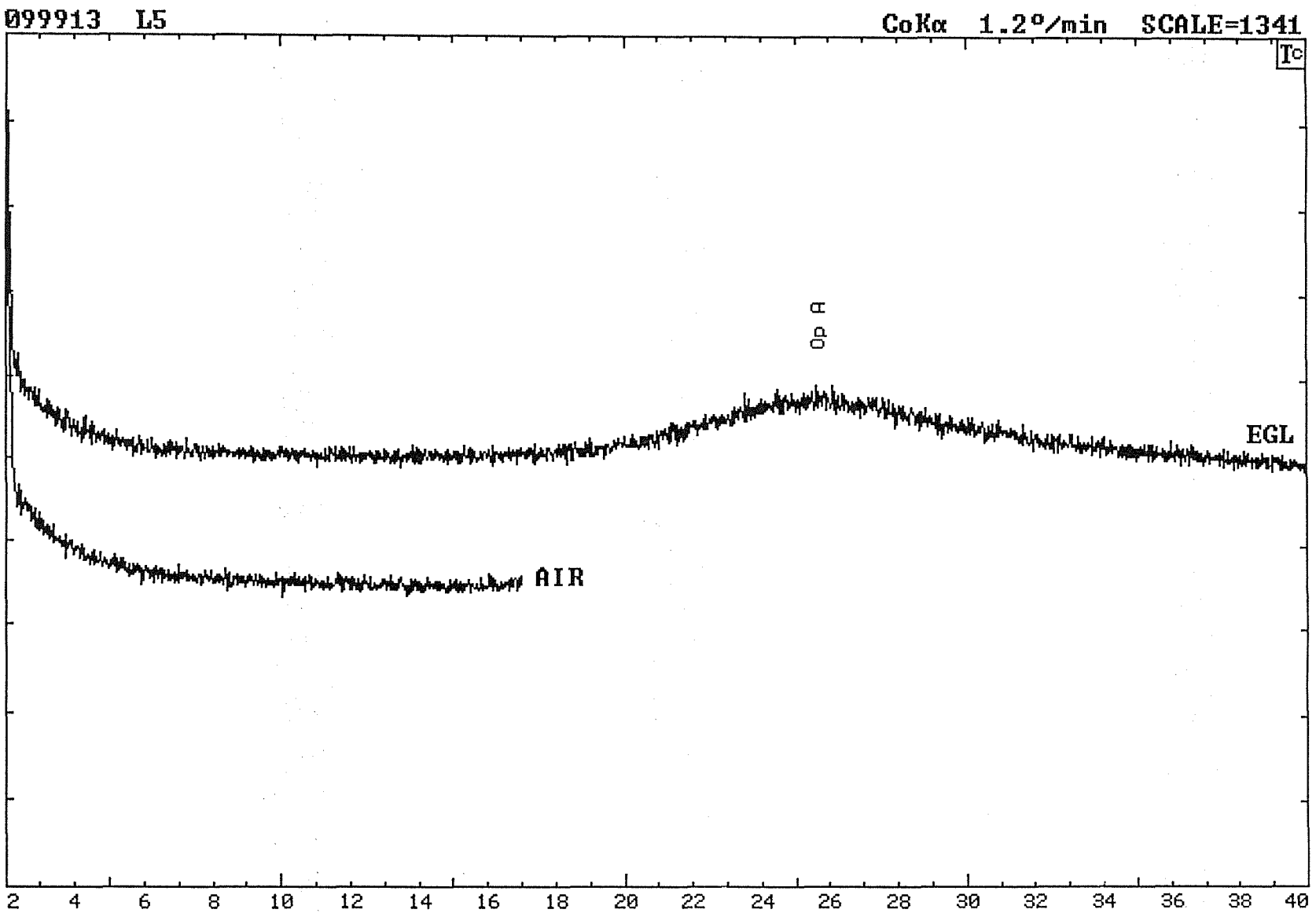

099911 L5
CoKα 1.2°/min SCALE=1823
Tc
Goe
Ba
Ba
Goe
Ba
Ba
Ba
Ba
Ba
Ba
Ba
Ba
EGL
AIR
2 4 6 8 10 12 14 16 18 20 22 24 26 28 30 32 34 36 38 40

Loc 1.

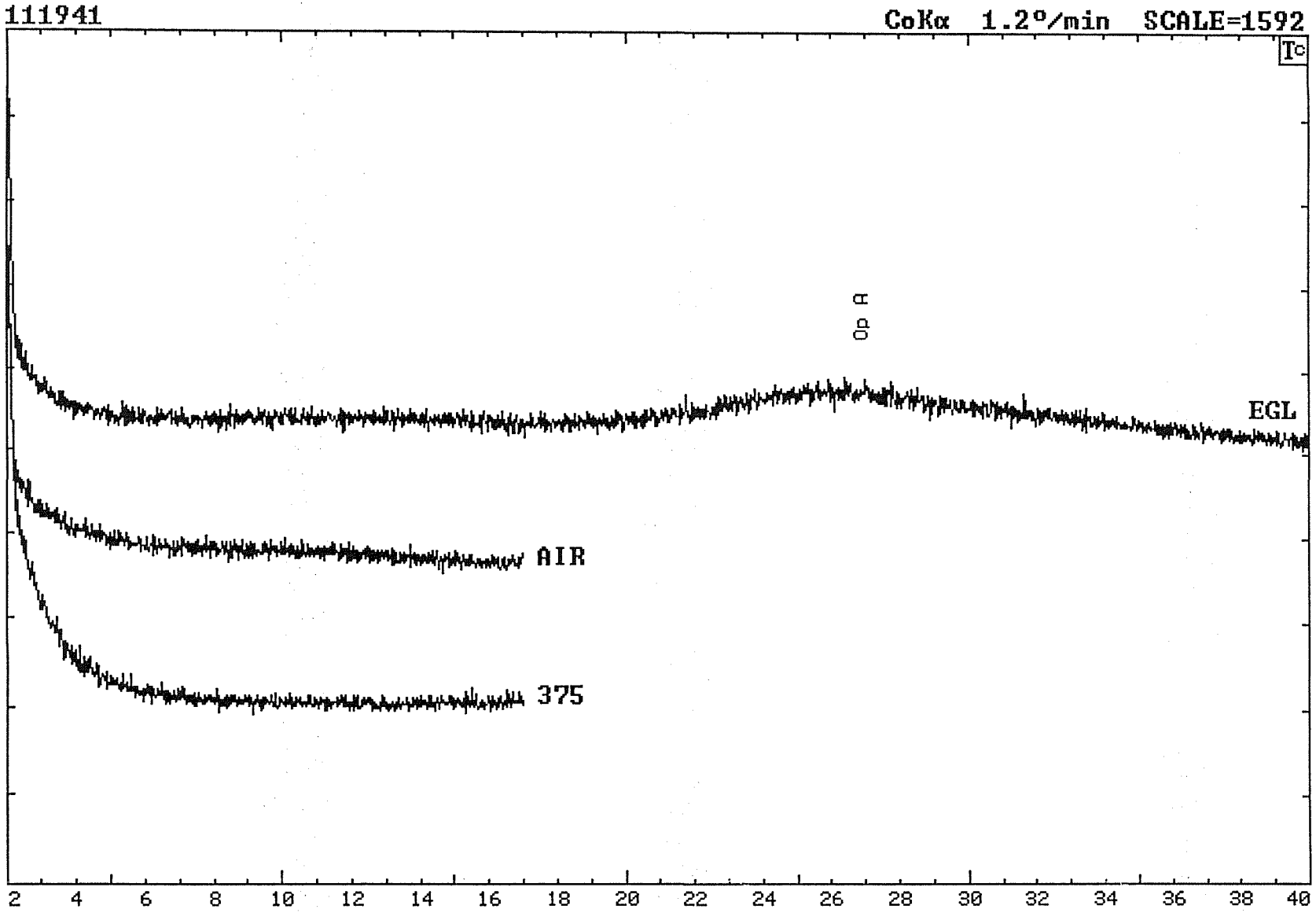

099905 L5
CoKα 1.2°/min SCALE=7700
Tc
Ka
Ka
I
I
EGL
AIR
375
550
2 4 6 8 10 12 14 16 18 20 22 24 26 28 30 32 34 36 38 40

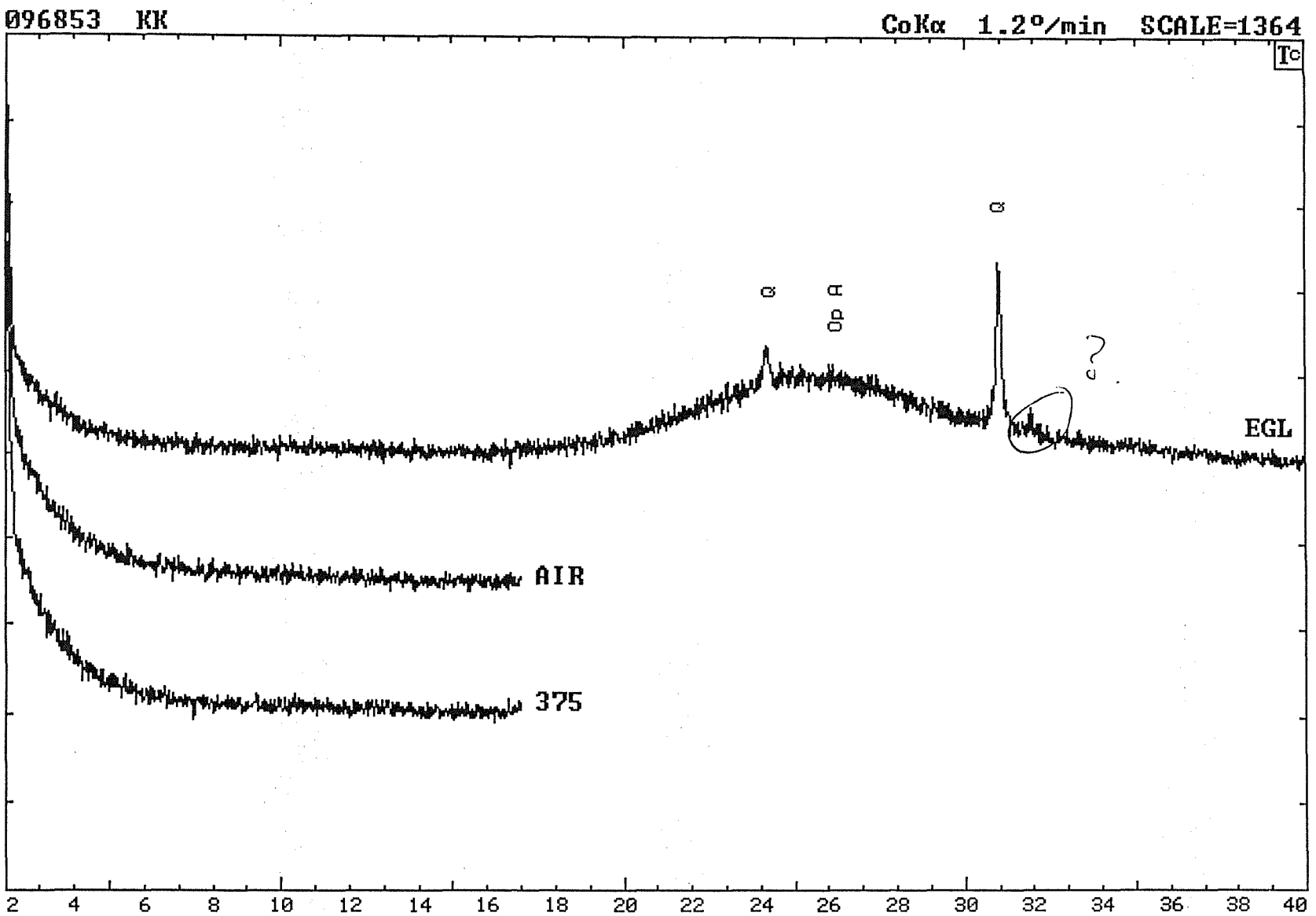

097201 L5
CoKα 1.2°/min SCALE=1386
Tc
I
Ja
Ja
I
Q
Op
?
I/Q
Ja
Ja
Ja
Ja
EGL
AIR
375
550
2 4 6 8 10 12 14 16 18 20 22 24 26 28 30 32 34 36 38 40


099910 L5
CoKα 1.2°/min SCALE=2050
Tc
I/Sm
I?
Ja
Ja
Ja
Op A?
Ja
Ja
Ja
EGL
AIR
375
550
2
4
6
8
10
12
14
16
18
20
22
24
26
28
30
32
34
36
38
40

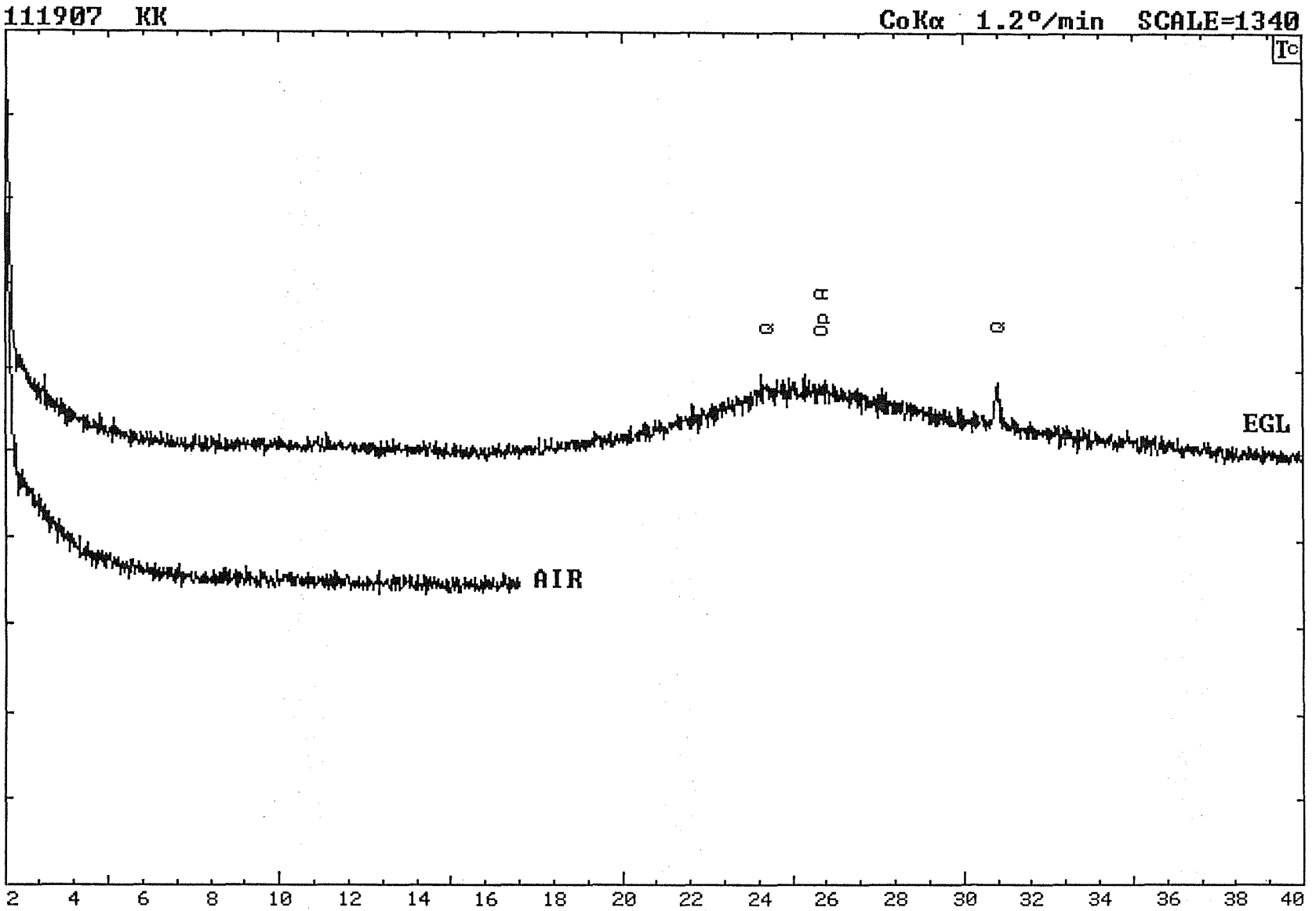

099913 L5
CoKα 1.2°/min SCALE=1341
Tc
Op A
EGL
AIR
2 4 6 8 10 12 14 16 18 20 22 24 26 28 30 32 34 36 38 40

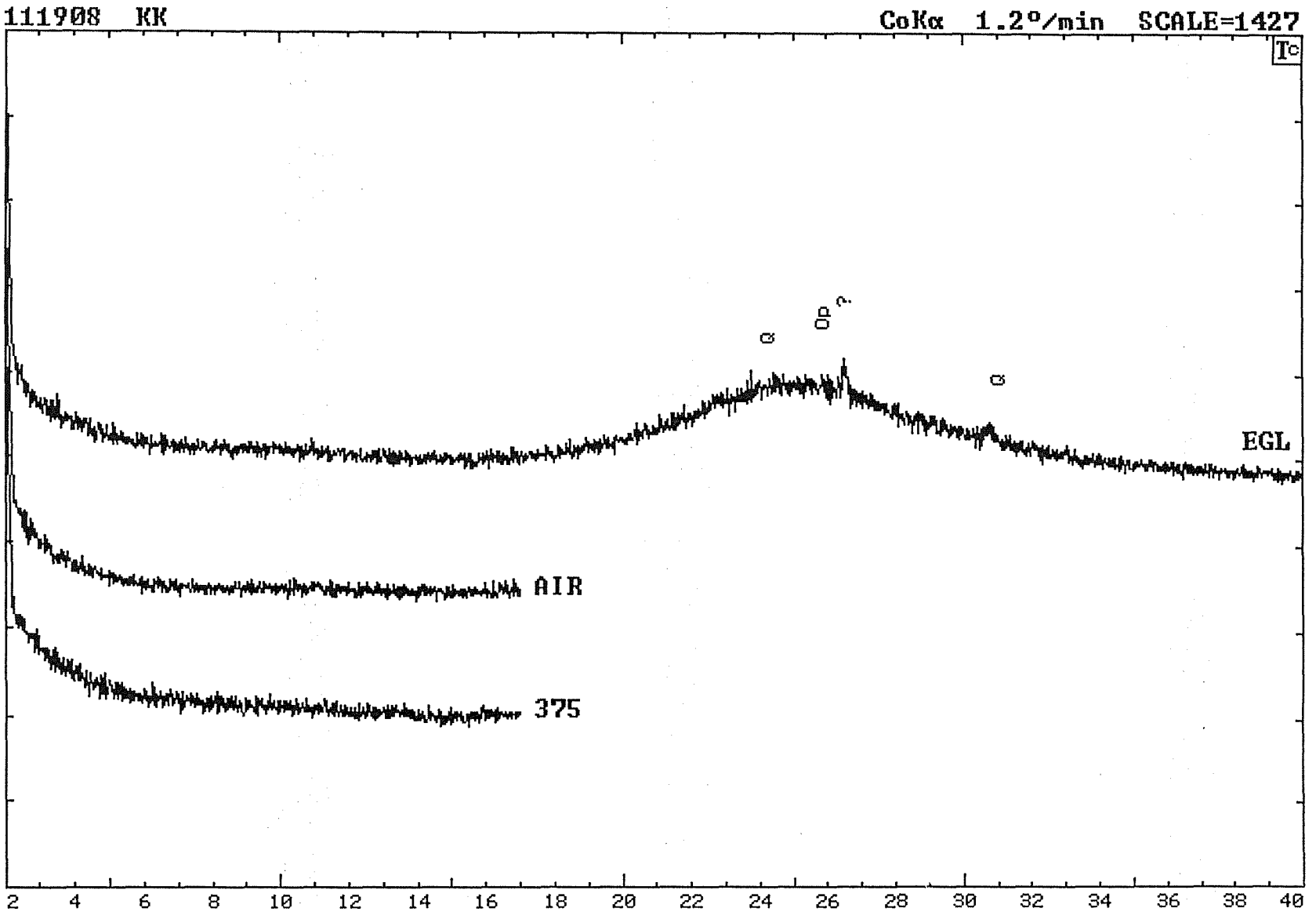
KK Loc 300

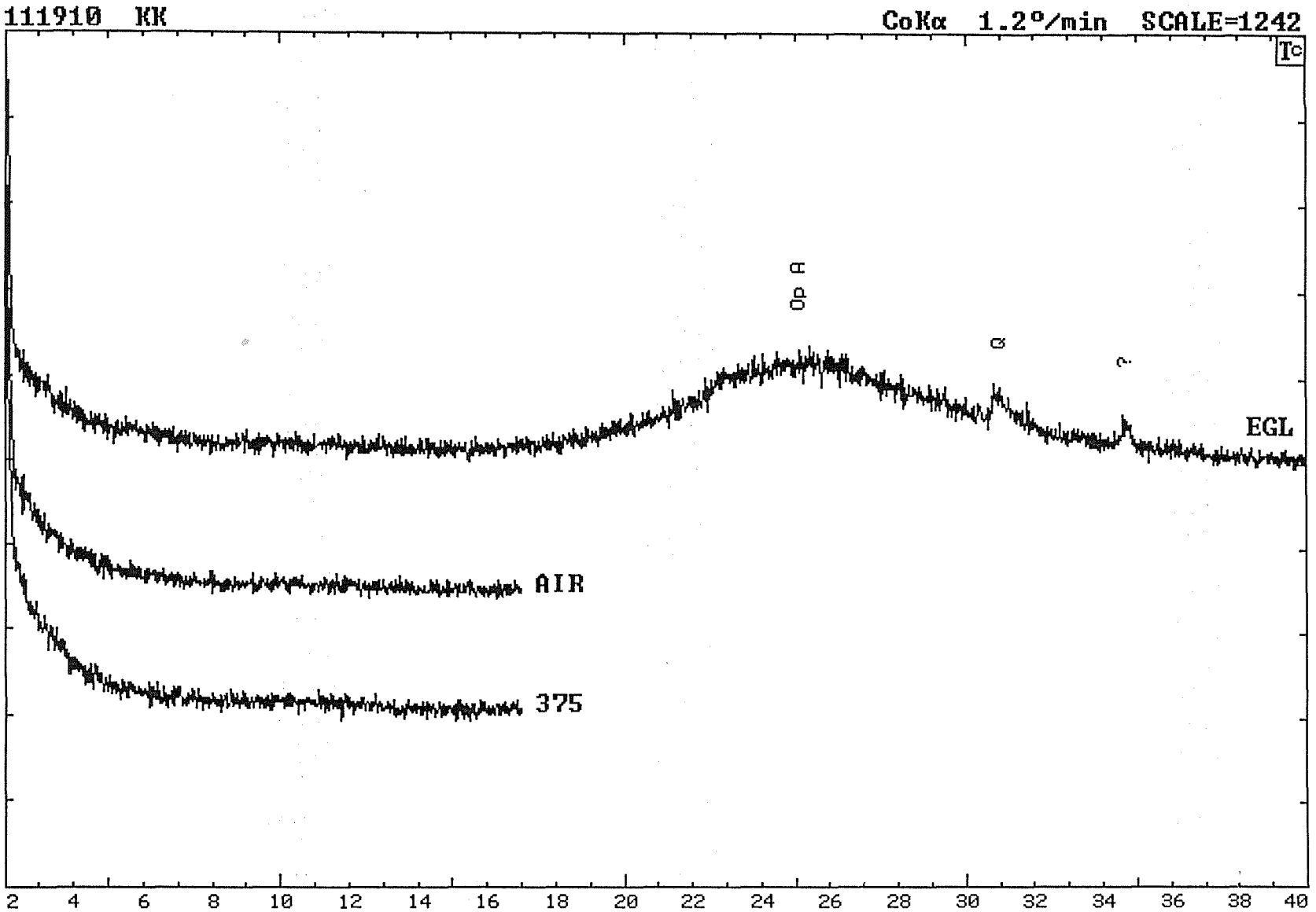

111941
CoKα 1.2°/min SCALE=1592
Tc
Op A
EGL
AIR
375
2 4 6 8 10 12 14 16 18 20 22 24 26 28 30 32 34 36 38 40

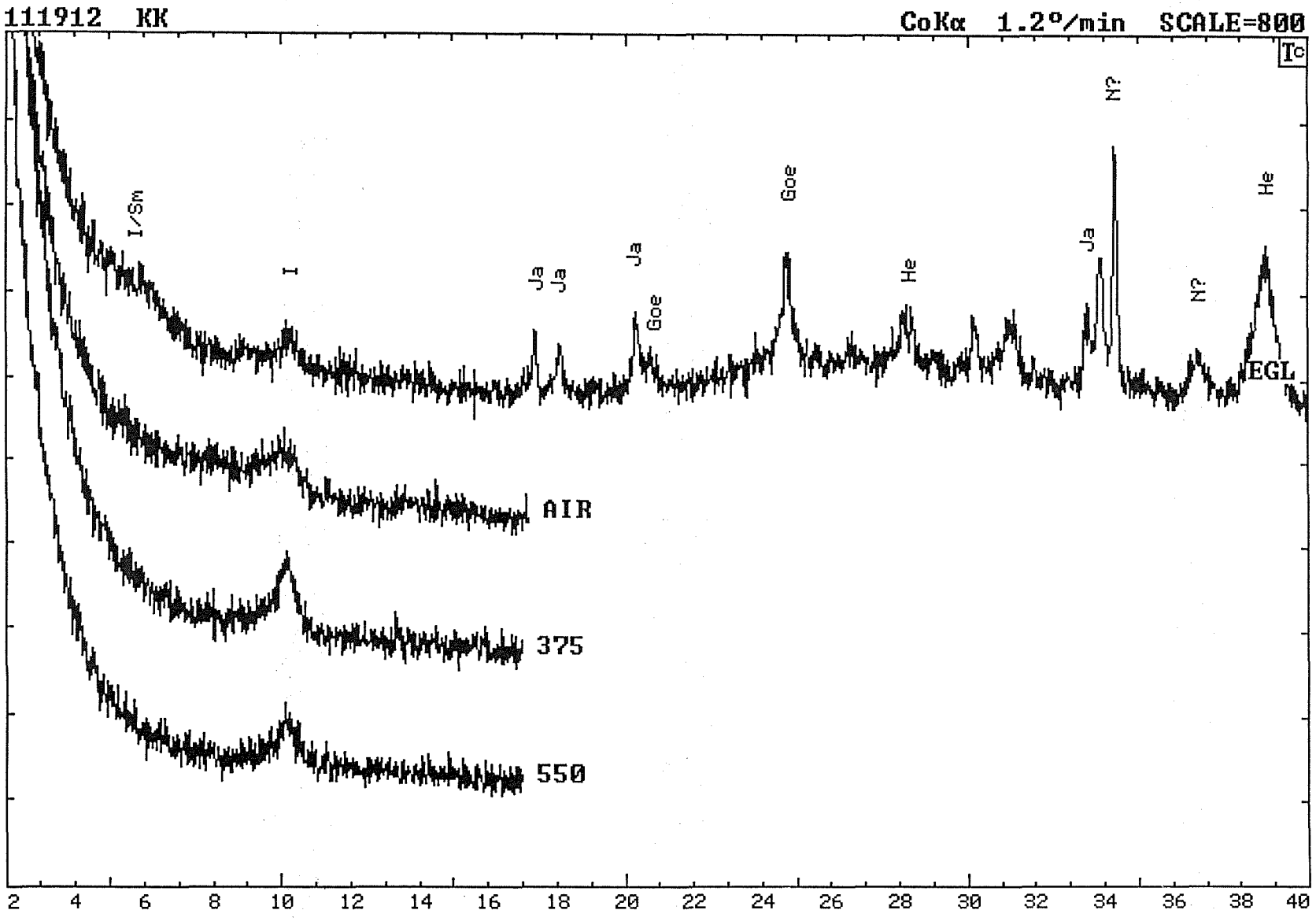

096853 KK
CoKα 1.2°/min SCALE=1364
Tc
α
Op α
α
c?
EGL
AIR
375
2 4 6 8 10 12 14 16 18 20 22 24 26 28 30 32 34 36 38 40

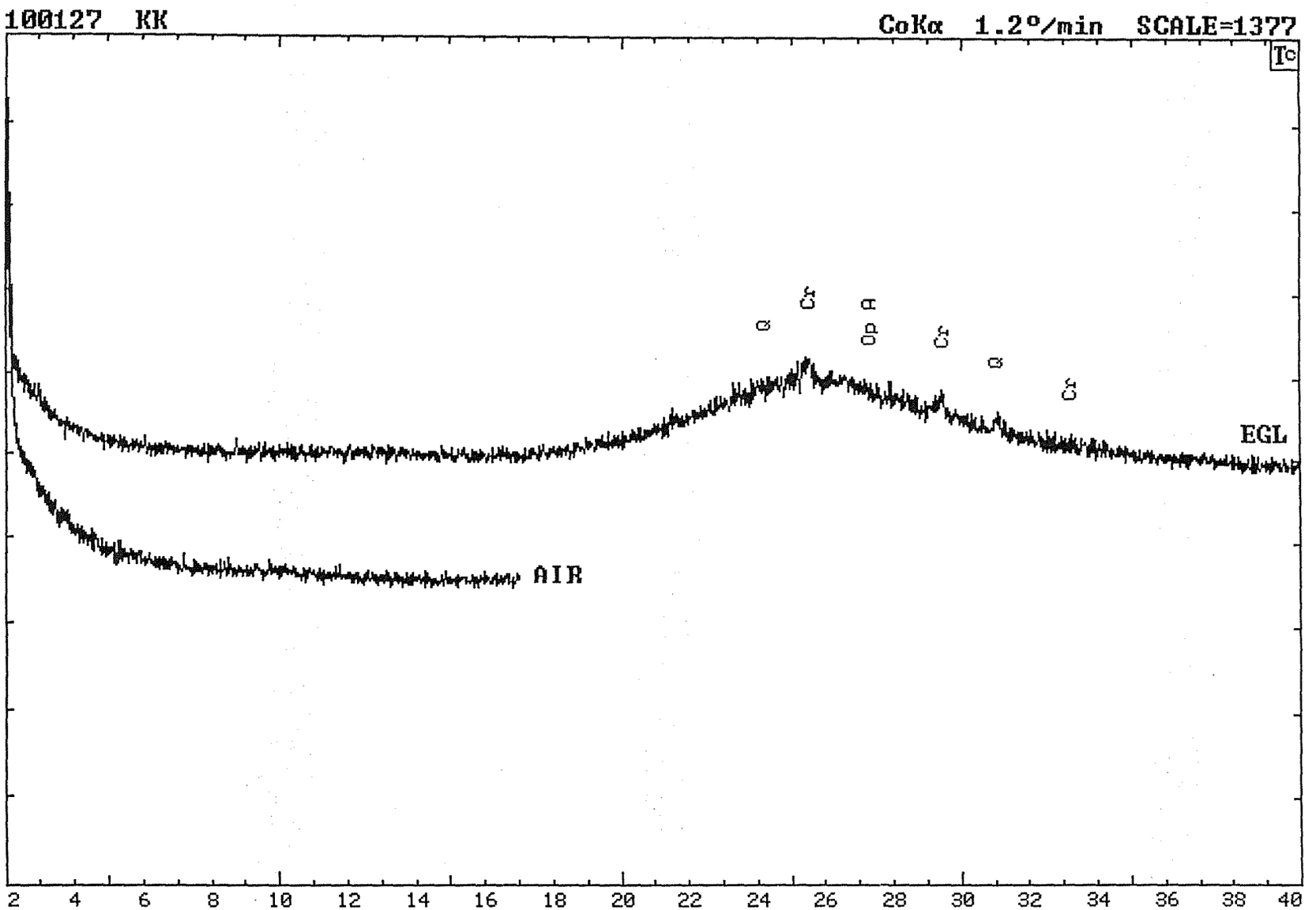
Loc 309

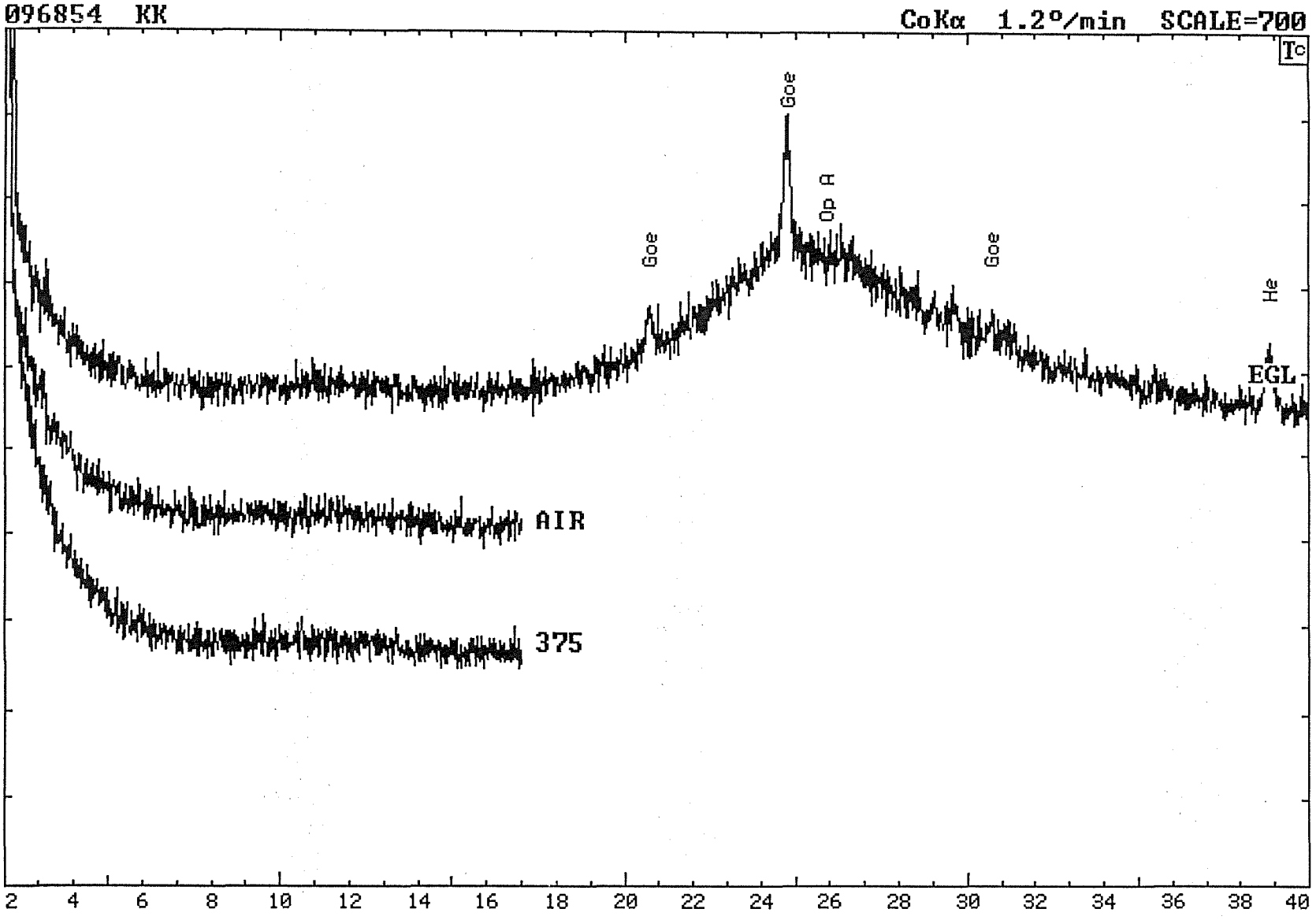

111907 KK
CoKα 1.2°/min SCALE=1340
Tc
α
α
α
EGL
AIR
2 4 6 8 10 12 14 16 18 20 22 24 26 28 30 32 34 36 38 40

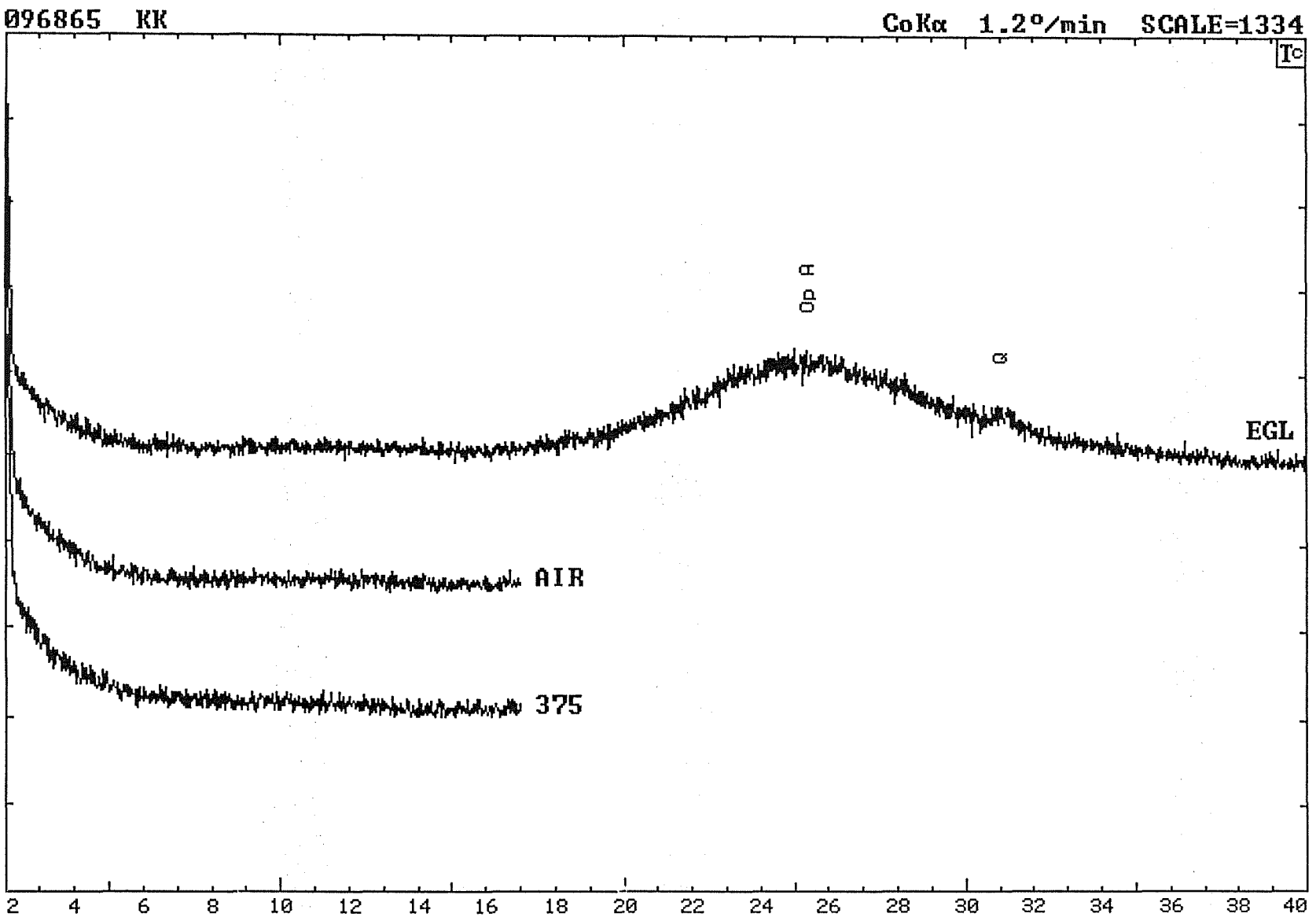

111908 KK
CoKα 1.2°/min SCALE=1427
Tc
α
Op ?
α
EGL
AIR
375
2 4 6 8 10 12 14 16 18 20 22 24 26 28 30 32 34 36 38 40

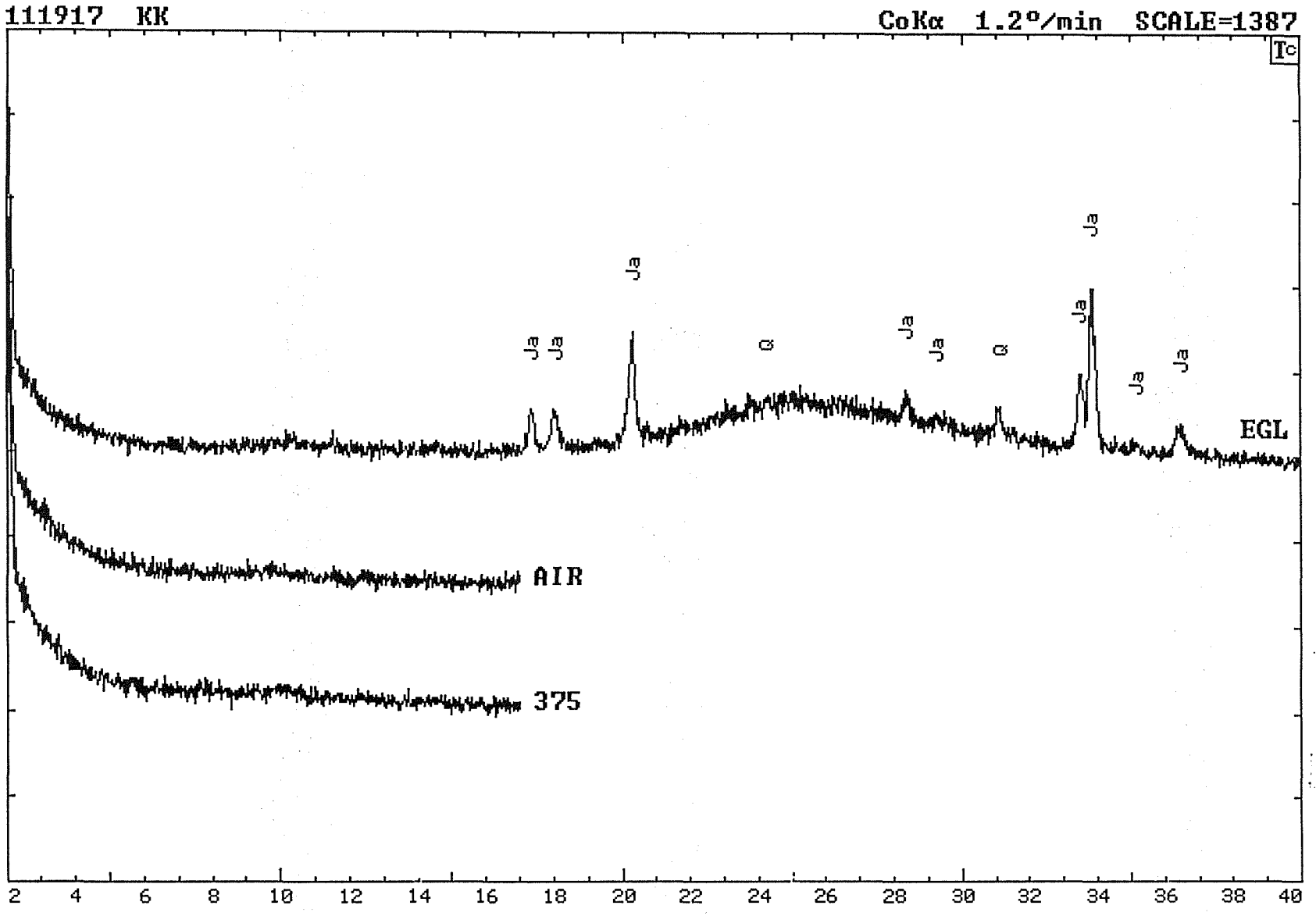

111910 KK
CoKα 1.2°/min SCALE=1242
Tc
Op a
a
c
EGL
AIR
375
2 4 6 8 10 12 14 16 18 20 22 24 26 28 30 32 34 36 38 40

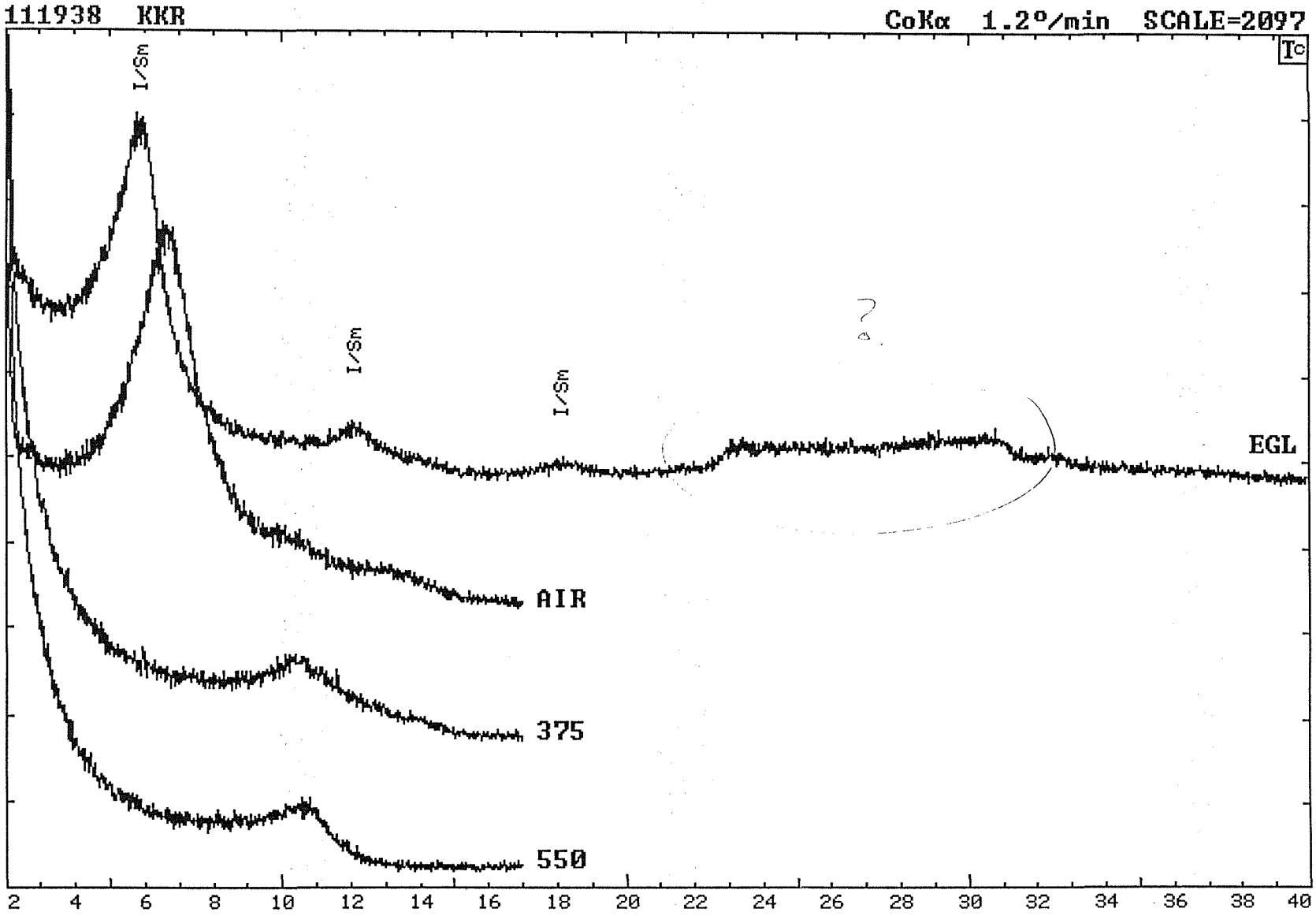

111912 KK
CoKα 1.2°/min SCALE=800
Tc
I/Sm
I
Ja
Ja
Ja
Goe
Goe
He
Ja
N?
N?
He
EGL
AIR
375
550
2
4
6
8
10
12
14
16
18
20
22
24
26
28
30
32
34
36
38
40


100127 KK
CoKα 1.2°/min SCALE=1377
Tc
Cr
α
α
Cr
α
Cr
EGL
AIR
2
4
6
8
10
12
14
16
18
20
22
24
26
28
30
32
34
36
38
40

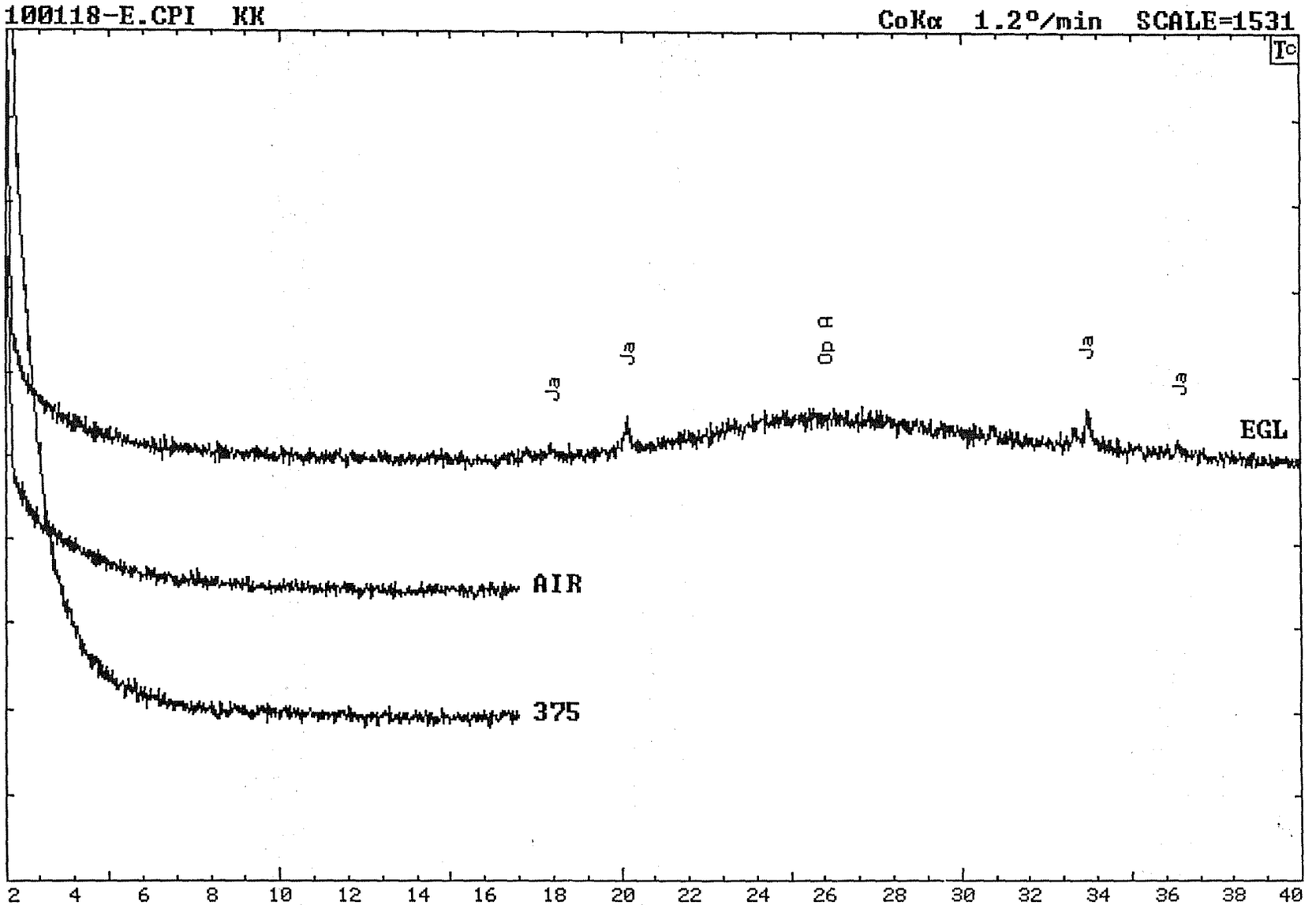

096854 KK
CoKα 1.2°/min SCALE=700
Tc
Goe
Goe
Op A
Goe
He
EGL
AIR
375
2 4 6 8 10 12 14 16 18 20 22 24 26 28 30 32 34 36 38 40

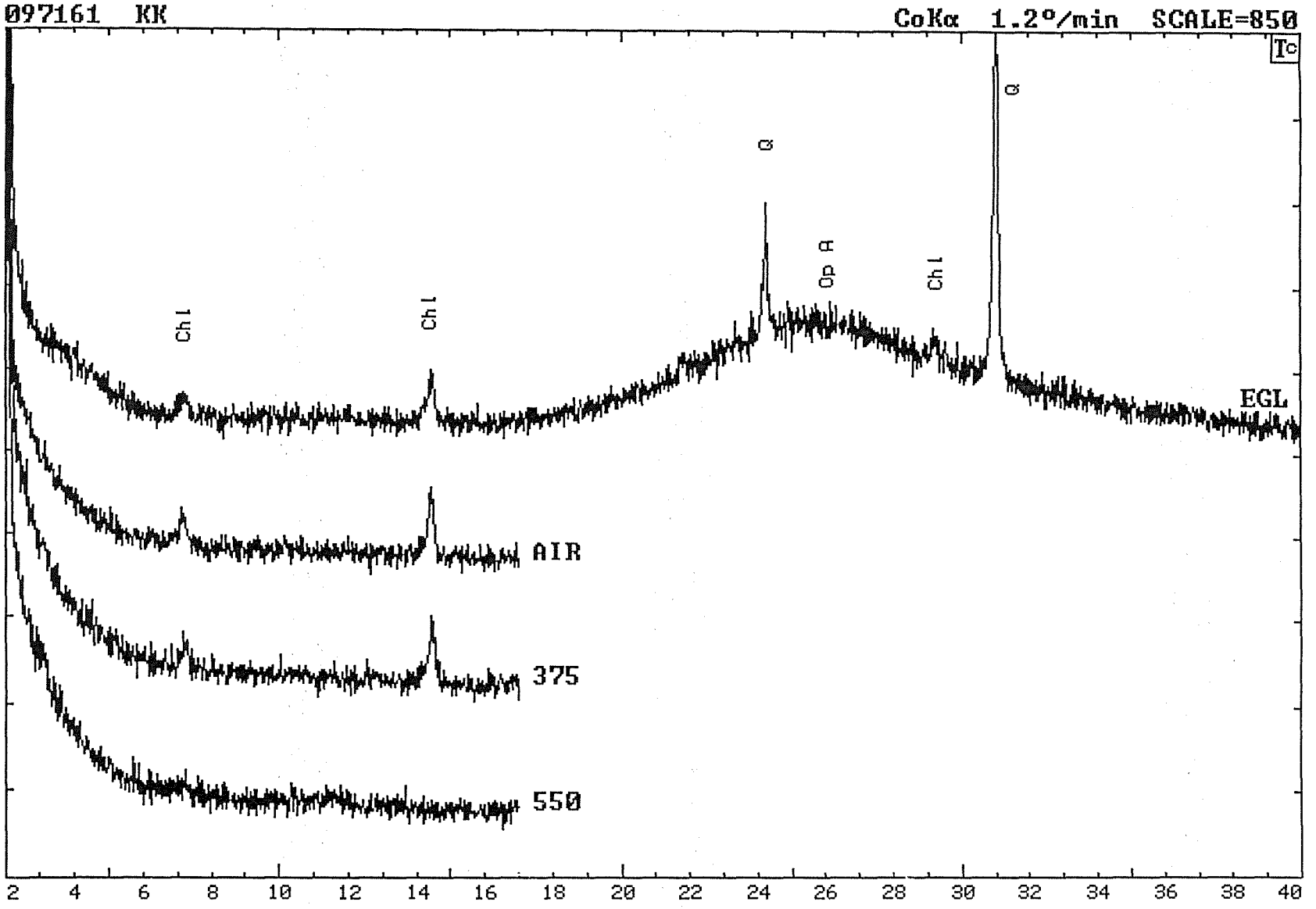

096865 KK
CoKα 1.2°/min SCALE=1334
Tc
Op A
α
EGL
AIR
375
2 4 6 8 10 12 14 16 18 20 22 24 26 28 30 32 34 36 38 40


111917 KK
CoKα 1.2°/min SCALE=1387
Tc
Ja
Ja
Ja
Q
Ja
Ja
Q
Ja
Ja
Ja
Ja
EGL
AIR
375
2
4
6
8
10
12
14
16
18
20
22
24
26
28
30
32
34
36
38
40

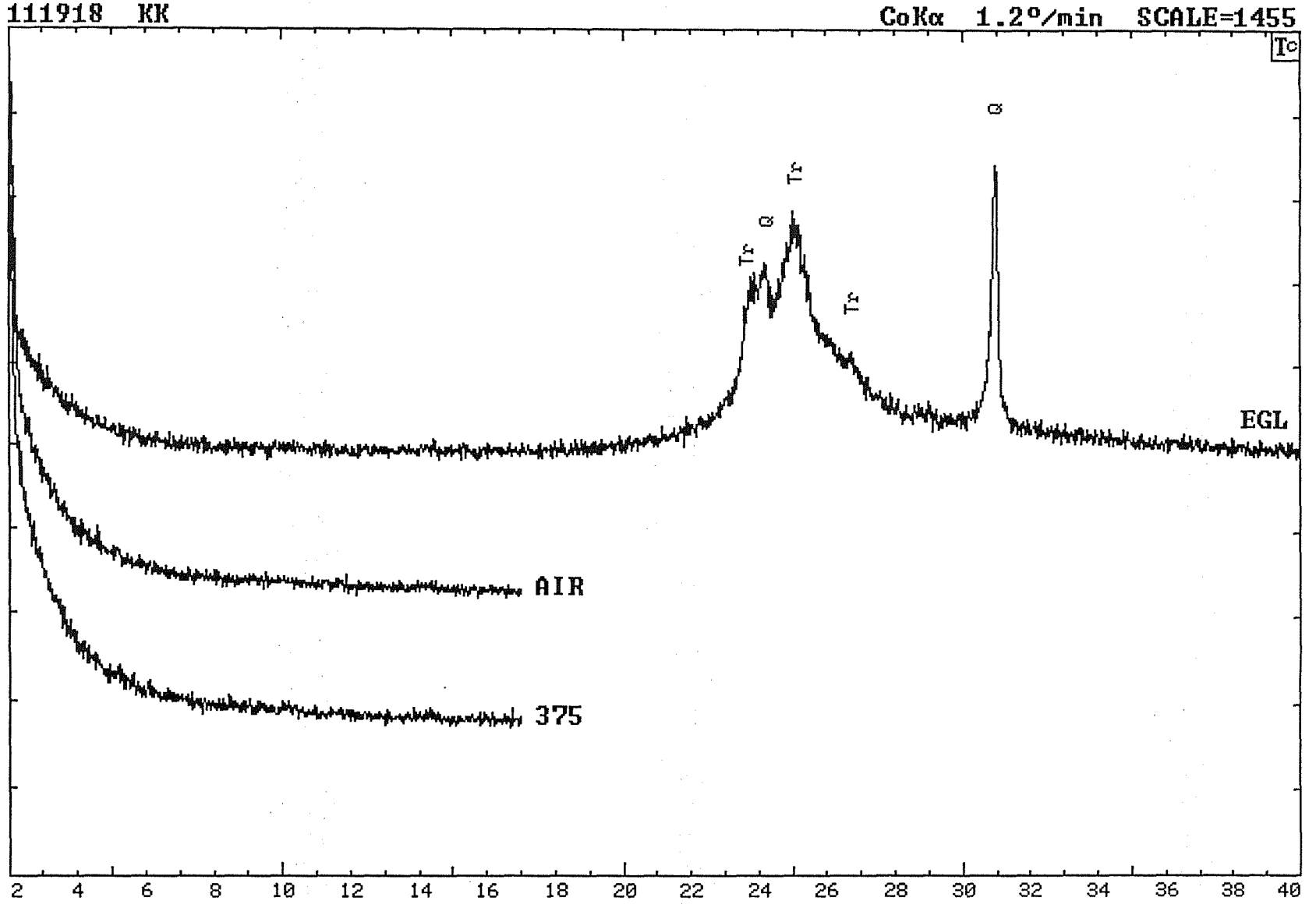

111938 KKR
CoKα 1.2°/min SCALE=2097
Tc
I/Sm
I/Sm
I/Sm
EGL
AIR
375
550
2 4 6 8 10 12 14 16 18 20 22 24 26 28 30 32 34 36 38 40

Lar 64.

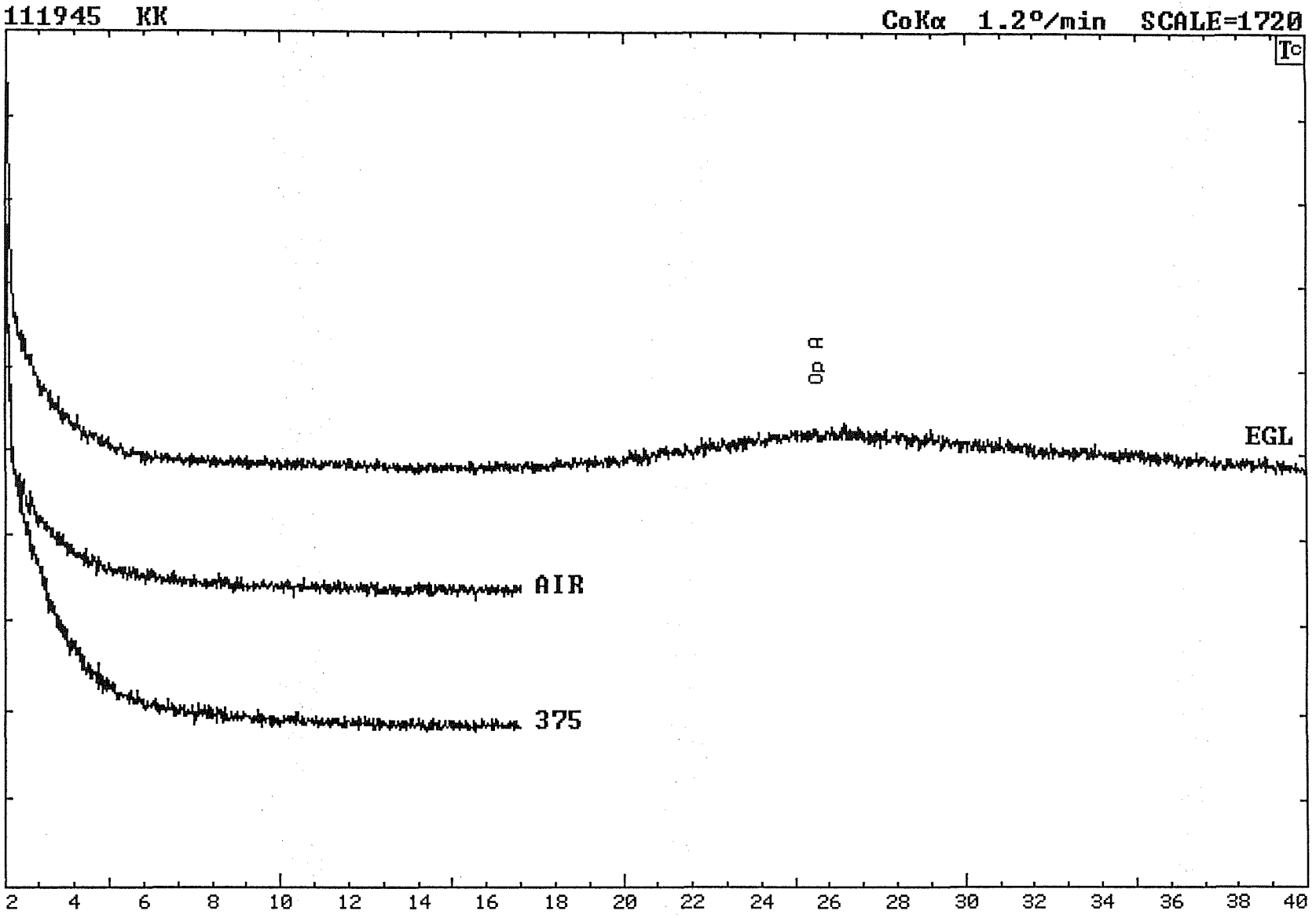

100118-E.CPI KK
CoKα 1.2°/min SCALE=1531
Tc
Ja
Ja
Op A
Ja
Ja
EGL
AIR
375
2 4 6 8 10 12 14 16 18 20 22 24 26 28 30 32 34 36 38 40

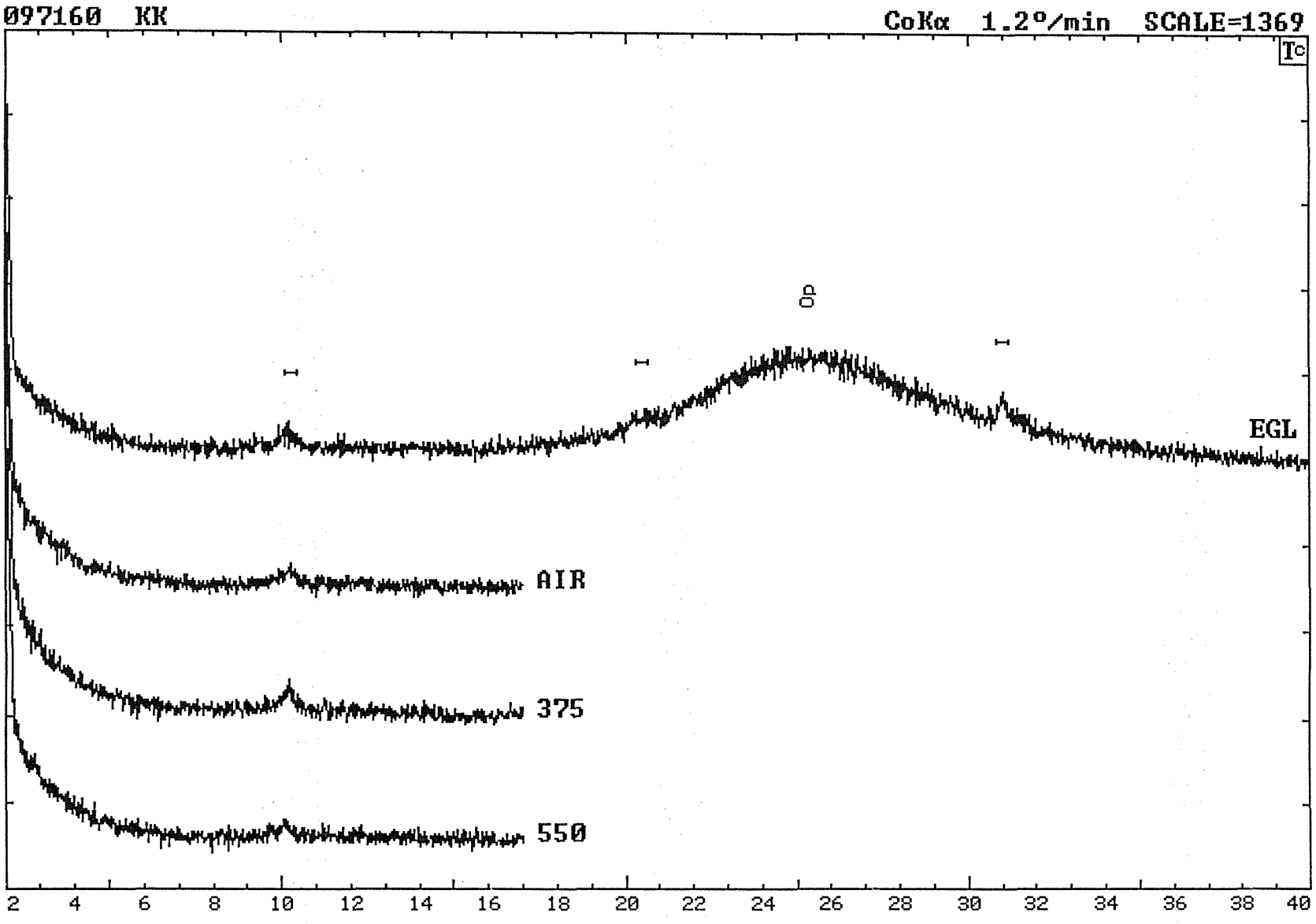

097161 KK
CoKα 1.2°/min SCALE=850
Tc
Q
Q
Op A
Chl
Chl
EGL
AIR
375
550
2
4
6
8
10
12
14
16
18
20
22
24
26
28
30
32
34
36
38
40

Loc 020

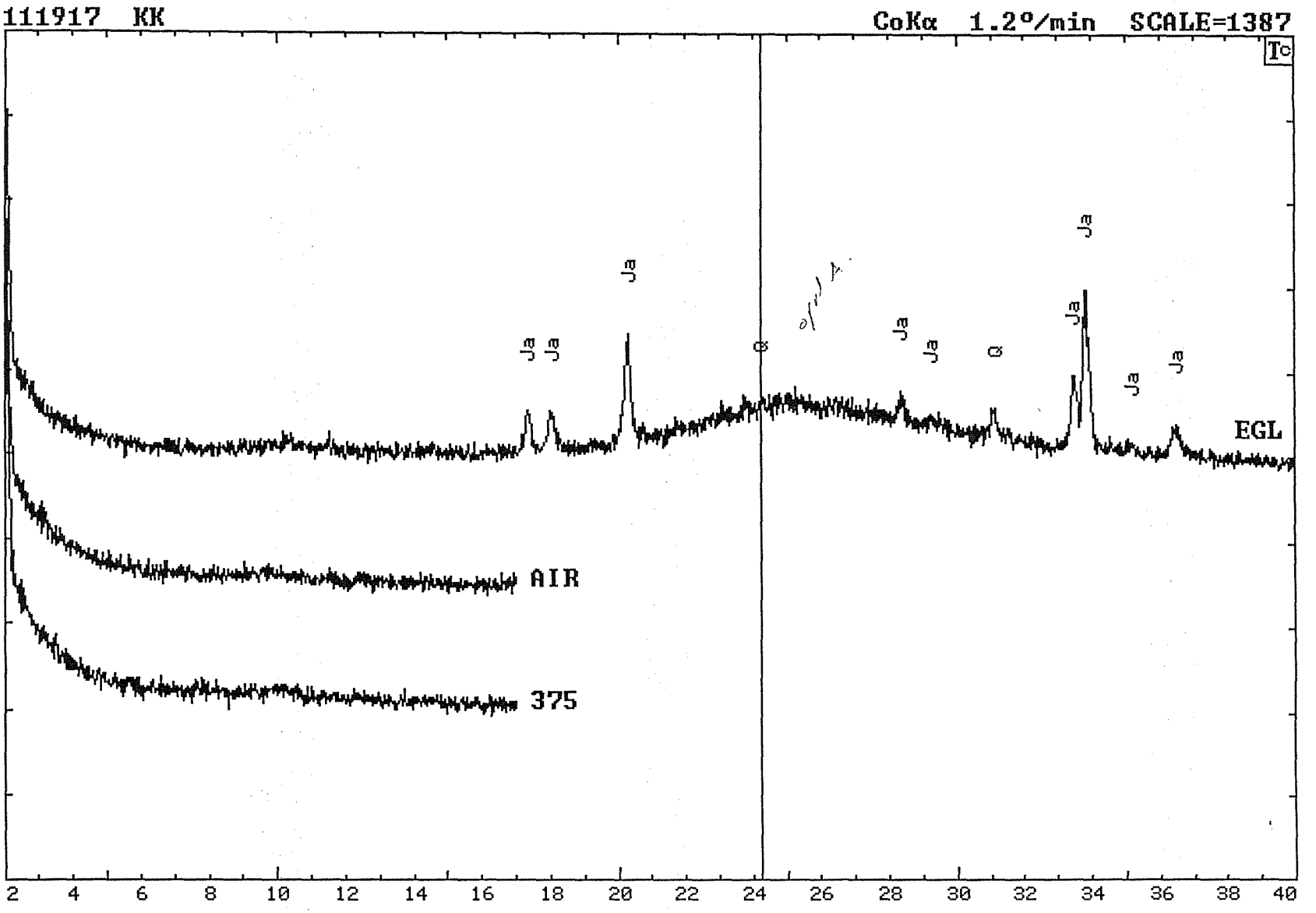

111918 KK
CoKα 1.2°/min SCALE=1455
Tc
Tr
α
Tr
Tr
α
EGL
AIR
375
2 4 6 8 10 12 14 16 18 20 22 24 26 28 30 32 34 36 38 40

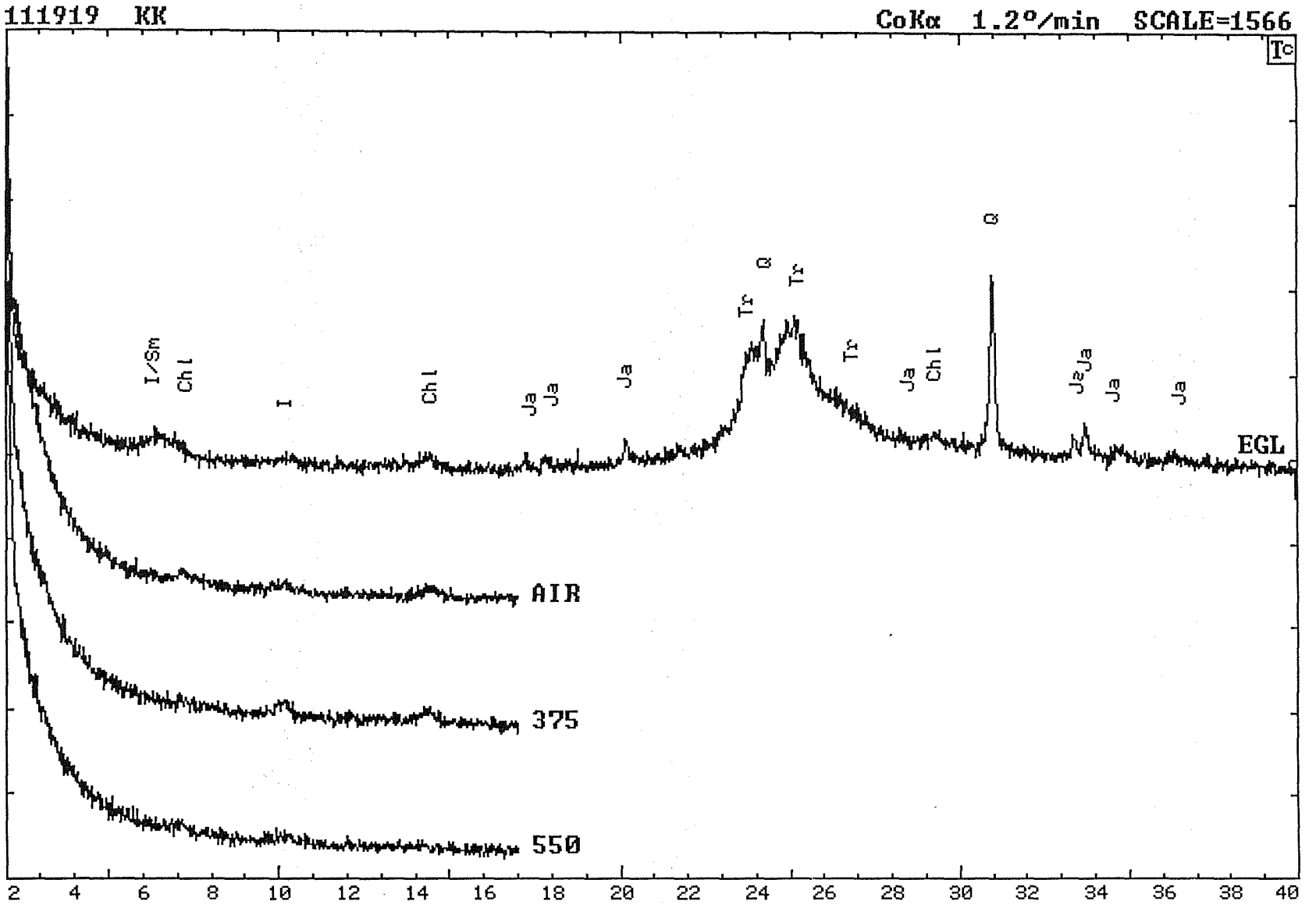
Loc 301

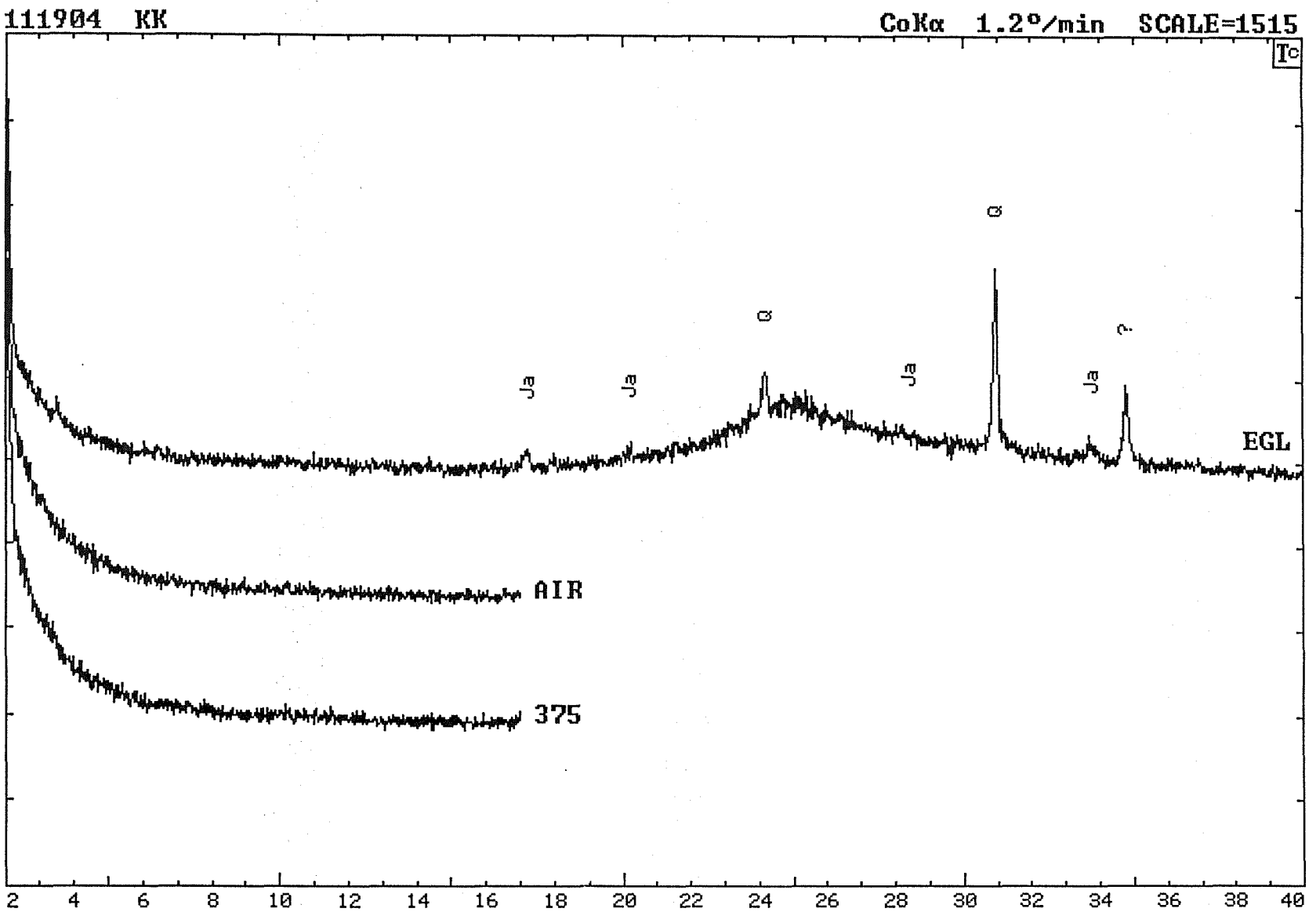

111945 KK
CoKα 1.2°/min SCALE=1720
Tc
Op A
EGL
AIR
375
2 4 6 8 10 12 14 16 18 20 22 24 26 28 30 32 34 36 38 40

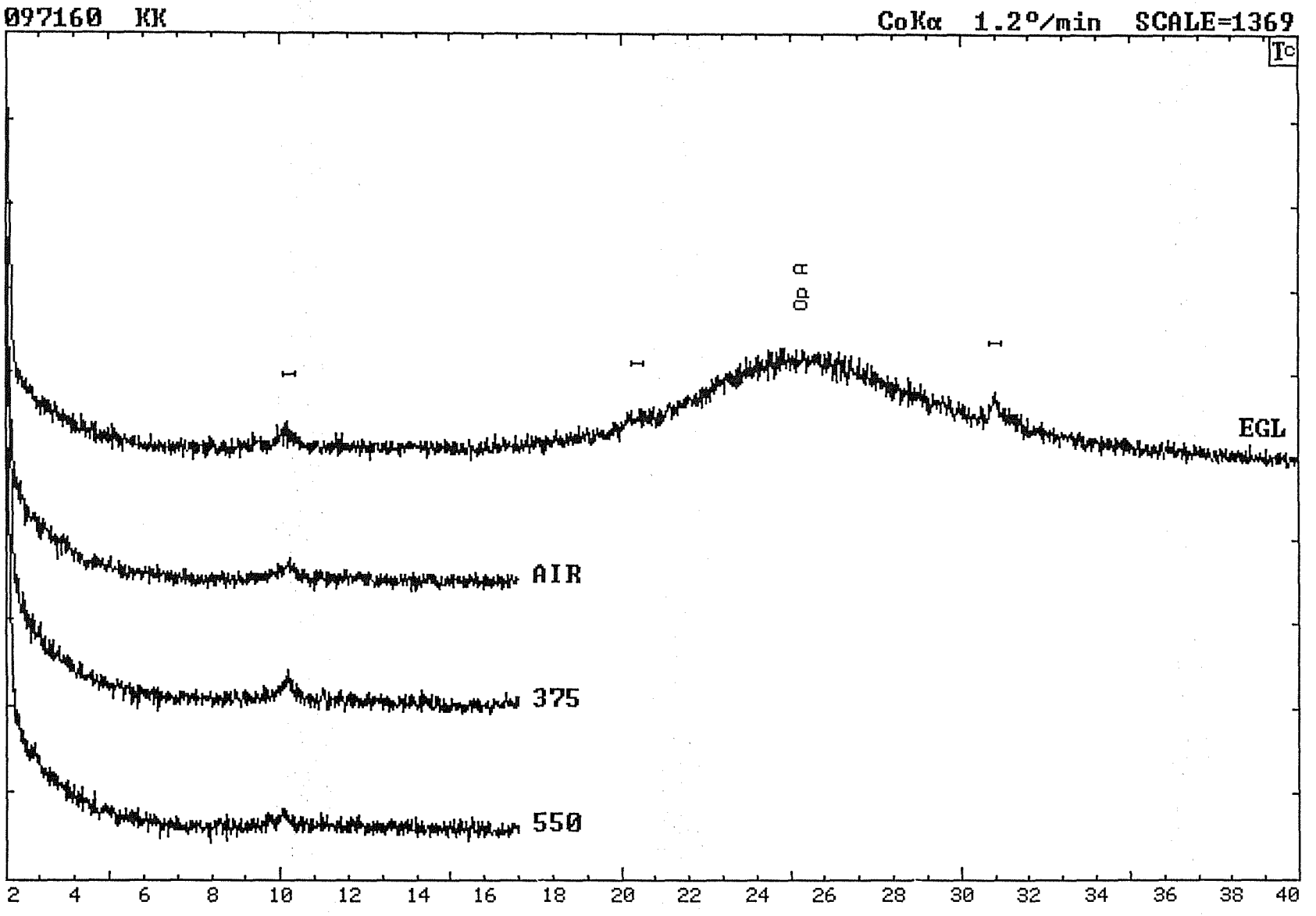

097160 KK
CoKα 1.2°/min SCALE=1369
Tc
I
I
Op
I
EGL
AIR
375
550
2
4
6
8
10
12
14
16
18
20
22
24
26
28
30
32
34
36
38
40

Loc 219

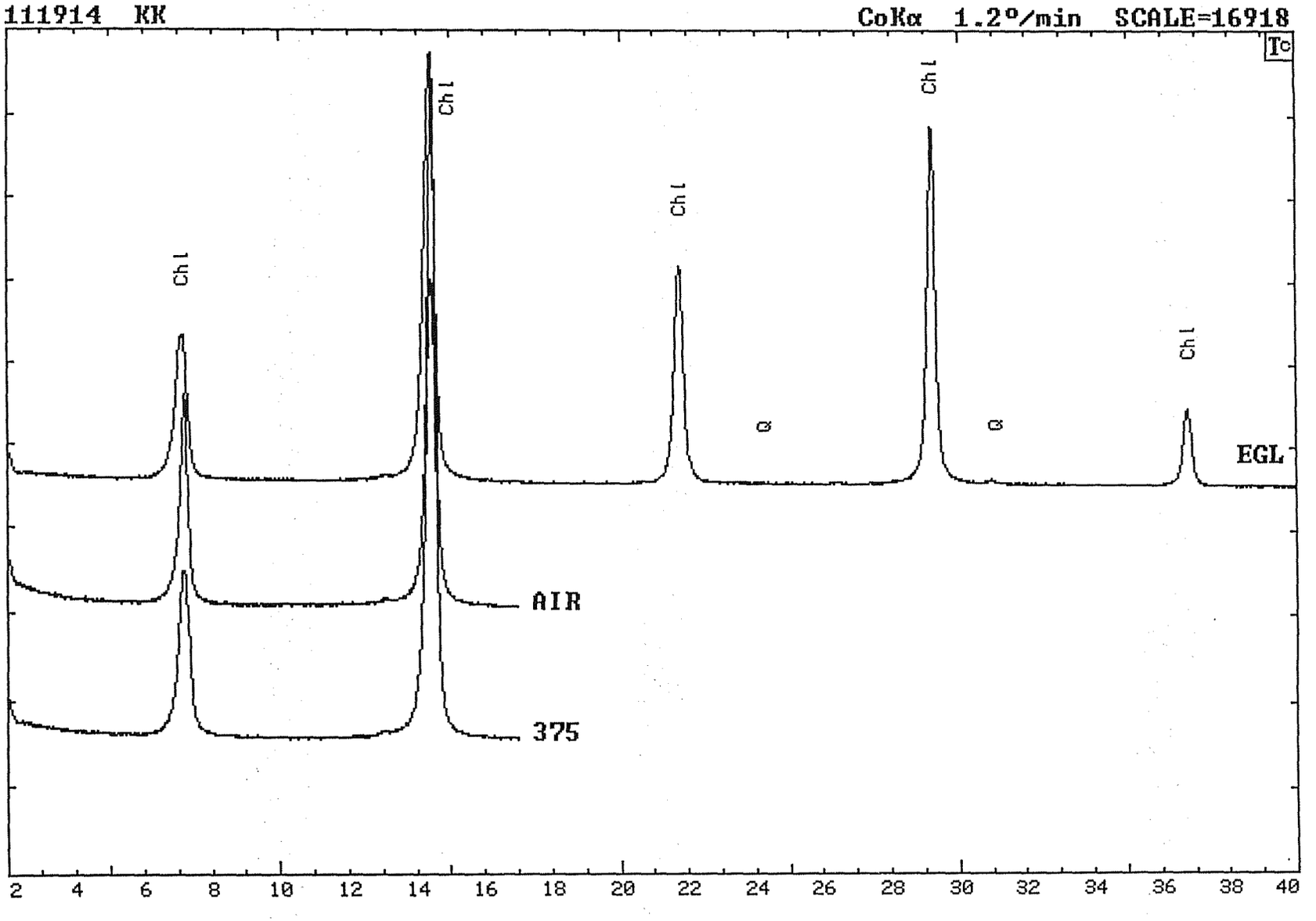

111917 KK
CoKα 1.2°/min SCALE=1387
Tc
Ja
Ja
Ja
Q
Ja
Ja
Q
Ja
Ja
Ja
EGL
AIR
375
2
4
6
8
10
12
14
16
18
20
22
24
26
28
30
32
34
36
38
40

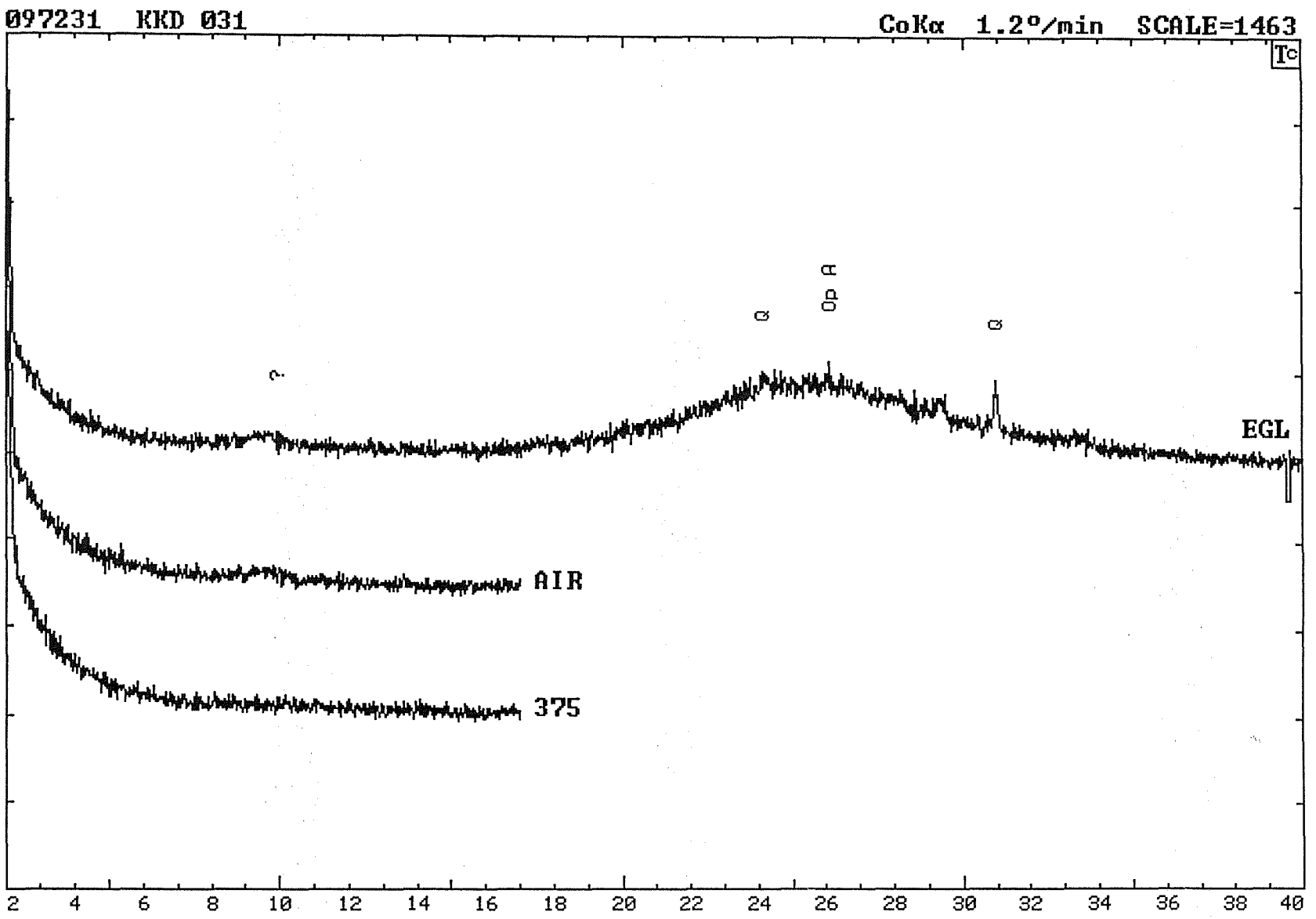

111919 KK
CoKα 1.2°/min SCALE=1566
Tc
I/Sm
Chl
I
Chl
Ja
Ja
Ja
Tr
Q
Tr
Tr
Ja
Chl
Q
Ja
Ja
Ja
Ja
EGL
AIR
375
550
2
4
6
8
10
12
14
16
18
20
22
24
26
28
30
32
34
36
38
40

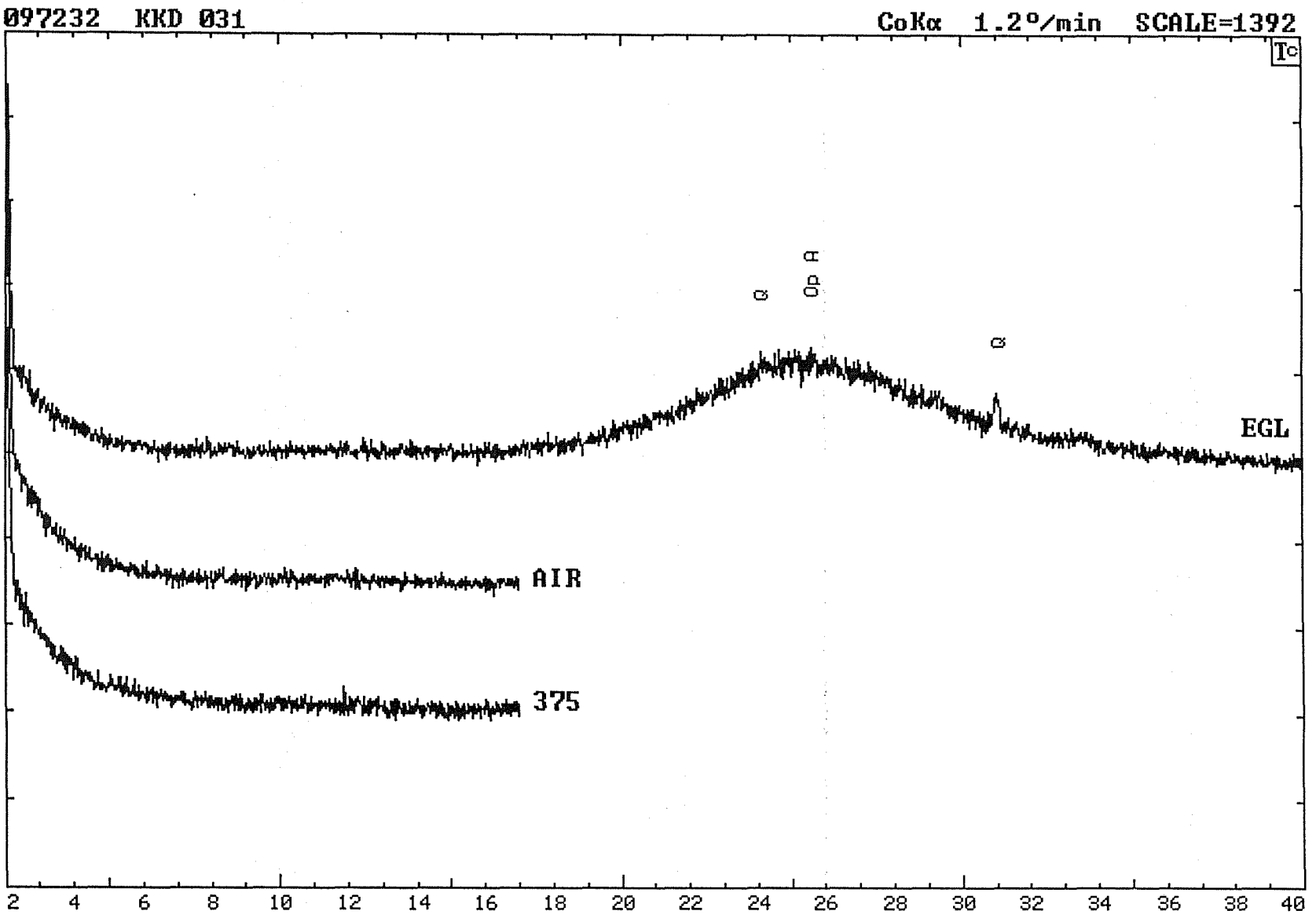

111904 KK
CoKα 1.2°/min SCALE=1515
Tc
Ja
Ja
α
Ja
α
Ja
?
EGL
AIR
375
2 4 6 8 10 12 14 16 18 20 22 24 26 28 30 32 34 36 38 40

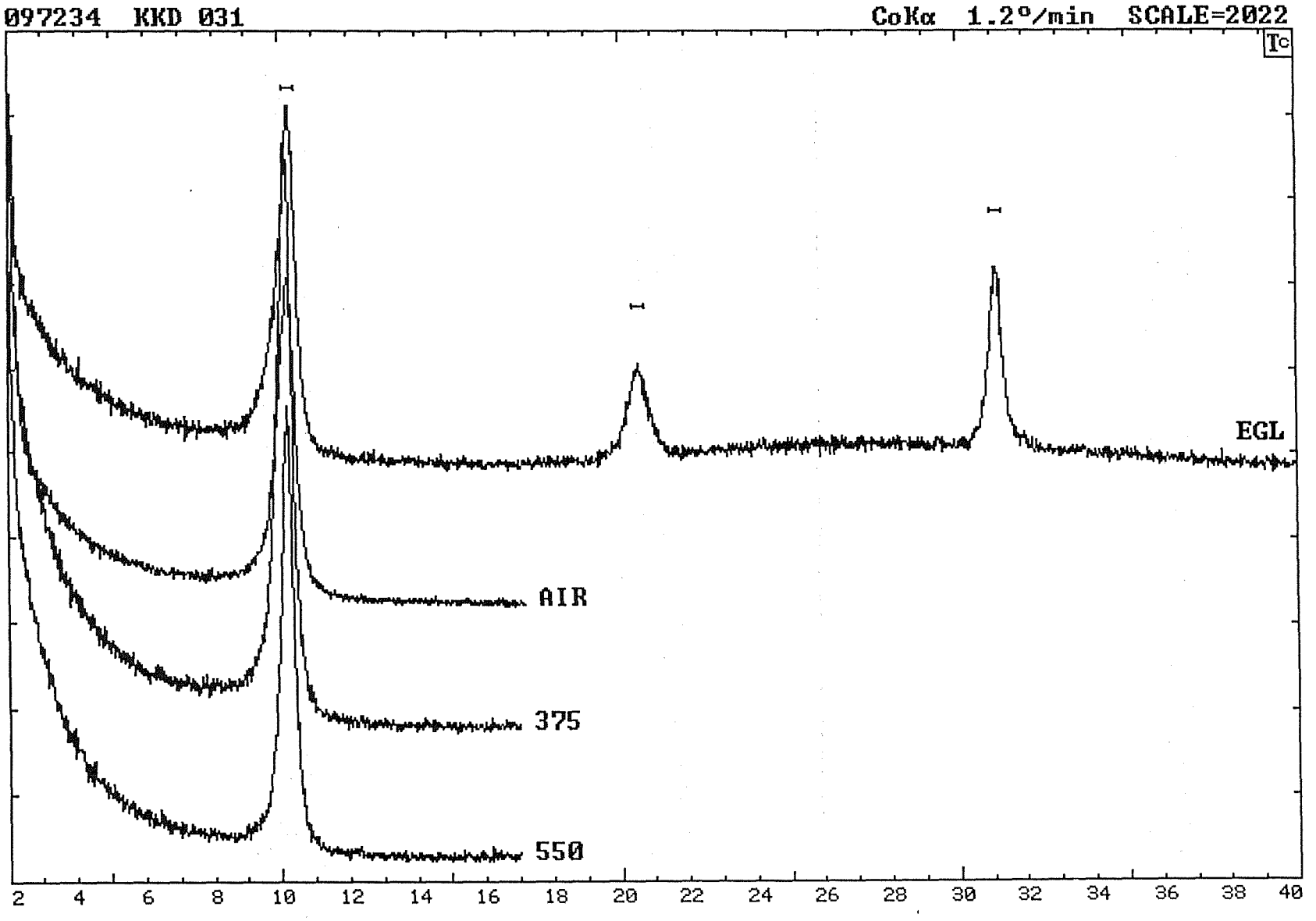

097160 KK
CoKα 1.2°/min SCALE=1369
Tc
Op A
I
I
I
EGL
AIR
375
550
2 4 6 8 10 12 14 16 18 20 22 24 26 28 30 32 34 36 38 40

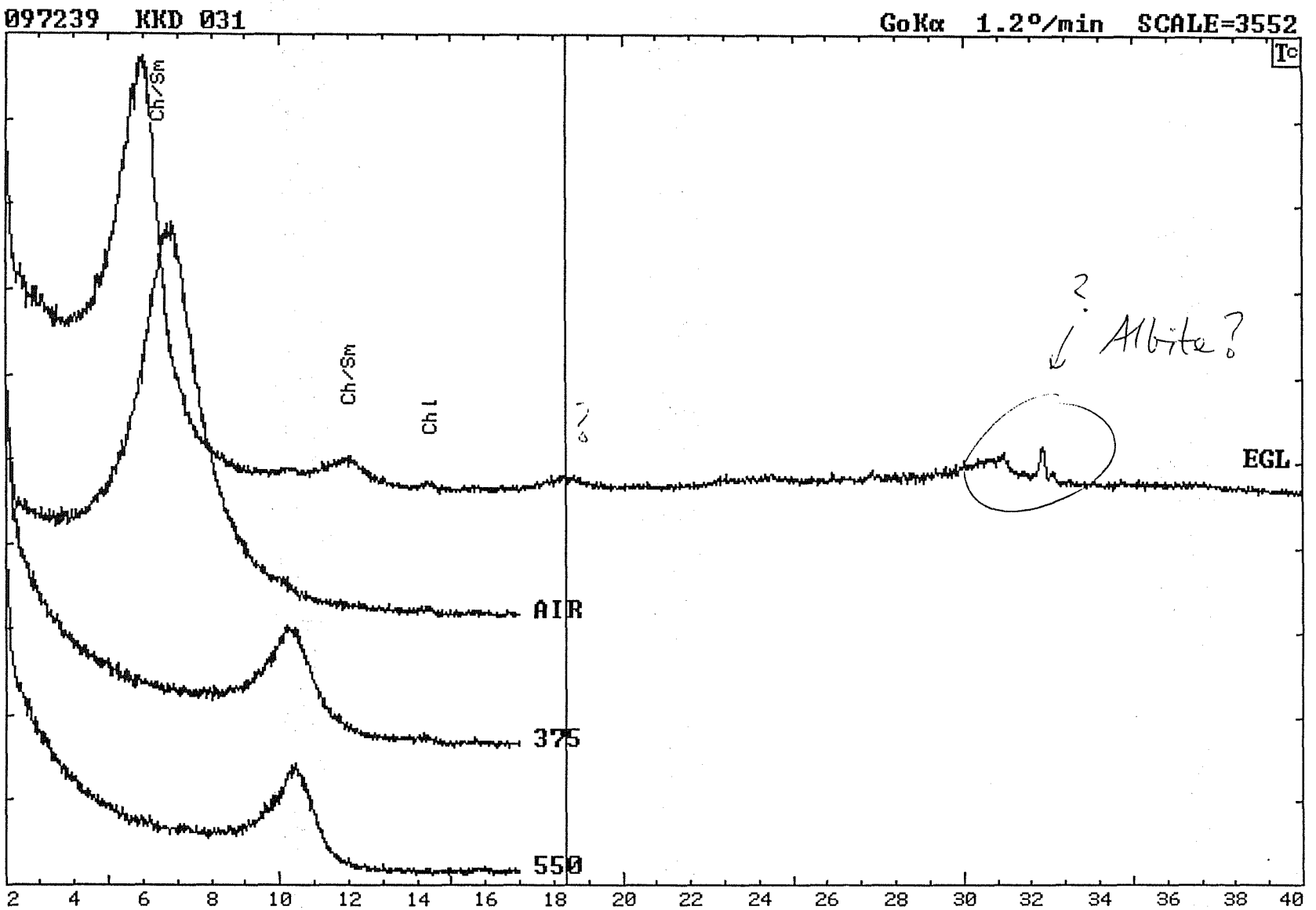
Lo. 316

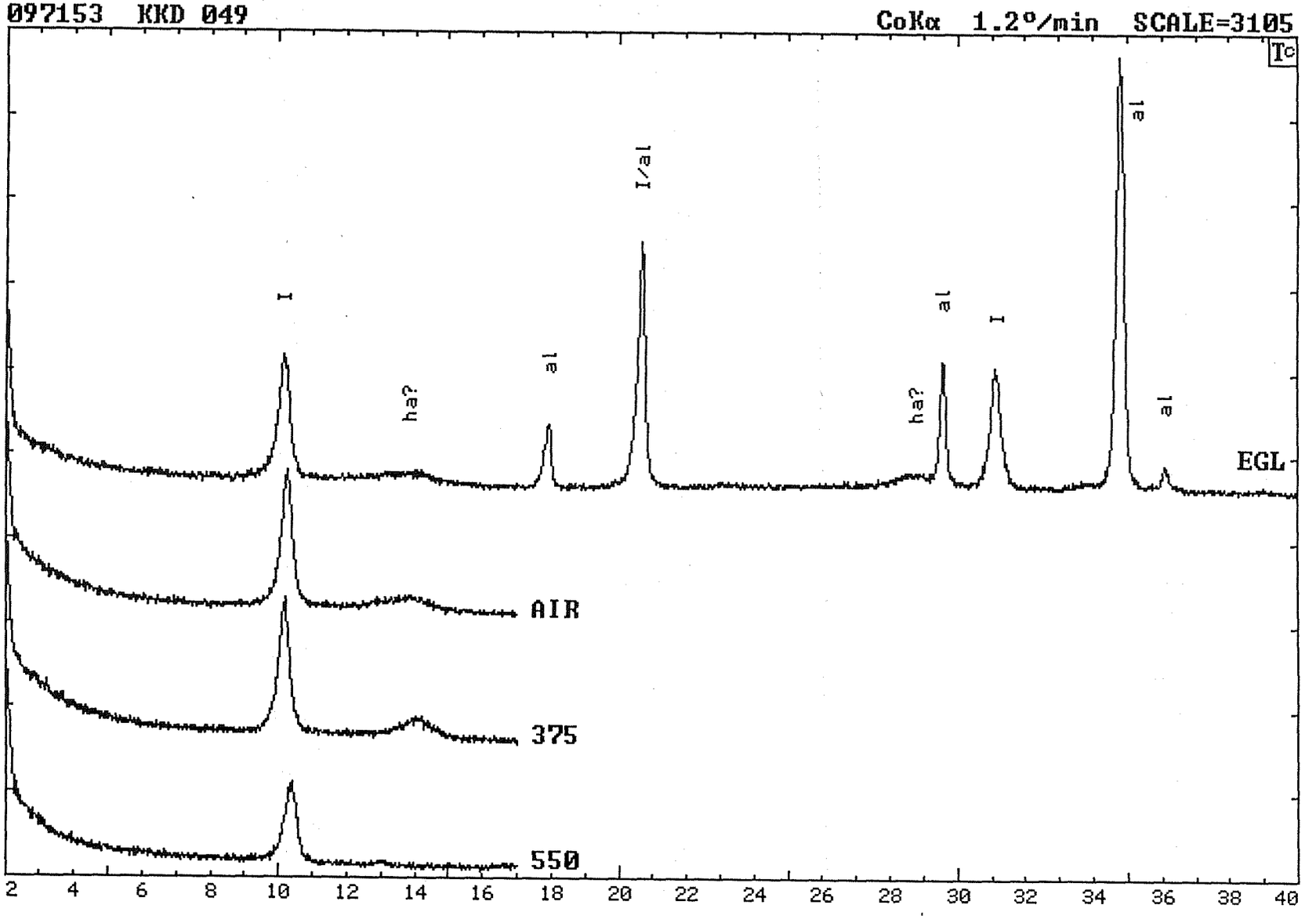

111914 KK
CoKα 1.2°/min SCALE=16918
Tc
Chl
Chl
Chl
Chl
Q
Q
EGL
AIR
375
2 4 6 8 10 12 14 16 18 20 22 24 26 28 30 32 34 36 38 40


097231 KKD 031
CoKα 1.2°/min SCALE=1463
Tc
EGL
AIR
375
2
4
6
8
10
12
14
16
18
20
22
24
26
28
30
32
34
36
38
40

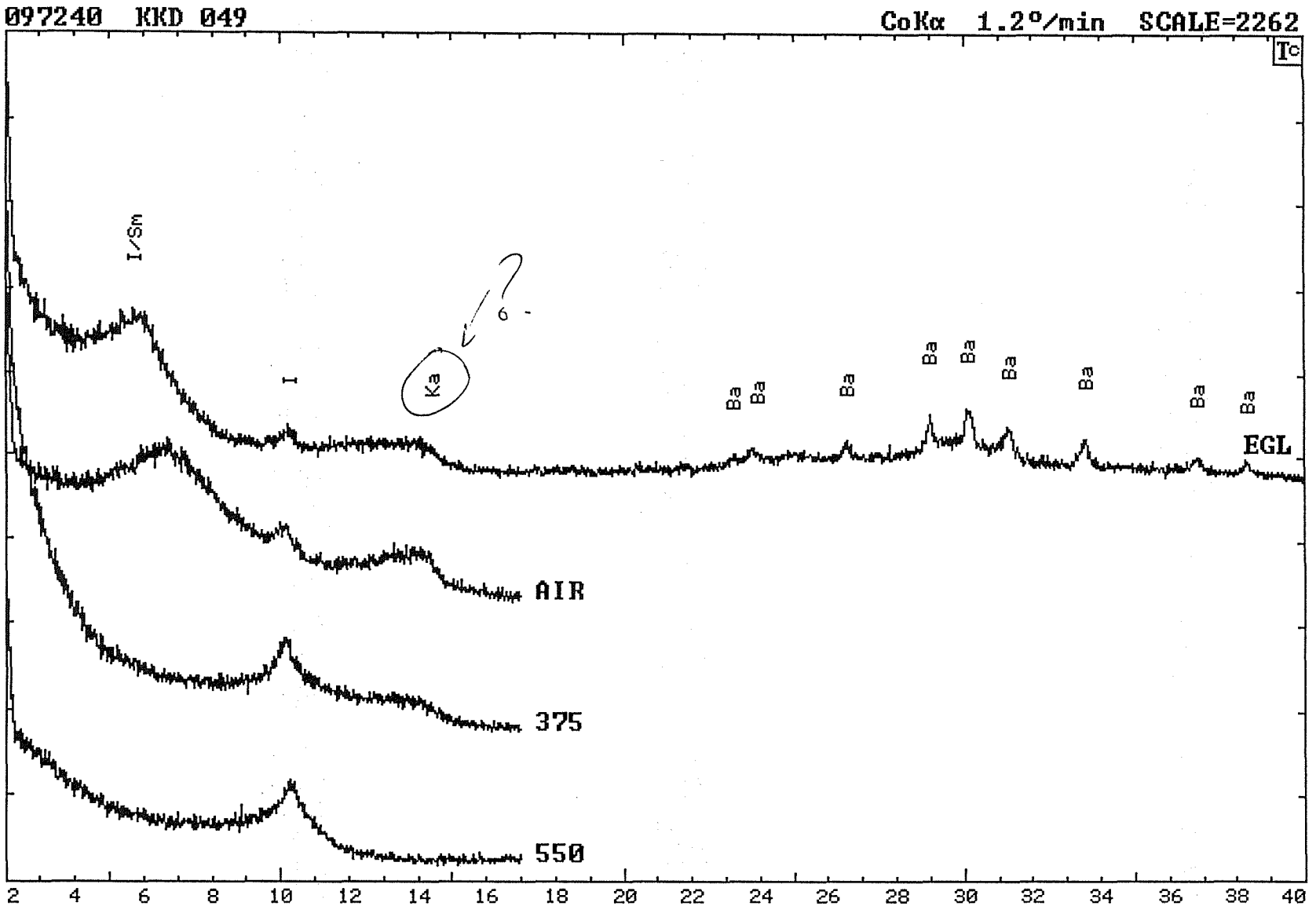

097232 KKD 031
CoKα 1.2°/min SCALE=1392
Tc
α
Op α
α
EGL
AIR
375
2 4 6 8 10 12 14 16 18 20 22 24 26 28 30 32 34 36 38 40

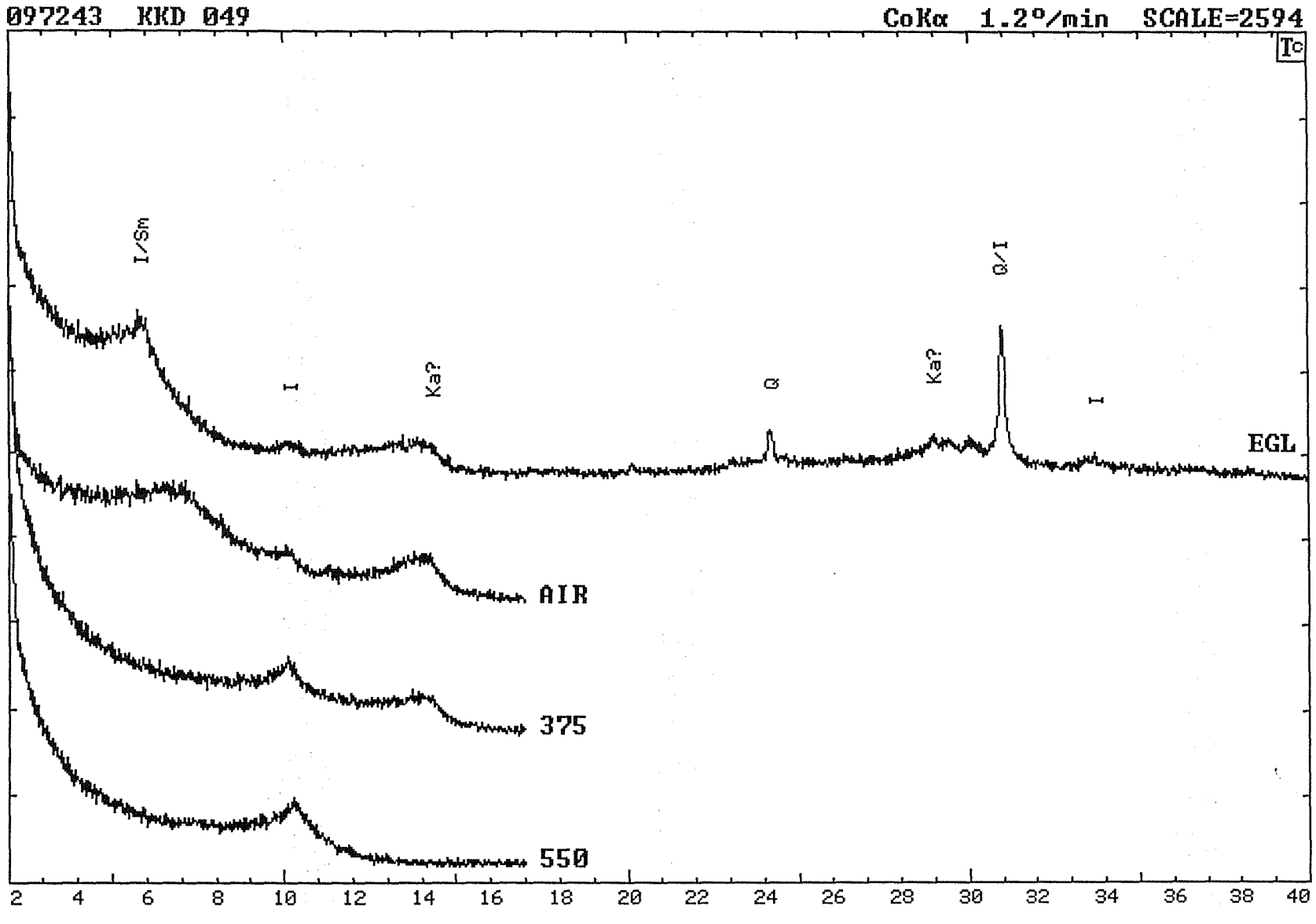

097234 KKD 031
CoKα 1.2°/min SCALE=2022
Tc
EGL
AIR
375
550
2 4 6 8 10 12 14 16 18 20 22 24 26 28 30 32 34 36 38 40

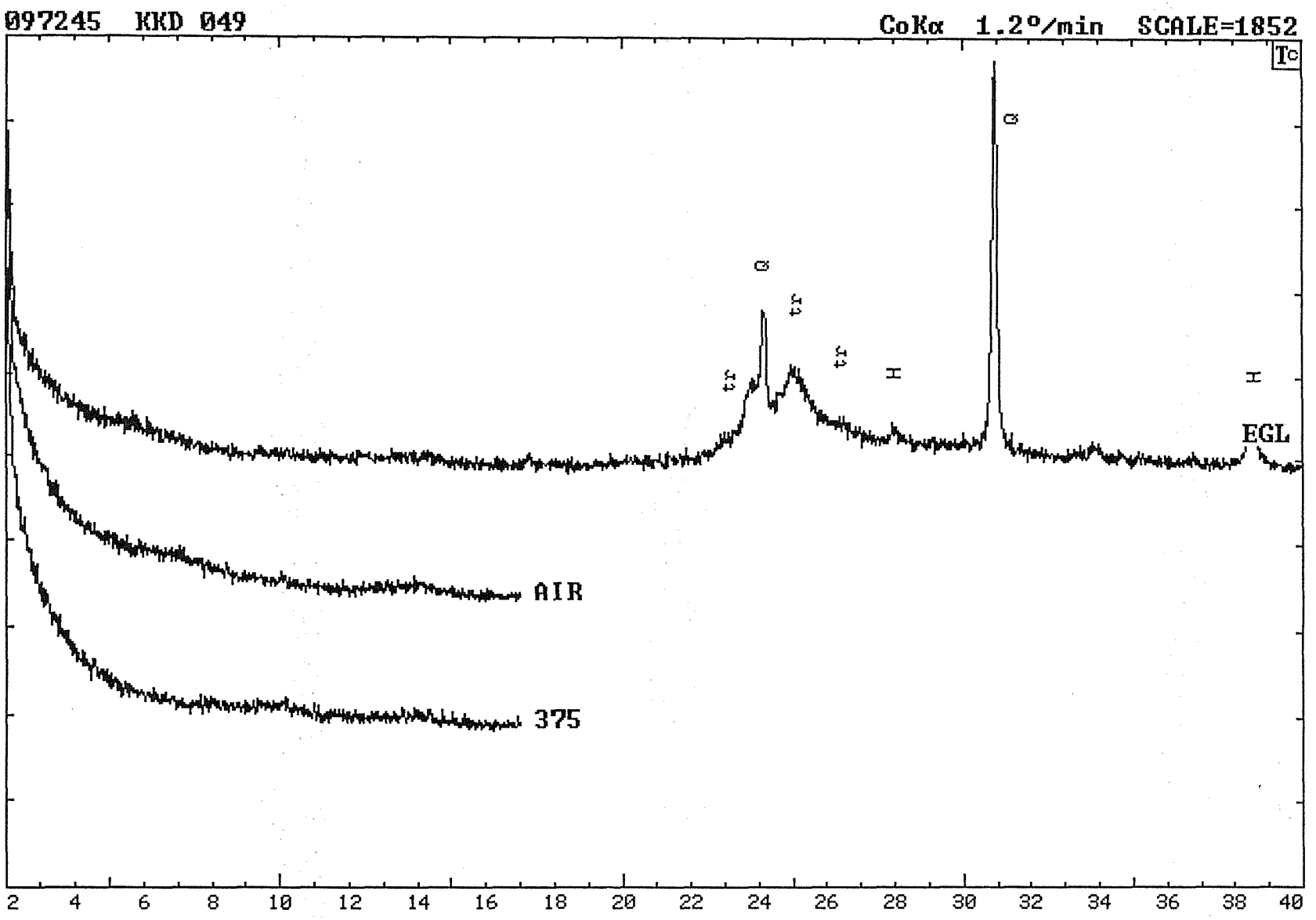

097239 KKD 031
GoKα 1.2°/min SCALE=3552
Tc
Ch/Sm
Ch/Sm
Chl
?
? Albite?
EGL
AIR
375
550
2 4 6 8 10 12 14 16 18 20 22 24 26 28 30 32 34 36 38 40

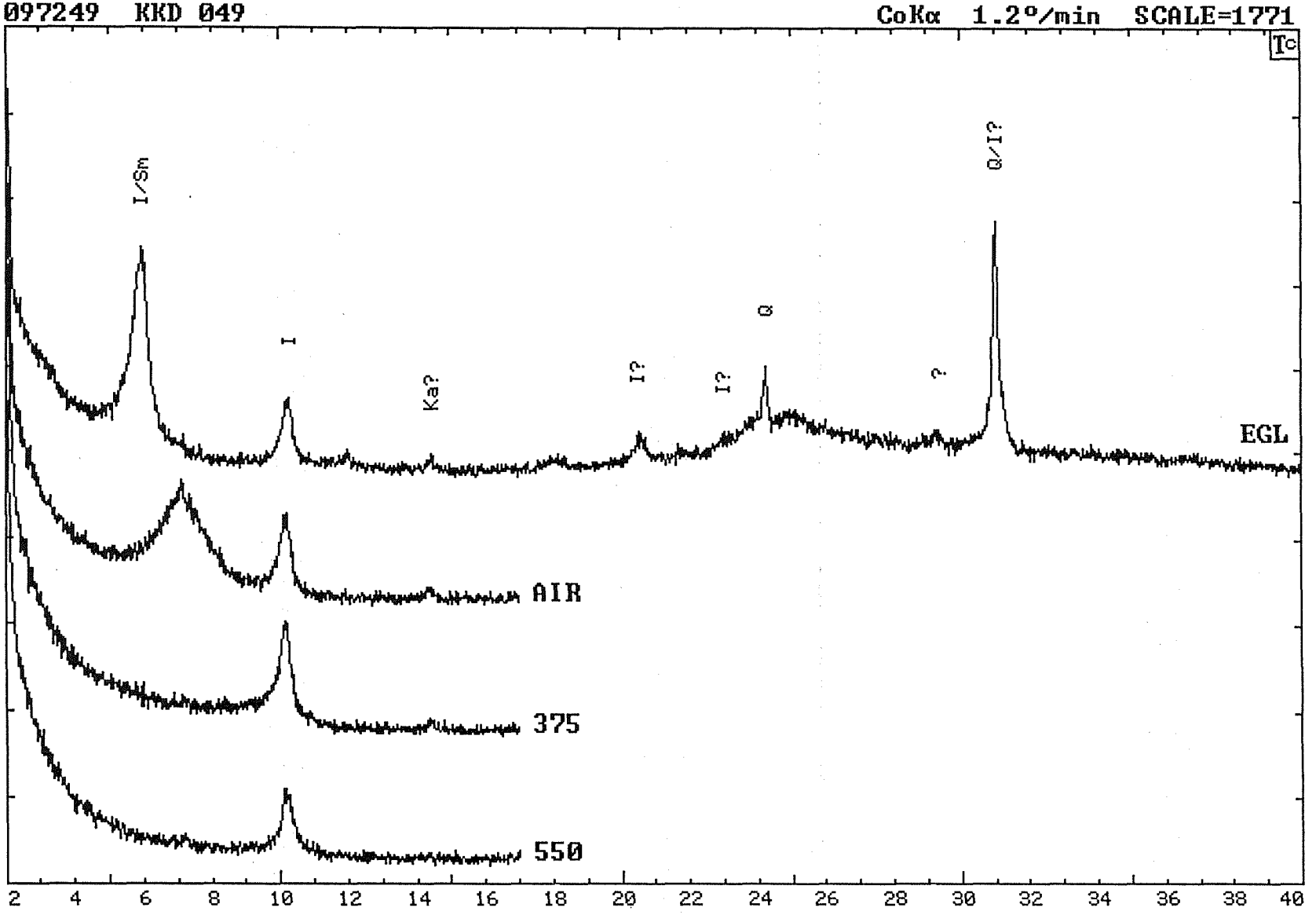

097153 KKD 049
CoKα 1.2°/min SCALE=3105
Tc
I
ha?
al
I/al
ha?
al
I
al
al
EGL
AIR
375
550
2 4 6 8 10 12 14 16 18 20 22 24 26 28 30 32 34 36 38 40

5m

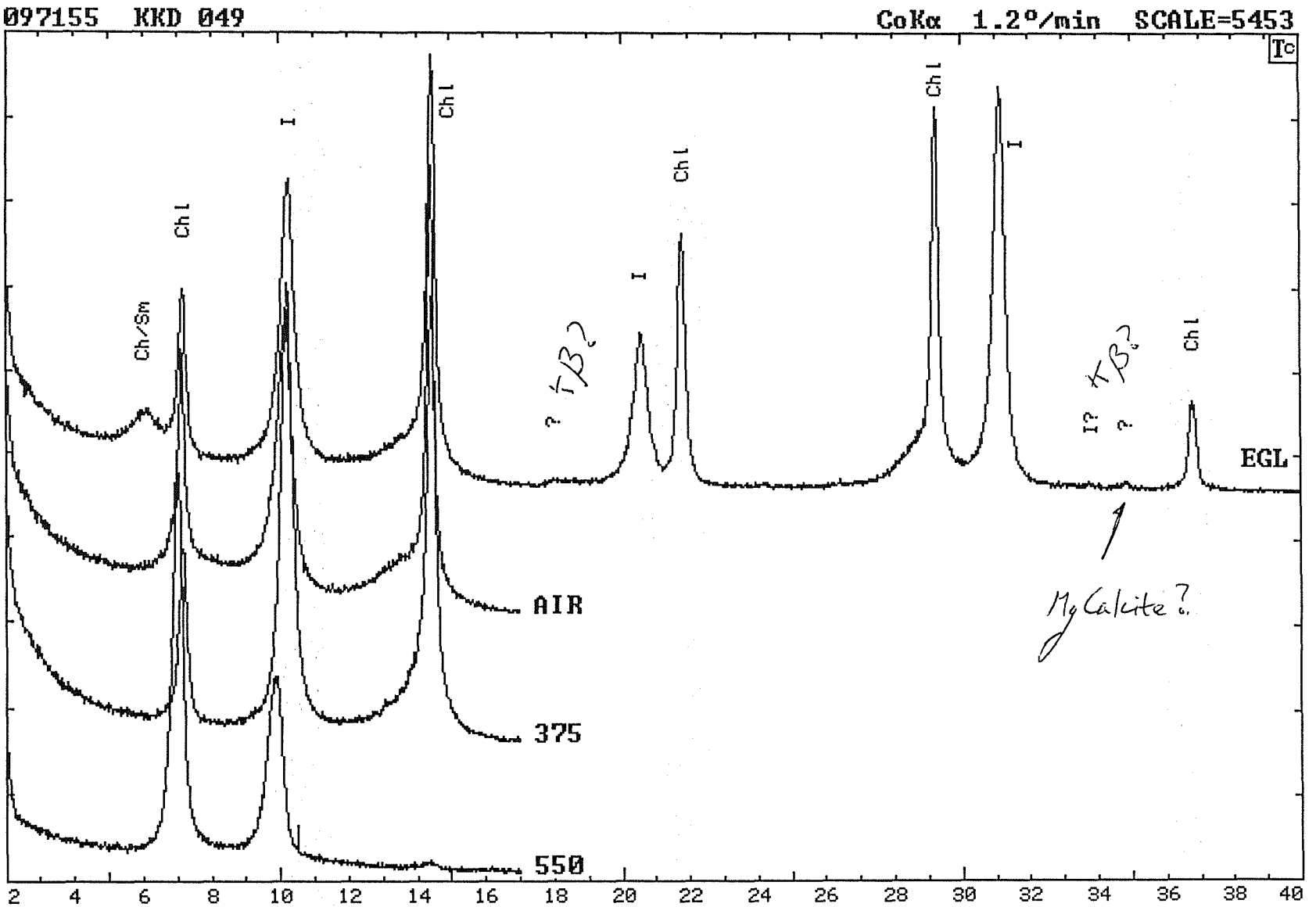

097240 KKD 049
CoKα 1.2°/min SCALE=2262
Tc
I/Sm
I
Ka
6
Ba
Ba
Ba
Ba
Ba
Ba
Ba
Ba
Ba
EGL
AIR
375
550
2
4
6
8
10
12
14
16
18
20
22
24
26
28
30
32
34
36
38
40

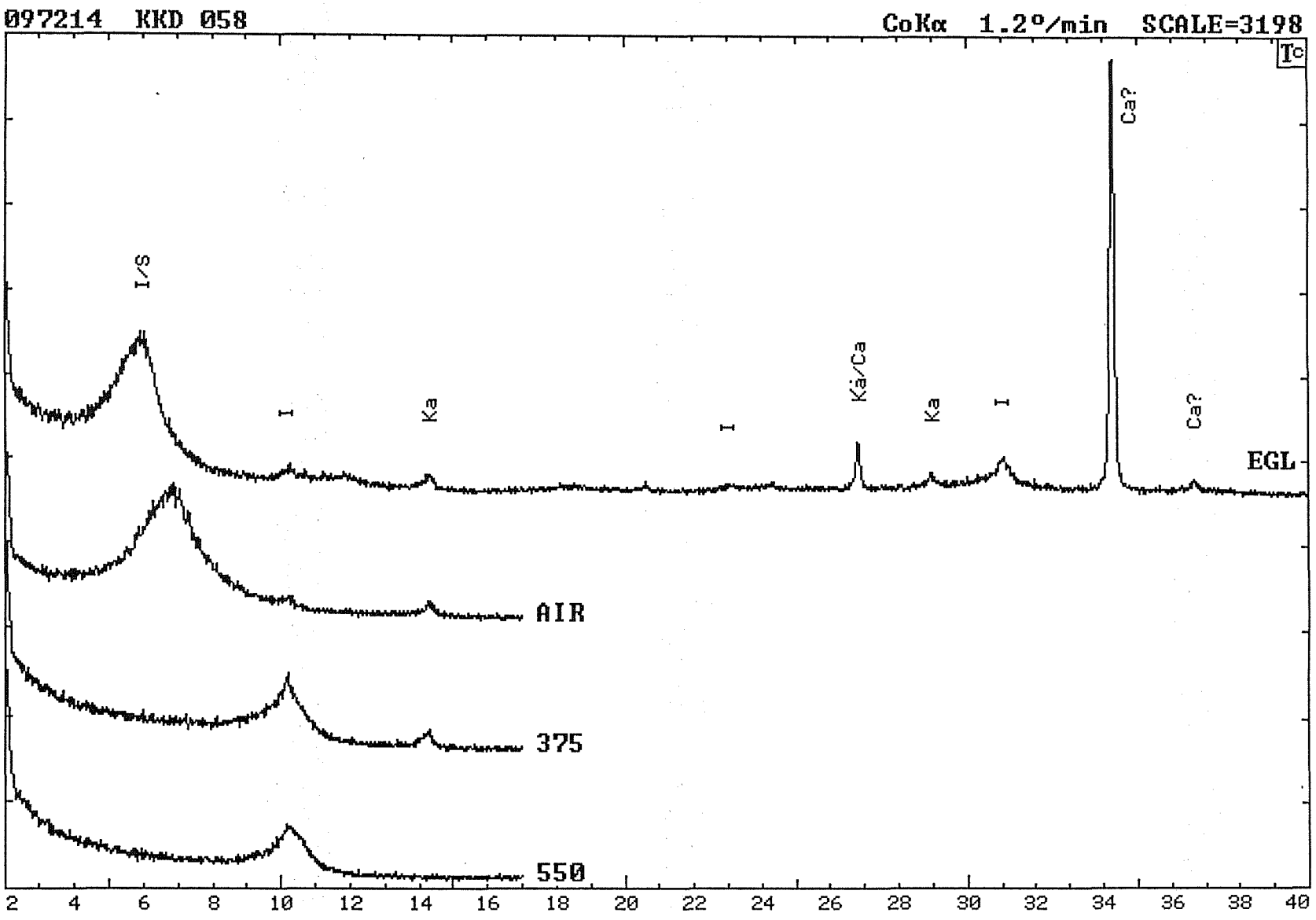

097243 KKD 049
CoKα 1.2°/min SCALE=2594
Tc
I/Sm
I
Ka?
Q
Ka?
Q/I
I
EGL
AIR
375
550
2
4
6
8
10
12
14
16
18
20
22
24
26
28
30
32
34
36
38
40

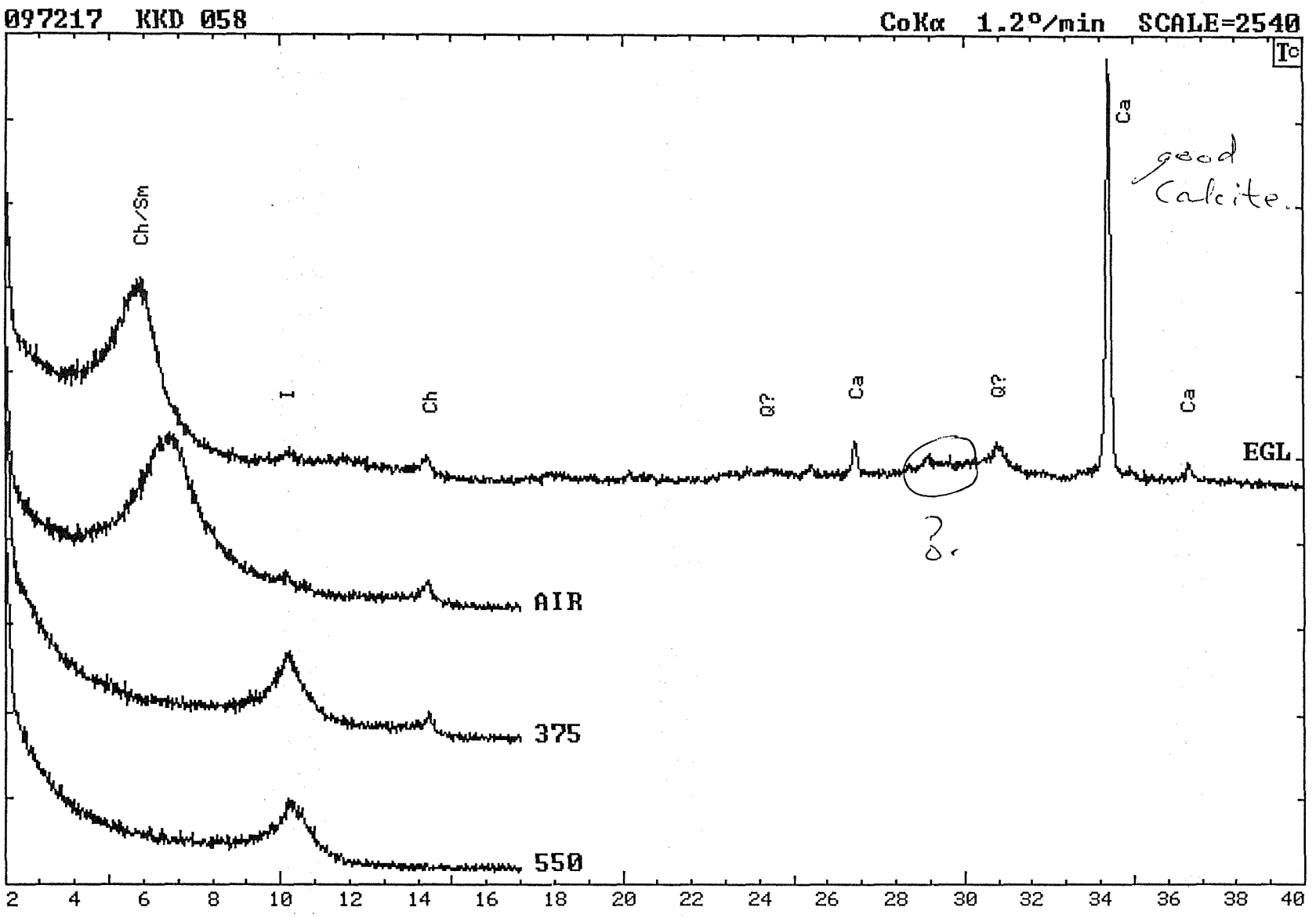

097245 KKD 049
CoKα 1.2°/min SCALE=1852
Tc
Q
tr
tr
tr
H
Q
H
EGL
AIR
375
2 4 6 8 10 12 14 16 18 20 22 24 26 28 30 32 34 36 38 40

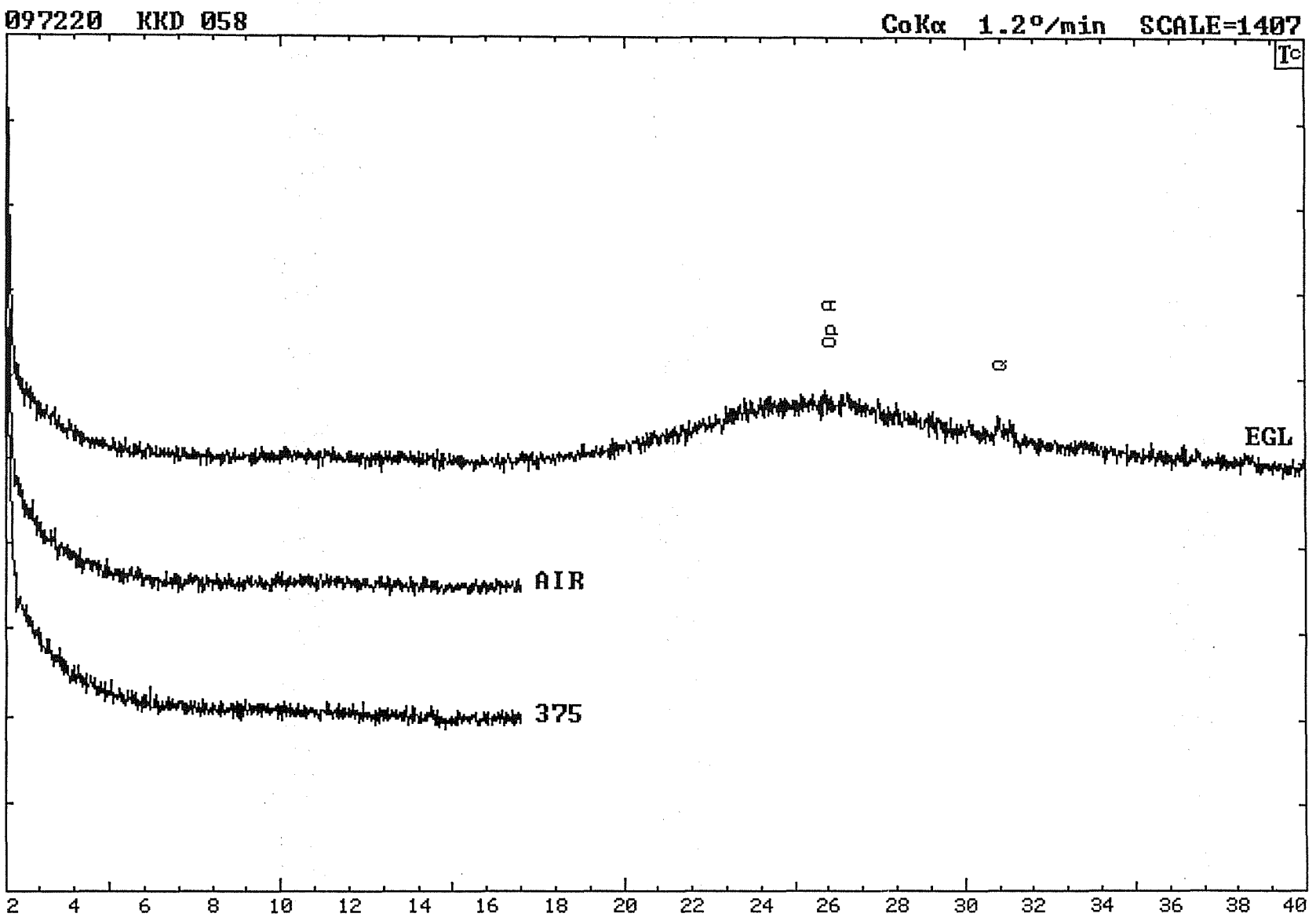

097249 KKD 049
CoKα 1.2°/min SCALE=1771
Tc
I/Sm
I
Ka?
I?
I?
Q
?
Q/I?
EGL
AIR
375
550
2
4
6
8
10
12
14
16
18
20
22
24
26
28
30
32
34
36
38
40

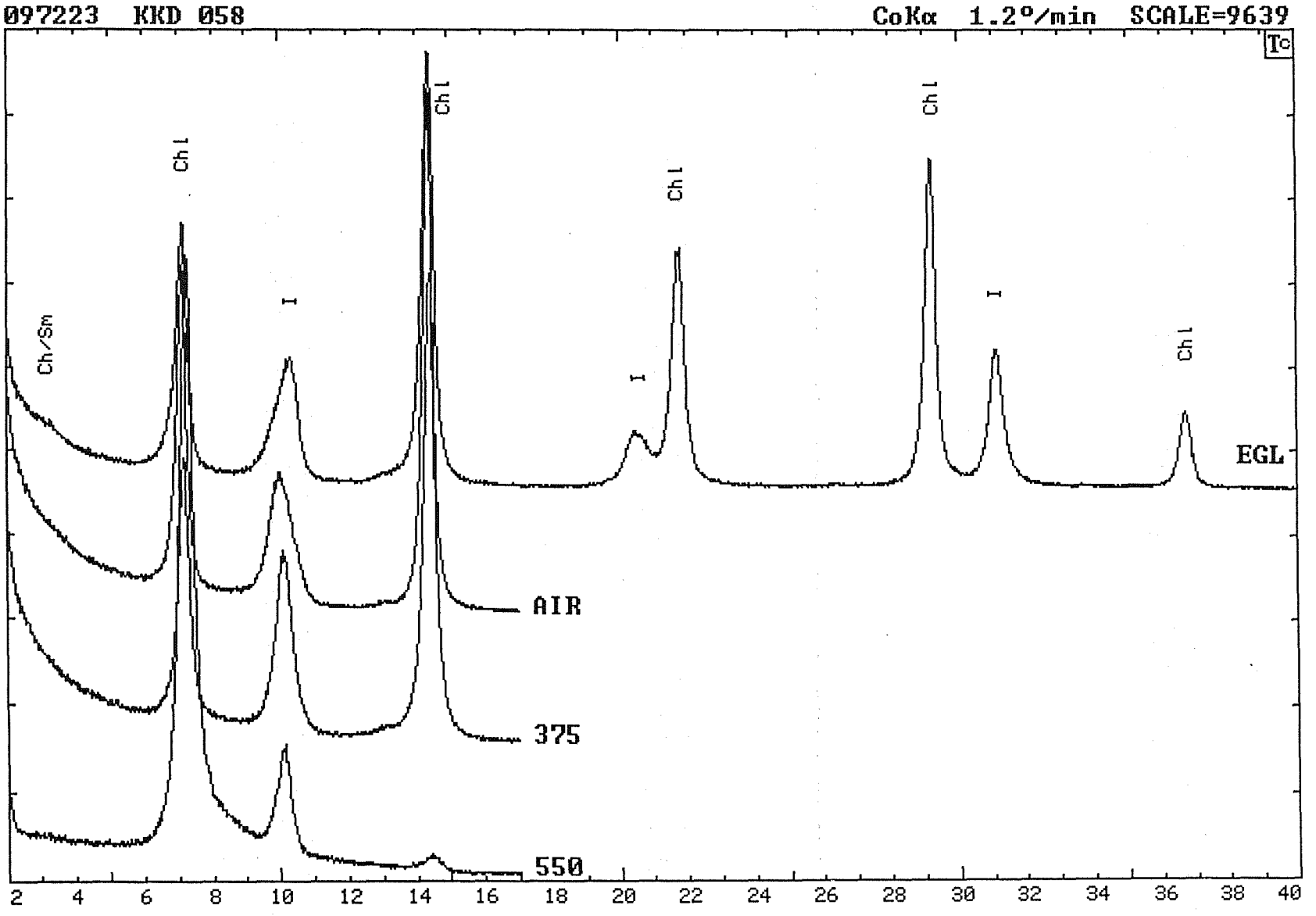
734

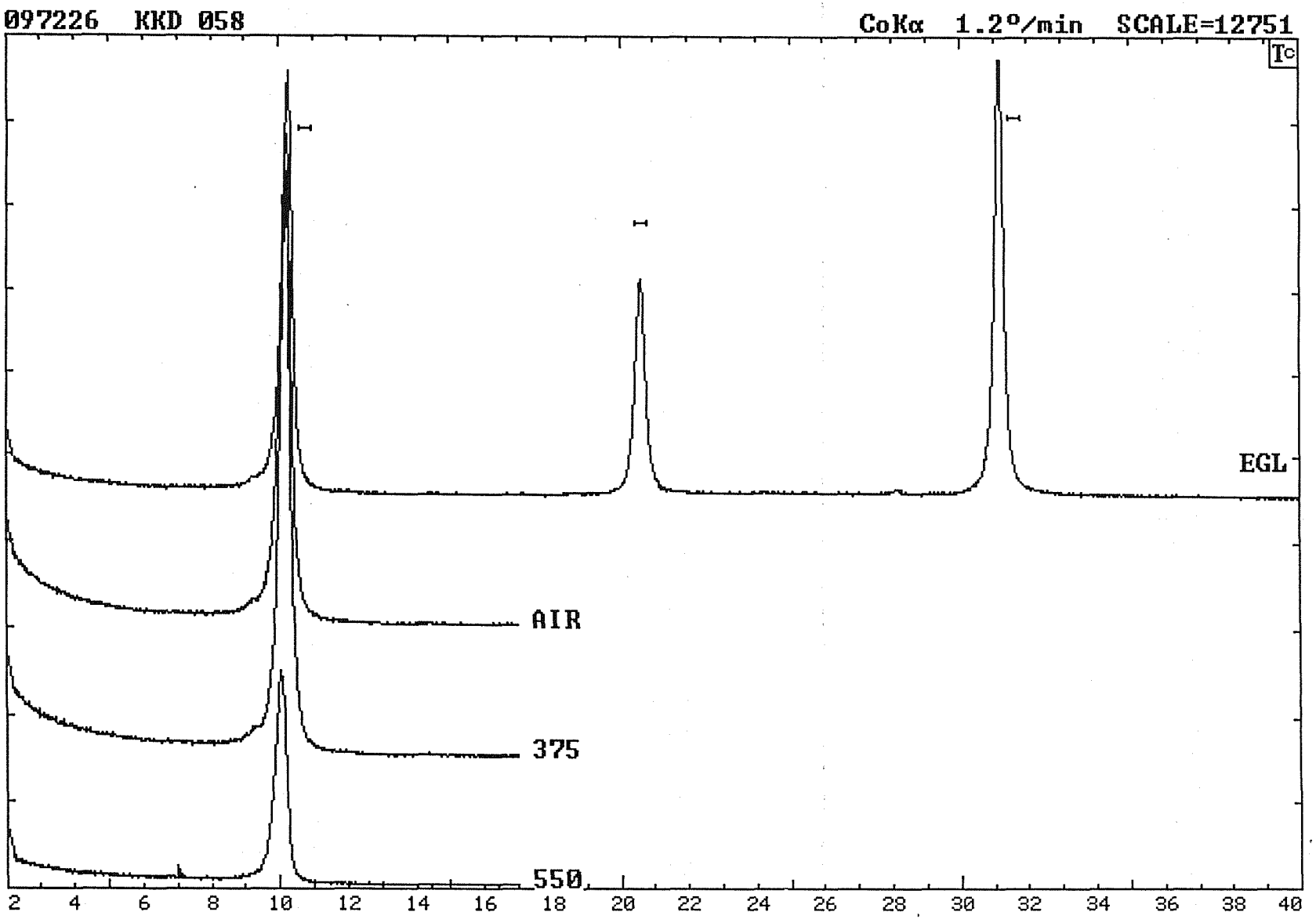

097155 KKD 049
CoKα 1.2°/min SCALE=5453
Tc
Ch/Sm
Chl
I
Chl
? KB?
I
Chl
Chl
I
I? KB?
?
Chl
EGL
AIR
375
550
Mg Calcite?
2 4 6 8 10 12 14 16 18 20 22 24 26 28 30 32 34 36 38 40

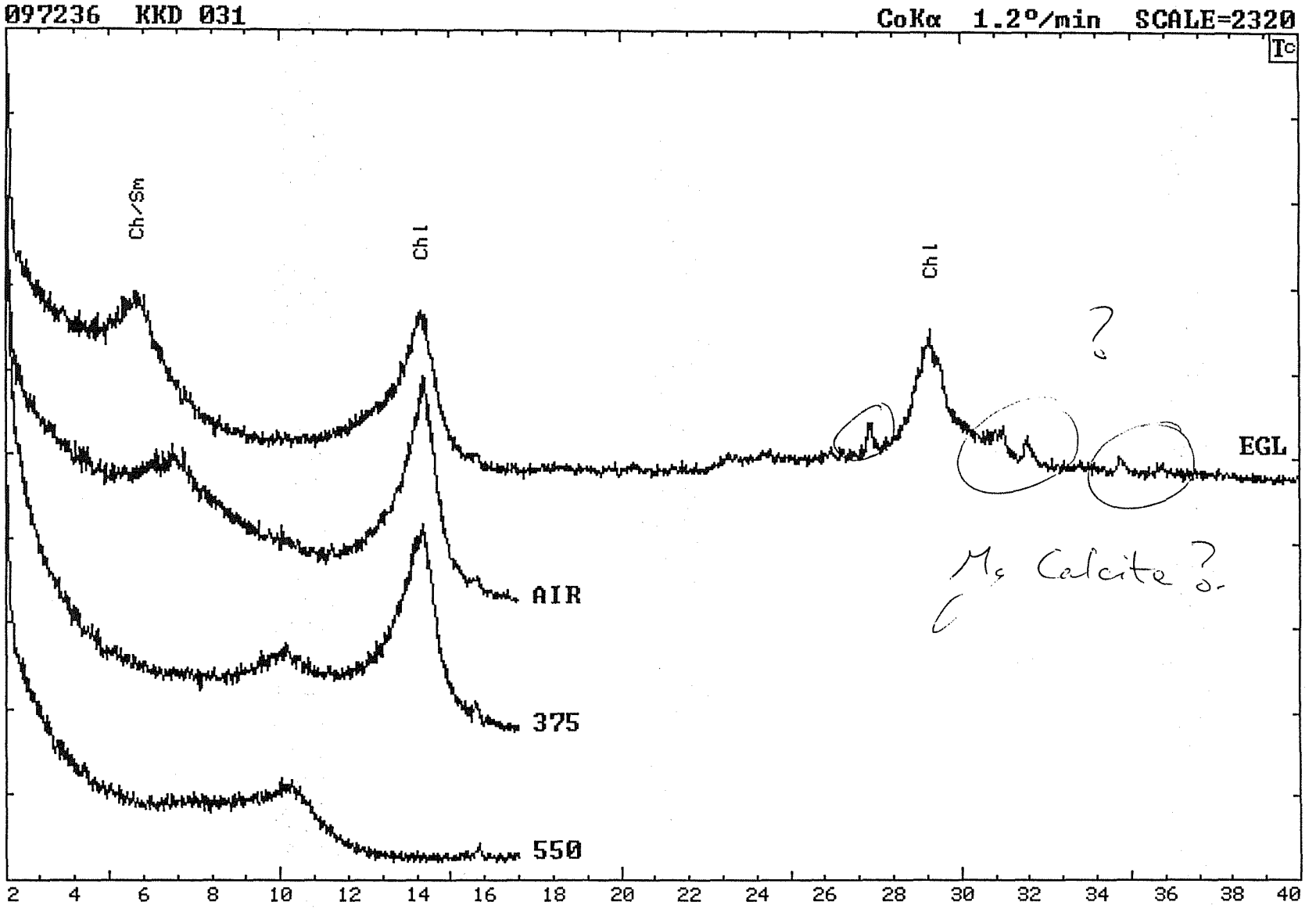

097214 KKD 058
CoKα 1.2°/min SCALE=3198
Tc
I/S
I
Ka
I
Kä/Ca
Ka
I
Ca?
Ca?
EGL
AIR
375
550
2 4 6 8 10 12 14 16 18 20 22 24 26 28 30 32 34 36 38 40


097217 KKD 058
CoKα 1.2°/min SCALE=2540
Tc
Ch/Sm
I
Ch
Q?
Ca
Q?
Ca
Ca
good
Calcite.
?
EGL
AIR
375
550
2 4 6 8 10 12 14 16 18 20 22 24 26 28 30 32 34 36 38 40

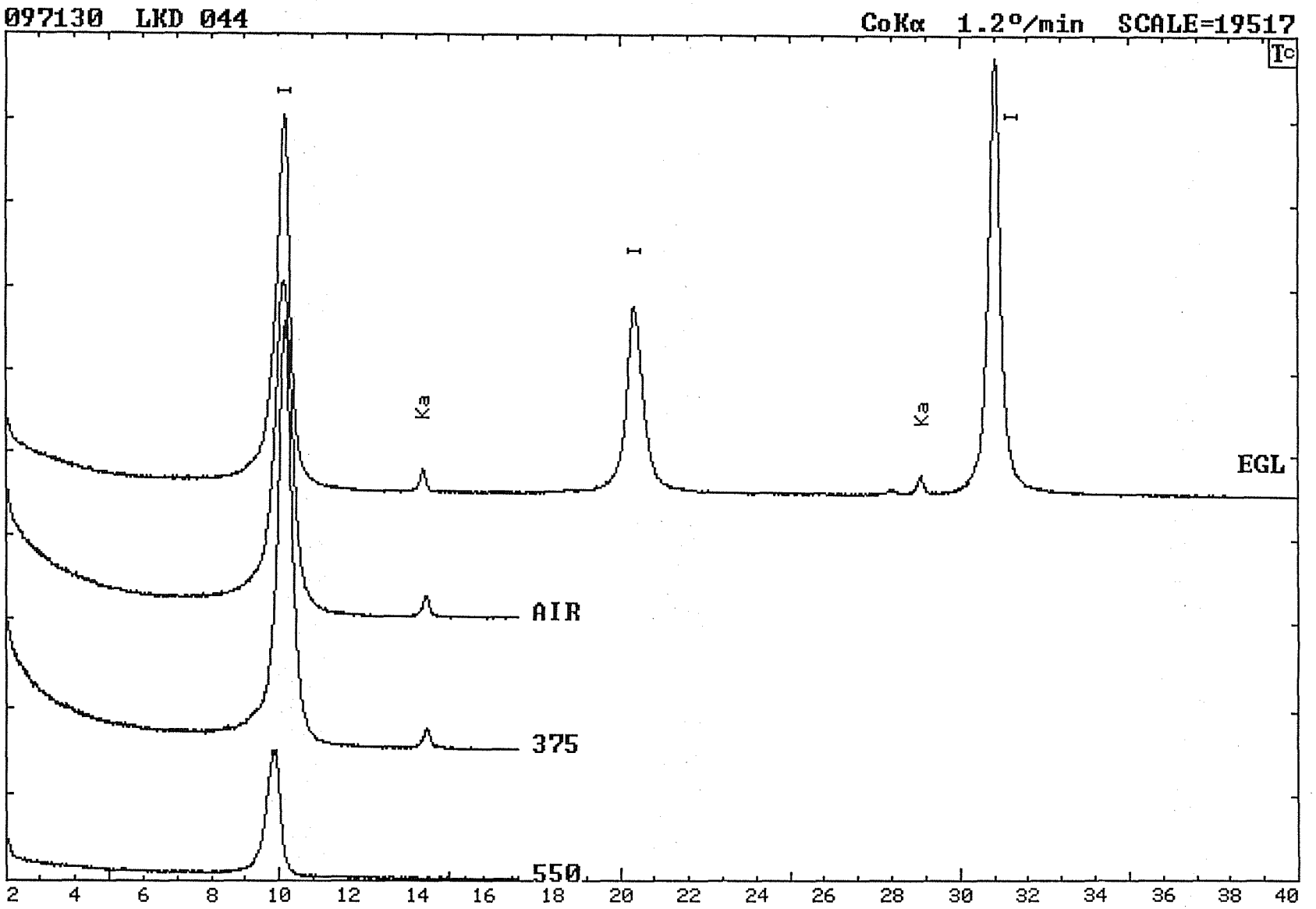

097220 KKD 058
CoKα 1.2°/min SCALE=1407
Tc
Op α
α
EGL
AIR
375
2 4 6 8 10 12 14 16 18 20 22 24 26 28 30 32 34 36 38 40


097223 KKD 058
CoKα 1.2°/min SCALE=9639
Tc
Ch/Sm
Chl
I
Chl
Chl
I
Chl
I
Chl
EGL
AIR
375
550
2 4 6 8 10 12 14 16 18 20 22 24 26 28 30 32 34 36 38 40

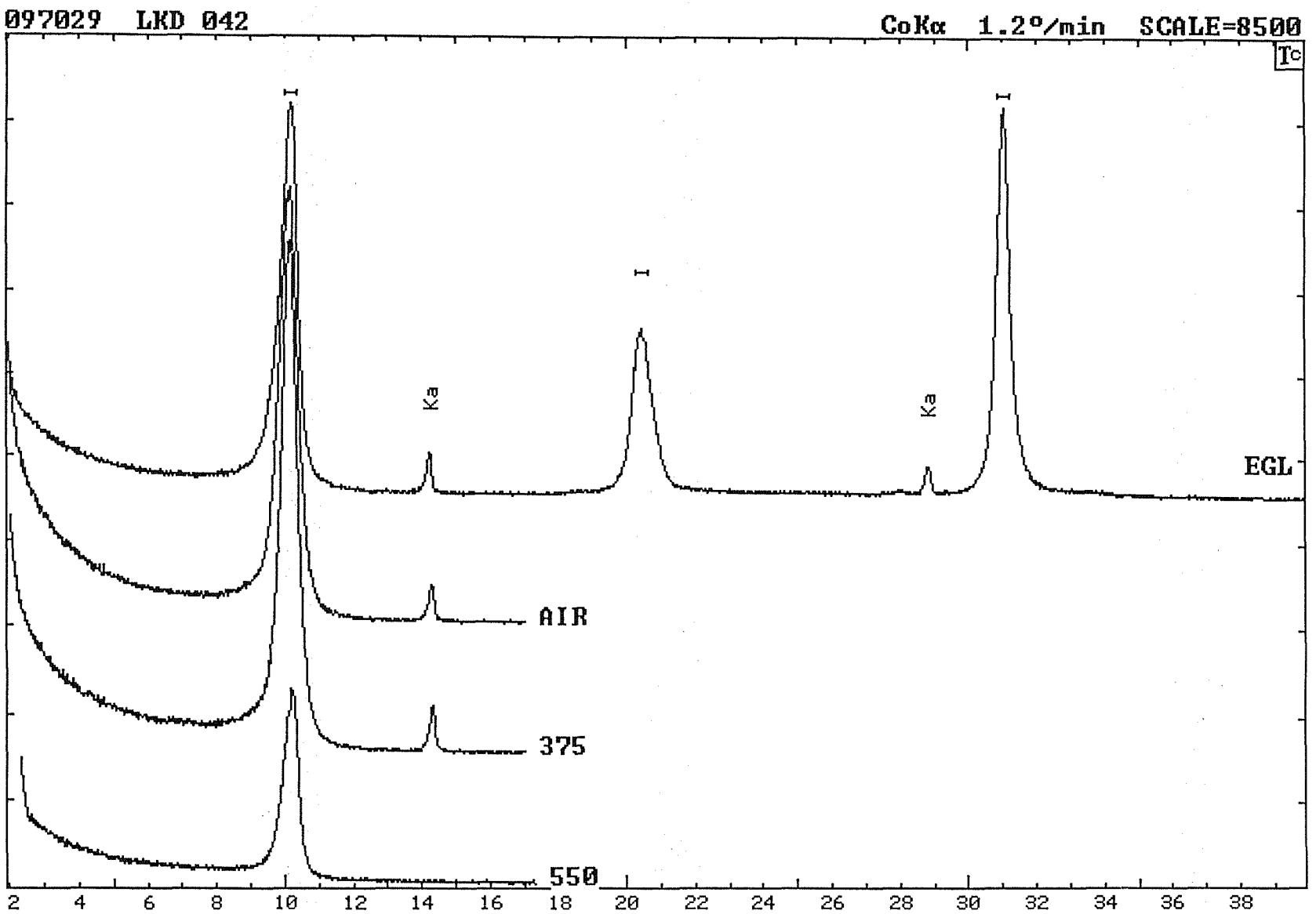

097226 KKD 058
CoKα 1.2°/min SCALE=12751
Tc
EGL
AIR
375
550
2 4 6 8 10 12 14 16 18 20 22 24 26 28 30 32 34 36 38 40

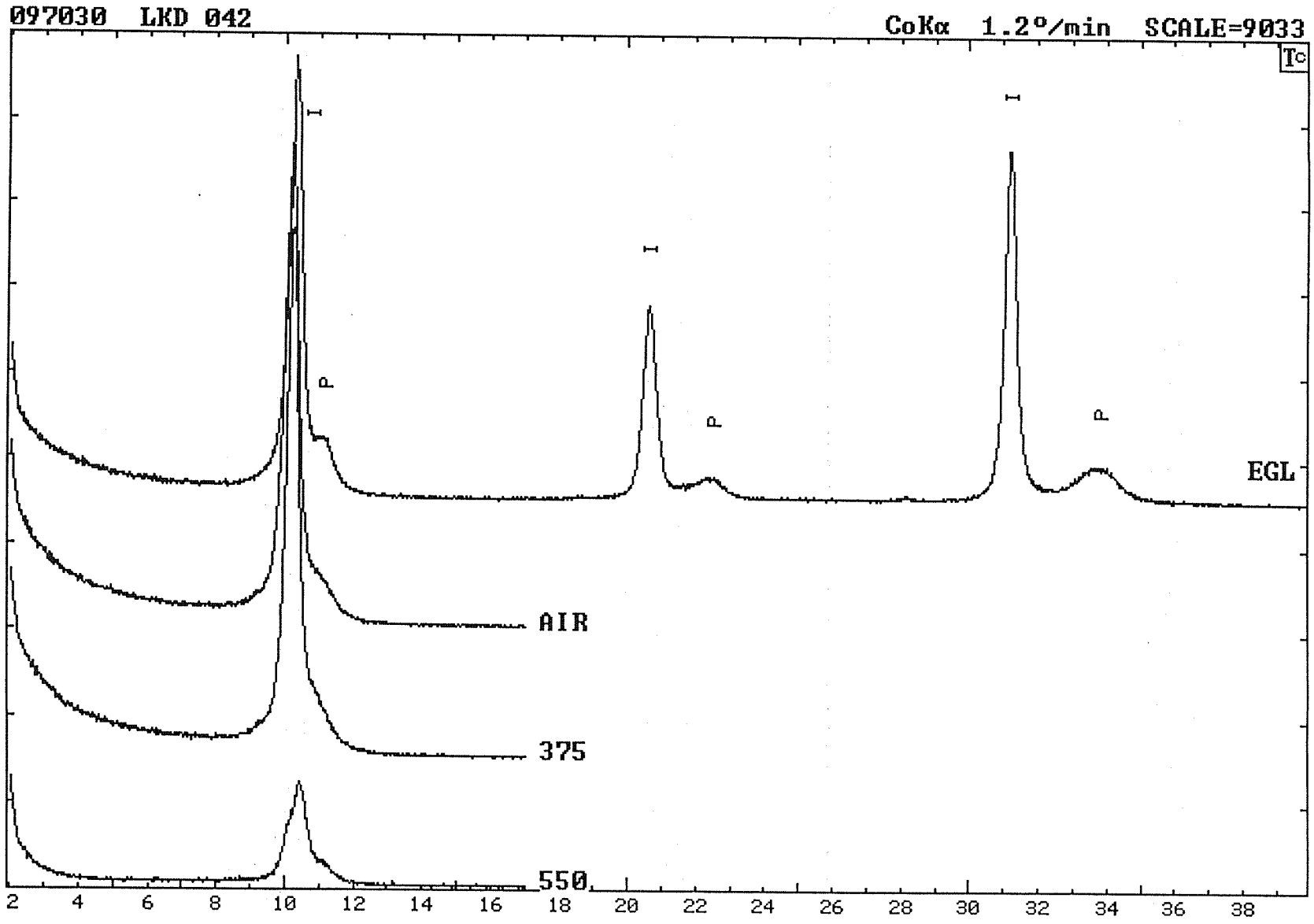

097236 KKD 031
CoKα 1.2°/min SCALE=2320
Tc
Ch/Sm
Chl
Chl
EGL
AIR
375
550
?
Mg Calcite?
2 4 6 8 10 12 14 16 18 20 22 24 26 28 30 32 34 36 38 40

85m

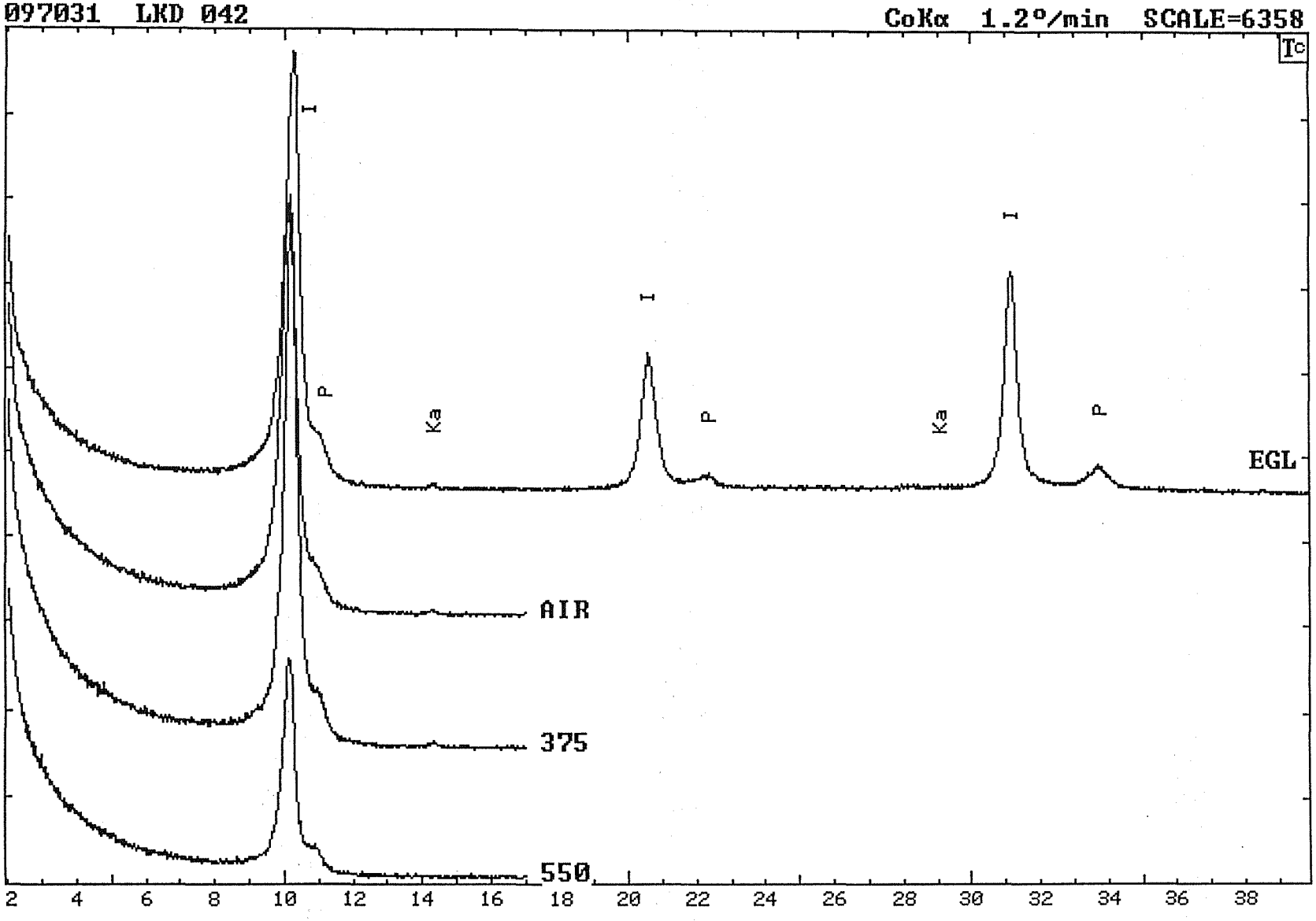

097130 LKD 044
CoKα 1.2°/min SCALE=19517
Tc
I
Ka
I
Ka
I
EGL
AIR
375
550
2 4 6 8 10 12 14 16 18 20 22 24 26 28 30 32 34 36 38 40

68.5m

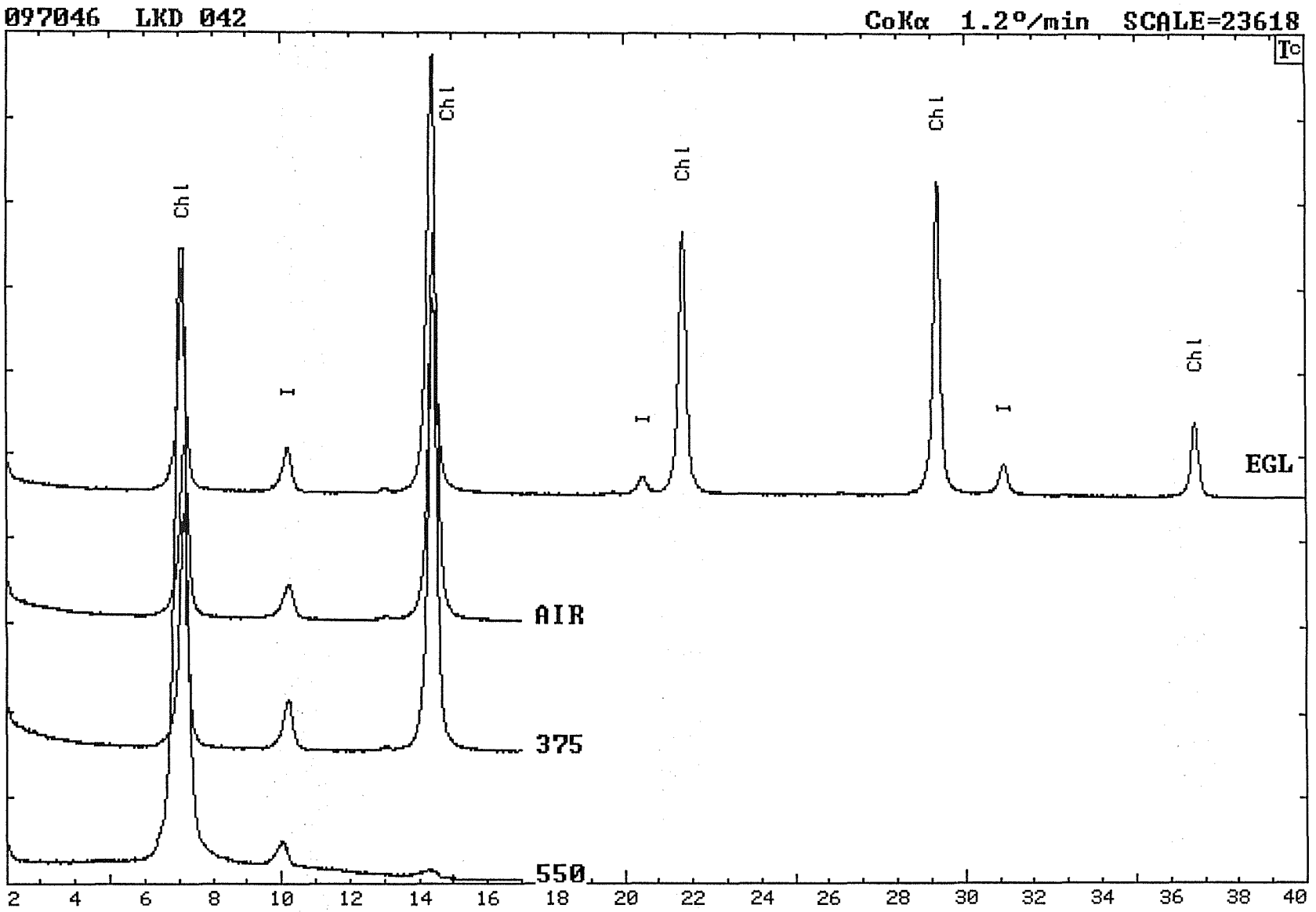

097029 LKD 042
CoKα 1.2°/min SCALE=8500
Tc
I
I
I
Ka
Ka
EGL
AIR
375
550
2 4 6 8 10 12 14 16 18 20 22 24 26 28 30 32 34 36 38


097030 LKD 042
CoKα 1.2°/min SCALE=9033
Tc
I
P
I
P
I
P
EGL
AIR
375
550
2
4
6
8
10
12
14
16
18
20
22
24
26
28
30
32
34
36
38

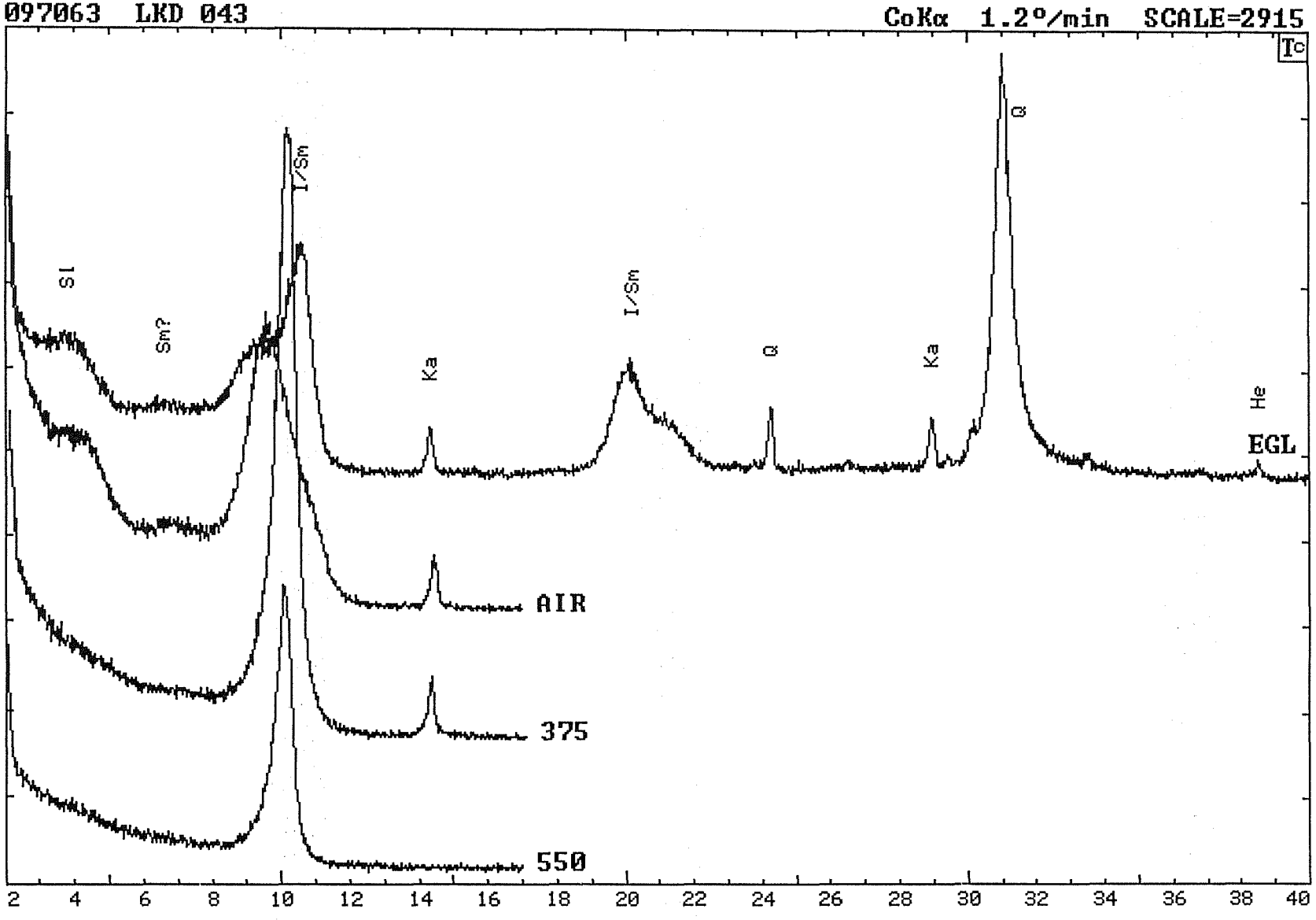
72 m


097031 LKD 042
CoKα 1.2°/min SCALE=6358
Tc
I
P
Ka
I
P
Ka
I
P
EGL
AIR
375
550
2 4 6 8 10 12 14 16 18 20 22 24 26 28 30 32 34 36 38

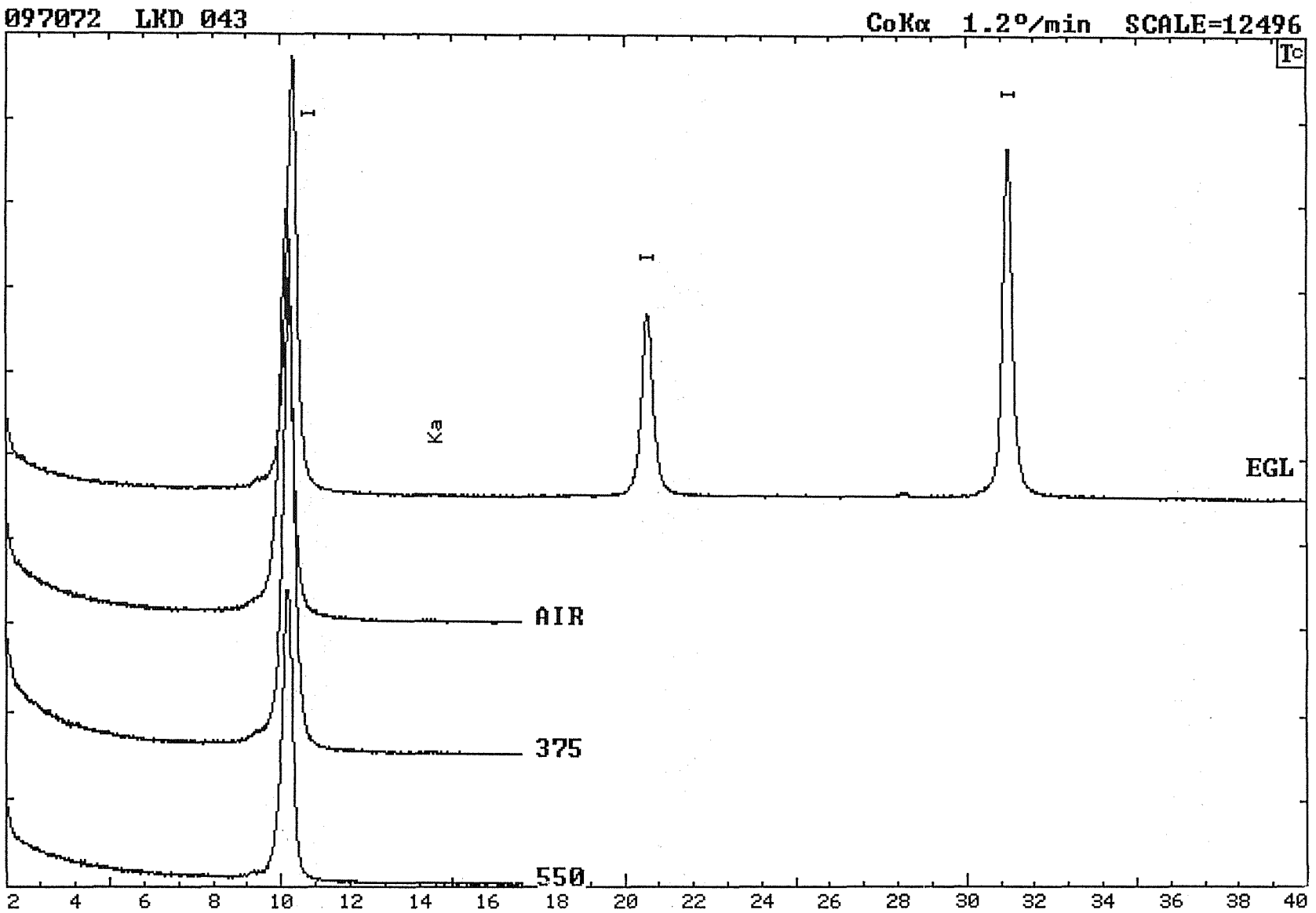
141m


097046 LKD 042
CoKα 1.2°/min SCALE=23618
Tc
Chl
I
Chl
I
Chl
I
Chl
EGL
AIR
375
550
2 4 6 8 10 12 14 16 18 20 22 24 26 28 30 32 34 36 38 40

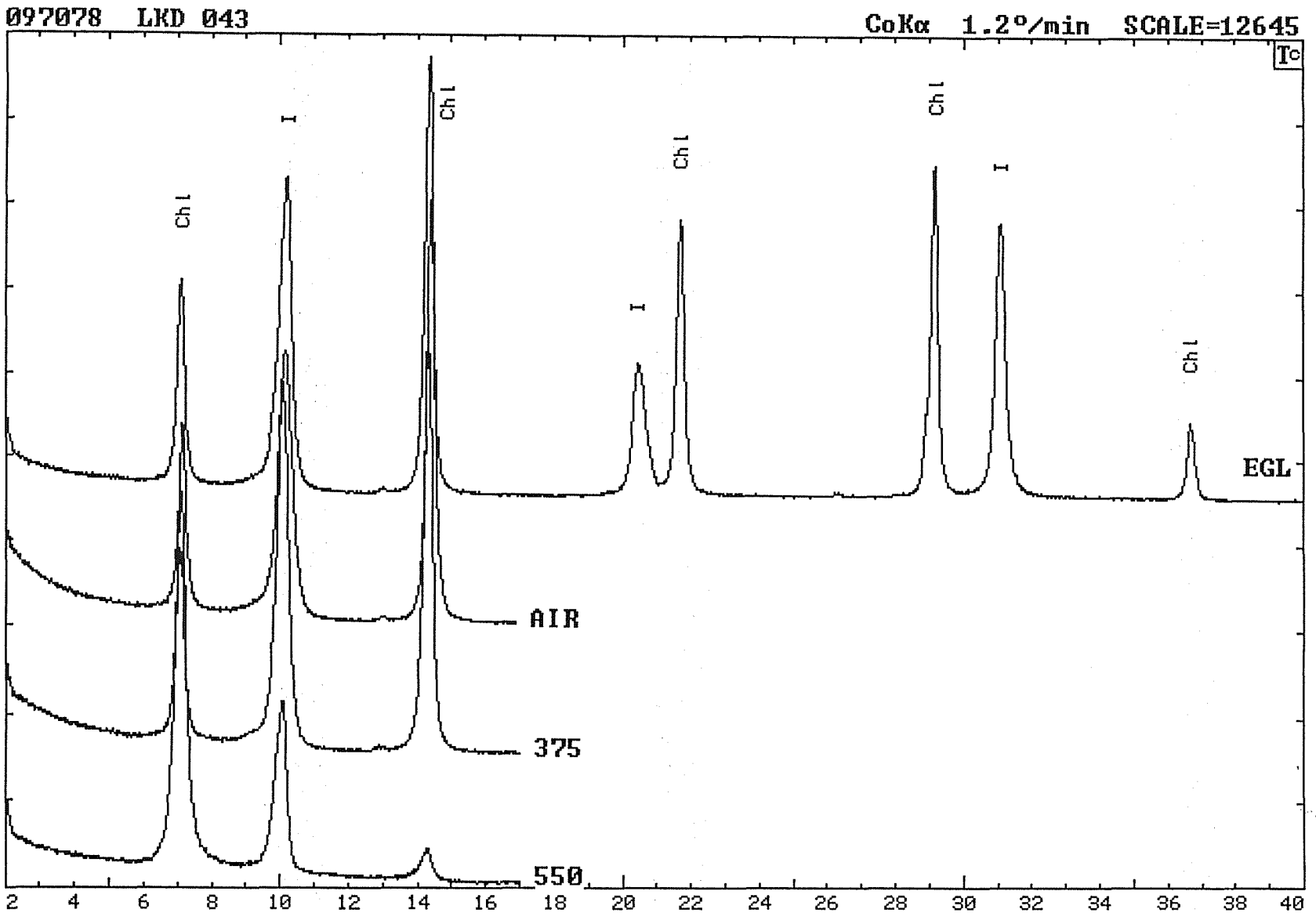
44.9 m


097063 LKD 043
CoKα 1.2°/min SCALE=2915
Tc
Sl
Sm?
I/Sm
Ka
I/Sm
Q
Ka
Q
He
EGL
AIR
375
550
2 4 6 8 10 12 14 16 18 20 22 24 26 28 30 32 34 36 38 40

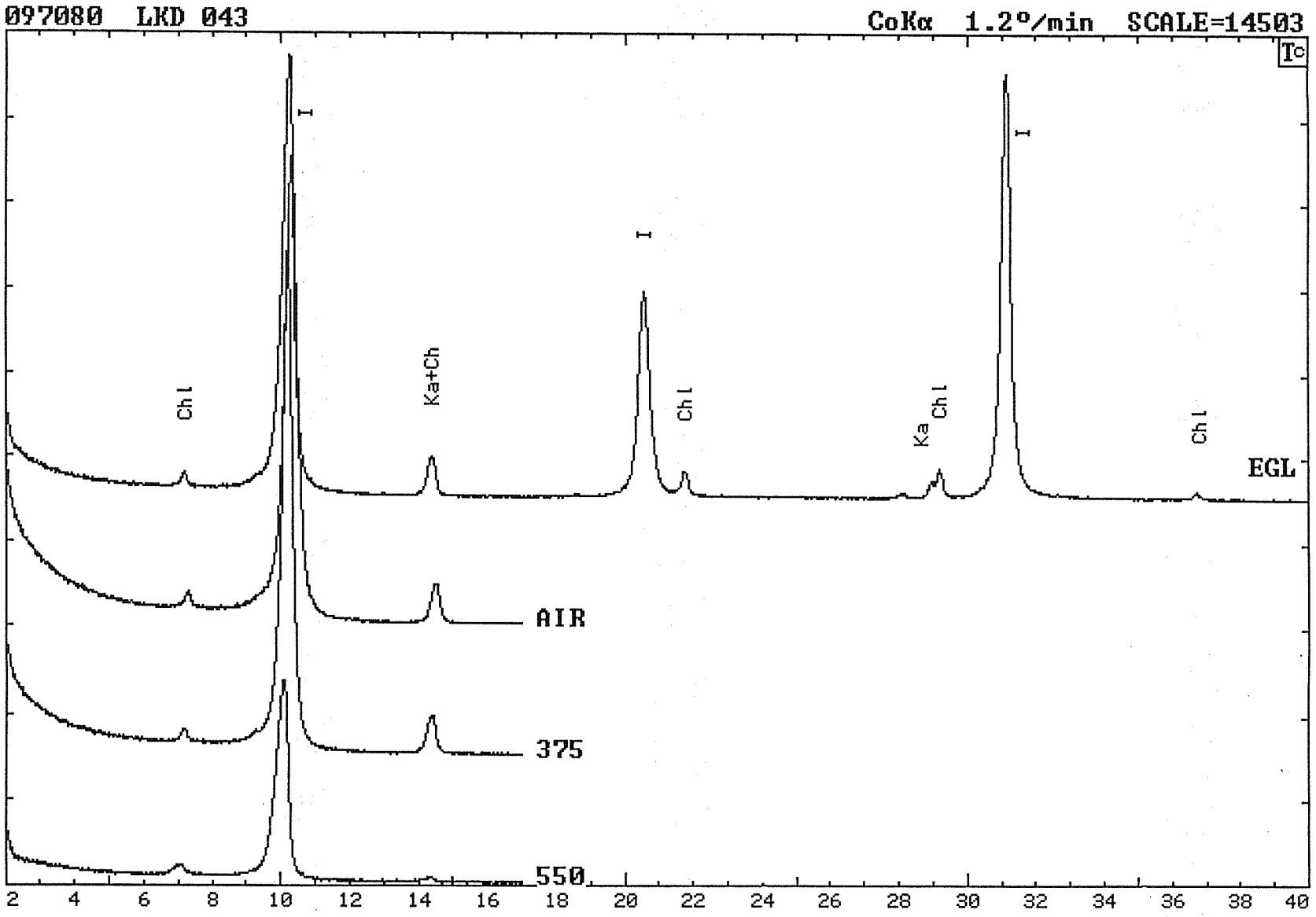
57-4 m

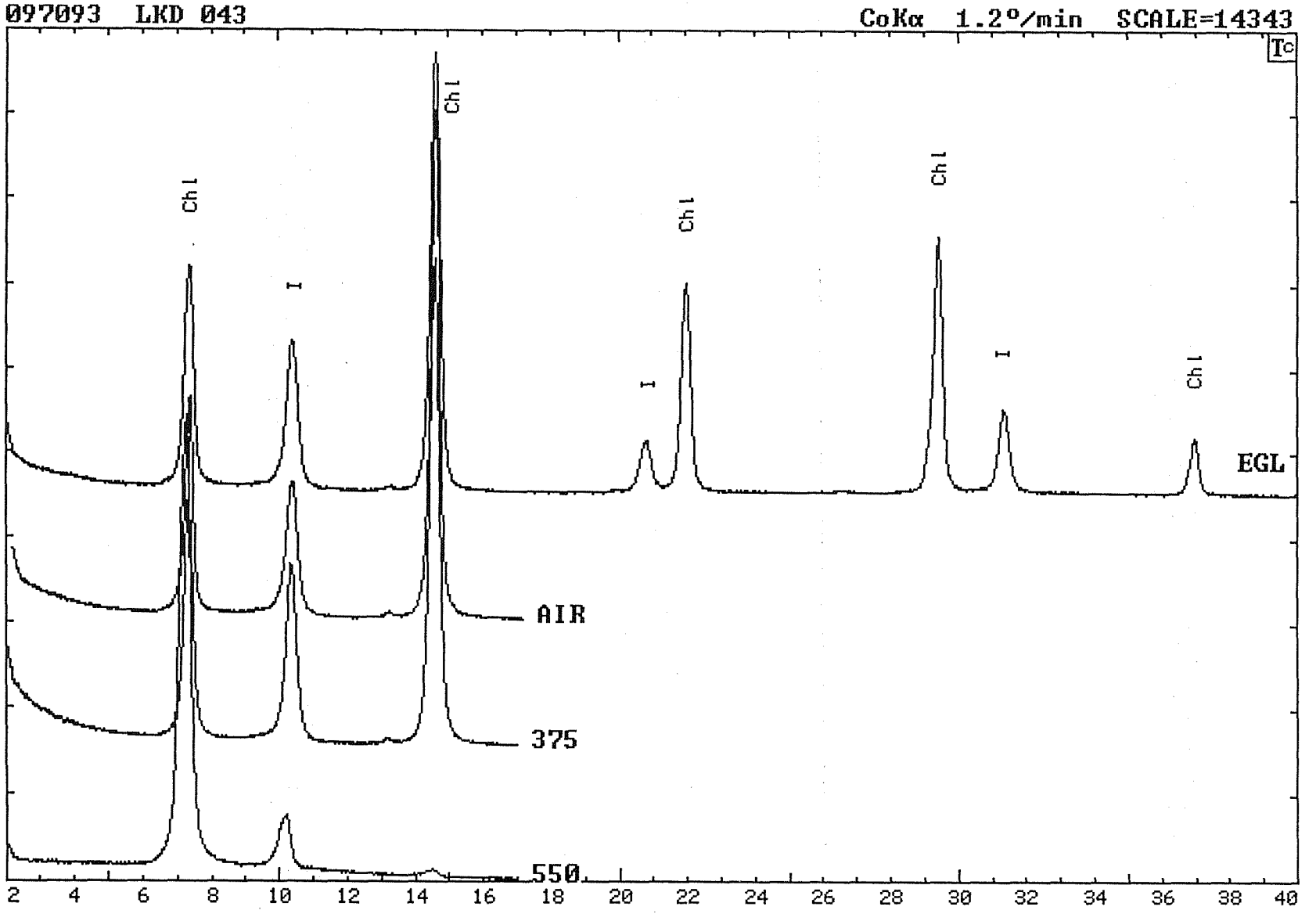

097072 LKD 043
CoKα 1.2°/min SCALE=12496
Tc
I
I
I
Ka
EGL
AIR
375
550
2 4 6 8 10 12 14 16 18 20 22 24 26 28 30 32 34 36 38 40

72.5m

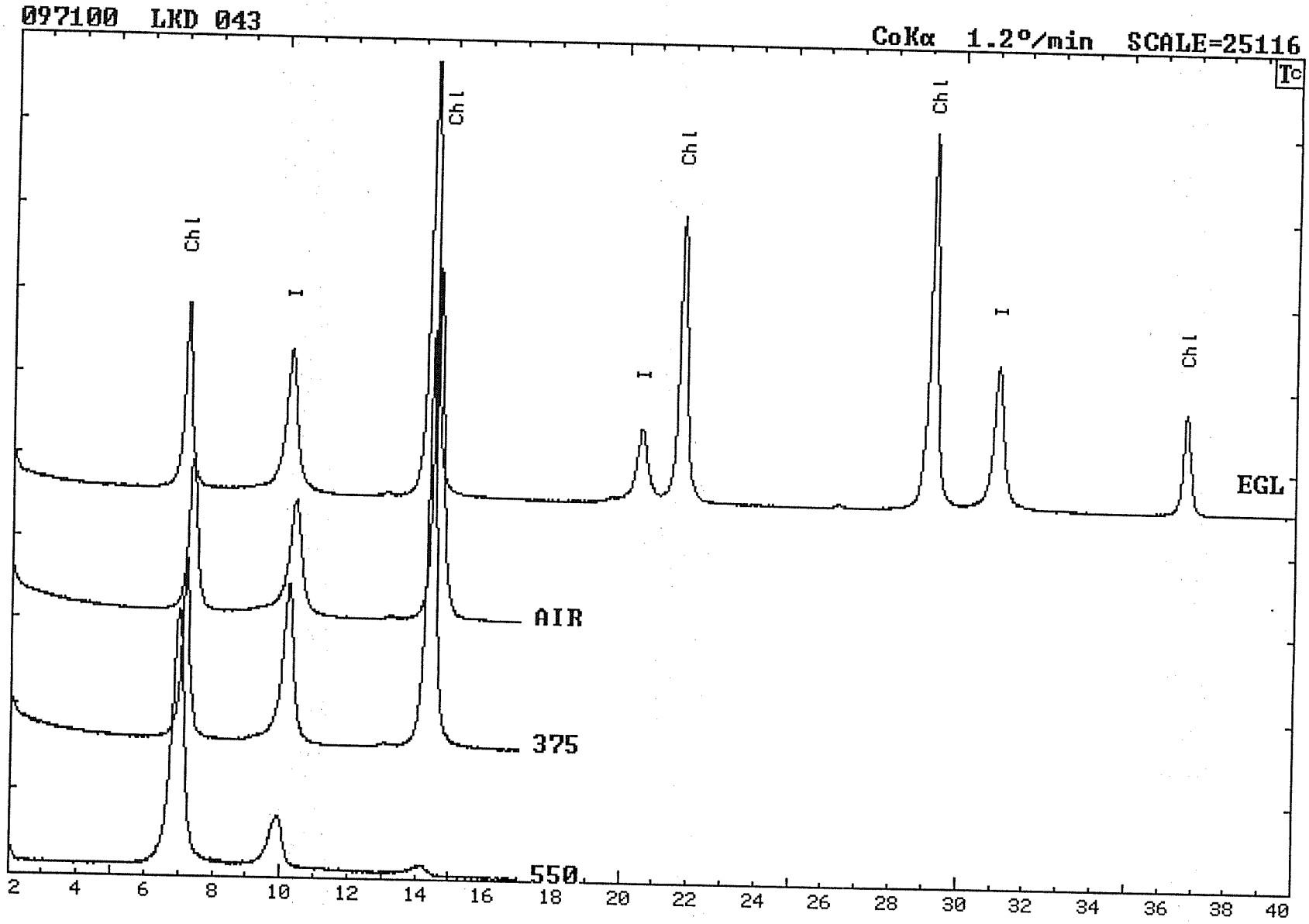

097078 LKD 043
CoKα 1.2°/min SCALE=12645
Tc
Chl
I
Chl
I
Chl
I
Chl
Chl
EGL
AIR
375
550
2 4 6 8 10 12 14 16 18 20 22 24 26 28 30 32 34 36 38 40

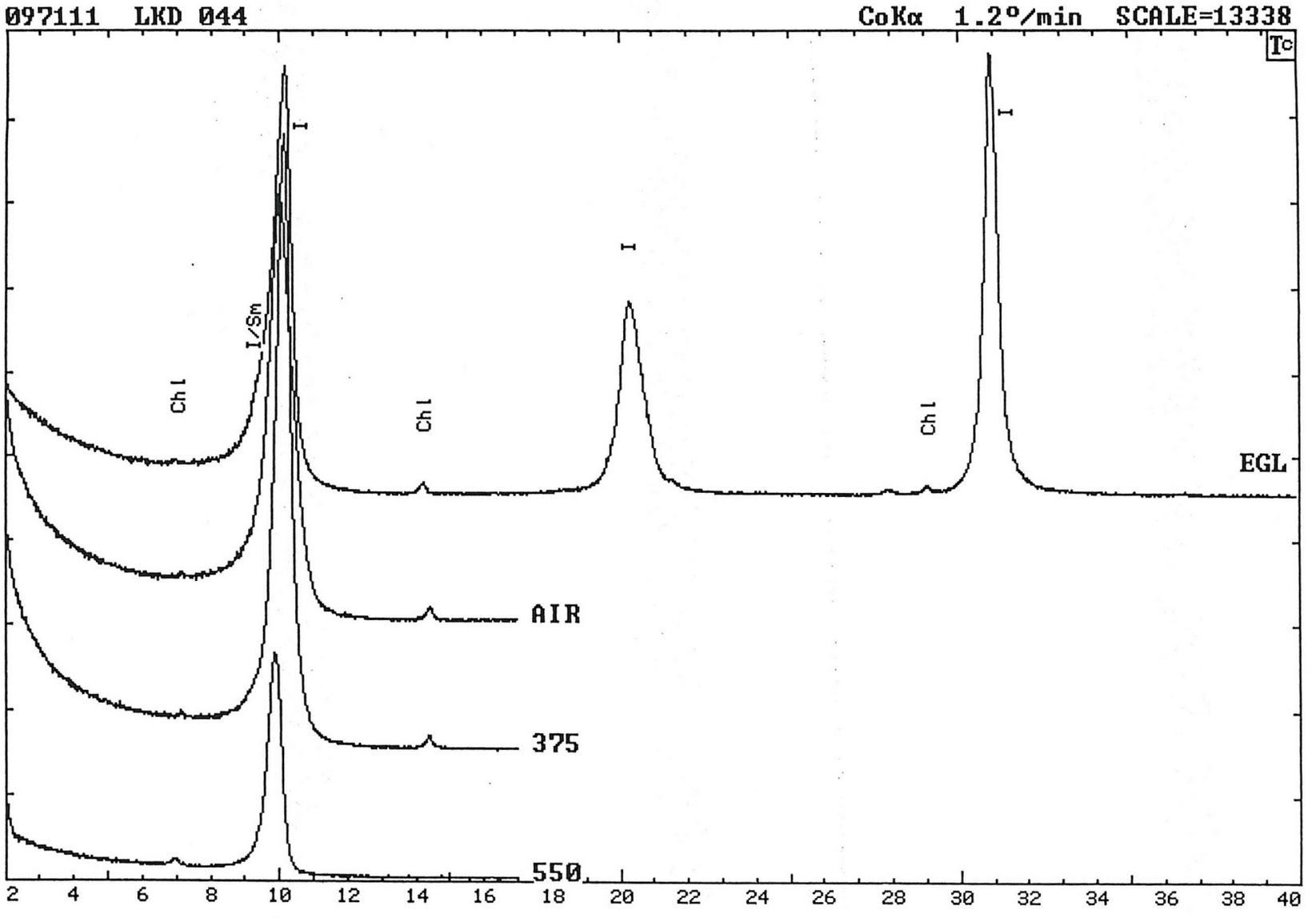
85m

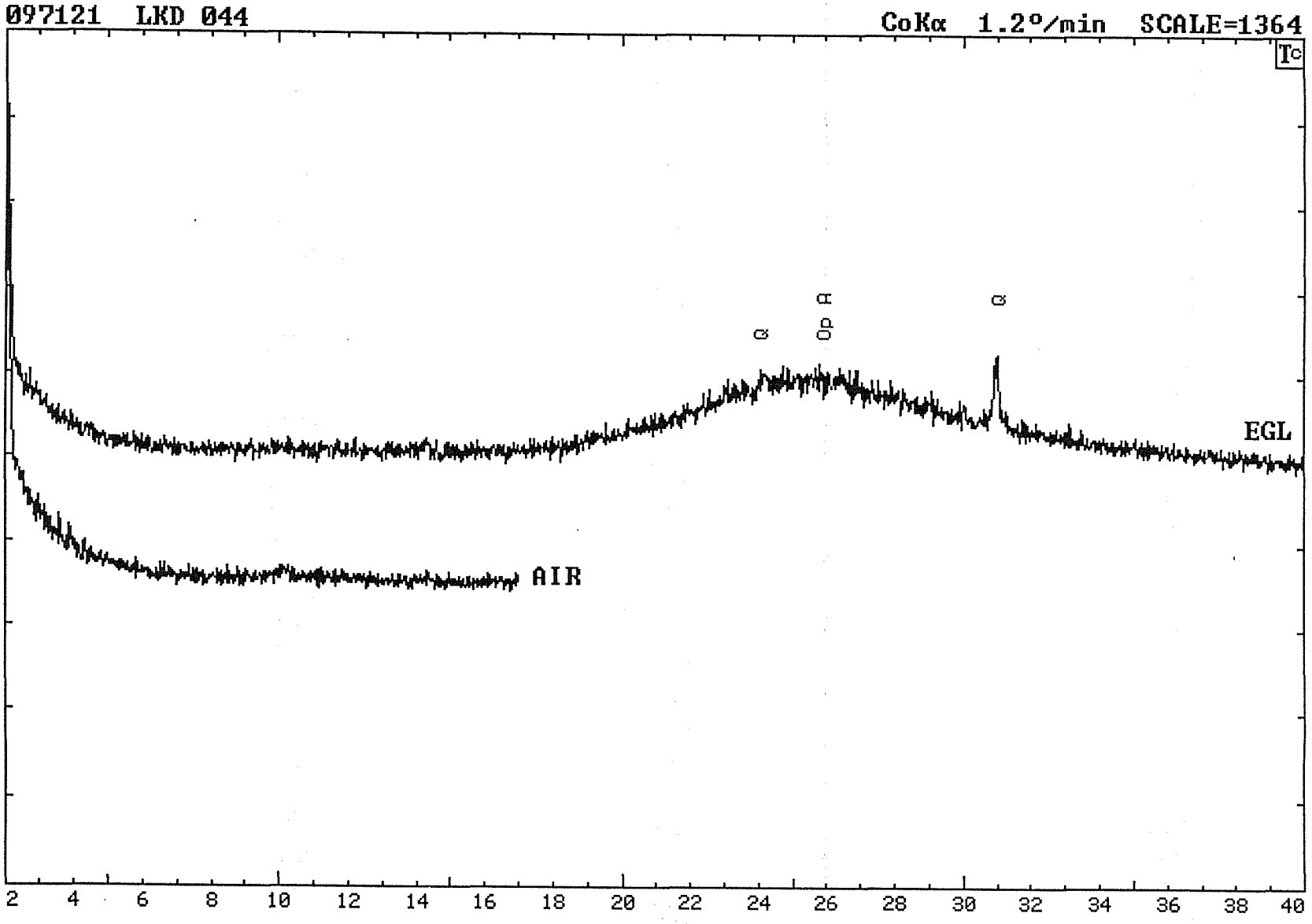

097080 LKD 043
CoKα 1.2°/min SCALE=14503
Tc
I
I
I
Chl
Ka+Ch
Chl
Ka
Chl
Chl
EGL
AIR
375
550
2 4 6 8 10 12 14 16 18 20 22 24 26 28 30 32 34 36 38 40

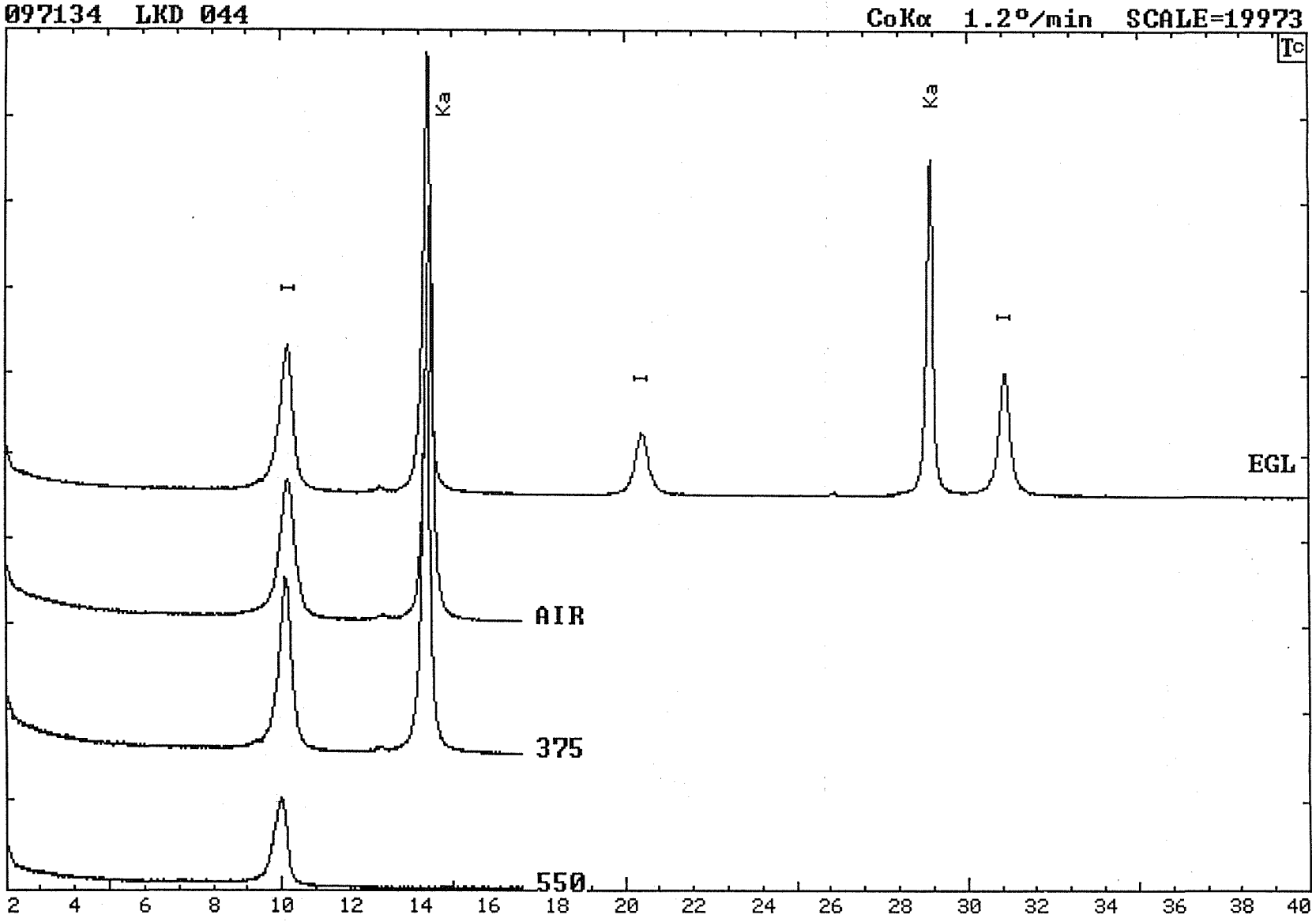

097093 LKD 043
CoKα 1.2°/min SCALE=14343
Tc
Chl
I
Chl
I
Chl
I
Chl
EGL
AIR
375
550
2 4 6 8 10 12 14 16 18 20 22 24 26 28 30 32 34 36 38 40

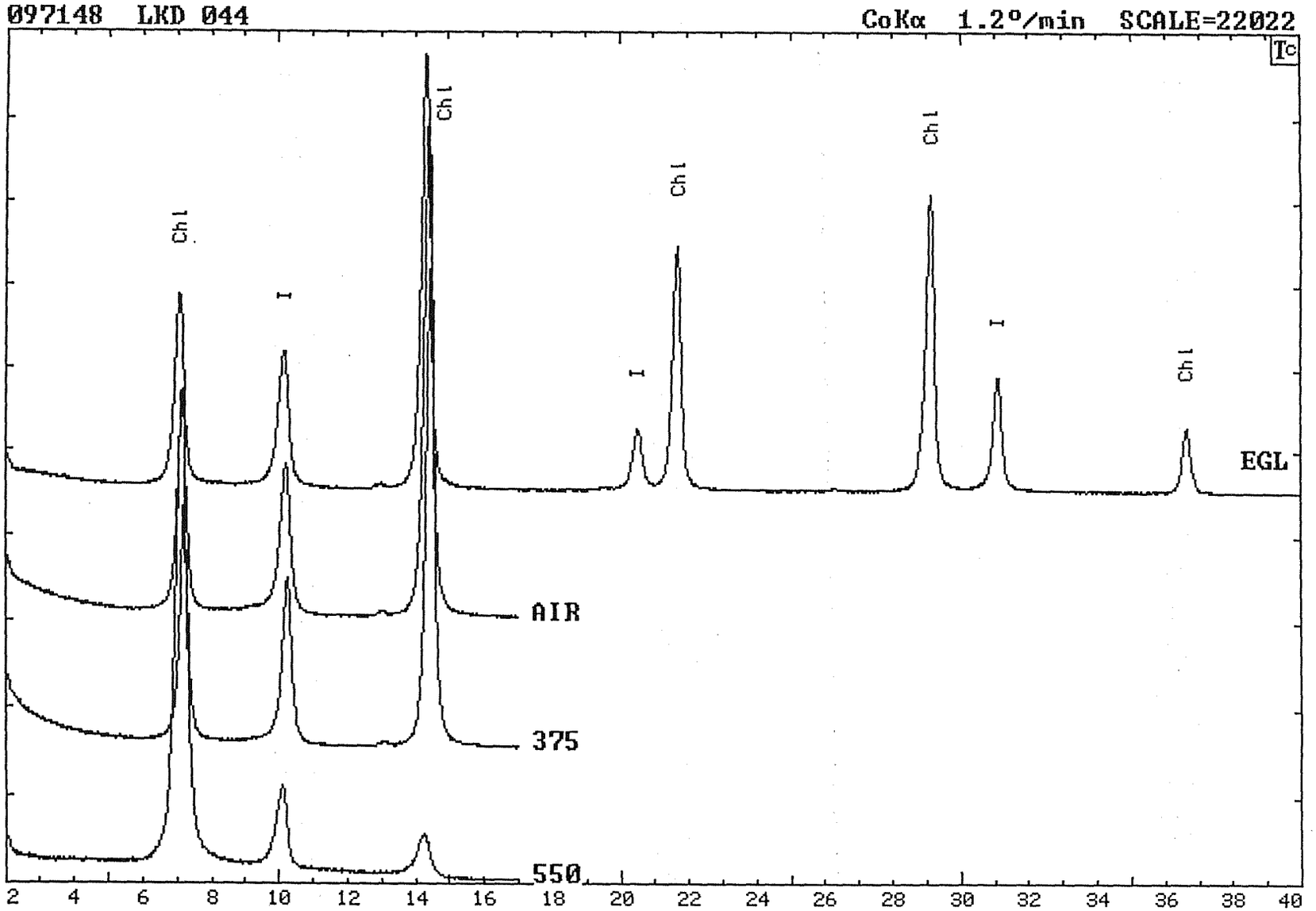
146m


097100 LKD 043
CoKα 1.2°/min SCALE=25116
Tc
Chl
I
Chl
I
Chl
I
Chl
Chl
EGL
AIR
375
550
2 4 6 8 10 12 14 16 18 20 22 24 26 28 30 32 34 36 38 40

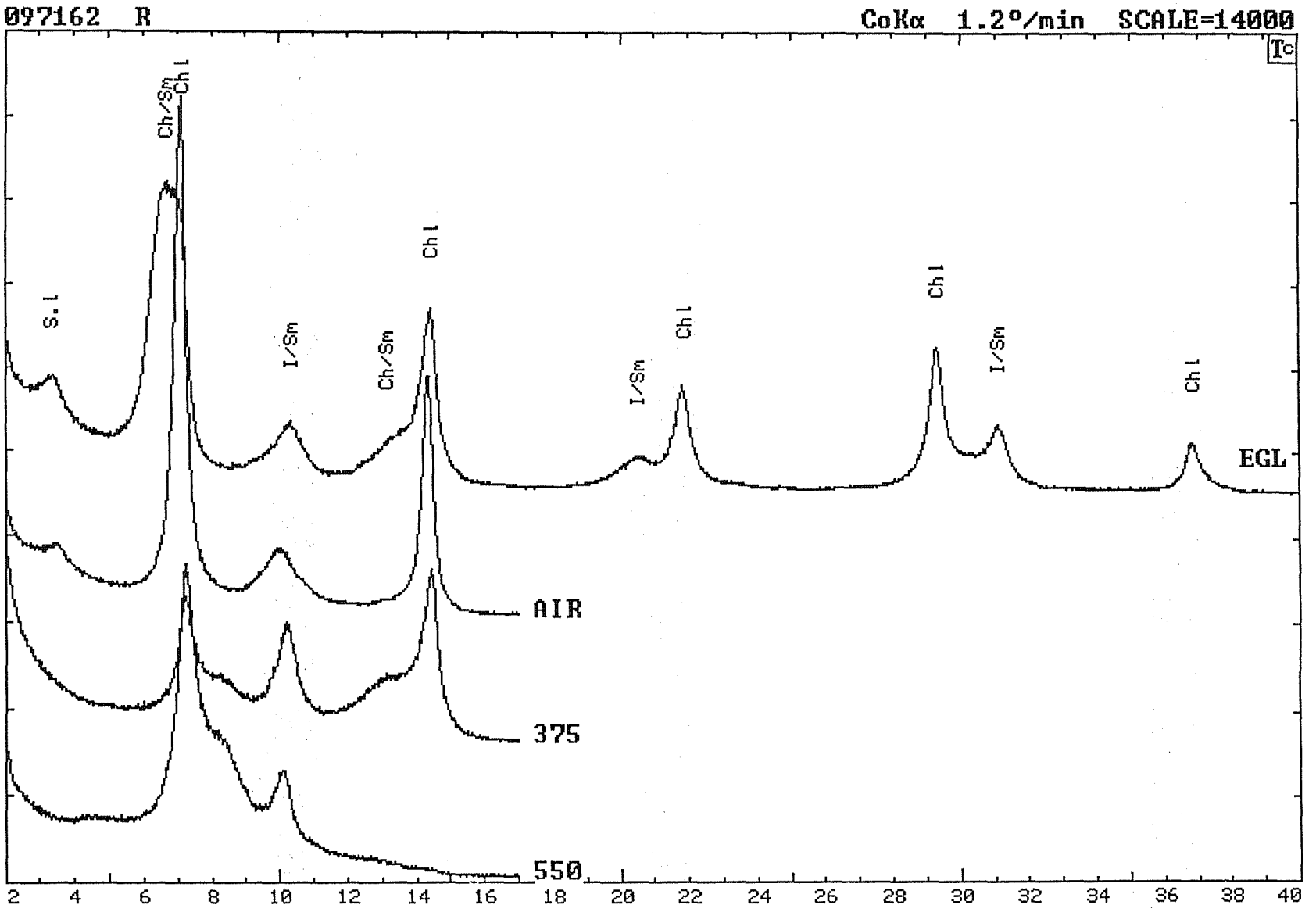

097111 LKD 044
CoKα 1.2°/min SCALE=13338
Tc
Chl
I/Sm
I
Chl
I
Chl
I
EGL
AIR
375
550
2 4 6 8 10 12 14 16 18 20 22 24 26 28 30 32 34 36 38 40

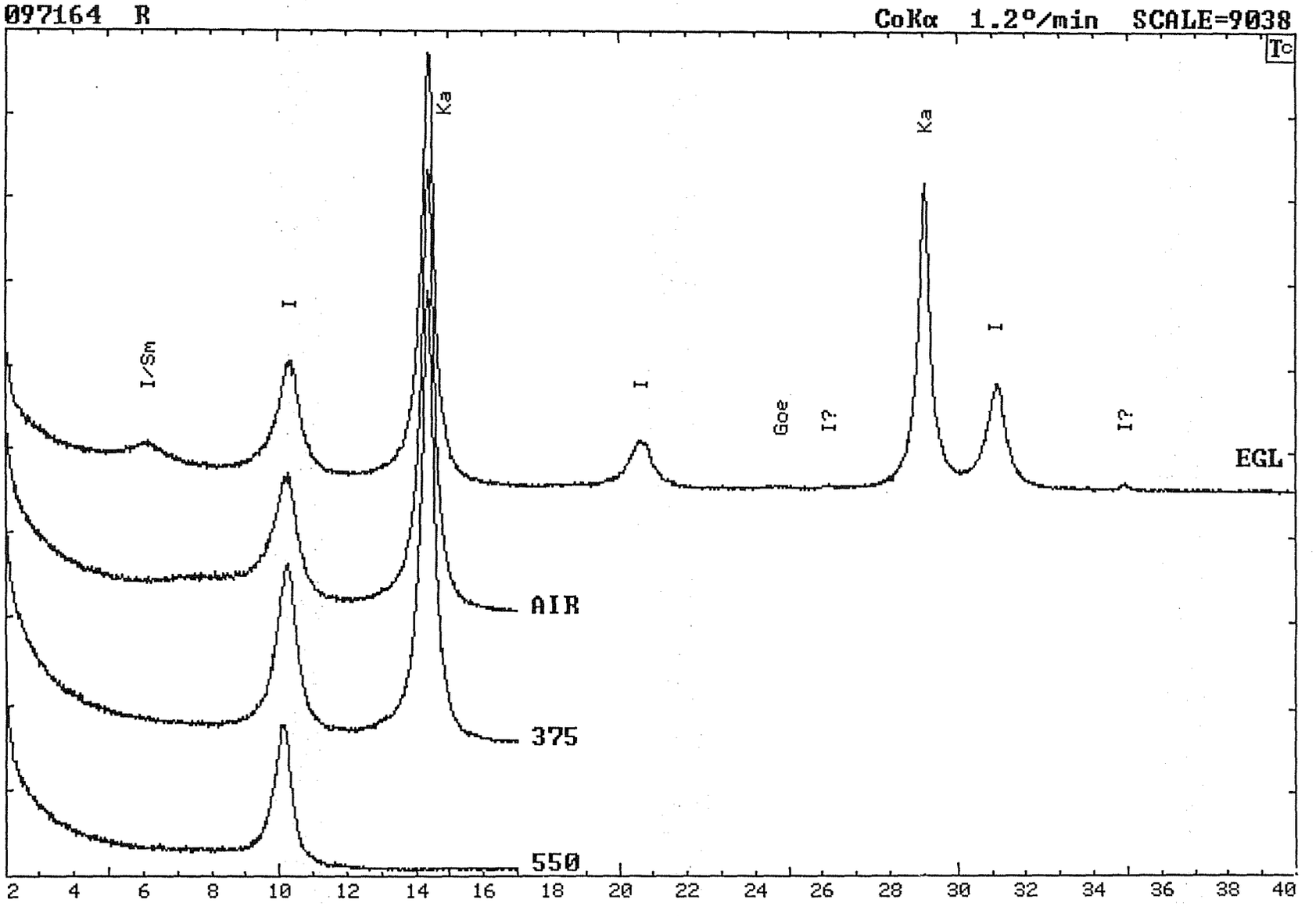

097121 LKD 044
CoKα 1.2°/min SCALE=1364
Tc
α
αp
α
EGL
AIR
2
4
6
8
10
12
14
16
18
20
22
24
26
28
30
32
34
36
38
40


097134 LKD 044
CoKα 1.2°/min SCALE=19973
Tc
Ka
Ka
I
I
I
EGL
AIR
375
550
2 4 6 8 10 12 14 16 18 20 22 24 26 28 30 32 34 36 38 40

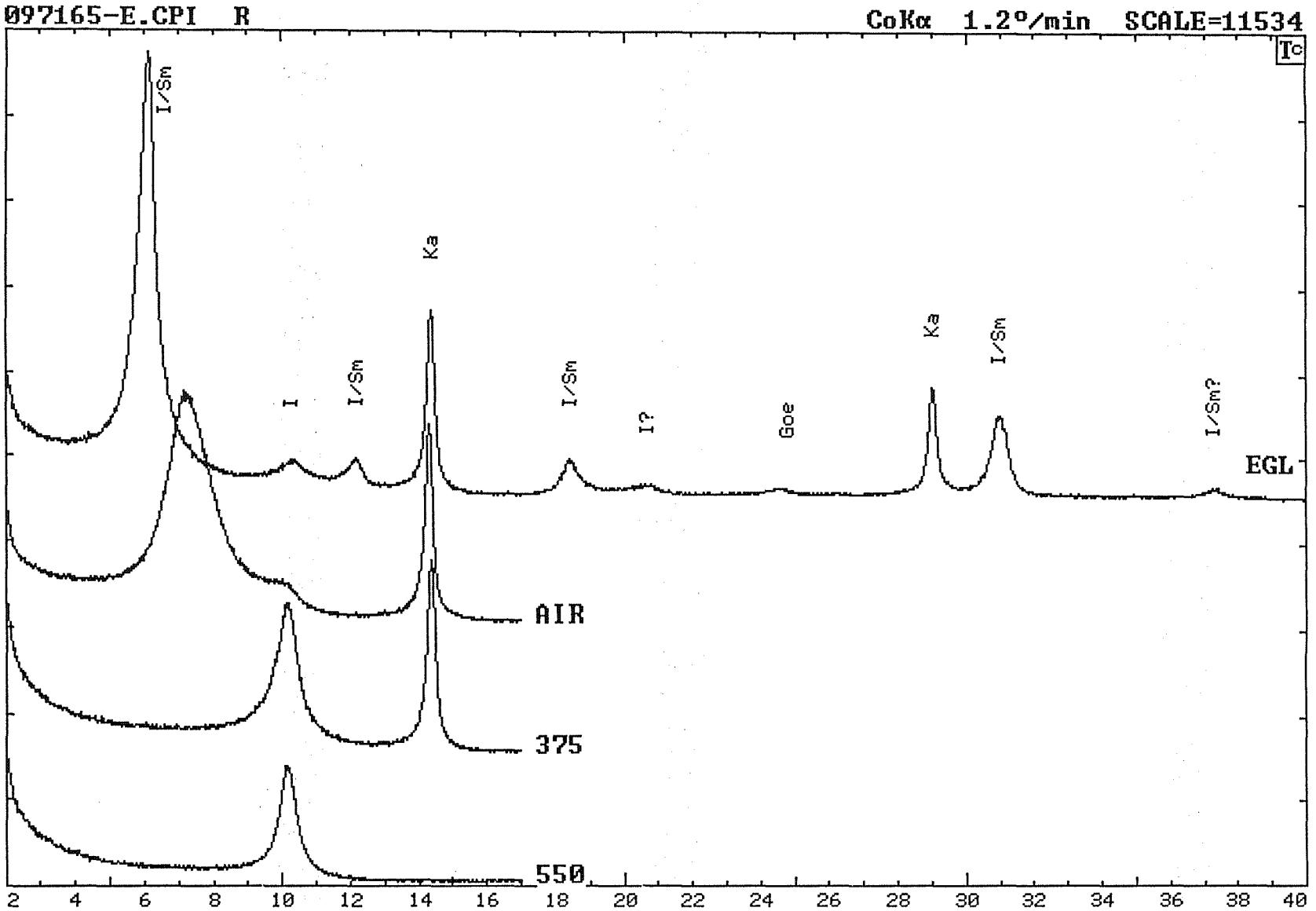

097148 LKD 044
CoKα 1.2°/min SCALE=22022
Tc
Chl
I
Chl
I
Chl
I
Chl
Chl
EGL
AIR
375
550
2 4 6 8 10 12 14 16 18 20 22 24 26 28 30 32 34 36 38 40

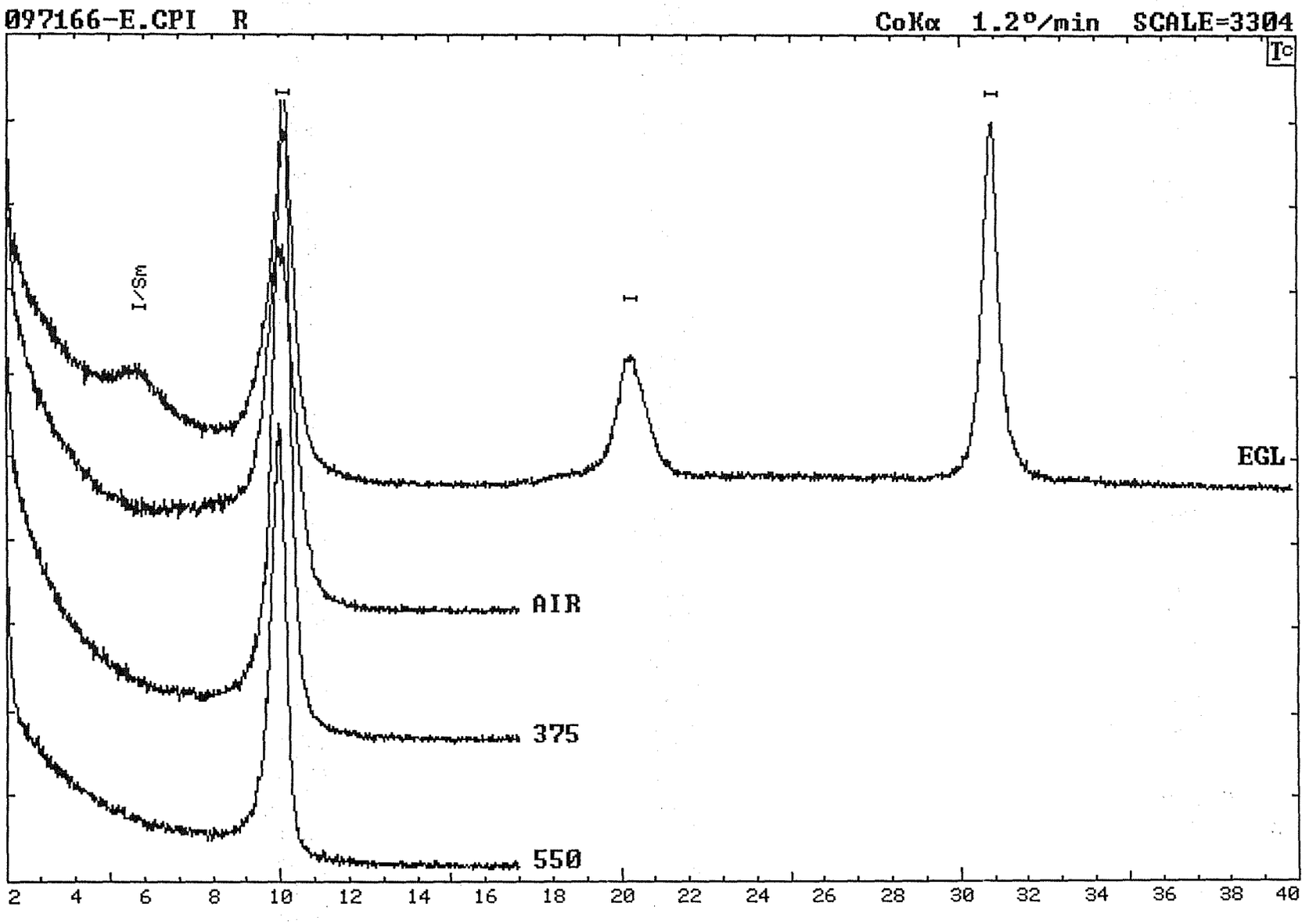
Loc 201

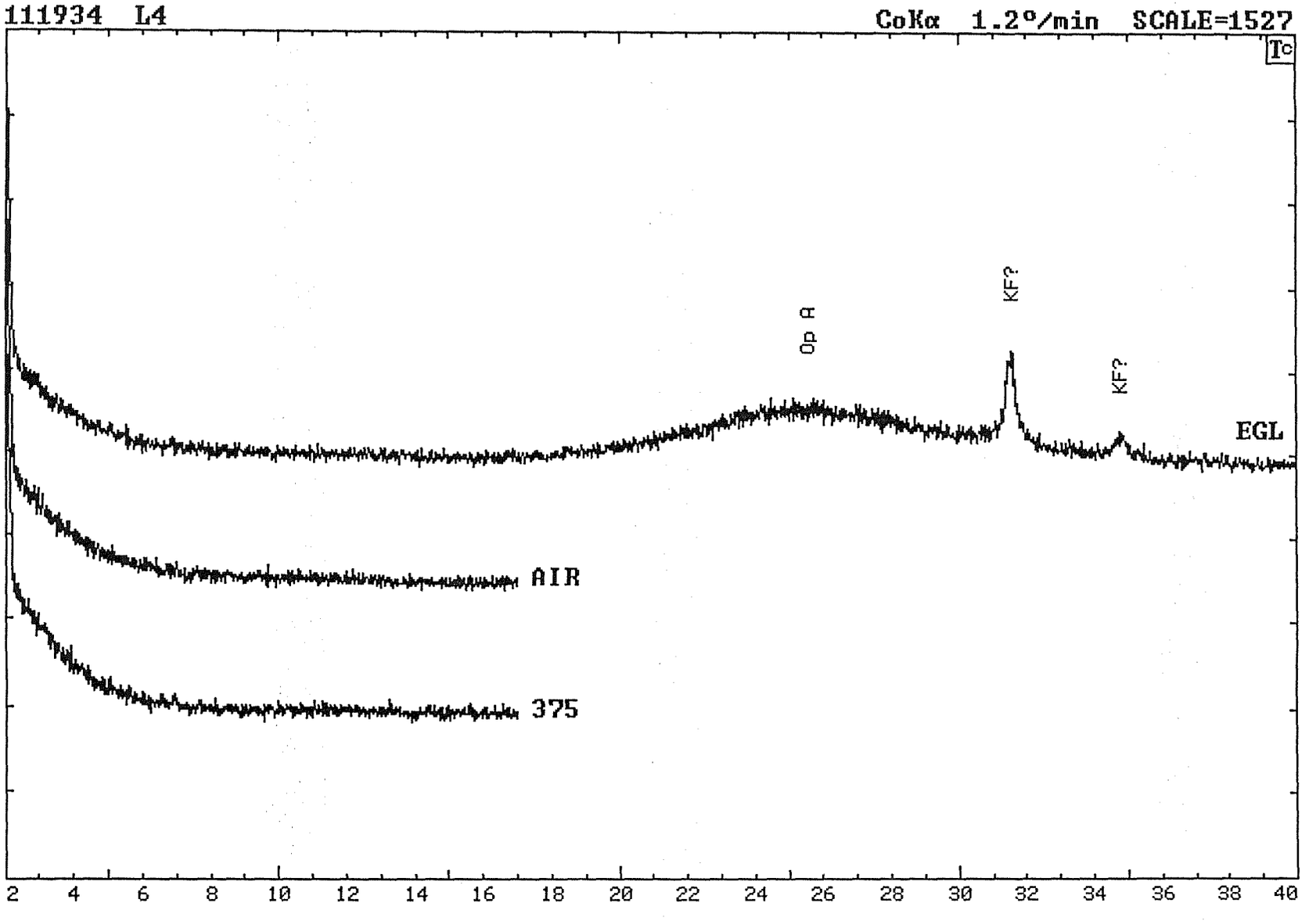

097162 R
CoKα 1.2°/min SCALE=14000
Tc
S.l
Ch/Sm
Chl
I/Sm
Ch/Sm
Chl
I/Sm
Chl
Chl
I/Sm
Chl
EGL
AIR
375
550
2 4 6 8 10 12 14 16 18 20 22 24 26 28 30 32 34 36 38 40

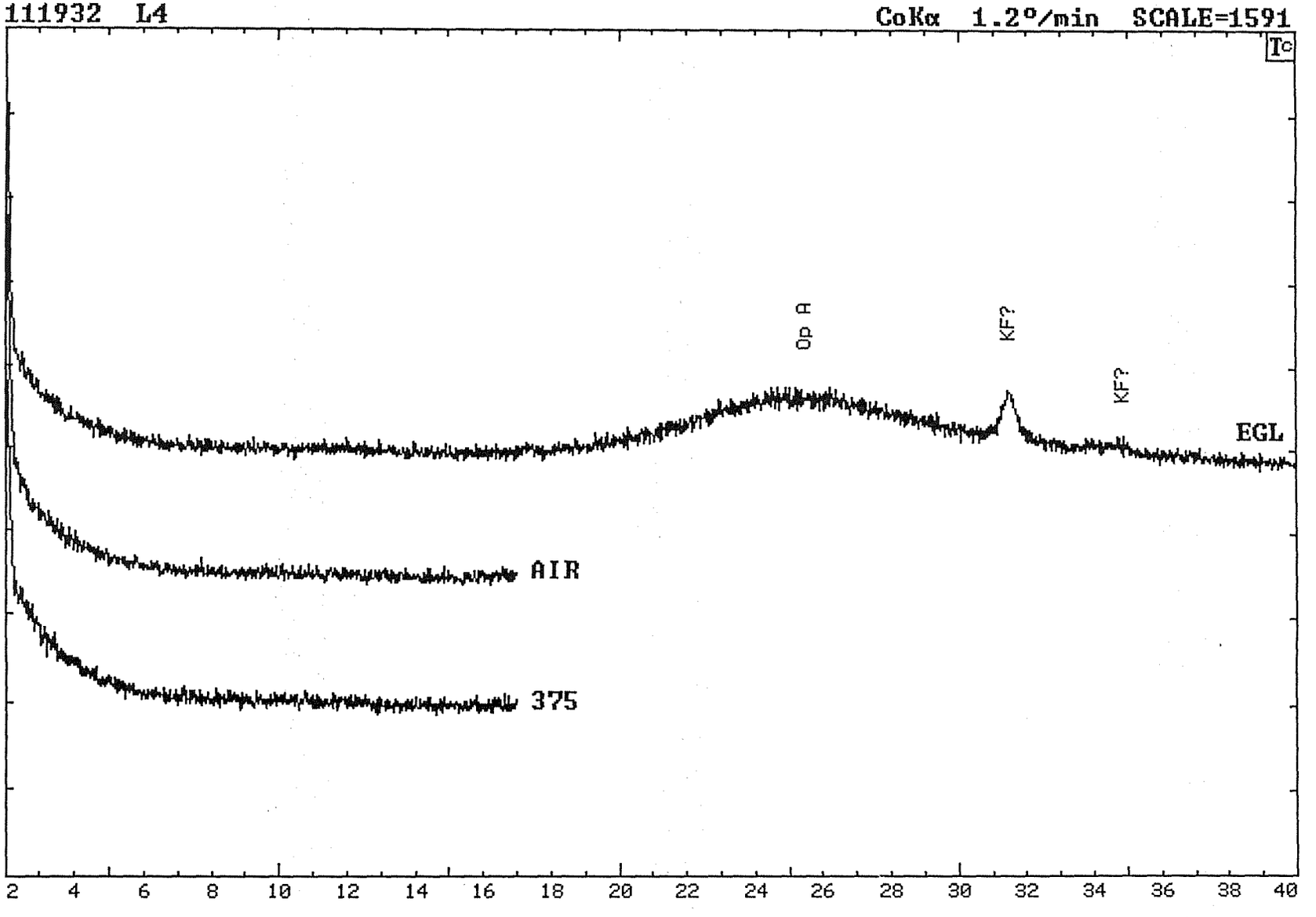

097164 R
CoKα 1.2°/min SCALE=9038
Tc
I/Sm
I
Ka
I
Goe
I?
Ka
I
I?
EGL
AIR
375
550
2 4 6 8 10 12 14 16 18 20 22 24 26 28 30 32 34 36 38 40

Loc 197


097165-E.CPI R
CoKα 1.2°/min SCALE=11534
Tc
I/Sm
I
I/Sm
Ka
I/Sm
I?
Goe
Ka
I/Sm
I/Sm?
EGL
AIR
375
550
2 4 6 8 10 12 14 16 18 20 22 24 26 28 30 32 34 36 38 40


097166-E.CPI R
CoKα 1.2°/min SCALE=3304
Tc
I/Sm
I
I
I
EGL
AIR
375
550
2 4 6 8 10 12 14 16 18 20 22 24 26 28 30 32 34 36 38 40


111934 L4
CoKα 1.2°/min SCALE=1527
Tc
Op a
KF?
KF?
EGL
AIR
375
2 4 6 8 10 12 14 16 18 20 22 24 26 28 30 32 34 36 38 40


111932 L4
CoKα 1.2°/min SCALE=1591
Tc
Op A
KF?
KF?
EGL
AIR
375
2 4 6 8 10 12 14 16 18 20 22 24 26 28 30 32 34 36 38 40

APPENDIX D

				From Unknown	From Calibration (I)								
			Element	Bk (c/s)	Pk (c/s/nA)	Counting time bk (s)	nA (pk)	% of Element in Std.	bk (counts)	Pk (counts)	3 * STD (bk counts)	Det. Limit (wt%)	Det. Limit (ppm)
			Test Values	100	100000	1000	1	100	100000	100100000	948.6832981	0.000947736	9
TAP	4	BAF	F	50	28.9	10	20	21.67	500	27172.81957	67.08203932	0.246871839	2469
PCI	2	AP4	F	50	24.566	10	20	3.4	500	145005.8824	67.08203932	0.046261599	463
TAP	4	JAD	Na	50	67.32	10	20	11.28	500	119861.7021	67.08203932	0.055966199	560
TAP	4	NAN	Na	50	75.649	10	20	14.03	500	108338.9166	67.08203932	0.061918691	619
TAP	4	MGO	Mg	50	885.546	10	20	60.32	500	294116.0477	67.08203932	0.022808017	228
TAP	4	COR	Al	50	1089	10	20	52.92	500	412064.6259	67.08203932	0.016279495	163
TAP	4	WOL	Si	50	510.977	10	20	23.8	500	429892.437	67.08203932	0.015604378	156
TAP	4	ZIR	Si	50	348.827	10	20	15.15	500	460997.6898	67.08203932	0.014551491	146
PET	1	SCP	P	50	77.349	10	20	22.13	500	70404.20244	67.08203932	0.0952813	953
PET	2	SCP	P	50	90.379	10	20	22.13	500	82180.0723	67.08203932	0.081628109	816
PET	1	FES	S	50	206.794	10	20	36.47	500	113904.9904	67.08203932	0.058892977	589
PET	2	FES	S	50	166.303	10	20	36.47	500	91699.89032	67.08203932	0.073153893	732
PET	1	HAL	Cl	50	443.871	10	20	60.65	500	146871.3108	67.08203932	0.045674025	457
PET	2	HAL	Cl	50	278.217	10	20	60.65	500	92245.09481	67.08203932	0.072721525	727
PET	1	KBR	K	50	369.9	10	20	32.86	500	225636.9446	67.08203932	0.029730078	297
PET	2	KBR	K	50	286.611	10	20	32.86	500	174943.7005	67.08203932	0.03834493	383
PET	1	WOL	Ca	50	459.67	10	20	34.17	500	269548.8733	67.08203932	0.024886782	249
PET	2	WOL	Ca	50	338.892	10	20	34.17	500	198856.453	67.08203932	0.033733901	337
PET	1	RUT	Ti	50	1017	10	20	59.95	500	339782.7356	67.08203932	0.019742627	197
PET	2	RUT	Ti	50	687.423	10	20	59.95	500	229832.1101	67.08203932	0.02918741	292
PET	1	STO	Ti	50	440.522	10	20	26.11	500	337935.4653	67.08203932	0.019850547	199
PET	2	STO	Ti	50	295.934	10	20	26.11	500	227182.4971	67.08203932	0.02952782	295
PET	?	PVV	V	50	958.32	10	20	100	500	192164	67.08203932	0.034908744	349
PET	1	PCR	Cr	50	1854	10	20	100	500	371300	67.08203932	0.018066803	181
PET	2	PCR	Cr	50	1089.432	10	20	100	500	218386.4	67.08203932	0.030717132	307
LIF	3	PMN	Mn	50	480	10	20	100	500	96500	67.08203932	0.069515067	695
LIF	3	PFE	Fe	50	524	10	20	100	500	105300	67.08203932	0.06370564	637
LIF	3	PCO	Co	50	550	10	20	100	500	110500	67.08203932	0.060707728	607
LIF	3	PNII	Ni	50	529	10	20	100	500	106300	67.08203932	0.06310634	631
LIF	3	PCU	Cu	50	475	10	20	100	500	95500	67.08203932	0.070242973	702
LIF	3	ZN2	Zn	50	416	10	20	100	500	83700	67.08203932	0.080145806	801
TAP	4	GAA	Ga	50	229	10	20	48.2	500	95520.74689	67.08203932	0.070227717	702
TAP	4	PGE	Ge	50	555	10	20	100	500	111500	67.08203932	0.060163264	602
TAP	4	GAA	As	50	166	10	20	51.8	500	64592.66409	67.08203932	0.10385396	1039
TAP	4	STO	Sr	50	374	10	20	47.74	500	157182.0276	67.08203932	0.042677932	427
PET	1	YYG	Y	50	6.553	10	20	11	500	12414.54545	67.08203932	0.540350346	5404
PET	2	YYG	Y	50	9.243	10	20	11	500	17305.45455	67.08203932	0.387635235	3876
PET	1	ZIR	Zr	50	46.8	10	20	49.1	500	19563.13646	67.08203932	0.342900227	3429
PET	2	ZIR	Zr	50	52.9	10	20	49.1	500	22047.86151	67.08203932	0.304256444	3043
PET	1	PNB	Nb	50	148	10	20	100	500	30100	67.08203932	0.222863918	2229
PET	2	PNB	Nb	50	143.442	10	20	100	500	29188.4	67.08203932	0.229824311	2298
PET	1	NAN	Nb	50	76.252	10	20	56.69	500	27401.39354	67.08203932	0.24481251	2448
PET	2	NAN	Nb	50	73.59	10	20	56.69	500	26462.25084	67.08203932	0.253500882	2535
PET	?	PRH	Rh	50	172.95	10	20	100	500	35090	67.08203932	0.191171386	1912
PET	?	PPD	Pd	50	167.16	10	20	100	500	33932	67.08203932	0.197695507	1977
PET	1	PAG	Ag	50	325	10	20	100	500	65500	67.08203932	0.102415327	1024
PET	2	PAG	Ag	50	165.627	10	20	100	500	33625.4	67.08203932	0.199498115	1995
PET	1	CDS	Cd	50	225	10	20	77.81	500	58333.1834	67.08203932	0.114998077	1150
PET	2	CDS	Cd	50	108.93	10	20	77.81	500	28498.97185	67.08203932	0.235384068	2354
PET	1	INP	In	50	315	10	20	78.75	500	80500	67.08203932	0.083331726	833

1000ppm = 0.1wt%

PET	2	INP	In	50	252.421	10	20	78.75	500	64606.92063	67.08203932	0.103831043	1038
PET	1	PSB	Sb	50	512	10	20	100	500	102900	67.08203932	0.065191486	652
PET	2	PSB	Sb	50	387.828	10	20	100	500	78065.6	67.08203932	0.085930345	859
PET	1	BAF	Ba	50	498	10	20	78.33	500	127654.347	67.08203932	0.052549749	525
PET	2	BAF	Ba	50	340.885	10	20	78.33	500	87538.17184	67.08203932	0.076631757	766
PET	1	LAG	La	50	75.8	10	20	14.15	500	107637.8092	67.08203932	0.062322004	623
PET	2	LAG	La	50	49.972	10	20	14.15	500	71131.80212	67.08203932	0.094306678	943
PET	1	CEG	Ce	50	93.9	10	20	16.83	500	112086.4528	67.08203932	0.059848481	598
PET	2	CEG	Ce	50	60.589	10	20	16.83	500	72501.18835	67.08203932	0.092525434	925
LIF	3	NDG	Nd	50	15.4	10	20	18.88	500	16813.55932	67.08203932	0.398975839	3990
LIF	3	SMG	Sm	50	22.8	10	20	17.42	500	26676.80827	67.08203932	0.251462014	2515
LIF	3	PHF	Hf	50	225.23	10	20	100	500	45546	67.08203932	0.147284151	1473
LIF	3	PTA	Ta	50	224.9	10	20	100	500	45480	67.08203932	0.147497888	1475
LIF	3	PWW	W	50	217.469	10	20	100	500	43993.8	67.08203932	0.152480666	1525
PET	1	TLB	Tl	50	56.8	10	20	71.89	500	16301.9196	67.08203932	0.411497793	4115
PET	2	TLB	Tl	50	50.224	10	20	71.89	500	14472.45792	67.08203932	0.46351518	4635
PET	1	GAL	Pb	50	101.23	10	20	86.3	500	23960.02317	67.08203932	0.279974852	2800
PET	2	GAL	Pb	50	81.549	10	20	86.3	500	19398.95713	67.08203932	0.345802297	3458
PET	1	PTH	Th	50	213.5	10	20	100	500	43200	67.08203932	0.155282498	1553
PET	2	PTH	Th	50	107.721	10	20	100	500	22044.2	67.08203932	0.30430698	3043
PET	1	UUO	U	50	173.407	10	20	88.15	500	39843.61883	67.08203932	0.16836332	1684
PET	2	UUO	U	50	139.456	10	20	88.15	500	32140.61259	67.08203932	0.208714253	2087

Table 1.

Cameca Quantitative Analysis
Label : Wetar sulphides
Wed Jun 10 14:22:55 1998
Normal Analysis

Weight Percents %

	Ag	Cd	S	Fe	Cu	Zn	As	Se	Sb	Pb	Total
#1	0	0.494	31.902	0.048	0.311	64.155	0.094	0.122	0.031	0	97.157
#2	0.042	0.401	31.429	0.018	0.241	64.785	0.031	0	0.038	0	96.985
#3	0.126	0.53	31.573	0.018	0.577	63.751	0.106	0	0.075	0	96.756
#4	0.024	0.742	31.422	0.051	0.616	63.721	0.124	0.014	0.115	0	96.829
#5	0	0.438	31.587	0.028	0.314	64.72	0.026	0	0.053	0	97.166
#6	0	0.478	31.425	0	0.281	63.798	0.054	0.068	0.026	0	96.13
#7	0	0.555	31.328	0.05	1.044	62.298	0.188	0.057	0.145	0	95.665
#8	0.096	0.547	32.049	0.078	1.428	62.53	0.055	0.018	0	0	96.801
#9	0	0	24.065	0.004	60.369	0.911	0.003	0.04	0.025	0	85.417
#10	0.082	0	29.257	0.014	62.577	1.196	0.074	0.078	0.006	0	93.284
#11	0.054	0.499	31.482	0.05	3.841	60.614	0.222	0.028	0.052	0	96.842
#12	0.018	0.734	31.399	0.037	0.504	64.459	0.077	0	0.027	0	97.255
#13	0	0.734	31.654	0	0.371	64.349	0.011	0	0.05	0	97.169
#14	0	0.904	31.524	0.007	0.523	62.786	0.015	0.02	0	0	95.779
#15	0	0.787	31.713	0.037	0.929	64.37	0.008	0.003	0	0	97.847
#16	0.154	0.458	26.77	0.029	5.471	58.675	0.08	0	0.08	0	91.717
#17	0	0.657	31.512	0.015	3.171	61.507	0.069	0.015	0.027	0	96.973
#18	0.059	0.091	28.41	0.005	57.33	9.771	0.052	0.058	0.057	0	95.833
#19	0	0.04	29.922	0.018	56.405	0.17	0.366	0	0.129	0	87.05
#20	0.227	0	26.584	0.005	64.714	0.412	0.357	0	0.606	0	92.905
#21	0.165	0.009	30.808	0.039	63.048	0.208	0.067	0.029	0.293	0	94.666
#22	0.11	0	21.633	0.084	50.051	0.635	3.518	0	2.526	0	78.557
#23	0	0	28.811	0.004	63.347	0.948	0.081	0	0.102	0	93.293
#24	0	0.03	25.213	0.004	60.055	2.007	0.073	0	0.404	0	87.786
#25	0.114	0.206	31.398	0.011	7.559	58.031	0.058	0.032	0.02	0	97.429
#26	0.096	0.176	31.709	0	0.771	64.019	0	0	0.02	0	96.791
#27	0.138	0.272	31.311	0.063	0.481	64.281	0	0.009	0.038	0	96.593
#28	0	0.209	27.485	0.057	0.249	62.091	0	0	0	0	90.091
#29	0.036	0.232	31.514	0.001	0.13	64.715	0	0.042	0	0	96.67
#30	0.048	0.312	31.341	0.015	0.293	64.317	0.054	0.06	0	0	96.44

#31	0.018	0.207	31.513	0.043	0.396	64.381	0.033	0	0.067	0	96.658
#32	0.024	0.201	31.547	0	0.338	64.905	0	0.031	0.023	0	97.069
#33	0.114	0.33	31.254	0	0.771	64.2	0.062	0.052	0	0	96.783
#34	0	0.113	28.712	0.007	48.204	14.568	0.045	0.018	0.213	0	91.88
#35	0.018	0	28.458	0.02	63.195	0.999	0.075	0.044	0.197	0	93.006
#36	0	0.154	30.042	0.06	9.16	55.825	0.049	0.023	0.036	0	95.349
#37	0.03	0.09	31.309	0	1.781	63.308	0.012	0.028	0	0	96.558
#38	0.06	0.142	31.289	0	0.934	64.186	0.041	0.046	0.019	0	96.717
#39	0	0.253	31.756	0.003	0.605	64.522	0	0	0	0	97.139
#40	0	0.235	31.5	0	0.296	64.682	0.041	0.048	0.006	0	96.808

Atomic %

	Ag	Cd	S	Fe	Cu	Zn	As	Se	Sb	Pb	Total
#1	0	0.221	50.008	0.043	0.246	49.328	0.063	0.078	0.013	0	100
#2	0.02	0.18	49.504	0.016	0.192	50.052	0.021	0	0.016	0	100.001
#3	0.059	0.239	49.801	0.016	0.459	49.323	0.071	0	0.031	0	99.999
#4	0.011	0.334	49.62	0.046	0.491	49.356	0.084	0.009	0.048	0	99.999
#5	0	0.196	49.621	0.025	0.249	49.869	0.018	0	0.022	0	100
#6	0	0.216	49.839	0	0.225	49.629	0.037	0.043	0.011	0	100
#7	0	0.253	49.933	0.046	0.839	48.704	0.128	0.037	0.061	0	100.001
#8	0.045	0.245	50.312	0.071	1.131	48.149	0.037	0.012	0	0	100.002
#9	0	0	43.753	0.004	55.387	0.812	0.002	0.03	0.012	0	100
#10	0.04	0	47.558	0.013	51.33	0.953	0.052	0.051	0.003	0	100
#11	0.025	0.225	49.611	0.045	3.054	46.851	0.15	0.018	0.022	0	100.001
#12	0.008	0.329	49.411	0.034	0.401	49.754	0.052	0	0.011	0	100
#13	0	0.329	49.745	0	0.295	49.603	0.007	0	0.021	0	100
#14	0	0.41	50.149	0.006	0.42	48.992	0.01	0.013	0	0	100
#15	0	0.351	49.547	0.033	0.732	49.329	0.006	0.002	0	0	100
#16	0.078	0.223	45.714	0.028	4.714	49.147	0.058	0	0.036	0	99.998
#17	0	0.295	49.609	0.014	2.519	47.496	0.046	0.01	0.011	0	100
#18	0.028	0.042	45.646	0.004	46.481	7.701	0.036	0.038	0.024	0	100
#19	0	0.019	50.992	0.017	48.506	0.142	0.267	0	0.058	0	100.001
#20	0.113	0	44.436	0.005	54.587	0.338	0.255	0	0.267	0	100.001
#21	0.078	0.004	48.966	0.035	50.567	0.162	0.046	0.019	0.123	0	100
#22	0.066	0	43.744	0.097	51.073	0.63	3.045	0	1.345	0	100
#23	0	0	46.995	0.004	52.143	0.758	0.056	0	0.044	0	100
#24	0	0.015	44.506	0.004	53.494	1.738	0.055	0	0.188	0	100
#25	0.053	0.092	49.199	0.01	5.977	44.602	0.039	0.02	0.008	0	100

#26	0.045	0.079	49.87	0	0.612	49.386	0	0	0.008	0	100
#27	0.065	0.123	49.502	0.057	0.384	49.847	0	0.006	0.016	0	100
#28	0	0.102	47.258	0.056	0.216	52.367	0	0	0	0	99.999
#29	0.017	0.104	49.693	0.001	0.103	50.055	0	0.027	0	0	100
#30	0.023	0.141	49.594	0.014	0.234	49.92	0.037	0.039	0	0	100.002
#31	0.008	0.093	49.695	0.039	0.315	49.8	0.022	0	0.028	0	100
#32	0.011	0.09	49.573	0	0.268	50.028	0	0.02	0.01	0	100
#33	0.053	0.149	49.367	0	0.614	49.741	0.042	0.034	0	0	100
#34	0	0.053	47.614	0.006	40.339	11.85	0.032	0.012	0.093	0	99.999
#35	0.009	0	46.686	0.019	52.316	0.804	0.053	0.029	0.085	0	100.001
#36	0	0.071	48.326	0.055	7.436	44.048	0.034	0.015	0.015	0	100
#37	0.014	0.04	49.453	0	1.42	49.047	0.008	0.018	0	0	100
#38	0.028	0.064	49.395	0	0.744	49.703	0.028	0.03	0.008	0	100
#39	0	0.113	49.787	0.003	0.478	49.618	0	0	0	0	99.999
#40	0	0.105	49.621	0	0.235	49.978	0.028	0.031	0.002	0	100

Peak c/s

	Ag	Cd	S	Fe	Cu	Zn	As	Se	Sb	Pb
#1	5.4	28.8	2257.1	13.4	27.5	1652.2	21.7	24.6	21.9	6
#2	6.5	26	2223.9	12.9	25	1669.5	16.9	20.6	22.3	6.5
#3	6.7	30	2235.9	11.8	36.5	1640.5	22	20.9	26.2	7.5
#4	5.6	33.5	2226	12.8	37.4	1640.6	24	22.1	27.5	6.2
#5	5.4	27.4	2236.2	13	30	1663.2	20.2	21.1	23.9	6.3
#6	7.5	28.9	2222.8	12.3	30.7	1639.6	20.1	22.4	23.3	7.3
#7	5.4	31.8	2214.7	13.2	52.5	1605.6	28.4	22.5	28.8	7.3
#8	7	32.1	2269.5	15.3	66.7	1607	17.9	20.6	21	6.3
#9	5.5	10.8	1725	11.6	1925.9	41.4	16.2	22.3	21.4	7.9
#10	7.4	11.6	2111.8	10.4	2010.5	51.5	20.5	27.1	22	8.3
#11	7.1	29.8	2230.6	13.2	143.6	1561.5	26.7	21.6	24.9	7.4
#12	7.1	36.4	2220	12.2	37.1	1659.5	20	21.4	22.1	6.2
#13	6.4	35.4	2241.9	12.3	30.3	1658	16.2	21.6	23.5	7.4
#14	6.1	42.3	2231.8	11.6	35.9	1612.8	18.8	24.7	21.1	6.3
#15	5.7	39.1	2241.8	12.9	50.5	1659.3	16.3	24	19.9	5.7
#16	6	24.8	1882	13.9	199.3	1517.8	23	22.6	22.8	7.8
#17	6.5	34.1	2231.4	11.4	120.5	1580.4	21.7	22.8	21.9	6.8
#18	7.2	18	2041.5	11.2	1863	269.9	20.2	23.5	23.1	12.2
#19	7	10.9	2161.6	11.8	1789.8	24.3	39.6	23.6	26.7	14.5
#20	8.9	9.7	1916.3	12.9	2085.9	28.8	36	19.6	51.1	14.7

#21	9	13.1	2235.6	11.3	2022.2	24.9	20.5	24.8	35.3	13
#22	6.1	10.7	1547.5	13.9	1619.2	36.1	216.6	17	148.2	8.2
#23	7	9.7	2078.7	11.4	2035.5	45.2	19	20.2	24.8	8.1
#24	5.8	11.8	1809.8	9.9	1919.9	67.5	23.2	21.1	38.9	16.7
#25	7.1	17.1	2224.2	11.2	263.6	1496.8	17.6	20.7	23.5	6.4
#26	7.8	19.1	2240.7	11.4	44.5	1645.3	17.2	21.3	21.9	6.9
#27	8.1	18.8	2212.3	13.8	33.1	1654	16.9	22	22.7	7.6
#28	4.3	15.4	1924.9	14.2	30.5	1587.7	7.9	8.1	21.4	4.9
#29	6.2	18.5	2225.6	12.4	22.3	1658.9	17.2	23.9	21.1	5.8
#30	6.6	19.5	2213.4	11.4	27.5	1654.8	19	24.7	22.4	6.9
#31	7.1	18.7	2227.5	13	32.1	1658.9	18.6	21.1	23.7	6.6
#32	6	18.9	2226.3	10.8	28.4	1669	17.4	24.2	21.7	6.1
#33	6.7	20.5	2207	12.2	44.7	1653.5	19.3	24	21.1	6.7
#34	7.5	14.5	2057.8	11.8	1565.1	391.9	18.6	21.8	30.4	15.6
#35	7.5	10.6	2050	11.6	2024.9	44.1	20.9	22.4	29.4	10.7
#36	6.3	17.8	2123.2	12.1	316.2	1440.1	19.1	21.7	24.5	9.5
#37	6.1	18.3	2211.6	11	79.4	1624.8	16.1	24	20.9	5.6
#38	6.6	16.6	2207.2	11.3	46.9	1649.6	18	20.4	21.8	7.1
#39	6.5	18.8	2244.9	11.6	38	1659.5	17.3	20.2	21.1	8.4
#40	8	17.8	2224.8	11.2	29.4	1667.8	18.1	21.9	22.1	6.3

Bacground c/s

	Ag	Cd	S	Fe	Cu	Zn	As	Se	Sb	Pb
#1	5.6	12.8	10.6	11	17.2	24	16.6	16.6	20.3	48
#2	5.8	13	11.6	12	17	23.8	15.2	25.6	20.4	41.6
#3	4.6	12.8	11.9	10.9	17.4	22.2	16.3	21	22.4	42.8
#4	5.2	9.4	11.6	10.2	17	21.4	17.3	21.2	21.7	45
#5	7.2	13.2	13.5	11.6	19.6	20.2	18.8	25	21.2	45.8
#6	8	13.4	12.9	12.3	21.4	23	17.2	18	22	44.4
#7	5.8	13.8	9.8	10.7	18	26.8	18.2	18.8	21.5	44.6
#8	5.4	14.4	10.8	11.4	19.6	22.2	14.9	19.4	21	44.4
#9	5.6	12	9.7	11.4	20	18	16	19.6	20.1	37.4
#10	6	11.8	10.4	9.6	26	21	16.3	21.8	21.7	43.4
#11	6.2	13.6	12.7	10.7	17	22.2	14.7	19.8	22.3	41.6
#12	6.8	12.6	10.6	10.4	20.4	22.4	15.8	22.8	20.7	43.6
#13	7	11.6	11.7	12.4	18	23.6	15.6	23	21	44.8
#14	7.4	13	10.7	11.3	18.6	22	18	23.4	22	46
#15	6.6	13.6	9.9	11	19.8	24.8	15.8	23.8	22.8	43
#16	3.4	9.8	12.5	12.4	18	26.6	18.8	24.6	18.7	41.2

#17	7	12.8	12	10.6	16	19	18	21.8	20.5	44.8
#18	6.2	15	10.7	11	25	19.8	17.3	19.6	20.2	36.8
#19	7.4	9.6	10.1	10.9	26.4	20	18.4	27.6	20.2	46.8
#20	5	11.8	9.9	12.6	19.6	18.2	16.1	24.8	20.1	44
#21	6.2	12.8	12.5	9.3	22.6	19.6	16.6	22.8	20.5	47.6
#22	4.2	12.2	8.6	9.5	22.6	19.6	13.4	17	18.7	29.6
#23	7	10.8	10	11.2	24.6	21	14.4	20.6	19.6	39.8
#24	6.2	10.8	9.6	9.7	16.4	16	19.1	23	18.3	32
#25	5.2	10.4	11.1	10.7	15.4	21.6	14.4	18.6	22.5	47
#26	6.2	13.4	10.7	11.7	19	22.8	18.6	22.4	20.9	43.6
#27	5.8	10	13.4	10.6	17.2	25.6	17.5	21.4	20.8	49
#28	5.2	8.6	9.7	11.3	22.2	23	7.9	8.2	21.5	30.8
#29	5.6	11	13.1	12.3	18	20.2	17.3	21.2	21.6	44
#30	5.8	9.4	10.5	10.6	17.8	24	16.1	20.8	23.2	39.6
#31	6.8	12	12.2	10.8	19	26.8	16.8	21.2	20.3	44.6
#32	5.6	12.4	10.7	12	17.2	23.8	17.8	22.2	20.5	40.4
#33	4.8	9.8	11.5	12.7	19.2	25.2	15.9	20.6	21.2	44.8
#34	8.4	10.8	9.9	11.4	25.8	20.6	16.1	20.6	19.6	42
#35	7.2	11.2	9.4	10.5	20	18.6	16.7	19.4	19.4	45.2
#36	7.2	12.8	11.7	9.1	15.6	22.4	16.4	20.2	22.7	38.8
#37	5.6	15.4	14.2	11.6	20.6	21.4	15.4	22.2	21.4	46.6
#38	5.6	12	10.5	14	16	22.6	15.8	17.4	20.8	44.4
#39	7.4	10.6	11.8	11.4	18	23.4	18.5	20.6	22.5	42.2
#40	9.2	10.2	11.2	12.3	19.6	27.6	15.9	18.8	21.8	39.8

Table 2.

Cameca Quantitative Analysis
Label : Wetar sulphides
Wed Jun 10 17:09:54 1998
Normal Analysis

Weight Percents %

	Ag	Cd	S	Fe	Cu	Zn	As	Se	Sb	Pb	Total
#1	0.094	0	27.57	0.627	42.127	6.736	18.967	0.024	0.815	0	96.96
#2	0.093	0.15	27.23	0.608	41.237	7.375	17.684	0.098	3.39	0	97.865
#3	0.129	0	26.95	0.389	41.759	7.635	18.864	0.156	1.835	0	97.717
#4	0.17	0.07	27.276	0.309	41.724	7.872	18.91	0	1.648	0	97.981
#5	0	0.13	27.385	1.25	41.472	6.711	19.246	0.061	1.09	0	97.345
#6	0.07	0.039	27.287	1.417	41.283	6.933	19.272	0.088	0.962	0	97.351
#7	0.006	0	25.158	2.195	38.556	5.216	7.017	0.048	19.871	0	98.067
#8	0	0	0.026	0	0.256	0.015	0.022	0.017	0	0	0.336
#9	0.036	0.383	31.602	0.086	0.983	64.989	0	0	0.003	0	98.082
#10	0.41	0	27.579	0.063	62.425	1.957	0.097	0.053	0.557	0	93.141
#11	0.072	0.386	31.492	0.041	0.559	64.791	0	0	0	0	97.341
#12	0	0.045	26.276	0.181	40.477	7.791	15.457	0.031	6.577	0	96.835
#13	0	0.054	27.035	0.566	40.609	7.813	17.339	0.106	3.723	0	97.245
#14	0.047	0.07	31.233	0.038	45.798	0.164	15.911	0.134	3.947	0	97.342
#15	0	0	26.56	0.114	41.236	8.297	17.792	0.059	3.099	0	97.157
#16	0.07	0.078	26.923	0.958	41.8	7.002	16.745	0	4.523	0	98.099
#17	0	0.241	31.635	0	1.109	64.66	0.023	0.043	0.055	0	97.766
#18	0	0.192	31.587	0.031	1.548	63.676	0.034	0	0.078	0	97 146
#19	0.158	0	27.071	0.638	41.411	7.433	18.174	0.143	2.383	0	97.411
#20	0	0.09	19.004	0.001	48.928	0	0.121	0	1.418	0	69.562

Atomic %

	Ag	Cd	S	Fe	Cu	Zn	As	Se	Sb	Pb	Total
#1	0.046	0	45.299	0.591	34.929	5.429	13.337	0.016	0.353	0	100
#2	0.046	0.071	44.95	0.577	34.351	5.972	12.494	0.066	1.474	0	100.001
#3	0.063	0	44.437	0.368	34.746	6.175	13.311	0.104	0.797	0	100.001
#4	0.083	0.033	44.741	0.291	34.534	6.333	13.274	0	0.712	0	100.001
#5	0	0.061	44.962	1.178	34.36	5.404	13.523	0.041	0.471	0	100

#6	0.034	0.018	44.804	1.336	34.206	5.583	13.542	0.059	0.416	0	99.998
#7	0.003	0	44.378	2.223	34.32	4.513	5.297	0.034	9.231	0	99.999
#8	0	0	14.488	0	72.408	4.035	5.202	3.867	0	0	100
#9	0.017	0.17	49.266	0.077	0.773	49.695	0	0	0.001	0	99.999
#10	0.202	0	45.655	0.06	52.147	1.589	0.068	0.036	0.243	0	100
#11	0.034	0.173	49.431	0.037	0.443	49.883	0	0	0	0	100.001
#12	0	0.022	44.536	0.176	34.62	6.477	11.212	0.022	2.936	0	100.001
#13	0	0.026	44.951	0.54	34.072	6.372	12.338	0.071	1.63	0	100
#14	0.023	0.032	50.066	0.035	37.046	0.129	10.916	0.087	1.666	0	100
#15	0	0	44.297	0.109	34.705	6.788	12.699	0.04	1.361	0	99.999
#16	0.034	0.037	44.574	0.91	34.922	5.686	11.864	0	1.972	0	99.999
#17	0	0.107	49.413	0	0.874	49.54	0.016	0.027	0.023	0	100
#18	0	0.086	49.58	0.028	1.226	49.025	0.023	0	0.032	0	100
#19	0.078	0	44.753	0.605	34.546	6.027	12.858	0.096	1.037	0	100
#20	0	0.058	43.048	0.001	55.929	0	0.117	0	0.846	0	99.999

Peak c/s

	Ag	Cd	S	Fe	Cu	Zn	As	Se	Sb	Pb
#1	6.8	13.1	1941.6	44.8	1406.8	199.8	1291.4	29.8	66	8.5
#2	6.2	16.2	1932.1	42.4	1383.2	217.4	1200.6	32.9	192.8	7.4
#3	7.6	12	1902.1	29.6	1398.1	221.2	1282.7	34.6	113.2	8.4
#4	6.7	12.3	1924.9	27.9	1398.2	229.5	1287.9	28.1	107.1	7.1
#5	5.6	17.5	1933.7	75.4	1386.6	201.8	1317	32.4	75.4	5.7
#6	6.8	13.5	1924.4	82.6	1386.2	204.3	1322	34.2	70.4	7.1
#7	7.5	12.4	1872.9	121.5	1312.2	166.7	467.8	28.6	1075.4	7.6
#8	1.4	2.5	3	1.8	13.2	4.4	5.2	8.6	5.4	1.4
#9	6.4	24.8	2232.6	15.2	49.3	1673.3	17	20	22.3	6.1
#10	9.8	12.2	1987.4	12.5	2012.2	69.1	22.9	24.4	49	18.9
#11	6.8	24.5	2223.9	12.4	37.5	1667.5	17.4	20.6	20.9	5.5
#12	6.8	14.7	1881	20.4	1361.5	232.2	1039.5	29.3	362.6	6.8
#13	6.1	14.2	1922.6	40	1361.2	226.4	1174.6	32	214.1	6
#14	7.8	11.5	2240.5	12.2	1517.8	21.9	1109.5	34.2	221.8	7
#15	4.9	11.7	1876.7	16.3	1384.3	243.4	1200.9	32.5	179.8	6.5
#16	5.8	15	1920.6	60.2	1401.4	205.1	1128.6	30.5	253.8	6.3
#17	6	18	2231	11.6	55.4	1663.2	16.6	24	21.1	7.2
#18	6.1	20.6	2227.8	13	70.1	1644.2	18.9	22.5	24.9	6.9
#19	7.7	12.9	1915.6	47.5	1385.6	218.5	1235.2	33.2	145.1	8.8
#20	5	10.6	1356.6	10.4	1540.9	18.8	14.8	12.6	90.8	7.9

Bacground c/s

	Ag	Cd	S	Fe	Cu	Zn	As	Se	Sb	Pb	
#1	5.2	14	9.2	12.9	22.8	22.2	27	28.2	24.6	39.4	
#2	4.6	11.2	9.9	11.5	23.6	22.4	28.4	26.4	19.5	35.6	
#3	5.4	13	10.1	9.8	20.6	19.2	29.4	24.4	19.5	36.8	
#4	3.8	10	10	12.1	23.4	21.4	32	28.8	23.1	38	
#5	7.4	13.2	11.7	11.9	22.2	24.6	28.4	28.4	19.9	35.4	
#6	5.6	12.2	9.6	10.5	27.6	21.2	32.3	28.4	21.4	38.8	
#7	7.4	13	11.3	11.8	25.6	27.2	23	25.2	25.8	35.4	
#8	1.4	3.4	1.2	1.9	4.6	4	4.1	7.6	6.2	1.4	
#9	5.8	12.4	11.4	10.9	16.8	22.8	18.6	23.2	22.1	42.8	
#10	2.8	13.2	10.4	9.2	24.6	19	17.5	20.8	20.7	41	
#11	5.6	12	10.7	10.3	19	23.8	18.4	23.4	21.5	44	
#12	7.2	13.2	11.7	11.2	21.8	25.4	30.6	27.2	23.8	35.6	
#13	7.8	12.4	13	11.3	21.4	19.6	28.4	25	23.5	39.8	
#14	7	9.2	11.7	10.3	26.6	17.6	27.3	25	22.1	37.8	
#15	8.6	13.8	8.8	10.5	23.6	23.8	31.4	28.6	21.3	37	
#16	4.6	12.4	12.5	11.6	21.8	19.8	26.9	30.8	21.8	37.8	
#17	6.6	10.2	11	11.6	18.8	24	15.3	21.2	18.3	47.4	
#18	7.4	14.4	9	11.4	19	30.4	17.1	23	21	45.4	
#19	5	14.2	10.6	15.1	20.8	22	29.8	23.8	23.4	39	
#20	5.2	7.6	8	10.3	20.8	19.2	8.1	13.8	18.1	24.2	

#65	7.4	11.8	11.2	10.8	20.8	18	32.5	32.4	19.3	38.6
#66	3.6	5.8	3.4	4.3	6.4	6.4	12.3	15.2	10.3	7
#67	3.4	7.2	8.2	9	19.8	15.2	15.6	21.6	17.7	29
#68	7.8	9.8	9.1	11.7	20.4	18	17.5	21	19.5	30.8
#69	6.2	12.6	10.2	10.1	24.4	19.8	17.8	21	18.8	42.8
#70	5.4	9.8	9.8	10.9	22.4	20.8	11.9	14.6	18.6	31.6
#71	5.2	8	8	9.3	22.6	18.4	7.7	11.6	18.6	27
#72	5.2	9.4	9.3	9.6	24.4	18.8	12.3	17.2	21.7	36.4
#73	4.6	9.4	9.7	10.4	20.2	16	17	21	18.6	37.8
#74	5.6	8.4	9.1	11.3	22	20.8	12	13.6	17.4	26.6
#75	6.6	12	11.6	11.1	22.4	17.8	19	19.8	22.5	43.8
#76	7	10.6	11.6	9.7	19	20.8	18.7	19.2	22.5	43.6
#77	4.2	11.4	12	11.6	21.6	23.2	16.4	20	22.9	44.6
#78	7.6	10.4	10.9	11.1	19	22.8	16.7	22.6	19.6	48.2
#79	7	13	10.1	10.5	17.6	25.2	16.2	21	20.4	45
#80	6.8	15	11.4	10.1	15.4	20.4	16.3	20	20	46
#81	6	8.2	10.1	12.4	16.8	23.2	17.8	23	20.2	46
#82	7.4	13.6	12.6	12.4	18.8	24	15.7	20.8	22.2	44.6
#83	6.4	13	13.5	11.9	13.6	25.2	16.6	18.6	20.8	43.6
#84	5.4	12.6	11.5	12	21	22.6	16.7	22	20.4	48.8
#85	4.4	12.6	11.4	10	25	18	14.6	25.4	19.5	47.2
#86	7.2	9.4	13	11.4	24.2	20.8	17.1	21.4	18.4	45.2
#87	4	10.8	11.5	11.5	24.8	21.2	18.6	20.2	20.2	49.4
#88	6.4	10	10.2	9.6	25.8	18	15.2	18.6	20.4	53.8
#89	5.8	12.8	9.9	11.2	21.6	16.2	18.2	22	21.5	46.2
#90	8.6	12.8	11.1	11	21.2	15.4	14.8	20.6	18.5	37.6
#91	5.6	7.6	9.4	9.5	25.4	17.8	15.4	17.8	17.1	40.4
#92	4	11.8	11.3	10.5	23.8	15.8	16.3	23.2	19.5	43.4
#93	5.6	12.2	10.2	10.9	20.4	18.2	15.7	18	20.3	38.4
#94	5.8	12	11.6	11.2	23.6	20.2	18.4	20.2	19.2	46.2
#95	4.4	12	9.1	9.9	21	19.4	16.9	22.4	21.2	36.8
#96	7.6	10.2	9.7	10.1	24.6	21	13.6	20.4	20.5	36.6
#97	4.4	11.2	8.6	9.4	23	17.4	16.6	20.6	17.6	38
#98	5	8.6	6.3	8.7	15.2	17.8	14.1	19.8	16.1	30.6
#99	4.4	10.8	10	10.5	20.6	16	13.1	14.4	16.7	33.2
#100	3.6	9.6	6.9	11	19.6	14.6	14.8	14.8	18	34.8
#101	5.4	8.4	10.4	10.2	23.6	17.8	15.9	19	19.3	35.8
#102	3.4	9.4	9	10	22.6	18.6	14.6	22	18.1	37.8
#103	4.4	6.8	6.5	9.2	24.2	18.4	4.9	9.2	17.7	25
#104	5.2	8.6	9.5	9.2	17	15.2	13.7	16	16.3	33.6

Table 3.

Cameca Quantitative Analysis
Label : Wetar sulphides
Thu Jun 11 09:28:47 1998
Normal Analysis

Weight Percents %

	Ag	Cd	S	Fe	Cu	Zn	As	Se	Sb	Pb	Total
#1	0	0	51.859	45.944	0	0.132	1.218	0.037	0.009	0	99.199
#2	0	0	51.508	45.904	0	0.077	0.627	0	0	0	98.116
#3	0	0	52.287	46.014	0	0.017	0.598	0.012	0.008	0	98.936
#4	0	0.042	51.841	45.459	0	0.132	0.5	0.022	0.014	0	98.01
#5	0	0.039	52.056	46.057	0	0	0.603	0.061	0.055	0	98.871
#6	0.044	0.039	52.34	46.591	0.038	0	0.132	0.031	0	0	99.215
#7	0.043	0	48.674	44.742	0	0.059	5.153	0.016	0.056	0	98.743
#8	0.043	0	47.66	43.858	0	0.008	6.657	0.084	0.036	0	98.346
#9	0	0	48.01	44.367	0.034	0.038	6.613	0.042	0	0	99.104
#10	0.037	0.035	52.141	45.222	0.017	0.072	0.54	0.019	0.009	0	98.092
#11	0	0	51.837	45.679	0	0.047	0.967	0.064	0	0	98.594
#12	0.136	0.102	49.651	43.742	0.111	0.025	5.446	0.043	0.047	0	99.303
#13	0	0	51.655	45.869	0	0	0.91	0	0	0	98.434
#14	0	0.07	49.741	45.233	0	0	3.47	0.078	0	0	98.592
#15	0.025	0.1	51.768	45.927	0	0.034	0.58	0.002	0	0	98.436
#16	0.006	0.182	32.274	9.586	3.246	49.019	0	0.001	0.174	0	94.488
#17	0.019	0	52.683	46.484	0.208	0	0.197	0.038	0	0	99.629
#18	0	0.006	51.061	44.625	0.332	0	2.84	0.06	0	0	98.924
#19	0	0.013	52.143	44.765	0.769	0.145	1.087	0.047	0	0	98.969
#20	0.05	0	51.794	45.38	0	0.047	1.17	0.002	0.02	0	98.463
#21	0	0.074	52.174	45.122	0.123	0.004	1.48	0	0	0	98.977
#22	0	0.055	52.21	45.295	0.092	0	1.265	0	0.04	0	98.957
#23	0	0.084	50.966	43.498	1.008	0.362	0.74	0	0.05	0	96.708
#24	0.094	0.026	52.217	45.36	0.44	0	0.683	0	0.006	0	98.826
#25	0.106	0.01	50.787	44.88	0.139	0.004	3.403	0.01	0.046	0	99.385
#26	0	0.096	51.701	44.863	0.197	0	1.92	0.035	0.042	0	98.854
#27	0.078	0	31.251	0.044	45.383	0.146	18.278	0.109	0.121	0	95.41
#28	0.024	0.012	30.916	0	46.497	0.191	18.294	0.086	0.012	0	96.032
#29	0.201	0	26.41	0	47.644	0.015	13.088	0.042	0.125	0	87.525
#30	0.042	0.028	31.337	0.041	45.946	0.088	18.565	0.065	0.108	0	96.22

#31	0.131	0.04	31.779	0.035	45.475	0.115	17.915	0.05	0.117	0	95.657
#32	0.035	0	21.048	0	35.344	0.131	8.868	0.001	1.79	0	67.217
#33	0.065	0.033	22.916	0	39.187	0.145	10.484	0.016	2.801	0	75.647
#34	0.029	0.021	28.81	0.042	59.516	0.094	1.3	0.019	0.768	0	90.599
#35	0.106	0	22.254	0.081	33.899	0	4.969	0.087	5.162	0	66.558
#36	0.035	0.046	27.659	0.498	41.792	8.057	19.514	0.052	0.437	0	98.09
#37	0.123	0.054	26.928	0.617	41.135	7.646	17.99	0.123	2.882	0	97.498
#38	0.164	0.073	16.119	0.064	21.621	0.178	9.466	0.077	3.326	0	51.088
#39	0.047	0.015	30.122	0.041	63.654	0.554	0.06	0.015	0.078	0	94.586
#40	0.042	0	31.177	0.018	47.21	0.188	17.354	0.11	0.162	0	96.261
#41	0.03	0	31.243	0.009	46.098	0	17.771	0.161	0.092	0	95.404
#42	0.041	0	25.559	0.154	43.8	0.057	13.419	0.055	1.032	0	84.117
#43	0.065	0	18.045	0.049	30.674	0.164	9.617	0.049	1.54	0	60.203
#44	0.03	0	28.28	0.085	41.319	0.004	16.644	0	1.401	0	87.763
#45	0.012	0.119	25.124	0.041	39.785	0	15.842	0.07	0.875	0	81.868
#46	0.101	0.052	24.478	0.045	42.813	0.089	10.953	0.135	0.255	0	78.921
#47	0.106	0.018	22.552	0.043	36.165	0.046	13.411	0.031	1.128	0	73.5
#48	0.025	0.032	1.489	0.004	1.225	0	0.235	0.014	0.158	0	3.182
#49	0	0	14.466	0.011	18.087	0.004	2.964	0	1.136	0	36.892
#50	0.148	0	29.471	0.032	47.01	0	16.286	0.073	0.171	0	93.191
#51	0	0	20.514	0.041	33.904	0.03	17.764	0.061	1.464	0	73.778
#52	0.064	0.033	6.07	0.083	10.064	0.019	4.542	0.003	1.57	0	22.448
#53	0.108	0.009	24.994	0.052	36.928	0.232	10.428	0.02	0.288	0	73.059
#54	0.137	0	27.347	0.002	38.114	0.027	16.645	0.131	1.173	0	83.576
#55	0.088	0	19.851	0.004	40.923	0.069	8.715	0.018	1.51	0	71.178
#56	0.115	0	21.496	0.03	23.728	0.058	12.444	0.049	0.822	0	58.742
#57	0.047	0	29.249	0.09	59.637	0.122	0.907	0.036	0.334	0	90.422
#58	0.065	0	29.415	0.088	56.802	0	1.482	0.069	0.428	0	88.349
#59	0.006	0.064	24.822	0	54.649	0.055	0.152	0.018	0.564	0	80.33
#60	0.024	0.049	25.015	0.049	36.435	0.12	10.324	0.055	0.779	0	72.85
#61	0.262	0.009	25.168	0.152	34.396	0.081	9.915	0.087	2.778	0	72.848
#62	0	0	24.011	0.258	43.474	0.258	9.007	0.031	1.57	0	78.609
#63	0.059	0	20.313	0.059	29.668	0.243	7.947	0.068	1.958	0	60.315
#64	0.107	0.015	27.647	0.068	43.904	0.291	15.122	0.08	1.299	0	88.533
#65	0	0	29.978	0.06	45.252	0.069	19.013	0.027	0.131	0	94.53
#66	0	0	4.782	0.251	4.15	0.07	0.708	0.003	1.739	0	11.703
#67	0.122	0.051	18.991	0.043	50.727	0.131	2.69	0.005	0.668	0	73.428
#68	0	0	23.575	0	48.799	0	1.808	0.038	0.543	0	74.763
#69	0.059	0	30.262	0.063	61.966	0.071	0.046	0	0.396	0	92.863
#70	0.121	0.063	21.632	0.043	65.865	0.05	0.106	0.015	0.401	0	88.296

#71	0.063	0.03	19.34	0.068	56.605	0.058	0.297	0	1.271	0	77.732
#72	0.018	0.036	26.218	0.068	56.888	0.165	0.263	0.013	0.643	0	84.312
#73	0.1	0.027	24.288	0.054	57.38	0.125	0.193	0.034	0.652	0	82.853
#74	0.041	0.057	24.226	0.014	60.631	0.129	0.161	0.004	0.389	0	85.652
#75	0.006	b	31.294	0.031	55.42	7.738	0.022	0.044	0.227	0	94.782
#76	b	0.073	30.754	0.042	56.313	6.364	0.043	0.058	0.225	0	93.872
#77	0.222	0.241	31.881	0.087	5.209	58.502	0.17	0.079	0.395	0	96.786
#78	0	0.412	31.952	0.053	1.221	62.908	0.093	0.018	0.109	0	96.766
#79	0.096	0.399	31.774	0.044	1.655	62.164	0.156	0.017	0.382	0	96.687
#80	0.054	0.426	31.673	0.084	2.612	60.583	0.377	0.038	0.745	0	96.592
#81	0	0.531	31.846	0.047	1.465	63.783	0.099	0	0.234	0	98.005
#82	0.03	0.34	31.521	0.009	1.55	62.498	0.138	0.028	0.307	0	96.421
#83	b	0.482	32.291	0.1	1.568	64.98	0.076	0.049	0.192	0	99.738
#84	0.096	0.401	31.762	0.051	6.088	59.409	0.227	0.031	0.641	0	98.706
#85	0.201	0.034	30.933	0.031	61.263	1.661	0.212	0	0.677	0	95.012
#86	b	0.055	31.784	0	61.535	1.149	0.07	0.013	0.215	0	94.821
#87	0.291	0.055	31.866	0	61.734	0.698	0.092	0.046	0.36	0	95.142
#88	0.042	0.086	31.508	0.035	62.029	0.58	0.101	0.033	0.209	0	94.623
#89	0.059	b	31.304	0.009	60.907	0.446	0.039	0	0.151	0	92.915
#90	b	b	27.516	0	60.316	0.385	0.231	0.053	0.226	0	88.727
#91	0.107	0.061	27.928	0.015	56.856	0.228	0.068	0.065	0.216	0	85.544
#92	0.212	b	28.94	0	62.491	0.302	0.043	0	0.159	0	92.147
#93	b	b	29.335	0.004	60.682	0.24	0.08	0.013	0.236	0	90.59
#94	0.053	b	30.419	0	61.717	0.02	0.061	0.042	0.199	0	92.511
#95	0.065	b	25.937	0.012	59.599	0	0.056	0	0.205	0	85.874
#96	b	0.054	26.358	0.016	61.662	0.012	0.131	0.009	0.271	0	88.513
#97	0.123	0.018	26.194	0.036	60.884	0.18	0.155	0.004	0.464	0	88.055
#98	0.006	0.058	22.565	0.035	49.057	0	0.052	0.054	0.554	0	72.381
#99	0.131	b	23.97	0	44.005	0.016	0.11	0.013	0.929	0	69.174
#100	0.149	0.049	26.004	0	45.154	0.146	0.145	0.052	0.875	0	72.574
#101	0	0.036	22.086	0	55.559	0.14	0.199	0	0.679	0	78.699
#102	0.216	0.009	24.088	0.004	61.242	0.074	0.124	0	0.346	0	86.103
#103	0.08	0.195	17.313	0.043	57.094	0.069	0.175	0	0.595	0	75.564
#104	0	0.08	23.385	0.01	41.243	0.044	0.159	0.034	0.909	0	65.864

Atomic %

	Ag	Cd	S	Fe	Cu	Zn	As	Se	Sb	Pb	Total
#1	0	0	65.777	33.458	0	0.082	0.661	0.019	0.003	0	100

#2	0	0	65.893	33.716	0	0.048	0.343	0	0	0	100
#3	0	0	66.205	33.451	0	0.011	0.324	0.006	0.003	0	100
#4	0	0.015	66.255	33.357	0	0.063	0.273	0.012	0.005	0	100
#5	0	0.014	66.055	33.554	0	0	0.327	0.031	0.018	0	99.999
#6	0.016	0.014	66.084	33.774	0.024	0	0.071	0.016	0	0	99.999
#7	0.017	0	63.518	33.522	0	0.038	2.878	0.009	0.019	0	100.001
#8	0.017	0	62.918	33.242	0	0.005	3.761	0.045	0.013	0	100.001
#9	0	0	62.869	33.356	0.022	0.024	3.706	0.023	0	0	100
#10	0.014	0.013	66.497	33.112	0.011	0.045	0.295	0.01	0.003	0	100
#11	0	0	66.013	33.398	0	0.029	0.527	0.033	0	0	100
#12	0.052	0.038	64.262	32.504	0.073	0.016	3.016	0.023	0.016	0	100
#13	0	0	65.904	33.6	0	0	0.497	0	0	0	100.001
#14	0	0.026	64.391	33.619	0	0	1.922	0.041	0	0	99.999
#15	0.009	0.036	65.998	33.617	0	0.021	0.317	0.001	0	0	99.999
#16	0.003	0.082	50.777	8.659	2.577	37.828	0	0.001	0.072	0	99.999
#17	0.007	0	66.2	33.536	0.132	0	0.106	0.019	0	0	100
#18	0	0.002	65.386	32.809	0.215	0	1.556	0.031	0	0	99.999
#19	0	0.005	66.178	32.619	0.493	0.09	0.591	0.024	0	0	100
#20	0.019	0	66.07	33.235	0	0.029	0.639	0.001	0.007	0	100
#21	0	0.027	66.212	32.877	0.079	0.003	0.804	0	0	0	100.002
#22	0	0.02	66.232	32.99	0.059	0	0.687	0	0.013	0	100.001
#23	0	0.031	66.207	32.442	0.661	0.23	0.411	0	0.017	0	99.999
#24	0.035	0.009	66.256	33.045	0.231	0	0.371	0	0.002	0	99.999
#25	0.04	0.004	65.001	32.978	0.09	0.003	1.864	0.005	0.015	0	100
#26	0	0.035	65.918	32.84	0.127	0	1.048	0.018	0.014	0	100
#27	0.037	0	50.267	0.04	36.837	0.115	12.582	0.071	0.051	0	100
#28	0.011	0.006	49.584	0	37.631	0.151	12.556	0.056	0.005	0	100
#29	0.106	0	47.017	0	42.803	0.013	9.972	0.03	0.058	0	99.999
#30	0.02	0.013	50.051	0.037	37.032	0.069	12.69	0.042	0.045	0	99.999
#31	0.062	0.018	50.788	0.032	36.675	0.09	12.253	0.033	0.049	0	100
#32	0.024	0	48.693	0	41.262	0.148	8.78	0.001	1.091	0	99.999
#33	0.04	0.02	47.72	0	41.179	0.148	9.343	0.014	1.536	0	100
#34	0.015	0.01	48.262	0.04	50.312	0.077	0.932	0.013	0.339	0	100
#35	0.073	0	51.803	0.109	39.819	0	4.95	0.083	3.164	0	100.001
#36	0.017	0.021	44.976	0.465	34.293	6.427	13.58	0.034	0.187	0	100
#37	0.06	0.026	44.62	0.587	34.395	6.215	12.757	0.083	1.258	0	100.001
#38	0.152	0.064	50.088	0.115	33.903	0.272	12.588	0.097	2.722	0	100.001
#39	0.022	0.007	48.11	0.038	51.305	0.434	0.041	0.009	0.033	0	99.999
#40	0.02	0	49.78	0.016	38.038	0.147	11.859	0.071	0.068	0	99.999
#41	0.014	0	50.219	0.008	37.39	0	12.224	0.105	0.039	0	99.999

#42	0.023	0	47.483	0.165	41.062	0.052	10.669	0.042	0.505	0	100.001
#43	0.05	0	47.248	0.074	40.527	0.211	10.776	0.052	1.062	0	100
#44	0.016	0	49.892	0.087	36.785	0.003	12.567	0	0.651	0	100.001
#45	0.007	0.065	48.038	0.046	38.387	0	12.963	0.054	0.441	0	100.001
#46	0.059	0.029	47.99	0.051	42.357	0.085	9.19	0.108	0.132	0	100.001
#47	0.067	0.011	48.049	0.053	38.883	0.048	12.228	0.027	0.633	0	99.999
#48	0.322	0.398	65.48	0.106	27.192	0	4.415	0.252	1.836	0	100.001
#49	0	0	57.341	0.025	36.18	0.008	5.027	0	1.419	0	100
#50	0.073	0	48.874	0.03	39.341	0	11.558	0.049	0.075	0	100
#51	0	0	44.914	0.052	37.458	0.032	16.645	0.054	0.844	0	99.999
#52	0.139	0.069	44.658	0.351	37.364	0.068	14.3	0.009	3.043	0	100.001
#53	0.066	0.005	51.689	0.061	38.538	0.236	9.23	0.017	0.157	0	99.999
#54	0.075	0	50.529	0.002	35.538	0.024	13.162	0.098	0.571	0	99.999
#55	0.058	0	44.411	0.005	46.199	0.076	8.344	0.016	0.89	0	99.999
#56	0.087	0	54.961	0.045	30.614	0.072	13.616	0.051	0.554	0	100
#57	0.023	0	48.781	0.086	50.191	0.1	0.647	0.025	0.147	0	100
#58	0.033	0	49.92	0.085	48.646	0	1.077	0.048	0.191	0	100
#59	0.003	0.035	47.13	0	52.361	0.051	0.124	0.014	0.282	0	100
#60	0.015	0.029	51.947	0.058	38.181	0.122	9.175	0.046	0.426	0	99.999
#61	0.163	0.005	52.716	0.182	36.356	0.083	8.888	0.074	1.532	0	99.999
#62	0	0	47.542	0.293	43.438	0.251	7.633	0.025	0.819	0	100.001
#63	0.045	0	51.556	0.086	37.999	0.303	8.632	0.07	1.309	0	100
#64	0.056	0.008	48.618	0.069	38.96	0.251	11.38	0.057	0.602	0	100.001
#65	0	0	49.092	0.057	37.396	0.055	13.325	0.018	0.057	0	100
#66	0	0	61.175	1.844	26.79	0.441	3.877	0.013	5.86	0	100
#67	0.079	0.031	41.233	0.053	55.579	0.14	2.499	0.004	0.382	0	100
#68	0	0	47.982	0	50.121	0	1.575	0.031	0.291	0	100
#69	0.028	0	49.012	0.058	50.644	0.056	0.032	0	0.169	0	99.999
#70	0.065	0.032	39.238	0.045	60.29	0.045	0.082	0.011	0.192	0	100
#71	0.039	0.018	39.908	0.08	58.943	0.059	0.263	0	0.691	0	100.001
#72	0.009	0.019	47.37	0.07	51.867	0.146	0.203	0.01	0.306	0	100
#73	0.055	0.014	45.279	0.057	53.98	0.114	0.154	0.026	0.32	0	99.999
#74	0.022	0.03	43.971	0.015	55.534	0.114	0.125	0.003	0.186	0	100
#75	0.003	0	49.545	0.028	44.277	6.009	0.015	0.028	0.095	0	100
#76	0	0.034	49.254	0.038	45.512	4.999	0.03	0.038	0.095	0	100
#77	0.104	0.108	50.129	0.078	4.133	45.12	0.114	0.051	0.164	0	100.001
#78	0	0.185	50.201	0.048	0.968	48.479	0.062	0.012	0.045	0	100
#79	0.045	0.179	50.083	0.04	1.316	48.062	0.105	0.011	0.159	0	100
#80	0.025	0.192	50.063	0.076	2.083	46.971	0.255	0.025	0.31	0	100
#81	0	0.236	49.641	0.042	1.152	48.767	0.066	0	0.096	0	100

#82	0.014	0.153	49.858	0.008	1.237	48.489	0.094	0.018	0.128	0	99.999
#83	0	0.211	49.486	0.088	1.212	48.845	0.05	0.031	0.077	0	100
#84	0.044	0.178	49.301	0.046	4.768	45.231	0.151	0.019	0.262	0	100
#85	0.095	0.015	49.086	0.028	49.057	1.292	0.144	0	0.283	0	100
#86	0	0.025	50.048	0	48.895	0.887	0.047	0.008	0.089	0	99.999
#87	0.136	0.025	50.091	0	48.97	0.538	0.062	0.029	0.149	0	100
#88	0.02	0.039	49.805	0.032	49.478	0.45	0.069	0.021	0.087	0	100.001
#89	0.028	0	50.217	0.008	49.305	0.351	0.027	0	0.064	0	100
#90	0	0	47.18	0	52.189	0.323	0.169	0.037	0.102	0	100
#91	0.056	0.031	49.082	0.015	50.422	0.197	0.051	0.047	0.1	0	100.001
#92	0.104	0	47.642	0	51.912	0.244	0.03	0	0.069	0	100.001
#93	0	0	48.747	0.004	50.884	0.196	0.057	0.009	0.103	0	100
#94	0.026	0	49.314	0	50.49	0.016	0.043	0.028	0.085	0	100.002
#95	0.034	0	46.22	0.013	53.594	0	0.043	0	0.096	0	100
#96	0	0.027	45.732	0.016	53.988	0.01	0.097	0.006	0.124	0	100
#97	0.064	0.008	45.747	0.036	53.658	0.154	0.116	0.003	0.213	0	99.999
#98	0.004	0.035	47.456	0.042	52.063	0	0.047	0.046	0.307	0	100
#99	0.084	0	51.527	0	47.734	0.017	0.101	0.011	0.526	0	100
#100	0.09	0.029	52.818	0	46.281	0.146	0.126	0.043	0.468	0	100.001
#101	0	0.02	43.764	0	55.556	0.136	0.169	0	0.355	0	100
#102	0.116	0.005	43.605	0.004	55.944	0.066	0.096	0	0.165	0	100.001
#103	0.051	0.12	37.237	0.053	61.968	0.073	0.161	0	0.337	0	100
#104	0	0.051	52.47	0.013	46.698	0.048	0.152	0.031	0.537	0	100

Peak c/s

	Ag	Cd	S	Fe	Cu	Zn	As	Se	Sb	Pb
#1	4.2	10.2	4018.4	2029.6	13.3	16.7	114.2	28.7	19.8	8.6
#2	5.4	10.6	3996.8	2021.6	14.6	14.4	65.7	24.7	18.4	7.9
#3	4.6	9.6	4055.6	2024.5	14.6	17.8	64.6	27.1	19.5	6.9
#4	4.4	10.1	4020.6	2000.3	15.6	17.1	59.2	27.4	19.7	8.4
#5	5.8	10	4041.2	2027.4	14.7	15.9	63.7	27.2	19.6	7.5
#6	5.7	10	4060	2052.1	13.3	15.8	28.9	25.4	19.3	8.8
#7	5.5	9.8	3729.3	1991.6	14.9	15.6	424.3	30.6	20.1	8.4
#8	5.9	9.8	3638.2	1956	14.7	17.6	550.1	31.7	21.6	8.9
#9	4	11.3	3665.7	1979.7	16.8	14.1	544.4	27.4	18.5	8.8
#10	4.8	10.9	4046.9	1992.1	14.9	15.1	61.4	24.7	17.1	9.2
#11	5.6	9.1	4016.5	2015.1	15.4	15.9	97.1	25.5	19.3	7.5
#12	7	11.8	3806.8	1946.4	17.9	17.6	450.8	28.7	20.8	9.2

#13	5.4	8.8	4000.3	2021.8	17.2	15.1	90.7	24.3	19.4	8
#14	4.8	10.2	3824.7	2003.8	13.5	16.1	289	28	18.8	9.3
#15	5.6	10.9	4012.9	2026.1	14.7	16	63.1	23.8	19.6	8.7
#16	5.3	19.3	2308	477.6	121.6	1251.2	19	21.1	29	11.2
#17	5.3	8.4	4092.1	2048.5	19.7	14.9	32.4	26.6	20	8.9
#18	4.4	9.4	3939.8	1975.5	23.8	15.2	240.8	28.5	18.7	8.5
#19	6.4	9.6	4039.6	1975.5	36.8	17.8	102.2	27	17.3	10
#20	7.4	9.8	4009.9	1998.7	14.2	14.9	110.4	23.8	20	6.4
#21	5.3	12.3	4037.9	1990.2	18.6	15.1	132.4	24.1	19.7	8.5
#22	5.1	10.5	4047.5	1996.9	15.7	14.6	116	23.9	19.8	7.4
#23	4.6	10.4	3940.7	1915.9	44	22.5	76.2	25.3	20.3	9.8
#24	6.1	11.6	4051.7	1998.5	26.1	15.1	72.1	25.7	20.4	8.7
#25	6.9	10.3	3912.8	1988.8	20.3	16.9	285.3	25.9	24.3	9.8
#26	4.1	12	3995.5	1978.3	22.6	15	167.9	26.7	28.3	9.4
#27	7.7	10.6	2215	11.6	1496.9	21.4	1292.6	33	25	9.5
#28	6.8	11	2189.1	11.2	1535.7	22.2	1281.7	34	22.3	8.1
#29	7.2	11.3	1866	12.6	1561.4	20	861.4	20.2	26.1	8.8
#30	6.5	10.7	2219	11.9	1517.1	20.1	1311.7	30.2	25.6	10.8
#31	8.4	12.1	2255.8	11.4	1496.3	19.6	1263.4	31.6	27.4	8.1
#32	6.4	8.9	1485.5	10.6	1146.3	20.4	578	17.7	106.1	9.4
#33	6.1	10.5	1623.2	10.6	1280.1	21.4	694.7	23.7	159.7	10
#34	6.5	11.7	2076	11.9	1907.1	21.4	90.1	20.7	59	9.7
#35	5.8	8.3	1602.1	10.6	1096	18.5	328.1	18.8	282.5	12
#36	5.6	13.1	1946.4	34	1398	230.1	1329.1	34.2	45.7	7.8
#37	7.3	15.4	1906	41.2	1379.3	220.8	1220.8	32.5	169.7	6.7
#38	6.6	8.8	1131.8	10.6	711.9	16.1	651	22.3	181.8	10
#39	6.8	11.9	2175.9	11.8	2036.6	35.5	18.8	23.8	24.8	10.2
#40	7.9	11.7	2209.6	12.5	1553.3	21.3	1207.6	33.2	26.5	8.6
#41	7.7	12.8	2214.5	11.6	1517.7	20.5	1247.9	35.7	24.3	8
#42	6.7	8.9	1804.1	18.1	1437.6	22.9	892.5	24.1	71.4	8
#43	5.3	7.3	1259.5	10.5	1000.3	17.9	630	22.1	93.8	6
#44	6.7	11.9	2001.7	13.7	1360.8	21.3	1166.1	30.6	89.9	6.9
#45	6.8	10.7	1765.8	12.5	1309.8	15.8	1091.5	29.9	64	8.3
#46	6.3	11.3	1725.1	11.4	1394.3	21.3	717.5	24.9	34.4	7.2
#47	5	8.8	1582.3	10.1	1184.3	16	907.8	25.7	70.5	7.9
#48	2	3.6	104.2	3.6	40.6	4.2	24.3	8.9	13.3	2.2
#49	4.4	7.7	1015.3	8.1	562.2	11.7	200.1	9.9	81.2	6.1
#50	8.1	10.9	2089	12.2	1548.5	18.3	1121.7	30.9	27.8	8.4
#51	5.1	8.9	1426.6	11.2	1131.2	17.4	1234.8	33	92.2	8.6
#52	2.5	6.7	420.3	8	336.7	9.3	296.3	11.4	88.7	2.6

#53	5.8	9.7	1759.1	12	1188.9	21.2	699	21.2	36	6.6
#54	5.7	10.7	1927.3	10.8	1252.1	19.1	1179.8	35.3	79.9	6.8
#55	6.3	9	1397	9.4	1328.1	15.4	556.3	28	93.2	8.8
#56	5.3	9.2	1494.3	10.8	772.5	16.3	896.7	24.4	56.6	9.1
#57	7.6	9.8	2106.2	15.6	1898.9	21.3	68.4	22.3	38.8	10.9
#58	6.7	10.5	2121.4	15	1809.6	17.3	105.1	28	41.3	11
#59	5.5	10.3	1778.5	11.1	1724.2	19.2	21.9	18.2	48.4	7
#60	6.8	9.6	1765.1	12.1	1176.5	18.9	693.3	18	57.9	7.2
#61	7.2	10.9	1791.9	16.2	1112.7	17.1	679.3	25.1	157.5	11.5
#62	5.6	9.4	1700.2	23.9	1413	21.7	582.4	24.9	97.2	12
#63	5.6	7.4	1431.7	10.6	956.4	18.9	528.4	16.5	114.4	7.8
#64	7.2	11.5	1956.9	15.7	1443.3	24.6	1030.5	27.6	83.6	14.8
#65	6.7	10.3	2117.4	13.9	1492	19.8	1341.2	34.2	25.9	8.7
#66	2.8	3.7	345.5	16.3	134.9	8.2	60.2	15.4	94.6	3.3
#67	5.5	8.9	1346.3	11.2	1618.4	18.6	166.2	21.9	52	11
#68	7.8	9	1682	10.6	1537.2	17.1	121.9	23.6	46.9	7.6
#69	7.2	11.6	2187.4	13.4	1960.2	21.6	20.4	20.7	38.8	8.9
#70	7.5	11.9	1544.3	13.2	2119.5	22.1	17.6	15.6	39.3	9.3
#71	6.3	9	1377.3	12.9	1803.2	19.9	23.9	11.6	84	6.6
#72	5.5	10.6	1881.7	13.1	1804.8	23	27.2	18.1	54.2	9.1
#73	6.3	10.3	1739.6	13.2	1818.5	19.2	27.8	23.3	51.8	10.1
#74	6.3	10.3	1735.1	12.1	1933	24.1	20.9	13.9	37.2	8.2
#75	6.7	11.7	2256.1	12.7	1780	21.4	20.3	22.8	33.9	12.5
#76	7	13	2218.2	11.9	1804.2	182.4	21.2	23.2	33.8	11.5
#77	7.9	19.2	2255.4	15.9	192.2	1503.6	25.6	25.2	42.6	8.5
#78	6	23.7	2254.3	13.8	59.2	1612.5	21.7	23.8	25	6.6
#79	8.6	25.9	2244.5	12.7	72.1	1598.8	24.6	22.1	39.4	7.1
#80	7.7	28.8	2240.7	14.3	101.3	1555.6	36.8	22.5	57.2	7.1
#81	6	25.4	2249.1	14.8	65.1	1641.1	23.1	21.4	31.9	6.9
#82	7.9	24.6	2227	12.9	69.9	1605.9	23.2	22.6	37.5	7.4
#83	4.7	28.6	2285.3	16.9	65.3	1677.3	20.7	21.8	30.4	5.7
#84	7	25.6	2249.2	14.6	220.8	1532.7	29	24	52.4	8.7
#85	7.8	13.7	2238.1	11.6	1966.3	60.2	26.7	22.4	53.6	18.3
#86	6.4	11.2	2300.4	10.7	1966.5	49.9	21.1	22.3	29.2	11.4
#87	8.9	12.6	2310.1	10.5	1976.9	38.9	23.9	23.4	38.3	9.9
#88	7.1	12.8	2277.6	11.4	1983.6	32.7	21	20.9	30.9	7.9
#89	6.8	11	2262.2	11.6	1938.1	27.5	20.5	21.1	29.1	8.9
#90	6.3	10.7	1978.1	10.1	1919.1	25.2	27.8	24.2	29.9	8.3
#91	7.4	9.6	2008.1	10.2	1800.7	23.6	19.3	22.3	28	7.7
#92	7.6	9.9	2087.8	10.4	1998.1	23.5	18.7	22.6	27.5	6.5

#93	5.4	11.4	2114.3	11.1	1928.8	24.3	20.3	18.9	32.2	9.7
#94	6.7	11.4	2197.7	9	1967.5	20.7	21.9	23.1	29.2	9
#95	5.5	10.6	1860.6	10.6	1890.9	19.2	20.1	21.7	31.6	7.3
#96	5.2	12	1893	10.9	1969	21.3	20.9	21	34.3	10.7
#97	6.5	11.7	1879.1	11.3	1941.5	22	25.3	20.9	41.1	9.6
#98	5.1	10.5	1608.5	10.5	1525.2	16.7	17.1	23.5	44.1	10.2
#99	6.6	10.3	1720.2	9.7	1367.1	16.4	19.5	15.3	63.3	9.8
#100	6.1	11.2	1866.7	10.8	1404.1	18.3	23.3	18.5	61.7	7.2
#101	5.4	9.6	1577.6	9.7	1758.6	21.4	26.9	19	54	10.7
#102	7.1	9.7	1723.2	10.2	1952.6	20.5	21.5	19.6	35.7	9.5
#103	5.8	13.4	1227.6	11.5	1817	20.2	14.3	9	48.5	8.2
#104	5.2	11.2	1673.4	9.7	1271.2	16.3	23	18.4	61.7	9.6

Bacground o/s

	Ag	Cd	S	Fe	Cu	Zn	As	Se	Sb	Pb
#1	5	10.6	15.2	16.4	14	13.6	20.8	25.4	19.3	74.6
#2	5.8	10.8	17.9	14.2	14.6	12.6	17.8	25.4	21.3	76.2
#3	7	10.4	14.7	13.4	15	17.4	18.8	26	19.1	68.6
#4	6	8.8	16.5	15.3	15.8	14	21	25.4	19	73.8
#5	6.6	8.8	16.6	12.5	16	16.4	17.6	21.8	16.9	71.4
#6	5	8.8	12.4	16.6	12.2	16.8	18.8	22.6	19.7	74.6
#7	4.8	11.2	15.1	16.1	16.2	14.2	23.1	29.2	17.4	69.8
#8	5.2	10.6	14.8	13.6	14.8	17.4	26.9	24.6	19.8	66
#9	4.8	12.4	16.4	15.5	15.8	13.2	25.9	23.8	19.6	67.6
#10	4.2	9.8	14.7	16.5	14.4	13.4	20	23	16.6	74.2
#11	6.4	9.4	14.2	16.6	16	14.8	22.9	19.8	20.8	76.6
#12	4.8	8.6	14.1	15.3	14.6	17	23.2	25	18.5	73.8
#13	6.8	9.4	12.6	15.7	17.2	19	21.1	28.6	21.4	77.8
#14	6	8	13.6	14.3	17.8	16.4	20.7	21.2	20	70.8
#15	5.2	7.8	15.4	13.6	16.2	15.2	18.8	23.6	20.4	75.4
#16	5.2	13.4	10.5	12.6	17.4	25	20.1	21	20.3	41.8
#17	5	13.2	15.7	15.7	13.6	16.2	17.4	23.2	21.7	74.4
#18	5.6	9.2	16	15.4	14	15.4	20.9	23.2	21.3	74.4
#19	6.4	9.2	17.6	15.2	14.2	14.4	18.9	22.8	17.7	67.4
#20	6.6	11.8	16	15.4	15.2	13.8	20.6	23.6	19	73.6
#21	5.6	10	14.5	16.4	15	15	18.5	24.2	21.2	74
#22	5.4	8.8	16.5	14.8	13	14.6	18.7	26	17.9	76.4
#23	4.6	7.8	14.9	14.6	14.4	14	19.8	26.8	17.9	71
#24	4.6	10.8	15.9	13.9	13.2	16.4	19.8	27.2	20.1	76.4

#25	5.2	10	16.6	16.3	16.2	16.8	21.5	25	22.1	74.2
#26	6.8	9	15.3	14.1	16.8	17.6	19.9	23.6	21.3	76.4
#27	6.4	10,6	11.7	9.4	25	17.6	32.4	25.6	18.9	47
#28	6.4	10.6	11.2	11.8	26.2	17.2	28.7	28.2	21.7	41.8
#29	3.8	12.6	10.2	12.6	23.4	19.6	21.7	17.4	19.8	34.2
#30	5.8	9.8	9.9	9.8	26	17.8	31.7	25.8	20.2	41.2
#31	6.2	10.8	11.9	9.6	23.6	16.6	28.6	28.2	21.5	40.8
#32	5.8	12.8	9.5	11.2	18.8	17	16.1	17.6	15.6	33.2
#33	5	9.4	8.1	10.9	17.6	17.6	24.3	22.6	17.5	35.4
#34	6	11	9.4	9.8	25.4	19	15.3	19.4	20.2	39.2
#35	4	9.4	9.3	6.6	21.2	19.8	14.7	12.6	22.4	41.4
#36	5	11.6	12.2	8.6	24.2	17.6	29.8	30.8	23.5	40
#37	5.2	13.6	10.6	9.9	23.6	18.6	30.3	24.4	22.5	36.8
#38	3.8	6.4	6.6	7.4	12.4	11.4	18.1	17	13.9	23.4
#39	6	11.4	11.6	9.6	20.4	21.4	15.4	22.8	20.8	41
#40	7.2	12.4	9.9	11.6	23.2	16.4	28.4	25.8	18.3	41.6
#41	7.2	14.6	10.9	11.2	23.6	22.2	29.1	24.8	19.7	40
#42	6	11.6	9.8	10.2	23	21.4	20.8	20.4	19.2	38.8
#43	4.2	7.4	6	8	17.2	13.6	17.5	18.8	15.8	24.6
#44	6.2	12.2	10.8	9.4	21.2	21.2	28.8	30.6	19.3	38.6
#45	6.6	6.8	9.7	10.4	19.2	17.2	28.1	25.2	19.8	34
#46	4.6	9.6	10.3	9.1	24.2	19	21.1	15.8	21.5	35.4
#47	3.2	8.2	9.5	7.9	16.4	14.8	23.4	23.6	13.5	31.6
#48	1.6	2.6	1.4	3.4	4	4.4	8.1	7.8	5.7	3
#49	4.6	8.8	5.2	7.5	10.6	11.6	9.7	10	14.1	27.4
#50	5.6	11.6	11.7	10.6	24.4	19.2	30.4	26	19.2	44
#51	5.6	10.4	9.1	9.1	17.6	16.6	29.4	29	17.6	30.2
#52	1.4	5.6	3.4	3.8	8.6	8.8	10.1	11.2	6.7	6.2
#53	4	9.4	8.4	9.4	17.6	15.2	19.6	19.8	21.6	39.4
#54	3.4	12	10.4	10.7	18.8	18.4	31.7	26.4	21	33
#55	4.8	9.4	7.7	9.2	15.4	13.6	23.4	26.8	16.2	24.6
#56	3.4	10	8.4	9.3	15.6	14.8	22.7	21	15.7	30.2
#57	6.8	14.2	10	10.9	20.6	18.2	16.4	19.8	22	35.2
#58	5.6	12.4	11.8	10.5	24.2	18.2	18.8	23.2	19.8	41
#59	5.4	8.2	8.8	11.7	22.2	17.8	13.3	17	19.9	37.8
#60	6.4	8	8.9	9.7	19.2	15.8	17.8	14.2	18.9	35.2
#61	2.8	10.6	10	8.6	15.4	15	22.2	19	18.3	29.2
#62	7.4	9.6	7.8	10.7	22.6	15	20.8	22.8	17.7	39.6
#63	4.6	10.4	9.2	7.7	17	12.6	15.6	11.8	16.1	26.6
#64	5.4	11	10.4	12.2	21.4	17	24.6	22.2	18	37

Table 4.

Cameca Quantitative Analysis
Label Barite sand cementing phases
Wed Mar-22 14:33:52 2000
Stoi Analysis

Weight%

	Cl	S	Fe	Zn	As	Se	Ag	Pb	Sb	Ba	Hg	Bi	O	Total
#1	0.051	0.037	0	0	0.015	28.62	0.122	71.92	0.105	0.122	0	0.101	17.24	118.333
#2	0.092	0.02	0	0.003	0	28.304	0.055	71.887	0.087	0.131	0.211	0.34	17.113	118.243
#3	0.061	14.425	0	0.144	0.023	0.024	0	86.643	0.075	0.091	0	0	21.155	122.641
#4	0.038	14.571	0	0	0.07	0.027	0.052	86.223	0.094	0	0	0	21.261	122.336
#5	2.491	0.306	0.13	0.003	14.605	0.041	0.888	68.108	0	0	0	0.244	12.948	99.764
#6	2.704	0.325	0.191	0.101	14.737	0.02	0.734	67.81	0.071	0.034	0	0.134	12.992	99.853
#7	2.603	0.053	0.194	0.103	15.034	0	0	69.341	0	0.156	0	0	12.945	100.429
#8	2.532	0.016	0.477	0.024	15.102	0.002	0.114	68.899	0.041	0.105	0	0.007	13.001	100.32
#9	0.05	0.175	15.173	0	21.153	0.077	0	36.157	0.078	0.202	0.027	0	18.667	91.759
#10	0.006	0.152	12.046	0.026	20.777	0.035	0	43.918	0.07	0	0	0	18.119	95.149
#11	0.045	0.135	13.174	0.164	21.283	0.124	0.023	41.889	0.012	0.135	0	0	18.606	95.59
#12	0.067	0.114	13.966	0.142	21.401	0	0.043	38.304	0	0	0	0.066	18.528	92.631
#13	0.064	3.364	22.128	0.165	11.371	0.016	0.066	22.005	0.435	2.11	0	0.059	17.841	79.624
#14	0.029	0.267	21.358	0.007	19.229	0	0.135	26.528	0.229	0.918	0.009	0	18.857	87.566
#15	0.022	0.31	11.022	0	19.859	0.083	0.003	44.529	0	0.123	0.079	0.016	17.559	93.605
#16	0.079	0.412	11.541	0.032	18.247	0.082	0.041	44.044	0.309	0.025	0	0.048	16.956	91.816
#17	0.075	2.631	20.762	0.099	13.363	0.112	0.081	24.69	0.425	0.921	0	0.008	17.864	81.031
#18	0.043	0.402	20.583	0.038	18.566	0.032	0.023	28.012	0.329	0.21	0	0.209	18.5	86.947
#19	0.336	0.443	11.4	0.029	17.202	0.065	0.026	37.586	0.074	0.19	0	0	15.791	83.142
#20	0.095	0.437	11.423	0	19.692	0.049	0.012	42.212	0.061	0.124	0	0.21	17.53	91.845
#21	0.033	0.229	12.934	0.089	20.847	0	0.017	40.605	0.053	0.021	0	0	18.227	93.055
#22	0.002	0.173	13.554	0.109	21.022	0.095	0.026	39.106	0	0.057	0.24	0	18.391	92.775
#23	0.167	0.334	9.338	0.057	19.493	0	0.038	49.114	0.207	0.068	0	0	17.235	96.051
#24	0.026	0.867	13.559	0.033	20.811	0.009	0.069	34.616	0.111	4.179	0	0.173	19.073	93.526
#25	2.557	0.173	0.266	0	14.81	0.059	0.41	69.026	0	0.085	0	0.253	13.002	100.641
#26	0.043	0.122	14.015	0.017	21.401	0	0.041	37.344	0.068	0	0	0	18.457	91.508
#27	0.056	0.228	11.392	0	20.433	0.047	0.017	45.318	0.113	0.096	0.026	0	17.942	95.668
#28	0.057	0.248	11.562	0	20.121	0.054	0.026	43.032	0.137	0.011	0.132	0.121	17.688	93.189
#29	0.264	0.228	10.897	0.055	19.992	0.015	0.139	47.015	0.037	0	0	0.296	17.664	96.602
#30	0.086	0.34	9.971	0.308	19.561	0.02	0.052	48.345	0.1	0	0	0.104	17.471	96.358

#31	0.062	0.166	12.879	0	20.576	0.094	0.113	42.229	0	0.323	0	0.097	18.182	94.721
#32	2.706	0.21	0.315	0.166	14.787	0	0.578	68.367	0.075	0.034	0	0.409	13.012	100.659
#33	0.061	3.315	20.494	0	11.012	0.009	0	20.67	0.417	2.195	0	0.067	16.99	75.23

Atomic%

	Cl	S	Fe	Zn	As	Se	Ag	Pb	Sb	Ba	Hg	Bi	O	Total
#1	0.08	0.064	0	0	0.011	20.212	0.063	19.357	0.048	0.05	0	0.027	60.089	100.001
#2	0.145	0.035	0	0.003	0	20.102	0.029	19.457	0.04	0.054	0.059	0.091	59.985	100
#3	0.078	20.485	0	0.1	0.014	0.014	0	19.042	0.028	0.03	0	0	60.209	100
#4	0.049	20.627	0	0	0.043	0.016	0.022	18.889	0.035	0	0	0	60.32	100.001
#5	4.93	0.67	0.163	0.003	13.679	0.036	0.578	23.068	0	0	0	0.082	56.791	100
#6	5.312	0.705	0.239	0.107	13.698	0.017	0.474	22.792	0.04	0.017	0	0.045	56.553	99.999
#7	5.15	0.116	0.244	0.111	14.074	0	0	23.474	0	0.08	0	0	56.751	100
#8	4.994	0.035	0.597	0.025	14.099	0.002	0.074	23.259	0.024	0.053	0	0.002	56.835	99.999
#9	0.074	0.286	14.259	0	14.818	0.051	0	9.159	0.034	0.077	0.007	0	61.235	100
#10	0.009	0.257	11.698	0.022	15.04	0.024	0	11.497	0.031	0	0	0	61.422	100
#11	0.067	0.223	12.442	0.132	14.983	0.083	0.011	10.664	0.005	0.052	0	0	61.339	100.001
#12	0.1	0.188	13.253	0.115	15.137	0	0.021	9.797	0	0	0	0.017	61.371	99.999
#13	0.095	5.525	20.869	0.133	7.994	0.011	0.032	5.594	0.188	0.809	0	0.015	58.734	99.999
#14	0.041	0.424	19.464	0.005	13.062	0	0.064	6.516	0.096	0.34	0.002	0	59.986	100
#15	0.035	0.541	11.041	0	14.828	0.059	0.002	12.023	0	0.05	0.022	0.004	61.395	100
#16	0.128	0.738	11.859	0.028	13.977	0.06	0.022	12.199	0.146	0.011	0	0.013	60.82	100.001
#17	0.112	4.355	19.733	0.08	9.467	0.075	0.04	6.325	0.185	0.356	0	0.002	59.268	99.998
#18	0.062	0.65	19.115	0.03	12.853	0.021	0.011	7.012	0.14	0.079	0	0.052	59.974	99.999
#19	0.582	0.849	12.531	0.028	14.095	0.051	0.015	11.137	0.037	0.085	0	0	60.59	100
#20	0.149	0.763	11.451	0	14.714	0.034	0.006	11.406	0.028	0.05	0	0.056	61.342	99.999
#21	0.05	0.386	12.483	0.073	14.997	0	0.009	10.563	0.023	0.008	0	0	61.407	99.999
#22	0.004	0.289	12.967	0.089	14.991	0.064	0.013	10.084	0	0.022	0.064	0	61.414	100.001
#23	0.267	0.591	9.499	0.05	14.781	0	0.02	13.467	0.097	0.028	0	0	61.2	100
#24	0.037	1.393	12.509	0.026	14.311	0.006	0.033	8.608	0.047	1.568	0	0.043	61.419	100
#25	5.037	0.378	0.332	0	13.802	0.052	0.266	23.262	0	0.043	0	0.084	56.744	100
#26	0.065	0.203	13.373	0.014	15.221	0	0.02	9.604	0.03	0	0	0	61.471	100.001
#27	0.086	0.389	11.158	0	14.919	0.033	0.009	11.965	0.051	0.038	0.007	0	61.346	100.001
#28	0.089	0.429	11.491	0	14.907	0.038	0.013	11.528	0.062	0.005	0.036	0.032	61.368	99.998
#29	0.411	0.393	10.77	0.046	14.73	0.011	0.071	12.526	0.017	0	0	0.078	60.946	99.999
#30	0.135	0.594	10.004	0.264	14.629	0.015	0.027	13.074	0.046	0	0	0.028	61.186	100.002
#31	0.095	0.278	12.416	0	14.785	0.064	0.056	10.973	0	0.127	0	0.025	61.181	100
#32	5.3	0.456	0.391	0.177	13.707	0	0.372	22.917	0.043	0.017	0	0.136	56.485	100.001
#33	0.095	5.742	20.38	0	8.163	0.006	0	5.541	0.19	0.888	0	0.018	58.977	100

Compoun(%

	Cl	SO2	FeO	ZnO	As2O5	SeO2	Ag2O	PbO	Sb2O3	BaO	HgO	Bi2O3	Total
#1	0.039	0.074	0	0	0.023	40.218	0.131	77.474	0.126	0.136	0	0.113	118.333
#2	0.071	0.04	0	0.004	0	39.774	0.059	77.438	0.104	0.146	0.228	0.379	118.243
#3	0.047	28.82	0	0.179	0.035	0.034	0	93.333	0.09	0.102	0	0	122.641
#4	0.029	29.112	0	0	0.107	0.038	0.056	92.881	0.113	0	0	0	122.336
#5	1.929	0.611	0.167	0.004	22.402	0.058	0.954	73.367	0	0	0	0.272	99.764
#6	2.094	0.649	0.246	0.126	22.604	0.028	0.788	73.046	0.085	0.038	0	0.149	99.853
#7	2.016	0.106	0.25	0.128	23.06	0	0	74.695	0	0.174	0	0	100.429
#8	1.961	0.032	0.614	0.03	23.164	0.003	0.122	74.219	0.049	0.117	0	0.008	100.32
#9	0.039	0.35	19.52	0	32.446	0.108	0	38.949	0.093	0.226	0.029	0	91.759
#10	0.005	0.304	15.497	0.032	31.869	0.049	0	47.309	0.084	0	0	0	95.149
#11	0.035	0.27	16.948	0.204	32.645	0.174	0.025	45.124	0.014	0.151	0	0	95.59
#12	0.052	0.228	17.967	0.177	32.826	0	0.046	41.262	0	0	0	0.074	92.631
#13	0.05	6.721	28.467	0.205	17.441	0.022	0.071	23.704	0.521	2.356	0	0.066	79.624
#14	0.022	0.533	27.477	0.009	29.495	0	0.145	28.576	0.274	1.025	0.01	0	87.566
#15	0.017	0.619	14.18	0	30.461	0.117	0.003	47.967	0	0.137	0.085	0.018	93.605
#16	0.061	0.823	14.847	0.04	27.988	0.115	0.044	47.445	0.37	0.028	0	0.054	91.816
#17	0.058	5.257	26.71	0.123	20.497	0.157	0.087	26.597	0.509	1.028	0	0.009	81.031
#18	0.033	0.803	26.48	0.047	28.478	0.045	0.025	30.175	0.394	0.234	0	0.233	86.947
#19	0.26	0.885	14.666	0.036	26.385	0.091	0.028	40.488	0.089	0.212	0	0	83.142
#20	0.074	0.873	14.695	0	30.205	0.069	0.013	45.472	0.073	0.138	0	0.234	91.845
#21	0.026	0.458	16.639	0.111	31.976	0	0.018	43.74	0.063	0.023	0	0	93.055
#22	0.002	0.346	17.437	0.136	32.245	0.133	0.028	42.126	0	0.064	0.259	0	92.775
#23	0.129	0.667	12.013	0.071	29.899	0	0.041	52.907	0.248	0.076	0	0	96.051
#24	0.02	1.732	17.443	0.041	31.921	0.013	0.074	37.289	0.133	4.666	0	0.193	93.526
#25	1.98	0.346	0.342	0	22.716	0.083	0.44	74.356	0	0.095	0	0.282	100.641
#26	0.033	0.244	18.03	0.021	32.826	0	0.044	40.228	0.081	0	0	0	91.508
#27	0.043	0.456	14.656	0	31.341	0.066	0.018	48.817	0.135	0.107	0.028	0	95.668
#28	0.044	0.495	14.874	0	30.863	0.076	0.028	46.355	0.164	0.012	0.143	0.135	93.189
#29	0.204	0.456	14.019	0.068	30.665	0.021	0.149	50.645	0.044	0	0	0.33	96.602
#30	0.067	0.679	12.827	0.383	30.004	0.028	0.056	52.078	0.12	0	0	0.116	96.358
#31	0.048	0.332	16.569	0	31.561	0.132	0.121	45.49	0	0.361	0	0.108	94.721
#32	2.095	0.42	0.405	0.207	22.681	0	0.621	73.646	0.09	0.038	0	0.456	100.659
#33	0.047	6.623	26.365	0	16.891	0.013	0	22.266	0.499	2.451	0	0.075	75.23

Peak c/s

	Cl	S	Fe	Zn	As	Se	Ag	Pb	Sb	Ba	Hg	Bi	O	
#1	18.4	11.2	22.4	50.5	39.6	2911.2	19.2	952.4	38	58.3	9.3	15.9	N/A	
#2	19	9.3	28.2	51.9	37	2879.1	20.1	952.4	36.9	57.9	9.1	18	N/A	
#3	17.4	1027.3	30.7	50.8	33.4	40.6	18.8	1245.1	38.5	58.9	7.8	19.3	N/A	
#4	16.4	1037.5	28.7	44.6	35.8	43.7	18.7	1234.8	35.6	54.3	8.9	17.6	N/A	
#5	221.2	30.1	31.4	41.7	1208.1	46.3	43.6	900.4	31.5	48.6	7.2	14.7	N/A	
#6	235.8	27.7	33.3	45	1219.7	45.6	39.1	894.7	32	51.1	7.4	15.4	N/A	
#7	228.9	11	33.9	41.7	1243.7	37.9	14.7	916.5	30.2	58	6.4	13.7	N/A	
#8	220.2	8.7	46.9	42.2	1246.1	41.4	18.3	909.9	32.3	55.1	7.4	13.9	N/A	
#9	12.1	15.7	770.6	26.1	1594.5	38.2	10.6	424.5	30.8	43.2	5.5	8.3	N/A	
#10	10.7	17.3	624.7	28	1599.7	41.9	12.3	528.4	28.4	41.2	5.1	10.4	N/A	
#11	12.6	16.8	678.3	31.6	1628.1	43.2	14	500.9	30.6	38.5	5.4	9.5	N/A	
#12	15.5	13	714.7	31.5	1626	34.7	13.9	452.3	28.7	38.3	6.1	8.6	N/A	
#13	16.4	209.9	1065.5	23.2	775.2	29.1	12.9	258.4	42.3	119.6	4.2	9.1	N/A	
#14	9.9	21.2	1049.5	24.6	1369.2	31.7	11.9	304.6	31.8	71	5.3	8.3	N/A	
#15	12.9	24.9	579.5	30.4	1540	41.4	14.3	538.5	28.5	43.2	6.7	9.2	N/A	
#16	16.3	32.2	604.5	31.2	1400	38.6	14.6	534	40.8	41.1	5.6	10.4	N/A	
#17	14.5	165.9	1006.8	25.4	933.7	32	11.4	288.6	42.1	72.1	4.8	8.5	N/A	
#18	13.1	29.6	1017.6	23.3	1329.6	34.4	11.8	325.9	38.7	41.7	3.5	8.7	N/A	
#19	38.5	30.7	589.4	28.1	1298.7	35.7	14.9	444.4	28.8	42.7	4.9	8.3	N/A	
#20	15.6	30.3	592.5	30.8	1513.4	39.5	14.2	505.8	28.3	37.4	5.7	10.2	N/A	
#21	12.4	19.2	665.4	27.1	1592.2	36.4	13.8	483.3	28.3	37.7	4.5	10.7	N/A	
#22	10.4	15.1	696.5	31.1	1602.1	41.7	13.1	465.4	25.2	37.9	5.9	8.9	N/A	
#23	23	28.2	498.8	34	1524.2	37.5	15.7	601.4	33	46.6	5.2	11.4	N/A	
#24	10.2	57.7	685.9	27.4	1545.3	39.6	12.6	409.3	30.7	216.3	4.5	9.5	N/A	
#25	221.9	16	33.9	39.3	1226.3	48	27.2	911.3	30.9	49	7.1	15.8	N/A	
#26	12.3	12.5	714.3	30.7	1616.5	35.7	13.6	441.3	26.3	37.8	5.2	8.3	N/A	
#27	12.7	19.5	597.9	29.2	1578.6	41.8	14.6	547.6	32.6	42	5.7	9.9	N/A	
#28	13.8	21.5	602	30.1	1552	38.5	11.3	514.8	31.2	41.5	6.7	10.3	N/A	
#29	31.7	21.2	573.3	32.9	1550.2	41.7	16.8	572.7	33.7	43	5.4	11.5	N/A	
#30	15	25.9	527.8	35	1519.2	38.5	15	589.5	30.3	37.5	4.5	10.5	N/A	
#31	13.7	17.1	663.7	29.2	1570.3	42.3	14.7	507.5	27	52.3	5.2	10.8	N/A	
#32	236.3	21.9	35.1	45.4	1219	44.2	37.1	903.1	33.4	47.5	7.2	17.9	N/A	
#33	13.1	205.9	986.3	21.2	750.6	27.6	8.1	241.2	40.7	126.8	3.7	8	N/A	

Backgrour c/s

	Cl	S	Fe	Zn	As	Se	Ag	Pb	Sb	Ba	Hg	Bi	O
#1	14.2	8.8	24.4	51.6	38.4	62.6	15	8.6	32.6	52.8	10.8	14.6	N/A
#2	11.4	8	29.2	51.8	42.8	62.8	18.2	8	32.4	52	6.6	13.6	N/A
#3	12.6	15.2	34.6	46.2	31.6	38.4	21.2	11.6	34.8	55	13.2	25.6	N/A
#4	13.4	16	37.6	50	30.4	41.2	17	9.4	31	61.2	11.8	21	N/A
#5	15.2	9.2	24.4	41.6	38.2	43	13.2	7.4	32.4	49.2	8.2	11.4	N/A
#6	12.2	5.6	23	41.6	41.2	44	14	7.6	28.4	49.6	7.4	13.6	N/A
#7	14.2	7.4	23.4	38.2	39.4	44.8	17.8	7	32.2	51	7.8	16.4	N/A
#8	11.4	7.6	21.2	41.4	38	41.2	14.4	7.8	30.2	50.4	9.6	13.8	N/A
#9	7.8	5	17.2	28.8	38.6	32.8	11.4	3.4	26.8	34.4	5.2	9.2	N/A
#10	10.2	7.8	16	27.2	35.4	39.4	12.6	4.6	24.8	41.4	5.8	13.4	N/A
#11	8.8	8.4	16.6	26.6	36	34.4	13.2	4.4	30	32.6	7.4	10.2	N/A
#12	9.8	6	17.6	27.2	37.8	37.6	12.4	3.6	29.8	40.8	8.2	7.8	N/A
#13	10.8	6.6	15.4	18.6	24	28	10.6	6.8	20	29.2	4.2	8.4	N/A
#14	7.4	5.2	13.4	24.4	33.4	34.4	7.2	2.4	20	31.2	5.2	8.4	N/A
#15	11	5.4	20	31.8	40	35.4	14.2	5.6	29.6	37.8	5.8	9	N/A
#16	9.6	6.2	19.2	30.2	37.8	32.6	13.2	7.2	25	40	8	9.8	N/A
#17	8	6.6	12.4	22.6	28.8	24.2	8.6	6.2	20.4	32.6	6.8	8.4	N/A
#18	9.4	5.4	16.2	22.2	33.4	32.2	11	5.6	21.8	32.6	5.4	6.2	N/A
#19	10	3	15.4	27.2	30	31	14	4.4	25	34.4	6.2	10	N/A
#20	7.6	3	16.2	31	36.6	36	13.8	4.8	25.2	32	7	7.6	N/A
#21	9.6	5	17	24.4	37.6	42.6	13.2	4.6	25.6	36.8	6.4	11.8	N/A
#22	10.2	4.4	18.4	27.8	38.8	35	12.2	6	26.2	35.4	3.2	10	N/A
#23	9	7	21	32.2	38.8	38.8	14.4	5.2	22.4	43.6	8.2	12.4	N/A
#24	8	4.8	15.4	26.4	31.4	39	10.2	6	25	34.2	7.2	7.4	N/A
#25	11.2	4.2	19.6	40.6	43	43.2	13.2	7	31.8	45.2	10.2	12.4	N/A
#26	8.6	5	16.6	30.2	31.6	38.2	12.2	5.8	22.8	38.6	9.8	9.2	N/A
#27	8	5.2	21	31.8	36.6	38.4	14	4.8	26.8	37.8	5.4	10.4	N/A
#28	9	6	18	33.8	40	34.6	10.4	3	24.2	41	5.2	8.8	N/A
#29	9.4	6.8	19.2	31.2	36.6	40.6	12	5.2	31.8	43.4	7.8	7.8	N/A
#30	7.8	4.4	19.4	25.4	37.6	37	13.2	4.6	25.2	40.2	5.8	9.2	N/A
#31	8.4	6.8	16.4	32	34.6	35.6	10.8	6.6	27	38.2	7	9.6	N/A
#32	13	7.6	18.2	39.8	40.6	47.4	17.4	8.6	29.6	46	10	12.4	N/A
#33	7.8	6	16	22.8	23.4	27	11.2	6.2	19.4	33	3.8	7.2	N/A

Table 5.

Cameca Quantative Analysis
Label Barite cementing phases .
Thu Mar-23 17:38:55 2000
Stoi Analysis

Weight%

	Cl	S	Fe	Zn	As	Se	Ag	Pb	Sb	Ba	Hg	Bi	O	Total	
#1	0.009	5.759	9.056	0.023	6.824	0	0.008	0	0.108	14.627	0.135	0.185	13.746	50.48	
#2	0.007	0.753	26.81	0	34.456	0.077	0.063	0	0.004	0.047	0	0.094	26.877	89.188	
#3	0.017	1.021	25.792	0.095	33.007	0	0	0.058	0	0	0.104	0	26.061	86.155	
#4	0.018	11.087	31.744	0	0.096	0.062	0.044	0.027	0.151	0.468	0	0.087	20.33	64.114	
#5	0.035	54.258	48.131	0.062	0.03	0	0.1	0	0	0.734	0	0.087	68.061	171.498	
#6	0	0.978	26.27	0	33.46	0.093	0	0.068	0	0.063	0	0.122	26.429	87.483	
#7	0	0.798	26.64	0	32.939	0.068	0.011	0	0.023	0.082	0	0.019	26.058	86.638	
#8	0	0.765	26.279	0	33.747	0.061	0.006	0	0.067	0.219	0.083	0.057	26.385	87.669	
#9	0.018	0.952	26.707	0.095	33.357	0	0.037	0.214	0.083	0.012	0.062	0.226	26.496	88.259	
#10	0	11.534	33.969	0	0.109	0.029	0.258	0	0.018	0.228	0.009	0	21.362	67.516	
#11	0	9.213	26.646	0	0.382	0	0.05	0	0.095	0.696	0.028	0.061	17.145	54.316	
#12	0.03	11.686	34.035	0	0.065	0.007	0.085	0	0.046	0.235	0	0	21.485	67.674	
#13	0.019	0.965	26.439	0	32.557	0.02	0	0.088	0	0.065	0	0	25.936	86.089	
#14	0.002	0.556	26.548	0	33.68	0.032	0.06	0.146	0.033	0.219	0	0	26.201	87.477	
#15	0.009	11.248	34.202	0.026	0.029	0	0.276	0	0	0.184	0	0.254	21.114	67.342	
#16	0.01	11.34	34.915	0	0.027	0	0.463	0	0	0.124	0.084	0.044	21.391	68.398	
#17	0	10.392	32.639	0	0.009	0	0.298	0	0	0.775	0.066	0.359	19.885	64.423	
#18	0.006	0.267	26.649	0.106	0.546	0.101	0	0	0.039	0.037	0	0.018	8.272	36.041	
#19	0	10.57	30.98	0.089	0.03	0.013	0.076	0	0.103	0.65	0.047	0.184	19.594	62.336	
#20	0	0.252	24.943	0	0.532	0.086	0	0	0.072	0.052	0.01	0.062	7.744	33.753	
#21	0	9.33	28.742	0.032	0.055	0.018	0.103	11.54	0.082	0.457	0.027	0.101	18.571	69.058	
#22	0	8.682	27.354	0.082	0.15	0	0.468	14.863	0.132	0.214	0.027	0.066	17.844	69.882	
#23	0	8.053	24.896	0.023	0.09	0.065	0.221	12.465	0.359	0.2	0.045	0.033	16.329	62.779	
#24	0.031	8.942	27.305	0.19	0.317	0	0.651	14.935	0.375	0.375	0	0.199	18.296	71.616	
#25	0.005	9.089	27.686	0	0.158	0.013	0.106	13.883	0.337	0.421	0	0.075	18.294	70.067	
#26	0.031	9.228	27.497	0.078	0.049	0	0.334	13.973	0.04	0.576	0	0.15	18.321	70.277	
#27	0.028	9.815	28.834	0.024	0.031	0.046	0.172	12.215	0.004	0.338	0	0.067	19.094	70.668	
#28	0.02	9.193	27.522	0.089	0.11	0.027	0.118	16.821	0.072	0.275	0.08	0.141	18.522	72.99	
#29	0.01	9.607	29.024	0.02	0.106	0.012	0.18	10.283	0.175	0.402	0	0.229	18.881	68.929	
#30	0.016	9.053	27.226	0.035	0.081	0	0.201	16.144	0.099	0.571	0	0.017	18.232	71.675	

#31	0.019	1.97	3.151	0.069	0.081	0.046	0.006	0	0.068	0	0.037	0.097	2.971	8.515
#32	0.04	3.066	7.804	0	0.083	0.001	0	0.144	0.072	0.11	0	0.053	5.376	16.749
#33	0.027	9.371	0.047	0	0	0	0	54.015	0.042	9.501	0	0.178	14.666	87.847
#34	0.048	8.592	1.159	0.05	0.4	0.02	0.024	0.192	1.568	43.968	0	0.254	14.606	70.881
#35	0.049	9.337	0.012	0.28	0	0	0.054	51.452	0	9.152	0	0.238	14.45	85.024
#36	0.017	12.134	0.05	0.125	0	0.031	0	0	0.024	59.37	0.158	0.169	19.116	91.194
#37	0.016	5.894	30.727	0	0.464	0	0	0.329	0.136	33.57	0.17	0.017	18.907	90.23
#38	0.003	0.294	56.584	0.074	0.428	0.018	0	0.382	0.119	0.898	0	0	16.914	75.714
#39	0	0.327	56.373	0.147	0.577	0.015	0	0.337	0.165	1.155	0	0	17.019	76.115
#40	0.02	0.352	54	0.012	0.686	0.063	0.03	0.653	0.532	1.001	0.134	0.432	16.545	74.46
#41	0.07	18.855	0	0.024	7.264	0	0.091	68.794	6.046	0.974	0	0.239	29.336	131.693
#42	0.017	0.237	62.214	0	1.763	0	0	0	0.091	0.004	0.154	0.355	19.068	83.903
#43	0.031	0.333	56.885	0.061	1.146	0.067	0	0.255	1.24	0.195	0	0.035	17.566	77.814
#44	0.009	1.233	50.16	0.004	2.67	0.061	0.059	4.572	0.239	0.265	0	0.316	17.521	77.109
#45	0	0.273	61.781	0.037	1.608	0.005	0.121	0.055	0.244	0.128	0.183	0.391	18.977	83.803
#46	0.024	2.339	45.632	0.028	1.828	0.014	0.098	5.183	1.995	0.306	0.056	0.182	17.251	74.936
#47	0.029	2.074	48.328	0	1.763	0.017	0.025	5.03	0.883	0.294	0	0.157	17.473	76.073
#48	0.022	14.56	0.436	0.286	0	0.04	0.07	84.786	0.291	0.494	0	0.088	21.414	122.487

Atomic%

	Cl	S	Fe	Zn	As	Se	Ag	Pb	Sb	Ba	Hg	Bi	O	Total
#1	0.017	12.814	11.569	0.025	6.498	0	0.006	0	0.063	7.598	0.048	0.063	61.298	99.999
#2	0.007	0.887	18.143	0	17.381	0.037	0.022	0	0.001	0.013	0	0.017	63.492	100
#3	0.018	1.241	17.999	0.057	17.17	0	0	0.011	0	0	0.02	0	63.484	100
#4	0.023	15.767	25.918	0	0.059	0.036	0.019	0.006	0.057	0.155	0	0.019	57.942	100.001
#5	0.014	24.822	12.642	0.014	0.006	0	0.014	0	0	0.078	0	0.006	62.403	99.999
#6	0	1.172	18.078	0	17.164	0.045	0	0.013	0	0.018	0	0.023	63.487	100
#7	0	0.968	18.546	0	17.093	0.034	0.004	0	0.007	0.023	0	0.004	63.322	100.001
#8	0	0.918	18.114	0	17.34	0.03	0.002	0	0.021	0.061	0.016	0.01	63.486	99.998
#9	0.019	1.135	18.29	0.056	17.028	0	0.013	0.039	0.026	0.003	0.012	0.041	63.338	100
#10	0	15.577	26.34	0	0.063	0.016	0.104	0	0.006	0.072	0.002	0	57.82	100
#11	0	15.549	25.819	0	0.276	0	0.025	0	0.042	0.274	0.008	0.016	57.99	99.999
#12	0.037	15.699	26.252	0	0.037	0.004	0.034	0	0.016	0.074	0	0	57.847	100
#13	0.021	1.175	18.487	0	16.969	0.01	0	0.017	0	0.019	0	0	63.304	100.002
#14	0.002	0.671	18.4	0	17.4	0.016	0.021	0.027	0.01	0.062	0	0	63.389	99.998
#15	0.011	15.325	26.754	0.017	0.017	0	0.112	0	0	0.059	0	0.053	57.652	100
#16	0.012	15.228	26.92	0	0.016	0	0.185	0	0	0.039	0.018	0.009	57.573	100
#17	0	14.991	27.032	0	0.006	0	0.128	0	0	0.261	0.015	0.079	57.488	100
#18	0.017	0.823	47.078	0.161	0.718	0.126	0	0	0.032	0.027	0	0.008	51.01	100

#19	0	15.562	26.186	0.065	0.019	0.008	0.033	0	0.04	0.224	0.011	0.042	57.811	100.001
#20	0	0.828	47.112	0	0.75	0.115	0	0	0.063	0.04	0.005	0.031	51.057	100.001
#21	0	14.341	25.363	0.024	0.036	0.011	0.047	2.745	0.033	0.164	0.007	0.024	57.205	100
#22	0	13.827	25.011	0.064	0.103	0	0.222	3.663	0.056	0.08	0.007	0.016	56.953	100.002
#23	0	14.055	24.947	0.02	0.067	0.046	0.115	3.367	0.165	0.081	0.012	0.009	57.116	100
#24	0.044	13.914	24.394	0.145	0.211	0	0.301	3.596	0.154	0.136	0	0.048	57.057	100
#25	0.007	14.178	24.797	0	0.105	0.009	0.049	3.351	0.138	0.153	0	0.018	57.194	99.999
#26	0.044	14.363	24.571	0.06	0.033	0	0.154	3.366	0.016	0.209	0	0.036	57.148	100
#27	0.038	14.707	24.805	0.018	0.02	0.028	0.076	2.833	0.002	0.118	0	0.015	57.34	100
#28	0.028	14.145	24.314	0.067	0.073	0.017	0.054	4.005	0.029	0.099	0.02	0.033	57.117	100.001
#29	0.014	14.556	25.248	0.015	0.069	0.008	0.081	2.411	0.07	0.142	0	0.053	57.333	100
#30	0.023	14.143	24.421	0.027	0.054	0	0.093	3.903	0.041	0.208	0	0.004	57.083	100
#31	0.171	19.945	18.312	0.343	0.35	0.188	0.018	0	0.181	0	0.061	0.151	60.28	100
#32	0.196	16.603	24.263	0	0.192	0.003	0	0.121	0.103	0.139	0	0.044	58.337	100.001
#33	0.05	18.958	0.055	0	0	0	0	16.911	0.022	4.488	0	0.055	59.461	100
#34	0.087	17.347	1.343	0.049	0.346	0.017	0.014	0.06	0.834	20.725	0	0.079	59.1	100.001
#35	0.092	19.198	0.014	0.283	0	0	0.033	16.372	0	4.393	0	0.075	59.541	100.001
#36	0.023	18.819	0.044	0.095	0	0.019	0	0	0.01	21.496	0.039	0.04	59.414	99.999
#37	0.02	8.469	25.349	0	0.285	0	0	0.073	0.052	11.261	0.039	0.004	54.447	99.999
#38	0.004	0.437	48.338	0.054	0.273	0.011	0	0.088	0.047	0.312	0	0	50.437	100.001
#39	0	0.485	47.955	0.107	0.366	0.009	0	0.077	0.064	0.399	0	0	50.537	99.999
#40	0.027	0.538	47.385	0.009	0.448	0.039	0.014	0.154	0.214	0.357	0.033	0.101	50.679	99.998
#41	0.068	20.196	0	0.012	3.33	0	0.029	11.403	1.706	0.244	0	0.039	62.973	100
#42	0.02	0.316	47.598	0	1.005	0	0	0	0.032	0.001	0.033	0.073	50.923	100.001
#43	0.041	0.481	47.203	0.043	0.709	0.039	0	0.057	0.472	0.066	0	0.008	50.881	100
#44	0.012	1.834	42.842	0.003	1.7	0.037	0.026	1.052	0.094	0.092	0	0.072	52.237	100.001
#45	0	0.366	47.476	0.024	0.921	0.003	0.048	0.011	0.086	0.04	0.039	0.08	50.905	99.999
#46	0.033	3.576	40.061	0.021	1.196	0.009	0.044	1.226	0.803	0.109	0.014	0.043	52.865	100
#47	0.039	3.107	41.577	0	1.131	0.01	0.011	1.166	0.349	0.103	0	0.036	52.471	100
#48	0.027	20.435	0.351	0.197	0	0.023	0.029	18.416	0.108	0.162	0	0.019	60.233	100

Compound%

	Cl	SO2	FeO	ZnO	As2O5	SeO2	Ag2O	PbO	Sb2O3	BaO	HgO	Bi2O3	Total
#1	0.007	11.506	11.65	0.029	10.467	0	0.009	0	0.129	16.331	0.146	0.206	50.48
#2	0.005	1.504	34.491	0	52.851	0.108	0.068	0	0.005	0.052	0	0.105	89.188
#3	0.013	2.04	33.181	0.118	50.628	0	0	0.062	0	0	0.112	0	86.155
#4	0.014	22.151	40.838	0	0.147	0.087	0.047	0.029	0.181	0.523	0	0.097	64.114
#5	0.027	108.404	61.92	0.077	0.046	0	0.107	0	0	0.82	0	0.097	171.498
#6	0	1.954	33.796	0	51.323	0.131	0	0.073	0	0.07	0	0.136	87.483

#7	0	1.594	34.272	0	50.524	0.096	0.012	0	0.028	0.092	0	0.021	86.638
#8	0	1.528	33.807	0	51.763	0.086	0.006	0	0.08	0.245	0.09	0.064	87.669
#9	0.014	1.902	34.358	0.118	51.165	0	0.04	0.231	0.099	0.013	0.067	0.252	88.259
#10	0	23.044	43.7	0	0.167	0.041	0.277	0	0.022	0.255	0.01	0	67.516
#11	0	18.407	34.28	0	0.586	0	0.054	0	0.114	0.777	0.03	0.068	54.316
#12	0.023	23.348	43.785	0	0.1	0.01	0.091	0	0.055	0.262	0	0	67.674
#13	0.015	1.928	34.013	0	49.938	0.028	0	0.095	0	0.073	0	0	86.089
#14	0.002	1.111	34.153	0	51.66	0.045	0.064	0.157	0.04	0.245	0	0	87.477
#15	0.007	22.473	44	0.032	0.044	0	0.296	0	0	0.205	0	0.283	67.342
#16	0.008	22.657	44.917	0	0.041	0	0.497	0	0	0.138	0.091	0.049	68.398
#17	0	20.763	41.989	0	0.014	0	0.32	0	0	0.865	0.071	0.4	64.423
#18	0.005	0.533	34.283	0.132	0.837	0.142	0	0	0.047	0.041	0	0.02	36.041
#19	0	21.118	39.855	0.111	0.046	0.018	0.082	0	0.123	0.726	0.051	0.205	62.336
#20	0	0.503	32.089	0	0.816	0.121	0	0	0.086	0.058	0.011	0.069	33.753
#21	0	18.641	36.976	0.04	0.084	0.025	0.111	12.431	0.098	0.51	0.029	0.113	69.058
#22	0	17.346	35.19	0.102	0.23	0	0.503	16.011	0.158	0.239	0.029	0.074	69.882
#23	0	16.089	32.028	0.029	0.138	0.091	0.237	13.428	0.43	0.223	0.049	0.037	62.779
#24	0.024	17.866	35.127	0.237	0.486	0	0.699	16.088	0.449	0.419	0	0.222	71.616
#25	0.004	18.159	35.617	0	0.242	0.018	0.114	14.955	0.403	0.47	0	0.084	70.067
#26	0.024	18.437	35.374	0.097	0.075	0	0.359	15.052	0.048	0.643	0	0.167	70.277
#27	0.022	19.61	37.094	0.03	0.048	0.065	0.185	13.158	0.005	0.377	0	0.075	70.668
#28	0.015	18.367	35.406	0.111	0.169	0.038	0.127	18.12	0.086	0.307	0.086	0.157	72.99
#29	0.008	19.194	37.339	0.025	0.163	0.017	0.193	11.077	0.209	0.449	0	0.255	68.929
#30	0.012	18.087	35.026	0.044	0.124	0	0.216	17.391	0.119	0.638	0	0.019	71.675
#31	0.015	3.936	4.054	0.086	0.124	0.065	0.006	0	0.081	0	0.04	0.108	8.515
#32	0.031	6.126	10.04	0	0.127	0.001	0	0.155	0.086	0.123	0	0.059	16.749
#33	0.021	18.723	0.06	0	0	0	0	58.186	0.05	10.608	0	0.198	87.847
#34	0.037	17.166	1.491	0.062	0.614	0.028	0.026	0.207	1.877	49.09	0	0.283	70.881
#35	0.038	18.655	0.015	0.349	0	0	0.058	55.425	0	10.218	0	0.265	85.024
#36	0.013	24.243	0.064	0.156	0	0.044	0	0	0.029	66.286	0.171	0.188	91.194
#37	0.012	11.776	39.53	0	0.712	0	0	0.354	0.163	37.481	0.184	0.019	90.23
#38	0.002	0.587	72.794	0.092	0.656	0.025	0	0.411	0.142	1.003	0	0	75.714
#39	0	0.653	72.523	0.183	0.885	0.021	0	0.363	0.198	1.29	0	0	76.115
#40	0.015	0.703	69.47	0.015	1.052	0.089	0.032	0.703	0.637	1.118	0.145	0.482	74.46
#41	0.054	37.671	0	0.03	11.142	0	0.098	74.106	7.238	1.087	0	0.266	131.693
#42	0.013	0.474	80.037	0	2.704	0	0	0	0.109	0.004	0.166	0.396	83.903
#43	0.024	0.665	73.181	0.076	1.758	0.094	0	0.275	1.484	0.218	0	0.039	77.814
#44	0.007	2.463	64.53	0.005	4.095	0.086	0.063	4.925	0.286	0.296	0	0.352	77.109
#45	0	0.545	79.48	0.046	2.466	0.007	0.13	0.059	0.292	0.143	0.198	0.436	83.803
#46	0.019	4.673	58.705	0.035	2.804	0.02	0.105	5.583	2.388	0.342	0.06	0.203	74.936

#47	0.022	4.144	62.173	0	2.704	0.024	0.027	5.418	1.057	0.328	0	0.175	76.073
#48	0.017	29.09	0.561	0.356	0	0.056	0.075	91.333	0.348	0.552	0	0.098	122.487

Peak c/s

	Cl	S	Fe	Zn	As	Se	Ag	Pb	Sb	Ba	Hg	Bi	O
#1	6.6	333.4	413.7	15.6	426.4	20.1	8.5	4	20.4	631.2	3.4	4.9	N/A
#2	6.8	43.5	1229.4	16.8	2402	33.1	9.8	2.9	18.4	29.2	3.1	4	N/A
#3	6.7	57.4	1174.3	18.3	2282.4	28.9	8.1	4.2	18.9	25.9	3.4	4.2	N/A
#4	6	647.6	1307.4	10.6	18.6	15.5	8.7	4.9	19.6	37.7	3	5	N/A
#5	6.3	3307.6	2041	17.6	20.7	19.7	10.6	8.1	19.5	51.3	4.4	7.4	N/A
#6	5.2	55.9	1197.9	13.3	2322.5	30.8	8.6	4.1	19	28.7	3.4	4.1	N/A
#7	5.9	47.1	1212.9	15	2269.9	29.8	9.2	3	20.4	27.1	3.8	3.4	N/A
#8	5.4	44.3	1199.8	14.5	2339.6	29	8	3.2	22.3	34.2	3.4	4.2	N/A
#9	6.4	54.6	1218.5	16.3	2308.9	30.5	9.5	3.6	18.9	26.1	3	4.6	N/A
#10	4.3	673.2	1399.8	8.9	17.5	18.2	16.4	3.3	13.3	26.1	2.7	4.6	N/A
#11	5.3	533.7	1086.5	10.6	30.6	15.7	6.9	4.2	19	45.6	2.3	3.5	N/A
#12	5.1	679	1398.8	11.1	16.4	17.7	8.9	3.6	14.1	25.4	2.8	3.3	N/A
#13	6.5	53.8	1202.3	15.3	2232.1	28.3	9.9	3.7	19.2	30	3.1	3.6	N/A
#14	6.8	32	1210.1	15.9	2327.4	32	9.5	3.7	19.3	29.4	2.7	4	N/A
#15	4.8	657.1	1409.9	11.2	14.4	16.1	14.6	2.7	12.5	26.3	3	5.7	N/A
#16	6.1	661	1440.6	8.7	14.7	15.3	21.8	2.9	13.3	22.6	3.7	3.5	N/A
#17	5.4	607.9	1346	10.6	14.7	17.1	15.4	4.4	12.3	49.4	2.9	7.7	N/A
#18	5.6	18.3	1081.7	10.2	38.6	17.8	6	2.2	16.1	18.1	1.7	2.2	N/A
#19	4.4	614.8	1274.8	11.1	14.7	13.1	7.8	4.7	21.4	44.1	3.5	5.9	N/A
#20	3.9	16.8	1010.4	9	37.6	17.5	4.8	2.3	13.3	19	1.9	3.3	N/A
#21	6	570.8	1271.4	15.8	16.5	18.9	13.9	141	20.9	40.2	3.9	6	N/A
#22	5.5	536.6	1232.8	19.1	22.4	19.9	23.3	178.2	23.4	31.5	4.1	5.4	N/A
#23	5.9	497.1	1115.5	13.4	21.1	19.4	14.3	150.7	34.7	33.7	4.5	7.2	N/A
#24	7.7	553.7	1232.7	18.1	33	18	30.1	179.8	33.9	39.2	2.3	8.4	N/A
#25	6.4	558.2	1237.5	14.4	21.8	20	14.4	167.4	34.6	41.7	3.2	6.5	N/A
#26	7.7	570.5	1233	15.4	17.4	21.5	19.7	165.8	19.4	48.9	3.6	7.4	N/A
#27	7	601.1	1272.6	16.2	16.5	17.6	14.8	147.9	18	39.4	3.2	6.8	N/A
#28	6.3	568.9	1245.5	15.5	22.4	21	11.4	201.9	21.6	39.6	3.3	7.7	N/A
#29	5.7	583.7	1269.1	15.1	15.9	17.3	13.5	125.4	24.3	42.6	3.6	6.7	N/A
#30	8.4	559.7	1228.1	15.5	19.8	18.5	12.6	195.2	21.7	49.5	3.2	5.4	N/A
#31	4	114	127.8	7.2	13.4	15.9	5.4	2	14.3	17	1.4	2.5	N/A
#32	5.1	178.4	312.7	7.1	16.9	13.5	5.6	3.6	15.4	19.9	2.1	2	N/A
#33	11.2	651.3	20.8	32.5	22.1	29	13	704.9	27.7	454.3	7	13.4	N/A
#34	11.2	516.6	62.8	19.6	38.7	22.3	11.7	9.2	112.7	1900.6	4.4	8.8	N/A

#35	13.8	648.7	18	32.8	22.3	30.4	14.6	666.2	25.3	437.7	5.8	13.4 N/A
#36	9.2	728.7	13.1	25.9	9.4	14.4	12.6	5.8	26.4	2681.8	5.3	9.4 N/A
#37	8.5	351.4	1413.8	18.2	38.3	21.2	10.2	7.5	29.8	1517.2	5	6 N/A
#38	6.7	20	2430.6	13.4	33.8	18.1	8.7	7.2	24.2	64.1	3	3.6 N/A
#39	5.4	19.3	2429.5	13.8	43.6	23.3	8.5	6.1	23.3	74.7	2.4	3.1 N/A
#40	6.5	23.2	2339	15.1	48.2	20.1	9.7	9.6	45.2	68.4	3.4	7.7 N/A
#41	15.4	1253.1	23.2	41.1	586.1	40	20.2	927.6	325.7	91.7	7.8	19.1 N/A
#42	6.6	18.1	2707.2	15.5	105.9	19.9	8.4	4.5	26.5	24.4	4.6	8 N/A
#43	7.4	22	2457.9	15.3	72.2	20.3	10	6.6	84.9	33.4	2.7	4.8 N/A
#44	7.8	76.5	2215.5	15.1	155.5	20.3	10.9	54.3	30	30.3	3.1	7.6 N/A
#45	6	20	2693.3	15.3	93.4	17.7	12.6	4.6	30.1	30.6	5.1	7 N/A
#46	8.2	142	2021.4	15.9	112.1	20.5	10.9	62.6	128.9	34.9	3.4	7.3 N/A
#47	7.7	125.7	2133.7	14.3	105.7	20.5	9.5	60.1	63	36.3	2.9	7 N/A
#48	15.7	1019.6	44.8	54.8	31.3	41.6	18.7	1200	47.4	77	9.5	21 N/A

Backgrour c/s

	Cl	S	Fe	Zn	As	Se	Ag	Pb	Sb	Ba	Hg	Bi	O
#1	5.8	5.8	9.6	15	17.4	24.2	8.2	5.4	14.6	25.6	2	2.8	N/A
#2	6.2	3.4	17.6	16.8	33	28.8	7.6	3.8	18.2	27.2	4.2	3	N/A
#3	5.2	3	11.4	15.8	32.8	30.6	9	3.6	20.8	28.2	2.4	4.8	N/A
#4	4.4	7.2	12	10.8	13.2	11.2	7.2	4.6	12	18.2	3.6	4	N/A
#5	3.4	13.8	11.8	16.2	18.8	21.6	7.4	17	20	22.8	5.2	6.4	N/A
#6	5.8	3.8	13.2	13.8	34.6	25.6	8.6	3.4	19	26	3.6	2.8	N/A
#7	8.2	4.6	12.2	17	35.2	26	8.8	3.6	19.2	23.6	4	3.2	N/A
#8	7.6	3.6	14.4	14.6	34	25.6	7.8	3.2	18.8	24.8	2.6	3.6	N/A
#9	4.8	3.8	13.4	13.8	32.6	32.2	8.2	1.4	14.6	25.6	2.4	2.2	N/A
#10	4.8	7.6	12.2	10	11.4	16.2	7.6	5.6	12.4	16.6	2.6	5	N/A
#11	5.4	3.8	7.6	12.8	9.2	15.8	5.2	4.4	14.2	16.6	2	2.8	N/A
#12	2.4	4.8	10	11.4	12.8	17.2	6	4.8	11.8	15.6	2.8	4	N/A
#13	4.8	2.4	11.8	17	26.6	27.2	11.2	2.8	19.6	27.2	3.2	4.4	N/A
#14	6.6	2.4	11.4	17.6	32.4	30.2	7.4	2.2	17.6	20	3	4.2	N/A
#15	4	7.2	10.8	10.6	12.8	16.6	5.2	7.8	14.8	18.6	3.2	2.8	N/A
#16	5.2	5.8	11.2	11.2	13.2	16.2	6	6.6	15.2	17.4	2.8	3	N/A
#17	5.6	7.4	9.4	11	14.2	20	5.2	4.8	14.2	17	2.2	3.6	N/A
#18	5	3	8.4	7.6	11.4	11.6	6.4	3.8	14	16.4	2.2	2	N/A
#19	4.6	5.2	12.4	9	13	12.2	5.2	8.4	16.2	17	3	3.8	N/A
#20	4.2	2.4	8.6	9.4	11	12.2	8.2	2.4	9.4	16.6	1.8	2.6	N/A
#21	7	7	12.6	15	13.2	17.6	10.4	8.6	16.8	21.2	3.6	4.8	N/A

#22	5.6	5.6	12.8	17	13.2	22.2	7.4	6.4	16.8	22.6	3.8	4.6	N/A
#23	7	6.6	13.6	12.8	15.6	14.6	6.8	7.4	16.8	25.4	4	6.8	N/A
#24	5	7	13.6	13.2	13.6	21.4	8	7	15.2	23.6	3.2	6	N/A
#25	6	5	11	18.2	12.2	19	10.8	7.4	17.8	24.2	3.8	5.6	N/A
#26	5	8.2	14.6	13.4	14.4	24.4	8.4	4.6	17.4	25	3.6	5.6	N/A
#27	4.6	8.2	11.4	15.6	14.6	14.2	9	7.8	17.8	25.4	4.8	6	N/A
#28	4.6	5.2	13.6	13.2	15.6	19	7.4	7	18	28.2	2.4	6	N/A
#29	4.8	7.6	10.6	14.6	9.6	16.4	7.4	8.2	15.6	26	5	4	N/A
#30	7	6	13	14.6	14.8	21.6	5.8	8.6	16.8	25.8	4.8	5.2	N/A
#31	2.4	2.4	4.8	5.6	8.6	12.6	5.2	2.8	11	17	1	1.4	N/A
#32	1.6	3.6	8.2	8.8	12.2	13.4	6	2	11.8	15.4	2.4	1.4	N/A
#33	9	8.8	18.4	37	26.2	29.4	16.8	10.2	25.6	42.4	8.8	11	N/A
#34	6.6	6.2	9	18.2	16	21	10.8	7	23	45	4.8	5.8	N/A
#35	9.8	10.4	17.4	24	24.2	35	12.8	9.6	26.4	42.2	9.8	10.2	N/A
#36	7.6	6.6	10.8	22.4	11.2	12.4	12.8	6.4	25	51.8	3.6	7.4	N/A
#37	7	6.6	15	22	13.4	23.2	11.6	3.8	22.2	31.8	3.2	5.8	N/A
#38	6.4	3.2	13.4	11.6	12.6	17	9.8	3	17.8	23.2	4.2	4.6	N/A
#39	7	0.6	15.8	10.2	15	22.4	10.4	2.4	14.4	22.2	3.4	4.2	N/A
#40	4.6	3	14.2	14.8	13.8	16.2	8.6	2.4	16.6	23.2	2	2.8	N/A
#41	9.8	12	24	40.4	33.6	41	17.2	11.6	30.2	51.4	9.2	16	N/A
#42	5	4.6	15	15.8	17.8	20.8	10	5	21.6	24.2	3	4	N/A
#43	4.4	3	13.2	13.8	15	16.2	10.8	3.8	18.2	24.6	3.6	4.4	N/A
#44	7	5.4	15.2	15	14.6	16.4	8.8	3.8	17.4	18.6	3.6	4	N/A
#45	6	4.4	18.2	14.4	13	17.4	8.2	4	17	24.8	3.2	2.6	N/A
#46	6	5.6	14.2	15.2	14.2	19.6	7.4	4.8	24.2	21.6	2.8	5.2	N/A
#47	5	5.2	16	17.8	12.2	19.4	8.6	4.2	16.6	23.4	3.6	5.2	N/A
#48	14	11.2	22.6	45.8	32.8	38	16.4	11.2	33.2	56	10.6	19.8	N/A

Table 6.

Cameca Quantitative Analysis
Label : sulphides inclusion phases
Fri Mar 24 16:02:48 2000
Normal Analysis

Weight%

	Fe	S	Cu	Zn	As	Se	Sb	Pb	Hg	Ag	Ba	Total
#1	0	13.107	0.13	0.132	0.058	0.002	0.145	85.171	0	0.231	0.173	99.149
#2	0.059	13.877	1.914	0.122	0.05	0.028	3.307	80.43	0	0.129	0.318	100.234
#3	0.052	19.356	12.781	0	1.831	0.031	22.572	41.082	0	0.055	0.164	97.924
#4	29.145	34.306	34.423	0.083	0.106	0	0.332	0	0.095	0.048	0.601	99.139
#5	5.338	12.339	0.029	0.209	0.227	0.012	0	0	0.317	76.793	0.497	95.761
#6	0	13.736	0.024	0.158	0.068	0.014	1.309	84.373	0	0.255	0.788	100.725
#7	29.068	34.315	34.618	0.071	0.1	0.003	0.117	0	0.137	0	0.869	99.298
#8	7.148	30.455	62.208	0	0	0.027	0	0	0.025	0.104	0.464	100.431
#9	27.966	34.388	35.083	0	0.023	0	0.059	0	0.073	0.043	0.645	98.28
#10	0.084	13.793	2.001	0.13	0	0.041	0.153	83.979	0	0.047	0.777	101.005
#11	4.354	32.361	1.814	54.204	0.104	0.038	0.661	0	0.131	0.027	0.597	94.291
#12	0.039	13.453	0.005	0	0.068	0.032	0.193	86.685	0	0.19	0.382	101.047
#13	0	7.868	0	0.093	0	0.019	0.075	56.889	0	0	7.048	71.992
#14	0.061	8.195	0	0	0.031	0	0.096	47.721	0	0.025	11.966	68.095
#15	1.255	12.004	0.062	0.013	0.055	1.203	0	0	0.654	80.338	2.628	98.212
#16	0.158	6.221	0.116	0.139	0.084	0.01	4.511	3.82	0.003	75.791	0.802	91.655
#17	0.023	8.351	0	0.011	0	0.01	0	50.915	0	0	9.723	69.033
#18	29.303	34.503	35.124	0.004	0.042	0.002	0.006	0	0	0.051	0.42	99.455
#19	0	17.935	0.03	0	11.123	0.047	0.643	69.484	0	0.001	0.422	99.685
#20	0	13.249	0.07	0.056	0.049	0.013	0.049	86.552	0	0.028	0.889	100.955
#21	44.858	51.641	0.226	0.178	1.419	0.04	0.039	0	0	0.016	0.666	99.083
#22	0.101	14.634	0.138	0.094	2.025	0.012	2.323	79.709	0	0.037	0.157	99.23
#23	6.119	32.613	0.234	56.282	0.002	0.025	0.034	0	0.059	0	0.116	95.484
#24	28.209	33.978	33.907	0.488	0	0.042	0	0	0.049	0.017	1.112	97.802
#25	0	13.858	0.034	0.128	0.046	0.015	2.977	81.246	0	0	0.325	98.629
#26	29.547	34.109	35.005	0.051	0.122	0.027	0	0	0.04	0	0.805	99.706
#27	0.283	9.259	0.132	0.115	0.009	0.046	0.021	24.172	0.014	0.049	35.692	69.792
#28	0.047	8.597	0.059	0	0.004	0	0.042	53.584	0	0.041	9.813	72.187
#29	29.023	34.643	34.588	0	0	0.012	0	0	0.051	0.014	0.696	99.027
#30	47.769	52.899	0.091	0.083	0.006	0.034	0.002	0	0.033	0	0.123	101.04

#31	0.44	0	0	0	0	0.357	0.01	0	79.207	12.986	0.111	93.111
#32	1.481	3.02	0	0.221	0.062	0.947	0.106	0	22.756	2.9	0.044	31.537
#33	1.426	7.828	0.13	0.055	0.06	2.114	0.137	0	47.526	17.922	0.103	77.301
#34	1.084	1.403	0	0.003	0.1	1.619	0.05	0	41.857	35.409	0.058	81.583
#35	1.503	0	0.122	0.127	0.008	0.483	0	0	27.97	19.062	0.185	49.46
#36	0.765	8.275	0.054	0	0	0.261	0	0	37.696	30.791	0.121	77.963

Atomic %

	Fe	S	Cu	Zn	As	Se	Sb	Pb	Hg	Ag	Ba	Total
#1	0	49.29	0.247	0.243	0.093	0.003	0.144	49.569	0	0.258	0.152	99.999
#2	0.119	48.863	3.401	0.211	0.076	0.04	3.066	43.827	0	0.135	0.261	99.999
#3	0.076	49.645	16.543	0	2.01	0.032	15.247	16.307	0	0.042	0.098	100
#4	24.338	49.897	25.265	0.059	0.066	0	0.127	0	0.022	0.021	0.204	99.999
#5	7.936	31.954	0.037	0.266	0.251	0.013	0	0	0.131	59.111	0.3	99.999
#6	0	49.909	0.044	0.281	0.106	0.021	1.253	47.442	0	0.276	0.669	100.001
#7	24.255	49.871	25.388	0.05	0.062	0.002	0.045	0	0.032	0	0.295	100
#8	6.208	46.07	47.488	0	0	0.017	0	0	0.006	0.047	0.164	100
#9	23.492	50.312	25.902	0	0.014	0	0.023	0	0.017	0.019	0.22	99.999
#10	0.171	48.975	3.586	0.227	0	0.059	0.143	46.146	0	0.05	0.644	100.001
#11	3.982	51.558	1.459	42.359	0.071	0.025	0.277	0	0.033	0.013	0.222	99.999
#12	0.082	49.585	0.009	0	0.107	0.048	0.187	49.444	0	0.208	0.329	99.999
#13	0	42.784	0	0.247	0	0.041	0.107	47.873	0	0	8.948	100
#14	0.19	44.404	0	0	0.073	0	0.138	40.017	0	0.04	15.138	100
#15	1.902	31.696	0.083	0.017	0.062	1.29	0	0	0.276	63.055	1.62	100.001
#16	0.292	20.084	0.188	0.22	0.116	0.013	3.835	1.909	0.002	72.736	0.605	100
#17	0.072	45.085	0	0.03	0	0.022	0	42.537	0	0	12.254	100
#18	24.317	49.869	25.618	0.003	0.026	0.001	0.002	0	0	0.022	0.142	100
#19	0	53.139	0.046	0	14.104	0.057	0.501	31.86	0	0.001	0.292	100
#20	0	49.14	0.131	0.102	0.078	0.02	0.048	49.68	0	0.031	0.769	99.999
#21	32.855	65.876	0.146	0.111	0.774	0.021	0.013	0	0	0.006	0.198	100
#22	0.201	51.037	0.242	0.161	3.022	0.018	2.134	43.02	0	0.038	0.128	100.001
#23	5.497	51.032	0.185	43.198	0.001	0.016	0.014	0	0.015	0	0.042	100
#24	23.883	50.105	25.232	0.353	0	0.025	0	0	0.011	0.007	0.383	99.999
#25	0	50.582	0.063	0.228	0.072	0.023	2.862	45.893	0	0	0.277	100
#26	24.578	49.418	25.593	0.036	0.076	0.016	0	0	0.009	0	0.272	99.998
#27	0.751	42.739	0.307	0.26	0.019	0.087	0.026	17.268	0.011	0.067	38.466	100.001
#28	0.139	44.633	0.154	0	0.009	0	0.057	43.051	0	0.064	11.894	100.001
#29	24.171	50.251	25.318	0	0	0.007	0	0	0.012	0.006	0.236	100.001

#30	34.085	65.743	0.057	0.051	0.003	0.017	0.001	0	0.006	0	0.036	99.999
#31	1.49	0	0	0	0	0.855	0.015	0	74.71	22.777	0.153	100
#32	9.528	33.824	0	1.216	0.295	4.308	0.311	0	40.746	9.657	0.115	100
#33	3.621	34.627	0.29	0.119	0.113	3.797	0.16	0	33.603	23.564	0.106	100
#34	3.118	7.027	0	0.007	0.215	3.291	0.066	0	33.503	52.704	0.068	99.999
#35	7.592	0	0.543	0.55	0.03	1.726	0	0	39.331	49.847	0.381	100
#36	1.827	34.4	0.113	0	0	0.44	0	0	25.051	38.05	0.118	99.999

Peak c/s

	Fe	S	Cu	Zn	As	Se	Sb	Pb	Hg	Ag	Ba
#1	24.7	1000.9	43.4	51.1	33.2	42	47	1568	8.2	24.5	70.3
#2	26.9	1047.1	120.1	51.3	35.9	40.2	201.7	1460.5	7.4	20	66.4
#3	21.3	1329.9	506.7	35.9	149.2	34.1	1226.8	706.6	6	15.8	55.5
#4	1377.2	2036.7	1062	22.1	18.6	20.1	35.8	7.6	4.2	10.6	55.6
#5	278.2	871.4	27.6	33.2	35.8	29.8	26.2	9.6	7.7	3122.4	61.2
#6	24.6	1045.2	45.8	50.4	35	41.3	105.4	1549.5	8.1	26.2	86.1
#7	1369.6	2037	1067.3	21	19.3	20.5	28.9	7.1	4.3	10.2	66.9
#8	367.5	1764.3	1960.9	21.3	15.8	20.4	22.8	14.3	4.6	14.2	49.5
#9	1322.2	2040.4	1077.5	17.8	17.8	20.1	22.2	9.8	4	11.6	56.4
#10	32.3	1040.4	121.4	51.6	31.8	42	40	1528	8.2	18.7	83.5
#11	220.2	1836.3	73.9	1424.3	20.5	20.6	51.4	23.4	5.5	11.7	56
#12	26.8	1023.6	44.6	46.5	35	41.3	47.2	1593.7	7.8	23.6	72.2
#13	16.9	595.3	30.8	36.3	24.9	33.2	29.5	993.2	5.9	13.2	365.6
#14	21.2	605.3	26.5	33.5	25.1	31.9	31.7	822	6.3	14.4	595.2
#15	78	850	27.4	32.4	25.3	130.4	23.9	9.7	12.8	3306.7	145.9
#16	26.4	449.9	34	35.7	29	30.9	246.2	80.2	6.1	3163.9	71.4
#17	18.3	622.9	27.8	33.2	22.5	30.2	27.2	883.1	6.1	13.1	487.6
#18	1382.3	2045.6	1079.3	19.1	17.6	20.7	21.1	7.5	3.6	11.2	48.5
#19	23.3	1280	35.8	39.8	954.7	45.9	67.2	1207.5	7.1	16.1	68.8
#20	24.7	1008.2	44.9	47.8	32.3	42.9	37.5	1583.3	7.9	17.8	93.7
#21	1950.4	3183.1	23.5	20.7	110	23.3	20.1	25.1	4	9.5	49.4
#22	31.8	1094.5	51.8	49.3	191	41.7	154	1443.4	8.4	18	61.7
#23	306.8	1844.1	27.4	1470.3	15.7	20.9	21.3	7.6	4	10.2	36
#24	1331.7	2012.2	1041.7	32.4	16.8	21.1	19.3	7.9	4.2	11.4	71.5
#25	24.3	1049.6	43.4	49.9	34	41.9	187.1	1479.4	7.5	17.6	67.7
#26	1397.1	2019.8	1077.1	19.3	18.8	21.3	19.6	9.7	4	9.7	60.4
#27	30.6	625.8	31.1	30	22.2	27.4	28	411.8	5.5	13.8	1717.1
#28	20.4	639.8	32.8	31.3	25.5	30.7	30.2	928.8	6.6	14.4	492.9

#29	1368.4	2051.4	1058.1	16.8	15.9	20.2	17.8	7.6	4.1	10.4	60.7
#30	2068.6	3270.1	14.4	17.8	19.2	22.1	18.7	10.5	4.1	8.6	33.2
#31	53.6	148.2	48.6	50.7	33.4	81.8	35.9	8.3	1043.7	457.4	60
#32	98.2	287.2	26.2	29.6	16.1	101.4	29.9	5.9	256.3	103.4	23.8
#33	98.9	729.2	43	47.1	33.9	218.6	34.4	7.5	581.9	616.7	40.8
#34	84	246.2	39	42.3	34.3	178.4	33.7	7.2	521.8	1294.6	48
#35	104.9	72.8	32.2	32.9	18.6	62.4	23.4	6.5	339.7	672.2	31
#36	60.1	702.9	33.9	34.8	23.8	51.2	25.5	9.6	467.2	1086.5	49.3

Bacground c/s

	Fe	S	Cu	Zn	As	Se	Sb	Pb	Hg	Ag	Ba
#1	26	10.2	38	46.4	28.6	41.8	39.6	50.8	11.5	16.7	62.4
#2	23.6	14	42	47	32	37.6	32.6	46	9.6	15.6	52
#3	18.6	9.8	33.2	37.4	25.4	31.6	37.8	46.6	8.2	13.9	48.4
#4	13.8	9.4	21.8	20	13	20.4	19	51.4	3.3	9	30.2
#5	15	8.4	26.6	27	20.6	28.8	27.8	24.6	4	32.3	40.8
#6	25.2	12	44.8	44.8	29.6	40	38.6	48.8	11.6	17.6	50.2
#7	11	12	22	19.2	14	20.3	23	52.4	3	10.9	30.2
#8	9.8	9.2	27.8	22.2	15.8	18.8	23.2	42.6	4.4	10.7	29.8
#9	14.2	12.2	19.2	21.6	16.6	20.1	19.2	61.8	3.3	10.1	29.2
#10	27.6	10.8	39.4	47	34	38.2	32.2	44.2	12.3	17.1	48.2
#11	11	9.8	16.4	25.2	15.6	18.4	18.4	49.2	4.2	10.8	31.2
#12	24.6	10.4	44.4	52.4	29.6	38.3	37.4	48.6	11	17.2	54.8
#13	17.4	9.8	33.8	33	27	31.6	25.6	45.4	8.2	14.2	40
#14	17.8	7.6	27	36	22.8	32.2	26.6	42.6	6.6	13.5	42
#15	15.8	9.8	25.2	32	21.6	31.3	27.4	29.8	5.2	33.3	37.6
#16	18.4	7.4	29.8	31.4	23.4	30.1	27.6	17.2	6.1	34.5	38
#17	17	8.6	33.4	32.8	24.6	29.3	30.8	46	8.7	13.3	39.2
#18	13.6	12.2	21	19	15.4	20.6	20.8	53.2	3.8	9.5	30.8
#19	25	14.6	34.6	43.2	33.8	41.8	34.8	49.6	10.4	16.1	50
#20	25.4	11.2	42	45.8	28.4	41.7	35	42	11.6	16.9	53.2
#21	16.6	12.6	17	16.4	17.8	20.2	18.2	63.6	4.2	9	22.4
#22	26.2	9.6	46.2	46	30.4	40.5	35.8	50.4	9.7	16.7	54.6
#23	13.6	8.4	20	23.4	15.6	19.5	19.6	51	3.4	12.3	31.2
#24	15.4	12	20	20	17.8	18.3	20.2	56.4	3.7	10.9	24.6
#25	26.2	12	42	45.4	30.4	40.4	35.4	47.2	11.7	18.8	53
#26	16.8	11.2	21.2	18	12.4	19.5	20	54	3.6	11.2	26.4
#27	15.6	7.4	26	26.2	21.6	24	26.8	38.6	5.4	12	52.4
#28	17.8	8	30.4	31.8	25.2	31.9	28	43.8	7.4	12.9	40.6

#29	15.4	10.4	17.2	22.8	17.6	19.4	19.4	52.2	3.6	9.9	31.4
#30	14	13.4	11.8	15.8	18.8	19.4	18.6	76.6	3.8	8.8	28.2
#31	27.8	162.7	51.2	53.6	35.2	47.3	35.4	11.6	19.8	19.7	54.8
#32	15.4	62.2	26.2	21.8	11.2	11.6	24.6	14.2	4.6	9.3	21.8
#33	20.8	150.9	37.8	45.2	29.2	19	27.6	11.8	9.4	13.6	36.2
#34	24	142.3	39.6	42.2	26.8	32.2	31.2	14.6	11.5	21.2	45.4
#35	20.6	92.2	27.2	28.4	18	19	29.2	10	6.2	13.1	22.6
#36	19.2	94.2	31.8	40.2	26.2	27.4	26.8	29.8	11.2	20.7	44

APPENDIX E

APPENDIX E. FLUID INCLUSION ANALYSIS

E1 SAMPLE PREPARATION

Hand picked barite samples were doubly polished to a thickness of 100 to 150μm, sample chips are generally 10 to 20mm in diameter.

E2. SAMPLE RUNNING

A linkam THM600 heating-freezing stage mounted on a Dialux microscope was used during the study, the barite chip to be studied was placed on a sapphire window and sealed. Liquid nitrogen is pumped to the heating-freezing stage and circulated around the sample via rubber hoses. Calibration of the stage is necessary to monitor and correct for any drift occurring throughout the day, pure CO_2 and H_2O inclusion standards were used for low temperature calibrations, a sodium nitrate sample was used for high temperatures. Low temperature calibrations were made on a daily basis, repeat analysis were performed on selected samples.

E3. MICROTHERMOMETRY

Standard microthermetric study has been used on all inclusions, using the heating and freezing methods described by Roedder (1984) and Shepherd et al., (1985). Heating-freezing runs were carried out on each fluid inclusion in order to establish first melt temperature (T_{fm}), final ice melt temperature (T_{mice}) and temperature of homogenisation (T_h). Criteria for recognition of phase changes within the fluid inclusions are given below.

Freezing

All inclusions were cooled to –120°C to ensure all phases are frozen, the analysed inclusions sometimes showed a evidence of freezing with a decrease in the size of the vapour bubble.

First Melt (T_{fm})

Occurs at the eutectic temperature for a chemical system where both liquid and solid are stable. The phenomena, like all of the measurements is made on slow ($1°min^{-1}$) heating. As "first melt" begins, some inclusions exhibit a granular appearance, described by Shepherd *et al.,* (1985).

Final Ice Melt (T_{mice})

Ice is easily observed in many inclusions analysed, generally clinging to the vapour bubble. Measurements are again made at very slow heating rates ($0.5°min^{-1}$) which is believed to be accurate to within 2°C.

Melting temperature of ice (freezing point depression) is representative of salinity (wt% NaCl equivalent) within the H_2O-NaCl system and is based on T_{mice}. Salinity of inclusions has been calculated using the equation of Bodnar (1993):

$$\text{Salinity (wt\% NaCl)} = 1.78\theta - 0.0442\theta^2 + 0.000557\theta^3$$

Where θ is the final ice melting temperature in degrees Celsius

Homogenisation (T_h)

In the two-phase (L+V) inclusions, homogenisation temperature is easily observed. The vapour bubble becomes "excited" on nearing homogenisation, again, heating is continued but at a slow rate until the vapour bubble disappears.

APPENDIX E.

WETAR ISLAND MICROTHERMETRIC DATA

Sample	097106								
	Degree of Fill	Tfm °C	Tmice °C	Wt% NaCl	Th °C	Td °C	Size µm	Inclusion Type	Comments
1	0.95	-20.0	-1.8	3		110	12	1B	
2	0.95		-2.7	4.5	260.1		10	1B	
3	0.9		-2.4	4.1	264		15	1B	
4	0.7					215.2	15	1A	
5	0.9		-2	3.4	258.1		10	1B	
6	0.7					201	20	1A	
7	0.9		-3.1	5.1	301.8		10	1B	
8	0.9					188.4	12	1B	
9	0.95		-1.6	2.8	241		20	1B	
10	0.95		-1.4	2.5	243.2		18	1B	
11	0.95					150	5	1B	
12	0.95				224.6		5	1B	
13	0.7					204.3	20	1A	
14	0.6					178	22	1A	
15	0.95				294		2	1B	
16	0.7		-1.8	3	277.8		22	1A	
17	0.95				265.2		20	1B	
18	0.95				216.7		5	1B	
19	0.9	-21.8	-2.1	3.6	297		22	1B	
20	0.9	-21.0	-1.9	3.2	250.6		10	1B	
21	0.95				219		10	1B	
22	0.95				263.6		10	1B	
23	0.95				205		8	1B	
24	0.7	-20.2	-2.5	4.2	262.7		8	1B	
25	0.95		-2	3.4	249		12	1B	
26	0.95		-1.4	3.2	259.3		8	1B	
27	0.95				247.2		5	1B	
repeat 16	0.7		-1.9	2.5	276.2		22	1A	
28	0.95		-2.1	3.6	249		12	1B	
repeat 24	0.7	-20.3	-2.6	4.3	262.8		10	1B	
29	0.95		-2.1	3.6	243.1		10	1B	
Mean	0.87258	-20.7	-2.0824	3.52941	255.46	178.13	12.581		
SD	0.1139	0.74	0.45858	0.7183	24.396	36.789	5.9876		
				decrepitated samples =			20.69	%	
Mode				3.6	249		10		

Sample	096948								
	Degree of Fill	Tfm °C	Tmice °C	Wt% NaCl	Th °C	Td °C	Size µm	Inclusion Type	Comments
1	0.9		-1.6	2.8	251.1		20	1B	
2	0.9	-23.0	-1.7	2.9	210		20	1B	
3	0.95		-2.4	4.1	207.8		10	1B	
4	0.9		-2.3	3.8	228		12	1B	
5	0.9		-1.8	3	231.6		15	1B	
6	0.95		-2.2	3.7	210.5		12	1B	
7	0.95		-1	1.7	279.1		10	1B	
8	0.95		-1.7	2.9	234.7		10	1B	
9	0.95		-1.4	2.5		185	15	1A	
10	0.9		-1.4	2.5	230.9		10	1B	
11	0.95		-1.5	2.6	205.2		10	1B	
12	0.9				256		8	1B	
13	0.95				209.2		6	1B	
14	0.95		-2	3.4	197.2		6	1B	
15	0.95				309		6	1B	
16	0.9				258.2		6	1B	
17	0.95		-0.9	1.6	262		10	1B	
18	0.95				264.6		10	1B	
repeat 16	0.9				256		6	1B	
19	0.9		-1	1.7		188	10	1B	
20	0.9		-1.5	2.6	257.2			1B	
21	0.7					194	12	1B	
22	0.95		-1.2	2.1	242.1		10	1B	
Mean	0.91739	-23	-1.6	2.7438	240.02	189	10.636		
SD	0.05353	-	0.4604	0.7519	28.809	4.5826	4.0065		
				decrepitated samples =			13.043	%	
Mode				2.9	256		10		

Sample	097122								
	Degree of Fill	Tfm °C	Tmice °C	Wt% NaCl	Th °C	Td °C	Size µm	Inclusion Type	Comments
1	0.9	-22.4	-2.2	3.7	185.9		20	1A	
2	0.9		-2.1	3.6	249		8	1B	
3	0.95		-2.8	4.6		192.6	10	1A	
4	0.95		-2.2	3.7	256.8		10	1B	
5	0.95		-2.4	4.1		197.1	8	1A	
6	0.7		-2.3	3.8	255.1		15	1A	
7	0.9				263		10	1B	
8	0.9					178.8	20	1B	
9	0.95	-22.4	-2.4	4.1	265		10	1B	
10	0.95		-2.4	4.1	294		8	1B	
11	0.9	-22.5	-2.2	3.7	261		6	1B	
12	0.7					173.1	30	1A	
13	0.95		-1.9	3.2	279.4		6	1B	
14	0.7		-2	3.4		183.2	25	1A	
15	0.95				273.1		6	1B	
16	0.95				274.4		8	1B	
17	0.95		-2.1	3.6	297.8		20	1B	
18	0.95		-2.4	4.1	285.2		10	1B	
19	0.9		-1.9	3.2	266.4		20	1B	
20	0.9		-2.1	3.6	281		8	1B	
21	0.95	-22.1	-2.3	3.8	231.4		8	1B	
22	0.9		-1.9	3.2	278		8	1B	
23	0.6		-2.1	3.6		176.9	20	1A	
24	0.95				301.2		10	1B	
25	0.7		-2.3	3.8	313.6		10	1B	
26	0.9				278.3		6	1B	
Mean	0.88077	-22.4	-2.2105	3.73158	269.48	183.62	12.308		
SD	0.104	0.17	0.2233	0.36064	27.518	9.3977	6.6439		
				decrepitated samples =			23.077	%	
Mode				3.6	278		8		

Sample	111943								
	Degree of Fill	Tfm °C	Tmice °C	Wt% NaCl	Th °C	Td °C	Size µm	Inclusion Type	Comments
1	0.9	-22.8	-1.7	2.9	203		24	1A	
2	0.95		-1.8	3	254.6		5	1B	
3	0.9	-22.1	-1.4	2.5		158.4	26	1A	
4	0.95		-1.8	3	254.5		10	1B	
5	0.9		-2	3.4	245.4		24	1B	
6	0.95		-1.9	3.2	233.2		12	1B	
7	0.9					247.4	10	1A	
8	0.7		-1.8	3	262.1		20	1B	
9	0.95		-1.4	2.5	244.4		10	1B	
10	0.95				231		10	1B	
11	0.95		-2.1	3.6	228.1		15	1B	
12	0.95		-2	3.4	245.4		5	1B	
13	0.95				264		15	1B	
14	0.9	-22.6	-2	3.4	227		8	1B	
repeat 14	0.9	-22.6	-2.3	3.8	228		8	1B	
15	0.95					199	10	1B	
17	0.95					197	15	1B	
18	0.9		-1.4	2.5	221.3		10	1B	
repeat 18	0.9		-2.3	3.8	218.3		10	1B	
19	0.95		-2.1	3.6	196		12	1B	
Mean	0.9175	-22.5	-1.8667	3.17333	234.77	200.45	12.95		
SD	0.05684	0.3	0.29681	0.44955	19.723	36.453	6.1342		
				decrepitated samples =			21.053	%	
Mode				3	245.4		10		

Sample	097024								
	Degree of Fill	Tfm	Tmice °C	Wt% NaCl	Th °C	Td	Size µm	Inclusion Type	Comments
1	0.9		-1.6	2.8		120.2	25	1A	
2	0.9		-1.9	3.2		184	20	1A	
3	0.9		-2.2	3.7	221.6		20	1B	
4	0.95		-2.4	4.1	222.5		10	1B	
5	0.95				217.2		5	1B	
6	0.95				237.3		5	1B	
7	0.95				222		10	1B	
8	0.95		-1.7	2.9	209.8		5	1B	
9	0.95				220		5	1B	
10	0.95				223.6		4	1B	
11	0.95				264		5	1B	
12	0.95				268.1		5	1B	
13	0.95				245.9		10	1B	
14	0.9		-2.2	3.7	258		8	1B	
15	0.9				294.5		4	1B	
16	0.7		-2.4	4.1	293.2		4	1B	
17	0.7				237		4	1B	
18	0.7		-2.1		239.2		10	1B	
repeat 18	0.7		-2.1		247.1		10	1B	
repeat 18	0.7		-2.3		251.7		10	1B	
repeat 18	0.7		-2.3		288.6		10	1B	
19	0.7					228	5	1B	
20	0.7					231.3	5	1B	
Mean	0.85217	-	-2.1091	3.5	245.33	190.88	8.6522		
SD	0.11528	-	0.27	0.53852	26.479	51.816	5.7652		
				decrepitated samples =			20	%	
Mode				3.7	237		5		

Sample	097084								
	Degree of Fill	Tfm	Tmice °C	Wt% NaCl	Th °C	Td	Size µm	Inclusion Type	Comments
1	0.9		-2.1	3.6	264.3		10	1B	
2	0.95				235.1		5	1B	
3	0.95				202.7		10	1B	
4	0.95		-1.8	3	231.6		10	1B	
5	0.95		-2	3.4	238		10	1B	
6	0.95	-21.4	-1.5	2.6	202		20	1A	
7	0.95				243.8		25	1B	
8	0.95		-1.9	3.2	241		20	1B	
9	0.9				238.6		10	1B	
10	0.95				218		12	1B	
11	0.9					230.3	10	1B	
12	0.95				229.9		10	1B	
13	0.95				246		10	1B	
14	0.95		-1.6	2.8	208.4		10	1B	
15	0.95		-1.7	2.9	187		12	1B	
16	0.95		-1.7	2.9	193		10	1B	
17	0.95		-1.9	3.2	228.5		10	1B	
18	0.95		-2	3.4			10	1B	
19	0.95		-1.9	3.2	238.1		10	1B	
20	0.9		-2.1	3.6	245		15	1B	
repeat 20	0.9		-2.1	3.6	244.8		15	1B	
21	0.95				286		10	1B	
23	0.7		-2	3.4			12	1B	
24	0.7		-1.9	3.2		189.1	15	1B	
25	0.95		-1	1.7	229.9		5	1B	
26	0.95				216.5		5	1B	
Mean	0.92115	-21.4	-1.825	3.10625	230.37	209.7	11.577		
SD	0.06808	-	0.284	0.47954	22.986	29.133	4.571		
					decrepitated samples =		7.7	%	
Mode				3.2	238		10		

Sample	096879								
	Degree of Fill	Tfm	Tmice °C	Wt% NaCl	Th °C	Td	Size µm	Inclusion Type	Comments
1	0.7	-22.5	-1.8	3	229.1		40	1A	
2	0.95				295		4	1B	
3	0.9	-21.2	-1.7	2.9	224.6		20	1A	
4	0.95		-1.4	2.5	208.7		20	1B	
5	0.95				236		22	1B	
6	0.95				232.1		10	1B	
7	0.95		-1.2	2.1	221		10	1B	
8	0.95		-1.6	2.8	237.9		10	1B	
9	0.95		-1.6	2.8	244		10	1B	
10	0.95				233		8	1B	
11	0.9					184	10	1B	
12	0.95		-1	1.7	217.8		10	1B	
13	0.95				262		6	1B	
14	0.95		-1.8	3	224		10	1B	
15	0.9		-1.9	3.2	242		10	1B	
16	0.95		-1.8	3	232.6		20	1B	
17	0.95		-1.7	2.9	239		8	1B	
repeat 16	0.95		-1.8	3	231		20	1B	
19	0.95					204.6	10	1B	
20	0.9		-1.5	2.6		207	8	1B	
21	0.95		-1.7	2.9	249.3		4	1B	
22	0.95		-1.6	2.6	272.1		4	1B	
23	0.95		-1.8	3	266.1		8	1B	
24	0.95		-1.8	3	288.9		10	1B	
Mean	0.93125	-21.9	-1.6294	2.76471	242.2	198.53	12.166667		
SD	0.05278	0.92	0.2392	0.37739	22.727	12.643	7.9981882		
				decrepitated samples =			12.5	%	
Mode				3	232		10		

Sample	099938								
	Degree of Fill	Tfm	Tmice °C	Wt% NaCl	Th °C	Td	Size µm	Inclusion Type	Comments
1	0.9	-22.5	-2.2	3.7		160	20	1A	
2	0.95		-1.6	2.8			12	1B	
3	0.9	-23.4	-2	3.4	207.4		24	1A	
4	0.95	-22.2	-2.7	4.5	188.2		16	1B	
5	0.95	-22.8	-2.5	4.2	200.6		15	1B	
6	0.95		-2.5	4.2	144.4		20	1B	
7	0.95	-22.8	-2.5	4.2	179.6		12	1B	
8	0.95		-2.6	4.3	182.4		5	1B	
9	0.95		-2.7	4.5	231		18	1B	
10	0.95	-24.4	-2.6	4.3	187.5		10	1B	
repeat 5	0.95	-22.9	-2.5	4.2	200.9		15	1B	
11	0.95		-2.5	4.2		144.8	12	1B	
12	0.95				211.7		10	1B	
13	0.95				197.2		4	1B	
14	0.9					162.1	15	1B	
15	0.9	-22.2	-1.4	2.5			10	2	Monophase L
16	0.9	-22	-1.6	2.8			15	2	Monophase L
17	0.9		-1.7	2.9			10	2	Monophase L
18	0.9		-1.4	2.5			8	2	Monophase L
19	0.95		-2.3	3.8	191		10	1B	
20	0.95		-2.5	4.2	204		8	1B	
21	0.95				181		8	1B	
22	0.9		-1.4	2.5			10	2	Monophase L
23	0.9		-1.5	2.6			10	2	Monophase L
24	0.7	-21.9	-2.5	4.2		151.5	18	1B	
25	0.9					147	15	1B	
26	0.9	-23			202.4		10	1B	
27	0.9		-2.7	4.5		166.2	10	1B	
Mean	0.9196429	-22.7	-2.177	3.6818	194	155.27	12.5		
SD	0.0497015	0.72	0.4937	0.7645	19.25	8.726	4.694		
					decrepitated samples =		23.81	%	
Mode				4.2	200		10		

Sample	111931								
	Degree of Fill	Tfm	Tmice °C	Wt% NaCl	Th	Td °C	Size µm	Inclusion Type	Comments
1	0.7					142.1	10	1B	
2	0.95				215.4		5	1B	
3	0.95		-1.1	1.9	238.2		12	1B	
4	0.95		-1.4	2.5	221.3		5	1B	
5	0.9				268.6		5	1B	
6	0.95				214.2		5	1B	
7	0.9				200		7	1B	
8	0.9				237.7		12	1B	
9	0.95				284.1		10	1B	
10	0.9				244.4		4	1B	
11	0.95	-21.1	-1.5	2.6	189.2		22	1B	
12	0.95		-2.1	3.6	196		18	1B	
13	0.7					202.4	12	1A	
14	0.95				226.1		10	1B	
15	0.7					204	15	1B	
16	0.95		-1.7	2.9	227.2		10	1B	
repeat 16	0.95		-1.6	2.8	224.9		10	1B	
17	0.95				194		6	1B	
18	0.7					198.9	10	1B	
19	0.95				264.9		5	1B	
20	0.95				237.1		5	1B	
Mean	0.892857	-21.1	-1.5667	2.71667	228.43	186.85	9.4286		
SD	0.212959	14.9	0.3327	1.14559	59.834	29.909	5.0427		
				decrepitated samples =			22.727	%	
Mode				#N/A	237		10		

Sample	099917								
	Degree of Fill	Tfm	Tmice °C	Wt% NaCl	Th	Td °C	Size µm	Inclusion Type	Comments
1	0.95	-20.4	-2.5	4.2	221		10	1B	
2	0.95	-21.8	-2.6	4.3	233.8		12	1B	
3	0.95		-2.2	3.7	182.7		5	1B	
4	0.95		-1.6	2.8	233		5	1B	
5	0.95				260		10	1B	
6	0.95				198.4		10	1B	
7	0.7					172.2	18	1B	
8	0.95		-2.1	3.6	215.2		10	1B	
repeat 8	0.95		-2.2	3.7	212.7		10	1B	
9	0.95		-2.5	4.2	237.4		12	1B	
10	0.7					199.1	15	1B	
11	0.95				223.1		20	1B	
12	0.95	-21.1	-2.5	4.2	199.9		5	1B	
13	0.95		-2.4	4.1	212.3		5	1B	
14	0.95				214.9		6	1B	
15	0.9					206.3	10	1B	
16	0.95		-2.1	3.6	228.8		4	1B	
17	0.7		-1.9	3.2		207	10	1B	
18	0.95		-1.8	3	228.6		10	1B	
Mean	0.90789	-21.1	-2.2	3.71667	220.12	196.15	9.8421		
SD	0.09319	0.7	0.3162	0.50782	18.608	16.361	4.4003		
				decrepitated samples =			22.222	%	
Mode				4.2	228		10		

Sample	099939								
	Degree of Fill	Tfm	Tmice °C	Wt% NaCl	Th °C	Td	Size µm	Inclusion Type	Comments
1	0.7		-1.8	3	248.8		10	1B	
2	0.95		-1.2	2.1		184.2	12	1B	
3	0.95		-1.5	2.6	222.2		6	1B	
repeat 3	0.95		-1.6	2.8	220.9		6	1B	
4	0.7					197.6	4	1B	
5	0.95				213		4	1B	
6	0.95		-1.8	3	260.2		10	1B	
7	0.9					216.7	12	1B	
8	0.95	-22.6	-1.6	2.8	212.5		10	1B	
9	0.9					186	20	1B	
10	0.95				199		15	1B	
11	0.95		-1.6	2.8	229.3		10	1B	
12	0.95		-1.7	2.9	244		10	1B	
13	0.95		-1.8	3	269		8	1B	
14	0.95		-1.5	2.6	238.4		8	1B	
15	0.95		-1.7	2.9	248		10	1B	
16	0.95		-1.3	2.3	213.1		15	1B	
17	0.9		-1.8	3	233		20	1B	
18	0.9		-1.7	2.9	251		15	1B	
19	0.95		-1.5	2.6	238		10	1B	
20	0.95		-1.7	2.9	221.9		10	1B	
repeat 19	0.95		-1.5	3	238.1		7	1B	
Mean	0.91818	-22.6	-1.6059	2.77647	233.36	196.13	10.545		
SD	0.07327	-	0.1749	0.26108	18.48	14.947	4.3504		
				decrepitated samples =			20	%	
Mode				3	238		10		

APPENDIX F

APPENDIX F. STABLE ISOTOPE ANALYSIS

SAMPLE PREPARATION

Sulphur analysis

Sulphates

The majority of barites were coarse enough to be separated from hand-specimen using small steel needles. Only pure barite grains were subsequently picked using fine tweezers with the aid of a binocular microscope thus to avoid any other sulphur bearing contamination.

- Approximately 10mg of sample were added to ~200mg CuO and 600mg of "lab-sand" for experimentation.

Sulphides

Sulphides were separated from hand-specimen using a fine tipped dental drill taking care not to involve any other sulphur bearing phases. The late-stage HS sulphide assemblage could not be separated so the drill was used to produce a "bulk" assemblage of covellite-tennantite (Zn rich and Zn poor)-Fe poor sphalerite. No other treatments were performed prior to $\delta^{34}S$ isotopic analysis.

- Approximately 10mg of sample were added to ~200mg CuO for experimentation.

Native Sulphur

One sample collected from Kali Kuning was analysed,

- ~3mg of sample were ground and added to ~200mg CuO for experimentation.

Oxygen analysis

Barite

A number of barite samples were contaminated with sulphur bearing phases.

- These were removed by adding 6ml of 6molar HCL and heating to 145°C for ~1.5 hr.
- HCL was then removed and the samples were rinsed and dried. The remaining samples were also cleaned in this way.

Gypsum

- Gypsum was prepared for $\delta^{18}O_{SO4}$ analysis by precipitating the sulphate as $BaSO_4$.

SAMPLE RUNNING

Sulphur

Sulphides

- Place sample in tube and screw in,
- Open LV1, Turn furnace on (5 minutes to reach ~1075°C)
- Open LV4, then CO2 finger, wait until vacuum to exceed 4, close LV4, open X3,
- When temperature reached, close LV1, open HV1,
- Close all HV and LV taps except for HV5,
- Open X1,2, 3 and CO2 trap,
- Using magnet, slide sample into furnace (gauges should all drop)
- Put liquid nitrogen on Pentane trap and leave for ~25 min (keep nitrogen topped up,
- Close X1, turn off furnace, close X3 and open LV3,
- When gauge 2 rises above 4, close LV3 and open HV3,
- Open LV4, when gauge 4 rises above 4, close LV4 and open HV4,
- Close after a few minutes,
- Take nitrogen off the Pentane trap and heat from top to bottom (gauge 4 will fall)
- Refreeze this trap and watch gauge 4 recover to greater than 6,
- Open HV4 for a few seconds, watch for gauge to cover and close HV4,
- Put nitrogen on CO2 finger, gauge 4 will fall and recover,
- Close CO2 finger and take off nitrogen, heat both Pentane and CO2 traps,
- Close HV5, open X4 and gauge 5 will fall,
- Put nitrogen on clod finger and wait for gauge 5 to recover, open X4,
- Open HV5 and watch gauge 5 recover to ~8, close X5,
- Remove nitrogen from cold finger and heat to room temperature ONLY!
- Record Baratron reading, close HV5, place label on bottle, open X5,
- After gauge falls, put nitrogen on sample bottle, open HV5 and close tap on sample bottle.
- Close X5 and remove sample.

Sulphates

- Place sample in tube and screw in, also add a coiled section (~5 cm) of copper wire,
- Leave copper wire half way out of the furnace, heat to ~1125°C,
- Repeat procedure as for sulphides.

HV, LV and X followed by numbers 1-5 relate to taps on the SURRC sulphur line.

Oxygen

- Place sample in platinum crucible and then into sample tube,
- Fit sample and collection tubes to the oxygen line, open taps,
- Make sure HV isolation valve is closed and HV taps are closed,
- Open LV1 and 4 in turn holding both sample tube then collection tube,
- Close LV1 and 4,
- Open HV isolation valve, then HV1, 2 and 3,
- Turn on RADYNE upto 10 and take reading after 5 minutes. Turn upto 15, the 17 recording after 5 minutes,
- Put nitrogen under sample and the 2 traps,
- Close HV1 and 2 (make sure tap is closed to the right of trap 3),
- Increase RADYNE to 25, read at every 5 minutes, continue upto ~67 or until plasma appears in sample tube,
- Turn off RADYNE and take nitrogen of sample tube,
- Heat sample and watch gauge for second recovery (to ~5),
- Open HV for a second, gauge should move to ~8, close HV,
- Switch off discharge tube and close tap to the right of the cold finger,
- Isolate gas in the two traps, open tap to the left of the cold finger,
- Take nitrogen off the traps and put on the clod finger,
- Switch to gauge 3 and heat both traps until gauge stops increasing,
- Close tap left of cold finger and remove nitrogen,
- Heat off the frost and take Baratron reading,
- Put nitrogen on collecting beaker, close HV3 and open tap right of the cold finger,
- Close tap on collection tube.

ANALYSIS

Sulphur isotope analysis were carried out using the conventional techniques of combustion with Cu2O. SO_2 was extracted from sulphide and sulphate samples following the methods of Robinson and Kusakabe (1975) and Coleman and Moore (1978) respectively. The resulting gas (SO2) were analysed on a VG SIRA II mass spectrometer.

Oxygen isotope ratios were measured on a VG SIRA 10 mass spectrometer.

All stable isotope analysis were carried out at SURRC, East Kilbride, and are presented as per mil (‰) deviations relative to CDT for δ34S and V-SMOW for δ18O.

APPENDIX F. STRONTIUM ISOTOPE ANALYSIS

SAMPLE PREPARATION

N.B. Use gloves at all stages

Barite

- Hand picked barite grains under binocular microscope achieved the cleanest samples,
- Grind ~100 g sample using an agate mortar and pestle and transfer to a Teflon beaker,
- Treat sample with aqua regia to remove any adhering sulphide phases, dilute with 1 ml of Milli-Q before adding acid
- Place on a hot plate for 3-4 hrs, pipette the aqua regia off, wash sample 3 times then dry,
- Barite sample is added to previously cleaned sodium carbonate solution at a ratio of ~1:10 (ratio needed for complete barite dissolution)
- Place in oven at 95°C for 1.5 days, occasionally shake the solution, remove and allow to cool,
- Filter off carbonates on 0.4 m polycarbonate membrane filter under vacuum,
- Dissolve carbonates, in ~10 ml of dilute HCL

Boil down sufficient mother solution to give about 1 microgram of strontium:

- Dissolve in 2 ml 6N Aristar Nitric HNO_3 for loading.

Silica gel may be present, centrifuge samples prior to loading.

Anhydrite / Gypsum

- Grind ~60 mg of sample and dilute with 3 ml of Milli-Q and add 1 drop of CONC 11N HCL,
- Place on hotplate (not greater than 70°C) for 24 hr in capped Savilex beakers,
- Evaporate samples to incipient dryness,
- Take up in 2 ml of 6N Aristar HNO_3 for loading.

Silica gel may be present, centrifuge samples prior to loading.

Whole Rock

- Crush and grind parent rock using a TEMA mill,
- Add ~0.5 g of sample to Savilex beaker and half fill with Milli-Q,
- Place capped beaker onto hot plate (140°C) for 1 hr (H_2O leach),

One sample of fresh basalt (096920) was also leached using HCL, one was placed on the hot plate for 1 hr, the other was left cold.

- Allow to cool, decant water, re-wash with Milli-Q, allow to settle and decant again,
- Place on to hot plate to dry and re-weigh.
- Add HF to samples, cap beakers and leave on hot plate for 24 hr,
- Evaporate to dryness, add 10 drops of HCL, evaporate and add 10 drops of HNO_3, evaporate again,
- Take up in 6 ml of 6N HNO_3 for loading.

Silica gel may be present, centrifuge samples prior to loading.

Column Preparation

~ 0.1 gm resin is used for each column,

- Mix the Sr-spec resin to a slurry with Milli-Q (18.2 MΩ), repeat procedure for the Anion exchange resin.
- Place clean, 4N HNO_3 acid soaked columns in to horizontal rack, using disposable pipettes, load the Sr-spec resin in to each column to a bed depth of 6 mm and allow it to settle.
- Add the Anion exchange resin on top to a depth of at least 3 mm. It is important that the ion exchange resin does not form down the side of the Sr-spec resin as this will allow strontium to bypass the Sr-spec resin.

Conditioning the Column

- Wash the columns through with 10 ml of Milli-Q water followed by 10 ml of 6N Aristar HNO_3 then repeat, the final wash should always be acid.
- Add small containers to each column to catch the subsequent wash (containing everything except lead and strontium).

Running the Columns

- Load the 2 ml / 6 ml sample solutions with care using disposable pipettes. When the sample has run through the resin, wash down the inside of the column with 2 ml 6N HNO_3 (as before, do not disturb the bed resin).
- Elute the column finally with 9 ml 6N HNO_3.
- Remove the containers (containing the wash) and place PTFE beakers under each column.
- Wash the strontium fraction from each column with 10 ml of Milli-Q.
- Evaporate to dryness and cover with parafilm ready for loading on to pre-degassed Tantalum Centre Filaments.

The Sr-spec resin is discarded after the run, columns are washed with Milli-Q water and left soaking in 4N HNO_3, new columns are prepared for each new set of samples.

SAMPLE RUNNING

Degassing Filaments

N.B use gloves at all stages,

- Strip filament posts and clean using sand paper,
- Spot weld Re filaments on to posts,
- Boil filaments in Milli-Q for ~1 hr, decant water,
- Dry filaments in a vacuum oven (80°C),
- Place filaments in degasser and pump down to 1×10^{-7} mbars,
- Increase amperage through filaments until they have spent at least 20 mins at 4.5A, do not allow pressure to degrade to more than 5×10^{-6} mbars,
- Flash filaments
- Allow to cool and remove.

Loading Filaments

- Fit a clean pipette tip to pipette, add tantalum activator to filaments at ~ 1A,
- Pipette ~ 0.5molar Nitric on to sample and mix,
- Pipette mixture on to the filament in small aliquots to avoid overbanking, (spreading of the load during evaporation) turn filament up to ~ 2.5A,
- Sample should change colour (glow red),
- Store sample for adding to turret.

ANALYSIS

Sr isotope ratios were measured at the SOC on a VG 354 thermal ionisation mass spectrometer (TIMS). Sr isotopic ratios were determined as the average of >100 ratios by measuring ion intensities in multidynamic collection mode (Taylor and Nesbitt, 1998). The standard used was NBS 987 with a ratio of 0.710045 $\pm$ 0.000015 (2 S.D., n=30) at the time of analysis.

APPENDIX F. HELIUM ISOTOPE ANALYSIS

SAMPLE PREPARATION

- Hand picked barites and sulphides under a binocular microscope achieved the cleanest samples.
- Massive pyrite samples were broken down to a size between 2-5mm.
- Clean samples ultrasonically with 20% HNO_3, de-ionised water and finally acetone.
- Load samples into screw type crusher.
- Bake crusher and neighbouring stainless steel extraction lines for 12 hours under vacuum (≤150°C)

SAMPLE RUNNING

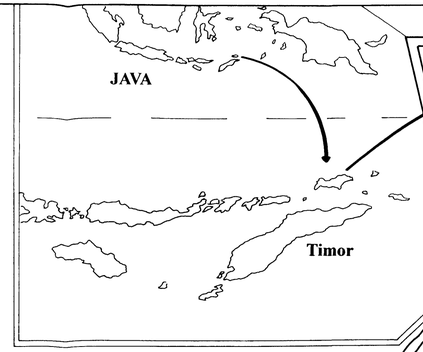
- Helium and Argon determinations were performed using a MAP 215 noble gas mass spectrometer at the University of Manchester.
- Extracted gases were exposed to a SAES Zr-Al getter operating at 250°C to clean up and remove any active gases (N_2, O_2, CO_2) released during crushing.
- After purification, gases were condensed onto an activated charcoal finger, held at liquid nitrogen temperature (-196°C). The non-condensable species including He, Ne and H_2 were exposed to another SAES Zr-Al getter operating at room temperature to reduce any H_2 prior to introduction into the mass spectrometer.
- A second charcoal finger (-196°C) adjacent to the source inlet valve was used to minimise and stabilise the background levels of any Ar, CO_2 and H_2O during the Helium analysis.
- Post Helium analysis, condensable gases are released off the charcoal finger for Argon analysis. Prior to expansion into the mass spectrometer, exposure to a room temperature SAES Zr-Al getter provides a secondary clean up.
- ^{4}He and $^{36,40}Ar$ isotopes were measured using a Faraday collector whilst ^{3}He was measured using an electron multiplier.
- Abundances were calculated by peak height comparison to a known calibrated gas and pressure. Errors for He ratios are quoted as 1σ.

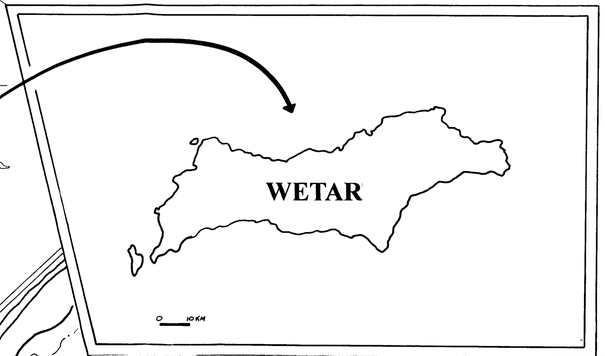
Appendix F: Ar-Ar step heating data of mineral seperates from Wetar Island, Indonesia.

	36Ar (cc)	±36Ar (cc)	Cl (moles)	±Cl (moles)	K (moles)	±K (moles)	40Ar (cc)	±40Ar (cc)	40Ar*/K	±40Ar*/K	Age (Ma)	± Age (Ma)
111999												
400	3.78162E-11	5.83901E-13	1.9898E-08	1.32302E-10	6.49197E-07	1.05932E-09	1.12E-08	7.01E-12	3.134E-08	1.140E-08	4.62	1.68
500	4.44749E-11	5.50383E-13	5.41569E-08	3.57991E-10	1.59532E-06	2.57433E-09	1.38E-08	2.11E-11	3.249E-08	4.407E-09	4.78	0.65
550	3.76075E-11	4.43307E-13	7.90711E-08	5.22601E-10	2.29034E-06	3.80421E-09	1.24E-08	8.69E-12	3.342E-08	2.455E-09	4.92	0.36
600	2.37679E-11	6.19947E-13	7.60886E-08	5.05626E-10	2.20671E-06	3.59821E-09	8.15E-09	4.32E-12	2.814E-08	3.562E-09	4.14	0.52
650	1.01915E-11	6.40375E-13	5.721E-08	3.78797E-10	1.67359E-06	2.60624E-09	4.12E-09	2.89E-12	3.255E-08	4.852E-09	4.79	0.71
700	8.75207E-12	4.67473E-13	4.03731E-08	2.68054E-10	1.18086E-06	1.83443E-09	3.29E-09	1.97E-12	3.050E-08	5.020E-09	4.49	0.74
800	1.71768E-11	7.41116E-13	6.41534E-08	4.24058E-10	1.88303E-06	2.97168E-09	6.13E-09	2.77E-12	2.955E-08	4.990E-09	4.35	0.73
900	4.76439E-11	3.97889E-13	2.54318E-07	1.68547E-09	7.35687E-06	1.23049E-08	1.90E-08	1.70E-11	3.334E-08	6.922E-10	4.91	0.10
1000	1.67173E-11	6.98306E-13	1.28268E-07	8.4688E-10	3.71317E-06	5.78888E-09	7.24E-09	9.39E-12	2.993E-08	2.387E-09	4.41	0.35
1400	1.57838E-11	8.89027E-13	7.40222E-10	3.22077E-11	2.09815E-08	1.09403E-10	4.69E-09	4.99E-12	4.384E-07	5.373E-07	63.52	76.50
097167												
400	2.33008E-11	6.23323E-13	3.72094E-08	2.45724E-10	8.91776E-07	1.39174E-09	6.86E-09	3.60E-12	1.166E-08	6.24E-09	2.41	1.29
500	2.2832E-11	5.90206E-13	4.78916E-08	3.20306E-10	1.02324E-06	1.6049E-09	6.89E-09	2.89E-12	1.755E-08	5.88E-09	3.17	1.06
600	1.36517E-11	5.42885E-13	6.94077E-08	4.58611E-10	1.46575E-06	2.32481E-09	4.35E-09	2.47E-12	1.435E-08	4.15E-09	2.36	0.68
700	1.06693E-11	1.00211E-12	9.04042E-08	5.96881E-10	1.9112E-06	2.96362E-09	3.15E-09	1.88E-12	2.673E-09	4.78E-09	0.54	0.97
800	1.22993E-11	7.42382E-13	1.57136E-07	1.03905E-09	3.29674E-06	5.24834E-09	4.65E-09	6.07E-12	1.556E-08	2.70E-09	2.39	0.41
850	9.82951E-12	8.02412E-13	2.03015E-07	1.3383E-09	4.28129E-06	6.62716E-09	4.52E-09	7.97E-12	1.803E-08	2.29E-09	2.72	0.35
900	7.73832E-12	5.52006E-13	2.53454E-07	1.67072E-09	5.35229E-06	8.25348E-09	4.41E-09	7.23E-12	1.843E-08	1.27E-09	2.75	0.19
950	6.48637E-12	6.16358E-13	1.96419E-07	1.30177E-09	4.0939E-06	7.04098E-09	3.00E-09	8.32E-12	1.261E-08	1.84E-09	1.90	0.28
1000	4.04049E-12	4.67937E-13	1.11173E-07	7.35082E-10	2.23663E-06	3.70127E-09	1.90E-09	2.52E-12	1.497E-08	2.56E-09	2.25	0.39
1200	1.15953E-11	6.45645E-13	5.94805E-08	3.94416E-10	1.04721E-06	1.72964E-09	3.36E-09	2.57E-12	2.842E-09	4.55E-09	0.71	1.14
056896												
200	1.96E-12	8.57E-13	3.86E-11	8.29E-12	3.90E-09	1.64E-10	2.83E-10	1.07E-12	nd		nd	
300	3.00E-12	6.41E-13	1.56E-09	3.56E-11	7.57E-07	1.19E-09	1.16E-09	2.17E-12	1.63E-08	1.12E-08	2.40	1.65
350	1.21E-12	7.17E-13	1.00E-09	2.08E-11	9.69E-07	1.54E-09	1.16E-09	1.70E-12	3.69E-08	9.73E-09	5.43	1.44
400	2.26E-12	9.72E-13	5.32E-10	3.60E-11	2.43E-06	3.81E-09	2.38E-09	3.97E-12	3.15E-08	5.27E-09	4.64	0.78
450	3.04E-12	7.76E-13	2.96E-10	3.85E-11	5.67E-06	8.89E-09	5.13E-09	5.92E-12	3.33E-08	1.80E-09	4.90	0.27
500	4.17E-12	9.19E-13	1.78E-10	4.48E-11	6.51E-06	1.02E-08	6.06E-09	7.51E-12	3.31E-08	1.86E-09	4.88	0.27
600	4.55E-12	9.54E-13	8.52E-12	2.94E-11	2.10E-06	3.34E-09	2.17E-09	3.64E-12	1.74E-08	5.97E-09	2.57	0.88
1200	1.27E-11	6.28E-13	7.26E-11	3.70E-11	3.06E-08	2.10E-10	9.68E-10	3.63E-12	nd		nd	
Total			*3.57E-09*	*8.58E-11*	*1.84E-05*	*1.45E-08*			3.07E-08	1.47E-09	*4.52*	*0.22*

Geological Map of the Kali Kuning, Lerokis and Meron area, Wetar Island, Indonesia.

By Philip Scotney





INDEX

DRIFT

Scree / recent

SOLID	FORMATION
R_L	Reef Limestone
L	Limestone
DF	Lahar / Debris Flow
DF_d	Lahar (+ dacite clasts)
T	Tuff
	Massive Sulphide
B	Barite Ore (pre-mined outline)
A_v	Altered Volcanics
V	Basalt / Andesite
D	Dacite
R	Rhyolite

GEOLOGICAL SYMBOLS

Lithological Boundary
- Definite
- Approximate
- Inferred

Bedding, Strike with Dip

Horizontal Bedding

Fault
Fault Inferred

A-A' Line of Section

Sample Location
Fossiliferous Locality

Axis of Dacite Rhyodaite dome

Scale = 1: 10 000

0 1km

N

S. Koreng

S. Kelapa Tiga

S. Kali Besar

S. Kali Kuning

CAMP

Lerokis Zone 4

Lerokis Zone 5

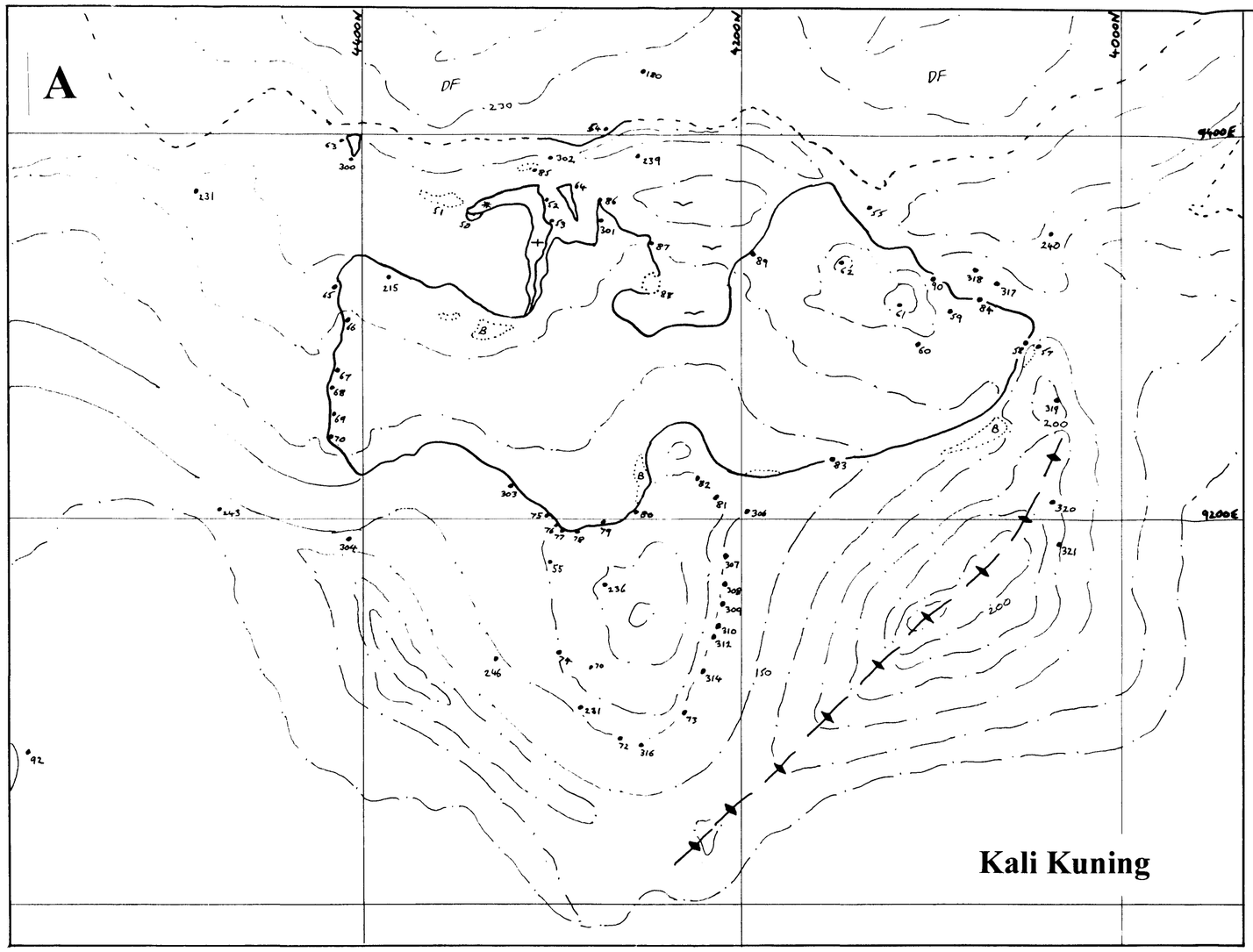
Kali Kuning

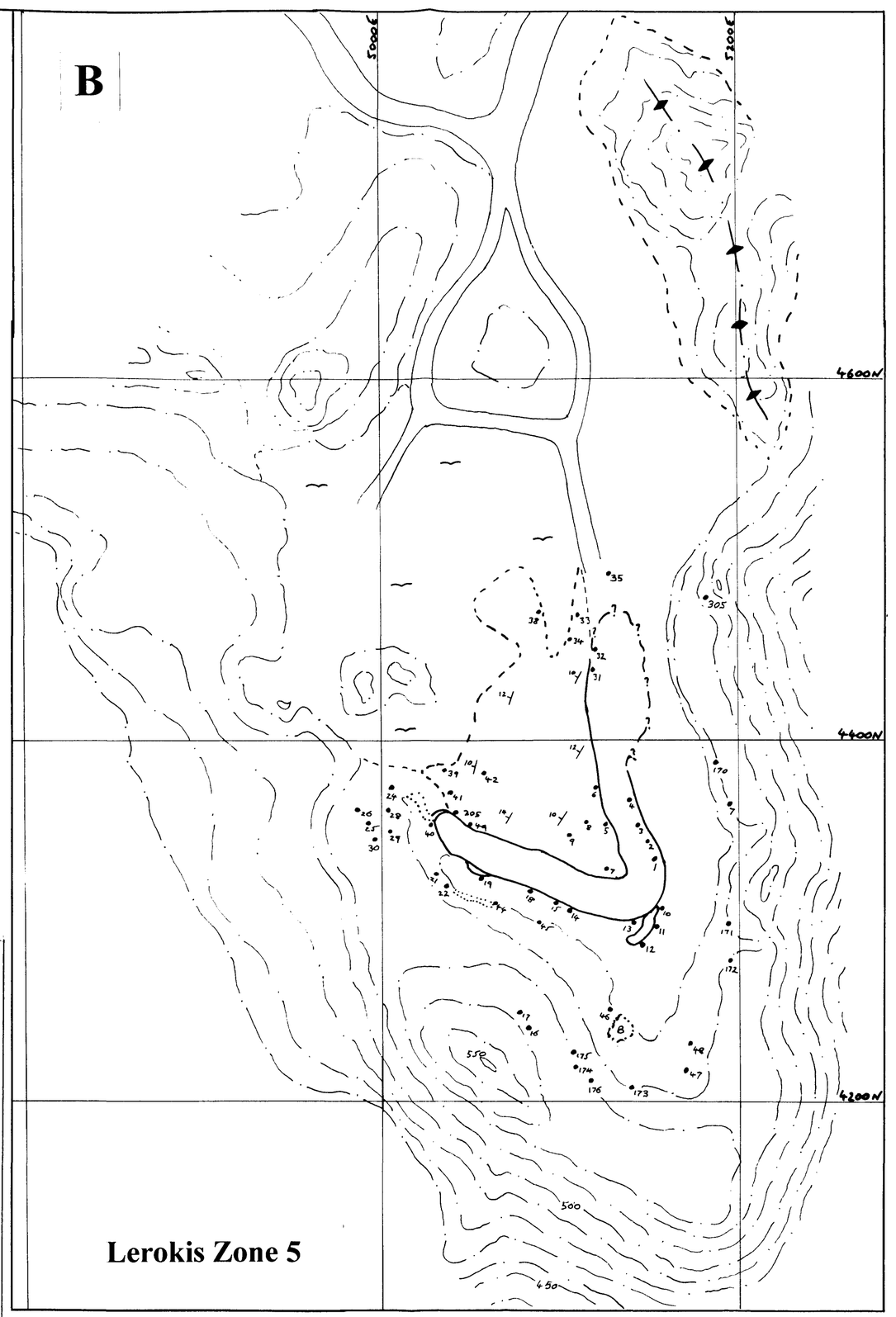
Baru Manu

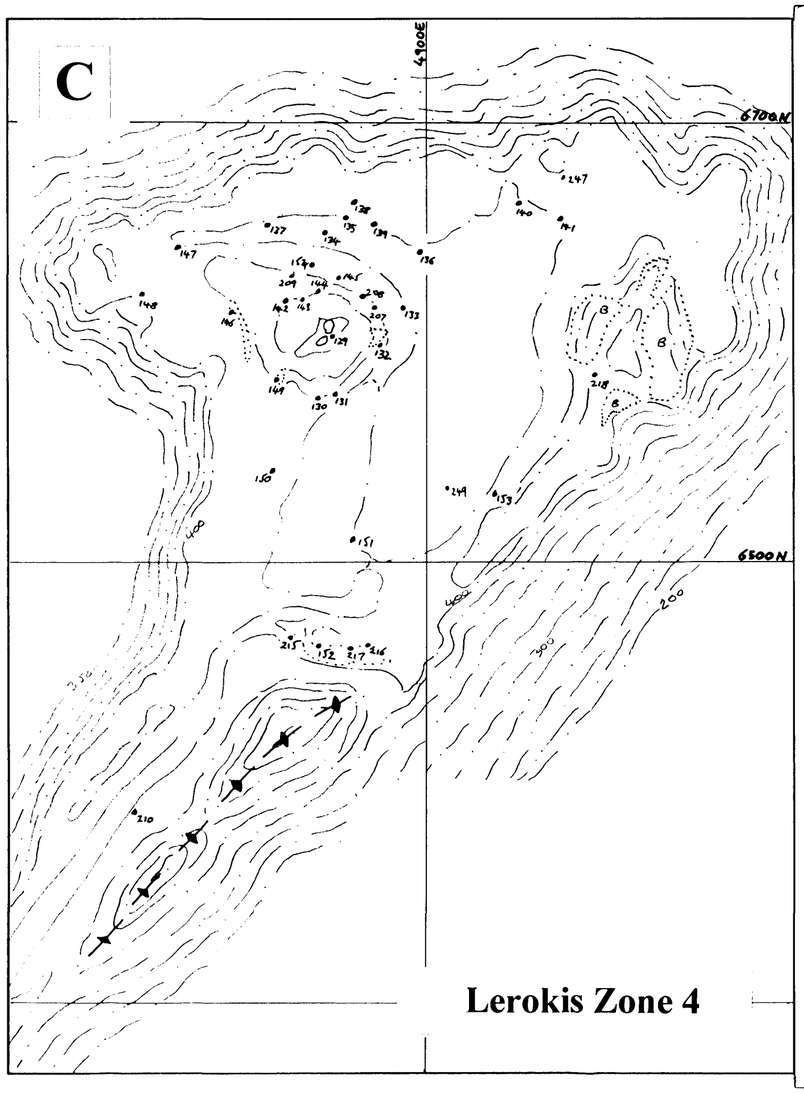
Meron

Geological Map of the Kali Kuning, Lerokis and Meron area, Wetar Island, Indonesia.

MAP INSERT SHEET 1







INDEX

DRIFT

~	Scree / recent

SOLID	FORMATION
L	Limestone
DF	Lahar / Debris Flow
DF_d	Lahar (+ dacite clasts)
T	Tuff / Volcanoclastic sediment
	Massive Sulphide
B	Barite Ore (in situ)
A_v	Altered Volcanics
D	Dacite

0 100m

GEOLOGICAL SYMBOLS

Lithological Boundary
- Definite
- Approximate
- Inferred

Bedding, Strike with Dip

Horizontal Bedding

Fault
Fault Inferred

A-A' Line of Section

Sample Location

Fossiliferous Locality

Axis of Dacite Rhyodaite dome

Geological Map of the Kali Kuning, Lerokis Zone 4 and 5 area, Wetar Island, Indonesia.

MAP INSERT SHEET 2